

Methods in  
Molecular Biology 2294

Springer Protocols

Ulrike S. Stein *Editor*

# Metastasis

Methods and Protocols

MOREMEDIA 

 Humana Press

# METHODS IN MOLECULAR BIOLOGY

*Series Editor*

John M. Walker

School of Life and Medical Sciences

University of Hertfordshire

Hatfield, Hertfordshire, UK

For further volumes:  
<http://www.springer.com/series/7651>

For over 35 years, biological scientists have come to rely on the research protocols and methodologies in the critically acclaimed *Methods in Molecular Biology* series. The series was the first to introduce the step-by-step protocols approach that has become the standard in all biomedical protocol publishing. Each protocol is provided in readily-reproducible step-by-step fashion, opening with an introductory overview, a list of the materials and reagents needed to complete the experiment, and followed by a detailed procedure that is supported with a helpful notes section offering tips and tricks of the trade as well as troubleshooting advice. These hallmark features were introduced by series editor Dr. John Walker and constitute the key ingredient in each and every volume of the *Methods in Molecular Biology* series. Tested and trusted, comprehensive and reliable, all protocols from the series are indexed in PubMed.

# **Metastasis**

## **Methods and Protocols**

Edited by

**Ulrike S. Stein**

*Translational Oncology of Solid Tumors Experimental and Clinical Research Center,  
Charité – Universitätsmedizin Berlin and Max-Delbrück-Center for Molecular Medicine, Berlin, Germany*

*Editor*

Ulrike S. Stein

Translational Oncology of Solid

Tumors Experimental and Clinical

Research Center

Charité – Universitätsmedizin Berlin

and Max-Delbrück-Center for Molecular Medicine

Berlin, Germany

ISSN 1064-3745

ISSN 1940-6029 (electronic)

Methods in Molecular Biology

ISBN 978-1-0716-1349-8

ISBN 978-1-0716-1350-4 (eBook)

<https://doi.org/10.1007/978-1-0716-1350-4>

© Springer Science+Business Media, LLC, part of Springer Nature 2021

This work is subject to copyright. All rights are reserved by the Publisher, whether the whole or part of the material is concerned, specifically the rights of translation, reprinting, reuse of illustrations, recitation, broadcasting, reproduction on microfilms or in any other physical way, and transmission or information storage and retrieval, electronic adaptation, computer software, or by similar or dissimilar methodology now known or hereafter developed.

The use of general descriptive names, registered names, trademarks, service marks, etc. in this publication does not imply, even in the absence of a specific statement, that such names are exempt from the relevant protective laws and regulations and therefore free for general use.

The publisher, the authors, and the editors are safe to assume that the advice and information in this book are believed to be true and accurate at the date of publication. Neither the publisher nor the authors or the editors give a warranty, expressed or implied, with respect to the material contained herein or for any errors or omissions that may have been made. The publisher remains neutral with regard to jurisdictional claims in published maps and institutional affiliations.

This Humana imprint is published by the registered company Springer Science+Business Media, LLC, part of Springer Nature.

The registered company address is: 1 New York Plaza, New York, NY 10004, U.S.A.

---

## Preface

Cancer metastasis is the most lethal attribute of cancer. *It is estimated that at least 90% of all cancer patients dying from any type of cancer are dying due to cancer metastasis.* Cancer metastasis is both the process and the outcome of the process, whereby cancer cells leave a tumor at the primary or original site, spread throughout the body, and seed tumors in new organs or secondary sites. It is mainly metastasis that makes cancer lethal. *Although there is no cure for metastasis,* only 5% of cancer research funding worldwide is devoted to metastasis research.

With this book edition we will enable current and future basic and translational researchers, clinical scientists, and oncologists to take the challenges and work in this field of research. This book series is devoted to disseminate Methods and Protocols, with focus on those indispensable for state-of-the-art metastasis research.

The first part introduces models useful for metastasis research, starting with Zebrafish models for cancer cell invasion and metastasis, the chicken egg chorioallantoic membrane (CAM) model for investigating invasion and the metastasis cascade, in vitro 3D models for tunable stiffness, patient-derived mouse xenografted (PDX) metastasis models from solid tumors for predicting therapy response, and organotypic hippocampal slices to analyze brain metastasis and primary brain tumor growth. In the second part, functional in vitro assays are described, illustrating the steps of the metastatic cascade, such as cancer cell mechanical properties, matrix degradation, cancer cell adhesion, migration, and invasion, platelet aggregation, blood-based pro-metastasis immune cells, bone marrow-derived macrophages, and cancer cell extravasation. The third part describes options for prognostication of metastasis, e.g., by using bioinformatics pipelines to identify metastatic biomarkers, barcoding technology and in vivo assessment for analyzing metastatic abilities and metastatic cell potential, as well as nucleolar contents and proteases to uncover metastatic progression. A last, fourth part complements the book outline with clinical methods, such as imaging procedures and the path toward metastasis research from the clinical setting showing a clinicians perspective.

Finally, we would very much appreciate if also the cancer patient her/himself—who certainly is the center of all efforts—might benefit from this book. Since when the patient is asking “Has it spread?,” she/he is actually asking: “What is my prognosis? Do I have therapy options? Will I survive?” The hope is that this book edition will contribute to a more often optimistic answer to the patient.

Berlin, Germany

Ulrike S. Stein

---

# Contents

Preface .....	v
Contributors .....	ix

## PART I METASTASIS MODELS

1 Cancer Cell Invasion and Metastasis in Zebrafish Models ( <i>Danio rerio</i> ) .....	3
<i>Sarah Martinez Roth, Eric B. Berens, Ghada M. Sharif, Eric Glasgow, and Anton Wellstein</i>	
2 The Chicken Egg Chorioallantoic Membrane (CAM) Model as an In Vivo Method for the Investigation of the Invasion and Metastasis Cascade of Malignant Tumor Cells .....	17
<i>Jörg H. Leupold, Nitin Patil, and Heike Allgayer</i>	
3 In Vitro 3D Models of Tunable Stiffness.....	27
<i>Elysse C. Filipe, Amelia L. Parker, Antonia L. Cadell, Gretel Major, David R. Croucher, and Thomas R. Cox</i>	
4 Patient-Derived Xenografts from Solid Tumors (PDX) for Models of Metastasis .....	43
<i>Annika Wulf-Goldenberg, Jens Hoffmann, Michael Becker, Bernadette Brzezicha, and Wolfgang Walther</i>	
5 Preparation and Culture of Organotypic Hippocampal Slices for the Analysis of Brain Metastasis and Primary Brain Tumor Growth .....	59
<i>Ellina Schulz, Tim Hohmann, Urszula Hohmann, Ralf-Ingo Ernestus, Mario Löhr, Faramarz Dehghani, and Carsten Hagemann</i>	

## PART II FUNCTIONAL MECHANISMS OF METASTASIS

6 Measuring Mechanical and Adhesive Properties of Single Cells Using an Atomic Force Microscope .....	81
<i>Tim Hohmann and Faramarz Dehghani</i>	
7 Analyzing the Roles of Rho GTPases in Cancer Cell Adhesion to Endothelial Cells Under Flow Conditions .....	93
<i>Camilla Cerutti and Anne J. Ridley</i>	
8 Probing Intravascular Adhesion and Extravasation of Tumor Cells with Microfluidics.....	111
<i>Naël Osmani, Gautier Follain, Valentin Gensbittel, María Jesús García-León, Sébastien Harlepp, and Jacky G. Goetz</i>	
9 Real-Time Cell Migration Monitoring to Analyze Drug Synergism in the Scratch Assay Using the IncuCyte System .....	133
<i>Dennis Kobelt, Wolfgang Walther, and Ulrike S. Stein</i>	
10 Measurement of Metabolites from Migrating Cells.....	143
<i>Demond Williams and Barbara Fingleton</i>	

11	Matrix Degradation Assay to Measure the Ability of Tumor Cells to Degrade Extracellular Matrix .....	151
	<i>Rosa Fontana and Jing Yang</i>	
12	Evaluation of Real-Time In Vitro Invasive Phenotypes .....	165
	<i>René M. DeLosh and Robert H. Shoemaker</i>	
13	Detection of Tumor Cell-Induced Platelet Aggregation and Granule Secretion .....	181
	<i>Svenja Schwarz, Martin Schlesinger, and Gerd Bendas</i>	
14	Fatty Acid-Driven Polarization of Suppressive Bone Marrow-Derived Macrophages Including Metabolic and Functional Analysis .....	197
	<i>Hao Wu and Rainer Glauben</i>	
15	From Whole Blood to Isolated Pro-Metastasis Immune Cells: An Ex Vivo Approach to Isolate and Manipulate Immune Cells Contributing to Tumor Metastasis .....	209
	<i>Amany Samir, Aya Aly El Khodiry, and Hend M. ElTayebi</i>	

### PART III PROGNOSTICATION OF METASTASIS

16	A Bioinformatic Pipeline to Identify Biomarkers for Metastasis Formation from RNA Sequencing Data .....	221
	<i>Mathias Dahlmann and Ulrike S. Stein</i>	
17	Barcode Technology for Multiplexed Analysis of Metastatic Ability In Vivo .....	239
	<i>Philip Dujardin and Barbara M. Grüner</i>	
18	In Vivo Assessment of Metastatic Cell Potential in Prostate Cancer .....	253
	<i>Marc Nunez-Olle, Marc Guiu, and Roger R. Gomis</i>	
19	Isolation of Nucleoli for Characterization of Nucleolar Contents to Uncover Clues to Metastatic Progression .....	269
	<i>Shannon E. Weeks and Rajeev S. Samant</i>	
20	Analyzing the Role of Proteases in Breast Cancer Progression and Metastasis Using Primary Cells from Transgenic Oncomice .....	275
	<i>Olga Vasiljeva, Lisa Sevenich, and Thomas Reinheckel</i>	

### PART IV CLINICAL METASTASIS

21	Nuclear Medicine Imaging Procedures in Oncology .....	297
	<i>Ajay-Mohan Mohan, Nicola Beindorff, and Winfried Brenner</i>	
22	From Operating Table to Laboratory Bench: The Path Toward Metastasis Research from the Clinical Setting .....	323
	<i>Miguel E. Alberto Vilchez and Beate Rau</i>	

<i>Index</i> .....	335
--------------------	-----

---

## Contributors

MIGUEL E. ALBERTO VILCHEZ • *Department of Surgery, Campus Virchow Klinikum—Campus Mitte, Charité—University Hospital Berlin, Berlin, Germany; Translational Oncology of Solid Tumors, Experimental and Clinical Research Center, Charité—University Hospital Berlin, Berlin, Germany; Max-Delbrück-Center for Molecular Medicine in the Helmholtz Association, Berlin, Germany*

HEIKE ALLGAYER • *Department of Experimental Surgery—Cancer Metastasis, Medical Faculty Mannheim, Ruprecht Karls University of Heidelberg, Mannheim, Germany; Centre for Biomedicine and Medical Technology Mannheim (CBTM), Medical Faculty Mannheim, Ruprecht Karls University of Heidelberg, Mannheim, Germany*

MICHAEL BECKER • *Experimental Pharmacology and Oncology (EPO), Berlin, Germany*  
NICOLA BEINDORFF • *Berlin Experimental Radionuclide Imaging Centre (BERIC), Charité—Universitätsmedizin Berlin, Berlin, Germany*

GERD BENDAS • *Pharmaceutical Department, University Bonn, Bonn, Germany*

ERIC B. BERENS • *Department of Oncology, Lombardi Comprehensive Cancer Center, Georgetown University Washington, Washington, DC, USA*

WINFRIED BRENNER • *Department of Nuclear Medicine, Charité—Universitätsmedizin Berlin, Berlin, Germany; Berlin Experimental Radionuclide Imaging Centre (BERIC), Charité—Universitätsmedizin Berlin, Berlin, Germany*

BERNADETTE BRZEZICHA • *Experimental Pharmacology and Oncology (EPO), Berlin, Germany*

ANTONIA L. CADELL • *The Garvan Institute of Medical Research and The Kinghorn Cancer Centre, Darlinghurst, NSW, Australia*

CAMILLA CERUTTI • *School of Cellular and Molecular Medicine, Biomedical Sciences Building, University of Bristol, Bristol, UK*

THOMAS R. COX • *The Garvan Institute of Medical Research and The Kinghorn Cancer Centre, Darlinghurst, NSW, Australia; Faculty of Medicine, St. Vincent's Clinical School, UNSW Sydney, Kensington, NSW, Australia*

DAVID R. CROUCHER • *The Garvan Institute of Medical Research and The Kinghorn Cancer Centre, Darlinghurst, NSW, Australia; Faculty of Medicine, St. Vincent's Clinical School, UNSW Sydney, Kensington, NSW, Australia*

MATHIAS DAHLMANN • *Experimental and Clinical Research Center, Charité—University Medicine Berlin and Max-Delbrück-Center for Molecular Medicine in the Helmholtz Association, Berlin, Germany; German Cancer Consortium (DKTK), Heidelberg, Germany*

FARAMARZ DEHGHANI • *Institute of Anatomy and Cell Biology, Martin Luther University Halle-Wittenberg, Halle (Saale), Germany*

RENÉ M. DE LOSH • *Leidos Biomedical Research, Frederick National Laboratory for Cancer Research, Frederick, MD, USA*

PHILIP DUJARDIN • *Department of Medical Oncology, West German Cancer Center, University Hospital Essen at the University of Duisburg-Essen, Essen, Germany*

AYA ALY EL KHODIRY • *Molecular Pharmacology Research Group, Department of Pharmacology and Toxicology, Faculty of Pharmacy and Biotechnology, German University in Cairo, Cairo, Egypt*

- HEND M. ELTAYEBI • *Molecular Pharmacology Research Group, Department of Pharmacology and Toxicology, Faculty of Pharmacy and Biotechnology, German University in Cairo, Cairo, Egypt*
- RALF-INGO ERNESTUS • *Department of Neurosurgery, Tumorbiology Laboratory, University of Würzburg, Würzburg, Germany*
- ELYSSA C. FILIPE • *The Garvan Institute of Medical Research and The Kinghorn Cancer Centre, Darlinghurst, NSW, Australia; Faculty of Medicine, St. Vincent's Clinical School, UNSW Sydney, Kensington, NSW, Australia*
- BARBARA FINGLETON • *Cancer Biology Program and Department of Pharmacology, Vanderbilt University, Nashville, TN, USA*
- GAUTIER FOLLAIN • *INSERM UMR\_S1109, Strasbourg, France; Université de Strasbourg, Strasbourg, France; Fédération de Médecine Translationnelle de Strasbourg (FMTS), Strasbourg, France; Turku Bioscience Centre, University of Turku and Åbo Akademi University, Turku, Finland*
- ROSA FONTANA • *Department of Pharmacology, University of California, San Diego, La Jolla, CA, USA*
- MARIA JESÚS GARCÍA-LEÓN • *INSERM UMR\_S1109, Strasbourg, France; Université de Strasbourg, Strasbourg, France; Fédération de Médecine Translationnelle de Strasbourg (FMTS), Strasbourg, France*
- VALENTIN GENSBITTEL • *INSERM UMR\_S1109, Strasbourg, France; Université de Strasbourg, Strasbourg, France; Fédération de Médecine Translationnelle de Strasbourg (FMTS), Strasbourg, France*
- ERIC GLASGOW • *Department of Oncology, Lombardi Comprehensive Cancer Center, Georgetown University Washington, Washington, DC, USA*
- RAINER GLAUBEN • *Medical Department for Gastroenterology, Infectiology and Rheumatology, Charité—Universitätsmedizin Berlin, Berlin, Germany*
- JACKY G. GOETZ • *INSERM UMR\_S1109, Strasbourg, France; Université de Strasbourg, Strasbourg, France; Fédération de Médecine Translationnelle de Strasbourg (FMTS), Strasbourg, France*
- ROGER R. GOMIS • *Cancer Science Program, Institute for Research in Biomedicine (IRB Barcelona), The Barcelona Institute of Science and Technology, Barcelona, Spain; CIBERONC, Madrid, Spain; School of Medicine, Universitat de Barcelona, Barcelona, Spain; ICREA, Institució Catalana de Recerca i Estudis Avançats, Barcelona, Spain*
- BARBARA M. GRÜNER • *Department of Medical Oncology, West German Cancer Center, University Hospital Essen at the University of Duisburg-Essen, Essen, Germany*
- MARC GUIU • *Cancer Science Program, Institute for Research in Biomedicine (IRB Barcelona), The Barcelona Institute of Science and Technology, Barcelona, Spain; CIBERONC, Madrid, Spain*
- CARSTEN HAGEMANN • *Department of Neurosurgery, Tumorbiology Laboratory, University of Würzburg, Würzburg, Germany*
- SÉBASTIEN HARLEPP • *INSERM UMR\_S1109, Strasbourg, France; Université de Strasbourg, Strasbourg, France; Fédération de Médecine Translationnelle de Strasbourg (FMTS), Strasbourg, France*
- JENS HOFFMANN • *Experimental Pharmacology and Oncology (EPO), Berlin, Germany*
- TIM HOHMANN • *Institute of Anatomy and Cell Biology, Martin Luther University Halle-Wittenberg, Halle (Saale), Germany*
- URSZULA HOHMANN • *Institute of Anatomy and Cell Biology, Martin Luther University Halle-Wittenberg, Halle (Saale), Germany*

- DENNIS KOBELT • *Experimental and Clinical Research Center, Charité—Universitätsmedizin Berlin, Berlin, Germany; Max-Delbrück-Center for Molecular Medicine, AG Translational Oncology of Solid Tumors, Berlin, Germany; German Cancer Consortium (DKTK), Heidelberg, Heidelberg, Germany*
- JÖRG H. LEUPOLD • *Department of Experimental Surgery—Cancer Metastasis, Medical Faculty Mannheim, Ruprecht Karls University of Heidelberg, Mannheim, Germany; Centre for Biomedicine and Medical Technology Mannheim (CBTM), Medical Faculty Mannheim, Ruprecht Karls University of Heidelberg, Mannheim, Germany*
- MARIO LÖHR • *Department of Neurosurgery, Tumorbiology Laboratory, University of Würzburg, Würzburg, Germany*
- GRETEL MAJOR • *The Garvan Institute of Medical Research and The Kinghorn Cancer Centre, Darlinghurst, NSW, Australia*
- AJAY-MOHAN MOHAN • *Department of Nuclear Medicine, Charité—Universitätsmedizin Berlin, Berlin, Germany; Berlin Experimental Radionuclide Imaging Centre (BERIC), Charité—Universitätsmedizin Berlin, Berlin, Germany*
- MARC NUNEZ-OLLE • *Cancer Science Program, Institute for Research in Biomedicine (IRB Barcelona), The Barcelona Institute of Science and Technology, Barcelona, Spain; CIBERONC, Madrid, Spain*
- NAËL OSMANI • *INSERM UMR\_S1109, Strasbourg, France; Université de Strasbourg, Strasbourg, France; Fédération de Médecine Translationnelle de Strasbourg (FMTS), Strasbourg, France*
- AMELIA L. PARKER • *The Garvan Institute of Medical Research and The Kinghorn Cancer Centre, Darlinghurst, NSW, Australia; Faculty of Medicine, St. Vincent's Clinical School, UNSW Sydney, Kensington, NSW, Australia*
- NITIN PATIL • *Department of Experimental Surgery—Cancer Metastasis, Medical Faculty Mannheim, Ruprecht Karls University of Heidelberg, Mannheim, Germany; Centre for Biomedicine and Medical Technology Mannheim (CBTM), Medical Faculty Mannheim, Ruprecht Karls University of Heidelberg, Mannheim, Germany*
- BEATE RAU • *Department of Surgery, Campus Virchow Klinikum—Campus Mitte, Charité—University Hospital Berlin, Berlin, Germany*
- THOMAS REINHECKEL • *German Cancer Consortium (DKTK), Partner Site Freiburg/Mainz, Germany; German Cancer Research Center (DKFZ), Heidelberg, Germany; Institute for Molecular Medicine and Cell Research, Medical Faculty, Albert-Ludwigs-University Freiburg, Freiburg, Germany; BIOSS Centre for Biological Signalling Studies, University of Freiburg, Freiburg, Germany*
- ANNE J. RIDLEY • *School of Cellular and Molecular Medicine, Biomedical Sciences Building, University of Bristol, Bristol, UK*
- SARAH MARTINEZ ROTH • *Department of Oncology, Lombardi Comprehensive Cancer Center, Georgetown University Washington, Washington, DC, U.S.A.*
- RAJEEV S. SAMANT • *Department of Pathology, University of Alabama at Birmingham, Birmingham, AL, USA; Birmingham VA Medical Center, Birmingham, AL, USA; Comprehensive Cancer Center, University of Alabama at Birmingham, Birmingham, AL, USA*
- AMANY SAMIR • *Molecular Pharmacology Research Group, Department of Pharmacology and Toxicology, Faculty of Pharmacy and Biotechnology, German University in Cairo, Cairo, Egypt*
- MARTIN SCHLESINGER • *Pharmaceutical Department, University Bonn, Bonn, Germany*

ELLINA SCHULZ • *Department of Neurosurgery, Tumorbiology Laboratory, University of Würzburg, Würzburg, Germany*

SVENJA SCHWARZ • *Pharmaceutical Department, University Bonn, Bonn, Germany*

LISA SEVENICH • *Georg-Speyer-Haus, Institute for Tumor Biology and Experimental Therapy, Frankfurt, Germany; German Cancer Consortium (DKTK), Partner Site Frankfurt/Mainz, Germany; German Cancer Research Center (DKFZ), Heidelberg, Germany; Frankfurt Cancer Institute (FCI), Goethe University Frankfurt, Frankfurt am Main, Germany*

GHADA M. SHARIF • *Department of Oncology, Lombardi Comprehensive Cancer Center, Georgetown University Washington, Washington, DC, USA*

ROBERT H. SHOEMAKER • *Division of Cancer Prevention, National Cancer Institute, Bethesda, MD, USA*

ULRIKE S. STEIN • *Translational Oncology of Solid Tumors Experimental and Clinical Research Center, Charité – Universitätsmedizin Berlin and Max-Delbrück-Center for Molecular Medicine, Berlin, Germany*

OLGA VASILJEVA • *Department of Biochemistry and Molecular and Structural Biology, Jozef Stefan Institute, Ljubljana, Slovenia; CytomX Therapeutics Inc., South San Francisco, CA, USA*

WOLFGANG WALTHER • *Experimental and Clinical Research Center, Charité—Universitätsmedizin Berlin, Berlin, Germany; Max-Delbrück-Center for Molecular Medicine, AG Translational Oncology of Solid Tumors, Berlin, Germany*

SHANNON E. WEEKS • *Department of Pathology, University of Alabama at Birmingham, Birmingham, AL, USA*

ANTON WELLSTEIN • *Department of Oncology, Lombardi Comprehensive Cancer Center, Georgetown University Washington, Washington, DC, USA*

DEMOND WILLIAMS • *Cancer Biology Program and Department of Pharmacology, Vanderbilt University, Nashville, TN, USA*

HAO WU • *Würzburg Institute of Systems Immunology, Julius-Maximilians-Universität Würzburg, Würzburg, Germany*

ANNIKA WULF-GOLDENBERG • *Experimental Pharmacology and Oncology (EPO), Berlin, Germany*

JING YANG • *Department of Pharmacology, University of California, San Diego, La Jolla, CA, USA; Moores Cancer Center, Department of Pediatrics, University of California, La Jolla, CA, USA*

# **Part I**

## **Metastasis Models**



# Chapter 1

## Cancer Cell Invasion and Metastasis in Zebrafish Models (*Danio rerio*)

**Sarah Martinez Roth, Eric B. Berens, Ghada M. Sharif, Eric Glasgow, and Anton Wellstein**

### Abstract

Cancer cell vascular invasion and extravasation at metastatic sites are hallmarks of malignant progression of cancer and associated with poor disease outcome. Here we describe an *in vivo* approach to study the invasive ability of cancer cells into the vasculature and their hematogenous metastatic seeding in zebrafish (*Danio rerio*). In one approach, extravasation of fluorescently labeled cancer cells is monitored in zebrafish embryos whose vasculature is marked by a contrasting fluorescent reporter. After injection into the precardiac sinus of 2-day-old embryos, cancer cells can extravasate from the vasculature into tissues over the next few days. Extravasated cancer cells are identified and counted in live embryos via fluorescence microscopy. In a second approach, intravasation of cancer cells can be evaluated by changing their injection site to the yolk sac of zebrafish embryos. In addition to monitoring the impact of drivers of malignant progression, candidate inhibitors can be studied in this *in vivo* model system for their efficacy as well as their toxicity for the host.

**Key words** Cancer, Extravasation, Zebrafish, Embryo, Fluorescence, Vascular Invasion, Metastasis

---

### 1 Introduction

Metastatic progression accounts for the majority of cancer-related deaths; however, the mechanisms underlying this complex process differ between cancer types and remain poorly understood [1]. The migration of cancer cells from primary tumors to distant tissues involves a multistep process named the invasion-metastasis cascade. The process begins with the local invasion of tumor cells into the surrounding tissues. These cells then intravasate into the circulatory system and survive hematogenous transport. Cancer cells arrest in the microvessels of distant tissues and extravasate through the vascular lining into the parenchyma to form metastatic seeds. Proliferation of these colonies leads to clinically detectable lesions [2]. Crucial rate-limiting steps in the metastatic cascade include intravasation and extravasation of cancer cells. Cancer cells disrupt and migrate through endothelial junctions while also interacting

with other circulating cells such as leukocytes and platelets that contribute to this process [3]. The tumor microenvironment (TME) also continually changes over the course of cancer progression, emphasizing the need to consider the TME's role in metastasis [4]. Developing an animal model that allows the tracking of single cells or cell subpopulations is essential to understanding the key components of the invasion-metastasis cascade.

Currently, there are various in vitro model systems that are employed to study cancer cell vascular invasion. The most common of in vitro assays include transwell assays to observe cancer migration through endothelial barriers [5] and electric cell-substrate impedance sensing (ECIS) assay to assess the disruption of an intact monolayer by cancer cells in real-time over a time lapse [6, 7]. However, there are limitations in these existing in vitro assays, in that they lack the fluid dynamics and stromal factors that physiologically impact cancer cell attachment to the endothelial wall. Microfluidic devices are at the forefront of studying metastasis in vitro. These devices create a perfusable vascular networks that arise from 3D cultures of endothelia cells with supporting stroma [8, 9]. Still, these techniques lack the microenvironment of a physiologically intact circulatory system.

Mouse models have been the most widely used animal model in cancer research because of the gene homology with humans and similar body organization, organ function, and immune system. Some limitations include the high number of animals needed to reach statistical significance. Still, mice remain the most widely used in vivo model to study vascular invasion because they closely mimic physiologic metastasis [10]. The assays in mice involve injection of cancer cells into the circulation to monitor extravasation and colonization of distant organs. Cancer cells injected into the tail vein will result mostly in seeding of the lungs, as a distant organ of metastasis [11, 12]. Intracardiac injection will result in metastatic seeding of the bone marrow [13–15] and brain [16]. Injection into the spleen or portal vein results in seeding of the liver [17] while carotid artery injection directs cancer cells to the brain [18, 19]. Monitoring and quantitation of organ colonization is generally determined via luminescence and can detect manifest metastases. Real-time imaging of extravasation can be very instructive though it requires surgical implantation and complex microscopy that has to adapt to the breathing of an anesthetized animal [20–22]. This complexity of the setup limits the extravasation analysis.

The zebrafish model has emerged as a system to study cancer cell metastasis that is easier to implement, accommodates higher throughput, and allows for state-of-the-art imaging [23, 24]. This model allows for the assessment of cancer cell invasion and extravasation in an intact circulatory system over a shorter timescale when compared with murine model [25–28]. The zebrafish genome

overlaps with the human genome by 70%, and most organs and cellular function are conserved. An overview of zebrafish in biomedical research is provided in an award-winning short movie for an educated lay audience [29] ([www.zebrafishfilm.org](http://www.zebrafishfilm.org)). One major benefit of the model is the potential for cost efficient, relatively high throughput using dozens of easy-to-visualize transparent embryos that can grow and develop in small volumes accommodated by 96-well format dishes in a single experiment [30]. The model also allows the observation of very few to single-cell behaviors that help elucidate the impact of subpopulations present in heterogeneous tumor cell populations (see, e.g., Fig. 3) [32]. Therefore, transplantation of cells in the optically clear, immune-permissive zebrafish embryos can provide a unique perspective to understand cancer metastasis and to visualize single-cell cancer progression in real time [33]. The zebrafish model of cancer invasion and metastasis can also be used to assess drug effects or screen for candidate inhibitors in an *in vivo* model. Drugs to be analyzed can be added to the growth media of the fish embryos at an appropriate time to read out the effect on the host embryo as well as the cancer cells transplanted for evaluation of invasion and metastasis. Several examples from different areas of study were published during the past years [34–37] including the application to individualized analysis of human cancer biopsies [38].

In the approach described, first we utilize a transparent zebrafish strain that has its endothelia tagged with a green reef coral fluorescent protein reporter driven by the kdrl promoter, the receptor for vascular endothelial growth factor [39]. The vascular invasive ability of a commonly used cancer cell line is shown as a representative example, and the general steps are outlined in Fig. 1. In this example, MDA-MB-231, a human breast cancer cell line, was labeled with a red fluorescent lipophilic dye and injected into the precardiac sinus of 2-day-old embryos. Between 48 and 96 h after the injection, cancer cells that have extravasated out of the vasculature and invaded into tissues in the caudal region of embryos can be scored efficiently on a fluorescent microscope (Fig. 2). In the experiment shown here, the breast cancer cell line was cultured at different cell densities for a few days resulting in inhibition of the Hippo pathway and *in vitro* invasion of an endothelial monolayer by cells grown at low density [31]. In the zebrafish, embryos cells grown at low density extravasated from the vasculature and invaded tissues at a significantly higher rate confirming the biologic significance of the *in vitro* findings (Fig. 2b, c).

In a second approach, in wild-type zebrafish embryos without fluorescent vasculature, the injection site of cancer cells is changed to the yolk sac (Fig. 3a, b). The approach allows for the study of heterogeneous cancer cell populations that are labeled with differently colored Q-dots (Fig. 3). Cancer cells that have extravasated in

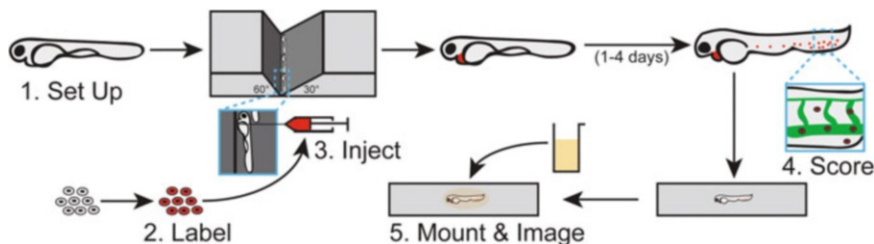


**Fig. 1** Overview of the cancer cell extravasation assay in zebrafish embryos. Cancer cells are incubated with Q-dots (Thermo Fisher) or a fluorescent dye that is taken up by the cells as a label (red). Cells in suspension are injected into the precardiac sinus of the embryos (2 days old). During the next 2–4 days, cancer cells traffic in the vasculature can invade tissues in the caudal region of the embryo and are imaged after mounting in an anesthetic agarose medium. The vascular endothelia in the embryos express GFP (Green Fluorescent Protein) to identify the location of cancer cells either inside the vasculature or inside the tissues by confocal microscopy. (Reproduced with permission; Ref. [40])

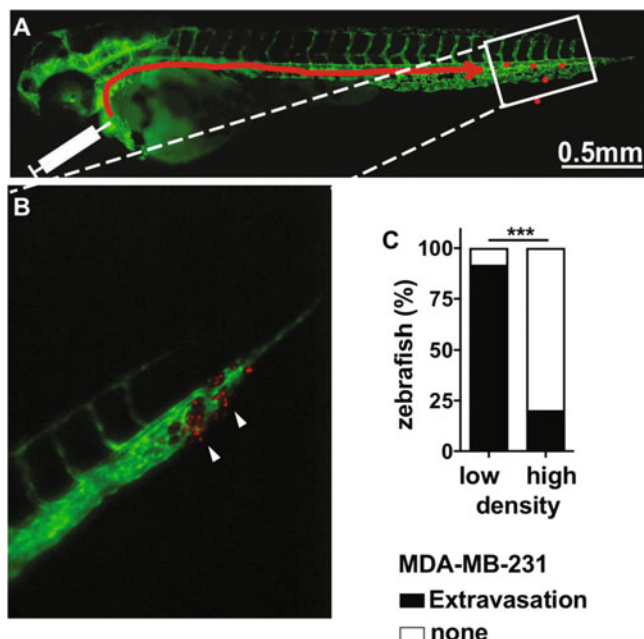


**Fig. 2** Extravasation of cancer cells (red) in zebrafish embryos with GFP-labeled vasculature (green). (a) Schematic of injection of cancer cells into the precardiac sinus. Note that some of the cancer cells have entered tissues 2 days after injection. (b) The embryo's caudal region is magnified to show extravasated cancer cells. Punctate fluorescent labeling is seen upon magnification. (c) Quantitation of extravasated cancer cells in tissues. Twelve and five Zebrafish were scored for extravasated cancer cells grown at low and high density, respectively (Original data in Ref. [31])

the yolk sac can traffic in the vasculature and are scored in the caudal region (Fig. 3c) 24–48 h after injection [31, 41]. In the example shown here, breast cancer cells grown at low or high cell density were labeled with green or red Q-dots, respectively and

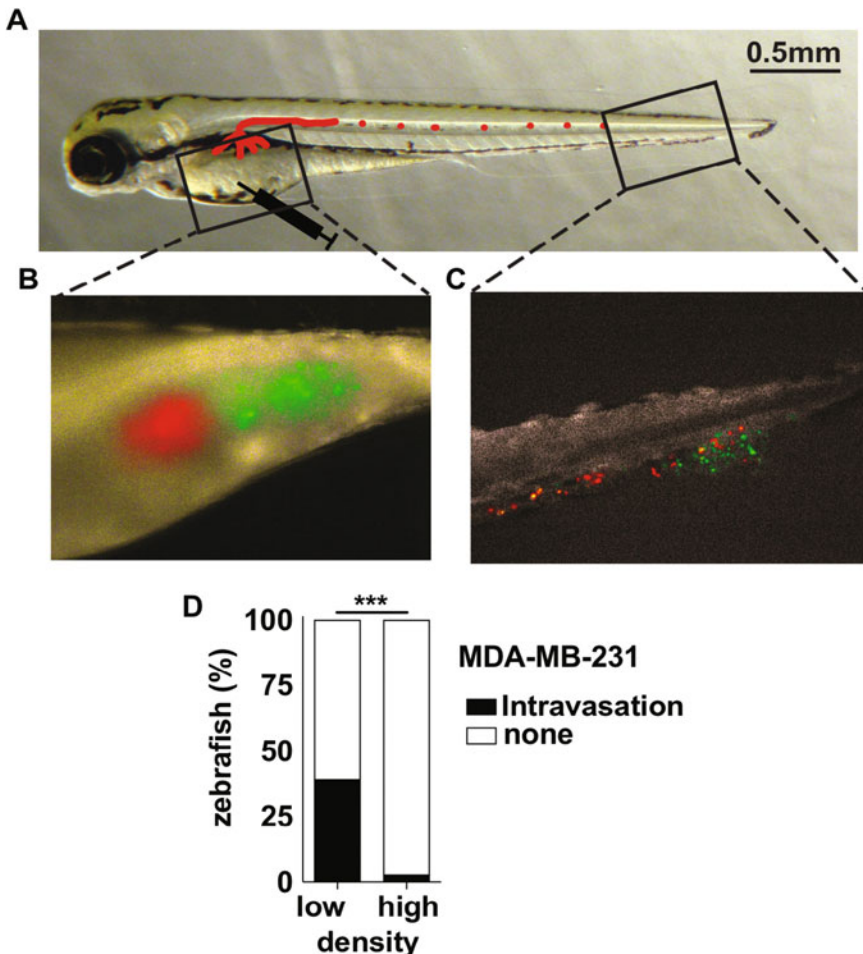


**Fig. 3** Intravasation of two distinct cancer cell populations after yolk sac injection. **(a)** Brightfield image of a wild-type zebrafish embryo 4 days after fertilization. The boxed areas indicate the yolk sac. **(b)** Yolk sac with green (invasive = low-density growth) and red (noninvasive = high-density growth) Q-dot labeled cancer cells. **(c)** The caudal region with cancer cells that intravasated into the vasculature and reached the tail region. **(d)** The percentage of embryos ( $n = 75$ ) with intravasated cells in the caudal region 2 days after injection (Original data in Ref. [31])

co-inoculated at the same time into the yolk sacs of embryos for a direct comparison (Fig. 3b). Cells grown at low density intravasated at a significantly higher rate than the high-density cells as evidenced by their appearance in the tail vasculature (Fig. 3c, d). The extravasation and intravasation assays from Figs. 2 and 3 provide complementary insights. Both approaches can also be used to assess the contribution of pathways by knockdown of candidate genes as well as treatment with small molecule or antibody-based inhibitors of potential driver molecules. Examples of such interventions can be found in [31, 41].

---

## 2 Materials

### 2.1 Injection Station

1. Needles: Capillary Glass, Standard, 1.2 MM × 0.68 MM, 4", A-M Systems, Inc., pulled using David Kopf 700C Vertical Pipette Puller, Hofstra Group. Pull long-tapered pipettes using 20 mAmp current and a two-coil heating element.
2. Machinery needed for injection station setup: Electrode storage jar, 1.0 MM, World Precision Instruments, Inc., latex rubber bulbs, 2 mL, Pack of 72, Heathrow Scientific and micromanipulator, Narishige, Picospritzer II, General Valve Corporation.

### 2.2 Manipulating Fish

1. Tools for manipulating embryos: Eyelash Brush, Ted Pella, Inc., transfer pipettes, and 5 3/4" disposable Pasteur pipettes, borosilicate glass.
2. Fish water: 0.3 g/L, Instant Ocean Salt, Sea Salt, Pentair. Store at room temperature for up to 3 months.
3. Tricaine stock solution: Ethyl 3-aminobenzoate methanesulfonate salt (Tricaine, MS-222), Fluka: (4 mg/mL, 10 mM Tris, pH 7) to 50 mL of fish water plus penicillin-G potassium and streptomycin sulfate.

### 2.3 Visualization

1. Microscopy method used: For visualizing cells, use Leica SP8 Confocal Microscope.
2. Staining cells:
  - (a) For staining cancer cells for pre-cardiac sinus injection, cancer cells were labeled with a lipophilic red fluorescent dye: Vybrant DiI Cell-Labeling solution (Thermo Fisher).
  - (b) For staining cancer cells for yolk sac injection, cells were labeled with 565 nm or 655 nm Q-dots using the Qtracker Cell-Labeling kit (Thermo Fisher).

---

## 3 Methods

Ethics statement: Experiments were carried out in compliance with recommendations by the Georgetown University Animal Care and Use Committee. Zebrafish embryos were generated under an approved IACUC protocol.

### 3.1 Set up Embryos for Injection and Make Stock Solutions

1. Separate males and females the night before experiment in a breeding cage. The goal is to develop enough zebrafish larvae to assess cancer cell vascular invasion.
2. Pull the gate on the breeding cage of pairwise or group in-cross mating with *Tg(kdrl:grcfp)zn1;mitfa<sup>b692</sup>;ednrb1<sup>b140</sup>* fish (see Note 1).

3. After about 30 min, collect eggs, and remove unfertilized, deformed embryos and debris the next day under the microscope.
4. Incubate embryos at 28.5 °C until ready for injection, 2 days postfertilization (2 dpf), make sure all embryos are dechorionated.
5. Make injection plates: Melt 25 mL of 1.5% agarose in dH<sub>2</sub>O for each plate.
6. Pour 12 mL of the agarose into a 100 mm × 15 mm petri dish and let it solidify.
7. Remelt then pour the remaining agarose in the plate.
8. Immediately position a cut glass mold (3 mm × 7.2 cm wide × 7.5 cm long) so that it is at a 30° angle to the agarose and positioned in the center of the plate (*see Note 2*).
9. Tape the glass mold in place and let the agarose set.
10. Slowly remove the glass mold (*see Note 3*).
11. Equilibrate injection plate with fish water (0.3 g/L sea salt) and store at room temperature.
12. Wash plate twice with distilled water.
13. Equilibrate plate by adding 10 mL of fish water to the plate and place on shaker for 10 min. Do this two times as well.
14. Split 2-day postfertilization (dpf) embryos into injection groups by transferring them into petri dishes containing fish water.
15. Set up recovery dishes for each group that will be used after injection. (*see Note 4*).
16. Prepare 2× tricaine solution by adding 4 mL of buffered tricaine stock (4 mg/mL, 10 mM Tris, pH 7) to 50 mL of fish water plus penicillin and streptomycin.
17. Dissolve 15 mg low-melting-point agarose in 10 mL of 2× tricaine solution to generate a mounting anesthetic medium that will immobilize live embryos for imaging (*see Note 5*).
18. Pull the microinjection needles.
19. Place glass capillary tubing in a vertical pipette puller. Pull long-tapered pipettes using 20 mAmp current and a two-coil heating element.

### **3.2 Labeling Cells with Red Lipophilic Fluorescent Dye**

1. Grow cells of interest in their recommended culture conditions (*see Note 6*).
2. Generate a single-cell suspension by dissociating an adherent culture of cancer cells.
3. Wash cells with 1× PBS and add 0.05% trypsin-EDTA solution (*see Note 7*).

4. Neutralize the trypsin solution with serum-containing cell culture media after the cells detach.
5. Centrifuge the cell suspension for 5 min at  $200 \times g$ , then resuspend the cell pellet in media for cell counting.
6. Count the cell suspension and prepare one million cells per 200  $\mu\text{L}$  of cell culture media (*see Note 8*).
7. Check cell viability with trypan blue dye before injection into zebrafish embryos (*see Note 9*).
8. Add 2  $\mu\text{L}$  of red lipophilic dye to the cell suspension for a 1:100 dilution, mix well, and then incubate the mixture at 37 °C for 20 min (*see Note 10*).
9. Following the incubation, add 1 mL of fresh media to the tube and then centrifuge again for 5 min at  $200 \times g$ .
10. Wash the residual fluorescent dye from the cells.
11. Aspirate the supernatant and resuspend the pellet in 1 mL of fresh culture media, and centrifuge for 5 min at  $200 \times g$ .
12. Repeat the washing step a second time: aspirate the supernatant, resuspend the cell pellet in 1 mL of fresh media, and then centrifuge again for 5 min at  $200 \times g$ .
13. Repeat the washing step: aspirate the supernatant, resuspend the cell pellet in 1 mL of fresh media, and then centrifuge for the third time for 5 min at  $200 \times g$ .
14. Aspirate the supernatant and resuspend the cell pellet containing one million labeled cancer cells in 500  $\mu\text{L}$  of fresh media (*see Note 11*).

### **3.3 Injecting Cells into the Precardiac Sinus of Zebrafish Embryos**

1. Attach microinjection dispense system to a pressurized air source and turn on the microinjection dispense system power.
2. Test pressure by depressing the foot pedal. A brief pulse of air should come out from the needle holder.
3. Equilibrate the injection plates twice with 2× tricaine solution.
4. For each equilibration step, add 20 mL of 2× tricaine solution to the injection plate and place on shaker for 10 min.
5. Use a transfer pipette to move a group of embryos to a small dish containing the 2× tricaine solution.
6. Fill the microinjection needle from the back with cancer cells using a gel-loading pipette tip.
7. Place the needle in an electrode storage jar with the pointed end facing down so cells settle near the tip, make sure to cut your tip so the appropriate number of cells are injected per embryo.

8. Transfer 20–30 anesthetized embryos to an injection plate with a transfer pipette with 2× tricaine.
9. Allow embryos to settle in the tip of the pipette.
10. Gently move embryos into the trough of the injection plate, spreading the fish along the length of the trough.
11. Align embryos with heads facing up and bellies facing the steep wall of the trough (*see Note 12*).
12. Inject 50–100 cancer cells (2–5 nL) into the precardiac sinus of the zebrafish embryos using the microinjection dispense system.
13. Attach the needle to the needle holder of a micromanipulator.
14. Position the injection plate under the stereoscope with the 60° wall to the left and focus on the top embryo at 25× magnification (Fig. 1).
15. Position the micromanipulator so that the needle will pierce the embryo.
16. Extend the needle until it is nearly touching the embryo.
17. Looking under the microscope, align the needle so that it will pierce the embryo upon further extension.
18. Pierce the embryo through the yolk sac placing the tip just at the pre-cardiac sinus.
19. Inject cells by depressing the foot pedal. *The force of the injection expels the cells into the cardiac sinus.* Retract the needle (Fig. 2b).
20. Extend and retract the injection needle with one hand. Make fine adjustments to position next embryo with your other hand.
21. Retract the needle as high as it goes while setting up to inject another plate.
22. Transfer the embryos to the recovery dish once the entire plate is injected.
23. Tilt the injection plate to pool the embryos at the bottom of the petri dish and wash embryos off the plate with fish water, collecting them with the transfer pipette.
24. Allow the embryos to settle in the bottom of the transfer pipette.
25. Transfer the embryos to the recovery dish.
26. Incubate recovery dish at 28 °C for 1 h. After the incubation, separate viable zebrafish embryos from dead embryos.
27. Incubate dish at 33 °C until ready for scoring, typically 24–96 h (*see Note 13*).

### **3.4 Scoring Extravasation of Cancer Cells in Zebrafish Embryos**

1. Anesthetize one batch of embryos at a time to be scored by placing them in a dish with  $2\times$  tricaine solution.
2. Place an anesthetized larva on a depression slide in a drop of  $2\times$  tricaine.
3. Orient larvae laterally for imaging of the caudal region (Fig. 2b).
4. Count the number of cancer cells that have successfully invaded out of the vasculature by focusing on the cell location to clearly discern an intact cell (*see Note 14*).
5. Score larvae on a Nikon compound fluorescence microscope with the  $10\times$  objective lens. Use the  $20\times$  objective for any difficult calls (Fig. 2c).

### **3.5 Mounting Zebrafish onto Slides and Subsequent Fluorescence Imaging**

1. Melt 1.5% agarose/ $2\times$  tricaine solution, and bring to  $37^{\circ}\text{C}$ .
2. Anesthetize the embryo by placing it in  $2\times$  tricaine solution.
3. Transfer the embryo in a drop of  $2\times$  tricaine solution to the imaging station (*see Note 15*).
4. Use a glass pipette to remove the excess  $2\times$  tricaine solution, retaining the embryo on the imaging surface.
5. Overlay one drop of melted agarose solution over the embryo.
6. Before the agarose polymerizes, use an eyelash brush, to orient the embryo laterally for imaging, making sure the embryo is flattened along the imaging surface.
7. Submerge the now polymerized agarose drop under  $2\times$  tricaine solution.
8. Image the zebrafish embryo using microscopy.

### **3.6 Alternative Application: Injecting Cancer Cells into the Yolk Sac**

1. Prepare the microinjection dispense system and injection plates as previously described in Subheading 3.3 of this protocol.
2. Label two cell populations with contrasting fluorescent Q-dots from the Qtracker Cell-Labeling kit (Thermo Fisher) or with fluorescent dyes as described in Subheading 3.2 above.
3. Inject  $5\text{--}10\text{ nL}$  of  $2 \times 10^7$  cells/mL into the yolk sac (Fig. 3b). Keep the injection volume constant to inject identical cell numbers (100–200 cancer cells) from each cell population (*see Note 16*).
4. Collect the injected embryos as previously described in Subheading 3.3 of this protocol and then screen for successful injections.
5. Screen and transfer viable embryos that were successfully injected to a new dish (*see Note 17*).
6. Transfer the viable embryos to a new petri dish if cancer cells are clearly seen in the yolk sac (Fig. 3b).

7. Incubate dish at 33 °C until ready for scoring, typically 24–48 h after injection (see Note 18).
8. To score intravasation in zebrafish embryos, follow the guidelines in Subheading 3.4 of this protocol, but instead count the number of cancer cells that have successfully invaded into the vasculature of the caudal region (Fig. 3c).

---

## 4 Notes

1. We generated *Tg(kdrl:grcfp)zn1;mitfa<sup>b692</sup>;ednrb1<sup>b140</sup>* zebrafish, by crossing *Tg(kdrl:grcfp)zn1<sup>25</sup>*, which express green reef coral fluorescent protein in endothelial cells, with a line that lacks pigment cells, *mitfa<sup>b692</sup>;ednrb1<sup>b140</sup>*, developed at the Zebrafish International Resource Center.
2. This will create a steep 60° wall with a 30° sloped ramp.
3. Molds can be stored in dH<sub>2</sub>O at 4 °C, edges wrapped with parafilm.
4. Recovery dish contains 10 mL fish water: penicillin (25 µg/mL) and streptomycin (50 µg/mL).
5. Mounting medium consists of 1.5% agarose.
6. This cell line was grown in DMEM +10% FBS: MDA-MB-231.
7. Time of trypsin exposure will depend on the cell line.
8. Cell number is determined with an automated counter, feel free to use whatever you have.
9. Only live cell populations should be injected into zebrafish embryos, as injection of dead cells will not reflect true vascular invasion.
10. We have found that DiI tends to produce the best labeling, yet its fluorescence level can vary between cell lines. Concentration and labeling time may need to be optimized for each cell line. It is critical that the excess dye is washed away from the cells after labeling. This is achieved by the centrifugation steps indicated in the labeling Subheading 3.2. Excess fluorescent dye can be toxic to cells or leak into the bloodstream, producing a faux fluorescent background.
11. 0.5 mM EDTA can be added to the media to prevent cell clumping.
12. Tricaine solution should cover both the trough length and the flat agarose surface, with embryos only residing in the trough.
13. This temperature is determined as a compromise between 37 °C, the ideal temperature for cancer cells, and 28.5 °C, the temperature for zebrafish.

14. It is best to have at least two individuals involved in this process, where one individual scoring the fish is blind to the experimental condition being assessed. It is imperative to generate consistent criteria that will be applied to all conditions.
15. A glass-bottom dish or microscope slide can be used.
16. A transparent zebrafish embryos lacking fluorescent vasculature can be used for this assay. Passive entry of particles into the vasculature can be controlled by injecting fluorescent beads ( $<10\ \mu\text{m}$ ).
17. All embryos should have a consistently sized mass of cells located in the yolk (Fig. 3b). Embryos are discarded if the mass size differs or if any cells are located outside of the yolk.
18. This temperature is considered a compromise between 37 °C, the ideal temperature for cancer cells, and 28.5 °C, the ideal temperature for zebrafish.

## Acknowledgments

We thank Peter Johnson of the Georgetown University Microscopy Core for assistance with imaging the zebrafish embryos. The Microscopy and Imaging Shared Resource and the Zebrafish Shared Resource are partially supported by NIH/NCI grant P30-CA051008. This work was also supported by NIH/NCI F31-CA235970-01 (SMR), R01CA231291-01(AW).

*Disclosures:* The authors have no conflicts of interest to disclose.

## References

1. Cummings MC, Simpson PT, Reid LE, Jayanthan J, Skerman J, Song S, McCart Reed AE, Kutasovic JR, Morey AL, Marquart L, O'Rourke P (2014) Metastatic progression of breast cancer: insights from 50 years of autopsies. *J Pathol* 232:23–31
2. Lambert AW, Pattabiraman DR, Weinberg RA (2017) Emerging biological principles of metastasis. *Cell* 168:670–691
3. Reymond N, d'Agua BB, Ridley AJ (2013) Crossing the endothelial barrier during metastasis. *Nat Rev Cancer* 13:858–870
4. Quail DF, Joyce JA (2013) Microenvironmental regulation of tumor progression and metastasis. *Nat Med* 19:1423
5. Hooper S, Marshall JF, Sahai E (2006) Tumor cell migration in three dimensions. *Method Enzymol* 406:625–643
6. Stylianou DC, Der Maur AA, Kodack DP, Henke RT, Hohn S, Toretsky JA, Riegel AT, Wellstein A (2009) Effect of single-chain antibody targeting of the ligand-binding domain in the anaplastic lymphoma kinase receptor. *Oncogene* 28:3296–3306
7. Rahim S, Üren A (2011) A real-time electrical impedance based technique to measure invasion of endothelial cell monolayer by cancer cells. *J Vis Exp* 50:e2792
8. Jeon JS, Bersini S, Gilardi M, Dubini G, Charlest JL, Moretti M, Kamm RD (2015) Erratum: human 3D vascularized organotypic microfluidic assays to study breast cancer cell extravasation. *Proc Natl Acad Sci U S A* 112:E818
9. Shin Y, Han S, Jeon JS, Yamamoto K, Zervantakis IK, Sudo R, Kamm RD, Chung S (2012) Microfluidic assay for simultaneous culture of multiple cell types on surfaces or within hydrogels. *Nat Protoc* 7:1247–1259
10. Vargo-Gogola T, Rosen JM (2007) Modelling breast cancer: one size does not fit all. *Nat Rev Cancer* 7:659–672

11. Mohanty S, Xu L (2010) Experimental metastasis assay. *J Vis Exp* 42:e1942
12. Minn AJ, Gupta GP, Siegel PM, Bos PD, Shu W, Giri DD, Viale A, Olshen AB, Gerald WL, Massagué J (2005) Genes that mediate breast cancer metastasis to lung. *Nature* 436:518–524
13. Campbell JP, Merkel AR, Masood-Campbell SK, Elefteriou F, Sterling JA (2012) Models of bone metastasis. *J Vis Exp* 67:e4260
14. Arguello F, Baggs RB, Frantz CN (1988) A murine model of experimental metastasis to bone and bone marrow. *Cancer Res* 48:6876–6881
15. Minn AJ, Kang Y, Serganova I, Gupta GP, Giri DD, Doubrovin M, Ponomarev V, Gerald WL, Blasberg R, Massagué J (2005) Distinct organ-specific metastatic potential of individual breast cancer cells and primary tumors. *J Clin Invest* 115:44–55
16. Bos PD, Zhang XH, Nadal C, Shu W, Gomis RR, Nguyen DX, Minn AJ, van de Vijver MJ, Gerald WL, Fockens JA, Massagué J (2009) Genes that mediate breast cancer metastasis to the brain. *Nature* 459:1005–1009
17. Soares KC, Foley K, Olino K, Leubner A, Mayo SC, Jain A, Jaffee E, Schulick RD, Yoshimura K, Edil B, Zheng L (2014) A pre-clinical murine model of hepatic metastases. *J Vis Exp* 91:e51677
18. Kienast Y, Von Baumgarten L, Fuhrmann M, Klinkert WE, Goldbrunner R, Herms J, Winkler F (2010) Real-time imaging reveals the single steps of brain metastasis formation. *Nat Med* 16:116
19. Hasegawa H, Ushio Y, Hayakawa T, Yamada K, Mogami H (1983) Changes of the blood-brain barrier in experimental metastatic brain tumors. *J Neurosurg* 59:304–310
20. Entenberg D, Voiculescu S, Guo P, Borriello L, Wang Y, Karagiannis GS, Jones J, Baccay F, Oktay M, Condeelis J (2018) A permanent window for the murine lung enables high-resolution imaging of cancer metastasis. *Nat Methods* 15:73
21. Dondossola E, Alexander S, Holzapfel BM, Filippini S, Starbuck MW, Hoffman RM, Navone N, De-Juan-Pardo EM, Logothetis CJ, Hutmacher DW, Friedl P (2018) Intravital microscopy of osteolytic progression and therapy response of cancer lesions in the bone. *Sci Transl Med* 10:eaao5726
22. Warren SC, Nobis M, Magenau A, Mohammed YH, Herrmann D, Moran I, Vennin C, Conway JR, Méléne P, Cox TR, Wang Y (2018) Removing physiological motion from intravital and clinical functional imaging data. *elife* 7: e35800
23. Amatruda JF, Shepard JL, Stern HM, Zon LI (2002) Zebrafish as a cancer model system. *Cancer Cell* 1:229–231
24. Feitsma H, Cuppen E (2008) Zebrafish as a cancer model. *Mol Cancer Res* 6:685–694
25. Stoletov K, Klemke R (2008) Catch of the day: zebrafish as a human cancer model. *Oncogene* 27:4509–4520
26. Stoletov K, Kato H, Zardouzian E, Kelber J, Yang J, Shattil S, Klemke R (2010) Visualizing extravasation dynamics of metastatic tumor cells. *J Cell Sci* 123:2332–2341
27. Kanada M, Zhang J, Yan L, Sakurai T, Terakawa S (2014) Endothelial cell-initiated extravasation of cancer cells visualized in zebrafish. *PeerJ* 2:e688
28. Teng Y, Xie X, Walker S, White DT, Mumm JS, Cowell JK (2013) Evaluating human cancer cell metastasis in zebrafish. *BMC Cancer* 13:453
29. Manner JA (2018) Zebrafish practically people, “Transforming the Study of Disease” Documentary Movie. [www.zebrafishfilm.org](http://www.zebrafishfilm.org)
30. Osman N, Goetz JG (2019) Multiscale imaging of metastasis in zebrafish. *Trends Cancer* 5:1–13
31. Sharif GM, Schmidt MO, Yi C, Hu Z, Haddad BR, Glasgow E, Riegel AT, Wellstein A (2015) Cell growth density modulates cancer cell vascular invasion via hippo pathway activity and CXCR2 signaling. *Oncogene* 34:5879–5889
32. Blackburn JS, Langenau DM (2014) Zebrafish as a model to assess cancer heterogeneity, progression and relapse. *Dis Model Mech* 7:755–762
33. Tang Q, Moore JC, Ignatius MS, Tenente IM, Hayes MN, Garcia EG, Yordán NT, Bourque C, He S, Blackburn JS, Look AT (2016) Imaging tumour cell heterogeneity following cell transplantation into optically clear immune-deficient zebrafish. *Nat Commun* 7:1–10
34. Çelik H, Hong SH, Colón-López DD, Han J, Kont YS, Minas TZ, Swift M, Paige M, Glasgow E, Toretsky JA, Bosch J (2015) Identification of novel ezrin inhibitors targeting metastatic osteosarcoma by screening open access malaria box. *Mol Cancer Ther* 14:2497–2507
35. Chen C, Choudhury S, Wangsa D, Lescott CJ, Wilkins DJ, Sripadhan P, Liu X, Wangsa D, Ried T, Moskaluk C, Wick MJ (2017) A multiplex preclinical model for adenoid cystic carcinoma of the salivary gland identifies

- regorafenib as a potential therapeutic drug. *Sci Rep* 7:1–15
36. Parasido E, Avetian GS, Naeem A, Graham G, Pishvaian M, Glasgow E, Mudambi S, Lee Y, Ihemelandu C, Choudhry M, Peran I (2019) The sustained induction of c-Myc drives nab-paclitaxel resistance in primary pancreatic ductal carcinoma cells. *Mol Cancer Res* 17:1815–1827
37. Spikol ED, Laverriere CE, Robnett M, Carter G, Wolfe E, Glasgow E (2016) Zebrafish models of prader-willi syndrome: fast track to pharmacotherapeutics. *Diseases* 4:13
38. Yan C, Brunson DC, Tang Q, Do D, Iftimia NA, Moore JC, Hayes MN, Welker AM, Garcia EG, Dubash TD, Hong X (2019) Visualizing engrafted human cancer and therapy responses in immunodeficient zebrafish. *Cell* 177:1903–1914
39. Cross LM, Cook MA, Lin S, Chen JN, Rubinstein AL (2003) Rapid analysis of angiogenesis drugs in a live fluorescent zebrafish assay. *Arterioscler Thromb Vasc Biol* 23:911–912
40. Berens EB, Sharif GM, Wellstein A, Glasgow E (2016) Testing the vascular invasive ability of cancer cells in zebrafish (*Danio Rerio*). *J Vis Exp* (117). <https://doi.org/10.3791/55007>
41. Berens EB, Sharif GM, Schmidt MO, Yan G, Shuptrine CW, Weiner LM, Glasgow E, Riegel AT, Wellstein A (2017) Keratin-associated protein 5-5 controls cytoskeletal function and cancer cell vascular invasion. *Oncogene* 36:593–605



# Chapter 2

## The Chicken Egg Chorioallantoic Membrane (CAM) Model as an In Vivo Method for the Investigation of the Invasion and Metastasis Cascade of Malignant Tumor Cells

Jörg H. Leupold, Nitin Patil, and Heike Allgayer

### Abstract

The CAM model enables an in vivo analysis of the individual sub-steps of the metastatic cascade like local invasion, intravasation, or the establishment of metastasis in particular organs. Incubated fertilized chicken eggs are inoculated with human tumor cells and further processed for up to 9–10 days. The invasion and metastasis of these cells is then detected quantitatively with high specificity and sensitivity by means of a PCR for human ALU sequences, using the genomic DNA isolated from distant portions of the CAM, as well as from diverse internal organs of the developing embryo.

**Key words** Chicken chorioallantoic membrane, ALU elements, DNA, Quantification, TaqMan, Primer, Probe, Real-time PCR, Metastasis, In vivo model

---

### 1 Introduction

The CAM, as an in vivo model to study tumor growth and metastasis, has a long history that goes back to the beginning of the twentieth century. At that time, scientists demonstrated the successful explantation of tumors isolated from various species, to the chorioallantoic membrane of bred chicken eggs, and found that these tumors could be maintained by continuous passage from egg to egg [1, 2]. Understandably, the effects of these transplantations to the CAM and the chicken embryo were further investigated and the potential of some of these chorioallantoic grafts to metastasize to chicken organs became apparent [3]. Subsequently, the most widely used procedure for optimal grafting of tissues on a CAM became the removal of a square of the shell and the choice of the junction point of two or more large blood vessels. Developmentally, it became obvious soon that the ideal host age for

transplanting to the CAM is 9 or 10 days of incubation. Before this time points, chicken embryos do not have sufficiently well-developed CAMs, and older growth stages will limit the length of time available for transplants growth and development, since the chorioallantoic circulation begins to dry up at about 18 days of incubation [4]. Moreover, by day 18, as chicken embryos progressively mature, the model becomes immunocompetent and loses its natural immunodeficiency, which prevents to accept transplantations from various tissues and species without any immune response [5, 6]. Over time, this concept became an established model to study not only grafted tissues but also the invasive and metastatic potential of various human tumor-derived cancer cell lines [7–9]. Moreover, the use of human cell lines provides the opportunity to take advantage of the abundantly present *ALU* family of short interspersed repeated DNA elements (SINES), which are distributed throughout the human genome, to perform *ALU*-PCR for the quantitative detection of intravasated tumor cells into the CAM and within chicken organs [10–12]. Today, the chicken embryo metastasis model became a convincing alternative to heterotopic or orthotopic carcinoma models of the nude mouse and a powerful *in vivo* replacement method to examine specific criteria of malignant progression [13]. Compared to the mouse model, it enables a relatively unproblematic analysis of the individual sub-steps of complex physiological processes of invasion and metastasis and thus ideally fulfils the aim of being reducible, replacing animals required for corresponding experiments [4]. In contrast to most animal models, the CAM model enables a specific differentiation of the step of intravasation of the tumor cells breaking into vessels. Typically, within a few day after inoculation, tumor cells can be identified in distant locations of the CAM, as well as in the internal organs of the developing embryo, such as lungs and liver [4]. In addition, the usage of fertilized eggs is much less cost-intensive, since neither the purchase nor the necessary accommodation in incubators results in high costs. Finally, the CAM model has a decisive advantage, since a test approach to spontaneous or experimental metastasis in the murine model usually lasts 4–10 weeks. In contrast, the same questions can be answered in the chicken embryo model after 11 days for intravasation studies to a maximum of 17 days for investigating metastasis.

Here we provide a concise protocol for the detection of human tumor cells within the lower CAM and internal organs of the chicken embryo that are colonized by as few as 10 invaded cells. Detection and quantification is performed using highly specific primer/probes designed to exclusively detect *ALU*-YB8 subfamily sequences in the background of chicken genomic DNA [10].

---

## 2 Materials

Unless otherwise stated, all reagents and chemicals used are of molecular biology grade. Genomic DNA from either cell lines was isolated using the DNeasy Blood and Tissue Kit (Qiagen, Hilden, Germany), and genomic DNA isolation from chicken was performed using a modified protocol based on the original Gentra Puregene Tissue Kit (Qiagen, Hilden, Germany). All plastic consumables unless otherwise stated were purchased sterile. Stainless steel instruments and distilled deionized H<sub>2</sub>O are sterilized by autoclaving at 15 psi for 15–20 min. For preparation of cleaning solution approximately 2000 ml water was added to a plastic or glass beaker. Then, 4 g SDS (*see Note 1*) and 16 g NaOH pellets were transferred to the beaker and mixed until completely dissolved. Finally, water was added to a volume of 4000 ml and the working solution stored at room temperature. All real-time PCR chemicals and master mixes were prepared using distilled deionized H<sub>2</sub>O. All chemicals and reagents were prepared and stored at the indicated temperatures. Make sure that before starting the different experimental sections, all surfaces and equipment are sterilized with 70% ethanol. Diligently follow all waste disposal regulations when disposing waste materials.

### 2.1 Equipment

1. Digital egg incubator for chicken, fully automatic turn system.
2. Scriber with pen-like handle and diamond tip.
3. Pencil.
4. Egg piercer tool.
5. Mini rotary tool with cutting wheel.
6. Set of nickel-plated steel cover glass tweezers, curved.
7. Dark room.
8. Egg candling lamp with LED light.
9. Workstation with white lamp and UV sterilization.
10. Set of nickel-plated steel microscopy scissors, pointed, straight.
11. Set of nickel-plated steel tweezers, curved.
12. Digital shaking thermo block.
13. Digital shaking water bath.
14. Laboratory rotor homogenizer with disposable, plastic-based generators.
15. Spectrophotometer.
16. Real-time thermal cycler.
17. Sterile work bench.
18. Vortexer.
19. Standard laboratory centrifuge or microfuge.

**2.2 Consumables**

1. Special pathogen-free (SPF) eggs.
2. Pipette sucker for standard Pasteur pipettes.
3. Adhesive tape, transparent.
4. 13 ml screw tubes, polypropylene, round bottom, assembled cap, suitable for liquid nitrogen.
5. 15 ml centrifuge tubes, polypropylene, conical bottom, assembled cap.
6. 1.5 ml tubes.
7. 96-well optical PCR plates.
8. Filtered pipet tips (10 µl, 20 µl, 200 µl, 1000 µl).
9. Pipettor, pipettes.
10. Serological pipettes (5 ml, 10 ml, 30 ml).
11. Surgical mask.

**2.3 Reagents**

1. Liquid nitrogen (in case of storage tissues).
2. Oligonucleotide primer for YB8-ALU-S68 was 5'-GTCAGGA GATCGAGACCATCCT-3'.
3. Oligonucleotide primer for YB8-ALU-AS244 was 5'-AGTGG CGCAATCTCGGC-3'.
4. Dual-labeled TaqMan® probe for YB8-ALU-167 was 5'-6-FAM-AGCTACTCGGGAGGGCTGAGGCAGGA-TAMRA-3'.
5. Proteinase K (20 mg/ml).
6. RNase A (4 mg/ml).
7. Ethanol.
8. Isopropanol.
9. Crushed ice.
10. TaqMan real-time PCR master mix that contains a thermostable DNA polymerase, dNTPs, MgCl<sub>2</sub>, and proprietary additives in a buffer optimized for this type of PCR.
11. DNeasy Blood and Tissue Kit (Qiagen, Hilden, Germany).
12. Gentra Purgene Tissue Kit (Qiagen, Hilden, Germany).
13. Appropriate serum-free cell culture medium containing 0.1% BSA.
14. Cleaning solution containing 0.1% SDS and 0.1 M NaOH.

**3 Experimental Procedure**

For each experiment, include a separate set of eggs that can be used for the isolation of genomic chicken DNA for standard curve preparation. For statistically valid results, a minimum of 10 eggs/group is recommended, and the experiment must be carried out as three independent biological replicates.

### 3.1 Incubation and Preparation of Eggs

1. Eggs should be incubated at 37.5 °C in a modern forced-draft incubator (*see Note 2*) and a relative humidity of 58–60%, ideally, in an incubator equipped with an automatic turning device.
2. At ninth day of incubation, eggs are removed from the incubator, and candled in order to see the vasculature of the CAM and the position of the air cell (*see Notes 3 and 4*).
3. Using the egg candling light, a highly vascular area on the side of the egg near a major blood vessel should be located, and a 1 cm<sup>2</sup> window marked on the shell at this site.
4. The egg is swabbed with 70% ethanol. Using an egg piercer tool, a small hole is made through the shell into the air cell at the large end of the egg.
5. While holding the egg in the hand, a hole is drilled into the shell within the marked window using a diamond drill pin, penetrating the shell but not the underlying shell membrane.
6. The egg is now turned in such a way that the marking is pointing upwards, and by applying a vacuum with a pipette sucker, the air is extracted from the air cell, causing the CAM to detach from the egg shell at the marked point.
7. A window is cut into the egg shell over the artificial airbag created in this way, using a mini rotary tool with cutting wheel (*see Notes 5 and 6*).
8. When the window has been cut, the piece of shell is lifted off very carefully using a cover glass tweezers to avoid any contamination of the membrane with shell parts or dust.
9. Finally, one to two million cells are placed on the CAM in 50 µl serum-free medium containing 0.1% BSA and with light touch of the CAM.
10. The open window is sealed with an adhesive tape, and the egg is incubated without rotation.

### 3.2 Isolation of Samples

1. For each sample, prepare a separate 13 ml round-bottom screw tube and add 4 ml of cell lysis solution (provided by Gentra Purgene Tissue Kit).
2. For isolation of the lower CAM only, the egg is incubated for additional 52 h after inoculation. The lower CAM is physiologically defined as the CAM of the opposite half of the egg in respect of the window cut for placing the cells. For isolation of chicken embryo organs, the egg is incubated for additional 8 days after inoculation of the cells on the CAM.
3. While holding the egg between the fingers, the egg is cut open horizontally with the inoculation point upwards using a pointed and straight microscopy scissor (*see Notes 7 and 8*).

4. The lower CAM is obtained with a curved steel tweezer after removal of the chicken embryo and the remaining egg content.
5. To obtain lungs and liver, the 17 days old embryo is sacrificed, removed from the egg and the desired organs harvested.
6. Carefully transfer the samples to the before prepared 13 ml round-bottom tubes without touching the outside of the tubes with your probes. Make sure that the samples are completely covered by the lysis buffer. Store on crushed ice or 4 °C for direct subsequent processing. Otherwise, the samples can be freshly frozen in liquid nitrogen and stored at –80 °C until isolation of genomic DNA is carried out.

### 3.3 Isolation of Genomic DNA

Preheat water bath to 55 °C for use in **step 4** and 37 °C for use in **step 6**. Prechill a centrifuge suitable for 13 ml round-bottom tubes and equipped with a swinging rotor to 4 °C for use in **step 9**. Preheat shaking thermo block to 65 °C for use in **step 19**.

1. Resolving cleaning solution.
2. Homogenize each tissue individually with a laboratory rotor homogenizer (*see Note 9*). Avoid extensive foam formation. If disposable, plastic-based generators are used, they should be immediately placed into “cleaning solution” to avoid later impurity from dried albumin and proteins.
3. Immediately add 20 µl proteinase K to the homogenate and invert the tube 25 times to mix the solution equally.
4. Place the tubes in a water bath with orbital shaking motion and incubate the samples overnight at 55 °C until the tissue has completely lysed.
5. Add 20 µl RNase A solution, and mix the samples by inverting 25 times.
6. Further incubate the samples at 37 °C for 1 h in a water bath with orbital shaking motion.
7. Cool down the samples on crushed ice up to 3 min.
8. Add 1.25 ml of protein precipitation solution (provided by Gentra Purgene Tissue Kit) to each sample and vortex vigorously for 20 s.
9. Centrifuge the samples in a swinging rotor at 4 °C for 15 min at 2000 × *g*. If the precipitated proteins do not form a tight pellet, incubate the tubes for additional 5 min on crushed ice and repeat centrifugation.
10. Transfer the supernatants to 15 ml centrifuge tubes without disturbing the pellet and add 4 ml of isopropanol to the supernatant.
11. Mix gently by inverting the tubes not less than 50 times or until a white, cloudy precipitate becomes visible.

12. Carefully transfer the precipitate using a 5 ml serological pipette to a 1.5 ml tube. The precipitate should be always pipetted within a small volume of solution to prevent adhesion to the plastic.
13. Centrifuge the samples in a standard laboratory centrifuge or microfuge at  $18,000 \times g$  at 4 °C for 5 min.
14. Discard the supernatant, drain the tube by pipetting remaining liquid using filtered pipette tips, and take care that the pellet remains in the tube.
15. Add 1 ml of 70% ethanol and carefully vortex the tube to release the pellet from the bottom. Invert the tube a few times to wash the pellet.
16. Centrifuge the samples in a standard laboratory centrifuge or microfuge at  $18,000 \times g$  at 4 °C for 5 min.
17. Discard the supernatant, drain the tube by pipetting remaining liquid using filtered pipet tips, and take care that the pellet remains in the tube. Allow to air-dry for 10 min.
18. Add 400 µl DNA hydration solution (provided by Gentra Purgene Tissue Kit) to the pellet and vortex for a few seconds at medium speed.
19. Incubate the tubes at 65 °C for 1 h in a shaking thermo block and further overnight at room temperature to dissolve the genomic DNA.
20. Measure the amount and quality of the obtained genomic DNA by spectrophotometric analysis.
21. Store the samples at 4 °C for direct subsequent processing. Otherwise the samples can be frozen and stored at –20 °C until the subsequent PCR analysis is carried out.

### **3.4 TaqMan®-Based Quantitative PCR of Samples and Standard Curve**

Make sure that your quantitative PCR machine is able to detect the fluorescent reporter dye *FAM* and the fluorescent quencher dye *TAMRA*. Dilute primers and probe to a working stock concentration of 10 µM. Hold available genomic DNA from untreated chicken eggs and each human cell line (concentration equal to  $2 \times 10^6$  cells/100 µl) used in your current experimental setup. It is generally recommended to use at least three technical replicates for each PCR.

1. Dilute the genomic chicken DNA of all test samples to a final concentration of 1 µg/5 µl in water.
2. Prepare a serial dilution using genomic DNA from the respective cell line (*see Note 10*). For this six 1.5 ml tubes are primed with 45 µl water containing 9 µg genomic chicken DNA isolated from untreated eggs. An additional 1.5 ml tube is pipetted in a way that it contains genomic human cell DNA

equivalent to  $1 \times 10^5$  cells and 10 µg genomic chicken DNA from untreated eggs. From this tube, 5 µl are stepwise diluted over the before prepared six 1.5 ml tubes, to obtain a progression of the genomic human cell DNA concentration in a logarithmic fashion in a constant background of 1 µg/5 µl genomic chicken DNA.

3. Prepare the reaction mix by combining the quantitative 1 × PCR master mix, 0.2 µM PCR primer FWD, 0.2 µM PCR primer REV, 0.18 µM probe, 1 µg template DNA, or 5 µl standard DNA equal to  $1 \times 10^5$ ,  $1 \times 10^4$ ,  $1 \times 10^3$ ,  $1 \times 10^2$ ,  $1 \times 10^1$ , or  $1 \times 10^{-1}$  cells and nuclease-free water to a final volume of 15 µl. It is recommended to prepare first a master mix without the template DNA and to add the template DNA after distribution of the master mix in the individual wells of a 96-well optical plates.
4. Seal the optical plates and centrifuge briefly to collect the contents of the well at the bottom.
5. Protect the samples from extended light exposure or elevated temperatures before cycling.
6. Each sample is subjected to an initial denaturation of 95 °C for 10 min, followed by 40 amplification cycles of denaturation at 95 °C for 15 s and 60 °C for 1 min to anneal, and extend or follow the standard optimized thermal cycling protocol for amplification with your current quantitative PCR master mix (*see Note 11*).

### **3.5 TaqMan®-Based Absolute Quantification of Invasive Cells**

1. Absolute quantification is performed by constructing a standard curve for each cell line used in an experimental setup, by plotting the quantification cycle (CQ) values against logarithmic quantity of the dilution series from the genomic cell DNA. Average the number of replicates and also consider the standard deviation. Finally, calculate the number of invaded cells in the test samples versus the number of invaded cells in the control group as a graph and use the linear regression line to generate the calibration curve (*see Note 12*).

---

## **4 Notes**

1. Prevent foam while making SDS containing buffer and use SDS pellets instead of powder to avoid inhaling of SDS dust leading to possible respiratory tract irritation.
2. Before even looking at incubator brands, it should be determined how many eggs can be incubated at once. Incubators come in many different sizes and shapes, starting with only a few eggs and running all the way up to a few thousand.

3. Always use gloves to prevent human contamination and change the gloves frequently.
4. Always use cleaned lab coat.
5. Always use eye protection while working with the mini rotary tool.
6. Always use surgical mask to avoid contamination and to breathing in egg shell dust.
7. Replace the instruments used for isolation of the lower CAM and organs after each experimental group.
8. Clean the instruments used for isolation after each sample with 70% ethanol.
9. We recommend disposable, plastic-based generators as an effective solution for researchers homogenizing highly sensitive samples to prevent contaminants, which can affect downstream applications.
10. Take precautions while making standard curve dilutions to avoid any cross contamination with actual samples.
11. Optimum primer annealing temperatures may be different in different qPCR master mixes.
12. Ideally, a new standard curve is generated each time a sample is quantified. This prevents inaccurate results as the efficiency of amplification may vary across samples, with time, or between the target used to generate the standard curve and the “real” target within a complex sample.

## Acknowledgments

H.A. was supported by the Alfried Krupp von Bohlen und Halbach Foundation, Essen, the Deutsche Krebshilfe, Bonn (70112168), the Deutsche Forschungsgemeinschaft (DFG, grant number AL 465/9-1), the HEiKA Initiative (Karlsruhe Institute of Technology/University of Heidelberg collaborative effort), Dr. Hella-Bühler-Foundation, the DKFZ-MOST Cooperation, Heidelberg (grant number CA149), the HIPO/POP-Initiative for Personalized Oncology, Heidelberg (H032 and H027).

## References

1. Murphy JB (1913) Transplantability of tissues to the embryo of foreign species: its bearing on questions of tissue specificity and tumor immunity. *J Exp Med* 17(4):482–493. <https://doi.org/10.1084/jem.17.4.482>
2. Rous P, Murphy JB (1911) Tumor implantations in the developing embryo. *J Am Med Assoc* 56:741
3. Dagg CP, Karnofsky DA, Roddy J (1956) Growth of transplantable human tumors in the chick embryo and hatched chick. *Cancer Res* 16(7):589–594
4. Komatsu A, Higashi Y, Matsumoto K (2019) Various CAM tumor models. *Enzyme* 46:37–57. <https://doi.org/10.1016/bs.enz.2019.10.001>

5. Janse EM, Jeurissen SH (1991) Ontogeny and function of two non-lymphoid cell populations in the chicken embryo. *Immunobiology* 182 (5):472–481. [https://doi.org/10.1016/s0171-2985\(11\)80211-1](https://doi.org/10.1016/s0171-2985(11)80211-1)
6. Jankovic BD, Isakovic K, Lukic ML, Vujanovic NL, Petrovic S, Markovic BM (1975) Immunological capacity of the chicken embryo. I. Relationship between the maturation of lymphoid tissues and the occurrence of cell-mediated immunity in the developing chicken embryo. *Immunology* 29(3):497–508
7. Leupold JH, Yang HS, Colburn NH, Asangani I, Post S, Allgayer H (2007) Tumor suppressor Pcd4 inhibits invasion/intravasation and regulates urokinase receptor (u-PAR) gene expression via Sp-transcription factors. *Oncogene* 26(31):4550–4562. <https://doi.org/10.1038/sj.onc.1210234>
8. Lokman NA, Elder AS, Ricciardelli C, Oehler MK (2012) Chick chorioallantoic membrane (CAM) assay as an *in vivo* model to study the effect of newly identified molecules on ovarian cancer invasion and metastasis. *Int J Mol Sci* 13 (8):9959–9970. <https://doi.org/10.3390/ijms13089959>
9. Rovithi M, Avan A, Funel N, Leon LG, Gomez VE, Wurdinger T, Griffioen AW, Verheul HM, Giovannetti E (2017) Development of bioluminescent chick chorioallantoic membrane (CAM) models for primary pancreatic cancer cells: a platform for drug testing. *Sci Rep* 7:44686. <https://doi.org/10.1038/srep44686>
10. van der Horst EH, Leupold JH, Schubbert R, Ullrich A, Allgayer H (2004) TaqMan-based quantification of invasive cells in the chick embryo metastasis assay. *BioTechniques* 37 (6):940–942, 944, 946. <https://doi.org/10.2144/04376ST02>
11. Zijlstra A, Mellor R, Panzarella G, Aimes RT, Hooper JD, Marchenko ND, Quigley JP (2002) A quantitative analysis of rate-limiting steps in the metastatic cascade using human-specific real-time polymerase chain reaction. *Cancer Res* 62(23):7083–7092
12. Batzer MA, Deininger PL (1991) A human-specific subfamily of Alu sequences. *Genomics* 9(3):481–487. [https://doi.org/10.1016/0888-7543\(91\)90414-a](https://doi.org/10.1016/0888-7543(91)90414-a)
13. DeBord LC, Pathak RR, Villaneuva M, Liu HC, Harrington DA, Yu W, Lewis MT, Sikora AG (2018) The chick chorioallantoic membrane (CAM) as a versatile patient-derived xenograft (PDX) platform for precision medicine and preclinical research. *Am J Cancer Res* 8(8):1642–1660



# Chapter 3

## In Vitro 3D Models of Tunable Stiffness

**Elysse C. Filipe, Amelia L. Parker, Antonia L. Cadell, Gretel Major, David R. Croucher, and Thomas R. Cox**

### Abstract

Three-dimensional models of spheroid formation have been routinely used in the cancer field to test the colony forming capacity of malignant cells in an in vitro setting. Use of such a model provides a robust surrogate for in vivo testing, enabling large-scale interrogation into the effect of certain treatment conditions. This adapted protocol describes a high throughput and readily accessible composite alginate hydrogel system for spheroid formation, within a biomechanically tunable three-dimensional environment. This model therefore allows users to examine the effect of certain treatment conditions while cells are embedded within a hydrogel of defined stiffness. This is particularly important in the context of cancer where cells experience a wide range of mechanical properties within their microenvironment, driven by widespread changes in the extracellular matrix composition and architecture.

This protocol describes a high-throughput method which results in homogeneous interpenetrating polymer networks of collagen and alginate. We show that this network readily supports single-cell spheroid formation in numerous malignant cell lines (breast cancer, lung cancer, and melanoma) and that these can be robustly analyzed for colony formation measures such as spheroid size, spheroid number, and overall cell viability; therefore, allowing users to undertake high-throughput, in vitro screening against a controlled biomechanical background.

**Key words** Alginate, Spheroid, Colony formation, Stiffness, Extracellular matrix, High throughput

---

### 1 Introduction

The three-dimensional environment of cells, constituting mechanical, physical, and chemical cues, is recognized as an important regulator of cellular behavior in both health and disease. Molecules that form this three-dimensional extracellular matrix provide anchor points for other matrix components as well as adhesion sites for cells that dictate the biomechanical properties of the tissue. Both the biomechanical stiffness and biochemical composition of tissues are sensed independently and interdependently by cells,

---

Elysse C. Filipe and Amelia L. Parker contributed equally to this work.

which respond by activating and suppressing critical intracellular pathways governing cellular proliferation, polarity, and differentiation in a cell type- and tissue-dependent manner. Disruption of the extracellular matrix architecture, and by extension its biomechanical properties, contributes to the development and severity of disease, including malignant invasiveness [1–3].

The importance of biomechanical properties in driving disease processes has led to the development of in vitro models that recapitulate the biomechanics of healthy and diseased tissues. Two-dimensional (clonogenic assay) and three-dimensional (soft agar, low attachment, or hanging drop spheroid formation) models of spheroid formation have been routinely used in the cancer field to test the colony forming capacity of disseminated malignant cells in an in vitro setting. The propensity of individual cancer cells to form colonies is a surrogate measure of their tumor initiating capacity at metastatic sites. The effect of tissue stiffness in supporting or suppressing cancer cell outgrowth can be modeled by embedding the cancer cells within a mechanically tunable three-dimensional matrix and monitoring their outgrowth into spheroids.

Both biologically active materials and bioinert matrices have been appropriated as in vitro three-dimensional models of tissue stiffness. However, since biologically active materials contain cellular adhesion sites, uncoupling the contribution of biomechanical stiffness and cellular interaction with ECM biochemistry in these models has proved challenging. For example, the stiffness of recombinant basement membrane, such as Matrigel, increases with the type I collagen concentration. However the collagen I density also dictates the ligand density for cellular attachment with recent work showing that ligand density activates diverse signaling pathways independently of matrix stiffness [4–9] and thereby confounds the effects of mechanical stiffness alone. Enzymatic cross-linking of matrices that do contain cellular adhesion sites, such as using transglutaminase to crosslink Matrigel, has been used to increase matrix stiffness without affecting ligand density [10], although achieving precise control over the mechanical stiffness of the resulting gel is challenging.

Bioinert matrices, which lack cellular adhesion sites, offer the opportunity to tune the biomechanical properties of a hydrogel independently of cellular adhesion. Bioinert matrices of alginate [11], polyethylene glycol [12], and agarose [13] have each been used to tune matrix stiffness independently of ligand density through manipulating the density of crosslinks between polymer chains. By using models that uncouple the biomechanical and adhesive matrix properties, these studies have demonstrated that increased matrix stiffness drives stem cell differentiation and renewal, increases cellular proliferation, modulates intracellular signaling, regulates the epigenome, promotes chemotherapy

resistance in cancer cells, and promotes their metastatic behavior in a context-dependent manner [10–14]. While these bioinert model systems have been extensively developed for tissue regeneration and drug delivery purposes, they have only more recently been adopted as tools in cancer research.

Of these bioinert polymers, alginate hydrogels have been widely employed as tunable and biocompatible models of tissue mechanics for the ease with which their biomechanical properties can be manipulated. Alginates are natural polysaccharides composed of blocks of 1–4-linked beta-D-mannuronic acid and alpha-L-guluronic acid monomers. The distribution of polymer molecular weights and the relative proportions of the mannuronic and guluronic monomers can vary substantially between alginate preparations, thereby influencing their gelation, stability, degradation, and crosslinking properties [11, 15].

Alginate hydrogels are most commonly gelled by the application of divalent cations such as calcium [15], which form ionic bonds between the anionic carboxylic acid groups of the G-block polymers. The most common approach is a single-step gelation procedure, where alginate solutions are immersed in a calcium chloride buffer (i.e., bead in bath method), and the high aqueous solubility of calcium chloride rapidly releases the calcium ions to crosslink and gel the alginate. Thus, higher calcium concentrations increase the density of crosslinks between alginate polymers and thereby increase hydrogel stiffness [3]. Similarly, since ionic crosslinks are formed between the G-block polymers, alginate formulations with a higher G-block composition form stiffer matrices [15]. Using this approach, alginates can be gelled quickly and efficiently at room temperature without the need for advanced chemical apparatus. It should be noted that monovalent cations such as sodium or potassium can compete with divalent cations for these crosslink sites during gelation, and care must be taken to minimize their presence during hydrogel gelation.

A key challenge with the use of calcium chloride as a cross-linking agent is that its high aqueous solubility results in the rapid formation of crosslinks in a poorly controlled manner. In larger hydrogels, this can result in a high crosslink density in outer hydrogel layers with a lower crosslink density in the center and non-uniform mechanical properties through the gel thickness. This limits the size of alginate hydrogels that can be formed by this single-step method. Therefore, approaches to slow and control the release of calcium ions have gained considerable attention. For example, the lower aqueous solubility of calcium carbonate and calcium sulphate releases the calcium more slowly compared with calcium chloride. This provides adequate time for diffusion of the calcium salt throughout the alginate and results in a more homogeneous crosslink density through the gel thickness [15]. As the solubility of calcium carbonate increases at lower pH, controlled

reduction of the pH of the alginate solution can further control the release of calcium [16]. Alternatively, covalent crosslinking of alginate polymers by chemical modification of the mannuronic and guluronic blocks limits hydrogel softening typically observed over extended periods of time in gels made using cationic crosslinking approaches [17, 18]. While these covalent crosslinks are maintained over time, controlling the density of covalent crosslinks to tune biomechanical stiffness remains difficult [17, 18]. Furthermore, such approaches require sophisticated chemical apparatus.

Two-step cation-based gelation procedures, such as the protocol described in this chapter, have been developed to improve the homogeneity and tunability of cation-based alginate crosslinks. The initial gelation stage involves controlled release of divalent cations from within the hydrogel with a subsequent stiffening step to fine-tune the hydrogel stiffness. In this protocol, the first stage utilizes D-glucono-delta-lactone (GDL) to lower the pH of the gel solution, inducing dissociation of the calcium carbonate and release of the calcium ions. By slowing the release of the calcium, this pH-controlled approach produces a homogeneous crosslink density throughout the gel thickness. The second stage involves fine-tuned hydrogel stiffening by immersion in a calcium chloride solution. By slowing and controlling the gelation process through the initial gelation and subsequent stiffening stages, this method produces a more homogeneous hydrogel with uniform fine-tuned biomechanical stiffness compared with single-step calcium chloride gelation [16, 19, 20]. This approach is compatible with a wide range of hydrogel sizes, including the 96-well format described in this protocol, which has the significant advantage of being conducive to high-throughput applications.

While cation concentration is used to control the elastic stiffness of alginates and model the elastic tissue biomechanics, a recent study has demonstrated that the viscoelastic behavior of the matrix can regulate chromatin remodeling and epigenetic signaling [21]. This tissue property can also be controlled within alginate hydrogels by modulating the composition (G-block to M-block ratio) as well as the molecular weight of alginate monomers [21] and such an approach is compatible with this protocol. In this manner, the composition of the alginate is of fundamental importance in determining its mechanical properties.

As a bioinert polymer, alginate hydrogels are typically generated as composites together with bioactive polymers that provide cellular adhesion sites. Since the frequency-dependent mechanical properties of alginate hydrogels are similar to many bioactive polymers, these alginate–bioactive polymer composite systems, which can form interpenetrating network hydrogels, behave as a single mechanically integrated network [3]. Collagen I [22], laminin-111 [23], and recombinant basement membrane such as Matrigel [3] have been mixed with alginates to form these composite gels.

Alternatively, alginates with covalently bound RGD sequences [22] have been used to provide integrin adhesion sites. The choice of functionalizing protein allows control over the engagement of different subsets of cell surface mechanoreceptors that regulate different cellular functions.

The protocol outlined in this chapter is an accessible and robust method for generating *in vitro* three-dimensional high-throughput alginate-based composite models of tunable stiffness that can be readily employed to dissect the contribution of mechanical stiffness to the maintenance of healthy cellular function and to the progression of disease. This adapted protocol describes an accessible and robust two-stage alginate hydrogel preparation method to culture cells within a biomechanically tunable three-dimensional environment. The sequential controlled gelation and stiffening steps improve both throughput and reproducibility. The gelation step exploits pH-dependent calcium carbonate solubility to generate a hydrogel with a uniform baseline stiffness. This is followed by immersion within a calcium chloride solution to fine-tune the hydrogel stiffness (Fig. 1). The importance of mechanical stiffness on spheroid formation in a panel of cancer cell lines is provided as one example of how this system may be applied to interrogate the contribution of mechanical stiffness in promoting cancer aggressiveness. We show that this alginate composite network readily supports spheroid formation from single cells in numerous malignant cell lines (breast cancer, lung cancer, and melanoma) and that these can be robustly analyzed for colony formation measures such as spheroid size, spheroid number, and overall cell viability. These mechanically tunable alginate–bioactive polymer composite hydrogels provide a controlled biomechanical background in a range of low- to high-throughput formats to dissect the role of mechanical stiffness in health and disease.

---

## 2 Materials

### 2.1 Reagents

Alginate (Pronova UP-MVG; NovaMatrix; cat no: P-1408-24).

Calcium carbonate (Sigma-Aldrich; cat no: C4830).

Calcium chloride (Sigma-Aldrich; cat no: C1016).

D-(+)-gluconic acid  $\delta$ -lactone (GDL salt; Sigma-Aldrich, cat no: G4750).

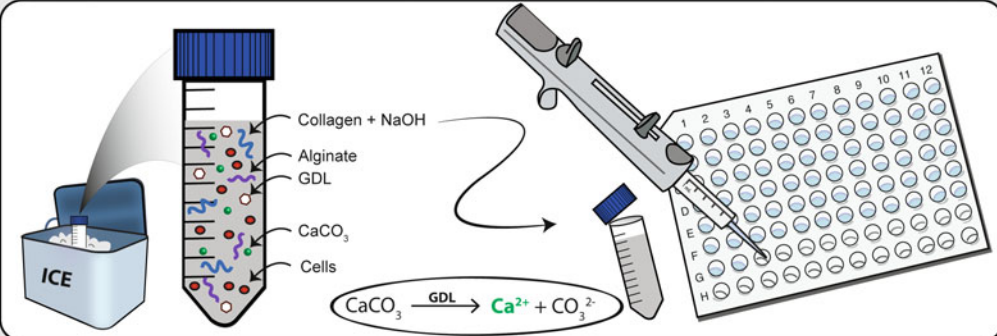
Rat tail collagen—for a detailed protocol for extraction of type I collagen from rat tail, see [24–26].

Sodium hydroxide (Sigma-Aldrich; cat no: S8045).

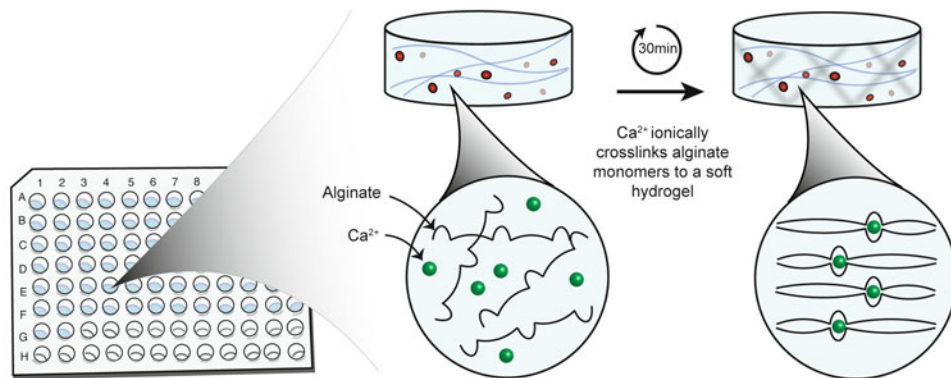
DMEM, high glucose (Gibco; cat no: 11995-065).

Fetal bovine serum: (Gibco; cat no: 16000-044).

### 1 Preparation



### 2 Gelation



### 3 Stiffening

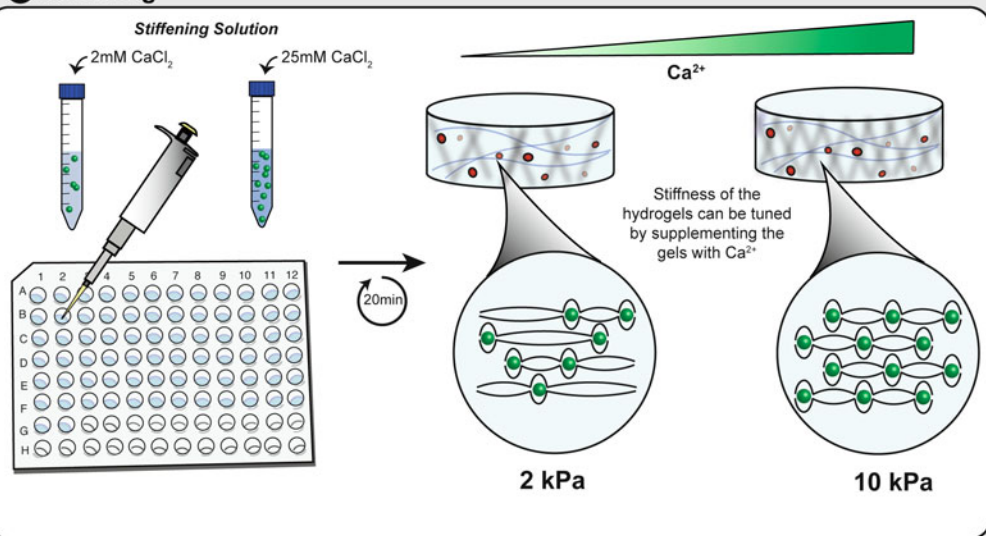


**Fig. 1** Alginate hydrogel workflow depicting the main stages of hydrogel gelation including (1) Preparation—where the alginate solution is mixed with cells, collagen, CaCO<sub>3</sub>, and GDL; (2) Gelation—where the low Ca<sup>2+</sup> ion concentration leads to a controlled crosslinking of the alginate monomers, yielding a soft hydrogel; (3) Stiffening—where hydrogels are immersed within a second Ca<sup>2+</sup>-containing CaCl<sub>2</sub> buffer to further crosslink the alginate and consequently increase hydrogel stiffness

Penicillin/streptomycin 100×: (Sigma-Aldrich; cat no: P4458).  
 Saline (0.9% NaCl<sub>2</sub> in water; Pfizer).  
 Acetic acid (Fisher Chemical; cat. no. A/040B/PB17).  
 Phosphate-buffered saline (Gibco; cat no: 14190-144).  
 Ultrapure water.

## **2.2 Equipment**

50 mL falcon tube (Corning; cat. no. 430829).  
 1.5 mL tubes (Eppendorf; cat no: 0030125150)  
 96-well flat-bottomed plate, tissue culture-treated (Costar; cat no 3599).  
 0.22 µm syringe filter (Sartorius; cat no: 16534)  
 0.44 µm syringe filter (Millipore; cat no: SLHV033RS).  
 1 L glass bottle  
 Pipettes and pipette tips (Sterile P10, P20, P200, and P1000).  
 Vortex.  
 Stepper pipette and tips.  
 Analytical balance.  
 Tissue culture laminar flow hood.  
 Cell incubator (37 °C, 5% CO<sub>2</sub>, and 21% oxygen).

## **3 Method**

### **3.1 Reagent Preparation**

1. Prepare a 2% alginate stock solution in saline and leave under gentle agitation overnight at room temperature. Once dissolved, solution should be filter-sterilized (0.45 µm filter) in a sterile working environment and stored at 4 °C for future use. We have successfully used alginate stock solutions prepared 3 weeks prior to an experiment and stored (maintaining sterility) at 4 °C until use (*see Note 1*).
2. Prepare a 1 M CaCO<sub>3</sub> stock solution in water and autoclave. In a sterile working environment, aliquot into smaller working stocks for routine use.  
*Note:* This should be prepared in a 1 L glass bottle to avoid over boiling during the autoclaving cycle.
3. Prepare a collagen working solution at 2 mg/mL collagen I in 17.4 mM acetic acid.  
*Note:* Ensure you work continuously on ice to avoid precipitation of the collagen.
4. Prepare a 220 mM NaOH stock solution in water. This solution should be filter-sterilized (0.22 µm) in a sterile working environment prior to use.

**Table 1**  
**Volumes to prepare 2, 5, or 10 mLs of alginate plugs**

Order	Solution	[Stock]	[Final]	μL		
1	2% alginate in 0.9% saline	2%	1%	1000	2500	5000
2	Saline	–	–	204.6	661.5	1423
3	2 mg/mL collagen working solution	2 mg/mL	0.5 mg/mL	500	1250	2500
4	220 mM NaOH stock solution	220 mM	3.9 mM	35.4	88.5	177
5	1 M CaCO <sub>3</sub> stock solution	1000 mM	5 mM	10	25	50
6	Cells in saline (to be added in step 4)	–	–	100	100	100
7	GDL working solution (to be added in step 6)	56 mg/mL	4.2 mg/mL	150	375	750
–	Total	–	–	2000	5000	10,000

5. Prepare a 1 M CaCl<sub>2</sub> stock solution in water. This solution should be filter-sterilized (0.22 μm) in a sterile working environment prior to use.
6. Prepare complete cell media compatible with your cell lines (*see Note 2*).

### 3.2 Alginate Hydrogel Preparation

*To be performed in a sterile environment such as a Biological Safety Cabinet.*

1. Prepare a bucket of ice containing your alginate stock solution, CaCO<sub>3</sub> stock solution, collagen working solution, NaOH stock solution, and saline. Keep these solutions on ice to avoid premature gelation of the collagen.
2. Trypsinize and count your cells. Calculate the number of cells necessary for your experiment (cell density of 1000–2000 cells/100 μL plug is optimal for spheroid formation in 96-well formats) and transfer to a new tube for centrifugation.
3. In the meantime, prepare your alginate mixture in a 50 mL tube as per Table 1, vortexing between each addition and always working on ice (*see Note 3*). The larger diameter of the 50 mL tube compared with a 15 mL tube allows for better homogenization.
4. Resuspend the cell pellet in 100 μL of ice-cold saline and add to your alginate mixture. Mix with a short burst of vortexing.
5. Prepare your GDL working solution by reconstituting the GDL salt in an appropriate volume of saline. Once completely dissolved, filter-sterilize with a 0.22 μm syringe filter (*see Note 4*).

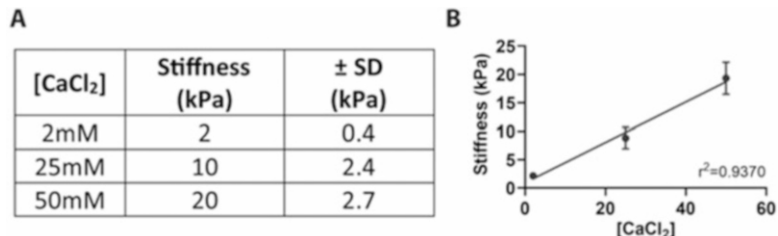


**Fig. 2** Elastic moduli of alginate hydrogels stiffened with various CaCl<sub>2</sub> concentrations. Values represent mean  $\pm$  SD of 20 individual gels (4 gels at 5 different time points)

6. Add appropriate volume of sterile GDL working solution into your alginate mixture and vortex immediately.
7. Pipette 100  $\mu$ L amounts of the alginate mixture into your 96-well plate. A stepper pipette will facilitate this and improve reproducibility. If a stepper pipette is unavailable, use sterile 200  $\mu$ L pipette tips with the top 1 cm of the tip cut off. This improves the accuracy/speed when pipetting viscous solutions.
8. Leave the plugs to gel for 30 min at room temperature. During this time, the cloudiness of the gels should dissipate. This can be monitored under a light microscope.
9. Prepare CaCl<sub>2</sub> supplemented media of required concentration, diluted in pre-warmed complete cell media (*see Notes 5–7*). See Fig. 2 to determine appropriate CaCl<sub>2</sub> concentrations for your specific applications.
10. Add 100  $\mu$ L (one gel volume) of the CaCl<sub>2</sub> supplemented cell media into each well and leave to incubate for 30 min at 37 °C.
11. Carefully remove the CaCl<sub>2</sub> containing media with a P200 pipette and wash gels twice with sterile PBS, 5 min each wash (200  $\mu$ L or equivalent to two gel volumes).
12. Add 125  $\mu$ L of complete cell media and place plate back into incubator.
13. Monitor plugs for spheroid formation and replace media (by pipetting) every 2 or 3 days or as necessary.

### 3.3 Monitoring Spheroid Formation

1. Ensure gels are touching the bottom on the plate, either by removing all cell media or gentle centrifugation (50  $\times$  *g*, 30 s).
2. On a standard inverted light microscope equipped with a camera, choose three regions of interest within the well and image all z-planes where a spheroid comes into focus.
3. Using standard imaging software, users can measure a variety of spheroid characteristics such as spheroid size by means of diameter or area, circularity, and spheroid number (Fig. 3) (*see Notes 8–9*).

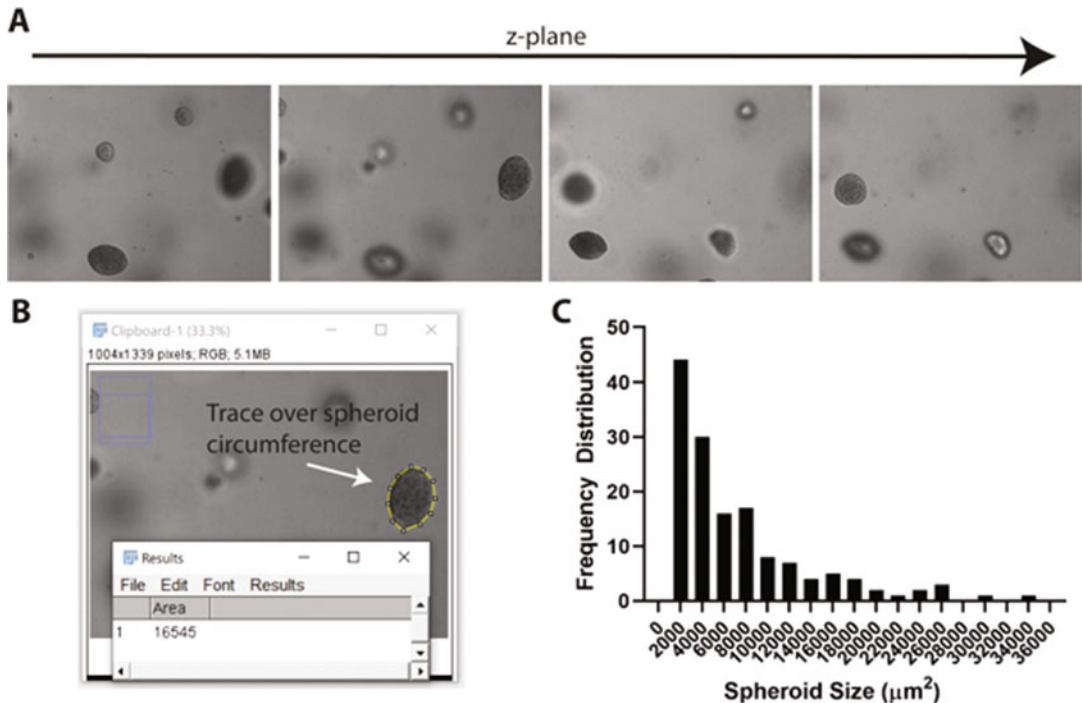


**Fig. 3** Spheroid formation analysis by microscopy **(a)** Images should be taken of all spheroids along the z-plane, within an ROI. **(b)** Spheroid area can then be measured by tracing over the spheroid circumference in an image analysis software. **(c)** Various measures of spheroid size can be plotted, including frequency distribution

#### 4 Notes

1. This protocol has been optimized using high purity alginate containing a minimum 60% G-block content. Alginates of different G-block content will yield solutions of very different viscosities, changing the gelation kinetics, and will also have different crosslink densities [15]. These alternative alginates may be used; however, optimization of the  $\text{CaCO}_3/\text{GDL}$  concentrations will need to be performed.
2. DMEM is the optimal base media for use with alginate hydrogels. Additives found in other media (i.e., RPMI 1640) can precipitate when in contact with  $\text{CaCl}_2$ .
3. The volumes in Table 1 can be changed according to your specific applications; however, care must be taken to keep the appropriate collagen/ $\text{NaOH}$  ratio (to completely neutralize the acidity of the collagen solution) and  $\text{CaCO}_3/\text{GDL}$  ratio (to completely dissociate all  $\text{CaCO}_3$  precipitate). Also note that any changes to these ratios will change the mechanical

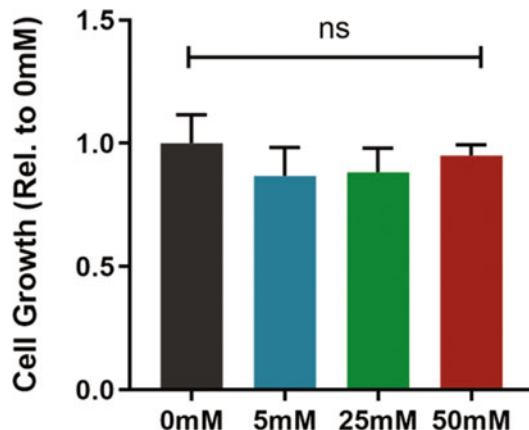


**Fig. 4** Cell growth of 4T1 breast cancer cells in an anchorage-independent assay. The addition of 5–50 mM CaCl<sub>2</sub> for 30 min immediately after gelation did not significantly influence cell growth. These values were collected at day 8 post seeding and are relative to control (0 mM CaCl<sub>2</sub>). Values represent mean  $\pm$  SD of 3 replicates

properties of the hydrogels, and further stiffness characterization will need to be performed. Mechanical characterization of the hydrogels can be performed using shear rheology [27], atomic force microscopy [28], or unconfined compression analysis [29].

4. GDL solution should be prepared immediately before use. Using an old GDL solution (i.e., GDL powder dissolved in saline more than 10 min prior to use) will cause the alginate to prematurely gel. GDL salt can be pre-weighed into 1.5 mL tubes and stored ready for dissolution. When needed, dissolve the GDL in saline and filter-sterilize with a 0.22  $\mu$ m syringe filter in a sterile working environment.
5. The DMEM recommended in this protocol contains a basal CaCl<sub>2</sub> concentration of 2 mM. The CaCl<sub>2</sub> concentrations in Fig. 2 are in addition to the 2 mM CaCl<sub>2</sub> in the media. If using other media, these concentrations may need optimization.
6. Using anchorage-independent agar gels (whose stiffness is unaffected by calcium), we tested the effect of CaCl<sub>2</sub> on cell proliferation and spheroid formation for 8 days. At end point, we observed no significant differences in the cell number in conditions with up to 50 mM of CaCl<sub>2</sub> confirming that alginate gelation conditions do not alter cell proliferation (*see* Fig. 4).
7. Due to the reversible nature of the ionic crosslinks, gels will experience a degree of hydrogel softening when cultured in normal cell media. We have characterized the dynamics of this loss of stiffness and shown that it occurs rapidly, within the first

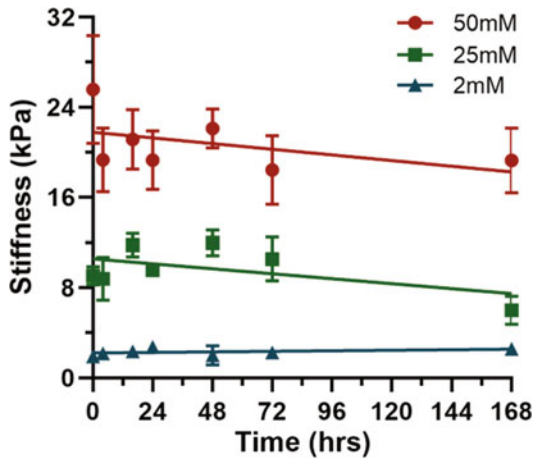


**Fig. 5** Profile of hydrogel stiffness over a 7-day period measured by shear rheology. After an initial decrease in hydrogel stiffness at 4 h post gelation, the mechanical properties do not significantly change over 7 days. Hydrogels stiffened with 2 mM, 25 mM, and 50 mM  $\text{CaCl}_2$  in steps 9–10 will reach an average stiffness of  $2 \pm 0.4$  kPa,  $10 \pm 2.4$  kPa, and  $20 \pm 2.7$  kPa. Values represent mean  $\pm$  SD of 4 gels per time point

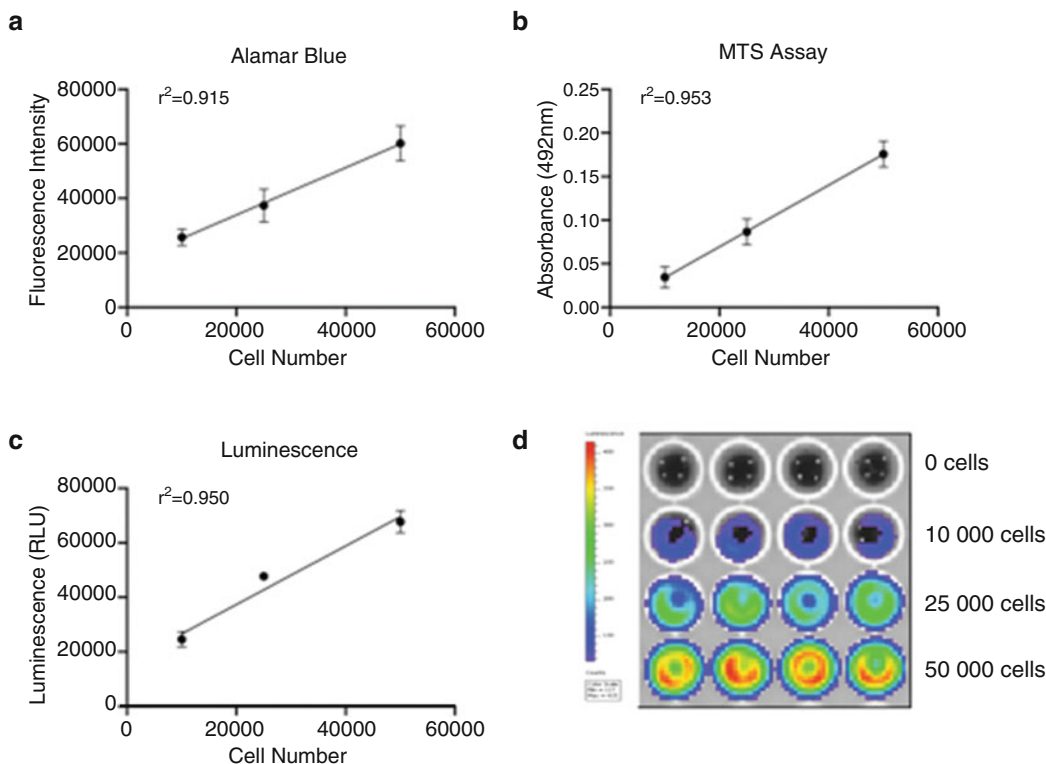


**Fig. 6** Luciferase-expressing A549 cells were embedded into alginate gels at 5000, 10,000, 25,000, and 50,000 cells per gel and stiffened in 2 mM  $\text{CaCl}_2$  for 30 min. Cell number was measured by alamarBlue (**a**), MTS (**b**), and luminescence assays (**c**) and by bioluminescence imaging (**d**) 24 h later. Data in **a**, **b**, and **c** are the mean  $\pm$  SD of three replicates. (**d**) Is a representative heatmap from one biological replicate with four technical replicates (one technical replicate per column)

2 h of hydrogel formation. Beyond the first 2 h, however, hydrogel stiffness remains stable (Fig. 5).

8. Further to the spheroid characterizations outlined in Subheading 3.3, cell viability can also be determined using colorimetric methods such as alamarBlue or MTS (Fig. 6). Longer incubation times compared with two-dimensional cultures may be necessary and should be optimized for your specific application [30, 31]. We have shown that the luminescence signal of luciferase-expressing cells contained within alginate hydrogels can be quantified either by bioluminescence imaging (e.g., IVIS system) or luminescence quantification on a plate reader. For all of the cell viability measures tested, we observed a linear relationship between cell number and signal, confirming robustness of the various approaches.
9. Using the protocol detailed in this manuscript for stiffness-controlled cell-containing alginate hydrogels, we demonstrate successful spheroid formation with multiple malignant cell lines, including breast (4T1), lung (H520), and melanoma (B16F10) (Fig. 7). We monitored spheroid formation over a 3-week period using an inverted light microscope. It is important to note that spheroid forming ability is a characteristic of only some cancer cell lines, and optimization of cell density, hydrogel properties, and assay length may be necessary for individual applications. For cell lines which do not demonstrate spheroid forming ability with the standard technique described in this manuscript, we have successfully added up to 25% Matrigel (substituting saline) into the hydrogels which was sufficient to support spheroid formation in some cell lines. Other additives can be used but care must be taken to avoid large volumes of additives in buffered solutions, as this will interfere with the pH and consequently the gelation of the hydrogels. Further, any additives (particularly ECM components) will likely cause changes in the mechanical properties of the hydrogels and revalidation of biomechanical properties should be performed.

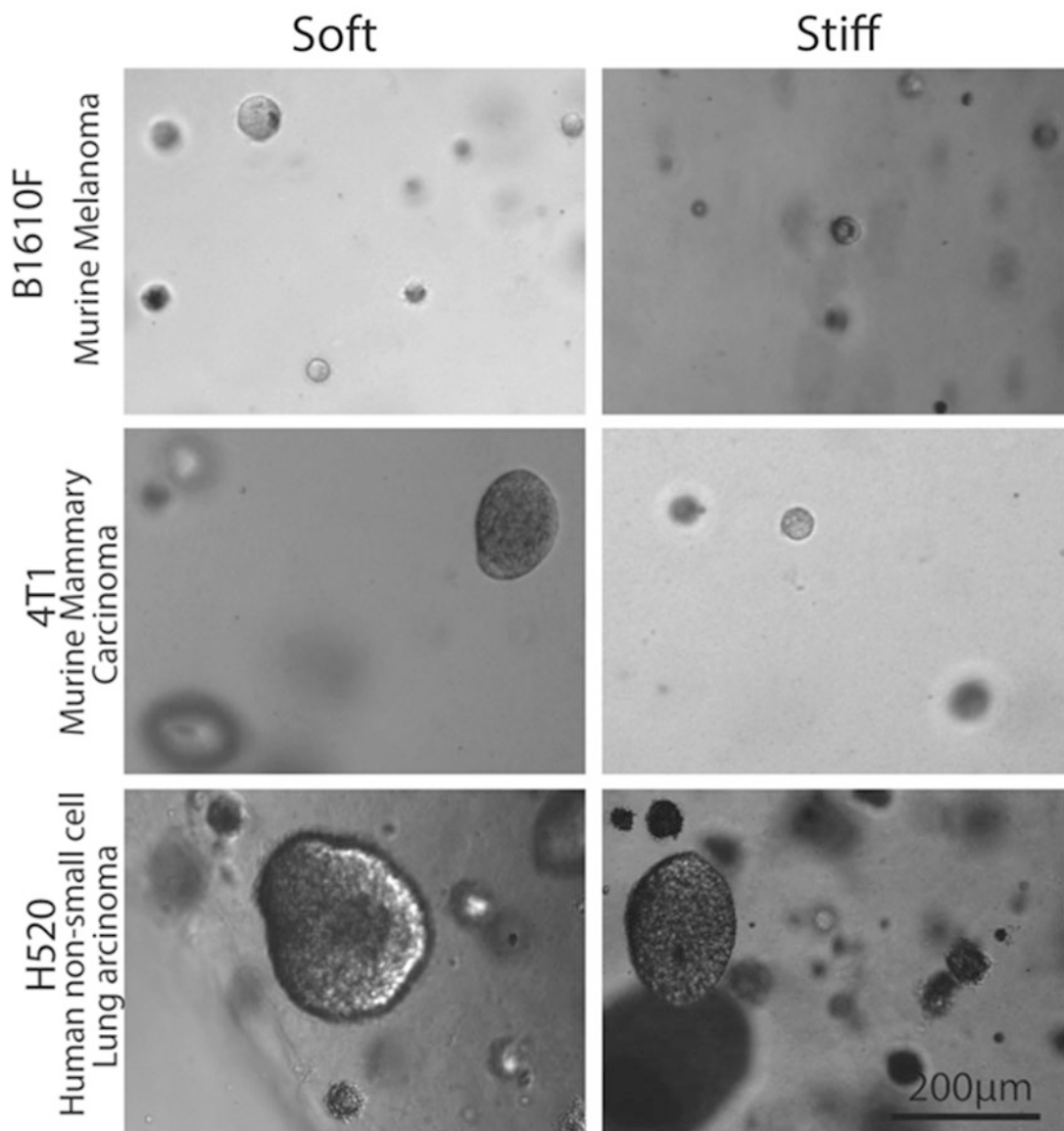


**Fig. 7** Spheroid formation in soft and stiff hydrogels for three distinct cell types, including murine melanoma (B1610F), murine mammary carcinoma, (4T1) and human non-small cell lung carcinoma (H520). Soft hydrogels are 2 kPa for all cell types, stiff hydrogels are 10 kPa for B1610F and 4T1, and 20 kPa for the H520. Scale bar = 200  $\mu$ m

## References

- Levental KR, Yu H, Kass L, Lakins JN, Egeblad M, Erler JT et al (2009) Matrix cross-linking forces tumor progression by enhancing integrin signaling. *Cell* 139(5):891–906
- Stowers RS, Shcherbina A, Israeli J, Gruber JJ, Chang J, Nam S et al (2019) Matrix stiffness induces a tumorigenic phenotype in mammary epithelium through changes in chromatin accessibility. *Nat Biomed Eng* 3 (12):1009–1019
- Chaudhuri O, Koshy ST, Branco da Cunha C, Shin J-W, Verbeke CS, Allison KH et al (2014)

- Extracellular matrix stiffness and composition jointly regulate the induction of malignant phenotypes in mammary epithelium. *Nat Mater* 13(10):970–978
4. Provenzano PP, Inman DR, Eliceiri KW, Keely PJ (2009) Matrix density-induced mechanoregulation of breast cell phenotype, signaling and gene expression through a FAK-ERK linkage. *Oncogene* 28(49):4326–4343
  5. Paszek MJ, Zahir N, Johnson KR, Lakins JN, Rozenberg GI, Gefen A et al (2005) Tensional homeostasis and the malignant phenotype. *Cancer Cell* 8(3):241–254
  6. Giancotti FG, Ruoslahti E (1999) Integrin signaling. *Science* 285(5430):1028–1032
  7. Engler A, Bacakova L, Newman C, Hategan A, Griffin M, Discher D (2004) Substrate compliance versus ligand density in cell on gel responses. *Biophys J* 86(1 Pt 1):617–628
  8. Brownfield DG, Venugopalan G, Lo A, Mori H, Tanner K, Fletcher DA et al (2013) Patterned collagen fibers orient branching mammary epithelium through distinct signaling modules. *Curr Biol* 23(8):703–709
  9. Nguyen-Ngoc K-V, Cheung KJ, Brenot A, Shamir ER, Gray RS, Hines WC et al (2012) ECM microenvironment regulates collective migration and local dissemination in normal and malignant mammary epithelium. *Proc Natl Acad Sci U S A* 109(39):E2595–E2604
  10. Mammo A, Connor KM, Mammo T, Yung CW, Huh D, Aderman CM et al (2009) A mechanosensitive transcriptional mechanism that controls angiogenesis. *Nature* 457 (7233):1103–1108
  11. Rowley JA, Madlambayan G, Mooney DJ (1999) Alginate hydrogels as synthetic extracellular matrix materials. *Biomaterials* 20 (1):45–53
  12. Peyton SR, Raub CB, Keschrumer VP, Putnam AJ (2006) The use of poly(ethylene glycol) hydrogels to investigate the impact of ECM chemistry and mechanics on smooth muscle cells. *Biomaterials* 27(28):4881–4893
  13. Ulrich TA, Jain A, Tanner K, MacKay JL, Kumar S (2010) Probing cellular mechanobiology in three-dimensional culture with collagen-agarose matrices. *Biomaterials* 31 (7):1875–1884
  14. Khetan S, Guvendiren M, Legant WR, Cohen DM, Chen CS, Burdick JA (2013) Degradation-mediated cellular traction directs stem cell fate in covalently crosslinked three-dimensional hydrogels. *Nat Mater* 12 (5):458–465
  15. Lee KY, Mooney DJ (2012) Alginate: properties and biomedical applications. *Prog Polym Sci* 37(1):106–126
  16. Gowney Kalaf EA, Flores R, Bledsoe JG, Sell SA (2016) Characterization of slow-gelling alginate hydrogels for intervertebral disc tissue-engineering applications. *Mater Sci Eng C Mater Biol Appl* 63:198–210
  17. Thornton AJ, Alsberg E, Hill EE, Mooney DJ (2004) Shape retaining injectable hydrogels for minimally invasive bulking. *J Urol* 172 (2):763–768
  18. Wang L, Shansky J, Borselli C, Mooney D, Vandenburgh H (2012) Design and fabrication of a biodegradable, covalently crosslinked shape-memory alginate scaffold for cell and growth factor delivery. *Tissue Eng Part A* 18 (19–20):2000–2007
  19. Qiao S-P, Zhao Y-F, Li C-F, Yin Y-B, Meng Q-Y, Lin F-H et al (2016) An alginate-based platform for cancer stem cell research. *Acta Biomater* 37:83–92
  20. Huebsch N, Arany PR, Mao AS, Shvartsman D, Ali OA, Bencherif SA et al (2010) Harnessing traction-mediated manipulation of the cell/matrix interface to control stem-cell fate. *Nat Mater* 9(6):518–526
  21. Nam J, Son S, Park KS, Zou W, Shea LD, Moon JJ (2019) Cancer nanomedicine for combination cancer immunotherapy. *Nat Rev Mater* 4:398–414
  22. Khavari A, Nydén M, Weitz DA, Ehrlicher AJ (2016) Composite alginate gels for tunable cellular microenvironment mechanics. *Sci Rep* 6:30854
  23. Lee GY, Kenny PA, Lee EH, Bissell MJ (2007) Three-dimensional culture models of normal and malignant breast epithelial cells. *Nat Methods* 4(4):359–365
  24. Rajan N, Habermehl J, Coté M-F, Doillon CJ, Mantovani D (2006) Preparation of ready-to-use, storable and reconstituted type I collagen from rat tail tendon for tissue engineering applications. *Nat Protoc* 1(6):2753–2758
  25. Conway JRW, Vennin C, Cazet AS, Herrmann D, Murphy KJ, Warren SC et al (2017) Three-dimensional organotypic matrices from alternative collagen sources as pre-clinical models for cell biology. *Sci Rep* 7 (1):16887
  26. Chitty JL, Skhinias JN, Filipe EC, Wang S, Cupello CR, Grant RD et al (2019) The Mini-Organo: A rapid high-throughput 3D coculture organotypic assay for oncology screening and drug development. *Cancer Rep* 3:e1209

27. Madsen CD, Cox TR (2017) Relative stiffness measurements of tumour tissues by shear rheology. *Bio Protoc* 7(9):e2265
28. Hadden WJ, Young JL, Holle AW, McFetridge ML, Kim DY, Wijesinghe P et al (2017) Stem cell migration and mechanotransduction on linear stiffness gradient hydrogels. *Proc Natl Acad Sci U S A* 114(22):5647–5652
29. Lueckgen A, Garske DS, Ellinghaus A, Desai RM, Stafford AG, Mooney DJ et al (2018) Hydrolytically-degradable click-crosslinked alginate hydrogels. *Biomaterials* 181:189–198
30. Zhou X, Holsbeeks I, Impens S, Sonnaert M, Bloemen V, Luyten F et al (2013) Noninvasive real-time monitoring by alamarBlue(®) during in vitro culture of three-dimensional tissue-engineered bone constructs. *Tissue Eng Part C Methods* 19(9):720–729
31. Eilenberger C, Kratz SRA, Rothbauer M, Ehmoser E-K, Ertl P, Küpcü S (2018) Optimized alamarBlue assay protocol for drug dose-response determination of 3D tumor spheroids. *MethodsX* 5:781–787



# Chapter 4

## Patient-Derived Xenografts from Solid Tumors (PDX) for Models of Metastasis

Annika Wulf-Goldenberg, Jens Hoffmann, Michael Becker,  
Bernadette Brzezicha, and Wolfgang Walther

### Abstract

In cancer research, availability of clinically relevant tumor models is still essential for drug testing, proof of concept studies, and also molecular analyses. To achieve this, models are of advantage, which more closely reflect heterogeneity of tumors. In this regard, patient-derived xenograft (PDX) models more closely recapitulate the native tumor biology, tissue composition, and molecular characteristics. Since metastasis is still the major challenge of tumor therapy, models are pivotal, which resemble this particular property. In this context, PDX model-derived metastasis is of particular interest for testing antimetastatic therapies for their efficacy to better target this systemic disease. This protocol describes the establishment of PDX models from tumor specimen and their applicability for PDX-derived metastasis at metastatic sites such as liver and lung, which are also clinically relevant for the systemic spread of cancer. Analysis of metastasis and methods for quantification of metastatic spread are provided.

**Key words** Metastasis, Patient-derived xenograft (PDX), Solid cancer, Lung cancer, Colorectal cancer, Breast cancer

---

### 1 Introduction

Patient-derived xenograft (PDX) models represent a powerful, experimentally rigorous, and clinically relevant approach in oncology, drug discovery, and development [1–3]. These models derived from solid as well as liquid cancers have been established during the last decades as important valuable platforms for drug screening, molecular analyses and biomarker, or drug target identification and validation [4]. Their advantage over cell line-derived models is based on preservation and stabilization of the genotypic and phenotypic features of the original patient tumor. PDX tumors maintain the primary tumor cell architecture and the inherent genetic heterogeneity of the original tumor [5–7]. Further, PDX retain the DNA methylation pattern of the original tumor and may therefore more faithfully mimic the response of human tumors to cancer

drugs [8]. In this regard, numerous studies conducted repeatedly showed a high degree of correlation between clinical response to cytotoxic agents in cancer patients and in PDX models generated from their respective tumor tissue [9–11]. In this context, correct prediction of clinical outcome was observed for both tumor resistance (97%) and tumor sensitivity (90%) in a large panel of PDX [12].

In recent years, there has been renewed interest in the development of PDX models from different tumor entities as the preferred preclinical tool to improve and to accelerate the drug development process. Recent studies confirmed and expanded the observations of similarities between patient outcome and PDX responses [13–15]. First reports of using PDX models to guide therapy include a pilot study in 14 patients with refractory advanced tumors in which patient's treatments were selected on the basis of chemosensitivity testing in their respective PDX. The objective response rate was 88% for treatments that showed activity in the PDX models and were then applied to the respective patients [13].

Although most PDX models are established as subcutaneous (s.c.) tumors, metastasis models are essential for testing new concepts of metastasis intervention or even prevention. This is explained by the fact that cancer metastasis is the lethal attribute of cancer, impacting outcome and survival of cancer patients [16, 17]. Therefore, clinically relevant metastasis models are essential for identification, validation of novel biomarkers, and, more importantly, testing new approaches to fight metastatic spread. To achieve this, PDX models are of great value to be used as clinically relevant models with potential to form metastasis in mouse models. This will then much closer mimic the clinical evolution of cancer disease, particularly if distant metastasis of the PDX will form in target organs, known to be the primary metastatic sites of a given tumor entity.

In general, there are seven main types of metastases, which are of major clinical relevance: liver, lung, brain, bone, lymph node, peritoneal, and skin metastases. As some tumors seem to preferentially follow certain paths of metastasis formation, it is helpful to address these in specific metastasis models.

For the establishment of such metastasis models, there are three main routes for developing metastases: the hematogenic, lymphogenic, and peritoneal dissemination. Although for some PDX models the development of distant metastases has been reported, the spontaneous PDX-derived metastasis is a rather rare event. Frequently the fast growth of the primary PDX hinders the follow-up on distant metastasis. Therefore, several “surrogate” models for metastasis have been developed, using special tumor transplantation technologies (orthotopic, intravenously, intra peritoneal, intra cerebral, and intracardiac) to better mimic the metastatic disease [18, 19].

In this chapter, we describe the establishment of metastatic PDX models in immune-compromised mice and provide a stepwise guide of how to use particular PDX models as metastasis models and their proper characterization. We describe the use of tumor cells or tumor fragments from our PDX models to metastasize to different organs after intravenous tumor cell application as model of hematogenous metastasis.

---

## 2 Materials

### **2.1 Materials for Collection of Primary Tumor Material and PDX Establishment**

#### **2.1.1 Media and Instruments**

#### **2.1.2 Material for Xenotransplantation of Tumor Samples**

#### **2.1.3 Materials for Cryoconservation**

All human primary tissue samples must be collected from informed, consenting patients under an approved Institutional Review Board of Ethics. Handling of any tumor tissue is performed under a safety hood (biosafety level S2).

1. Human primary tumor tissue (surgical specimen), metastasis tissue, effusion samples.
2. Transport tubes (any sterile 10 mL polypropylene tubes with tight cup).
3. Cooled transport medium (10 mL RPMI-1640 medium with L-glutamine, supplemented with gentamicin solution of 100 $\mu$ g/mL), supplement is added shortly prior use (use is recommended within 4 weeks due to stability/sterility restrictions).
4. Disinfectant Antifect®N.
5. Dissection mat.
6. Dissection needles.
7. Sterile surgical scissors and tweezers.
8. Sterile wound clips (7 mm, Henry Schein, Melville, NY, USA).
9. Sterile wound clip applicator (Henry Schein).
10. Sterile wound clip remover (Henry Schein).
11. Heating pad.
12. Anesthesia reagent Etomidate®Lipuro.
13. Isopropanol (70% v/v).
14. Digital caliper (Mitutoyo, Neuss, Germany).
15. Cryoconservator (X-cube).
16. Ice machine for crushed ice.
17. Thermocontainer (True North®, 1 L, Roth, Germany).
18. Cryovials (Cryo.s™, 2 mL, Greiner-bio-one, Kremsmünster, Austria).
19. Sterile surgical scissors and tweezers.

6. Sterile petri dish.
7. Dissection mat.
8. Pipetboy (Integra, Fisher Scientific, Schwerte, Germany).
9. Multipette® M4 (Neolab, Heidelberg, Germany).
10. Combitips® Biopur, 10 mL (Neolab).
11. Sterile pipettes 5 mL (Costar Stripette, Corning Incorp., Wiesbaden, Germany).
12. FBS (fetal bovine serum, Gibco-Invitrogen, Schwerte, Germany).
13. DMSO HYBRI-MAX® (Sigma, Taufkirchen, Germany).
14. DPBS (1×) (Gibco® by Life Technologies™).

## **2.2 Mouse Strains for PDX Establishment and Formation of Metastasis**

1. 4–7-week-old NOG-F (NOD.Cg-Prkdcscid Il2rgtm1Sug/Jic-Tac) mice (Taconic, Leverkusen, Germany) are used for first engraftment studies from human to mouse (*see Note 1*) and formation of metastases.
2. 5–7-week-old NMRI nu/nu (Rj: NMRI-Foxn1nu/nu) mice (Janvier Labs, France) are used for further engraftment passages from mouse to mouse.
3. Housing conditions for mice: IVC System Tecniplast DCC (Tecniplast, Hohenpeißenberg, Germany) strictly controlled and standardized barrier conditions (RT 22 °C ± 1 °C, RH 50% ± 10%), artificial light period: 12 h dark/12 h light rhythm (light 06.00–18.00 h).
4. Autoclaved tap water or HCL acidified water (pH 4).
5. Autoclaved rodent pellets (V1724-300, ssniff Spezialdiäten GmbH, Germany) ad libitum.

## **2.3 Materials for Generation of PDX-Derived Metastasis**

### **2.3.1 Media and Supplements**

1. TS3N agar plate (Biomerieux, France).
2. Enzymes contained in the human Tumor Dissociation Kit (Miltenyi, Bergisch Gladbach, Germany).
3. DNase I (5 MU/mL).
4. RPMI 1640 medium.
5. PBS buffer (Invitrogen).
6. 70% ethanol.
7. 4% formaldehyde.

### **2.3.2 Instruments for Generation of Single Cells, Inoculation of Cells and Collection of Samples**

1. Sterile scissor.
2. Sterile petri dish.
3. Sterile forceps.
4. gentleMACS C-Tubes (Miltenyi).

5. gentleMACS Dissociator (Miltenyi).
6. MACSmix Tube Rotator (Miltenyi).
7. Cell strainer (70µm).
8. 15 mL tube.
9. 20-gauge needle (Braun, Melsungen, Germany).
10. 1 mL Luer Syringe (Fisher Scientific).
11. Scale.
12. Magnifying glasses.

## **2.4 Materials for Molecular Analyses of Metastasis**

### **2.4.1 DNA Isolation**

1. DNeasy Blood & Tissue Kit (#69504, Qiagen, Hilden, Germany).
2. Ethanol absolute (96%), analytical grade (Serva, Heidelberg, Germany).
3. Vortexer.
4. Thermomixer (Eppendorf, Hamburg, Germany) at 56 °C.
5. Tube (1.5 mL).
6. Microcentrifuge with rotor for 1.5 mL tubes.
7. Peqlab NanoDrop®1000 Spectrophotometer (Peqlab, Erlangen, Germany).

### **2.4.2 PCR, Primer and Probes**

1. Custom-designed (Applied Biosystems, Germany) primer-probe assay (*see Table 1*).
2. TaqMan® Universal PCR Master Mix, No AmpErase® UNG (Applied Biosystems, Prod-No. 4324018).
3. StepOnePlus™ Real-Time PCR System (Applied Biosystems, Prod-No. 4376600).
4. 96-well microtiter plates.

**Table 1**  
**Oligonucleotides and probes for human satellite-specific PCR**

Name	5'-3' sequence	Localization <sup>a</sup>
Cr17_1a <sup>b</sup>	GGG ATA ATT TCA GCT GAC TAA ACA G	15.0.39
Cr17_4b <sup>c</sup>	AAA CGT CCA CTT GCA GAT TCT AG	472.0.494
TMsat_probe	6FAM <sup>d</sup> -CAC GTT TGA AAC ACT CTT XT TTG CAG GATC p <sup>e</sup> (X = Tamra <sup>f</sup> )	109.0.137

<sup>a</sup>nucleotide positions correspond to the sequence HSSATA17 (Gene-Bank Acc.-No. 13882)

<sup>b</sup>forward primer

<sup>c</sup>reverse primer

<sup>d</sup>fluorescent reporter dye FAM (6-carboxy-fluoresceine)

<sup>e</sup>probe extension during PCR is blocked by a 3'-phosphate

<sup>f</sup>quencher dye Tamra (Tetramethylrhodamine)

---

### 3 Methods

#### 3.1 Establishment of PDX Models

##### 3.1.1 Collection, Shipment and Processing of Primary Tumor Material

All human patient tissue samples must be collected from informed, consenting patients under an approved Institutional Review Board of Ethics (*see* Subheading 2.1.1).

1. Label the transport tube (allocation of the material, the date, and time of sampling).
2. Collect vital tumor tissue in the hospital shortly after surgical removal.
3. Collect five maximal  $5 \times 5 \times 5$  mm pieces.
4. Transfer the tumor sample into the transport tube filled with cooled ( $4^{\circ}\text{C}$ ) transport medium.
5. At arrival, fresh human tumor samples must be kept on ice and processed immediately under sterile conditions using a bio-safety hood (*see* Note 2).

##### 3.1.2 Xenotransplantation

1. Disinfect the surgical bench by wiping with the disinfectant Antifect®N.
2. Place autoclaved surgical instruments (scissors and tweezers).
3. Solid tumor sample is transferred with the transport medium in a petri dish.
4. Cut the tissue in  $3 \text{ mm} \times 3 \text{ mm} \times 3 \text{ mm}$  fragments and keep the fragments moist and cool.
5. Immobilize a mouse in a strainer.
6. Anesthetize intravenously (0.15 mL/mouse) with Etomidate®-Lipuro (0.3 mg/mouse).
7. Place the animal sideward on the dissection mat.
8. Disinfect the skin with isopropanol (70% v/v).
9. Perform a superficial vertical incision in the skin of 5–8 mm of the left flank.
10. Insert the tip of a surgical scissor into the incision to form a pocket in the subcutaneous space.
11. Implant one tumor fragment per mouse into the pocket by means of tweezers.
12. Close the incision with wound clips.
13. Transfer the animal to a clean cage on a heating pad.
14. Monitor the animal according to the approved IACUC protocol daily post-surgery. One week later, remove the wound clips.
15. Monitor the engraftment and the propagation of the tumor in the mice at least twice weekly by means of palpation. When the tumor is palpable, measure the tumor diameters by means of a digital caliper and record the data (*see* Note 3).

16. At the stage of stable PDX growth (after passage 0), the model can be used for characterization. In this regard, proper tumor histology (which is evaluated by an experienced pathologist) and also sensitivity of the PDX towards standard of care drugs is determined (*see* Fig. 1a). Furthermore, molecular analyses for mutational status and gene expression can be performed.

### 3.1.3 Harvesting of PDX Tumor Tissue

1. Sacrifice mice by cervical dislocation at stable tumor growth and if a tumor volume of approx. 1 cm<sup>3</sup> is reached.
2. Place the mouse backwards on a dissection mat.
3. Fix the paws with dissection needles.
4. Disinfect the skin with isopropanol.
5. Make an incision on the tumor-bearing flank and remove the upper skin.
6. Dissect the tumor with new sterile surgical material.
7. Place the tumor in a cool petri dish filled with medium at 4 °C.
8. Dissected tumors are either implanted into further immunodeficient mice for further *in vivo* propagation using the same procedure of xenotransplantation or are used for preparation of a single-cell suspension (*see* Subheading 3.2.1) or sample conservation (*see* Subheading 3.1.4).

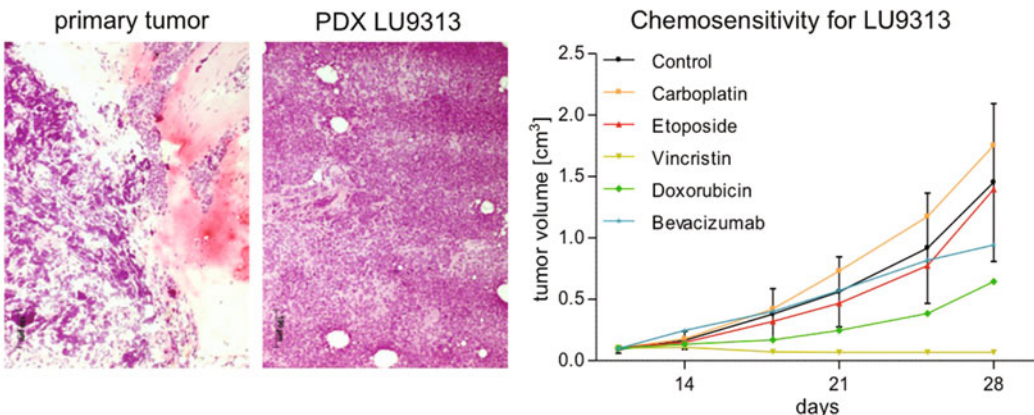
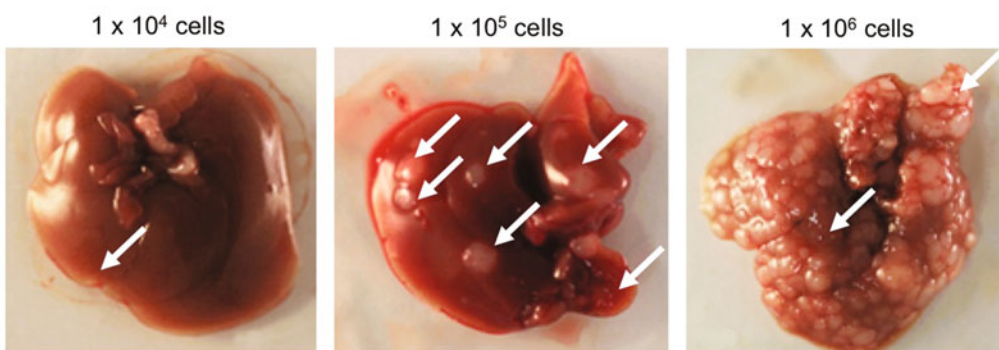
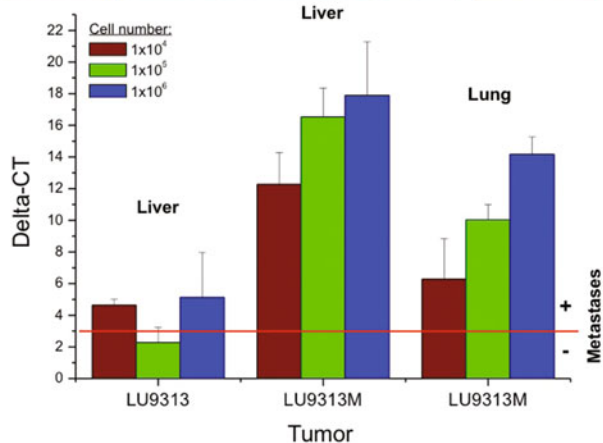
### 3.1.4 Cryoconservation and Biobanking of PDX Specimen

1. All steps have to be performed under a biosafety hood (S1).
2. Prepare the cryoconservation medium by pipetting 40 mL cooled FBS and 10 mL DMSO together.
3. Keep the cryovials cool at 2–8 °C, FBS and cryoconservation medium.
4. Add 0.75 mL cooled FBS per cryovial and keep cool.
5. Cut the moist and cooled tumor equally into 2–4 mm fragments.
6. Transfer 5 fragments per cryovial by using tweezer.
7. Mix gently the cryovial.
8. Add 0.75 mL cryoconservation medium per filled cryovial and close it.
9. Mix gently once again the cryovial and keep it cool at least for 15 min to max. 1 h.
10. Meanwhile the cryoconservator is started and cooled to a temperature of about 8–10 °C.
11. Enter the cryovial into the cryoconservator and start the program for cryoconservation (stepwise by 1 °C/min to minimal temperature of –80 °C).

**a**

## Clinical and molecular data on small cell lung cancer model (LU9313)

Histology	TNM	Gender	Age	Variations detected by Illumina TSACP
Pleural carcinosis, small cell lung carcinoma	cT3 cN2 M1a	female	57	KDR, TP53

**b****c**

**Fig. 1** Engraftment and use of PDX derived from small-cell lung carcinoma (LU9313) for establishment of metastasis models. (a) Primary lung carcinoma samples (patient's clinical and molecular characteristics of the established PDX model LU9313 are summarized in the table, top panel) were processed rapidly under stringent sterile conditions. After stable tumor engraftment during at least 2 or 3 passages, the lung PDX

**Table 2**  
**Scoring system, based on metastasis size, for reproducible semiquantification of metastases (see Note 6)**

Diameter (mm)	Score
1	1
1–2	8
2–3	27
3–4	64
4–5	125
5–8	512
10	1024
12	2048

12. After this process, the frozen sample is stored in the gas phase of liquid nitrogen at about  $-176^{\circ}\text{C}$  for long-term ( $>5$  years) storage. During this period, a tumor sample can be thawed and used for generation of vital PDX tissue by *in vivo* passaging. The thawing process is the same as for any living cells in the common cell culture laboratory.

### 3.2 Generation of PDX-Derived Metastasis Models

#### 3.2.1 Generation of Single-Cell Suspensions from PDX Tumor Tissue

For establishment of metastasis models derived from PDX, best results are obtained by use of PDX-derived cell suspension. For this, all procedures have to be carried out under sterile conditions.

1. Dissociate tumor tissues mechanically with sterile scissors in a sterile petri dish. Cut the tissues into small pieces of 2–4 mm. Transfer 0.2–1.0 g tumor tissue into gentleMACS C-tube

---

**Fig. 1** (continued) LU9313 was established. In the histology, the patient tumor (left panel) and xenograft (right panel) indicated comparable histopathology. The established xenograft model was characterized for its response to a panel of clinically used standard of care drugs. (b) Metastasis formation of lung carcinoma PDX LU9313 in mouse livers in correlation to cell counts applied i.v. Number of liver metastasis increases by increase in cell counts applied i.v. (corresponding to groups A-C in Table 3) shown for representative metastatic livers (metastasis are indicated by the arrows) for group A ( $1 \times 10^4$  LU9313 cells, left panel), group B ( $1 \times 10^5$  LU9313 cells, middle panel), and group C ( $1 \times 10^6$  LU9313 cells, right panel). Liver weight, numbers of metastases, calculation of the metastasis score (see Table 2), and quantification of human DNA in the liver are summarized in Table 3, indicating positive correlation between cell counts applied and number of liver metastasis. (c) Increase of metastatic potential of PDX subclone LU9313M after reapplication to mice and influence of cell numbers used for i.v. injection into NOG mice. For this, LU9313M cells were obtained from one liver metastasis of the LU9313 PDX, which was inoculated i.v. Human LU9313 PDX-derived tumor cells were quantified in the mouse liver and lung by quantitative PCR (see Subheading 3.3.2). Indicated is the mean delta CT value ( $\pm$  S.D.) for 3 mice, each analyzed in duplicate. The threshold for unambiguous signals of human DNA is set to a delta-CT value of 3. This study revealed increased metastatic potential of cells derived from *in vivo* metastasis of this PDX model

**Table 3**

**Liver weight, numbers of metastases, calculation of the metastasis score, and quantification of human DNA in the liver for the metastatic PDX model LU9313**

Group of cells	Number of cells	Liver weight (g)	Liver metastases (n)	Liver metastases Scores	Human DNA in the liver (ct norm)
A	$10^4$	$1.73 \pm 0.45$	$3 \pm 3$	$12 \pm 10$	$12.3 \pm 2.0$
B	$10^5$	$1.88 \pm 0.45$	$15 \pm 1.4$	$140 \pm 22$	$16.5 \pm 1.8$
C	$10^6$	$6.47 \pm 1.94$	Not countable (high load)		$17.9 \pm 3.4$

containing the enzyme mix. Follow all steps of dissociation by manufacturers' protocol. Attach the tube into the gentleMACS Dissociator. Start the dissociation by running the gentleMACS Program m\_impTumor-03. After termination of the program, perform a short centrifugation step. Incubate for 40 min at 37 °C under continuous rotation. Run the next gentleMACS Program m\_impTumor-03. After termination, filtrate the cell suspension through a cell strainer (70µm) placed in a 15 mL tube. Add 2µL DNase I to the suspension. Centrifuge cell suspension at  $300 \times g$  for 10 min, 4 °C and aspirate the supernatant.

2. Resuspend the cells in medium and count the cell number. Take samples for sterile control by inoculation on TS3N agar plates and incubate the sterile control probe at 37 °C for 2 days; check for potential bacterial growth. Centrifuge cell suspension again for in vivo inoculation at  $300 \times g$  for 10 min, 4 °C.
3. Resuspend the cells in PBS in an appropriate cell number and volume for further application.

### 3.2.2 Inoculation of Tumor Cells for Metastasis Generation

For modeling of hematogenic metastasis, the PDX-derived cell suspensions (*see* Subheading 3.2.1) are intravenously (i.v.) transplanted into female immune-deficient NOG mice. The objective of the studies is to evaluate and compare the metastasis potential of a panel of PDX-derived metastasis models.

1. Immune-deficient NOG mice are acclimated at least for 1 week in the animal facility before cell inoculation. During the cell inoculation, the mice are marked (e.g., by earmarks). Anesthetics are not essential for the intravenous application of tumor cells. The tail is disinfected with isopropanol before injection.
2. 0.2 mL cell suspension (suspension contains cell counts in the range of  $1\text{--}100 \times 10^6$  cells/0.2 mL) is slowly applied intravenously with a 20-gauge syringe. Enzymatically prepared cells are kept on ice until application into the mice.

3. The body weight of the mice is measured twice per week and the health status twice daily. The duration of each experiment depends on the tumor growth of the individual model. Body weights and lethality are recorded throughout the whole study. Tumor volume is not available as a parameter for measurement (*see Note 4*).

### 3.2.3 Collection of Liver and Lung Samples for Metastasis Analysis

For proper determination and quantification of PDX-derived metastases, tissues of metastatic sites (e.g., liver, lung) need to be collected and analyzed. For this, all procedures have to be carried out under sterile conditions.

1. Sacrifice the anesthetized female mice. Swab the fur with 70% ethanol. Make a midline incision of the skin anterior the vaginal opening toward the sternum using dissection scissors. The peritoneum is cut in the midline afterward and fixed laterally.
2. Carefully examine the liver and other organs to identify metastatic lesions. Harvest liver for determination of macroscopic metastasis. Harvest further organs if gross metastatic lesions are visible. Dissect the chest for examining and harvesting the lung.
3. Put liver and lung on the scales and determine the weight of the organs. Calculate the mean weight of each organ and standard deviations.
4. Determine, quantify, and document (e.g., by photo images) macroscopic metastasis. Figure 1b shows an example of metastasis formation in liver by small-cell lung cancer PDX. The study shows the correlation of cell counts injected and number of metastases formed (*see Fig. 1b*). Such experimental approach for PDX-derived metastasis is also applicable for PDX models of other tumor entities.
5. After the determination of metastasis, cut liver and lung into two pieces. Place one piece in medium for isolation of tumor cells and place one piece into a cryovial and snap-freeze in liquid nitrogen. Store at –80 °C for molecular analysis.
6. Organs with metastatic lesions are taken and single-cell suspensions are generated as described in Subheading 3.2.1, to obtain tumor cells with evidenced metastatic potential. These single-cell suspensions of tumor cells with metastatic potential are inoculated into mice as described in Subheading 3.2.2, to evaluate potentially increased capability of these cells to form metastases (*see Note 5*). Figure 1c shows the increased metastatic potential of small-cell lung carcinoma PDX (LU9313M) cells—derived from metastases of this PDX. After reimplantation of these cells from the metastasis (LU9313M), determination of metastasis by human satellite DNA PCR revealed an up to threefold increased metastasis formation in liver and lung, which is dependent on cell counts injected (*see Fig. 1c*).

### **3.2.4 Determination of Macroscopic Metastasis by Metastatic Counts and Scoring**

Macroscopic metastasis is measured by means of metastasis counts and metastasis size. Use the magnifying glass to see spots of tumor cells in the freshly prepared lung and liver tissues (*see* Subheading 3.2.3). Count each metastatic spot and determine the size of each metastatic spot. The size of a spot is defined by its diameter as listed in Table 2.

1. Calculate the score of each organ according to total score = (number of n spot x score of n spot) + (number of nn spot x score of nn spot) + (etc.). For example, in a liver 3 spots of 1 mm and 2 spots of 1–2 mm are detected. This will result in a total score of 19 by calculation of:  $(3 \times 1) + (2 \times 8) = 19$ .
2. Calculate the mean score and standard deviations thereafter (*see* Table 2).
1. Isolate DNA by using the Qiagen DNeasy Blood & Tissue Kit and perform the following steps according to the protocol provided by the manufacturer.
2. Use <20 mg tissue sample per isolation (sample size of approx.  $3 \times 3$  mm). Avoid complete pre-thawing of samples to minimize DNA degradation. Cut frozen tissue samples into small pieces. Add 180 $\mu$ L buffer ATL and 20 $\mu$ L proteinase K to disrupt and lyse the tissue (*see Note 7*). Mix thoroughly to homogenize the tissue. Incubate and vortex at 56 °C until the tissue is completely lysed using a thermomixer (*see Note 8*). Next, add 200 $\mu$ L of buffer AL (provided by the kit), mix thoroughly by vortexing, add 200 $\mu$ L of 96% ethanol, and mix again.
3. Load the sample on a DNeasy Mini spin column where DNA selectively binds to the silica membrane, and contaminants are efficiently washed away by following the manufacturer's protocol.
4. Elute the DNA with the Qiagen AE elution buffer (*see Note 7*) in a volume of 200 $\mu$ L in two steps. Use 100 $\mu$ L for each step, incubate for 1 min at room temperature. Centrifuge for 1 min at  $>6000 \times g$ , 4 °C.
5. Determine the concentration of DNA via UV measurement at 260 nm in a volume of 2 $\mu$ L using a NanoDrop® 1000 Spectrophotometer. Concentration is calculated under the assumption that 1 optical density (OD) represents approx. 50 $\mu$ g DNA/mL. The elution typically yields 2–10 $\mu$ g DNA from the lung and 5–25 $\mu$ g DNA from the liver. The purity of the isolated DNA is determined by the OD 260/280 ratio.
6. Store DNA at –20 °C until further analysis.

## **3.3 Molecular Analyses for Metastasis**

### **Detection and Quantification by Human-Specific PCR**

#### **3.3.1 Isolation of DNA from Metastatic Sites (E.g., Liver and Lung)**

### 3.3.2 qPCR for Detection of Human Satellite DNA in Mouse Tissue

- The determination of human satellite DNA in mouse tissue is used to quantify the extent of metastasis of human PDX-derived cells in the mouse organs, such as liver or lung. The quantification of human satellite DNA represents a reproducible metastasis parameter in mouse models (*see Note 9*).
- Thaw frozen genomic DNA. Perform amplification and quantitative detection of the centromere-specific fragments of human chromosome 17 by using a custom-designed (Applied Biosystems, *see Table 1*) primer-probe assay targeting a region described by Warburton et al. [20, 21].
- Use the ready-to-use primer-probe assay and the TaqMan® Universal PCR Master Mix, No AmpErase® UNG for Real-Time PCR amplification applying the standard protocol supplied by the manufacturer. The exonuclease probe is 5'-labeled with the reporter fluorescent dye FAM (6-carboxy-fluoresceine) and carries Tamra as quencher dye. Probe extension during PCR is blocked by a 3'-phosphate.
- Pipette 5µL of the DNA (containing 25 ng/µL DNA) to the PCR mix consisting of 10µL Universal Master Mix, 1µL primer-probe mix, and 4µL water to get a final reaction volume of 20µL.
- Perform the PCR and quantification in a StepOnePlus™ Real-Time PCR system.
- Perform the PCR with an initial denaturation step of 10 min at 95 °C followed by 40 cycles of 95 °C denaturation and 60 °C annealing/extension each. Do not perform a final elongation step. Test each sample thrice in parallel.
- Use genomic DNA from the respective patient-derived xenograft as a positive control, liver or lung from immune-deficient mice as a negative control as well as a water sample as a reagent control in parallel.
- To normalize and quantify the PCR results, calculate a delta-CT by subtracting the CT value of the tested sample from that of the negative-control sample.
- To take into account a possible blur of the CT value, the threshold is set above a delta-CT value 3.0 for positive signals of human DNA (*see Fig. 1c*).

---

## 4 Notes

- For PDX establishment, immune-deficient mice NOG-F® (*see Subheading 2.2*) or NSG mice without mature T-, B-, and NK-cells are used as first choice. They display reduced complement activity, and they have dysfunctional macrophages and

dendritic cells. Once the human tumor grew on NOG-F mice, the next passage is performed with NOG-F or with NMRI nu/nu mice. NMRI nu/nu mice are also immune-deficient mice with lack of T-cells, whereas B-cells remain. Both mouse strains are well suited for the engraftment and expansion of PDX. Use most immune-deficient mice for the transplantation of primary tumor tissue for successful engraftment of tumor samples. If the mice have less murine T-, B-, and NK-cells, the engraftment rate increases.

2. For effective engraftment of primary tumor tissue, the samples have to be processed in short time between clinical surgery and transplantation into immune deficient mice. The transplantation within 24 h is obligatory, since low processing time correlates with good engraftment. The samples should be free of necrotic, fat, muscle, and other connective tissue. If larger tissue samples are available, these should be divided/dissected into smaller pieces of 5 × 5 mm to avoid emergence of autolytic reactions in the tissue during transportation.
3. Use only tumors with stable tumor growth for passage. If xenograft tumors with heterogeneous tumor growth are retransplanted, no homogenous and reproducible tumor growth of a patient-derived xenograft (PDX) can be achieved.
4. Termination criteria are dependent on the health status of the animals and the original s.c. tumor growth of the PDX models in mice and vary between the PDX models.
5. Evident metastatic tumor cells are selected for analysis of their metastatic potential. It might be possible that tumor cells show a less or higher degree of metastasis compared to the original PDX tumor. The potential is a characteristic of the each individual PDX model.
6. The scoring system defines the size and frequency of spots and enables a comparison of PDX models. But, nevertheless, scores have to be considered with caution. Small spots could be overlooked and underrepresented, and large spots can be overrepresented.
7. The necessary buffers (ATL, AL, and AE) and proteinase K are part of the Qiagen DNeasy kit. The DNA isolation procedure described here adheres exactly to the detailed protocol supplied by Qiagen.
8. A complete lysis of tissue samples is crucial for the quality of isolated DNA. Lysis time may vary depending on the type of tissue processed. Lysis at 56 °C is usually complete in 1–3 h, but can be extended overnight with no adverse effect for DNA integrity.

9. In contrast to target gene sequences, the targeting of the chromosomal centromere region ensures a high degree of human specificity, since these structures are sufficiently different from similar loci in the mouse genome. Here we use an optimized primer-probe assay targeting the alpha-satellite region of the human chromosome 17 [21]. Genome regions suitable for this have been previously described by Warburton et al. [20].

---

## Acknowledgements

This work was supported by the BMBF funded Nanodiater project and the EuroNanoMed project funded by the European Commission. We thank Andrea Orthmann, Annika Hoffmann, and Nadine Bäsler for assistance with animal studies, tumor cell preparation, and molecular analysis. Furthermore, we thank the Evangelische Lungenklinik, Berlin-Buch, Germany for providing the tumor material for PDX establishment.

## References

1. Böck BC, Stein U, Schmitt CA, Augustin HG (2014) Mouse models of human cancer. *Cancer Res* 74:4671–4675
2. Fichtner I, Klinghammer K, Behrens D et al (2017) Animal models for personalized treatment options. *Int J Clin Pharmacol Ther* 55:698–700
3. Klinghammer K, Walther W, Hoffmann J (2017) Choosing wisely - Preclinical test models in the era of precision medicine. *Cancer Treat Rev* 55:36–45
4. Siolas D, Hannon GJ (2013) Patient-derived tumor xenografts: transforming clinical samples into mouse models. *Cancer Res* 73:5315–5319
5. Fichtner I, Slisow W, Gill J et al (2004) Anticancer drug response and expression of molecular markers in early-passage xenotransplanted colon carcinomas. *Eur J Cancer* 40:298–307
6. Fiebig HH, Maier A, Burger AM (2004) Clonogenic assay with established human tumour xenografts: correlation of in vitro to in vivo activity as a basis for anticancer drug discovery. *Eur J Cancer* 40:802–820
7. DeRose YS, Wang G, Lin Y-C et al (2011) Tumor grafts derived from women with breast cancer authentically reflect tumor pathology, growth, metastasis and disease outcomes. *Nat Med* 17:1514–1520
8. HogenEsch H, Nikitin AY (2012) Challenges in pre-clinical testing of anti-cancer drugs in cell culture and in animal models. *J Control Release* 164:183–186
9. Berger DP, Fiebig HH, Winterhalter BR et al (1990) Preclinical phase II study of ifosfamide in human tumour xenografts *in vivo*. *Cancer Chemother Pharmacol* 26(Suppl):S7–S11
10. Tentler JJ, Tan AC, Weekes CD et al (2012) Patient-derived tumour xenografts as models for oncology drug development. *Nat Rev Clin Oncol* 9:338–350
11. Julien S, Merino-Trigo A, Lacroix L et al (2012) Characterization of a large panel of patient-derived tumor xenografts representing the clinical heterogeneity of human colorectal cancer. *Clin Cancer Res* 18:5314–5328
12. Burger AM (2004) Preclinical screening for new anticancer agents. In: McLeod WDFHL (ed) *Anticancer pharmacokinetic pharmacodynamics*. Humana Press Inc., Totowa, NJ, pp 29–45
13. Hidalgo M, Bruckheimer E, Rajeshkumar NV et al (2011) A pilot clinical study of treatment guided by personalized tumorgrafts in patients with advanced cancer. *Mol Cancer Ther* 10:1311–1316
14. Zhang X, Claerhout S, Prat A et al (2013) A renewable tissue resource of phenotypically stable, biologically and ethnically diverse, patient-derived human breast cancer xenograft models. *Cancer Res* 73:4885–4897

15. Topp MD, Hartley L, Cook M et al (2014) Molecular correlates of platinum response in human high-grade serous ovarian cancer patient-derived xenografts. *Mol Oncol* 8:656–668
16. De Santis CE, Lin CC, Mariotto AB et al (2014) Cancer treatment and survivorship statistics. *CA Cancer J Clin* 64:252–271
17. Guan X (2015) Cancer metastases: challenges and opportunities. *Acta Pharm Sin B* 5:402–418
18. Hoffmann J, Fichtner I, Lemm M et al (2009) Sagopilone crosses the blood-brain barrier in vivo to inhibit brain tumor growth and metastases. *J Neurooncol* 11:158–166
19. Strube A, Hoffmann J, Stepina E et al (2009) Sagopilone inhibits breast cancer bone metastasis and bone destruction due to simultaneous inhibition of both tumor growth and bone resorption. *Clin Cancer Res* 15:3751–3759
20. Warburton PE, Greig GM, Haaf T, Willard HF (1991) PCR amplification of chromosome-specific alpha satellite DNA: definition of centromeric STS markers and polymorphic analysis. *Genomics* 11:324–333
21. Becker M, Nitsche A, Neumann C et al (2002) Sensitive PCR method for the detection and real-time quantification of human cells in xenotransplantation systems. *Br J Cancer* 87:1328–1335



# Chapter 5

## Preparation and Culture of Organotypic Hippocampal Slices for the Analysis of Brain Metastasis and Primary Brain Tumor Growth

**Ellina Schulz, Tim Hohmann, Urszula Hohmann, Ralf-Ingo Ernestus, Mario Löhr, Faramarz Dehghani, and Carsten Hagemann**

### Abstract

Brain metastasis is a major challenge for therapy and defines the end stage of tumor progression with a very limited patients' prognosis. Experimental setups that faithfully mimic these processes are necessary to understand the mechanism of brain metastasis and to develop new improved therapeutic strategies. Here, we describe an *in vitro* model, which closely resembles the *in vivo* situation. Organotypic hippocampal brain slice cultures (OHSCs) prepared from 3- to 8-day-old mice are well suited for neuro-oncology research including brain metastasis. The original morphology is preserved in OHSCs even after culture periods of several days to weeks. Tumor cells or cells of metastatic origin can be seeded onto OHSCs to evaluate micro-tumor formation, tumor cell invasion, or treatment response. We describe preparation and culture of OHSCs including the seeding of tumor cells. Finally, we show examples of how to treat the OHSCs for life-dead or immunohistochemical staining.

**Key words** Organotypic hippocampal slice cultures (OHSCs), Metastasis, Brain tumor, Glioblastoma, Invasion, Glioma, Life-dead staining, Cryosection, Immunohistochemistry

---

### 1 Introduction

#### 1.1 Brain Metastases and Other Brain Tumors

Brain metastases (BM) represent a significant portion of intracranial neoplasms outnumbering all other intracranial tumors combined. Conservative estimates suggest that 100,000–170,000 new cases of BM are diagnosed every year in the United States. The ratio of BM vs. primary brain tumors like, e.g., glioblastoma (GBM) is 10:1. Whereas the improvement of systemic therapies has led to a longer survival in extracranial disease, BM are still an end stage in cancer progression which provokes a major limitation of life expectancy and is frequently associated with neurological impairments. Despite

---

Faramarz Dehghani and Carsten Hagemann contributed equally to this work.

their treatment by surgical resection that is applicable only in a minority of patients with a single and superficial lesion, and radiotherapy, the median survival is 7.1 months and even worse in patients with multiple BM which are found in more than 50% of cases. Thus, 20% to 40% of all patients with different metastatic cancer types will have BM at autopsy [1].

Intensive research has led to recent impressive advances in the treatment of different primary cancers, i.e., through the development of immune or targeted therapies [2–4]. However, despite this success, disseminated disease remains the most lethal aspect of cancer with a particularly dire situation for patients suffering from BM or primary brain tumors [5]. This paucity is partially attributed to the complexity of the underlying mechanisms that drive BM and brain cancer growth. Interactions between tumor cells and their surrounding tissue environment are increasingly recognized as critical regulators of organ-specific metastasis [6, 7]. The brain metastatic cascade comprises a multitude of unique and complex tumor stroma interactions for central nervous system (CNS) colonization [8]. Each step requires tumor cells to adapt to or even exploit the foreign and hostile environment for successful colonization [9]. Proliferation, deregulated adhesion, increased motility, invasiveness, resistance to apoptotic signals, and the ability to induce angiogenesis are such characteristics of metastatic cells [10], but very similarly also of the highly malignant GBM cells.

To understand the mechanisms behind and to develop novel therapeutic strategies to improve prognosis and quality of life of brain tumor and BM patients, *in vitro* and *in vivo* models that faithfully mimic these processes are necessary.

## **1.2 Use of Cell Culture 3D Models and Animal Experiments**

Experiments in two-dimensional cell culture are easy, quick, and less expensive. However, unfortunately such cultures only partially reflect the *in vivo* situation [11–13]. Animal experiments, on the other hand, offer the complexity of an organism but should be reduced to a minimum due to ethical aspects [14, 15]. Three-dimensional cell culture models, as well as organoids, could bridge two-dimensional cell culture and the *in vivo* system, closing in on the latter due to their cellular composition of different cell types [16, 17]. In neuroscience research, however, the generation of organoids is extremely demanding, because different brain regions must reconstitute by self-organization [18, 19]. Although some research groups have succeeded in designing such brain organoids, not all neuronal structures are reproducible and their culture is still very tricky and time-consuming [20, 21]. Therefore, an obvious alternative is taking an already functioning, well-developed organ, and culture it further under *ex-vivo* conditions. Even if not all physiological functions are retained, such as blood flow through the vessels, it currently is the best available option [22, 23].

### 1.3 Organotypic Hippocampal Slice Cultures (OHSCs)

Organotypic hippocampal slice cultures have been introduced in the early 1990s [24]. Several slices can be generated from a single brain and cultured for an extended time period. This option is very advantageous, since control and treatment experiments can be performed with slices originating from the same animal, immensely increasing the comparability of results. Therefore, brain slice cultures offer an innovative experimental setup that is very close to the *in vivo* situation [25, 26]. A further advantage is that their preparation and culture are considered as organ removal and not as a full animal experiment (*see Note 1*).

Initially, OHSCs were cultured in roller tubes [27]. Later, culture on semipermeable membranes was established and proven as more efficient in comparison to the latter [24]. Different brain areas like cortex, forebrain, and midbrain have been tested for cultivation [28–30]. However, the hippocampus was found the most suitable one of the best explored brain areas, as its principal structure and neuronal organization remains conserved after preparation [31–34]. OHSCs consist of the cornu ammonis (CA1, CA2, CA3), dentate gyrus, and entorhinal cortex. The neuronal circuit between the entorhinal cortex, dentate gyrus, CA3, and CA1 back to entorhinal cortex remains intact after preparation and behave in most aspects similar to the *in vivo* situation (Fig. 1). Additionally, cytostructural degeneration of neuronal regions is almost absent. Thus, OHSCs can be used to investigate neurodegenerative diseases such as Alzheimer's or functional disorders like epilepsy [35, 36]. Under specific culture conditions, even epileptic activity can be induced and investigated [37]. Slice cultures are also employed for neurotoxicological screenings either to test effects of toxic substances on brain development or to evaluate new tumor treatment modalities [38, 39]. Furthermore, the analysis of primary or metastatic tumor cell development or their microenvironment is another

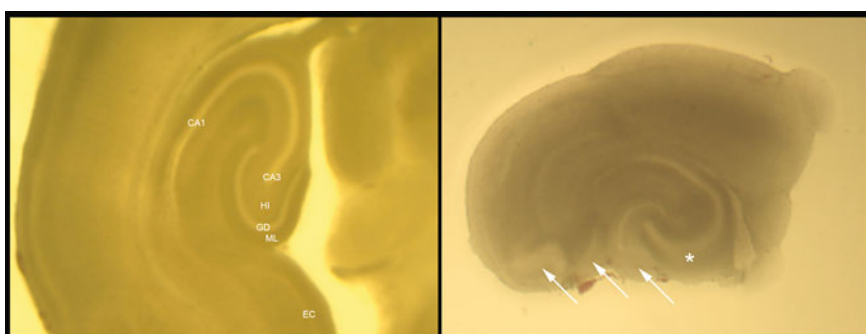


**Fig. 1** Examples of OHSCs in culture. Left: Structure of a well-growing OHSC. CA1: cornu ammonis layer 1, CA3: cornu ammonis layer 3, DG: dentate gyrus (granular cell layer), EC: entorhinal cortex, HI: hilus, ML: molecular layer. Right: Example of a degenerating OHSC after 3 days in culture. Arrows indicate zones of degeneration in the region of the EC and DG, and the asterisk highlights enlargement of the CA3 region

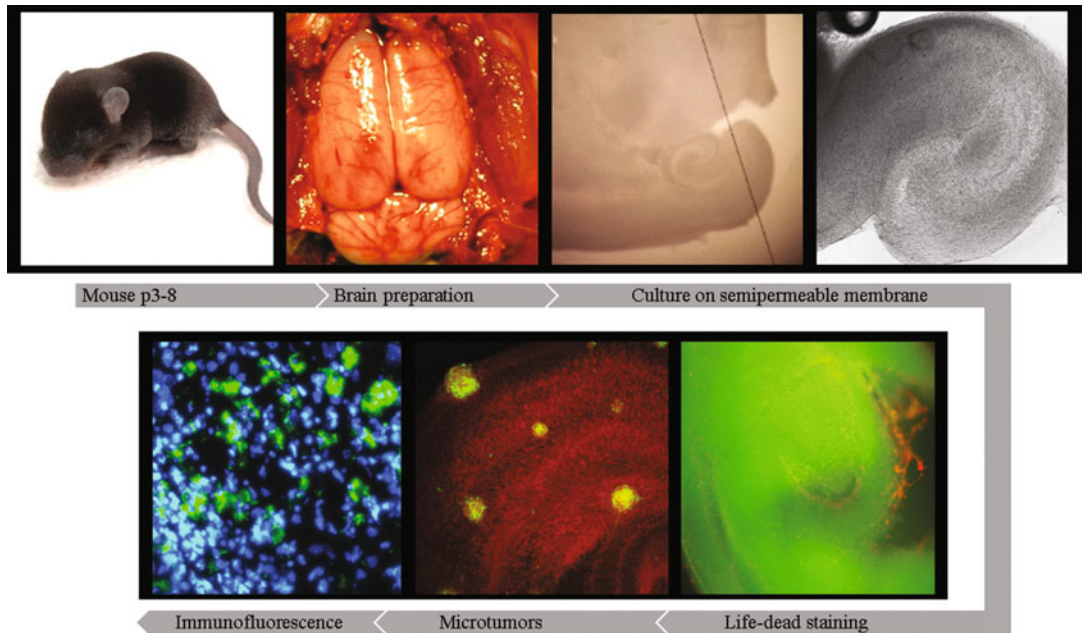


**Fig. 2** Scheme of the experimental procedures. The brain of a 3–8-day-old mouse is exposed and prepared. Brain slices of 350  $\mu\text{m}$  thickness are cut using a vibratome. After isolation of the hippocampus, the slices are cultured on a semipermeable membrane for several days. Life–dead staining is performed on exemplary slices to check for the quality of the OHSCs. In this example, the pia mater and fissure are shown. Only very few dead cells are visible. Tumor cells or cells of metastatic origin can be seeded onto the OHSCs to form microtumors. Cryosections can be prepared for immunohistochemical staining

application for OHSCs [26, 40–43]. Thus, slice cultures are particularly well suited for neurological and neuro-oncology research including brain metastasis.

To prepare good OHSCs, one requires healthy postnatal mice. It was shown that 3–8 days old mice are best suited for this purpose (Fig. 2). Such cultures have a high survival rate, are stable in handling, and show a good morphology compared to brain slices derived from embryonic mice [34, 35, 44]. To evaluate the success of preparation and culture, we usually perform life–dead staining of some exemplary slices to estimate the ratio of living and dead cells (Fig. 2). In our setting, we start with followup experiments 6 days after preparation, because inflammatory reactions associated with the slicing procedure disappear by this time, microglial cells show a ramified morphology, and synaptic connections have matured [26]. Tumor cells or cells of metastatic origin can be seeded onto such OHSCs to evaluate micro-tumor formation, tumor cell invasion, or treatment response (Fig. 2) [42]. Although the OHSCs thin out during the culture period, their thickness does not allow the penetration of many antibodies and adequate microscopic analysis. Cryosections must be prepared for immunohistochemical staining. Nevertheless, the structures of the slices remain relatively well preserved (Fig. 2) [22, 45].

## 2 Materials

### 2.1 OHSC Preparation

1. Laminar flow hood.
2. Agarose, bioreagent for molecular biology, low electroendosmosis (EEO).
3. Phosphate-buffered saline (PBS).
4. Preparation medium: Minimal Essential Medium (MEM, including Earle's Salts, 25 mM 4-(2-Hydroxyethyl)piperazine-1-ethanesulfonic acid (HEPES), without L-glutamine) supplemented with 1% w/v L-glutamine (final concentration 2 mM), 1% v/v of a 45% w/v glucose solution, 100 U/ml penicillin, and 0.1 mg/ml streptomycin (*see Note 2*).
5. Culture medium: MEM supplemented with 1% w/v L-glutamine (final concentration 2 mM), 1% v/v of a 45% w/v glucose solution, 25% v/v normal horse serum (NHS), 25% v/v Hanks' balanced salt solution (HBSS), 0.08% w/v vitamin C, 100 U/ml penicillin, and 0.1 mg/ml streptomycin (*see Note 3*).
6. Water bath set to 35 °C.
7. C57BL/6 mice, other wild-type or genetically modified mouse strains, postnatal 3–8 days. Alternatively, postnatal 7–9-day-old rats can be used.
8. Tweezers (surgical and tissue), scalpel, and very sharp scissors (a large one for decapitation of the mice and a smaller one for preparation).
9. Cell culture dishes (6 cm) and filter paper.
10. Vibratome (*see Note 4*).
11. Spatula with a flat and wide surface.
12. Histoacryl or other tissue adhesive.
13. Pasteur pipettes and rubber sucker (*see Note 5*, Fig. 3).
14. Stereomicroscope.
15. Inserts for 6-well cell culture cluster with 0.45 µm membrane. Optional: a second membrane (0.45 µm) to place on top of the first membrane for easier transportation of the slices (*see Note 6*).
16. 6-well cell culture cluster, flat bottom with lid.

### 2.2 Seeding of Cells

1. Cell culture medium (*see Note 7*).
2. Vent cap canted neck cell culture flasks (75 cm<sup>2</sup>).
3. 0.25% trypsin-EDTA.
4. Carboxyfluorescein diacetate (CFDA) (*see Note 8*).

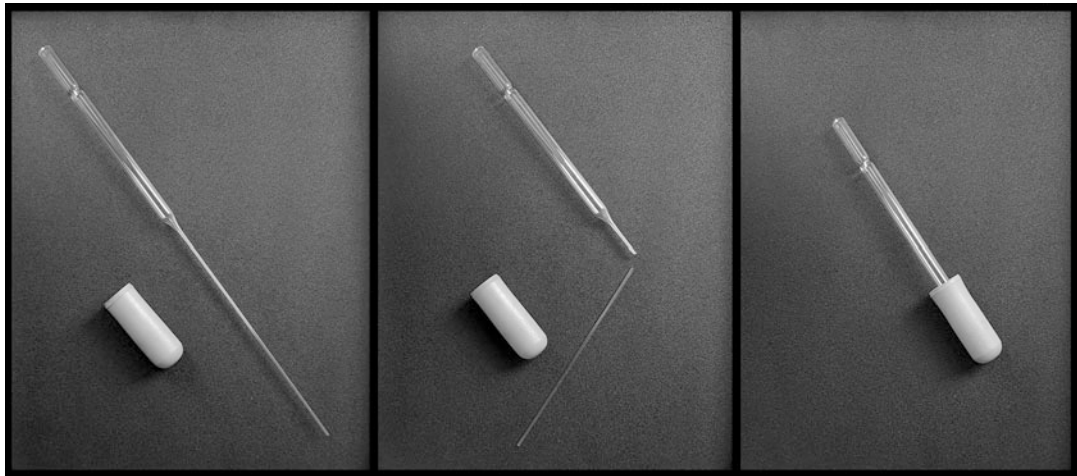


**Fig. 3** Preparation of a Pasteur pipette for slice transfer. The tip of a Pasteur pipette is broken off and placed upside down into a rubber sucker. The wide opening now is an ideal tool for sucking the brain slices for lifting and transferring them without causing damage

- 5. Phosphate-buffered saline (PBS) without  $\text{Ca}^{2+}$  and  $\text{Mg}^{2+}$ , low endotoxin.
- 6. Glass pipettes.
- 7. 15 ml tubes and 1.5 ml Eppendorf cups.
  
- 2.3 ***Life–Dead Staining***
- 1. Tinfoil.
- 2. 6-well cell culture cluster, flat bottom with lid.
- 3. Black Eppendorf reaction tubes.
- 4. Paintbrush (round, fine hair, size 0).
- 5. PBS without  $\text{Ca}^{2+}$  and  $\text{Mg}^{2+}$ , low endotoxin.
- 6. Staining solution: After diluting the stock solution of GelRed Nucleic Acid Gel Stain ( $10,000\times$  in water) with water to a  $30\times$  solution, add it in a dilution of 1:10 together with fluorescein diacetate (FDA, 5 mg/ml in dimethyl sulfoxide (DMSO)) in a dilution of 1:100 to PBS.
- 7. Shaker.
- 8. Fluorescence microscope.
  
- 2.4 ***Fixing and Staining of OHSCs with Seeded Cells***
- 1. Phosphate-buffered saline (PBS) without  $\text{Ca}^{2+}$  and  $\text{Mg}^{2+}$ , low endotoxin.
- 2. 4% w/v paraformaldehyde (PFA) in PBS (*see Note 9*).
- 3. PBS containing 0.03% v/v Triton X-100 (PBS-T).
- 4. 5  $\mu\text{g}/\text{ml}$  propidium iodide (PI) (*see Note 9*).
- 5. Distilled water.
- 6. Scalpel.

7. Dako fluorescent mounting medium.
8. Microscope slides.
9. Confocal laser scanning microscope (CLSM).

## **2.5 Cryosection**

1. PBS Dulbecco without  $\text{Ca}^{2+}$  and  $\text{Mg}^{2+}$ , low endotoxin.
2. Tweezers.
3. Tissue-Tek embedding medium.
4. Cryomold.
5. Cryostat.
6. SuperFrost slides.
7. Glass cuvette.
8. Acetone.

## **2.6 Immuno-fluorescence Staining**

1. Glass cuvette.
2. Washing solution: 0.1% v/v Tween-20 in PBS.
3. Permeabilization solution: 0.5% v/v Triton X-100 in PBS.
4. Blocking solution: 10% v/v donkey serum in PBS containing 1% BSA.
5. Antibody according to the protein of interest diluted in 0.1% v/v bovine serum albumin (BSA) (*see Note 10*).
6. PBS Dulbecco without  $\text{Ca}^{2+}$  and  $\text{Mg}^{2+}$ , low endotoxin.
7. Distilled water.
8. Fluoroshield with DAPI.
9. Coverslip.
10. Paper tissue.
11. Dark box.
12. Microscope slide folder.

## **3 Methods**

### **3.1 Preparation of OHSCs**

1. A couple of days before starting the preparation, mix 100 ml PBS with 5 g agarose and autoclave. Pour 5–6 ml of the melted agarose under aseptic conditions into cell culture plates (6 cm), each. After polymerization, store in the refrigerator.
2. Freshly prepare 100 ml preparation medium as outlined in Subheading 2.1. and cool it down to 4 °C (*see Note 11*).
3. Prepare 50 ml cultivation medium as outlined in 2.1. and preheat the medium in a water bath to 35 °C (*see Note 3*).
4. Take and decapitate a mouse with a sharp scissor by a precise cut directly behind the ears. Discard the body (*see Note 12*).

5. Remove the skin from the skull using a tweezer (*see Note 13*).
6. All following steps have to be performed under the laminar flow hood to ensure sterile conditions.
7. Make a T-section from caudal into the skull, open the skull, and remove the bone and cartilage tissue with a surgical tweezer. Work very carefully, not to damage the brain tissue.
8. Temporarily place the brain into a cell culture dish filled with preparation medium to wash away the blood.
9. Place a filter paper into a cell culture dish and drop the brain onto the paper (*see Note 14*).
10. Cut off the most rostral part of the frontal pole and the cerebellum using a scalpel.
11. Apply Histoacryl tissue glue onto the plate to fix and stabilize the brain. The plate is attached in the middle of the tub of the vibratome (Fig. 4).

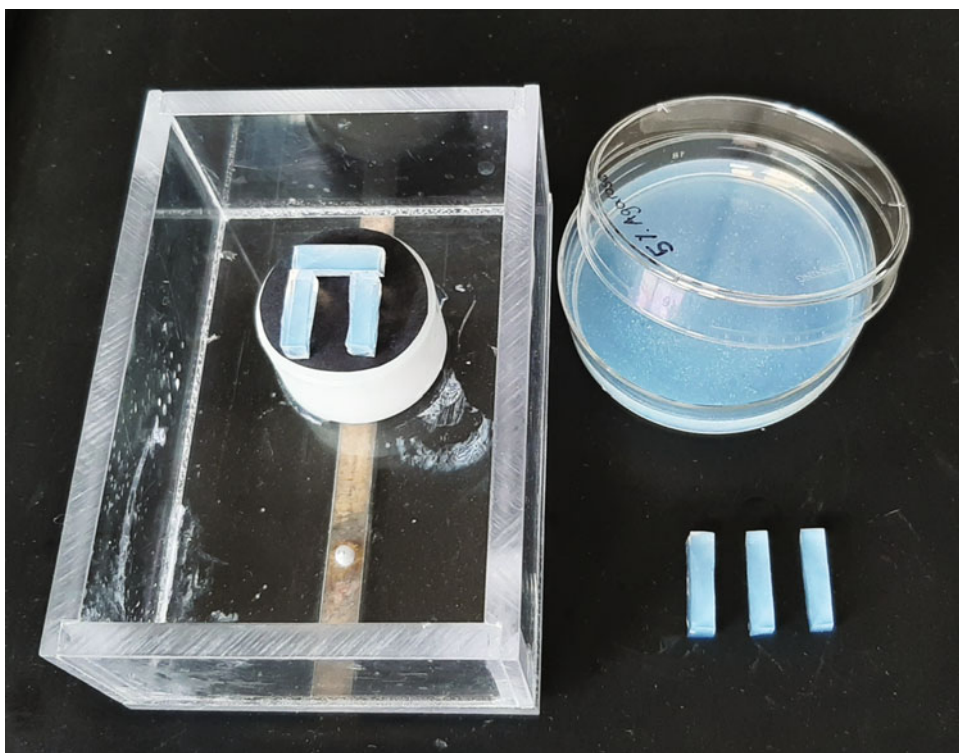


**Fig. 4** Usage of agarose blocks to fix the brains for preparation. Rectangles of  $0.5\text{ cm} \times 1.5\text{ cm}$  cut from polymerized 5% agarose are glued to the vibratome plate with Histoacryl tissue glue. The pads will support the brain attached in the middle (not shown) from three sides, preventing it from uncontrolled moving during the slicing procedure. Through the open area, the blade will enter to cut the brain. In our setting, the plate which will carry the brain is already attached inside the tub, which will be filled with preparation medium and inserted into the bracket of the vibratome

12. Use a wide spatula and tweezer to transfer the brain from the filter membrane onto the Histoacryl tissue glue on the plate of the vibratome. Position the brain with the caudal side to the blade of the slicer. Make sure to cut the brain from caudal to rostral to get slices in the horizontal plane.
13. Cut small rectangles ( $0.5\text{ cm} \times 1.5\text{ cm}$ ) out of the initially prepared 5% agarose gel and glue them onto the plate with Histoacryl tissue glue to fix the brain from three sides (Fig. 4).
14. Fill the vibratome tub with preparation medium to cover the whole brain and insert the tub onto the bracket of the vibratome.
15. Cut slices with a thickness of  $350\text{ }\mu\text{m}$  (*see Note 15*).
16. Carefully transfer the slices with the wide opening of a Pasteur pipette into a cell culture dish containing 3 ml preheated ( $35\text{ }^{\circ}\text{C}$ ) culture medium (*see Note 5*).
17. After each cut, check your slices under the stereomicroscope (Fig. 1) (*see Note 16*).
18. Under the stereomicroscope, carefully cut out the hippocampal area with a scalpel (*see Note 17*).
19. Using a Pasteur pipette (*see Note 5*), transfer the slices from the medium onto the membrane of the inserts, and ensure to transfer as little medium as possible (*see Note 6*).
20. Allow the brain slices to expand and ensure that there is no air bubble and no medium on the slice surface (*see Note 18*).
21. Place the insert into the 6-well cell culture cluster.
22. Fill the 6-well cell culture cluster wells with 1 ml culture medium that the surface of the inserts will just slightly immerse in the medium (*see Notes 18 and 19*).
23. The slices are incubated at  $35\text{ }^{\circ}\text{C}$  in a humidified atmosphere with 5% CO<sub>2</sub>.
24. Change medium every other day.

### **3.2 Seeding of Cells**

1. Maintain cell lines of interest in  $75\text{ cm}^2$  cell culture flasks, containing 15–20 ml of cell culture medium, at  $37\text{ }^{\circ}\text{C}$ , 5.0% CO<sub>2</sub> and 100% humidity. Cells are passaged when they reach subconfluence with trypsin-EDTA (*see Note 7*).
2. Label the cells with CFDA (*see Note 8*). Add 10 µl of CFDA to a 10 ml culture flask with tumor cells (*see Note 20*).
3. Incubate overnight at  $37\text{ }^{\circ}\text{C}$  in a humidified atmosphere with 5% CO<sub>2</sub>.
4. Discard the medium with CFDA, wash the cells once with PBS, and add 2 ml of trypsin-EDTA.

5. Incubate the cells for about 8 min (cell type dependent) at 37 °C in the incubator. Then check microscopically whether all cells are detached and add 8 ml of cell culture medium to the flask.
6. Transfer the cells with a 10 ml glass pipette into a 15 ml tube.
7. Count the cells, e.g., by using a Neubauer chamber, hemocytometer, or other cell counting device.
8. Centrifuge the cells 9 min at 200 × g.
9. Discard the supernatant by carefully inverting the tube or by aspirating it using a pipette.
10. Resuspend the cells in cell culture medium at a concentration of  $10^5$  cells per 10 µl.
11. Seed 10 µl of cell culture medium containing  $10^5$  cells onto each OHSC. Exact cell numbers may vary depending on the used cell line.
12. Incubate OHSCs with the cells for 1–5 days as described in Subheading 3.1. at 35 °C in a humidified atmosphere with 5% CO<sub>2</sub> (*see Note 21*).

### 3.3 Life–Dead Staining

1. Prepare tinfoil to cover the samples.
2. Use a tiny brush to detach the OHSCs from the membranes and transfer them into a 6-well cell culture cluster (*see Note 22*).
3. Wash the OHSCs once with PBS (*see Note 23*).
4. From now on, work in the dark.
5. Prepare the staining solution in a black Eppendorf cup.
6. Add 500 µl of the staining solution per well.
7. Cover the cell culture cluster with tinfoil and incubate the samples for 10 min.
8. Remove the staining solution.
9. Wash the OHSCs with 1 ml PBS 2 times for 10 min while they are on the shaker.
10. The OHSCs can now be covered with PBS and examined using a fluorescence microscope with filters for FDA with Excitation BP480/40 and Emission BP527/30 and for GelRed with Excitation BP545/25 and Emission BP605/70 (*see Note 24*).

### 3.4 Fixing and Staining of OHSCs with Seeded Cells

1. Remove the cell culture medium, wash once with PBS, and add 4% PFA to the cell culture cluster and in the insert. Ensure the OHSC is surrounded by the PFA solution. Incubate overnight.
2. Wash the OHSCs in the cell culture insert with PBS for 10 min and with PBS-T for another 10 min.

3. Add 5 µg/ml PI onto the OHSCs and incubate for 24 h (*see Note 25*).
4. On the next day, wash the OHSCs with PBS-T for 10 min and then for 5 min in distilled water.
5. If OSHCs grow on a second membrane (*see Note 6*), they can be removed using tweezers. Otherwise, cut off the OHSCs with a scalpel together with the membrane. Coverslip the OHSCs with DAKO fluorescent mounting medium on microscope slides.
6. Investigate the samples using a CLSM. For CFDA-labeled tumor cells, use monochromatic light at 488 nm with dichroic beam splitter (FT 488/543) and an emission band-pass filter of 505–530 nm. For detection of PI, use monochromatic light at 543 nm and emission band-pass filter of 585–615 nm (*see Note 26*).

### 3.5 Cryosection

1. Gently wash the OHSCs with PBS.
2. Remove the membrane together with the OHSCs from the insert using tweezers.
3. Fill a thin layer of Tissue-Tek into the cryomold. Place the sample into the mold with the OHSC facing down and then fill the mold completely with Tissue-Tek (Fig. 5) (*see Note 27*).
4. Place the cryomold into a freezer and let the sample cooldown to –20 °C (*see Note 28*).
5. Prepare 7 µm thick sections utilizing the cryostat (Fig. 5) (*see Note 29*).
6. Transfer the cryosections onto SuperFrost slides and let them air-dry overnight (*see Note 30*).

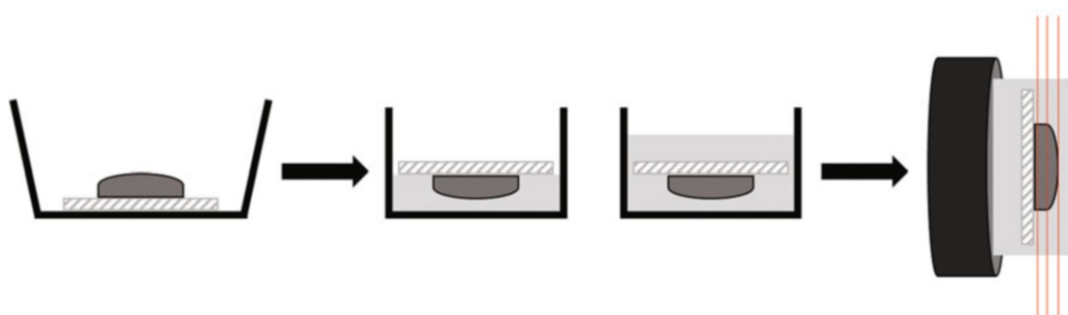


**Fig. 5** Scheme of OHSC embedding and cryosectioning. The OHSCs are detached from the insert together with the membrane and transferred with the OHSC facing down to the cryomold containing a thin layer of Tissue-Tek. Then the cryomold is filled up with Tissue-Tek. The solid sample is attached to the platform of the cryostat with the OHSC facing forward

7. If working with OHSCs with pre-stained seeded tumor cells (*see Subheading 3.3*), **steps 8** and **9** must be omitted. Otherwise proceed with step 8.
8. Fill a glass cuvette with ice-cold acetone ( $-20^{\circ}\text{C}$ ) and then let the samples slide in slowly. Incubate for 2 min at  $-20^{\circ}\text{C}$  for fixation.
9. Let the sections air-dry at room temperature for 30 min (*see Note 31*).
10. Store the samples in the freezer at  $-20^{\circ}\text{C}$  until performing the staining procedure.

### **3.6 Immuno-fluorescence Staining**

1. Thaw the sample at room temperature for 20 min (*see Note 32*).
2. Fill a glass cuvette with washing solution and wash the samples for 5 min at room temperature while shaking.
3. Place the samples on a tray (*see Note 32*).
4. Add 1  $\mu\text{l}$  permeabilization solution to each sample for exactly 7 min at room temperature to permeabilize the cell membranes.
5. Allow the samples to air-dry for 5 min (*see Note 33*).
6. Prepare a dark box, laid out with tissue paper moistened with distilled water and place the slides into this box (Fig. 6).
7. Add 100  $\mu\text{l}$  blocking solution to each sample and incubate for 90 min inside the dark box (*see Note 34*).
8. Remove the blocking solution, add 100  $\mu\text{l}$  antibody in 0.1% BSA solution on top of each sample, and incubate overnight in the fridge (*see Notes 35 and 10*).



**Fig. 6** Outline of the dark box used for immunofluorescence staining. The spaces between the slide carrier are covered with distilled water-moistened tissue paper to prevent the slices from drying out during the blocking time

9. Place the slides into a glass cuvette.
10. Wash the samples twice with PBS for 30 min and once with distilled water for 20 min while shaking.
11. Air-dry the samples for 5 min.
12. Use one drop of Fluoroshield with DAPI for each slide and place a coverslip on top.
13. Place the slides into a microscope slide folder and leave the samples in the refrigerator for at least 2 days before examining them using a fluorescence microscope.

---

## 4 Notes

1. Organ removal was performed in accordance with the Policy of Ethics and the Policy on the Use of Animals in Neuroscience Research as approved by the European Communities Council Directive 2010/63/EU of the European Parliament and of the Council of the European Union on the protection of animals used for scientific purposes. In addition, we followed the recommendations of the local animal welfare committee.
2. Prepare this medium freshly for each preparation.
3. Store the culture medium at 4 °C during the brain slice culture. However, it must be preheated to 35 °C each time before using. Alternatively, to a water bath, an incubator set to 35 °C could be used for preheating the medium. Even when stored at 4 °C, do not use this medium for longer than 1 week.
4. We are using the vibratome Slicer HR 2. However, any vibratome is suitable, as long as a cutting thickness of 350 µm is adjustable.
5. Break off the tip of a Pasteur pipette and insert it with this end into the rubber sucker. Be careful to not become injured, since the breakpoint of the Pasteur pipette may be very sharp. The wide opening at the upper end of the pipette now can be used to easily suck the brain slices for lifting and transferring them (Fig. 3).
6. The OHSCs will become thinner and grow into the membrane. For subsequent experiments, it might be difficult to transfer them and embed them into Tissue-Tek without causing damage. Therefore, it is advisable to culture the OHSCs on a second membrane (0.45 µm) which is placed on top of the first membrane in the insert. This might simplify their transfer for followup experiments.
7. The required cell culture medium depends on the cell line to be used. For human glioblastoma cell lines (e.g., U87MG, U138MG, U343, U373MG, GaMG, SNB19, or DKMG),

we apply Dulbecco's Modified Eagle's Medium (DMEM) containing 1 g/l glucose, sodium pyruvate, 3.7 g/l NaHCO<sub>3</sub>, and L-glutamine supplemented with 10% v/v heat-inactivated fetal calf serum (FCS), 2× nonessential amino acids (NEA, 100× stock, add 10 ml to 500 ml medium), 3 mM L-glutamine, 100 U/ml penicillin, and 100 mg/ml streptomycin. However, other cell lines may require different medium compositions and culture conditions.

8. We recommend using a CFDA kit, e.g., the Vybrant® CFDA SE Cell Tracer Kit, which has been used for the example image shown in Fig. 2. However, any other CFDA kit from other manufacturers will be as suitable as the system mentioned here.
9. Caution: PFA and PI are toxic and suspected carcinogens. Work under the fume hood and wear personal protective equipment.
10. The antibody dilution required for best staining results may vary depending on antibody, cells, and targets. They have to be evaluated in preliminary experiments. For most of our antibodies, a dilution of 1:100 was optimal.
11. Cooling down the medium to 4 °C will slowdown biochemical processes within the tissue while sectioning the mouse brains.
12. Make sure the mice are healthy. It will affect the quality of OHSCs immensely.
13. For a better grip, fix the mouth of the mouse with a big tweezer while removing the skin with a second tweezer.
14. The filter paper absorbs the liquid so that the Histoacryl glue sticks better while gluing it onto the vibratome plate. Do not leave the brain on the filter paper for a too long time period, otherwise it sticks.
15. The first slices can be done quickly and a bit thicker. After 3–4 cuts one has to be more careful and cut the slices slowly. If the blade runs too fast over the brain, the slices may rupture. Also make sure that the vibration of the vibratome is turned off while the blade is moving back to the start position. Otherwise the brain might tear. The exact settings of the vibratome may differ from different manufacturers and therefore have to be optimized in preliminary experiments.
16. It is important to ensure cuts are made in the right plane. The hippocampus should be nicely curved and looks like two "C" facing each other. If the area looks more like a duck's beak, one is already too far. Thus, sections should be microscopically examined after each cut. Discard slices of low quality immediately and only proceed with those with intact cytoarchitecture (Fig. 1).

17. Pay attention, even a slightly damaged hippocampus will not grow.
18. Make sure that there is no medium on top of the OHSCs, otherwise they will disintegrate. Nutrient absorption from the medium in the well takes place via the membrane of the insert.
19. The medium required is approximately 1 ml but will vary depending on the manufacturer of plates and inserts.
20. CFDA passively diffuses into the cells, reacting with intracellular compounds forming fluorescent conjugates, which are inherited by daughter cells. Thus, after CFDA removal, the fluorescence intensity will roughly be halved after each cell division.
21. To conserve viability of OHSC, the exact incubation time needs to be determined before the experiments. This may vary depending on the cell lines used. Keep in mind that CFDA fluorescence intensity will roughly be halved after each tumor cell division, thus limiting upper incubation times.
22. Alternatively, one can take the whole membrane with the OHSC on its top using a tweezer.
23. Remove the medium carefully, otherwise cells may detach and could be washed away.
24. Using the correct filters, living cells appear green and dead cells red, because the latter have a permeable membrane. Slices cannot be used for other staining or evaluations after the life-dead staining. Therefore, do not use all, but only exemplary OHSCs for evaluation of cell death, except this is your main experiment.
25. PI is a polar fluorescent dye, normally excluded from healthy cells by the intact plasma membrane. After fixation, the plasma membrane permeability is breached; the dye enters the cell and binds to DNA, thereby visualizing the cytoarchitecture of the brain slices.
26. The evaluation of the microtumors growing on OHSCs is not the topic of this chapter and highly depends on the scientific question to be answered by the specific experiment. However, to give some examples, the number of formed tumors, their volume, radius, and eccentricity can be determined. To do so, we obtain images using the 10 $\times$  objective using a z-stack with a step width of 2  $\mu\text{m}$ . The images are first analyzed with the Image J plugin Ovuscule [46] that fits an ellipse to the tumor visible on a CLSM image. A cell cluster is regarded as micro-tumor when it has a minimal diameter of at least 25  $\mu\text{m}$ . This is done for every image of the according z-stack. The mean planar radius of the tumor is defined as the ratio of the major and the minor axis of the fitted ellipse on every image on the z-stack

and the eccentricity is calculated. The eccentricity and the mean planar radius are then plotted over the depth, as well as a normalized radius and eccentricity defined as the ratio between radius and eccentricity divided by its mean value subtracted by one. The tumor volume is calculated, approximated by multiplying the step width with the summed up area of the tumor. The number of tumors is counted per slice and in relation to the  $10^5$  cells seeded.

27. Avoid embedding the OHSC carrying membrane into Tissue-Tek in an angle, ensuring that they are straight.
28. Make sure that all necessary utensils are precooled to  $-20\text{ }^\circ\text{C}$ .
29. Since the OHSCs thin out during culture, only very few usable cryosections can be obtained from each OHSC.
30. It is best to place the SuperFrost slide like a stamp on top the freshly cut cryosection, then remove the slide quickly. By this way, crushing and slipping of the cryosection is prevented.
31. The drying time varies from sample to sample, but should approximately take 30 min.
32. To dry the thawed slides, drain the liquid from the slide onto a tissue and shake it off by gently tapping. Alternatively, the bottom of the slide can be wiped and the surface carefully dabbed around the section.
33. Check samples under the microscope and proceed only with the good ones.
34. Circle the section with a Pap pen so that the liquids applied cover the section and do not flow away.
35. If working with conjugated antibodies, work in the dark. Depending on the size of the section, one has to use more antibody solution. Make sure that the whole sample is covered by antibody solution. Do not move the box with the samples.

---

## Acknowledgments

We thank the Jörg-Bernards-Stiftung, Cologne, Germany, for generous funding of this project. We are very grateful to Andreas Bahmer for providing the vibratome and to Siglinde Kühnel and Elisabeth Karl for excellent technical assistance.

## References

1. Weidle UH, Birzele F, Kollmorgen G et al (2016) Dissection of the process of brain metastasis reveals targets and mechanisms for molecular-based intervention. *Cancer Genomics Proteomics* 13(4):245–258
2. Slamon DJ, Leyland-Jones B, Shak S et al (2001) Use of chemotherapy plus a monoclonal antibody against HER2 for metastatic breast cancer that overexpresses HER2. *N*

- Engl J Med 344(11):783–792. <https://doi.org/10.1056/NEJM200103153441101>
3. Mayer IA, Abramson VG, Isakoff SJ et al (2014) Stand up to cancer phase Ib study of pan-phosphoinositide-3-kinase inhibitor buparlisib with letrozole in estrogen receptor-positive/human epidermal growth factor receptor 2-negative metastatic breast cancer. J Clin Oncol 32(12):1202–1209. <https://doi.org/10.1200/JCO.2013.54.0518>
  4. Elion DL, Jacobson ME, Hicks DJ et al (2018) Therapeutically active RIG-I agonist induces immunogenic tumor cell killing in breast cancers. Cancer Res 78(21):6183–6195. <https://doi.org/10.1158/0008-5472.CAN-18-0730>
  5. Ekici K, Temelli O, Dikilitas M et al (2016) Survival and prognostic factors in patients with brain metastasis: single center experience. J BUON 21(4):958–963
  6. Pavlides S, Tsirigos A, Vera I et al (2010) Transcriptional evidence for the “reverse Warburg effect” in human breast cancer tumor stroma and metastasis: similarities with oxidative stress, inflammation, Alzheimer’s disease, and “neuron-glia metabolic coupling”. Aging (Albany NY) 2(4):185–199. <https://doi.org/10.1863/aging.100134>
  7. Chuang HN, van Rossum D, Sieger D et al (2013) Carcinoma cells misuse the host tissue damage response to invade the brain. Glia 61(8):1331–1346. <https://doi.org/10.1002/glia.22518>
  8. Wingrove E, Liu ZZ, Patel KD et al (2019) Transcriptomic hallmarks of tumor plasticity and stromal interactions in brain metastasis. Cell Rep 27(4):1277–1292.e7. <https://doi.org/10.1016/j.celrep.2019.03.085>
  9. van der Weyden L, Arends MJ, Campbell AD et al (2017) Genome-wide *in vivo* screen identifies novel host regulators of metastatic colonization. Nature 541(7636):233–236. <https://doi.org/10.1038/nature20792>
  10. Hanahan D, Weinberg RA (2011) Hallmarks of cancer: the next generation. Cell 144(5):646–674. <https://doi.org/10.1016/j.cell.2011.02.013>
  11. Duval K, Grover H, Han LH et al (2017) Modeling physiological events in 2D vs. 3D cell culture. Physiology (Bethesda) 32(4):266–277. <https://doi.org/10.1152/physiol.00036.2016>
  12. Kaisar MA, Sajja RK, Prasad S et al (2017) New experimental models of the blood-brain barrier for CNS drug discovery. Expert Opin Drug Discov 12(1):89–103. <https://doi.org/10.1080/17460441.2017.1253676>
  13. Hoarau-Véchot J, Rafii A, Touboul C et al (2018) Halfway between 2D and animal models: are 3D cultures the ideal tool to study cancer-microenvironment interactions? Int J Mol Sci 19(1):E181. <https://doi.org/10.3390/ijms19010181>
  14. Ferdowsian HR, Gluck JP (2015) The ethical challenges of animal research. Camb Q Healthc Ethics 24(4):391–406. <https://doi.org/10.1017/S0963180115000067>
  15. Andersen ML, Winter LMF (2019) Animal models in biological and biomedical research - experimental and ethical concerns. An Acad Bras Cienc 91(Suppl. 1):e20170238. <https://doi.org/10.1590/0001-3765201720170238>
  16. Lovitt CJ, Shelpet TB, Avery VM (2014) Advanced cell culture techniques for cancer drug discovery. Biology (Basel) 3(2):345–367. <https://doi.org/10.3390/biology3020345>
  17. Trujillo CA, Muotri AR (2018) Brain organoids and the study of neurodevelopment. Trends Mol Med 24(12):982–990. <https://doi.org/10.1016/j.molmed.2018.09.005>
  18. Lancaster MA, Corsini NS, Wolfinger S et al (2017) Guided self-organization and cortical plate formation in human brain organoids. Nat Biotechnol 35(7):659–666. <https://doi.org/10.1038/nbt.3906>
  19. Renner M, Lancaster MA, Bian S et al (2017) Self-organized developmental patterning and differentiation in cerebral organoids. EMBO J 36(10):1316–1329. <https://doi.org/10.1522/embj.201694700>
  20. Lancaster MA, Renner M, Martin CA et al (2013) Cerebral organoids model human brain development and microcephaly. Nature 501(7467):373–379. <https://doi.org/10.1038/nature12517>
  21. Linkous A, Balamatsias D, Snuderl M et al (2019) Modeling patient-derived glioblastoma with cerebral organoids. Cell Rep 26(12):3203–3211.e5. <https://doi.org/10.1016/j.celrep.2019.02.063>
  22. Bendfeldt K, Radojevic V, Kapfhammer J et al (2007) Basic fibroblast growth factor modulates density of blood vessels and preserves tight junctions in organotypic cortical cultures of mice: a new *in vitro* model of the blood-brain barrier. J Neurosci 27(12):3260–3267. <https://doi.org/10.1523/JNEUROSCI.4033-06.2007>
  23. Kovács R, Papageorgiou I, Heinemann U (2011) Slice cultures as a model to study neurovascular coupling and blood brain barrier *in vitro*. Cardiovasc Psychiatry Neurol

- 2011:646958. <https://doi.org/10.1155/2011/646958>
24. Stoppini L, Buchs PA, Muller D (1991) A simple method for organotypic cultures of nervous tissue. *J Neurosci Methods* 37(2):173–182. [https://doi.org/10.1016/0165-0270\(91\)90128-m](https://doi.org/10.1016/0165-0270(91)90128-m)
25. Ebrahimi F, Koch M, Pieroh P et al (2012) Time dependent neuroprotection of mycopheolate mofetil: effects on temporal dynamics in glial proliferation, apoptosis, and scar formation. *J Neuroinflammation* 9:89. <https://doi.org/10.1186/1742-2094-9-89>
26. Grabiec U, Hohmann T, Hammer N et al (2017) Organotypic hippocampal slice cultures as a model to study neuroprotection and invasiveness of tumor cells. *J Vis Exp* 126:e55359. <https://doi.org/10.3791/55359>
27. Gähwiler BH (1981) Morphological differentiation of nerve cells in thin organotypic cultures derived from rat hippocampus and cerebellum. *Proc R Soc Lond B Biol Sci* 211 (1184):287–290. <https://doi.org/10.1098/rspb.1981.0007>
28. Giesing M, Zilliken F (1980) Lipid metabolism of developing central nervous tissues in organotypic cultures. III. Ganglionic control of glycerolipids and fatty acids in cortex grey matter. *Neurochem Res* 5(3):257–270. <https://doi.org/10.1007/bf00964614>
29. Sørensen JC, Ostergaard K, Zimmer J (1994) Grafting of dopaminergic ventral mesencephalic slice cultures to the striatum of adult rats. *Exp Neurol* 127(2):199–206. <https://doi.org/10.1006/exnr.1994.1096>
30. Robertson RT, Baratta J, Kageyama GH et al (1997) Specificity of attachment and neurite outgrowth of dissociated basal forebrain cholinergic neurons seeded on to organotypic slice cultures of forebrain. *Neuroscience* 80 (3):741–752. [https://doi.org/10.1016/s0306-4522\(97\)00067-5](https://doi.org/10.1016/s0306-4522(97)00067-5)
31. Zhabotinski YM, Chumasov EI, Chubakov AR et al (1979) Development of synaptic structure and function in organotypic cultures of the rat hippocampus. *Neuroscience* 4(7):913–920. [https://doi.org/10.1016/0306-4522\(79\)90175-1](https://doi.org/10.1016/0306-4522(79)90175-1)
32. Gähwiler BH (1981) Organotypic monolayer cultures of nervous tissue. *J Neurosci Methods* 4(4):329–342. [https://doi.org/10.1016/0165-0270\(81\)90003-0](https://doi.org/10.1016/0165-0270(81)90003-0)
33. Takano T, He W, Han X et al (2014) Rapid manifestation of reactive astrogliosis in acute hippocampal brain slices. *Glia* 62(1):78–95. <https://doi.org/10.1002/glia.22588>
34. Bakmand T, Troels-Smith AR, Dimaki M et al (2015) Fluidic system for long-term in vitro culturing and monitoring of organotypic brain slices. *Biomed Microdevices* 17(4):71. <https://doi.org/10.1007/s10544-015-9973-6>
35. Marksteiner J, Humpel C (2008) Beta-amyloid expression, release and extracellular deposition in aged rat brain slices. *Mol Psychiatry* 13 (10):939–952. <https://doi.org/10.1038/sj.mp.4002072>
36. Croft CL, Kurbatskaya K, Hanger DP et al (2017) Inhibition of glycogen synthase kinase-3 by BTA-EG4 reduces tau abnormalities in an organotypic brain slice culture model of Alzheimer's disease. *Sci Rep* 7(1):7434. <https://doi.org/10.1038/s41598-017-07906-1>
37. Magalhães DM, Pereira N, Rombo DM et al (2018) Ex vivo model of epilepsy in organotypic slices—a new tool for drug screening. *J Neuroinflammation* 15(1):203. <https://doi.org/10.1186/s12974-018-1225-2>
38. Moon KH, Tajuddin N, Brown J 3rd et al (2014) Phospholipase A2, oxidative stress, and neurodegeneration in binge ethanol-treated organotypic slice cultures of developing rat brain. *Alcohol Clin Exp Res* 38 (1):161–169. <https://doi.org/10.1111/acer.12221>
39. Gerace E, Landucci E, Totti A et al (2016) Ethanol toxicity during brain development: alterations of excitatory synaptic transmission in immature organotypic hippocampal slice cultures. *Alcohol Clin Exp Res* 40 (4):706–716. <https://doi.org/10.1111/acer.13006>
40. Eyüpoglu IY, Hahnen E, Tränkle C et al (2006) Experimental therapy of malignant gliomas using the inhibitor of histone deacetylase MS-275. *Mol Cancer Ther* 5 (5):1248–1255. <https://doi.org/10.1158/1535-7163.MCT-05-0533>
41. Hölsken A, Eyüpoglu IY, Lueders M et al (2006) Ex vivo therapy of malignant melanomas transplanted into organotypic brain slice cultures using inhibitors of histone deacetylases. *Acta Neuropathol* 112(2):205–215. <https://doi.org/10.1007/s00401-006-0082-8>
42. Hagemann C, Fuchs S, Monoranu CM et al (2013) Impact of MACC1 on human malignant glioma progression and patients' unfavorable prognosis. *Neuro-Oncology* 15 (12):1696–1709. <https://doi.org/10.1093/neuonc/not136>
43. Hohmann T, Feese K, Greither T et al (2019) Synthetic cannabinoids influence the invasion of glioblastoma cell lines in a cell- and receptor-

- dependent manner. Cancers 11(2):E161. <https://doi.org/10.3390/cancers11020161>
44. Ostergaard K, Schou JP, Zimmer J et al (1990) Rat ventral mesencephalon grown as organotypic slice cultures and co-cultured with striatum, hippocampus, and cerebellum. Exp Brain Res 82(3):547–565. <https://doi.org/10.1007/bf00228796>
45. Hutter-Schmid B, Kniewallner KM, Humpel C (2015) Organotypic brain slice cultures as a model to study angiogenesis of brain vessels. Front Cell Dev Biol 3:52. <https://doi.org/10.3389/fcell.2015.00052>
46. Thévenaz P, Delgado-Gonzalo R, Unser M (2011) The ovoidule. IEEE Trans Pattern Anal Mach Intell 33(2):382–393. <https://doi.org/10.1109/TPAMI.2010.112>

## **Part II**

### **Functional Mechanisms of Metastasis**



# Chapter 6

## Measuring Mechanical and Adhesive Properties of Single Cells Using an Atomic Force Microscope

Tim Hohmann and Faramarz Dehghani

### Abstract

Atomic force microscopy allows the determination of both mechanical and adhesive properties of living single cells and generation of high-resolution surface images. Here, we describe a method to determine the Young's modulus of a cell and adhesion between a coated cantilever and a cell, as well as an overview of the analysis of the data obtained. Additionally, we point out typical and important pitfalls during the measurement and analysis.

**Key words** Atomic force microscopy, AFM, Young's modulus, Elasticity, Biomechanics, Biomechanical properties, Adhesion

---

### 1 Introduction

The atomic force microscope (AFM) was first experimentally implemented in 1986 by Binnig et al. [1] and afterwards applied to many questions regarding surface topography and measurement of elastic properties of solid materials. The AFM consists of a small cantilever that might contain a sharp tip, a spherical bead or no further modifications and is typically made of silicon nitride. Silicon nitride is often used because it is chemically inert, combines low elastic moduli with high mechanical strength, and shows only little mechanical attrition. When the cantilever or its tip is brought into contact with a sample, the occurring forces lead to a deflection of the cantilever following Hooke's law and a deformation of the sample [2]. Given a finite contact time between cantilever and sample adhesive forces can be detected when retracting the cantilever.

For measuring specific adhesions between the cantilever and a cell, the cantilever can easily be coated with various molecules such as fibronectin or laminin, as the cantilevers material silicon nitride is inert. Based on the achieved spatial ( $<1$  nm) and force resolution ( $<30$  pN in aqueous solution), single and specific adhesion events

between the cantilever and a cell can be resolved and quantified. Such an approach allows, for example, the determination of interactions between tumor cells and specific substances of their micro-milieu. As migration of tumor cells depends on such interactions, AFM measurements yield valuable information for their understanding [3].

A second crucial parameter obtainable by AFM measurements is the elastic modulus of single cells. As the cantilever contacts the sample, it gets deformed. As the force exerted onto the sample can finely be tuned and measured, the resulting deformation allows estimating the Young's modulus of a cell. Previous studies demonstrated that cells of many malignant tumor types are more compliant than benign tumors and healthy cells of the corresponding tissue [4–12]. This idea was expanded to the assumption of associating the effect of treatments on single tumor cells with their mechanical properties, showing similar effects, even though data is limited [13–15].

Consequently, AFM measurements can provide valuable information about two important aspects of tumor cell biology: the interaction/adhesion with their surroundings and the mechanical properties, both potentially being related to tumor migration and invasion.

Thus, we here provide a protocol covering measurements of the mechanical properties and adhesion to fibronectin of single cells. We furthermore introduce the basics of data analysis for the obtained measurements and hint to possibilities on modifications of the given experimental setup.

---

## 2 Materials

Materials and instructions are fitted to the Bioscope Catalyst AFM. Device-specific components are marked with #.

### 2.1 Mechanical Measurements

1. 60 × 15 mm plastic petri dish. #
2. Arrow<sup>TM</sup> TL2 (for round cells just starting to adhere) or CP-CONT-BSG-A/B/C (for fully adhered cells) cantilever.
3. Cell culture medium.
4. Forceps.

### 2.2 Adhesive Measurements

1. 60 × 15 mm plastic petri dish. #
2. Arrow<sup>TM</sup> TL2 (for round cells just starting to adhere) or CP-CONT-BSG-A/B/C (for fully adhered cells) cantilever.
3. Fibronectin. Store at –20 °C (*see Note 1*).
4. Phosphate-buffered saline (sterile).
5. 96-well plate.

6. Cell culture medium.
7. Forceps.

### 3 Methods

Methods are fitted to the Bioscope Catalyst AFM. Steps that are (potentially) device-specific are marked with <sup>#</sup>. Times, cell numbers, and measurement parameters are adjusted to the U138-MG glioblastoma cell line.

#### 3.1 Cell Seeding

1. Seed  $\approx$  50,000 cells onto the petri dish (*see Note 2*).
2. Cover petri dish with culture medium.
3. Allow cells to adhere for  $\approx$  15 min (*see Note 3*), if measuring cells in the process of adhesion otherwise wait till the next day.
4. Transfer petri dish to the microscope and place it into the magnetic holder. <sup>#</sup>

#### 3.2 Cantilever Coating

This step is only necessary if adhesion measurements are to be performed.

1. Dilute fibronectin with PBS to working concentration. Here: 10 mg/ml (*see Note 1*).
2. Use forceps to place the cantilever into the 96-well plate.
3. Pipette  $\approx$  100  $\mu$ l of fibronectin solution onto the cantilever. Take care that the cantilever is not floating on the fibronectin solution.
4. Incubate for 24 h and mount the cantilever.

#### 3.3 Cantilever Mounting and Calibration

1. Use the forceps to place the cantilever onto the cantilever holder and place the cantilever holder onto the scan head. Use the Arrow™ TL2 cantilever for measuring cells that just started to adhere or the CP-CONT-BSG-A/B/C cantilever for fully adherent cells.
2. Place the scan head on the Easy Align. <sup>#</sup>
3. Position the laser on the cantilever in such a way that the sum signal is maximal (*see Fig. 1a*).
4. Adjust the photodetector such that noncontact deflection is very close to 0 V.
5. Retract the cantilever to maximize distance between cantilever and sample in order to avoid damage to the cantilever when placing it above the sample. Transfer scan head onto the microscope to the previously placed sample.

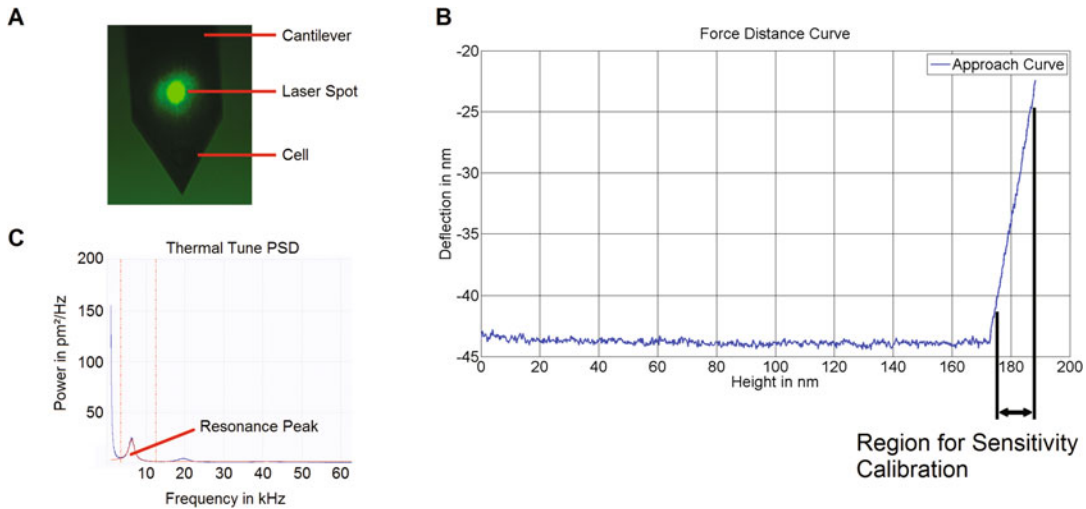


**Fig. 1** Positioning and calibration of a cantilever. (a) Shows the cantilever placed upon a single cell and a typical laser spot alignment. (b) Illustrates a typical sensitivity calibration curve and the region used for calculating the cantilevers sensitivity. (c) Depicts a thermal noise measurement used for determining the cantilevers spring constant. The first resonance peak is not fully visible. Thus, the second resonance peak is marked and used for fitting and calculating the spring constant

6. Engage the cantilever to the surface of the petri dish (*see Note 4*). Engage to an area without cells, as the following calibration needs to be performed on a hard surface.
7. Calibrate the deflection sensitivity using a force distance curve over a deflection of less than 1 V (*see Fig. 1b*). This step can be repeated several times, and the mean deflection sensitivity be used as final value. Typical measurement parameters are maximal deflections of  $\approx 40$  nm, approach velocity of 400 nm/s, ramp size of 200 nm, and at least 1024 measurement points. Denote that the exact values may vary for cantilevers with different spring constants.
8. Withdraw the cantilever from the surface at least 100  $\mu\text{m}$ .
9. Use the thermal tune calibration and acquire the respective data.
10. Set the markers for the fit to include the first visible resonance peak only, fit the data, and calculate the spring constant (*see Fig. 1c*) <sup>#</sup>. Please denote the presence of correction factors that depend on the geometry of the cantilever and the used resonance peak (*see Note 5*).
11. Repeat steps 9 and 10 several times and use the mean spring constant as final value.

### 3.4 Mechanical Measurements

#### 3.4.1 Weakly Adherent Cells

This paragraph describes the measurement for cells that just started to adhere and have thus a spherical shape.

1. After calibration, move the cantilever above one cell. Take care to have a separated cell, so that the cantilever cannot make contact with more than one cell when engaged (*see Fig. 1a*).
2. Engage the cantilever (*see Note 4*).
3. Generate a force–distance curve. Use the following settings: ramp size of 7 µm, a maximal force of 3 nN, approach speed of 5 µm/s, and at least 1024 measurement points (*see Note 6*).
4. If the approach curve looks satisfactory, without inflection points, indentations, or other discontinuities (*see Fig. 2a, b*), save the approach curve and an image of the cell or measure its diameter. If the cell seems to slip away under the cantilever, the measurement has to be discarded, as this would yield a seemingly lower elastic modulus (*see Note 7*).
5. Continue to measure the next cell.

#### 3.4.2 Fully Adherent Cells

Measurements on fully adherent cells are conducted in the same way as for weakly adherent cells, with one major difference: Instead of a single force curve a force volume scan is recommended. Therefore, define a region of interest and an adequate spacing for a mesh grid. The force volume scan generates force–distance curves at every grid point, allowing the determination of spatially resolved elastic moduli or adhesion energies. Necessary forces may be adjusted to different values, depending on the defined regions of interest, as, e.g., the lamellipodium is significantly softer and very thin. Thus, high forces may yield too high elastic moduli of the lamellipodium because the cantilever “feels” the hard substrate below the cell.

### 3.5 Adhesive Measurement

#### 3.5.1 Weakly Adherent Cells

This paragraph describes the measurement for cells that just started to adhere and have thus a spherical shape.

1. After calibration, move the cantilever above one cell. Ensure to have separated cells, so that the cantilever cannot make contact with more than one cell when engaged (*see Fig. 1a*).
2. Engage the cantilever (*see Note 4*).
3. Generate a force–distance curve. Use the following settings: ramp size of 7 µm, a maximal force of 1 nN, approach speed of 5 µm/s, surface delay of 30 s, and at least 1024 measurement points (*see Note 8*).
4. If the approach and retract curve look satisfactory, without inflection points, indentations, or other discontinuities (*see Fig. 2a–c*), save the retract curve and an image of the cell or measure its diameter. If the cell seems to slip away under the cantilever, the measurement has to be discarded, as this would alter the result.
5. Continue to measure the next cell.

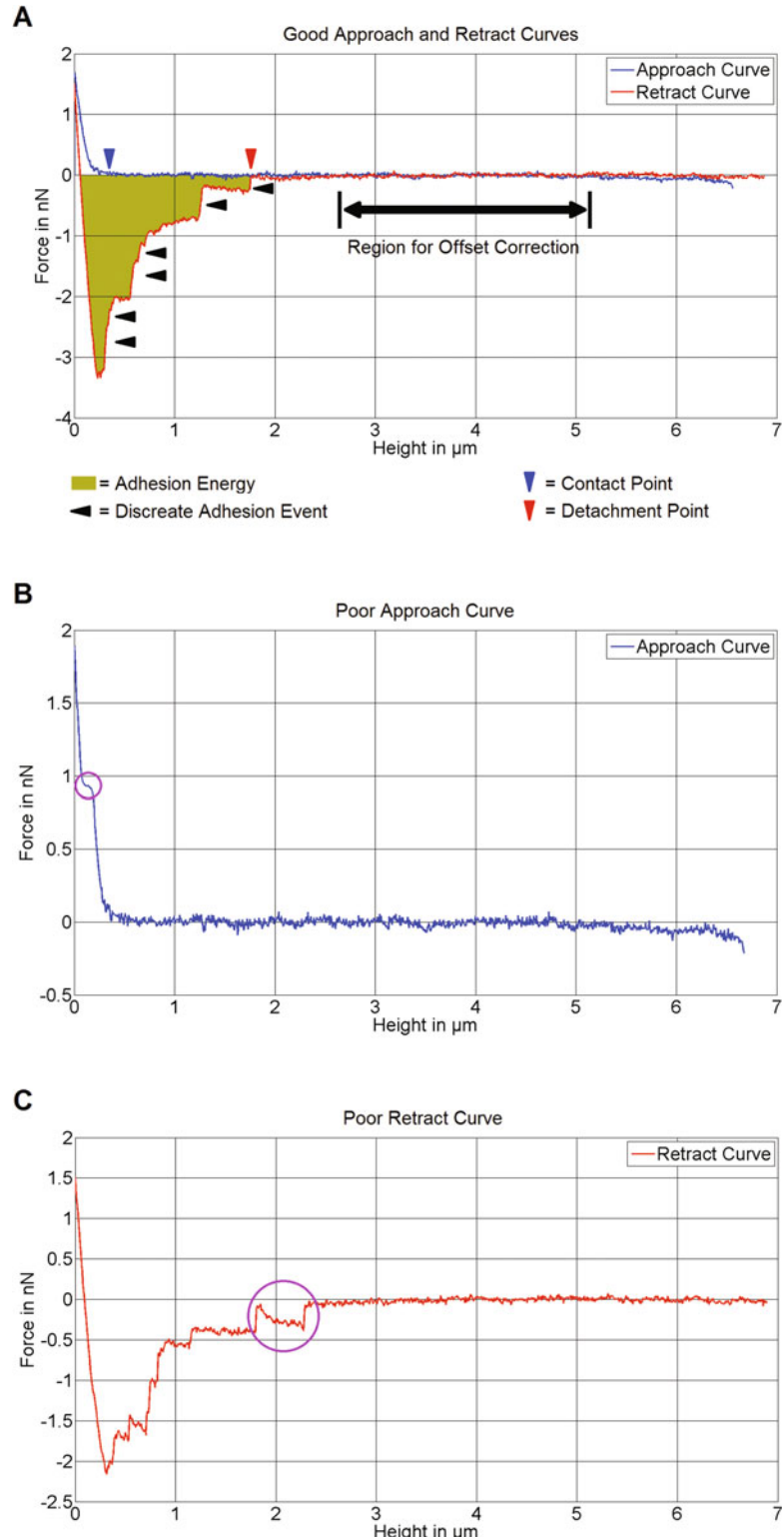


**Fig. 2** Typical good and poor approach and retract curves. (a) Example of a good approach and retract curve. Please denote the marked contact point between

### 3.5.2 Fully Adherent Cells

Adhesion measurements on fully adherent cells are conducted similarly as those performed with weakly adherent cells. Instead of a single force curve a force volume scan is recommended, with the same restrictions for the choice of maximal indentations forces as for the mechanical measurements on adhesive cells. Furthermore, the surface delay times need to be lowered, as cells might significantly reshape during the measurement time, if multiple points with a surface delay of 30 s are measured.

## 3.6 Data Analysis

### 3.6.1 Mechanical Measurements: Calculating the Young's Modulus

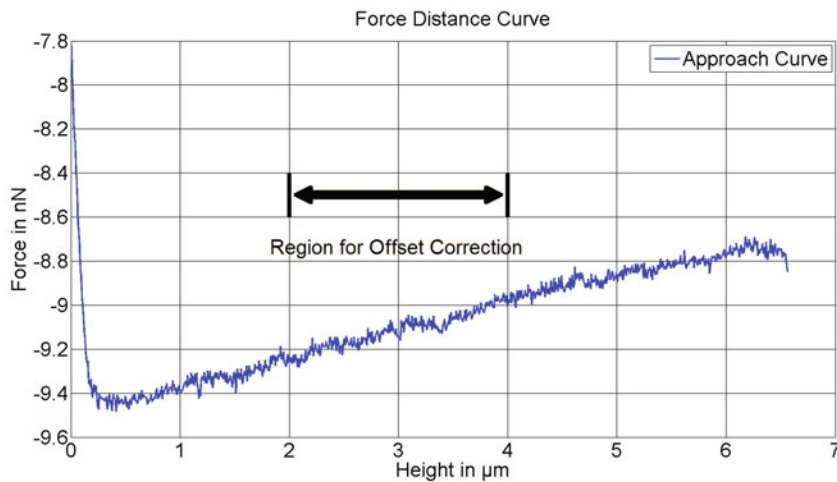
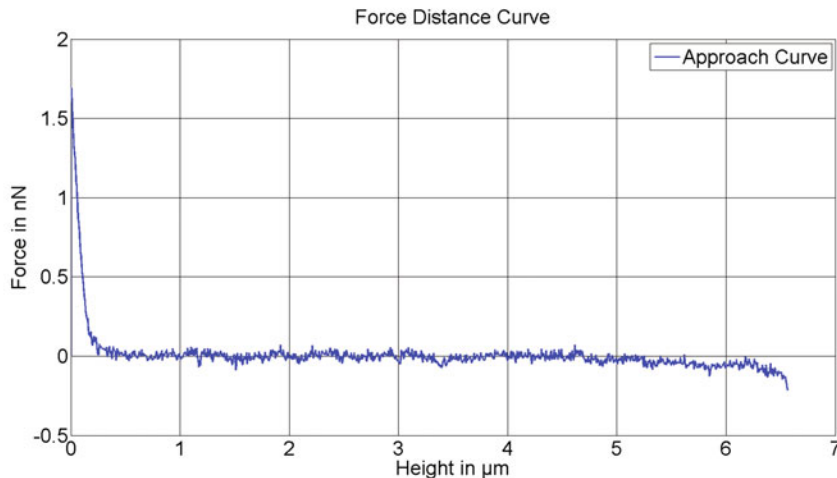
This paragraph describes the analysis for measurement of cells that just started to adhere and have thus a spherical shape.

1. Import approach curves into an adequate software, e.g., MatLab or NanoScope.
2. Correct the offset of the approach curve using a linear fit. Denote that the offset correction should be calculated in a region that is reasonably above the cell, as this region should on average display no signal (*see Figs. 2 and 3*).
3. Determine the contact point between cantilever and cell, as the first point the offset corrected force–distance curve has a force value significantly larger than zero (*see Fig. 2*).
4. Fit the Hertz model to the respective data and extract the effective Young's modulus  $E^*$ . The Hertz model is given by the following equation:  $F = \frac{4}{3} E^* \sqrt{R\delta^3}$ , with  $E^* = \frac{E}{1-\mu^2}$ . Here  $F$  denotes the measured force values,  $R$  the radius,  $E$  the Young's modulus,  $\mu$  the Poisson's ratio, and  $\delta$  the central indentation (deformation) of the cell (*see Note 9*).
5. It is best practice to use the effective Young's modulus  $E^*$  as final value, as the Poisson's ratio  $\mu$  is often unknown but supposed to be around  $\mu \approx 0.45\text{--}0.5$ .

Data analysis for fully adherent cells is performed almost identically to the one performed for weakly adherent cells, with only a slight difference in the used Hertz model. It now reads as follows:  $F = \frac{4}{3} E^* \sqrt{R\delta^3}$ , with  $E^* = \frac{E}{1-\mu^2}$ , and  $\frac{1}{R} = \frac{1}{R_1} + \frac{1}{R_2}$ . Here  $F$  denotes the measured force values,  $E$  the Young's



**Fig. 2** (continued) cantilever and cell (blue arrowhead) in the approach curve, as well as the detachment point in the retract curve (red arrowhead). Furthermore, discrete adhesion events are marked with black arrowheads. The yellowish area corresponds to the total adhesion energy. A typical region used for offset correction is also displayed. (b) Shows an approach curve of poor quality. The region marked with the violet circle is a clear anomaly and likely caused by a slippage of the measured cell under the cantilever. Such measurements should be discarded. (c) Depicts a retract curve of poor quality. The violet circle marks an anomalous region with decreasing force values during the detachment process. Such measurements need to be discarded

**A****Without Offset Correction:****B****With Offset Correction:**

**Fig. 3** Illustration of the offset correction process. (a) Shows an approach curve without offset correction and the region used for calculating the offset correction that is applied in (b). Note that the region above the cell can be clearly identified in (b) but not in (a)

modulus,  $\mu$  the Poisson's ratio, and  $\delta$  the central indentation (deformation) of the cell.  $R_{1/2}$  depicts the curvature of the cell or the radius of the bead glued to the cantilever, respectively.

### 3.6.2 Adhesive Measurement: Calculating Total Adhesion Energies

Evaluation of adhesion measurements for weakly and fully adherent cells is identical. For weakly adherent cells, the results represent a global adhesion parameter while the measurements for fully adherent cells give a spatial resolution of the adhesion.

1. Import retract curves into adequate software, e.g., MatLab or NanoScope.
2. Correct the offset of the retract curve using a linear fit. Denote that the offset correction should be calculated in a region that is reasonably above the cell, as this region should on average display no signal (*see* Figs. 2 and 3).
3. Determine the detachment point between cantilever and cell, as the first point the offset corrected force–distance curve has a force value significantly lower than zero (*see* Fig. 2).
4. Calculate the area of the retract curve that is below zero, using, for example, the Trapezoidal rule, using the given height resolution as step size. This gives the total measured adhesion energy. Additionally, the number of discrete rupture events, corresponding to a specific unbinding event between the cell and the cantilever coating, can be determined (*see* Fig. 2). Both are measures for adhesion.

## 4 Notes

1. Avoid multiple freeze–thaw cycles when using fibronectin, to maintain high quality. This is also valid for many other extracellular matrix components.  
Coatings with other adhesion molecules are also very well possible.
2. The exact cell number is not fixed. It needs to be adjusted in such a way that there is enough space between single cells, so that measurements can be performed without the cantilever touching multiple cells. Keep in mind that a too low cell number results in time-consuming searches for a cell.
3. The waiting time is necessary to allow partial adhesion so that cells do not slip away if brought into contact with the cantilever. For different cell lines, the time needed might be significantly prolonged or a coating of the petri dish with, e.g., poly-L-lysine is needed.
4. If engage was not successful, retract the cantilever and check whether the photodetector shows 0 V. If not, adjust it to 0 V and try to reengage. If the photodetector shows approximately 0 V, increase the set point and reengage.
5. Please denote that the obtained spring constant has to be corrected for the cantilever geometry and the used resonance

peak. For measurements in aqueous solution, the first resonance peak might not be fully visible. Enter necessary information into the respective input mask or multiply the resulting spring constant with the respective correction factor and change it manually. See, e.g., the “Practical Advice on the Determination of Cantilever Spring Constants” by Ben Ohler and sources within for more information [16]. For the Arrow TL-2 cantilevers, the correction factor for using the second resonance peak is 0.2511.

6. Denote that the models for calculating the elastic modulus presented here are valid in the linear elastic regime only. Consequently, adequate force values are cell type dependent, as too high forces may induce, e.g., strain hardening, rendering most elastic models invalid. Furthermore, the elastic modulus might depend on the approach velocity, thus this parameter has to be kept constant.

As the turnover times of the cytoskeleton can be in the order of 1 min and remodeling is induced by external forces multiple measurements of the same cell should be avoided.

7. If a high percentage of cells slip away under the cantilever try to either reduce the set point for engaging, the maximal forces applied to the cells or allow cells to adhere for longer times. If none of these approaches is successful, coat the petri dish with pro-adhesive substrates before cell seeding.
8. Keep in mind that the measured adhesion energies scale with the contact area between cantilever and cell. Consequently, the applied force should be kept constant and determined based on the elastic properties of the cell line. This is necessary in order to stay in a linear deformation regime and thus reduce measurement variance.

Furthermore, the surface delay should be chosen with care. Even though it is tempting to use long delay times, one has to consider that the cantilever starts to drift, distorting the measurement results. Additionally, due to turnover times of the cytoskeleton, applying forces for longer than 1 min may result in an adaptation of the cytoskeleton and thus alters measurements. For the same reason, multiple adhesion measurements of the same cell should be avoided.

9. Please note that the Hertz model has certain assumptions and limitations. It assumes that the contact between cell and cantilever is free of adhesion, which is mostly valid if the approach curve is used for determination of the Young’s modulus, as the contact time for full contact is low and thus adhesion can be neglected. If the retract curve is supposed to be used for calculation of the Young’s modulus, this assumption might be questionable, especially if the cantilever is coated or a surface

delay is used. Furthermore, the contact area between cantilever and cell needs to be small compared to the cell radius. This assumption is fulfilled, if measurement parameters are chosen adequately (*see also Note 6*), meaning a force that is adjusted to match the cells elastic modulus. As a rule of thumb, the indentation should not be larger than 10% of the cells height.

Additionally, the Hertz model assumes contact of two half-spheres, thus if a different combination of cell and cantilever (one spherical, one flat) is used, the model has to be adjusted. One critical requirement is the assumed isotropy of the Young's modulus, but without further a priori knowledge or severe modeling effort this issue cannot be easily resolved. Nevertheless, the Hertz model gives very good and reproducible results.

For more complex and sophisticated models, the interested reader is referred to the literature [6, 17–23].

## References

1. Binnig G, Quate CF, Gerber C (1986) Atomic Force Microscope. *Phys Rev Lett* 56 (9):930–933
2. Cappella B, Dietler G (1999) Force-distance curves by atomic force microscopy. *Surf Sci Rep* 34(1–3):1–104
3. De Pascalis C, Etienne-Manneville S (2017) Single and collective cell migration: the mechanics of adhesions. *Mol Biol Cell* 28 (14):1833–1846
4. Guck J, Schinkinger S, Lincoln B et al (2005) Optical deformability as an inherent cell marker for testing malignant transformation and metastatic competence. *Biophys J* 88 (5):3689–3698
5. Cross SE, Jin Y-S, Rao J et al (2007) Nanomechanical analysis of cells from cancer patients. *Nat Nanotechnol* 2(12):780–783
6. Iyer S, Gaikwad RM, Subba-Rao V et al (2009) AFM detects differences in the surface brush of normal and cancerous cervical cells. *Nat Nanotechnol* 4(6):389–393
7. Lekka M, Gil D, Pogoda K et al (2012) Cancer cell detection in tissue sections using AFM. *Arch Biochem Biophys* 518(2):151–156
8. Lekka M, Pogoda K, Gostek J et al (2012) Cancer cell recognition - mechanical phenotype. *Micron* 43(12):1259–1266
9. Li QS, Lee GYH, Ong CN et al (2008) AFM indentation study of breast cancer cells. *Biochem Biophys Res Commun* 374(4):609–613
10. Ochalek T, Nordt FJ, Tullberg K et al (1988) Correlation between cell deformability and metastatic potential in B16-F1 melanoma cell variants. *Cancer Res* 48(18):5124–5128
11. Remmerbach TW, Wottawah F, Dietrich J et al (2009) Oral cancer diagnosis by mechanical phenotyping. *Cancer Res* 69(5):1728–1732
12. Darling EM, Zauscher S, Block JA et al (2007) A thin-layer model for viscoelastic, stress-relaxation testing of cells using atomic force microscopy: do cell properties reflect metastatic potential? *Biophys J* 92(5):1784–1791
13. Swaminathan V, Mythreye K, Tim O'Brien E et al (2011) Mechanical stiffness grades metastatic potential in patient tumor cells and in cancer cell lines. *Cancer Res* 71 (15):5075–5080
14. Xu W, Mezencev R, Kim B et al (2012) Cell stiffness is a biomarker of the metastatic potential of ovarian cancer cells. *PLoS One* 7(10): e46609
15. Watanabe T, Kuramochi H, Takahashi A et al (2012) Higher cell stiffness indicating lower metastatic potential in B16 melanoma cell variants and in (2)-epigallocatechin gallate-treated cells. *J Cancer Res Clin Oncol* 138 (5):859–866
16. Ohler B (2007) Practical advice on the determination of cantilever spring constants. pp 1–12
17. Sokolov I, Iyer S, Subba-Rao V et al (2007) Detection of surface brush on biological cells in vitro with atomic force microscopy. *Appl Phys Lett* 91(2):2–4
18. Guz N, Dokukin M, Kalaparthi V et al (2014) If cell mechanics can be described by elastic modulus: study of different models and probes used in indentation experiments. *Biophys J* 107 (3):564–575

19. Smeets B, Cuvelier M, Pešek J et al (2019) The effect of cortical elasticity and active tension on cell adhesion mechanics. *Biophys J* 116 (5):930–937
20. Ding Y, Wang J, Xu GK et al (2018) Are elastic moduli of biological cells depth dependent or not? Another explanation using a contact mechanics model with surface tension. *Soft Matter* 14(36):7534–7541
21. Cartagena-Rivera AX, Logue JS, Waterman CM et al (2016) Actomyosin cortical mechanical properties in nonadherent cells determined by atomic force microscopy. *Biophys J* 110(11):2528–2539
22. Sneddon IN (1965) The relation between load and penetration in the axisymmetric boussinesq problem for a punch of arbitrary profile. *Int J Eng Sci* 3(1):47–57
23. Ding Y, Xu GK, Wang GF (2017) On the determination of elastic moduli of cells by AFM based indentation. *Sci Rep* 7:1–8



# Chapter 7

## Analyzing the Roles of Rho GTPases in Cancer Cell Adhesion to Endothelial Cells Under Flow Conditions

Camilla Cerutti and Anne J. Ridley

### Abstract

Adhesion between cancer cells and endothelial cells, lining the blood vessels, is an important event in tumor progression and metastasis formation. The expression of Rho GTPases is frequently altered in cancers, and they are known to regulate cell migration through their effects on adhesion and cytoskeletal dynamics. Several different types of assays are used to investigate how cancer cells attach to and cross the endothelium. Here, we describe an *in vitro* technique to study the effects of Rho GTPases on human cancer cell adhesion to endothelial cells under shear stress coupled to live cell imaging.

**Key words** Rho GTPases, Cancer cells, Endothelial cells, Cell adhesion, Shear stress, Live cell imaging, siRNA-mediated knockdown

---

### 1 Introduction

The interaction of circulating immune cells with endothelial cells lining the blood stream is essential for immunosurveillance, defense against pathogens, and repair of tissue damage [1]. In cancer progression, the ability of circulating tumor cells to interact with target organ endothelial cells [2] under blood shear stress [3] is an important step in the metastatic process. A variety of cell adhesion molecules and signaling proteins have been implicated in cancer cell attachment to endothelial cells. These include Rho GTPases, which are well known to regulate cell adhesion molecules [2, 4].

Most Rho GTPases cycle between an active GTP-bound and inactive GDP-bound form [5]. When bound to GTP, they interact with their effectors to stimulate signaling networks involved in cell adhesion in both endothelial cells [4] and cancer cells [2, 6]. The expression of Rho GTPases and/or their regulators and their targets is frequently altered in a variety of cancer types [7–9], including prostate cancer [10–13]. The Rho GTPases RhoA, RhoB, and Rac1 are also mutated in some cancers [14]. Rho GTPases have been implicated in several steps of cancer progression, including

proliferation, invasion, and metastatic dissemination [15–18]. Several studies have investigated the contribution of Rho GTPases in cancer cells to their adhesion to endothelial cells under static conditions [19, 20], as well as to crossing the endothelium either in endothelial cell-coated Transwells or in 3D assays [21, 22].

Here, we describe a method to study the role of Rho GTPases in cancer cell adhesion to endothelial cells, using transient depletion via siRNAs to reduce Rho GTPase expression in PC3 prostate cancer cells. The technique described in this chapter is adapted from previous assays described in [23] and [24, 25], to study the dynamic interaction and firm adhesion between cancer cells and endothelial cells in real time under shear-stress. The shear stress component is similar to the *in vivo*-like mechanical forces of the blood in the vasculature (hemodynamic forces) which has been shown to be crucial for immune cell and cancer cell adhesion [25–28]. Using a commercially available ibidi® flow chamber that accommodates human endothelial cell monolayers in channels, we set up a system that mimics circulating cancer cells in the vasculature. In the assay, cancer cells are perfused into the endothelial monolayer-coated channels at controlled speeds to study their shear stress-resistant firm adhesion with live cell imaging. This technique allows the real-time visualization of control and Rho GTPase-depleted human cancer cells interacting with and adhering to human endothelial cells, which is one of the steps in the complex process of metastasis formation. Furthermore, this technique can be easily adapted to a variety of different studies aimed to quantify cancer cell behavior with endothelial cells under shear stress conditions produced by fluid flow.

---

## 2 Materials

### 2.1 Cell Culture

1. PC3 prostate cancer cells (ATCC) (*see Note 1*).
2. PC3 complete medium: Roswell Park Memorial Institute 1640 medium (RPMI-1640) with L-glutamine, 25 mM Hepes, 100 µg/ml streptomycin, and 100 U/ml penicillin supplemented with 10% heat-inactivated fetal calf serum (FCS). Store at 4 °C.
3. Trypsin–EDTA to detach cells (store at 4 °C).
4. Phosphate-buffered saline (PBS) without magnesium ( $MgCl_2$ ) and calcium ( $CaCl_2$ ) ( $PBS^{-/-}$ ).
5. Phosphate-buffered saline (PBS) with magnesium ( $MgCl_2$ ) and calcium ( $CaCl_2$ ) ( $PBS^{+/+}$ ).
6. ibidi® µ-Slide VI<sup>0.4</sup> (ibidi® GmbH), tissue culture treated uncoated. For technical features and specifications, see <https://ibidi.com/channel-slides/57%2D%2Dslide-vi-04.html>.

7. Pooled primary human umbilical vein endothelial cells (HUVECs), P0 purchased from Lonza.
8. HUVEC complete medium: EBM™-2 basal medium (Lonza) with SingleQuots™ kit supplements rhEGF, VEGF, IGF, rhFGF, gentamycin, ascorbic acid, hydrocortisone, and fetal bovine serum (FBS) (as per manufacturer's instructions—concentrations not disclosed; Lonza). Store at 4 °C (*see Note 2*).
9. 10 µg/ml fibronectin (Calbiochem, Merck Millipore) in PBS<sup>+</sup> (50 ml, store at 4 °C) to coat flasks and ibidi® µ-Slide VI<sup>0.4</sup> for HUVEC culture.
10. Tissue culture light microscope.
11. Neubauer chamber to count cells.

## **2.2 siRNA Nucleofection**

1. Lonza nucleofection kit for PC3 cells (*see Note 3*) (store at 4 °C) with supplied certified cuvettes and supplied plastic pipettes.
2. Amaxa Nucleofector II device (Lonza).
3. 75 nM of siGENOME individual siRNAs, control siRNA, and siRNAs targeting Rho GTPase mRNAs (Dharmacon, Horizon Discovery); prepare a stock at 20 µM as per the manufacturer's instructions (i.e., 1 nmol siRNA in 50 µl 5x siRNA buffer for 20 µM stock) and store at –20 °C in 10–50 µl aliquots (*see Note 4*).

## **2.3 Cancer Cell Fluorescent Labeling**

1. 5 mM 5-chloromethylfluorescein diacetate (CMFDA) green (Ex = 495 nm, Em = 521 nm), (Life Technologies) in DMSO. Store at –20 °C in 10–20 µl aliquots.
2. RPMI-1640 with L-glutamine, 25 mM Hepes, 100 µg/ml streptomycin, and 100 U/ml penicillin (store at 4 °C).
3. Nonenzymatic cell dissociation buffer (Merck Millipore), store at 4 °C.

## **2.4 Flow Adhesion Assay**

1. Inverted time-lapse microscope with environmentally controlled chamber (37 °C, 5% CO<sub>2</sub>) and digital camera for fast acquisition. A Nikon Eclipse TE2000-E microscope (Nikon Plan Fluor 10×/0.30 Ph1 DL objective), equipped with a Hamamatsu ORCA-ER digital camera, was used to perform the assay described here. Place a clean piece of absorbent paper on top of the environmental chamber or in the space adjacent to the microscope (*see Note 5*).
2. Micromanager software for imaging acquisition, free to download from <https://micro-manager.org/> (*see Note 6*).
3. Hamilton glass syringes (5 or 10 ml) coupled to a high precision pump with withdraw/pull option (*see Note 7*) (placed on

microscope table/bench on the side/small trolley stand). A PHD ULTRA (Harvard Apparatus) was used here.

4. Rack for 50 ml tubes.
5. Two tubing hose clips (ibidi®).
6. Three timers.
7. Tubing and connectors to assemble the “flow system” as described in Fig. 1:

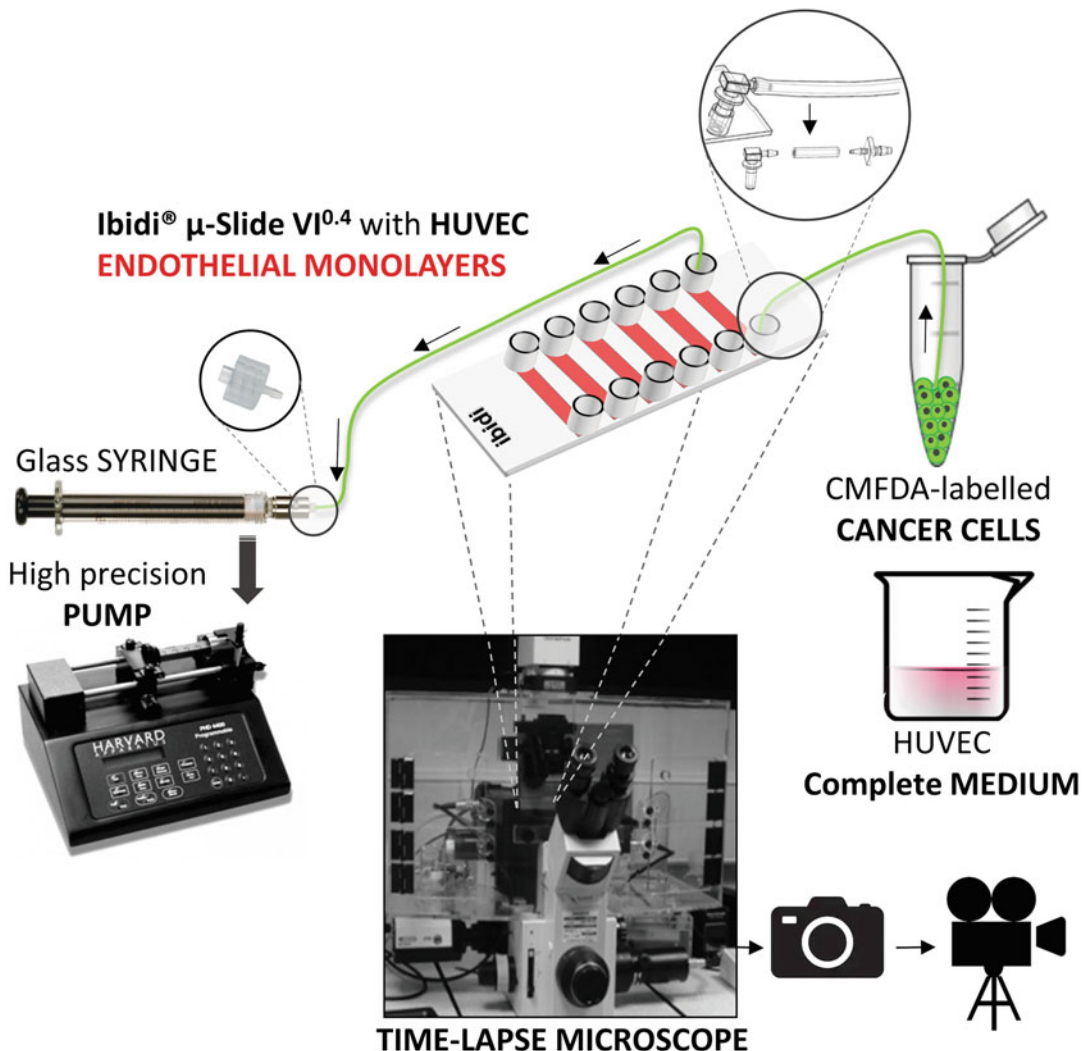


**Fig. 1** Flow-based assay of cancer cell adhesion to endothelial cells coupled to live cell imaging. Schematic representation of how the system of connectors/tubing/ibidi® μ-Slide<sup>VI</sup> is assembled and connected to the pump/syringe, with an enlargement to illustrate the ibidi® connectors for the μ-Slide<sup>VI</sup> channel inlet and glass syringe to create the “flow system” (taken from [www.ibidi.com](http://www.ibidi.com)). Once assembled, the system is placed inside an inverted time-lapse microscope environmentally controlled chamber for live cell imaging where one frame/s is captured and rendered as a movie.

- (a) ibidi®  $\mu$ -Slide channel elbow male Luer connectors for  $\mu$ -slide VI 0.4 flow kit (ibidi®).
- (b) Female Luer Lock Coupler (ibidi®).
- (c) Y connectors with 400 Series Barbs 3/32" Natural Polypropylene (Value Plastic, Inc.).
- (d) Female Luer Lug Style to classic series barb 1/16" Natural Polypropylene (Value Plastic, Inc.).
- (e) Tubing Tygon 3350 Sanitary Silicone Tubing (Saint-Gobain).
- (f) Three-way stopcock with male Luer lock adapter and port covers (Kendall Argyle™EZ-FLO™).

## 2.5 Quantification

1. ImageJ (NIH) or FIJI (they are the same program), free to download from <https://imagej.nih.gov/ij/>, with cell counter plug-in (downloadable from <https://imagej.nih.gov/ij/plugins/cell-counter.html>).

## 3 Methods

### 3.1 PC3 Cell Culture

1. Thaw PC3 cells from frozen aliquots in a water bath at 37 °C.
2. Seed into a 75 cm<sup>2</sup> flask containing 15 ml of PC3 complete medium.
3. Maintain cells at 37 °C in a tissue culture incubator (37 °C, 5% CO<sub>2</sub>) and change medium after 24 h.
4. When cells reach 80% confluence, passage them by removing the medium from the flask and washing cells with 5 ml of PBS<sup>+/+</sup>.
5. Aspirate the PBS<sup>+/+</sup> and add 5 ml of PBS<sup>-/-</sup>.
6. Aspirate the PBS<sup>-/-</sup> and add 5 ml of trypsin-EDTA and leave the flask in the incubator (37 °C, 5% CO<sub>2</sub>) for 5 min.
7. Add 10 ml of PC3 complete medium (37 °C) to inactivate the trypsin-EDTA.
8. Centrifuge cells for 7 min at 200  $\times$  g.
9. Resuspend cells in PC3 complete medium and seed PC3 cells into culture flasks to maintain the cells or for use in experiments.
10. Split cells at between 1:3 and 1:5 and change the medium every 2–3 days.
11. To improve experimental consistency, discard PC3 cells after 1 month of culture and defrost a fresh cell aliquot.

### **3.2 siRNA Transfection of PC3 Cells**

1. siRNA transfection is carried out 72 h before the flow assay.
2. Prepare a  $75\text{ cm}^2$  flask for each siRNA condition with 8 ml of PC3 complete medium in a tissue culture hood and put the flasks in a tissue culture incubator ( $37^\circ\text{C}$ , 5% CO<sub>2</sub>).
3. Thaw siRNAs on ice (control siRNA and siRNAs targeting Rho GTPase of interest).
4. Trypsinize a  $75\text{ cm}^2$  flask of PC3 cells (*see Subheading 3.1*), count the cells in a Neubauer chamber, centrifuge  $2 \times 10^6$  PC3 cells in a 15 ml tube per siRNA, and aspirate the medium leaving the pellet untouched.
5. Prepare the nucleofection mix as per the manufacturer's instructions: for each siRNA, use 82  $\mu\text{l}$  of Nucleofector® Solution plus 18  $\mu\text{l}$  of supplement to make 100  $\mu\text{l}$  of "nucleofection mix" total reaction volume in an RNase-free centrifuge tube. For PC3 cells, the Cell Line Nucleofector™ Kit V (Lonza) is recommended (*see Note 8*).
6. Mix  $2 \times 10^6$  PC3 cells with each "nucleofection mix."
7. Add 75 nM of each siRNA to each "nucleofection mix" and transfer to a cuvette (*see Note 9*).
8. Insert the cuvette in the Amaxa Nucleofector II device and run with the T-013 program, as per the manufacturer's instructions, and press "start."
9. Quickly take a flask from the incubator into the tissue culture hood, and then transfer all the nucleofected PC3 cells into the flask as per the manufacturer's instructions with the provided single-use plastic pipette.
10. Tilt the flask to distribute the cells and put it back in the incubator ( $37^\circ\text{C}$ , 5% CO<sub>2</sub>).
11. Repeat steps 8–10 for each siRNA "nucleofection mix."
12. Change the medium after 12–16 h with fresh PC3 complete medium ( $37^\circ\text{C}$ ).
13. Use PC3 cells 72 h after siRNA nucleofection.

### **3.3 HUVEC Cell Culture**

1. Coat a  $75\text{ cm}^2$  flask with 4 ml of 10  $\mu\text{g}/\text{ml}$  fibronectin for 1 h in a tissue culture incubator ( $37^\circ\text{C}$ , 5% CO<sub>2</sub>).
2. Aspirate the fibronectin and add 15 ml of HUVEC complete medium at  $37^\circ\text{C}$ .
3. Put the flask in the incubator ( $37^\circ\text{C}$ , 5% CO<sub>2</sub>) to equilibrate the medium.
4. Thaw HUVECs from frozen aliquots in a water bath at  $37^\circ\text{C}$ .
5. Take the fibronectin-coated  $75\text{ cm}^2$  flask from the incubator, add the thawed HUVECs, and put it back in the incubator.

6. Maintain cells at 37 °C in a tissue culture incubator (37 °C, 5% CO<sub>2</sub>) and change medium after 6 h.
7. When cells reach 100% confluence, passage them by removing the medium from the flask and washing cells with 5 ml of PBS<sup>+/+</sup>.
8. Aspirate the PBS<sup>+/+</sup> and add 5 ml of PBS<sup>-/-</sup>.
9. Aspirate the PBS<sup>-/-</sup> and add 2 ml of trypsin–EDTA and leave the flask in the incubator (37 °C, 5% CO<sub>2</sub>) for 5 min.
10. Add 10 ml of HUVEC complete medium (37 °C) to inactivate the trypsin–EDTA.
11. Count the cells with a Neubauer chamber.
12. Centrifuge cells for 5 min at 200 × g.
13. Resuspend cells in HUVEC complete medium and seed HUVECs into culture flasks to maintain the cells or for use in experiments.
14. Use HUVECs at passage P1 to P4 (times of cell trypsinization) and change the medium every 2 days.

### **3.4 HUVEC Seeding in Ibidi® μ-Slide VI<sup>0.4</sup> 48 H Pre-Assay**

1. Coat all 6 channels of the ibidi® μ-Slide VI<sup>0.4</sup> with 30 µl of 10 µg/ml fibronectin, using a p200 micropipette, then incubate for 1 h in a tissue culture incubator (37 °C, 5% CO<sub>2</sub>).
2. Prepare HUVECs (*see* Subheading 3.3) in HUVEC complete medium (warmed to 37 °C) at a concentration of 2 × 10<sup>6</sup>/ml.
3. Wash the ibidi® μ-Slide VI<sup>0.4</sup> channels with 120 µl of warm (37 °C) PBS<sup>+/+</sup>.
4. Aspirate the PBS<sup>+/+</sup> from the channel inlets.
5. Seed 30 µl of HUVECs (2 × 10<sup>6</sup>/ml) per channel making sure to add the cells in one single go, to allow cells to reach the other end of the channel and distribute equally in the channel area (*see* Note 10).
6. Check the cells are distributed equally in the channel area under a microscope and then repeat step 5 for the other 5 channels.
7. Put the ibidi® μ-Slide VI<sup>0.4</sup> chamber in the incubator (37 °C, 5% CO<sub>2</sub>) for 30 min.
8. Replenish the ibidi® μ-Slide VI<sup>0.4</sup> chamber channels with 120 µl of HUVEC complete medium heated to 37 °C.
9. Change medium after 12 h (24 h after seeding) with fresh HUVEC complete medium (37 °C).
10. Put the chamber back in the incubator (37 °C, 5% CO<sub>2</sub>).
11. Put a 50 ml tube with HUVEC complete medium in the incubator (37 °C, 5% CO<sub>2</sub>) overnight to equilibrate it for the flow-based adhesion assay.

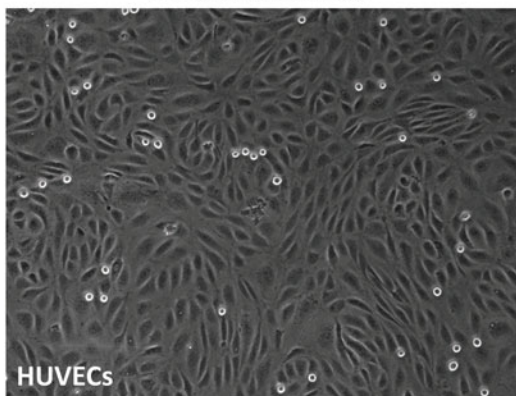
### 3.5 Microscope Setup for Live Imaging

1. Turn on the microscope to allow the stage to reach the indicated environmental conditions ( $37^{\circ}\text{C}$ , 5%  $\text{CO}_2$ ) for at least 2 h.
2. Set the magnification for the time-lapse movie acquisition. Here, we used a  $10\times$  objective (Fig. 2).
3. Set the acquisition channels to capture images of cancer cells (labeled with the fluorophore CMFDA;  $\text{Ex} = 495\text{ nm}$ ,  $\text{Em} = 521\text{ nm}$ ) and endothelial cells using fluorescence and phase contrast detection simultaneously. Here we use a configuration where we use one single fluorescent filter cube to allow rapid acquisition time. The acquisition of fluorescence and phase contrast images could be sequential as long as they are very close in time (1 frame/s).
4. Customize the exposure (ms) time of the bright field and fluorescence channels based on the intensity of your sample. We keep the lamp power between 0 and 18% to minimize fluorophore bleaching.
5. Set the acquisition time at 1 frame/s for 10 min (the adhesion assay is 6 min in total, then after the end of the experiment some extra acquisition time is required to take pictures of different field of views; however, it should not take more than 1 min) (see Note 11).
6. In the acquisition setting of memory function, set “record while acquiring.”
7. In the acquisition setting of live stream recording, set “allow stage movement while acquiring”—to take ten different pictures along the ibidi®  $\mu$ -Slide channel.
8. In the acquisition setting, set “save as” always in the acquisition software file format (for example, ome or .lif).
9. Save these settings (steps 2–8), to apply them to all the experimental technical replicate acquisitions.

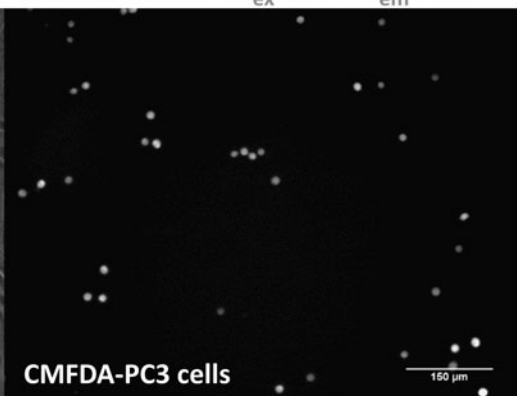
### 3.6 “Flow System” Setup

1. Connect the silicon tubing with Female Luer Lug Style classic series barb 1/16 connectors to the Hamilton glass syringe, coupled to the PHD ULTRA pump, to start create the “flow system,” as shown in Fig. 1, enlargement on the syringe.
2. Connect the other end of silicon tubing with an elbow male Luer connector, then the female Luer Lock Coupler, and another male Luer connector (ibidi®), as shown in Fig. 1.
3. Connect the Luers (enlarge in Fig. 1) to the ibidi®  $\mu$ -Slide VI<sup>0.4</sup> chamber channel inlet and outlet as shown in the ibidi movie: <https://ibidi.com/content/150-mv-21>.

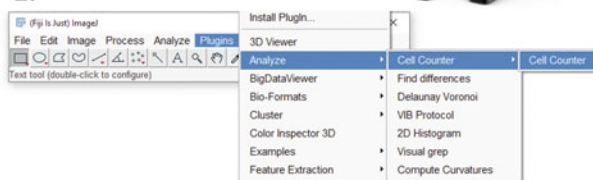
## Phase contrast



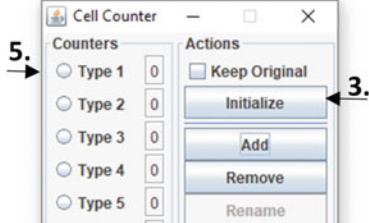
## Fluorescence $\lambda_{\text{ex}} = 495 \text{ nm}$ , $\lambda_{\text{em}} = 521 \text{ nm}$



2.



1. Open file microscope acquisition in ImageJ or Fiji

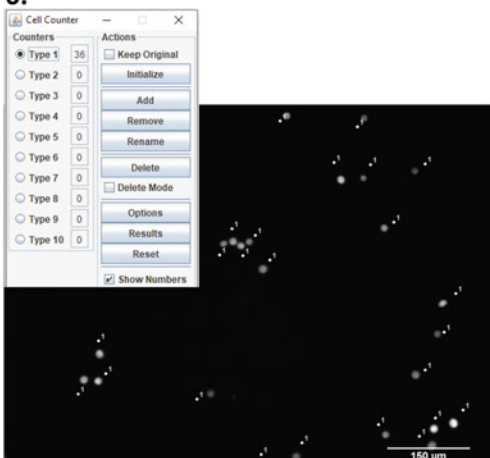


2. Open in ImageJ or Fiji  
Plugins> Analyse>Cell counter

3. Click initialize  
on the counter window

4. Click on the open movie and select the  
frame to analyse  
in the fluorescent channel  
i.e. right panel in the picture (top)

6.



5. Select Type 1 in the cell counter window

6. To quantify the number of cancer cells  
adhered on endothelial cells,  
clicking on the cells in the movie window,  
a 1 will appear on cells quantified.

7. To quantify the next field of view, select  
the frame in the movie and click Type2 on  
cell counter and repeat 6.

4. Finally, connect another piece of tubing of the desired length, which connects the “flow system” with the tube containing cancer cells or medium (Fig. 1).
5. Wash the “flow system” with 70% ethanol, and then wash with PBS<sup>+/+</sup> (37 °C) withdrawing with the pump at 1 or 2 dyn/cm<sup>2</sup> (see Note 12).
6. Introduce the “flow system” (except the pump, which can be placed on the microscope table/bench on the side/small trolley stand; Fig. 1) into the environmentally controlled chamber (37 °C, 5% CO<sub>2</sub>) of the time-lapse microscope and perform another wash with warm PBS<sup>+/+</sup> at 0.5 dyn/cm<sup>2</sup> (see Note 13). After the wash, leave the “flow system” inside the environmentally controlled chamber and switch off the pump (see Note 14).
7. Take the 50 ml tube with HUVEC complete medium equilibrated overnight in the incubator (see Subheading 3.4, step 3) and use it to perform another two washes of the “flow system” in the time-lapse microscope environmentally controlled chamber.
8. Set the flow rate ( $\theta$ ) applied to produce the required shear stress  $\tau$  (dyn/cm<sup>2</sup>).
  - (a) For the ibidi® μ-slide VI, the flow rate is calculated according to the equation:

$$\tau \text{ [dyn/cm}^2\text{]} = \eta \text{ [(dyn*s)/cm}^2\text{]} \cdot 176.1 \Phi \text{ ml/min}.$$

where the relationship between shear stress ( $\tau$ ) and flow rate ( $\Phi$ ) is based on the dynamic viscosity ( $\eta$ ) of water at 22 °C,  $\eta = 0.01$  dyn·s/cm<sup>2</sup> and other parameters specific to the geometry of the system based on the ibidi® μ-Slide geometry.

- (b) Shear stress ( $\tau$ ) is calculated according to  $\tau = 176.1 \eta \Phi$  ( $\eta = 0.01$ ,  $\Phi$  = volumetric flow rate). For more detailed information on the parameters to determine shear stress for vessel blood flow, see [23] Table S1 in Additional file 2.
- (c) Based on the ibidi® μ-Slide VI<sup>0.4</sup> geometries, cancer cells are pulled through the system for:  
30 s at 0.5 dyn/cm<sup>2</sup> (0.28 ml/min) to allow PC3 cells to enter in the channel,  
4 min and 30 s at 0.05 dyn/cm<sup>2</sup> (1.7 ml/h): ACCUMULATION TIME,  
1 min at 1 dyn/cm<sup>2</sup> (0.57 ml/min): CELL CHALLENGE TIME.

### **3.7 Cancer Cell Preparation for the Flow Assay**

1. Dye-label the siRNA-transfected PC3 cells: Aspirate the culture medium, wash once with PBS<sup>+/+</sup>.

2. Add 4 ml per flask of 5 mM CMFDA cell tracker green in RPMI without FCS and leave the flasks in the incubator (37 °C, 5% CO<sub>2</sub>) for 30 min.
3. Confirm that the PC3 cells are treated with CMFDA fluoresce green when excited at 488 nm under the time-lapse microscope.
4. Wash the PC3 cells twice with PBS<sup>-/-</sup>, 4 ml/flask.
5. Add 4 ml per flask of warm (37 °C) nonenzymatic cell dissociation buffer and leave the flasks in the incubator (37 °C, 5% CO<sub>2</sub>) for 30 min (*see Note 15*).
6. Take the flask containing PC3 cells from the incubator, gently tap on the side of the flask, and observe with a tissue culture microscope to determine whether all the PC3 cells are detached. If not, leave them 5–10 min longer.
7. Once PC3 cells are all detached, add 6 ml of warm (37 °C) PC3 complete medium to the flask, and transfer all the cells into a 50 ml tube.
8. Count the PC3 cells with a Neubauer chamber.
9. Take  $2 \times 10^5$  cells for siRNA transfection efficiency test (Western blot or qPCR, if there is not good antibody for the chosen Rho GTPase) and centrifuge the remaining cells for 7 min at 200 × g at room temperature.
10. Remove medium then resuspend PC3 cancer cells well in 1 ml of fresh warm (37 °C) HUVEC complete medium.
11. Add fresh warm (37 °C) HUVEC complete medium to PC3 cells at a concentration of  $2 \times 10^6$  cells/ml (*see Note 16*). Place the fluorescently labeled PC3 cells in the time-lapse microscope environmentally controlled chamber for the flow assay.

### **3.8 Endothelial Cell Preparation for the Flow Assay**

1. Take the ibidi® μ-Slide VI<sup>0.4</sup> chamber with HUVECs from the tissue culture incubator and change medium with 120 µl fresh warm (37 °C) HUVEC complete medium.
2. Connect the ibidi® μ-Slide VI<sup>0.4</sup> chamber to the “flow system” set in Subheading 3.6 (*see Note 17*) as follows:
3. Take the “flow system” out of the time-lapse microscope environmentally controlled chamber, and place it on top of a clean piece of absorbent paper (*see Note 18*).
4. Clip the tubing near the ibidi® μ-Slide VI<sup>0.4</sup> chamber inlet and outlet with the two tubing hose clips (ibidi®) as per the manufacturer’s instructions (see movie at min 7:46 <https://ibidi.com/content/150-mv-21>).
5. Open the ibidi® μ-Slide VI<sup>0.4</sup> chamber containing HUVECs and add 30 µl of fresh HUVEC complete medium to the first channel, closing the lids on the five remaining channels (in this

step, you lose the sterility working in the microscope area) (*see Note 19*).

6. Carefully detach the inlet and outlet Luer connectors (as shown in the manufacturer's instructions movie at min 8) and plug it into the ibidi®  $\mu$ -Slide VI<sup>0.4</sup> chamber with HUVEC first channel inlets (*see Note 20*).
7. Make sure the system is without air bubbles.
8. Unclip the tubing hose clips.
9. Put the system back with the ibidi®  $\mu$ -Slide VI<sup>0.4</sup> chamber containing HUVECs inside the time-lapse microscope environmentally controlled chamber making sure that the chamber is not wet.
10. Secure the ibidi®  $\mu$ -Slide VI<sup>0.4</sup> chamber containing HUVECs on the microscope stage and position the stage in order to visualize the middle of the channel using a 5 $\times$  objective first, then with 10 $\times$  objective. This will be the field of view of the experiment for PC3 cell adhesion to HUVECs under flow.

### **3.9 Flow-Based Adhesion Assay Coupled to Live Cell Imaging**

1. In the time-lapse microscope environmentally controlled chamber, connect the tube containing CMFDA-labeled PC3 cells ( $2 \times 10^6$  cells/ml) to the "flow system" (Fig. 1) and the HUVEC complete medium tube left overnight in the incubator to equilibrate (*see Subheading 3.3, step 3*), beside the PC3 cell tube.
2. Set the inverted fluorescence time-lapse microscope for acquisition (setting in Subheading 3.5).
3. Set the pump in withdraw/pull direction at 0.5 dyn/cm<sup>2</sup> (*see Subheading 3.6, step 8c*) (*see Note 21*).
4. Set 3 timers: two for the pump (30 s, timer 1; and 4 min and 30 s; timer 2), and the third for the microscope acquisition (6 min, timer 3) (*see Note 22*).
5. Start the pump, the microscope acquisition, and timer 1 (30 s) and timer 3 (6 min).
6. While the pump is pulling cells at 0.5 dyn/cm<sup>2</sup>, set the pump to 0.05 dyn/cm<sup>2</sup> (Harvard pumps allow this option).
7. After 30 s (timer 1) switch to 0.05 dyn/cm<sup>2</sup> (by this time, cancer cells should have reached the channel of the ibidi®  $\mu$ -Slide, and cancer cells will be observed to flow into the channel and interact with the endothelial cell monolayer), and start timer 2.
8. While the pump is pulling cells at 0.05 dyn/cm<sup>2</sup>, set the pump to 1 dyn/cm<sup>2</sup> (Harvard pumps allow this option). Just before 4 min and 30 s (timer 2), switch the connection from PC3 cell tube to the HUVEC complete medium tube. At 4 min and 30 s

(timer 2), increase the speed of the pump to 1 dyn/cm<sup>2</sup> set previously to wash off loosely adhered PC3 cells (*see Note 23*) for 1 min, until timer 3 goes off.

9. The movie will end at 6 min (timer 3), resulting in 360 frames (1/s) until this point.
10. At 6 min (timer 3), move the stage/chamber vertically along the middle of the ibidi® μ-Slide channel to acquire images of ten different fields of view while the microscope acquisition is still ongoing.
11. When ten different fields of view are acquired, stop the acquisition in the microscope software and the pump. Repeat **step 2** of Subheading 3.8 and **steps 1–10** of Subheading 3.9 for each ibidi® μ-Slide VI<sup>0.4</sup> chamber channel/siRNA condition/technical replicate (we normally perform two technical replicates for each siRNA).
12. Perform strong washes with warm (37 °C) PBS<sup>-/-</sup> between each ibidi® μ-Slide VI<sup>0.4</sup> chamber channel/experimental replicate.

### **3.10 Quantification of Images**

1. Keep the file in the acquisition software file format (for example, ome or .lif) and then save a copy in TIFF if you have limited data storage space (*see Note 24*).
2. For quantification, firm adhesion of PC3 cells to endothelial cells is defined by PC3 cells that remain adhered to HUVECs in the fields of view throughout the accumulation time (5 min), and after increasing the flow to 1 dyn/cm<sup>2</sup> (1 min), the cell challenge time.
3. Firmly adhered cells (as shown in Fig. 2) are manually counted on fluorescence images with ImageJ software in 10 different fields of view per condition in a single ibidi® μ-Slide VI<sup>0.4</sup> chamber channel (for each of the two technical replicates per siRNA).
4. Open the movie to analyze with ImageJ (Fig. 2.1).
5. Open> Plugins> Analyse>Cell counter (Fig. 2.2).
6. Click initialize on the counter window (Fig. 2.3).
7. In the movie window, go to the frame number 360 (last frame at min 6) of the acquisition in the FITC channel (Fig. 2.4).
8. Select cell type 1 in the cell counter (Fig. 2.5).
9. Click on each of the cells in the frame to count them (Fig. 2.6).
10. After finishing the first frame, go to the next frame (field of view), click on cell count type 2, and repeat **step 9**. Repeat to quantify cells in all 10 fields of view (Fig. 2.7).

To quantify the number of PC3 cells firmly adhered to HUVECs, calculate the mean number of PC3 cells firmly adhered per field of view from the number in each of the 10 different fields of view of one ibidi® μ-Slide channel (one condition/one technical replicate). You can perform two technical replicate per siRNA condition with nucleofected PC3 cells from one 75 cm<sup>2</sup> flask. For quantification, average the means of each technical replicate.

---

## 4 Notes

1. We use human PC3 prostate cancer cells, but you can use any cancer cells of your interest, provided they can attach to endothelial cells from the same organism (human, mouse).
2. It is possible to buy HUVECs from another company and/or to use any type of endothelial cells of choice; however, you must titrate the concentration of endothelial cells seeded and coat the ibidi chambers with extracellular matrix recommended by the manufacturer. It is also possible to purchase ibidi® μ-Slides coated with different extracellular matrix components.
3. Based on the cancer cells you intend to use for the assay, you must select the appropriate nucleofection kit. For this assay, we tested Oligofectamine to transfect siRNAs into PC3 cells; however, it increased PC3 cell:cell attachment (clumping), not ideal for this type of assay.
4. siRNAs targeting each Rho GTPase can be purchased from other companies.
5. It is recommended to have a long working distance objective to capture the endothelial monolayer and the adhered cancer cells within one focal plane. The acquisition can be performed with either a 10× or 20× objective, depending on the microscope and camera you use for acquisition. The field of view size can change drastically depending on the camera you use, for example.
6. It is possible to use any precision pump of your choice and to use two separate pumps to change the flow rate.
7. Use a pump with this option available as a setting.
8. Leave the Nucleofector at room temperature and do not keep the mix longer than 15 min (as per the manufacturer's instructions).
9. Be careful not to produce air bubbles while mixing.
10. As described in the manufacturer's instructions at min 4:56 in this movie: <https://ibidi.com/content/150-mv-21>.
11. If your microscope has high-performance specifications, it is possible to acquire multiple positions within a channel or

z-stacks in a single position. The assay can be modified based on the scientific question and/or the available instrumentation.

12. In this process, no air bubbles should enter in the system. If air bubbles form along the system, in the tubing, for example, they must be removed from the system with continuous washouts, until they reach the glass syringe. A three-way stopcock can be used to connect the tubing to the syringe to empty the syringe, without removing it from the pump. See application note 31 of ibidi® to learn how to avoid forming bubbles during the slide preparation and how to recognize air bubbles trapped in the in the system reservoirs: [https://ibidi.com/img/cms/support/AN/AN31\\_Serial\\_Connection\\_muSlideVI04.pdf](https://ibidi.com/img/cms/support/AN/AN31_Serial_Connection_muSlideVI04.pdf).
13. Based on the tubing length, you can calculate how long one cycle of wash takes to pass through all the connectors/tubing/chamber system.
14. Keep an eye on the syringe capacity: empty it via the Luer connector into a “waste” tube with some 70% ethanol or 1% Virkon (Dupont).
15. Depending on the cancer cell line, the time needed for cell dissociation may vary.
16. For the flow-based adhesion assay, only HUVEC complete medium is used as endothelial cells require more supplements than cancer cells and are more susceptible to changes in medium composition.
17. It is recommended to take the system out of the environmentally controlled chamber of the time-lapse microscope as it may be difficult to operate inside with precision. We recommend setting a secure small area near the microscope chamber doors or on top of the environmentally controlled chamber.
18. Make sure the pump is off (!). If you clip the tubing while the pump is pulling medium and once the clips are released, the endothelial monolayer in that channel will be compromised/detached. Always stop the pump before clipping the tubing.
19. As described in the manufacturer's instructions at min 7:50 in the movie: <https://ibidi.com/content/150-mv-21>.
20. To avoid excess medium entering the chamber, it is possible to use sterile cotton buds or absorbent paper, without touching the inlet borders. This is shown in the manufacturer's instructions at min 8 in the movie: <https://ibidi.com/content/150-mv-21>.
21. Make sure that the syringe in the pump is empty.
22. These times are optimized for the tubing size/length and cell types. Here you can resuspend the cancer cells again to make

sure they are not in groups and to avoid them forming clumps that may spoil the adhesion experiment.

23. It is possible to use a second pump to perform the washes with medium. It is also possible to use a Y connector and/or a three-way stopcock Luer for the PC3 cells and medium connection to the system.
24. Movies may be larger than 3 Gb each depending on a range of parameters like the pixel binning.

## References

1. Ousman SS, Kubes P (2012) Immune surveillance in the central nervous system. *Nat Neurosci* 15:1096–1101
2. Reymond N, d'Agua BB, Ridley AJ (2013) Crossing the endothelial barrier during metastasis. *Nat Rev Cancer* 13:858–870
3. Wirtz D, Konstantopoulos K, Searson PC (2011) The physics of cancer: the role of physical interactions and mechanical forces in metastasis. *Nat Rev Cancer* 11:512–522
4. Cerutti C, Ridley AJ (2017) Endothelial cell-cell adhesion and signaling. *Exp Cell Res* 358:31–38
5. Hodge RG, Ridley AJ (2016) Regulating Rho GTPases and their regulators. *Nat Rev Mol Cell Biol* 17:496–510
6. Lawson CD, Ridley AJ (2018) Rho GTPase signaling complexes in cell migration and invasion. *J Cell Biol* 217:447–457
7. Sahai E, Marshall CJ (2002) RHO-GTPases and cancer. *Nat Rev Cancer* 2:133–142
8. Vega FM, Ridley AJ (2008) Rho GTPases in cancer cell biology. *FEBS Lett* 582:2093–2101
9. Haga RB, Ridley AJ (2016) Rho GTPases: regulation and roles in cancer cell biology. *Small GTPases* 7:207–221
10. Engers R, Ziegler S, Mueller M, Walter A, Willers R, Gabbert HE (2007) Prognostic relevance of increased Rac GTPase expression in prostate carcinomas. *Endocr Relat Cancer* 14:245–256
11. Sequeira L, Dubyk CW, Riesenberger TA, Cooper CR, van Golen KL (2008) Rho GTPases in PC-3 prostate cancer cell morphology, invasion and tumor cell diapedesis. *Clin Exp Metastasis* 25:569–579
12. Yao H, Dashner EJ, van Golen CM, van Golen KL (2006) RhoC GTPase is required for PC-3 prostate cancer cell invasion but not motility. *Oncogene* 25:2285–2296
13. Tajadura-Ortega V, Garg R, Allen R, Owczarek C, Bright MD, Kean S, Mohd-Noor A, Grigoriadis A, Elston TC, Hahn KM, Ridley AJ (2018) An RNAi screen of Rho signalling networks identifies RhoH as a regulator of Rac1 in prostate cancer cell migration. *BMC Biol* 16:29
14. Ridley AJ (2013) RhoA, RhoB and RhoC have different roles in cancer cell migration. *J Microsc* 251:242–249
15. Kazanietz MG, Caloca MJ (2017) The Rac GTPase in cancer: from old concepts to new paradigms. *Cancer Res* 77:5445–5451
16. Orgaz JL, Herraiz C, Sanz-Moreno V (2014) Rho GTPases modulate malignant transformation of tumor cells. *Small GTPases* 5:e29019
17. Pandya P, Orgaz JL, Sanz-Moreno V (2017) Modes of invasion during tumour dissemination. *Mol Oncol* 11:5–27
18. Rodriguez-Hernandez I, Cantelli G, Bruce F, Sanz-Moreno V (2016) Rho, ROCK and actomyosin contractility in metastasis as drug targets. *F1000Res* 5(F1000 Faculty Rev):783
19. Reymond N, Im JH, Garg R, Vega FM, Borda d'Agua B, Riou P, Cox S, Valderrama F, Muschel RJ, Ridley AJ (2012) Cdc42 promotes transendothelial migration of cancer cells through beta1 integrin. *J Cell Biol* 199:653–668
20. Reymond N, Im JH, Garg R, Cox S, Soyer M, Riou P, Colombe A, Muschel RJ, Ridley AJ (2015) RhoC and ROCKs regulate cancer cell interactions with endothelial cells. *Mol Oncol* 9:1043–1055
21. Georgouli M, Herraiz C, Crosas-Molist E, Fanshawe B, Maiques O, Perdrizzi A, Pandya P, Rodriguez-Hernandez I, Ilieva KM, Cantelli G, Karagiannis P, Mele S, Lam H, Josephs DH, Matias-Guiu X, Marti RM, Nestle FO, Orgaz JL, Malanchi I, Fruhwirth GO, Karagiannis SN, Sanz-Moreno V (2019) Regional activation of myosin II in cancer cells drives tumor progression via a secretory cross-talk with the immune microenvironment. *Cell* 176:757–774

22. Okada T, Sinha S, Esposito I, Schiavon G, Lopez-Lago MA, Su W, Pratillas CA, Abele C, Hernandez JM, Ohara M, Okada M, Viale A, Heguy A, Soccia ND, Sapino A, Seshan VE, Long S, Inghirami G, Rosen N, Giancotti FG (2015) The Rho GTPase Rnd1 suppresses mammary tumorigenesis and EMT by restraining Ras-MAPK signalling. *Nat Cell Biol* 17:81–94
23. Cerutti C, Soblechero-Martin P, Wu D, Lopez-Ramirez MA, de Vries H, Sharrack B, Male DK, Romero IA (2016) MicroRNA-155 contributes to shear-resistant leukocyte adhesion to human brain endothelium in vitro. *Fluids Barriers CNS* 13:8
24. Cerutti C, Edwards LJ, de Vries HE, Sharrack B, Male DK, Romero IA (2017) MiR-126 and miR-126\* regulate shear-resistant firm leukocyte adhesion to human brain endothelium. *Sci Rep* 7:45284
25. Wirtz D (2012) MO-C-BRCD-02: physics of cancer cell migration. *Med Phys* 39:3864
26. Yan WW, Liu Y, Fu BM (2010) Effects of curvature and cell-cell interaction on cell adhesion in microvessels. *Biomech Model Mechanobiol* 9:629–640
27. Yan WW, Cai B, Liu Y, Fu BM (2012) Effects of wall shear stress and its gradient on tumor cell adhesion in curved microvessels. *Biomech Model Mechanobiol* 11:641–653
28. Follain G, Herrmann D, Harlepp S, Hyenne V, Osman N, Warren SC, Timpson P, Goetz JG (2020) Fluids and their mechanics in tumour transit: shaping metastasis. *Nat Rev Cancer* 20:107–124



# Chapter 8

## Probing Intravascular Adhesion and Extravasation of Tumor Cells with Microfluidics

Naël Osmani, Gautier Follain, Valentin Gensbittel,  
María Jesús García-León, Sébastien Harlepp, and Jacky G. Goetz

### Abstract

Cancer metastasis is a multistep process during which tumor cells leave the primary tumor mass and form distant secondary colonies that are lethal. Circulating tumor cells (CTCs) are transported by body fluids to reach distant organs, where they will extravasate and either remain dormant or form new tumor foci. Development of methods to study the behavior of CTCs at the late stages of the intravascular journey is thus required to dissect the molecular mechanisms at play. Using recently developed microfluidics approaches, we have demonstrated that CTCs arrest intravascularly, through a two-step process: (a) CTCs stop using low energy and rapidly activated adhesion receptors to form transient metastable adhesions and (b) CTCs stabilize their adhesions to the endothelial layer with high energy and slowly activated adhesion receptors. In this methods chapter, we describe these easy-to-implement quantitative methods using commercially available microfluidic channels. We detail the use of fast live imaging combined to fine-tuned perfusion to measure the adhesion potential of CTC depending on flow velocities. We document how rapidly engaged early metastable adhesion can be discriminated from slower activated stable adhesion using microfluidics. Finally, CTC extravasation potential can be assessed within this setup using long-term cell culture under flow. Altogether, this experimental pipeline can be adapted to probe the adhesion (to the endothelial layer) and extravasation potential of any circulating cell.

**Key words** Microfluidics, Circulating tumor cells (CTCs), Adhesion, Extravasation, Metastasis, Live imaging

---

### 1 Introduction

Metastasis is the leading cause of cancer death in patient [1]. Metastatic progression is a multistep process whereby tumor cells disseminate using body fluids and colonize distant organs to ultimately develop life-threatening secondary tumors [2, 3]. As they develop into an *in situ* tumor, cancer cells will eventually acquire an invasive potential and breach through the extracellular

---

Naël Osmani and Gautier Follain contributed equally to this work.

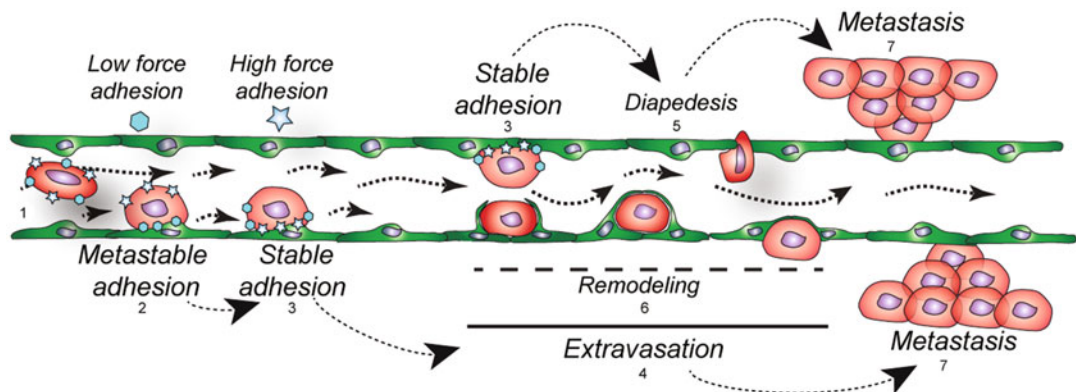


**Fig. 1** The metastatic cascade during hematogenous dissemination. Schematic representation of the metastatic cascade. (1) Circulating tumor cells (CTCs) are disseminated through blood circulation. (2) As CTCs reach vessels with lower and adhesion permissive flow velocities, they form metastable adhesions with low energy and fast to engage adhesion receptors which allow their transient arrest. (3) Once arrested, CTCs strengthen their adhesion to the luminal side of endothelial cells by clustering high energy and slow to engage adhesion receptors. This is essential for CTCs to resist to the shear-ripping forces of the blood flow. (4) CTCs' stable adhesions further permit cells to engage different strategies to escape circulation. (5) CTCs can extravasate by actively migrating through the endothelial layer using diapedesis. (6) The endothelium can also favor CTC passive extravasation by remodeling in order to restore blood flow after CTC arrest. (7) Once extravasated, CTCs will colonize the perivascular niche and ultimately form secondary colonies in distant organs

matrix of their organ of origin. (a) These escaping tumor cells will invade the surrounding stroma and reach neighboring vessels. (b) Cancer cells will then enter blood circulation by crossing the endothelial barrier (intravasation). (c) As they become circulating tumor cells (CTCs), they are transported to distant organs by blood circulation. (d) CTCs will stop into the capillary beds of distant organs in regions of adhesion-permissive flows and exit blood stream by crossing the endothelial layer (extravasation) either through active transendothelial migration or through flow-dependent endothelial remodeling [3]. (e) Finally, they will invade the organs and settle to secondary metastatic sites into metastatic niches where they either enter dormancy or form secondary colonies [4, 5] (Fig. 1).

Adhesion receptors at the surface of CTCs have been involved in the ability of CTC to roll or to arrest on the surface of endothelial cells using receptors of different binding energies [6] in a mechanism that is highly reminiscent of leukocytes rolling, arrest, and adhesion steps preceding their extravasation [7, 8] (Fig. 1). Among those, glycoproteins involved in leukocytes rolling at the surface of the endothelium, such as selectins, are required for the adhesion of CTCs to endothelial cells [9, 10]. CD24, CD44, PODXL, and mucins are involved in CTC adhesion to the endothelium [9, 11–15]. Finally, ECM adhesion receptors of the integrin family such as

integrins  $\alpha v\beta 3$ ,  $\beta 1$ , and  $\beta 4$  are also involved in adhesion of CTCs to endothelial cells [15–20]. These experimental approaches probed the role of specific adhesion receptors in CTC arrest or extravasation by various means. They used either parallel plate chambers with ligand-coated dish or Boyden chamber covered with a HUVEC monolayer, respectively, which unfortunately does not fully recapitulate the complex interaction between CTCs and endothelial cells in flow during arrest and extravasation. Thus, the respective contributions of these different receptors in early intravascular arrest versus stable adhesions have rarely been probed simultaneously. Hence, the correlation between the adhesive and the metastatic potentials of CTCs remains elusive. Furthermore, the important function of the biomechanical cues from blood flow during CTC arrest and extravasation has also been understudied [15, 21].

Microfluidics have long been used as a tool to study cells in flow from leukocyte to cancer biology and to probe their biological and mechanical properties [6, 8]. Recent developments in microfluidic tools now allow both biomechanical and biochemical characterization of CTCs [22–27]. Our recent work as demonstrated that the use of *in vitro* microfluidics in parallel with intravital imaging in the zebrafish embryo is a fast, efficient, and cost effective experimental metastasis framework that can be ultimately validated in mouse experimental metastasis models and patients [15, 21, 28, 29].

In this chapter, we propose an original framework using microfluidic microchannels as an *in vitro* experimental metastasis model to study the different steps of hematogenous dissemination. These methods are based on commercially available systems that require little/no expertise in microfluidics microfabrication or PDMS (polydimethylsiloxane) handling and are thus easy to implement in any cell biology laboratory. These methods enable to probe the potential of hematogenous dissemination of CTCs in physiological conditions where the vascular wall (endothelial cells) and the underlying hemodynamics (with some limitations) can be easily reproduced.

---

## 2 Materials

### 2.1 Cell

Classical cancer cell lines from human and mouse origin can be used. These can be easily genetically modified using CRISPR/Cas9, stably transfected or virally transduced with gene expression vectors or shRNA expression vectors, or transiently transfected with gene expression vectors or siRNA. We are using the metastatic mouse mammary carcinoma cell line D2A1 as shown in our recent reports [15, 21], which we fluorescently label at will when fluorescence analysis is required. Endothelial cells of primary origin either commercially available or from homemade purification should be

used. In the methods we present here, we are using human umbilical vein endothelial cells (HUVEC) from a single donor as they are easy to culture.

## 2.2 Cell Culture

1. Endothelial cell culture medium containing fetal calf serum 0.02 ml/ml, endothelial cell growth supplement 0.004 ml/ml, epidermal growth factor (recombinant human) 0.1 ng/ml, basic fibroblast growth factor (recombinant human) 1 ng/ml, heparin 90 µg/ml, hydrocortisone 1 µg/ml, penicillin-streptomycin 100 U–0.1 mg/ml.
2. Fibronectin from bovine plasma.
3. PBS–EDTA: 0.2 g/l.
4. Trypsin–EDTA: 0.05% for HUVEC and trypsin adapted to the cancer cell line of interest.
5. Cancer cell line medium: The appropriate medium for the cell line of interest, supplemented with all additives.
6. Hepes 1 M sterile.

## 2.3 Microfluidic Equipment (Fig. 2a–d)

1. Peristaltic pump. In the methods we present here, we use the Reglo Digital with 2 or 4 channels and 12 rollers (ISMATEC) (*see Note 1*).
2. Tygon® LMT-55 3-Stop Tubing 0.38 mm, 12-pack, Wall Thickness = ~0.86 mm (IDEX Corporation) to drive medium and cell perfusion.
3. 23G × 1" (0.6 × 25 mm) hypodermic needles extracted from their Luer adaptors are used to connect the 3-stop tubing to normal tubing (*see Note 2*).
4. Silicon tubing 0.5 mm (ibidi).
5. Fitting reducer 0.5–1.6 mm (ibidi).
6. Silicon tubing 1.6 mm (ibidi).
7. Elbow Luer connector (ibidi).

## 2.4 Microchannels (Fig. 2e)

1. µSlide I 0.4 Luer ibiTreat: #1.5 polymer coverslip (ibidi).
2. µSlide VI 0.4 ibiTreat: #1.5 polymer coverslip (ibidi).
3. sticky-Slide I Luer (ibidi).
4. Dow Corning® high-vacuum silicone grease is used to seal sticky-Slide I to rectangular glass coverslips (*see Note 3*).

## 2.5 Live Microscopy (Fig. 2f)

1. Any inverted live imaging compatible microscope can be used.
2. A heating system (we use a thermo-controlled heating box OKO Lab Cage from Okolab).
3. A dry 10× objective (we use a UPLFLN-P 10×/0.3 objective from Olympus).

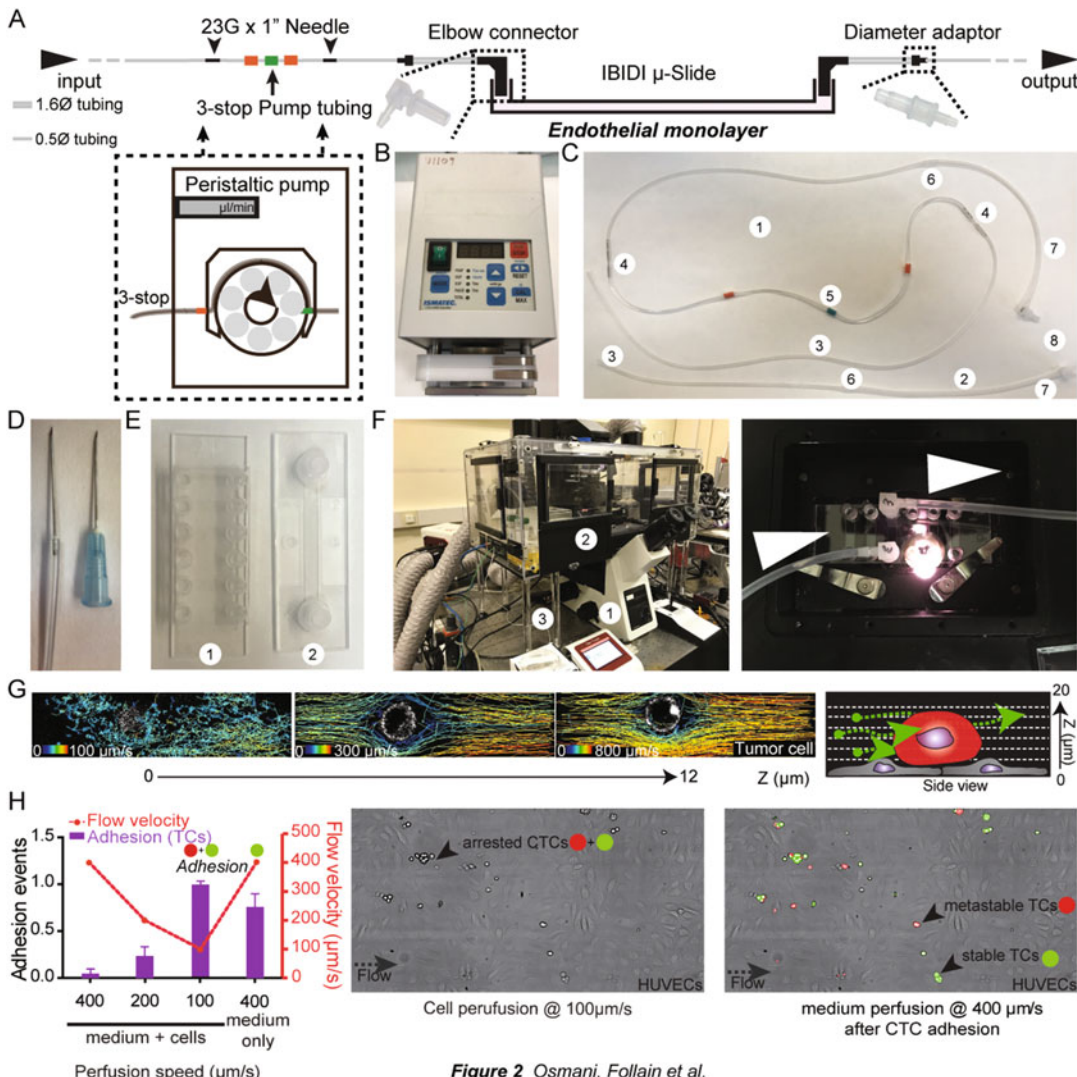


Figure 2\_Osmani, Follain et al.

**Fig. 2** Live adhesion assay. **(a)** Scheme of the microfluidic setup. **(b)** Peristaltic pump (here Ismatec Reglo Digital MS/2). **(c)** Tubing used for all microfluidic experiments: (1) 3-stop containing tubing. (2) Tubing without 3-stop. (3) 0.5 mm tubing. (4) Needle junction. (5) 3-stop tubing. (6) 0.5 to 1.6 fitter. (7) 1.6 mm tubing. (8) Elbow Luer. **(d)** 23G × 1" hypodermic needle without Luer inserted into the 3-stop tubing next 23G × 1" hypodermic needle with luer. **(e)** Commercially available μSlide I (1) and IV (2) 0.4. **(f)** **(Left)** Live microscopy setup: (1) Inverted microscope (Olympus). (2) Thermo-controlled heating box with 5% CO<sub>2</sub> atmosphere (Okolab). (3) CCD fast camera (Thorlabs). **(Right)** μSlide inserted into the stage. White arrows highlight medium flow direction. **(g)** **(left)** Examples of flow pattern analysis and flow velocities quantification using fast confocal imaging and automated tracking. CTCs are shown in gray. **(right)** Scheme of the sequential fast confocal acquisition performed along the z axis. (Adapted from [21]). **(h)** Data analysis: **(left)** chart showing increased evaluation inversely correlated to flow speed. The final washing step allows to assess the stability of CTC adhesions engaged with endothelial cells. Pictures showing **(center)** arresting CTC at 100 μm/s and **(right)** CTC discriminated during the washing step as stably adhered (stable) and transiently adhered (metastable). (Adapted from [15])

4. A camera able to image at 24 frame per second (we use a CMOS fast camera DCC3240M from Thorlabs).
5. A 5% CO<sub>2</sub> atmosphere is also recommended but can be replaced by supplementing medium with 20 mM of sterile Hepes.

## **2.6 Confocal Microscopy**

Any inverted confocal microscope of choice would be appropriate. We are using a TCS SP5 inverted confocal microscope systems (Leica) with an immersion oil 63× objective (HCX PL APO 63×/1.4 OIL).

## **2.7 Fluorescent Beads for Flow Calibration**

FluoSpheres™ Carboxylate-Modified Microspheres, 0.1 μm, yellow-green fluorescent (505/515), 2% solids (Thermo Fischer).

## **2.8 Scanning Electron Microscopy Reagents**

1. 1,1,1,3,3-hexamethyldilazane (HDMS).
2. 25, 4 mm EM Aluminum Mounts for AMRAY (EMS, Hatfield).
3. Leit-C conductive carbon cement (CCC, Plano GmbH, Germany).
4. Cressington Sputter Coater 208HR coupled to a Pfeiffer Vacuum (Germany).

## **2.9 Scanning Electron Microscopy Reagents**

Image acquisition can be performed with any desktop SEM microscope. We use a Phenom-World SEM desktop microscope (Phenom-World B.V, The Netherlands) (collaboration with EFS, Strasbourg, INSERM U1255).

## **3 Methods**

### **3.1 Endothelial Cell Seeding in Microchannels**

1. A single P0 vial is expended for 4 passages in 100 cm petri dishes. The P4 vials are then stored in liquid nitrogen. A single vial will be used for each experiment.
2. μSlide microchannels are coated with fibronectin to favor HUVEC seeding. Fibronectin is diluted at 10 μg/ml in PBS. 100 μl or 30 μl of this solution are added in μSlide I or VI, respectively. Microchannels are incubated 1 h at 37 °C (alternatively, μSlide can be incubated O/N at 4 °C). Microchannels are then washed three times with sterile PBS (*see Note 4*).
3. Freshly thawed HUVEC are lifted and resuspended in pre-heated ECGM. Cells are centrifuged 5 min at 100 × g and room temperature. The supernatant is discarded. The cell pellet is resuspended in ECGM at a concentration of 10<sup>6</sup> cells/ml. 100 μl or 30 μl of this solution are added in μSlide I or VI, respectively (*see Note 4*).

- Medium should be changed twice a day in the microchannels as long as it is not perfused. Each change of medium consists of two steps of wash with preheated medium to ensure that the used one is washed away and a final step of adding fresh medium to fill the microchannels and both wells. The gap time between two change of medium should not exceed 15–16 h (*see Note 4*).

### **3.2 Tubing Setup (Fig. 2a, c)**

To ensure sterility, this step should be performed under a sterile cell culture hood.

- For the 3-stop tubing, insert 23G × 1" hypodermic needles extracted from their Luer in each side of the 3-stop tubing. Connect the 0.5 mm tubing to the 3-stop tubing using the needles on each side. We recommend adapting the tubing length to the specificity of your microscope and keep the tubing as short as possible. Connect a 0.5 to 1.6 fitting reducer on one side of the 3-stop tube. Connect 1.6 mm tube to the fitting reducer. We advise to reduce the length of this part as much as possible (5–10 cm maximum).
- For the short tubing, cut a piece of 0.5 mm tubing adapted to the specificity of your microscope setup. We advise to use a tubing as short as possible. Connect a 0.5 to 1.6 fitting reducer on one side of the 3-stop tube. Connect 1.6 mm tube to the fitting reducer. We advise to reduce the length of this part as much as possible (5–10 cm maximum).

### **3.3 Calibrating the Microfluidic Perfusion and Probing Flow Profiles**

100 nm fluorescent beads can be used to assess flow speed within the channel at each given flowrate. We advise to measure the flow speed from the bottom to the middle of the channel at several  $z$  heights (using a piezoelectrical caliper) to characterize the Poiseuille flow (*see Note 5*).

- Prepare the live imaging microscope. Heat the setup at 37 °C and 5% CO<sub>2</sub> (if available).
- Prepare cells for perfusion. Wash cells with PBS–EDTA. Trypsinize cells and resuspend them in ECGM. Centrifuge cells to remove trypsin and resuspend them in ECGM at a concentration of 10<sup>6</sup> cells/ml (*see Note 6*).
- Inject a volume of cells equivalent to the microchannel volume (*see Note 4*). Tilt the channel along its length to homogenize. Incubate 5 min at 37 °C to favor CTC stable adhesion.
- Prepare the μSlide for perfusion. Perfuse ECGM-containing fluorescent beads at 0.02% in the 3-stop containing tubing using “pushing perfusion” (Fig. 3c). Connect the elbow Luer to the microfluidic channel, once the medium starts to drip. *This is essential to avoid bubbles as it would eventually destroy*

*endothelial cells*. Connect then the elbow Luer of the outlet tubing (without the 3-stop tubing) and put the outlet tubing into a liquid bin (*see Note 6*).

5. Microchannels are imaged at high speed (50 ~ 100 fps) using a Leica SP5 confocal microscope equipped with resonant scanner at different height from the bottom of the microchannel, where cells are sitting (0  $\mu\text{m}$ ) up to +20  $\mu\text{m}$ . Each movie contains at least 1000 frames.  
The tubing should not be reused for other experiments besides calibration as they will be filled with fluorescent beads.
6. To analyze data, we advise using the TrackMate plugin available in ImageJ (<https://imagej.net/TrackMate>). Use the metadata from the confocal to calibrate pixel size ( $x, y-z$  will not be considered as acquisition is performed on single planes) as well as the time between each frame.
7. Use the LoG detector and indicate the size of the beads.
8. Adjust spot detection using the thresholding from the plugin. We suggest using the autodetection as a first step and to manually filter aberrant detection.
9. Use Hyperstack displayer.
10. We do not use filters on spot.
11. We use the simple LAP tracker. We advise using parameters adapted to your experiments. You should measure the average distance traveled by the beads during each frame, and use this average value for linking max distance and gap-closing max distance. We advise using 1 as gap-closing max frame gap. This will be the most stringent and unbiased detection methods which, while it results in the loss of many events, is compensated by increasing their number.
12. On the “Set filter on tracks” page, use “Set color by mean velocity.” Extra filters can be applied to manually filter out biased trajectories.
13. On the “Display” page, check “Display tracks” and select “Set color by mean velocity.”
14. Spots and tracks can be manually modified to remove artifacts using “TrackScheme.”  
Data can be recovered using “Analysis” for further quantification (*see Note 7*).
15. Select “Capture overlay” to create the movie containing tracks and click on “Execute.”
16. Flow profiles and speeds can be analyzed using the rendered view of TrackMate (Fig. 2g).
17. Pump perfusion speed corresponding to flow velocities within the channel can be estimated for pump calibration. We provide

**Table 1**  
**Chart showing the flow rates for the setup using Ismatec Reglo Digital MS 2 or 4/12 pumps,  $\mu$ Slide I 0.4 or VI 0.4 and the tubing described in 3.2**

Mean flow velocity ( $\mu\text{m/s}$ )	$\mu$ Slide I 0,4 Flow rate ( $\mu\text{l/min}$ )	$\mu$ Slide VI 0,4 Flow rate ( $\mu\text{l/min}$ )
100	12	9
200	24	18
300	36	27
400	48	36
500	60	45
600	72	54
700	84	63
800	96	72
900	108	81
1000	120	90
1100	132	99
1200	144	108
1300	156	117
1400	168	126
1500	180	135

the flow rates for the Ismatec Reglo Digital MS 2 or 4/12 and  $\mu$ Slide I 0.4 or VI 0.4 and the tubing described in Subheading 3.2 in Table 1.

### 3.4 Microfluidic Shear Stress Resistance Assay

Prior to adhering and extravasating, CTCs transit in the blood circulation, which represents a key step of the metastatic cascade [3]. Their survival is threatened by mechanical stresses such as cell–cell collisions and most importantly fluid shear stress. Multiple parameters are critical to CTCs surviving these threats during their transit in the blood flow: cell–cell collision probability, shear stress level, exposition duration [30], and mechanical properties of CTCs [31]. Microfluidics, in the form of closed tubing circuits, offer simple approaches to recapitulate and probe the effects of all those parameters on CTC survival. Here, we propose a simple protocol that allows exposing tumor cells to various levels of shear stress (see Notes 8 and 9). Our setup allows probing physiologically relevant shear stress levels ranging from 0.1 Dynes/cm<sup>2</sup> (level found in interstitial flow *in vivo*) to 16 Dynes/cm<sup>2</sup> (found in capillaries and some small arteries) for relatively short but physiologically relevant durations (<10 h).

1. To prepare the specific tubing, *see* steps in Subheading 3.2.1. We recommend adapting the tubing length to the volume of medium that is intended to be put in circulation (*see Note 10*). Connect a 0.5 to 1.6 fitting reducer on both 0.5 mm tubing ends. Use a short piece of 1.6 mm tubing to connect both fitting reducers and close the circuit.
2. Prepare a large volume (roughly 2.5 times the volume that is intended to be put in circulation) of cells in medium supplemented with Hepes, at desired concentration. Split it into two different tubes.
3. Turn on the pump and open the circuit by disconnecting one of the 0.5 mm tubing ends from its fitting reducer.
4. Perfuse the content of one of the two tubes containing cells. Reconnect the 0.5 mm tubing end to its fitting reducer once liquid starts dripping at the other end to close the circuit.
5. Put the other tube containing cells on a shaker to keep the cells in suspension.
6. Leave the cells in circulation and under agitation for the duration of shear stress exposure of interest (*see Note 11*).
7. Disconnect one of the 0.5 mm tubing ends from its fitting reducer to open the circuit and collect the cells that have been circulating in a tube. Retrieve the tube of cells that have been kept in suspension.
8. Assess cell viability in both tubes. This can be done using the classical Trypan blue exclusion test. We provide as an example the shear stress values for the setup using Ismatec Reglo Digital MS 2 or 4/12 pumps and 0.5 mm or 1.6 mm diameter ibidi silicon tubing in Table 2.

### **3.5 Live Cell Adhesion Assay**

The aim of this approach is to quantify both the arrest potential of perfused cancer cells through specific receptors and to assess the stability of these adhesions. It is essential to perform the experiment when the endothelial monolayer is fully confluent as CTCs adhere with high affinity to the underlying fibronectin and can thus potentially bias the results. The monolayer should be carefully checked using a standard cell culture microscope, and HUVEC should be confluent before starting the experiment. Given that the microfluidic channel cannot be customized and also the peristaltic pump and the tubing presented in this protocol have a limited perfusion capacity, CTC perfusion can only be performed at flow speeds that are typically found in capillary vessels (0–1000  $\mu\text{m}/\text{s}$ ).

1. Prepare the live imaging microscope. Heat the setup at 37 °C and 5% CO<sub>2</sub> (if available).
2. Fix the  $\mu$ Slide VI on the microscope stage and the  $\mu$ Slide VI containing confluent HUVEC for perfusion. Perfuse ECGM in

**Table 2**

**Chart showing the shear stress values for the setup using Ismatec Reglo Digital MS 2 or 4/12 pumps and 0.5 mm or 1.6 mm diameter ibidi silicon tubing**

Flow rate setting ( $\mu\text{l}/\text{min}$ )	Tubing 1.6 mm Shear stress (Dynes/cm $^2$ )	Tubing 0.5 mm Shear stress (Dynes/cm $^2$ )
4	0.016	0.511
9	0.035	1.149
18	0.070	2.298
27	0.105	3.447
36	0.140	4.596
45	0.175	5.745
54	0.210	6.894
63	0.245	8.043
72	0.281	9.192
81	0.316	10.341
90	0.351	11.490
99	0.386	12.639
108	0.421	13.788
117	0.456	14.937
126	0.490893942	16.086

the 3-stop containing tubing using “pushing perfusion” (Fig. 3c). Connect the elbow Luer to the microfluidic channel once medium starts to drip (*see Note 12*). This is essential to avoid bubbles as it would eventually destroy endothelial cells. Connect the elbow Luer of the outlet tubing (without the 3-stop tubing) and put the outlet tubing into a liquid bin. Perfuse medium while preparing cells for perfusion.

3. Prepare cells for perfusion. Wash cells with PBS–EDTA. Trypsinize cells and resuspend them in ECGM. Centrifuge cells to remove trypsin and resuspend them in ECGM at a concentration of  $10^6$  cells/ml (*see Note 6*).
4. Put the inlet from the 3-stop containing tubing into medium. Perfuse using “pushing perfusion” (Fig. 2a, c, f). This step should be adapted to the cells of interest.

We use D2A1 mouse mammary carcinoma cells. In our experiments, we perform three steps of perfusion at physiologically relevant speeds with decreasing values to favor cancer cell adhesion to the endothelial monolayer.

- 400  $\mu\text{m}/\text{s}$  for 2 min.
- 200  $\mu\text{m}/\text{s}$  for 2 min.
- 100  $\mu\text{m}/\text{s}$  for 2 min.

We perform a final wash step of ECGM medium at 400  $\mu\text{m}/\text{s}$  for 2 min. This final step is essential to probe the stability of CTC adhesion (*see Note 6*).

5. The tubing can be reused for cell perfusion in series by connecting to new channels for each new set of cell perfusion. We recommend washing the tubing with PBS–EDTA to remove cells that might adhere to the tubing. Once done repeat **steps 2–4**, for each set of cell perfusion.

The tubing can be reused for following experiments. We advise cleaning the tubing using the pump by performing a wash with Milli-Q grade Ultrapure water for at least 2 min, a wash with absolute ethanol for at least 2 min, a wash with Milli-Q grade Ultrapure water for at least 2 min to remove ethanol. Dry the tubing by aspiring air through the tubing using the pump.

6. This method can be adapted to probe the adhesion properties of specific cell surface receptors either by transient siRNA or stable shRNA knockdown, using antagonist antibodies or chemical compounds directly within the perfusion medium.
7. To analyze data, we count the number of cells adhering at each step of perfusion (400  $\mu\text{m}/\text{s}$ , 200  $\mu\text{m}/\text{s}$ , and 100  $\mu\text{m}/\text{s}$ ) to quantify the flow dependence of cell adhesion. The number of cells remaining adhered after the washing step should also be quantified in order to assess the stability of cancer cell adhesion to the endothelial layer. In order to compare different conditions (i.e., the role of adhesion receptors as in [15] or comparing cell types), we advise normalizing all values to the mean value of control cells adhesion after perfusion at 100  $\mu\text{m}/\text{s}$  (Fig. 2h).

### **3.6 Microfluidic Extravasation Assay**

Once endothelial cells have been seeded in microchannels as described in Subheading 3.1, this method allows to study extravasation of CTCs either through active transendothelial migration or the active role of the endothelium in extravasating cancer cells. The flow-dependence of cancer cell extravasation can be studied by culturing endothelial cells with various flow conditions. Specific drugs can be added to the medium to assess the biological function of specific cellular pathways during CTC extravasation. This method is compatible with live imaging, chemical fixation and fluorescent immunostaining, or chemical fixation and scanning electron microscopy.

1. For the “no-flow” condition, keep changing medium twice a day as described in Subheading 3.1 **step 4** until performing experiments.
2. For the “flow” condition, 1 ~ 1.5 day after seeding, micro-channels containing endothelial cells can be connected to the microfluidics setup. We advise to perform this step under a cell culture hood to maintain sterility (*see Note 13*).
3. Preheat ECGM medium (without Hepes) at 37 °C in a Falcon tube. Cover it with parafilm under the cell culture hood. Open a hole with a hypodermic needle (Fig. 3a) and insert the inlet from the 3-stop containing tubing into medium through parafilm (Fig. 3b) (*see Note 13*).
4. Perfuse ECGM in the 3-stop containing tubing using “pushing perfusion” (Fig. 3c). Connect the elbow Luer to the microfluidic channel once medium starts to drip. *This is essential to avoid bubbles as it would eventually destroy endothelial cells.* Connect then the elbow Luer of the outlet tubing (without the 3-stop tubing) and put the outlet tubing into a liquid bin until it starts to drip (*see Note 12*).
5. Stop medium perfusion. Open a second hole with a hypodermic needle into the parafilm and insert the outlet tubing with medium through the parafilm. Seal and maintain tubing using tape (*see Note 14*).
6. Resume perfusion using “pushing perfusion” until no bubbles are seen coming out of the outlet (Fig. 3d). *This is essential to avoid bubbles.*
7. Reverse the rotation direction of the peristaltic pump and switch to “aspiration perfusion” (Fig. 3d). *This is essential to avoid bubbles during long-term culture under flow (see Note 15).*
8. Endothelial cells should be flow-activated for 24 h.
9. Proceed with the experimental workflows described in Subheadings 3.7–3.9.

### 3.7 Live Imaging

1. Prepare the live imaging microscope. Heat the setup at 37 °C and 5% CO<sub>2</sub> (if available).
2. Stain endothelial cells using lipidic dyes following the manufacturer’s protocol.
3. Prepare cancer cells for perfusion at a concentration of 10<sup>6</sup> cells/ml in ECGM as described in Subheading 3.5 **step 3** (*see Notes 6 and 16*).
4. Disconnect the “flow” condition microchannel from the tubing.

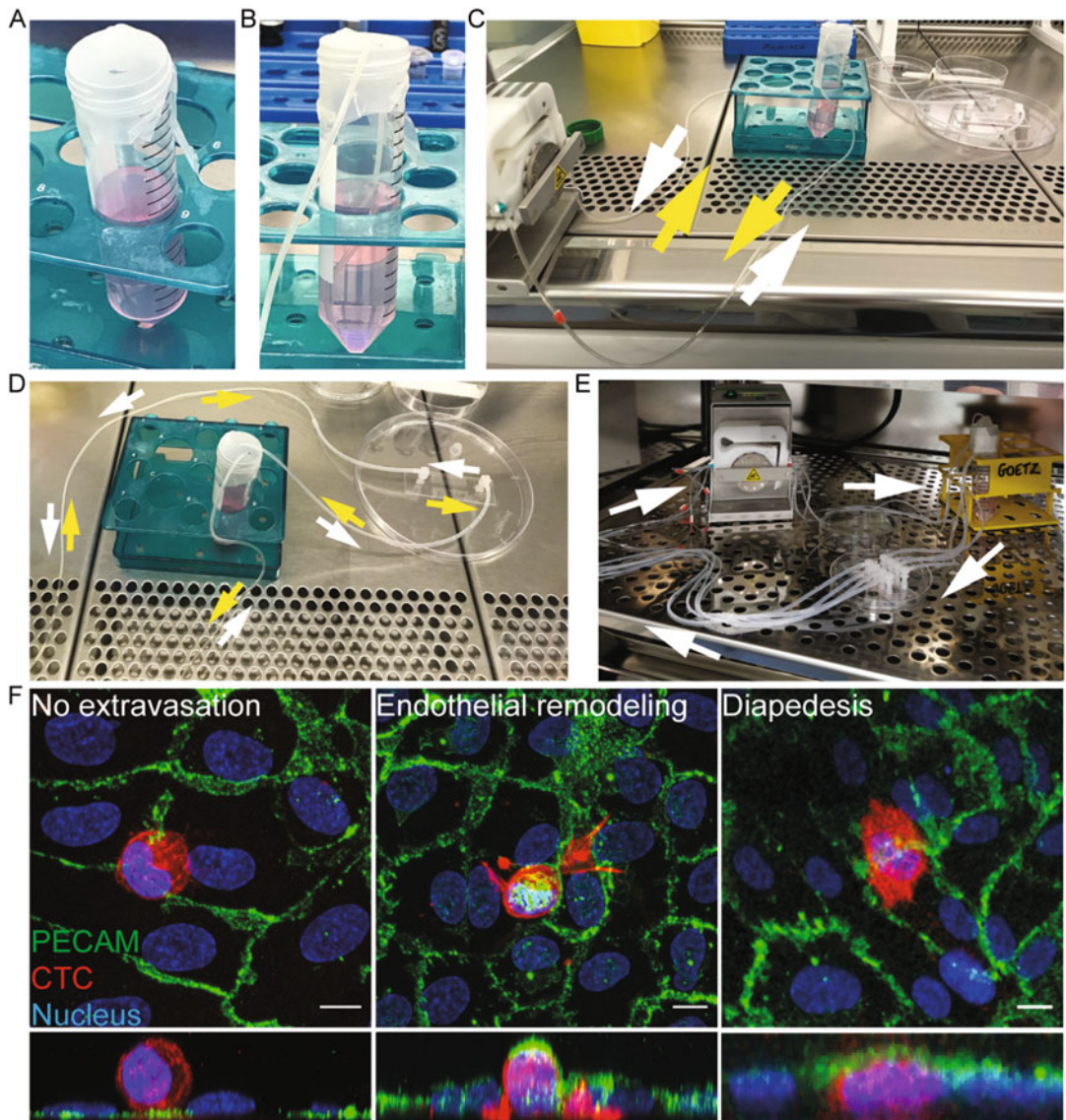


**Fig. 3** Extravasation assay. (a) Picture showing a 50 ml tube containing ECGM covered with parafilm with a hole pierced. (b) a 50 ml tube containing ECGM covered with parafilm with tubing going through. (c) Picture showing the microfluidic setup associated to the pump. Yellow arrows show “pushing” perfusion. White arrows show “aspiration” perfusion. (d) Picture showing a larger view of the microfluidic setup. Yellow arrows show “pushing” perfusion. White arrows show “aspiration” perfusion. (e) Picture showing the microfluidic setup associated to the pump within the cell culture incubator. White arrows show “aspiration” perfusion. (f) 3D confocal pictures showing cell staying intravascular or that underwent extravasation through endothelial remodeling or diapedesis. Endothelial cells are stained for PECAM (green), CTCs (D2A1 cell line) express Td-Tomato-LifeAct, nuclei are stained with DAPI. Scale bar = 10  $\mu\text{m}$

5. Add 100  $\mu\text{l}$  of cancer cells at  $10^6$  cells/ml in “flow” and “no flow” conditions. Homogenize them by tilting left-right from one well to the other.

6. Let cancer cells adhere for the required time to engage stable adhesions with the endothelial layer (in our case, with D2A1 cells, at least 5 min).
7. Resume perfusion in “flow” conditions as described in Subheading 3.6 steps 4–7.
8. Fix the  $\mu$ Slide I on the microscope stage. Resume medium “pushing perfusion.”
9. Perform confocal 3D imaging. We suggest using an immersion objective with high magnification ( $63\times$  or  $100\times$ ) and large numerical aperture (NA > 1.3 ~ 1.4). Excitation/integration parameters are adjusted depending on the samples and a  $0.5\text{ }\mu\text{m}$  Z-step is used to maximize 3D resolution. Acquisition parameters should be fixed throughout experimental dataset for statistical analysis (*see Note 17*).

### **3.8 Immunostaining and 3D Confocal Imaging**

1. Prepare cancer cells for perfusion at a concentration of  $10^6$  cells/ml in ECGM as described in Subheading 3.5 step 3 (*see Note 15*).
2. Disconnect the “flow” condition microchannel from the tubing.
3. Add  $100\text{ }\mu\text{l}$  of cancer cells at  $10^6$  cells/ml in “flow” and “no flow” conditions. Homogenize them by tilting left-right from one well to the other.
4. Let cancer cells adhere for the required time to engage stable adhesions with the endothelial layer (in our case, with D2A1 cells, at least 5 min).
5. Change medium in all microchannels as described in Subheading 3.1 step 4.
6. Resume perfusion in “flow” conditions as described in Subheading 3.6 steps 4–7.
7. Incubate the required amount of time depending on your cell line of interest (in our case, with D2A1 cells, 16 h). If the required time exceeds overnight incubation, the medium should be changed in “no flow” conditions as described in Subheading 3.1 step 4. (Fig. 3e).
8. Fix cells using PFA 4% at room temperature for 10 min (*see Note 18*). Wash three times with PBS 1 $\times$ .
9. Permeabilize cells using PBS-0.2% Triton X-100 at room temperature for 10 min (*see Note 18*). Wash three times with PBS 1 $\times$ .
10. Quench PFA cells using PBS-NaBH<sub>4</sub> 2 mg/ml or NH<sub>4</sub>Cl 50 mM at room temperature for 10 min (*see Note 18*). Wash three times with PBS 1 $\times$ .

11. Add primary antibody against a specific endothelial marker (we recommend using anti-PECAM/CD31 or anti-VE-cadherin) diluted in PBS at the manufacturers' recommended dilution. Incubate 1 h at room temperature on a tilting shaker (*see Notes 18* and **19**). Wash three times with PBS 1×.
12. Add secondary antibody against the primary antibody and DAPI diluted in PBS at the manufacturers' recommended dilution. Incubate 30 min at room temperature on a tilting shaker (*see Notes 18–20*). Wash three times with PBS 1×.
13. Add non-polymerizing mounting medium with antifading properties (we use VectaShield, Vectorlabs) (*see Note 18*).
14. We suggest using 3D confocal imaging with an immersion objective with high magnification (63× or 100×) and a large numerical aperture (NA > 1.3 ~ 1.4). Excitation/integration parameters are adjusted depending on the samples and a 0.5 µm Z-step is used. Acquisition parameters should be fixed throughout the experimental dataset for statistical analysis.
15. To analyze data, we count the number of intravascular-like cells (i.e., still adhering over the endothelial monolayer) and the total number of extravascular-like cells (i.e., present between the endothelial monolayer and the bottom of the microchannel). Within this last population, we discriminate between diapedesis-extravasation with no obvious endothelial remodeling and endothelial remodeling as observed with specific markers such as PECAM or VE-cadherin (Fig. 3f).

### **3.9 Scanning Electron Microscopy (Fig. 4)**

Use sticky-Slide. We advise to preferentially manipulate chambers under sterile conditions.

1. Gently remove the glue from the bottom part of the chamber by 5 min immersion on pure acetone (Fig. 4a).
2. Remove acetone-soaked glue by using sterile gauze. If not all the glue is removed by these means, do a second 5 min acetone immersion (*see Note 21*).
3. Stick the µSlide I on a sterile rectangular glass coverslip using vacuum grease by gently pressing the coverslip around the chamber to ensure proper vacuum (Fig. 4a) (*see Note 22*).
4. Seed HUVEC as described in Subheading 3.1.
5. Prepare the experiment as described in Subheading 3.6 steps 1–8.
6. Run experiment as described in Subheading 3.8 steps 1–7.
7. Fix with glutaraldehyde 2.5% in 0.1 M sodium cacodylate buffer (pH 7.4) for 15 min at room temperature or overnight at 4 °C.

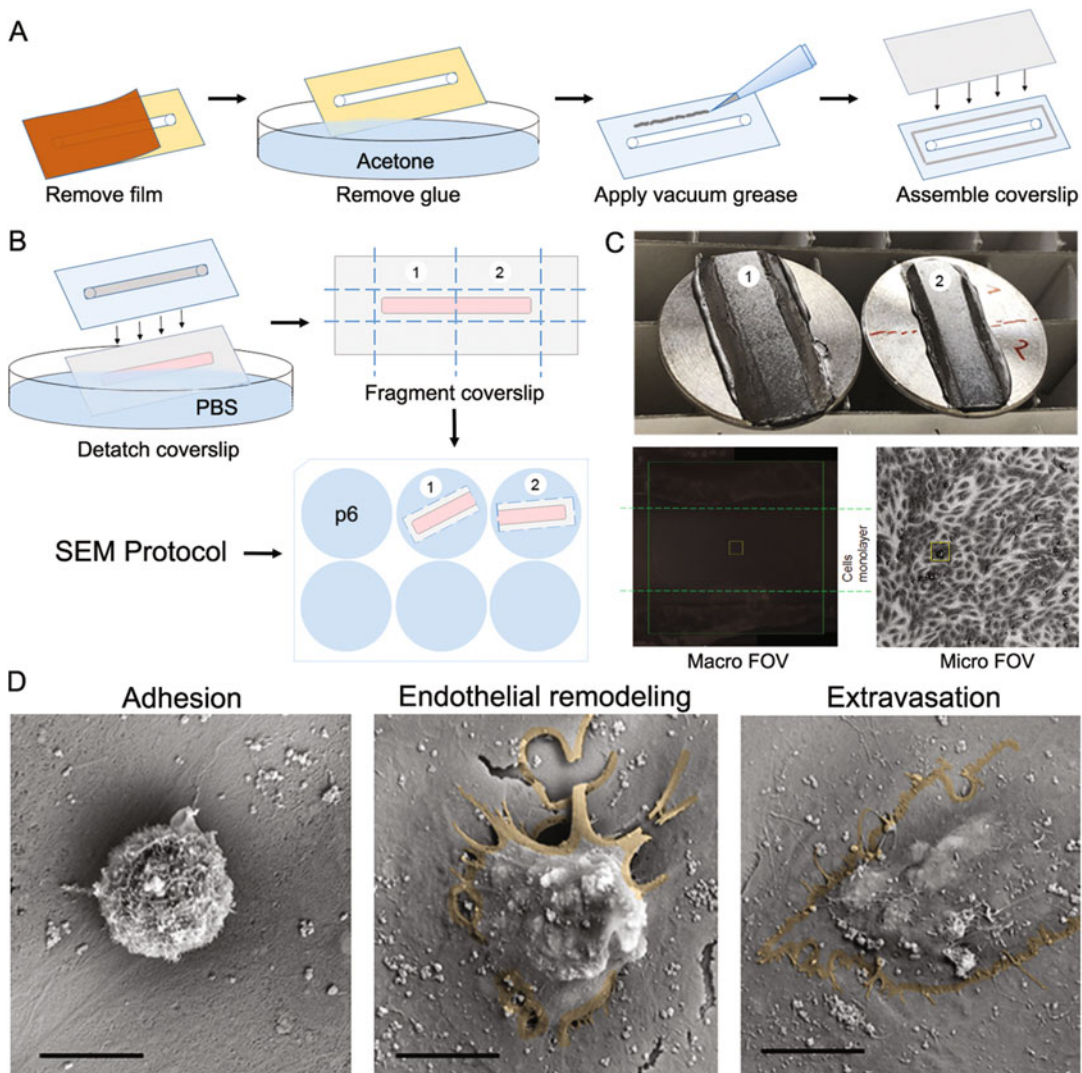


**Fig. 4** Scanning electron microscopy analysis of extravasation using microfluidics. **(a)** Scheme showing the procedure for microchannel setup. **(b)** Scheme showing the procedure for microchannel unmounting prior to EM processing. **(c)** **(top)** Picture showing the samples mounting before acquisition. Picture showing the field of view (FOV) observed with desktop SEM **(bottom left)** at small and **(bottom right)** larger magnification. **(d)** Pictures of scanning electron microscopy at larger magnification showing adhered “intravascular-like” CTC **(left)**, endothelial remodeling **(center)**, and fully extravasated cell **(right)**. Scale bar = 10  $\mu$ m

8. Wash the channel with Milli-Q grade Ultrapure water for 5 min.
9. Immerse the whole chamber on a 10 cm petri dish filled with Milli-Q grade Ultrapure water and proceed to carefully remove the glass coverslip with precision tweezers. Keep glass coverslip always immersed in water.

10. Once detached, place the glass coverslip in a clean 10 cm petri dish containing Milli-Q grade Ultrapure water containing. Carefully cut the cell-containing portion of the coverslip with a diamond knife in two pieces (Fig. 4b) (*see Note 23*).
11. Place the two cell-containing glass fragments into two wells of a 6-well plate filled with Milli-Q grade Ultrapure water. Wash at least of three times.
12. Dehydrate samples by sequential washes on ethanol-graded series ( $3 \times 5$  min on 70%,  $1 \times 5$  min on 80% and 90%, and  $2 \times 30$  min on 100%).
13. Irreversibly dehydrate samples with 5–10 min baths on 1,1,1,3,3,3-hexamethyldilazane (HMDS)/ethanol-graded series (1:2, 2:1, 100% HDMS).
14. Mount samples onto EM Aluminum Mounts using carbon sticky tabs or cement (Fig. 4c).
15. Dry overnight at room temperature.
16. Metalize samples by platinum vaporization under vacuum up to 12 nm.
17. Acquire images on a SEM desktop microscope (Fig. 4c, d).

---

#### 4 Notes

1. The number of rollers is essential for controlling and fine-tuning the flow. We advise using a peristaltic pump with at least 12 rollers. Each roller will induce a small pulsation. Thus, the more roller, the smoother the flow will be. Also, using a digital pump is a plus for fine control of flow perfusion. Pulsatile flows can also be performed, but this should be carefully assessed as it can be perturbed by the rollers (especially fast pulsatility).
2. The 23G  $\times$  1" hypodermic needle should be removed from their Luer using ethanol-sterilized needle-nose pliers. First, remove the white glue sticking the needle to the Luer by scratching it with the plier. Second, pull the needle out of the Luer. During this step, it is essential to avoid bending the needle as this might clog it.
3. We advise using  $\mu$ Slide with a height of 0.4 mm to maximize the efficiency of HUVEC growth. We observed that HUVEC do not grow efficiently at lower height. We also advise not to use larger heights as this would reduce shear stress on HUVEC.
4. To avoid bubbles within microchannels, it is essential to avoid making bubbles when pipetting and removing bubbles. We advise to add at least 10% of volume to any required pipetting volume when loading microchannels. Preheated medium will also prevent bubble formation.

5. The Poiseuille law states that flow speed is maximal in the center of the channel and decreases linearly as it gets closer to the border, where the flow is null.
6. For live imaging experiment, we advise using a 5% CO<sub>2</sub> atmosphere. This can be replaced by using ECGM supplemented with 20 mM of Hepes. In that situation, ECGM supplemented to Hepes should be added to the channel prior to starting experiments, and cells for perfusion should be prepared in ECGM supplemented with Hepes.
7. Tracking can be performed in regions of interest using the Mosaic plugin in ImageJ (<https://imagej.net/MOSAICsuite>).
8. The two most interesting parameters that can be tuned in this setup are the exposure time to shear stress and the strength of the shear stress.
9. The level of shear stress depends on multiple parameters such as viscosity of the medium, radius of the tubing, and the fluid flow that is set on the pump. Poiseuilles' equation linking these parameters is as follows:

$$SS = 4\mu Q / \pi r^3$$

with:

SS the shear stress in Pa.

$\mu$  the viscosity of the medium in Pa.s (In our case, 0.0094 with DMEM).

$Q$  the fluid flow in m<sup>3</sup>.s<sup>-1</sup>.

$r$  the radius of the tubing in m (in our case, 0.0025).

10. The formula linking the tubing length to the volume of cells that can be perfused is  $v = \pi r^2 L$ , with  $v$  the volume in m<sup>3</sup>,  $r$  and  $L$ , respectively the radius and the length of the tubing in m. Convert  $v$  from m<sup>3</sup> to  $\mu$ L for easy assessment of pipetting volumes needed.
11. Hepes is a reliable buffer that can replace CO<sub>2</sub> input for maximum 10 h. For studying longer shear stress exposure durations, a reservoir allowing O<sub>2</sub>/CO<sub>2</sub> entry in the system while preventing medium evaporation is required.
12. When connecting the microfluidics tubing to the microchannel, we advise to let medium drip into a bin to rinse the tubing with medium.
13. When connecting the tubing to the microchannel for long-term cell culture under the cell culture hood, we advise letting the pump outside.

14. For a single channel and overnight flow cell culture, 20 ~ 25 ml of medium is enough. For more channels or longer flow cell culture, 40 ~ 50 ml of medium should be used. For long-term flow culture, medium should be checked on a daily basis and changed if required.
15. We advise using “aspiration”-based medium perfusion (i.e., the pump is located after the microchannel and aspire medium from the medium container through the channel). This maintains elbow Luer in position by creating a depression and avoid air entry and bubbles formation.
16. We advise using a cell line stably expressing a genetically encoded fluorescent marker or alternatively stain cells with stable lipid markers such as DiI/DiO or MemBright [32].
17. For live imaging, we advise using a heating chamber with 5% CO<sub>2</sub> for long-term experiment (more than 9–10 h).
18. Each loading of reagent consists of three steps of wash with medium to ensure that the former liquid is washed away and a final step of adding the reagent to fill the microchannels and both wells.
19. During antibody incubation, the channel should be constantly tilted. Use a tilting stage and attach channels to it using tape. We advise putting the channel into the same direction as the tilt of the stage if bidirectional to maximize antibody homogenization.
20. Fluorescent secondary antibody should be incubated while the microchannels are protected from light (using aluminum foil, for instance).
21. Complete glue removal without chamber surface damage is capital for assuring further grease vacuum and avoid leakiness during perfusion.
22. Avoid grease entering into the channel.
23. It is very important to remove all vacuum grease present on the glass before starting EM procedure.

---

## Acknowledgments

We thank all members of the Goetz Lab for helpful discussions throughout the development of this technology, and to Florent Colin for careful proofreading. We are grateful to INSERM U1255 (EFS, Strasbourg) for providing access to the SEM microscope. This work has been funded by Plan Cancer (OptoMetaTrap and Nanotumor) and CNRS IMAG'IN to S.H. and J.G., by INCa (National Cancer Institute, PLBIO 2015-140) to J.G and by institutional funds from INSERM and University of Strasbourg to

J.G. N.O was supported by Plan Cancer 2014-2019 (OptoMetaTrap) and the Association pour la Recherche contre le Cancer. G.F. was supported by La Ligue Contre le Cancer and University of Strasbourg. V.G. is supported by INSERM and Region Alsace. M.J.G.L. is funded by INCa and University of Strasbourg.

## References

1. Valastyan S, Weinberg RA (2011) Tumor metastasis: molecular insights and evolving paradigms. *Cell* 147:275–292
2. Massagué J, Obenau AC (2016) Metastatic colonization by circulating tumour cells. *Nature* 529:298–306. <https://doi.org/10.1038/nature17038>
3. Follain G, Herrmann D, Harlepp S et al (2020) Fluids and their mechanics in tumour transit: shaping metastasis. *Nat Rev Cancer* 20:107–124. <https://doi.org/10.1038/s41568-019-0221-x>
4. Nguyen DX, Bos PD, Massagué J (2009) Metastasis: from dissemination to organ-specific colonization. *Nat Rev Cancer* 9:274–284. <https://doi.org/10.1038/nrc2622>
5. Obenau AC, Massagué J (2015) Surviving at a distance: organ-specific metastasis. *Trends Cancer* 1:76–91. <https://doi.org/10.1016/j.trecan.2015.07.009>
6. Reymond N, d'Água BB, Ridley AJ (2013) Crossing the endothelial barrier during metastasis. *Nat Rev Cancer* 13:858–870. <https://doi.org/10.1038/nrc3628>
7. Eibl C, Grigoriu S, Hessenberger M et al (2012) Structural and functional analysis of the NLRP4 pyrin domain. *Biochemistry* 51:7330–7341. <https://doi.org/10.1021/bi3007059>
8. McEver RP, Zhu C (2010) Rolling cell adhesion. *Annu Rev Cell Dev Biol* 26:363–396. <https://doi.org/10.1146/annurev.cellbio.042308.113238>
9. Aigner S, Ramos CL, Hafezi-moghadam A et al (1998) CD24 mediates rolling of breast carcinoma cells on P-selectin. *FASEB J* 12:1241–1251
10. Laferrière J, Houle F, Taher MM et al (2001) Transendothelial migration of colon carcinoma cells requires expression of E-selectin by endothelial cells and activation of stress-activated protein kinase-2 (SAPK2/p38) in the tumor cells. *J Biol Chem* 276:33762–33772. <https://doi.org/10.1074/jbc.M008564200>
11. Dallas MR, Liu G, Chen W-C et al (2012) Divergent roles of CD44 and carcinoembryonic antigen in colon cancer metastasis. *FASEB J* 26:2648–2656. <https://doi.org/10.1096/fj.12-203786>
12. Hanley WD, Napier SL, Burdick MM et al (2006) Variant isoforms of CD44 are P- and L-selectin ligands on colon carcinoma cells. *FASEB J* 20:337–339. <https://doi.org/10.1096/fj.05-4574fje>
13. Rahn JJ, Chow JW, Horne GJ et al (2005) MUC1 mediates transendothelial migration in vitro by ligating endothelial cell ICAM-1. *Clin Exp Metastasis* 22:475–483. <https://doi.org/10.1007/s10585-005-3098-x>
14. Shea DJ, Wirtz D, Stebe KJ, Konstantopoulos K (2015) Distinct kinetic and mechanical properties govern mucin 16- and podocalyxin-mediated tumor cell adhesion to E- and L-selectin in shear flow. *Oncotarget* 6:24842–24855. <https://doi.org/10.18632/oncotarget.4704>
15. Osmani N, Follain G, García León MJ et al (2019) Metastatic tumor cells exploit their adhesion repertoire to counteract shear forces during intravascular arrest. *Cell Rep* 28:2491–2500.e5. <https://doi.org/10.1016/j.celrep.2019.07.102>
16. Felding-Habermann B, O'Toole TE, Smith JW et al (2001) Integrin activation controls metastasis in human breast cancer. *Proc Natl Acad Sci* 98:1853–1858. <https://doi.org/10.1073/pnas.98.4.1853>
17. Laferrière J, Houle F, Huot J (2004) Adhesion of HT-29 colon carcinoma cells to endothelial cells requires sequential events involving E-selectin and integrin beta4. *Clin Exp Metastasis* 21:257–264
18. Klemke M, Weschenfelder T, Konstandin MH, Samstag Y (2007) High affinity interaction of integrin alpha4beta1 (VLA-4) and vascular cell adhesion molecule 1 (VCAM-1) enhances migration of human melanoma cells across activated endothelial cell layers. *J Cell Physiol* 212:368–374. <https://doi.org/10.1002/jcp.21029>
19. Reymond N, Im JH, Garg R et al (2012) Cdc42 promotes transendothelial migration of cancer cells through β1 integrin. *J Cell Biol*

- 199:653–668. <https://doi.org/10.1083/jcb.201205169>
20. Barthel SR, Hays DL, Yazawa EM et al (2013) Definition of molecular determinants of prostate cancer cell bone extravasation. *Cancer Res* 73:942–952. <https://doi.org/10.1158/0008-5472.CAN-12-3264>
21. Follain G, Osmani N, Azevedo AS et al (2018) Hemodynamic forces tune the arrest, adhesion, and extravasation of circulating tumor cells. *Dev Cell* 45:33–52.e12. <https://doi.org/10.1016/j.devcel.2018.02.015>
22. Nagrath S, Sequist LV, Maheswaran S et al (2007) Isolation of rare circulating tumour cells in cancer patients by microchip technology. *Nature* 450:1235–1239. <https://doi.org/10.1038/nature06385>
23. Stott SL, Hsu C-H, Tsukrov DI et al (2010) Isolation of circulating tumor cells using a microvortex-generating herringbone-chip. *PNAS* 107:18392–18397. <https://doi.org/10.1073/pnas.1012539107>
24. Yu M, Bardia A, Wittner BS et al (2013) Circulating breast tumor cells exhibit dynamic changes in epithelial and mesenchymal composition. *Science* 339:580–584. <https://doi.org/10.1126/science.1228522>
25. Aceto N, Bardia A, Miyamoto DT et al (2014) Circulating tumor cell clusters are oligoclonal precursors of breast cancer metastasis. *Cell* 158:1110–1122. <https://doi.org/10.1016/j.cell.2014.07.013>
26. Bagnall JS, Byun S, Begum S et al (2015) Deformability of tumor cells versus blood cells. *Sci Rep* 5:18542. <https://doi.org/10.1038/srep18542>
27. Au SH, Storey BD, Moore JC et al (2016) Clusters of circulating tumor cells traverse capillary-sized vessels. *Proc Natl Acad Sci U S A* 113:4947–4952. <https://doi.org/10.1073/pnas.1524448113>
28. Follain G, Osmani N, Fuchs C et al (2018) Using the zebrafish embryo to dissect the early steps of the metastasis cascade. In: *Cell migration*. Humana Press, New York, NY, pp 195–211
29. Osmani N, Goetz JG (2019) Multiscale imaging of metastasis in zebrafish. *Trends Cancer* 5:766–778. <https://doi.org/10.1016/j.trecan.2019.10.003>
30. Regmi S, Fu A, Luo KQ (2017) High shear stresses under exercise condition destroy circulating tumor cells in a microfluidic system. *Sci Rep* 7:39975. <https://doi.org/10.1038/srep39975>
31. Xin Y, Chen X, Tang X et al (2019) Mechanics and actomyosin-dependent survival/chemoresistance of suspended tumor cells in shear flow. *Biophys J* 116:1803–1814. <https://doi.org/10.1016/j.bpj.2019.04.011>
32. Hyenne V, Ghoroghi S, Collot M et al (2019) Studying the fate of tumor extracellular vesicles at high spatiotemporal resolution using the zebrafish embryo. *Dev Cell* 48:554–572.e7. <https://doi.org/10.1016/j.devcel.2019.01.014>



# Chapter 9

## Real-Time Cell Migration Monitoring to Analyze Drug Synergism in the Scratch Assay Using the IncuCyte System

Dennis Kobelt, Wolfgang Walther, and Ulrike S. Stein

### Abstract

Drug-mediated interference with metastasis represents a key approach to improve cancer therapy. In this regard, appropriate in vitro assays are needed to identify drugs, which inhibit cell migration as one feature for metastatic potential of cancer cells. One such migration assay is the wound healing or scratch assay, designed to allow cells for closure of an artificially generated gap (wound/scratch) in the monolayer. To identify possibly effective anti-migratory drugs as monotherapy or as synergistic drug combination, novel screening tools besides viability measurements at the experimental endpoint are needed. In this context, particularly drug combinations allow to increase treatment efficacy paralleled by lowered side effects. Here, a protocol for real-time monitoring cellular motility and its inhibition by anti-migratory drugs and combinations by the IncuCyte system and a 96-well scratch assay is described. A pipetting scheme allowing data collection for synergy calculation using one plate per replicate is provided. Using the IncuCyte System 2, drug combinations built of three biological replicates each using three technical replicates can be tested in parallel within hours to few days to accelerate identification of efficient antimetastatic drugs.

**Key words** Drug interaction, Synergy, IncuCyte, Combenefit, Scratch assay, Cell motility

---

### 1 Introduction

The scratch assay is one of simplest methods to study cellular movement in vitro. The technique dates back more than 60 years ago, although not initially described as an independent method [1]. Some years later, this assay was already used to analyze cell migration [2]. Despite all drawbacks and limitations like missing the extracellular matrix and 3D organization of cells, it is still a method that is widely used to analyze drug effects on motility. In addition, the impact of oncogenes using overexpression or inhibition via mi/siRNA or CRISPR/Cas experiments on motility can be assessed.

The scratch assay is based on the cell's behavior to start proliferation and movement towards space that is artificially applied to a confluent monolayer [1]. This space is likely called a wound in the

monolayer and the assay therefore referred as wound healing assay. It is to some extent comparable to the physiologic processes during wound healing. During wound healing, different cell types migrate towards the lesion. Here, for example, integrins play a pivotal role during physiological wound healing and migration. In the scratch assay, cells have to migrate in the direction of new space. In comparison to another popular assay, the Boyden chamber migration assay, the scratch assay can be more easily multiplexed and combined with microscopic techniques and monitoring tools. Furthermore, the scratch assay allows assessing cells attached to a surface and with limited cell–matrix and cell–cell contacts. This assay is therefore useful to monitor drug action interfering with cell migratory capabilities. In fact, this provides useful hints, if a given drug or drug combination has antimetastatic potential.

Due to technical development of devices capable to monitor cellular behavior in upscaled numbers involving several multiwell plates in parallel, it is possible to use the scratch assay as screening tool. In this protocol, the IncuCyte system is used to monitor cell movement. The monitoring of living cells with the help of the IncuCyte Zoom can be carried out over short (hours to few days) but also long periods (weeks) without any user access. The movable optics enable the trouble-free representation of the cells, which will be carried out at each time point at the very same position. This is supported by an autofocus. In this way, quantitative cell biology analyses are possible. The system is housed in an incubator with controlled humidity and CO<sub>2</sub> level, so that the analyses can be performed on living cells using standard cell culture conditions without disturbance while moving cells to a conventional microscope. The system takes bright field pictures, but offers fluorescence channels for green and red fluorescence. The system can accommodate a variety of testing formats, with 96-well plates for this particular protocol. These plates allow the minimum required concentrations and technical replicates in one plate greatly facilitating mid-scale drug testing and synergy calculation. Since six plates can be monitored in parallel, biological replicates can run in parallel. It is strongly recommended to use the 96-well IncuCyte® ImageLock Plates to facilitate monitoring the same spot at each time point. The scratches in 96-well format are applied using the IncuCyte® WoundMaker tool. It is a pin-based tool that applies one scratch per well in all wells in parallel. The IncuCyte® ImageLock Plates provide a trace mark so that the scratch is always centered, and pictures can be taken at the same position each time point.

Furthermore, software packages like Combenefit enables researchers to calculate possible beneficial or detrimental drug–drug interactions. This allows, for example, in cancer therapy, to identify possible beneficial drug combinations that target cancer drivers and downstream signals enhancing therapy success, omit or delay resistance, and avoid side effects in a way that the net efficacy

exceeds just the sum of the two drugs applied [3]. Since here new drugs not necessarily have to be developed, this allows optimizing therapeutic schedules within comparatively short time frames and low costs starting *in vitro* employing screening approaches. Most drug combinations were developed empirically. However, the possibility to study drug combinations *in vitro* should foster this process [4]. Alternatives are, for example, SynergyFinder [5], CompuSyn [6], Synergy [7], and Chalice or Genedata Screener (both commercial). The theory behind synergy and antagonism calculation is extensively discussed elsewhere [8].

---

## 2 Materials

All buffers and media should be pre-warmed before use. The requirements are based on the cell lines and conditions used. HCT116 human colorectal cancer cells are kept in RPMI with 10% fetal calf serum without antibiotics. The cells are passaged and collected using trypsin using standard cell culture protocols. The cells in the assay should be used at low passage and come from a defined pre-culture (e.g.,  $5 \times 10^6$  cells in a T175 cell culture flask grown for 48 h before the experiment, *see Note 4*) to increase reproducibility of the starting conditions. They can be kept using standard culture conditions unless the experimental setup requires special conditions like starvation. All treatment substances should be of high quality with low concentrations of contaminating side products. If the drugs cannot be dissolved in growth medium, we recommend preparation of stock solutions and all dilutions thereof as highly concentrated (e.g., 2000 $\times$  fold stocks in solvent, e.g., DMSO. This leads to a fixed DMSO concentration for all conditions.

### 2.1 Cell Cultivation

Test cell lines (HCT116, LGC Standards/ATCC, Wesel, Germany).

Growth medium (RPMI 1640, Thermo Fisher, Waltham, MA, USA).

Serum (fetal calf serum (FCS) Bio&Sell, Feucht, Germany).

Growth factors (optional, if needed).

Cell dissociation reagent (trypsin–EDTA, Thermo Fisher).

Phosphate-buffered saline (PBS).

Additives, e.g., antibiotics, amino acids, vitamins if needed.

### 2.2 Materials for

#### Preparation of Cells for Scratch Assay

Cell culture flasks (Sarstedt, Nümbrecht, Germany).

Cell counting equipment, e.g., hemocytometer, automated cell counter (Juli BR, NanoEnTek, Seoul, Korea).

Multichannel pipette, minimum volume per channel 100  $\mu$ l, electronic pipettes with stepping and larger volumes will facilitate seeding (EDP3 100–1200  $\mu$ l, Rainin, Oakland, CA, USA) (*see Note 1*).

IncuCyte® ImageLock Plates (Essen Bioscience, Ann Arbor, MI, USA).  
 IncuCyte® WoundMaker (Essen Bioscience).  
 IncuCyte® System (Essen Bioscience) (*see Notes 2 and 3*).

### **2.3 Software for Qualitative and Quantitative Migration Analysis**

IncuCyte® Zoom (analysis of cell movement).  
 Scratch wound plugin for the IncuCyte® Zoom software.  
 Combefit [9] (calculation of synergy).  
 Statistic software package of choice (GraphPad Prism 6.0, San Diego, CA, USA).  
 The materials or suppliers in brackets were used in this protocol and have to be adjusted to the experimental needs.

## **3 Methods**

### **3.1 Preparation of Cell Cultures, Seeding of Assay Plates, Scratch Assay, Drug Treatment**

In this basic protocol, the human colorectal cancer cell line HCT116 is used. Please adapt critical steps needed for the cell line used, based on your established protocols.

1. Cells are harvested from standard cultures. Briefly, cells are washed with PBS and incubated with trypsin–EDTA for 3–5 min at 37 °C in the incubator until the cells are completely dissociated. The cells are washed out of the flask with complete growth medium. After forming a pellet (centrifugation at  $200 \times g$ , 5 min), the old medium is replaced by fresh complete growth medium (RPMI 1640 + 10% FCS). Following counting,  $5 \times 10^6$  HCT116 cells are seeded in T175 flasks in 30 mL of complete growth medium. The cells are cultivated at 37 °C in a humidified incubator for 48 h. This results in a reproducible cell culture for starting the experiment (*see Note 4*).
2. The seeded cells should be sub confluent after 48 h of incubation. The cells are harvested as described above (*see step 1*). After centrifugation at  $200 \times g$ , 5 min and medium change, the cells are counted using the JuLI Br device. For seeding, the cells have to be diluted to  $1.1 \times 10^6$  cells per mL medium. The cell number is critical to obtain a monolayer after cultivation and has to be determined before the experiment is started for each specific cell line (*see Note 5*).
3. The cells are seeded into the inner 60 wells of the 96-well IncuCyte® ImageLock Plates (*see Fig. 1, see Note 6*). Each well is filled with 100 µL cell suspension resulting in a cell density of  $1.1 \times 10^5$  cells per well. The volume of 100 µL is recommended for the IncuCyte® WoundMaker tool and should not be increased or decreased. The outer 36 wells are filled with 100 µL PBS to avoid evaporation effects of the neighboring wells (*see Note 6*). Electronic and multichannel pipettes will aid the seeding process (*see Note 1*).

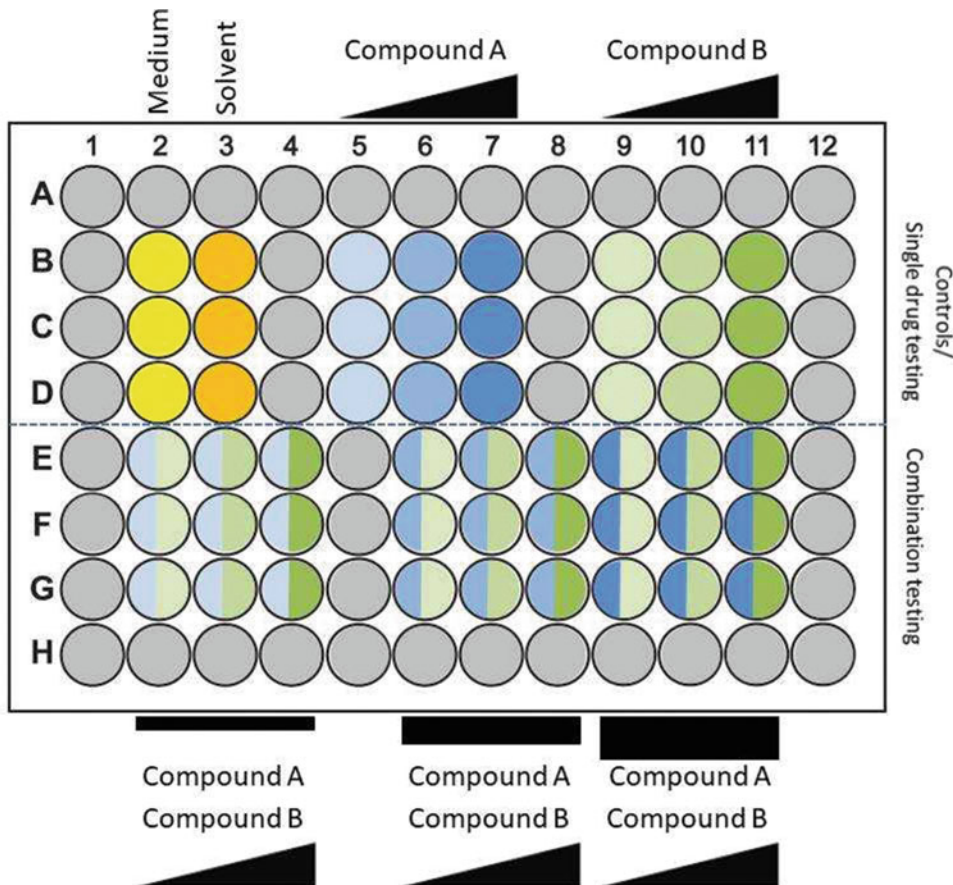


**Fig. 1** 96-well template for drug distribution. This test format allows to obtain data for calculation of possible drug synergies. Only the inner 60 wells (colored) are used. All unused wells of plate margins (gray) are filled with PBS. In the upper part, controls (medium [yellow], solvent [orange]) and the single drugs are applied. At least three concentrations are needed to generate dose-response curves. In the lower part (dual color area), the single drugs are combined. In each part, one drug is kept at a constant concentration while the other is applied in increasing concentrations

4. The plates are incubated at 37 °C in a humidified incubator for 6 h. The time here is critical and has to be determined before the experiment. The cells have to get enough time to settle down and adhere. But it has to be short enough that the cells do not form extensive cell-cell contacts that would lead to significant damage of the monolayer during scratching (*see Note 7*).
5. In parallel, the desired drug dilutions can be prepared. It is recommended to prepare high concentrated (2000×) stocks. The stock solutions are serially diluted in solvent. For example, 2, 1, and 0.5 mM stocks in solvent are needed to apply a drug with concentrations of 1, 0.5, and 0.25 µM, respectively. As a minimum to generate dose-response curves and calculate

possible synergistic effects, three concentrations per drug and all combinations thereof are needed (*see Fig. 1*). These 2000× fold stocks are diluted 1000× in medium, e.g., 1 µL stock solution per 1 mL medium. 100 µL diluted drug in medium is added to the cells in 100 µL medium per well. This results in a final 2× dilution giving rise to the desired drug concentration. If cells are washed (optional **step 7**), 1000× stocks have to be prepared and 200 µL diluted drug in medium should be added per well. For single drugs, an additional supply of solvent (e.g., 1 µL solvent per mL medium) is needed to get the same solvent concentration as in the drug combination samples. Solvent dilutions without drugs at appropriate concentrations serve as controls. If needed, at this step, further reagents to monitor cell death can be added (*see Note 3*).

6. Before applying the scratches to the cell monolayer, the IncuCyte® WoundMaker tool needs to be cleaned. The tool comes with three holders: two for liquids, one for the 96-well plates. One holder has to be filled with 80% ethanol, the other one with sterile PBS. After incubation of the wounding tool first for 5 min in ethanol and washing in sterile PBS, it can be used for scratch application. One IncuCyte® ImageLock assay plate without lid is placed in the plate holder, and the scratch applicator is placed on top. Leave one hand at the handle, with the other press the button with a constant force to move the scratch applicator once over the monolayer (*see Note 8*). After applying the scratch, remove the applicator without releasing the button. The last step is critical to avoid uneven scratches (*see Note 7*).
  7. Optional step: Dependent on the cell line used, the wells can be washed with PBS to remove floating cells.
  8. Directly after applying the scratches, the drugs (*see step 5*) can be applied. If the cells were not washed, 100 µL of a 2× concentrated drug/medium solution is added. After washing with PBS, 200 µL containing the final drug concentration is used. Medium and appropriate solvent dilutions serve as controls.
  9. The plates are placed in the IncuCyte® System (*see Note 2*). The software is set up to monitor the cells every second hour (*see Note 9*). To monitor scratch closure, preestablished image collections of the utilized cells and the scratch wound option are used. Dependent on the cell line, scratches will close within less than 1 day to several days.
- 3.2 Data Analysis**
1. The data of wound (scratch) confluence over time can be exported as averages of the technical replicates. Using the three biological replicates, growth curves can be generated using a statistics program (*see Fig. 2a*). For better visualization,

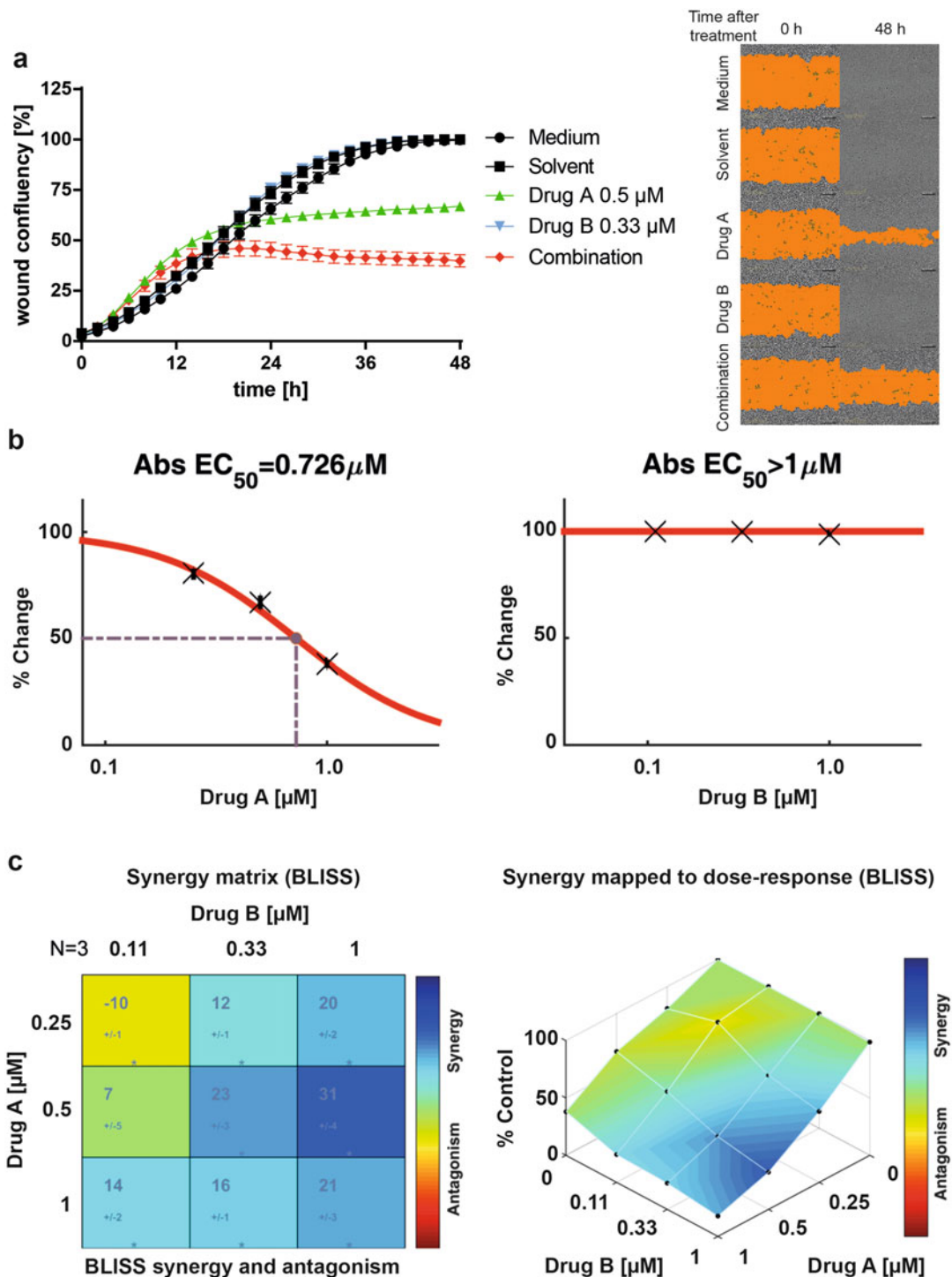


**Fig. 2** Representative results for a synergistic drug combination in the scratch assay. This experiment shows how single drugs and combination thereof can be evaluated for their ant-migratory efficacy in the IncuCyte scratch assay. **(a)** Growth curves for human HCT116 colon carcinoma cells treated with two different

only one concentration per drug and respective combination is shown. Drug effects of the lower and higher concentrations are summarized in the dose-response curves (*see* Fig. 2b).

2. The single averages for one time point are grouped in a matrix format defined by the program. For Combenefit, one matrix table (provided with the program) per experiment is needed in order to obtain significance calculations of biological replicates (*see Note 10*). In this matrix table, the control expressed in percent is expected in the upper left corner. In columns in ascending concentration order, the values for one drug are placed. In rows again for increasing concentrations, the values for the second drug are placed (*see* Fig. 2). The measurement values for the combinations are placed at their respective position defined by the applied drug concentration.
3. The tables for each biological replicate have to be placed in one folder. All tables will be used as replicate, if they fit in concentration, unit, and data number. At the front screen of Combenefit, the project folder containing the data tables can be chosen at the top. After choosing the synergy model(s) (HSA, Loewe, Bliss) and the outputs for dose-response, model and synergy distribution, the analysis can be started. Combenefit will generate figures for the selected output automatically. If the option for data storage is activated, all figures will be saved in the project folder in automatically generated subfolders (*see Note 10*).

### 3.3 Anticipated Results

1. The generated growth curves (*see* Fig. 2a) should show that the medium and solvent controls close the scratch with nearly the same speed (black curves). Since the solvent control could show different closure behavior, this is the appropriate control for the matrix table used to calculate drug interaction effects. If there is an extensive cellular reaction in the solvent control, the solvent itself or the concentration should be considered to change (higher concentrated stocks, another solvent if possible). The single drugs can show an effect. In the presented example, one drug shows no activity on scratch closure, while

---

**Fig. 2** (continued) experimental drugs. Three biological replicates for medium (black circle), solvent control (black squares), single drug A (green triangle), drug B (blue triangle), and the combination (red diamond) were used. Representative pictures showing the scratched monolayer 0 h and 48 h after drug application for the different treatment groups are depicted. The area that is not covered by cells is colored orange using the scratch wound mask. The area covered with cells is left uncolored and appears gray. (b) Dose-response curves for this experiment at three different single drug doses are shown. Drug A successfully delays scratch closure while drug B is not showing this effect at the tested concentrations. (c) Synergy matrix and synergy mapped to dose-response for the synergy model BLISS. Blue color represents synergistic effects of the drug combination regarding anti-migratory efficacy. Data are shown as mean  $\pm$  SEM for three biological replicates measured in three technical replicates

the other drug does (blue curve behind the controls, green curve). The drug combination shows a stronger effect than the single drugs, and the resulting sum of these single drug effects is giving hint to possible synergistic effects (red curve).

2. The dose-response curves (*see* Fig. 2b) confirm the impression for the single drugs examples above. In this example, drug A actively inhibits scratch closure with an IC<sub>50</sub> of 0.726 μM with nearly no activity at the very lowest concentration, while drug B does not inhibit scratch closure until a concentration of 1 μM when applied as single agent.
3. The Synergy matrices provided in Fig. 2c show that the two drugs applied here are indeed acting synergistically. At very low concentrations, where both drugs are nearly inactive, synergism is lost due to missing drug activity.

---

#### 4 Notes

1. The electronic and multichannel pipettes can be replaced by standard laboratory equipment. But pipetting manually numerous wells and plates is a source of error.
2. The IncuCyte® System can be replaced by other devices. This might lead to an increased number of experimental runs if only one plate can be assessed per time. If no automated monitoring equipment is available, standard microscopes with camera can be used. An automated stage will allow monitoring constant positions. Scratch closure can be calculated using an ImageJ plugin [10]. To date, the IncuCyte® WoundMaker is the most convenient tool to apply scratches in the 96-well format. V&P Scientific Inc. is providing wound making tips for robots and Poon et al. have provided a protocol using a multichannel-based installation [11].
3. To monitor cytotoxic effects, fluorescent reagents (for example, Essen Bioscience) for caspase 3/7 activity, surface Annexin V, or dead cells staining can be added to the experiment. They should be tested if they interfere with the experimental conditions.
4. The pre-culture in a cell culture flask allows to minimize uncertainties of culture conditions like cell density, pH, nutrient supply.
5. Cells might appear to be moved to one side in the assay plate. Possible solutions are: plates should be incubated in a leveled incubator to avoid cell movement to the lower side. Longer incubation times after seeding will allow the cells to adhere more tightly to the growth surface to avoid flushing cells to one side while pipetting drugs. Similarly, slower pipetting, especially with electronic pipettes, can reduce this effect as well.

6. The outer 36 wells should not be used for experimental conditions to avoid artifacts due to medium evaporation. Instead, they should be filled with 100 µL PBS.
7. Uneven scratches might result from cells that formed extensive, tight cell–cell contacts. Shorter incubation times between seeding and scratch application can reduce this effect and improves experimental outcome.
8. The IncuCyte® WoundMaker tool is optimized for the IncuCyte® ImageLock 96-well Plates. Other plates could be used, but they might damage the WoundMaker tool. In addition, uneven scratches can result if the plate is slightly lower or higher compared to the recommended plates.
9. It is recommended to monitor the cells every second hour. This allows the system to cooldown between measurements but generates enough data to draw growth curves and prepare animations/videos with reasonable frame rates. This time can be adjusted dependent on the actual movement speed of the cells analyzed.
10. Usage of locally stored data increases software stability and working speed of Combenefit.

## References

1. Todaro GJ, Lazar GK, Green H (1965) The initiation of cell division in a contact-inhibited mammalian cell line. *J Cell Physiol* 66 (3):325–333. <https://doi.org/10.1002/jcp.1030660310>
2. Burk RR (1973) A factor from a transformed cell line that affects cell migration. *Proc Natl Acad Sci U S A* 70(2):369–372. <https://doi.org/10.1073/pnas.70.2.369>
3. Al-Lazikani B, Banerji U, Workman P (2012) Combinatorial drug therapy for cancer in the post-genomic era. *Nat Biotechnol* 30 (7):679–692. <https://doi.org/10.1038/nbt.2284>
4. Bijnsdorp IV, Giovannetti E, Peters GJ (2011) Analysis of drug interactions. *Methods Mol Biol* 731:421–434. [https://doi.org/10.1007/978-1-61779-080-5\\_34](https://doi.org/10.1007/978-1-61779-080-5_34)
5. Ianevski A, He L, Aittokallio T, Tang J (2017) SynergyFinder: a web application for analyzing drug combination dose-response matrix data. *Bioinformatics* 33(15):2413–2415. <https://doi.org/10.1093/bioinformatics/btx162>
6. Chou T, Martin N (2005) CompuSyn for drug combinations: PC software and user's guide: a computer program for quantitation of synergism and antagonism in drug combinations, and the determination of IC50 and ED50 and LD50 values. ComboSyn Inc, Paramus, NJ
7. Kong M, Lee JJ (2008) A semiparametric response surface model for assessing drug interaction. *Biometrics* 64(2):396–405. <https://doi.org/10.1111/j.1541-0420.2007.00882.x>
8. Chou TC (2006) Theoretical basis, experimental design, and computerized simulation of synergism and antagonism in drug combination studies. *Pharmacol Rev* 58(3):621–681. <https://doi.org/10.1124/pr.58.3.10>
9. Di Veroli GY, Fornari C, Wang D, Mollard S, Bramhall JL, Richards FM, Jodrell DI (2016) Combenefit: an interactive platform for the analysis and visualization of drug combinations. *Bioinformatics* 32(18):2866–2868. <https://doi.org/10.1093/bioinformatics/btw230>
10. Schneider CA, Rasband WS, Eliceiri KW (2012) NIH image to ImageJ: 25 years of image analysis. *Nat Methods* 9(7):671–675. <https://doi.org/10.1038/nmeth.2089>
11. Poon PY, Yue PY, Wong RN (2017) A device for performing cell migration/wound healing in a 96-well plate. *J Vis Exp* (121). <https://doi.org/10.3791/55411>



# Chapter 10

## Measurement of Metabolites from Migrating Cells

Demond Williams and Barbara Fingleton

### Abstract

Metastasis is a multistep process that involves responses to extrinsic and intrinsic signals at every step. It is thus only truly appreciated in the context of a whole organism. Nevertheless, *in vitro* studies can be used to facilitate understanding of the possible factors contributing to any phenotype that is associated with metastatic competence. The use of migration assays—where monolayers of cells migrate to cover gaps or “wounds”—has been described for decades to identify signaling pathways that regulate motile competence and to screen for ways of interfering with this ability. Here we depict the combination of such an assay with assessment of indicators of carbon metabolism using commercially available assays. This enables identification of changes in cellular metabolism associated with actively migrating cells.

**Key words** Metastasis, Migration, Scratch assay, Glucose consumption, Lactate production

---

### 1 Introduction

The multiple steps of metastasis have been well described (1) and include both tumor cell autonomous behaviors and microenvironmental interactions. Thus, studying cell cultures *in vitro* cannot give a complete assessment of metastatic ability. Nevertheless, reductionist approaches enable evaluation of complex changes within cells under specific conditions. Here we use a straightforward two-dimensional (2D) cell migration assay as a means of assessing metabolic changes within tumor cells. We chose migration as one of the quintessential behaviors linked to metastatic potential and used an assay protocol that slows us to separate the metabolic changes associated with this single behavior. In the method described below, we describe the use of commercially available cell culture inserts. These enable the creation of a space for cells to migrate into without having to “wound” a cell monolayer. This is considered better than the traditional scratch assay where a pipette tip is used to literally scratch through the monolayer, thus creating an empty space (2). In creating the scratch, cells are damaged and can release factors that may impact cell behavior (3). Additionally,

use of inserts allows direct comparison of the same number of cells since removal of inserts should not significantly reduce cell numbers and reproducibility is improved (4). In contrast, the creation of scratches or wounds directly removes cells that were part of the monolayer. Nevertheless, the method described below can be easily adapted for a scratch assay format, as indicated.

For assaying metabolic activity, there are a number of different commercially available assays, and many of them are appropriate for use in the method described below. The optimal method, which we describe, is to assay the medium thus allowing multiple timepoints from the same set of specimens. It is also possible to set up multiple parallel sets of specimens that can be used at different timepoints if cell lysates are needed for the assays chosen.

---

## 2 Materials

### 2.1 Materials for Migration Assays

1. Actively growing culture of cells of interest.
2. Trypsin (0.25% with EDTA) or whatever is standard for dissociation and collection of the cells used.
3. Growth medium with glucose concentration of up to 5 mM, preferably serum-free (*see Note 1*).
4. Sterile PBS.
5. Trypan blue.
6. Cell counter and necessary slides or hemocytometer.
7. 24-well cell culture plates.
8. Silicone 2- or 3-well migration inserts, available from ibidi.
9. Sterile forceps.
10. Inverted microscope with camera that can capture phase contrast images.
11. ImageJ software—freely available from NIH (<https://imagej.nih.gov>).

### 2.2 Materials for Metabolic Assays

1. Promega-Glo assay kits for glucose uptake, lactate production, glutamine uptake, and glutamine production or other equivalent biochemical assay kits.
2. Microfuge tubes.
3. Micro-centrifuge.
4. -20°C freezer.
5. 96-well non-cell culture treated assay plates.
6. Microplate luminometer (*see Note 2*).
7. Optional if assaying cell lysates: Deproteinization kit such as Biovision Deproteinization Sample Preparation kit.

8. Optional if preparing lysates for assay of total protein content: Radioimmunoprecipitation assay (RIPA) buffer for protein lysis (0.1% sodium dodecyl sulfate, 0.5% sodium deoxycholate, 1% Triton X, 10 mM Tris pH 7.5, 150 mM NaCl).
9. Optional if conducting total protein assay for normalization: Bicinchoninic acid assay or other standard assay for determination of total protein content.

---

### 3 Methods

#### 3.1 Migration Assay and Sample Collection

1. If using migration inserts, use sterile forceps to transfer a 2- or 3-well migration chamber into multiple wells of a 24-well plate. Ensure the inserts adhere to the bottom of the well by gently tapping all around the top with the forceps and checking that they do not slip when the plate is moved (*see Note 3*).
2. Prepare cells by trypsinizing, counting, and diluting to ~200,000/ml of viable cells (trypan blue excluding) (*see Note 4*).
3. Place 1 ml of the cell suspension into each well, making sure it is as homogenous as possible before pipetting. If using a treatment, prepare it a 2× final concentration in the same medium as the cells are in and also make cell suspension at double cell concentration, e.g.,  $4 \times 10^5$ /ml, then mix together before adding to the appropriate wells. Use pipette tip to mix and ensure cells are evenly dispersed within insert (*see Note 5*).
4. Incubate 15–24 h under standard culture conditions (*see Note 6*).
5. After incubation, observe under microscope and ensure cells within insert and well are confluent.
6. If using migration inserts, use sterile forceps to gently remove inserts from each well to be used for migration assay; pull up so as not to disturb edges of cell layers. If using scratch assay, carefully scratch a single line down the center of the well with a sterile pipette tip (*see Note 7*).
7. Gently rinse each well with 1 ml of sterile PBS—add to side of well and rock plate carefully before aspirating from side of well. Repeat. This will remove any accidentally dislodged cells.
8. Gently add 0.6 ml of medium to well so that cell layer is completely covered. If using a treatment, add it to this medium. Save 30 µl samples as the t0 medium for metabolism assays. The medium samples should be stored at –20°C for later analysis (*see Note 8*).
9. Under phase contrast and 4× magnification, take time zero (t0) pictures along length of gap between cell sheets. At least

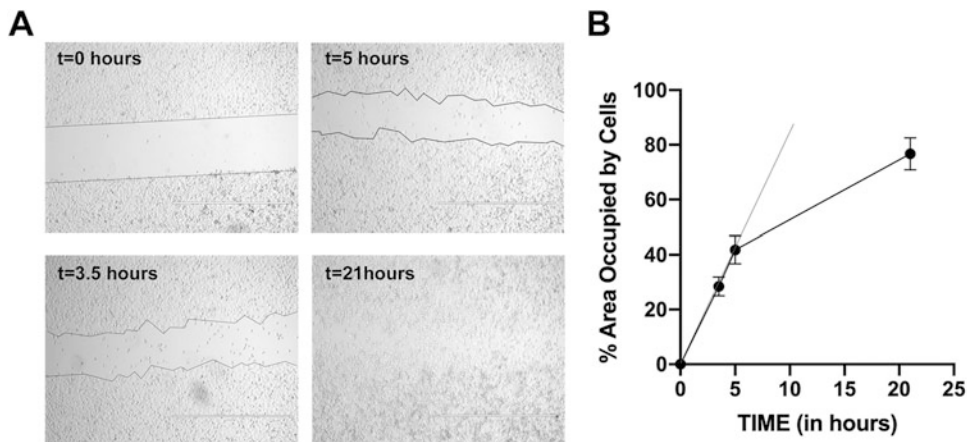


**Fig. 1** Migration assay using 4 T1 mammary cancer cells. (a) Sample images of a gap at times 0, 3.5, 5, and 21 h post-plating with area of gap outlined. Note no obvious gap remains at the final timepoint. (b) Graph showing area covered by cells over time. There is a clear change in the kinetics of migration between the 5 and 21 h timepoints, thus the initial rate of migration was calculated from the slope of the line for the 0, 3.5, and 5 h timepoints and is shown as a gray line

four images should be taken for each gap. Ensure that all images show the cells on either side of the gap (example in Fig. 1a). Save each image as a tif file.

10. Return plate to incubator and remove to image as above at 2–3 timepoints over 24 h (*see Note 9*). Continuing the assay for longer than 24 h is not recommended since proliferation of cells could then play a significant role in the apparent filling of the gap.
11. At each timepoint of interest, collect 30  $\mu$ L of medium from each well, spin at 10,000  $\times \ddot{\gamma}$  to remove any cellular debris, and snap-freeze the supernatant at  $-20^{\circ}\text{C}$  until ready to use for metabolism assays. Make sure to freeze in aliquots of 5–10  $\mu\text{l}$  if anticipating needing to perform multiple assays at different times so that individual samples do not undergo multiple rounds of freeze–thaw.
12. Analysis of the ability of cells to fill the gap can be done using ImageJ. Use a freehand tool to outline the area in each picture that has no cells—this should get smaller over time. The percent coverage is calculated as  $[(\text{Area at time } 0 - \text{Area at time } x)/\text{Area at time } 0] \times 100$ . The average for each timepoint can be plotted against time, and the slope gives the rate of migration (area covered per unit time). *See Fig. 1* for an example.

### 3.2 Metabolism Assays

1. Optional: If cell lysates will not be prepared for the metabolic assays, a standard lysis buffer such as RIPA buffer can be used to collect lysates from each well from the migration assay to enable normalization between wells based on protein concentration.

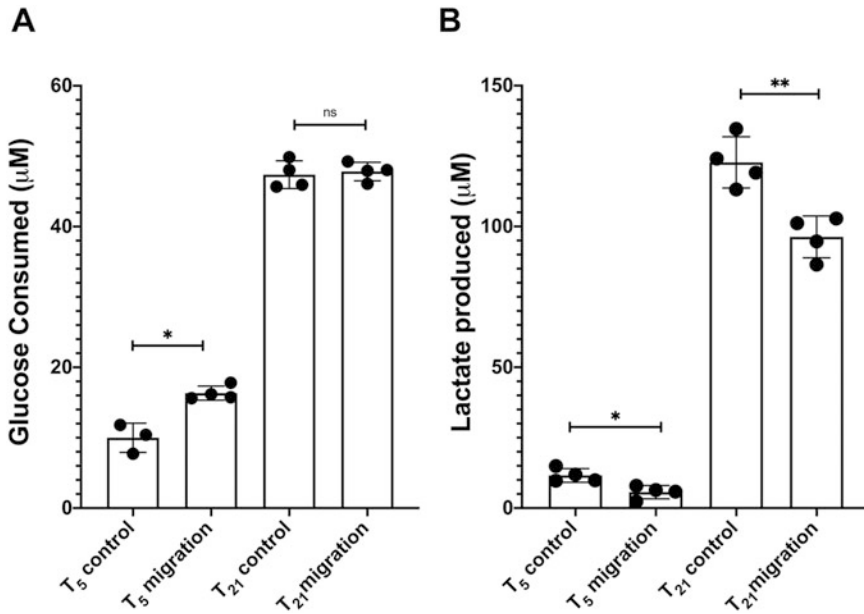


**Fig. 2** Changes in (a) glucose consumption and (b) lactate production between wells with actively migrating cells versus intact monolayers at the 5 and 21 h timepoints from the cells shown in Fig. 1. The migrating cells show increased glucose consumption that is not matched by increased lactate production suggesting that the glucose is used for oxidative phosphorylation rather than glycolysis

This is recommended if performing a scratch assay where cell numbers may be different between migrating and non-migrating wells, or if cell proliferation is possible.

2. Gently thaw all the medium samples to be analyzed on ice.
3. Dilute media collected with assay buffer (provided in assay kit) in order to bring concentration of metabolites of interest within the linear range of the assay being used (*see Note 10*). For the samples shown in Fig. 2, the cells were in medium containing 5 mM glucose and the dilution used was 1:200.
4. Optional: If analyzing intracellular concentration of metabolites, harvest cells and wash with PBS before resuspending cells in assay buffer and homogenizing by trituration with a pipette.
5. Optional: If using lysates, deproteinize using a standard deproteinization protocol such as perchloric acid precipitation (*see Note 11*). Do not deproteinize the entire lysate so that a protein assay can be performed on a fraction to enable normalization between samples.
6. Follow specific assay instructions given with each kit to determine the amount of metabolic substrate or product in medium or lysate sample at each timepoint (*see Note 12*).
7. To calculate substrate consumption, use the standard curve to determine the amount of glucose in each sample at time x and

at time 0, and correct for any dilution factors. Glucose consumption = concentration at time 0 – concentration at time  $x$ . Levels of metabolic products present in medium, e.g., lactate, can be determined directly from the standard curve with correction for any dilution factors. Example values from the migration assay shown in Fig. 1 are shown in Fig. 2. If lysates were analyzed for total protein content, the levels of substrate or product can be further divided by the protein concentration from that well to report the metabolite level per mg of total cellular protein.

---

## 4 Notes

1. When analyzing metabolism in cell culture, the concentration of metabolic substrates in the medium is an important consideration. For example, the concentration of glucose in most cell culture media is 25 mM, far out of the detection range of commercially available assays. Many assays will suggest using media with reduced concentration, for example, DMEM with 5 mM glucose as opposed to normal formulation, in order to limit how much samples must be diluted before they can be processed. Additionally, serum contains both metabolic substrates and products from the donor animal, thus minimizing the serum level is advantageous. We use serum-free or 2% serum (depending on cell line) for our assays. Since the medium is changed at the start of the migration assay, it is possible to use different media for initial plating and for the actual assay. This maybe especially important for cells that are sensitive to reduced serum levels.
2. For the Glo assays used here, the signal is luminescence and a luminometer is needed; however, other biochemical assays may require a fluorimeter or spectrophotometer.
3. The numbers of wells for each condition should be a minimum of three to enable statistical testing, but more may be needed. With practice, variability among wells should be minimal. To compare migrating versus non-migrating cells, we can either use wells with no inserts or use wells in which inserts will not be removed the next day.
4. The optimal cell concentration can change depending on the cell line and will need to be empirically determined. The aim is to have a confluent layer after 15–24 h of plating in the insert. Try  $0.75\text{--}4 \times 10^5/\text{ml}$ .
5. It is absolutely key that the cells are evenly distributed both within and around the migration inserts and the well in general. The plate can be swirled gently to aid in achieving a homogeneous layer of cells.

6. The length of time for incubation is based on obtaining an even monolayer within each well. Another factor is the timepoints for the ensuing migration assay. In our experience, we typically plate in the late afternoon on one day and start the migration assay in the morning of the following day after ~16 h of incubation.
7. For making a scratch, we have found a smaller size tip (for a 1–20  $\mu$ l pipettor) to be easiest to control. Hold directly with fingers rather than with forceps. While it is possible to make multiples scratches in each well to obtain multiple data points for the migration assay, this will impact the interpretation of any metabolic assays since each scratch removes cells from the well thus reducing overall cell number.
8. At this point, the medium can be changed from that used for the initial plating as indicated in **Note 1**. If any wells are receiving different treatments, e.g., addition of a growth factor or a drug or vehicle, separate samples must be collected for each of these as such additives could potentially affect the metabolic assays.
9. This is very cell-line dependent. Highly motile cells should be imaged at shorter timepoints, e.g., 2, 4, and 6 h; while others may only show movement beginning at 12–14 h.
10. We often perform serial dilutions with new samples when processing new cell lines or assaying for different metabolites. While the kit instructions make suggestions regarding dilutions, there is still cell-line dependence and thus the optimal dilution for each timepoint may have to be determined empirically. To minimize kit usage, we suggest that for dilution testing, only two standards (low and high concentration) be used. We aim for a dilution that puts the samples in the middle of the detection range for the assay being used in order to account for the natural variability in metabolism that can occur between replicate samples.
11. Protein in samples can often interfere with assays for small molecules such as metabolites. In order to prevent this interference samples such as lysates that may contain protein must be deproteinized; however, different methods are possible. Some methods such as perchloric acid precipitation will not necessarily be compatible with every commercially available metabolism assay. As such, it is important to test compatibility and consider alternative methods of deproteinizing samples such as trichloroacetic acid protocols.
12. We typically perform three technical replicates for each sample to be assayed; however, since there will be multiple biological replicates if three or more wells were plated for each condition, it is acceptable to do a single assay well for each of the samples.

## References

1. Hunter KW, Crawford NP, Alsarraj J (2008) Mechanisms of metastasis. *Breast Cancer Res* 10:S2. <https://doi.org/10.1186/bcr1988>
2. Justus CR, Leffler N, Ruiz-Echevarria M, Yang LV. (2014) In vitro cell migration and invasion assays. *J Vis Exp* (88):51046. <https://doi.org/10.3791/51046>
3. Kramer N, Walzl A, Unger C, Rosner M, Krupitza G, Hengstschläger M, Dolznig H (2013) In vitro cell migration and invasion assays. *Mutat Res* 752:10–24. <https://doi.org/10.1016/j.mrrev.2012.08.001>
4. Pijuan J, Barceló C, Moreno DF, Maiques O, Sisó P, Martí RM, Macià A, Panosa A (2019) In vitro cell migration, invasion, and adhesion assays: from cell imaging to data analysis. *Front Cell Dev Biol* 7:107. <https://doi.org/10.3389/fcell.2019.00107>



# Chapter 11

## Matrix Degradation Assay to Measure the Ability of Tumor Cells to Degrade Extracellular Matrix

Rosa Fontana and Jing Yang

### Abstract

During the metastatic process, carcinoma cells form invadopodia, F-actin enriched protrusive structures, to degrade the extracellular matrix (ECM) in order to invade the surrounding stroma and intravasate into the circulatory system. In this chapter, we describe the 2D-fluorescent matrix degradation assay, a highly sensitive and reproducible *in vitro* method used to measure invadopodia-mediated ECM degradation. We provide a detailed protocol on how to prepare the glass coverslips with fluorescent gelatin matrix and a standardized method to quantify gelatin degradation and invadopodia formation in order to evaluate cell invasion.

**Key words** Invadopodia, Invasion, Cancer metastasis, ECM, Fluorescent gelatin degradation assay, Podosome, Invadosome, Rosettes, ImageJ

---

### 1 Introduction

The invasion–metastasis cascade is a multistep process by which cancer cells acquire the ability to invade and migrate into the surrounding tissue, intravasate through the endothelium into the circulatory system, extravasate through vascular walls, and colonize distant organs. Both invasion and intravasation processes require degradation of the extracellular matrix (ECM), including basement membranes of epithelial, endothelial, and connective tissues [1, 2].

Invadopodia are actin-rich membrane protrusions in carcinoma cells that differentiate from other actin-based structures (i.e., focal adhesion, lamellipodia) [3, 4] by concentrating various matrix proteases (i.e., metalloproteases—MMPs and the ADAM family members—[5–7] and membrane-bound serine proteases—FAP and DPP4—[8, 9]) to cell-matrix contacts in order to promote focal ECM degradation [10–13].

While the classical method used to study cancer cell invasion can measure the degradation ability of the bulk cell population [14–16], the 2D-fluorescent matrix degradation assay described in this

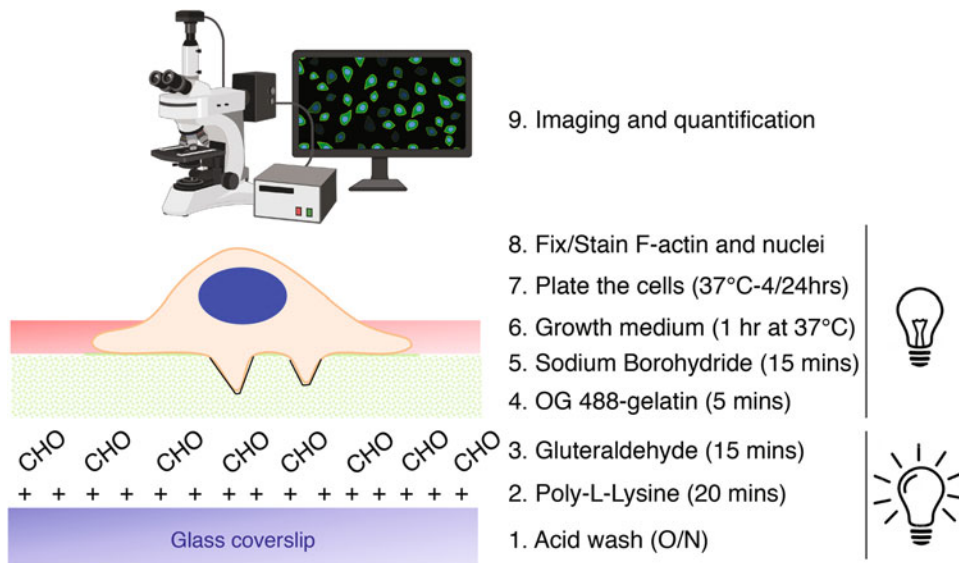


**Fig. 1** Schematic representation of the individual steps of the 2D-fluorescent matrix degradation assay: glass coverslips cleaning, Oregon green (OG) 488-gelatin coating, cell plating, fixing and fluorescence assay, imaging and quantification of invadopodia formation and function. The lit light bulb indicates all the steps carry out at the light, while the turned off bulb represents the ones that need to be conducted in the darkness to avoid photobleaching of fluorescently labeled gelatin

chapter is extremely useful to specifically quantify the ability of carcinoma cells to form invadopodia and degrade the ECM at both single and multicellular levels. Moreover, it can be used to analyze whether the expression of a specific protein or drug treatment can affect invadopodia formation and/or activity. In this assay, the cells are seeded on coverslips coated with an even layer of Oregon green (OG) 488-conjugated gelatin matrix that stimulates invadopodia formation and allows the identification of the degradation foci, detected as dark spots over the green background, by fluorescent microscopy. Here we provide a detailed protocol on preparing the OG 488-conjugated gelatin matrix coating of the glass coverslips and quantifying the assay by fluorescent microscopy. In the latter part, we describe in detail how to use the software ImageJ to quantify the gelatin degradation (Fig. 1 for protocol overview).

## 2 Materials

Prepare all the solutions using sterile double distilled water and store them at room temperature unless indicated otherwise. Carefully follow all the waste disposal regulations.

**2.1 Cell Culture**

1. Cells (i.e., SCC61 head and neck carcinoma cells, MDA-MB-231 SRC Y527F triple-negative breast cancer cell line).
2. Tissue culture media (i.e., DMEM).
3. Sterile Dulbecco's phosphate-buffered saline (DPBS) without calcium and magnesium.
4. Trypsin 0.05%–EDTA.
5. Penicillin–streptomycin solution.
6. Tissue culture incubator.
7. Sterile cell culture hood.
8. Hemocytometer.

**2.2 Acid Wash*****Coverslips Cleaning and Gelatin Coating***

1. Round 12 mm diameter glass coverslips (#1 thickness).
2. Forceps and needle.
3. Virgin fiber tissue wiper.
4. 24-well tissue culture plates.
5. Water bath sets at 37 °C.
6. Parafilm.
7. Plastic box.
8. 30% nitric acid.
9. 70% ethanol.
10. 50 µg/mL poly-L-lysine solution in DPBS.
11. 0.5% glutaraldehyde in DPBS.
12. Unlabeled 0.2% porcine skin gelatin type A: Add 20 mg of gelatin in 9 mL of DPBS. Vortex the solution and warm it in a 37 °C water bath for at least 30 min. When the gelatin is entirely melted, make up to 10 mL with DPBS and filter the solution through a 0.22 µm filter in a new tube. Store at 4 °C for 1 month.
13. Gelatin from pig skin, Oregon green (OG) 488 conjugate (Invitrogen): Dissolve the stock solution by following the manufacturer's instruction at 1 mg/mL. Warm the gelatin at 50 °C to completely dissolve the powder, then aliquot the solution in working stocks. Store at –20 °C and protect the stocks from light.
14. 5 mg/mL sodium borohydride (NaBH<sub>4</sub>) in DPBS.

***2.3 Gelatin Degradation Assay, Fluorescence/Immunocytochemistry Assay***

1. 4% paraformaldehyde (PFA).
2. PBS.
3. 0.05% Triton X-100 in PBS.
4. PBST.
5. 1% BSA in PBST.

6. Primary antibody anti-invadopodia marker protein (Tks5 or Cortactin) diluted in 1% BSA in PBST.
7. Fluorophore-conjugated secondary antibody diluted in 1% BSA in PBST.
8. Alexa Fluor 546 Phalloidin diluted in 1% BSA in PBST.
9. Mounting medium with DAPI and anti-fading agents (Vector Lab).
10. Microscope glass slides (75 × 25 mm).
11. Nail polish.
12. Fluorescence microscope.
13. Vacuum pump.

---

### 3 Methods

Carry out all the following steps in a sterile biosafety cabinet at room temperature unless otherwise specified. Make all the solutions fresh right before use.

#### 3.1 Glass Coverslips Cleaning (Acid Wash)

1. Prepare 30% nitric acid in double distilled water in a glass container and put the coverslips in it (*see Note 1*). Cover the container and incubate overnight.
2. Remove the nitric acid and wash the coverslips extensively with double distilled water on a shaker (*see Note 2*).
3. Transfer the coverslips in a clean container by using tweezers and store them in 70% ethanol.

#### 3.2 Fluorescent Gelatin Coating

1. Use the tweezers to separate and place the coverslips on a virgin fiber tissue wiper.
2. After ethanol has completely evaporated, use the tweezers to transfer the coverslips in a 24-well plate (*see Note 3*) and expose them to the UV light to sterilize the coverslips for 20–30 min.
3. Warm the unlabeled 0.2% porcine skin gelatin type A and the Oregon Green (OG) 488-conjugated porcine skin gelatin in a 37 °C water bath.
4. Coat the coverslips with 500 µL of 50 µg/mL poly-L-lysine (prepared from 0.1% stock solution and diluted in DPBS) for 20 min (*see Note 4*).
5. Aspirate the solution and wash three times with DPBS (*see Note 5*).
6. Incubate the coverslips with 500 µL of 0.5% glutaraldehyde (prepared from 25% stock solution and diluted in DPBS) for 15 min (*see Note 6*).

7. Discard the glutaraldehyde accordingly and wash as in **step 5**.
8. Prepare the OG 488–gelatin solution by diluting one part of fluorescent gelatin into ten parts of unlabeled porcine gelatin and mix well (i.e., 50 µL of OG 488–gelatin into 500 µL of 0.2% porcine skin gelatin to coat 24 coverslips). Warm the solution in a 37 °C water bath (*see Note 7*).
9. Spray 70% ethanol on a plastic lid, then cut and attach a piece of parafilm on it. The ethanol will help the attachment of the parafilm to the plastic surface.
10. Pipette 20 µL of OG 488–gelatin solution on the parafilm (*see Note 8*).
11. Use a needle and tweezers to gently pull up and invert the coverslips over the gelatin drop (*see Note 9*). Incubate for 5 min in the dark.
12. Use tweezers and a needle to carefully transfer the coverslips into a 24-well plate (*see Note 10*).
13. Wash as in **step 5**.
14. Repeat the **steps 10–13** to coat all the desired coverslips.
15. Incubate the coverslips with 500 µL of 5 mg/mL sodium borohydride (NaBH<sub>4</sub>) and gently shake the plate for 15 min (*see Note 11*).
16. Discard the sodium borohydride solution accordingly and wash three times with PBS by gently shaking the plate.
17. Add 1 mL of the complete medium appropriate to the specific cell type used in the assay in the 24-well plate and incubate at 37 °C in a tissue culture incubator for 1 h prior to seed the cells (*see Note 12*).

### **3.3 Fluorescent Gelatin Degradation Assay**

1. Seed the target cells onto gelatin-coated coverslips in a 24-well plate and incubate in a tissue culture incubator at 37 °C with 5% (v/v) CO<sub>2</sub> for 4–24 h (*see Note 13*).
2. 30 min before the end of the cell incubation period, warm PBS and 4% PFA in a 37 °C water bath (*see Note 14*).
3. At the end of the incubation time, aspirate the media from each well and wash the cells with 1 mL of pre-warmed PBS (*see Note 15*).
4. Fix the cells by adding 1 mL of pre-warmed 4% PFA in each well. Incubate the plate for 15 min at 37 °C in a tissue culture incubator (*see Note 16*).
5. Discard the PFA accordingly and wash the cells three times with PBS (*see Note 17*).

6. Permeabilize the cells by adding 1 mL of 0.05% Triton X-100 (prepared from 0.25% stock solution and diluted in PBS). Incubate for 10 min in the dark.
7. Wash as in **step 5**.
8. In order to visualize the invadopodia in the cells, incubate the coverslips with 300  $\mu$ L of Alexa Fluor 546 Phalloidin (diluted 1:1000 in 1% BSA in PBST) for 1 hour in the dark (*see Note 18*).
9. Wash as in **step 5**.
10. Mount maximum three coverslips on one glass microscope slide. Use a needle and tweezers to gently pull up and then take the coverslips. Adsorb the excess of PBS by gently touching the extreme edge of the coverslips with a virgin fiber tissue wiper. Then invert the coverslips on 5  $\mu$ L of mounting medium containing DAPI.
11. Aspirate the excess of mounting medium.
12. Fix and seal the edges of the coverslips by nail polish and store them at 4 °C in the dark (*see Note 19*).

### **3.4 Imaging and Quantification of Invadopodia Formation and Function**

1. The slides can be imaged by using a conventional fluorescent microscope to detect the nuclei (DAPI-stained), the gelatin matrix (Oregon green 488-stained), and the F-actin cytoskeleton (Alexa Fluor 546 Phalloidin-stained). Use a 40 $\times$  magnification and randomly image 30 fields for each coverslip to quantify the degradation area and invadopodia formation of the cell population (*see Notes 20 and 21*). Invadopodia are detected as F-actin positive dots localized on the ventral surface of the cells (SCC61 cells) or at the cell edges (big rosettes in MDA-MB-231 SRC Y527F cells), while the gelatin degradation is detected as dark spots over the green background (Fig. 2).
2. To quantify invadopodia formation, count the number of cells forming more than five F-actin positive invadopodia and normalize to the number of total cells for each field. Perform the appropriate statistical analysis to determine the significant differences between the samples. The result will be represented as “% of cells forming invadopodia” (*see Note 22*).
3. To quantify invadopodia function, the images are analyzed by using ImageJ [17].
4. Select the right measurements to track by choosing the menu command *Analysis*→*Set Measurements* and check *Area fraction* and *Limit to threshold*.
5. Open all the DAPI and fluorescent gelatin images in ImageJ.

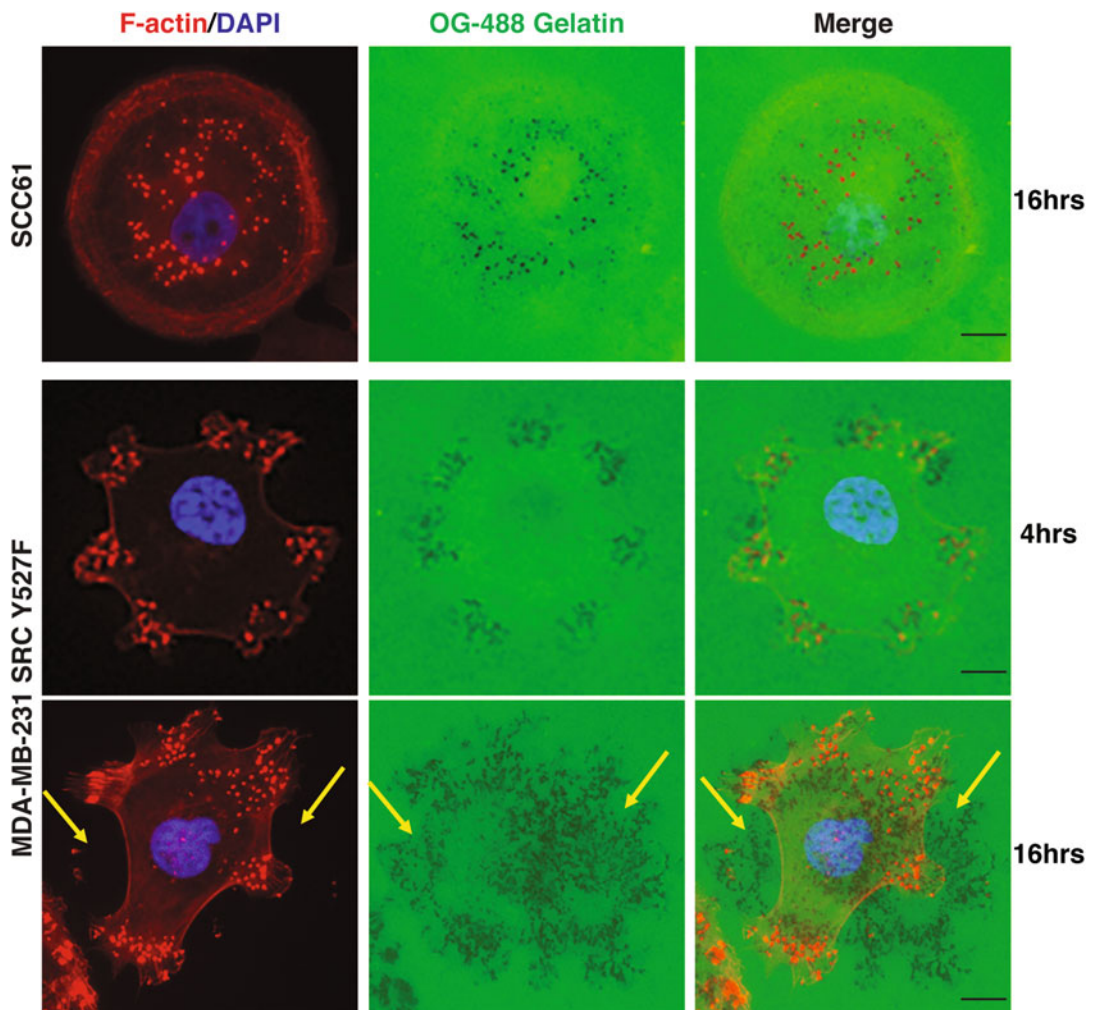


**Fig. 2** Representative examples of 2D-fluorescent matrix degradation assay in SCC61 and MDA-MB-231 SRC Y527F cells. The cells were plated on OG 488–gelatin coated coverslips and fixed at the indicated time points. The F-actin cytoskeleton and nuclei were stained with Alexa Fluor 546 Phalloidin (in red) and with DAPI (blue), respectively. The coverslips were imaged using a conventional fluorescent microscope with 40 $\times$  objective. The dark spots in the OG 488–gelatin pictures represent the invadopodia-mediated gelatin matrix degradation. Invadopodia are identified by F-actin positive dots (in SCC61 cells) or big rosettes at the cell edge (in MDA-MB-231 SRC Y527F cells). After 16 h, the degradation area shows no co-localization with the F-actin positive invadopodia and is diffused outside the cell body (yellow arrows) in MDA-MB-231 SRC Y527F cells, suggesting that cells responsible for degrading this area have migrated away

6. Stack the images by choosing the menu command *Image→Stacks→Image to stack*.
7. Convert the image in 8-bit to have it in black and white.
8. Create a square by using the rectangular tool (*see Note 23*).

9. Then cut the stacked images by using the shortcut *Cmd-Shift-X*.
10. Remove the stack by choosing the menu command *Image→Stacks→Stack to Image*.
11. Adjust the brightness and contrast by choosing the menu command *Image→Adjust→Brightness/Contrast→Auto→Apply*.
12. To quantify the % of degradation area (Area fraction), threshold the fluorescent gelatin image by using *Image→Adjust→Threshold* (see Note 24). Use the *Default* thresholding method and adjust the maximum threshold value while the minimum is set at 0. The degradation area will be displayed in red. By using this method, you need to set the threshold for each image (see Note 25) (Fig. 3a).
13. In the menu, *Analyze→Analyze particles*, choose the particle *Size 0–Infinity* to remove noise from the selection, the *Circularity 0.00–1.00*. Then check *Summarize* and *Exclude edge* to show the results. The % Area or Area fraction value represents the degradation area and can be saved as a Microsoft Excel file.
14. To count the number of cells in each field, threshold the DAPI image as reported in step 12. Adjust the minimum threshold while the maximum is set to the highest value.
15. To obtain the result, follow step 13 but set the particle *Size 15–Infinity* because the nuclei are bigger than the degradation dots. The number of cells in the field is represented by the value in the column *Count* (see Note 26) (Fig. 3a).
16. The final gel degradation index is the average % Area fraction normalize to total cell number in all the analyzed fields (see Notes 27 and 28). Perform the appropriate statistical analysis (Fig. 3b).

---

## 4 Notes

1. Acid washing of coverslips is an important step to remove any grease on them and helps polypeptides to adhere to the glass by enhancing polyamino acids coating, thus promoting cell adhesion/spreading too. Although the nitric acid washing method that we use is much more aggressive than the one with hydrochloric acid, it works better for the poly-L-lysine/gelatin coating because it is stronger and removes more contaminants [18].
2. Wash the coverslips for at least 2 h. Change the wash regularly and use a shaker help to efficiently remove the nitric acid between the coverslips.

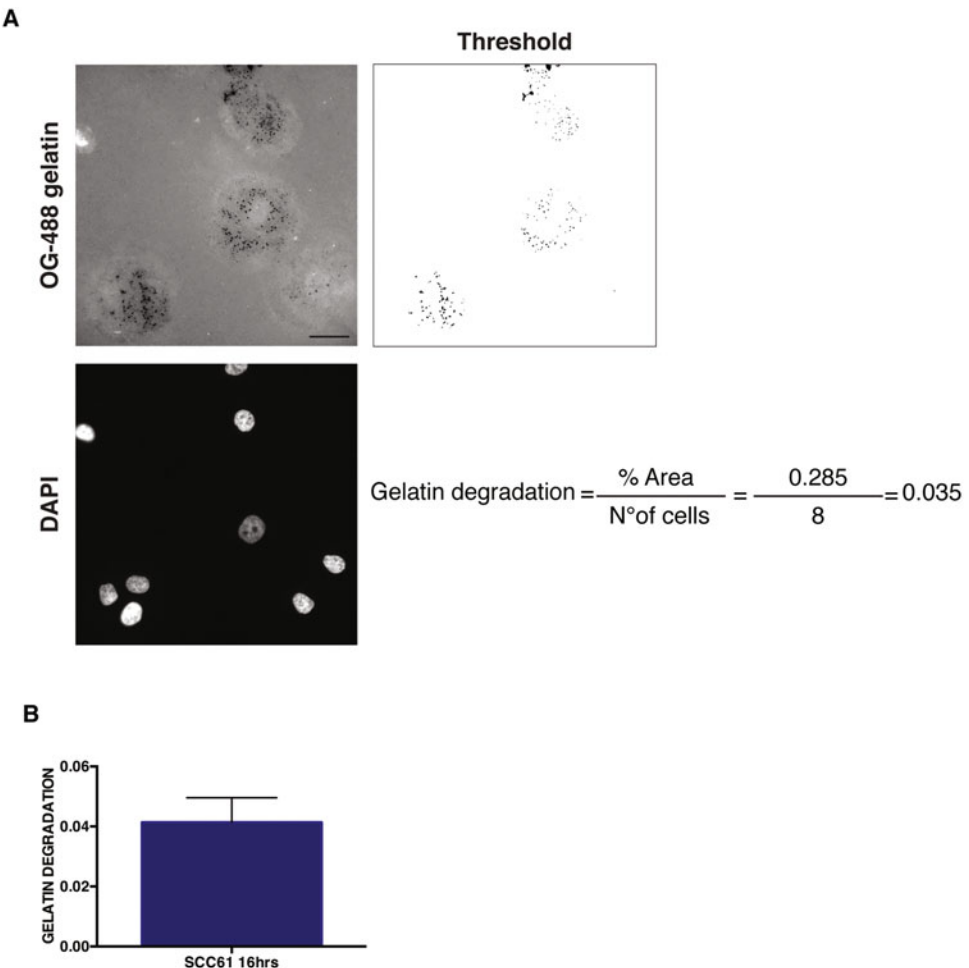


**Fig. 3 (a)** Example of gelatin degradation image analysis with ImageJ software. The OG 488–gelatin and DAPI images were converted in gray scale to better show the thresholding area. The *Default* thresholding method was applied to quantify both % area of degradation and number of cells. Thresholded gelatin image is shown in black and white by using the option *Converted to mask* in the menu *Process*→*Binary* in ImageJ to better display the thresholding area. The figure represents typical images of SCC61 cells fixed after 16 h. **(b)** Quantification of gelatin degradation in SCC61 cells after 16 h  $N = 154$  cells. Error bar is standard error of mean (SEM)

3. We always prepare three coverslips for each sample to perform the technical replicate in our experiment.
4. When the poly-L-lysine is adsorbed to the glass substratum, it increases the number of positively charged sites on the coverslips. This improves the coating and the bounding of the gelatin.
5. Do not dry the coverslips during and after the coating process as this affects cell attachment. Leave the coverslips in the last DPBS wash and make the required solution.

6. The glutaraldehyde catalyzes the cross-linking between the poly-L-Lysine and the gelatin with the reactive aldehyde ( $-CHO$ ) groups.
7. It is important to keep the OG 488–gelatin solution always warm at 37 °C to avoid premature solidification.
8. From here, perform all the following steps while keeping the coverslips protected from the light to avoid potential photo-bleaching of the OG 488–gelatin.
9. The main goal of this step is to obtain a thin uniform gelatin coating of the coverslips. To achieve this aim, we process maximum six coverslips at a time and repeat the process for the required number of coverslips. The partial solidification of the OG 488–gelatin solution can cause an uneven coating so we always keep this solution warm at 37 °C.
10. Try to touch only the extreme edge of the coverslips with the tweezers to avoid the scratch of the fluorescent gelatin matrix.
11. Sodium borohydride is used for reduction and quenching of the residual reactive aldehyde groups in the gelatin matrix. The reaction of the sodium borohydride with water produces hydrogen, which causes the formation of bubbles that tend to push up the coverslips. In order to keep the coverslips covered by the solution, we gently shake the plate during the incubation time.
12. The gelatin-coated coverslips can be used in the same day or can be stored at 4 °C in the growth medium for up to 1 week. The primary amines of the amino acids contained in the growth medium help quenching the free residual aldehydes groups in the gelatin matrix.
13. The number of cells seeded in each well and the length of the assay need to be empirically determined for the cell line of interest. We usually plate the cells to reach 50–60% of cell confluence at the end of the assay because a higher cell number can affect invadopodia formation. The length of the assay is affected by the invasiveness of the cell line used. For example, in our experience, the squamous cell carcinoma SCC61 cells require 16 h for invadopodia degradation while the breast cancer MDA-MB-231 SRC Y527F cells required only 4 h because they express the constitutively active form of SRC that induces the formation of large invadopodia rosettes that are more aggressive (Fig. 2). A longer assay for the MDA-MB-231 SRC Y527F cells results in the migration of the cells (Fig. 2, 16 h panel). To synchronize invadopodia formation or activity, the cells can be seeded in presence of PP2 (a Src family kinases inhibitor) [10, 19] or GM6001(broad spectrum MMPs inhibitor) [11], respectively. After a specific time, the inhibitor is washed off to induce invadopodia formation and/or function.

14. We noted that in particular cell lines (such as SCC61 cells), sudden drop of the temperature can cause the partial or complete F-actin depolymerization, which results in smaller invadopodia or their complete disappearance. In order to prevent this, we always keep the PBS and the 4% PFA solution warm at 37 °C.
15. Remember to always keep the plate protected from the light by using aluminum foil. From **step 3**, all the following steps are carried out outside the biosafety cabinet.
16. For the same reason reported in the **Note 14**, we perform the fixation step at 37 °C in a cell culture incubator.
17. From this step, all the solutions can be used at RT because the cells are fixed.
18. It is also possible to visualize the localization of one of the invadopodia marker proteins (i.e., cortactin [20] or TKS5 [21]) in addition to the F-actin. To achieve this, before to stain for the F-actin, incubate the coverslips with 1 mL of 1% BSA in PBST blocking solution for 1 h at RT. Then add a piece of parafilm in a humidified chamber and pipette 35 µL of diluted primary antibody. Use a needle and tweezers to gently pull up and invert the coverslips over the antibody and incubate overnight at 4 °C. The day after, transfer the coverslips from the chamber to a 24-well plate by using tweezers and wash three times with the blocking solution. Incubate the coverslips with 1 mL of 1% BSA in PBST blocking solution for 1 h at RT. Then dilute the fluorophore-conjugated secondary antibody and the Phalloidin in 1% BSA in PBST and incubate the coverslips for 1 h at RT as described before. Follow the protocol from **step 9**.
19. This step is important to prevent bacterial contamination of the sample. Moreover, if you use an oil immersion object for imaging, performing this step will prevent the oil from diffusing inside the coverslips and quenching the signal.
20. If you perform a co-localization study as reported in **Note 18**, higher magnification/resolution visualization (e.g., 60× oil objective and confocal microscope) is required.
21. In order to ensure random acquisition of the fields, we always move from one field to the next one by using the DAPI channel. In this way, we can also identify areas of the coverslips with the same number of cells to image.
22. From the same images, it is also possible to determinate the number of invadopodia per cell and the % of active invadopodia per cell. The definition of “active invadopodia” is given by the co-localization of F-actin and/or Cortactin (or Tks5) positive dots with the degradation area (*see Note 20*).

23. The size of the rectangle can be chosen by the user but it should be the same for all the images. We quantify the area of degradation only in this rectangle in order to exclude the edges of the field that can contain scratches from the analysis.
24. Thresholding the image means that you can choose a cutoff value (threshold) in a way that all the pixels greater than this value are considered features of interest and appear in red (degradation dots), while all the pixels less than this value represent the background and are displayed in grayscale.
25. It is important to set the threshold carefully to avoid false positive. For this reason, we always make sure that the chosen threshold value does not oversaturate the area of degradation and does not recognize specific areas of the image (i.e., due to irregular coating) as features of interest.
26. We recommended to always check if the cell number calculated by ImageJ is accurate in each field because sometimes the cells can be multinucleated or show nuclei with irregular shape and intensity, thus affecting the count. If the nuclei are not well separated, round and with a uniform intensity, we suggest to perform manual counting.
27. An alternative approach is to normalize the % of degradation area to the area of the cells. We do not use this method because cell morphology may not be uniform in the population or the specific treatment performed in the experiment (i.e., siRNA, drug) can affect cell shape. Normalizing to the cell number also allows compare different cell lines.
28. The gelatin degradation can also be analyzed at the single-cell level in a mixed population (i.e., transfected versus non-transfected cells). In this case, it is required to mark the transfected cells with a fluorescent tag. The result can be presented as % of degradation area normalize to the number of transfected cells in the population.

---

## Acknowledgments

This work was supported by an American-Italian Cancer Foundation Post-Doctoral Research Fellowship to R.F. and grants from NCI (1R01CA174869, 1R01CA206880, and 1R01CA236386) and California Tobacco-Related Disease Research Program (TRDRP-587107) to J.Y.

## References

1. Lambert AW, Pattabiraman DR, Weinberg RA (2017) Emerging biological principles of metastasis. *Cell* 168(4):670–691
2. Fontana R, Vivo M (2018) Dynamics of p14ARF and focal adhesion kinase-mediated autophagy in cancer. *Cancers (Basel)* 10 (7):221
3. Linder S (2007) The matrix corroded: podosomes and invadopodia in extracellular matrix degradation. *Trends Cell Biol* 17(3):107–117
4. Vivo M, Fontana R et al (2017) p14ARF interacts with the focal adhesion kinase and protects cells from anoikis. *Oncogene* 36 (34):4913–4928
5. Furmaniak-Kazmierczak E, Crawley SW et al (2007) Formation of extracellular matrix-digesting invadopodia by primary aortic smooth muscle cells. *Circ Res* 100 (9):1328–1336
6. Abram CL, Seals DF et al (2003) The adaptor protein fish associates with members of the ADAMs family and localizes to podosomes of Src-transformed cells. *J Biol Chem* 278 (19):16844–16851
7. Fontana R, Ranieri M et al (2019) Dual role of the alternative reading frame ARF protein in cancer. *Biomolecules* 9(3):87
8. Monsky WL, Lin CY et al (1994) A potential marker protease of invasiveness, seprase, is localized on invadopodia of human malignant melanoma cells. *Cancer Res* 54 (21):5702–5710
9. Ghersi G, Dong H et al (2002) Regulation of fibroblast migration on collagenous matrix by a cell surface peptidase complex. *J Biol Chem* 277(32):29231–29241
10. Paz H, Pathak N, Yang J (2014) Invading one step at a time: the role of invadopodia in tumor metastasis. *Oncogene* 33(33):4193–4202
11. Mueller SC, Artym VV, Kelly T (2008) Invadopodia: interface for invasion. In: Edwards D, Høyer-Hansen G, Blasi F, Sloane BF (eds) *The cancer Degradome*. Springer, New York, NY, pp 403–431
12. Eckert MA, Lwin TM et al (2011) Twist1-induced invadopodia formation promotes tumor metastasis. *Cancer Cell* 19(3):372–386
13. Eddy RJ, Weidmann MD et al (2017) Tumor cell invadopodia: invasive protrusions that orchestrate metastasis. *Trends Cell Biol* 27 (8):595–607
14. Hendrix MJ, Seftor EA et al (1989) Comparison of tumor cell invasion assays: human amnion versus reconstituted basement membrane barriers. *Invasion Metastasis* 9 (5):278–297
15. Le MN, Bruyneel E (1996) Comparison of in vitro invasiveness of human breast carcinoma in early or late stage with their malignancy in vivo. *Anticancer Res* 16(5A):2767–2772
16. Waller CA, Braun M, Schirrmacher V (1986) Quantitative analysis of cancer invasion in vitro: comparison of two new assays and of turnout sublines with different metastatic capacity. *Clin Exp Metastasis* 4(2):73–89
17. Abramoff MD, Magalhaes PJ, Ram SJ (2004) Image processing with ImageJ. *Biophoton Int* 11(7):36–42
18. Heit B (2017) Phagocyte Biology Wiki. [http://129.100.26.202/index.php?title=Acid\\_Washing\\_Coverslips&oldid=119](http://129.100.26.202/index.php?title=Acid_Washing_Coverslips&oldid=119). Accessed 1 July 2020
19. Creed SJ, Le CP et al (2015)  $\beta 2$ -adrenoceptor signaling regulates invadopodia formation to enhance tumor cell invasion. *Breast Cancer Res* 17(1):145
20. Ayala I, Baldassarre M et al (2008) Multiple regulatory inputs converge on cortactin to control invadopodia biogenesis and extracellular matrix degradation. *J Cell Sci* 121 (Pt 3):369–378
21. Seals DF, Azucena EF et al (2005) The adaptor protein Tks5/fish is required for podosome formation and function, and for the protease-driven invasion of cancer cells. *Cancer Cell* 7 (2):155–165



# Chapter 12

## Evaluation of Real-Time In Vitro Invasive Phenotypes

René M. DeLosh and Robert H. Shoemaker

### Abstract

The methods described here provide a standardized process for assessing in vitro tumor cell migration and invasion in real time. The kinetic data generated under these standardized conditions are reproducible and characteristic of individual tumor cell lines. The complex kinetic features of the data can be analyzed using parameters modeled after pharmacokinetic data processing. Application of the method to the array of tumor types included in the National Cancer Institute's sixty cell line panel (NCI60) revealed distinct modes of invasion with some tumor cell lines utilizing a mesenchymal mode and generating information-rich kinetic profiles. Other cell lines utilized an amoeboid mode not suitable for detection with this method. The method described will be useful as a guide for tumor cell line selection and as a starting point in designing experiments probing migration and invasion.

**Key words** In vitro, Migration, Invasion, Tumor cell line, NCI60

---

### 1 Introduction

Cancer cell migration and invasion are fundamental to the lethal process of metastasis. For a review of metastasis, see Talmadge and Fidler, 2010 [1]. While many factors critical to this process, such as dissemination via vascular and lymphatic channels, angiogenesis, are not readily modeled in cell culture, studies of in vitro migration and invasion have provided insight into many phenomena which are fundamental to metastasis. The introduction of the “Boyden chamber” [2], originally designed for in vitro studies of neutrophil chemotaxis, led to a range of modifications for studies of tumor cell migration. A method using an artificial basement membrane material, now marketed as Matrigel, was developed in George Martin’s lab at NIH [3] and gained wide acceptance as an in vitro model of tumor cell invasion. Further modifications to this method were made to enhance throughput and quantitation [4, 5]. Indeed, it

---

**Electronic Supplementary Material** The online version of this chapter ([https://doi.org/10.1007/978-1-0716-1350-4\\_12](https://doi.org/10.1007/978-1-0716-1350-4_12)) contains supplementary material, which is available to authorized users.

is now possible to purchase commercial kits for conduct of migration or invasion assays in 96-well plates. A fundamental limitation of these methods is the requirement to evaluate the process at a fixed time point. Thus, insight into the kinetics or comparison of migration or invasion rates between tumor cell populations was limited. The development of technology for real-time kinetic monitoring of in vitro cell migration and invasion based on detection of cell-induced changes in electrical impedance [6, 7] has made it possible to characterize the phenotypes of individual tumor cell lines in great detail. Our results, generated using this novel technology applied to a diverse panel of human tumor cell lines, reveal complex kinetic phenotypes which are characteristic for individual tumor cell lines.

The NCI60 tumor cell line panel was introduced decades ago as an anticancer drug screening model [8] and was rapidly recognized to convey information related to mechanism of drug action [9]. A detailed review of the rationale, history, and applications of the NCI60 has been published [10]. Molecular characterization of the tumor cell line panels has been shown to enable informatic analyses linking patterns of gene expression to drug response and many other applications. Publicly available tools for database searching and analysis are available at: [https://dtp.cancer.gov/databases\\_tools/data\\_search.htm](https://dtp.cancer.gov/databases_tools/data_search.htm). We reasoned that a detailed characterization of the in vitro migration or invasion phenotypes could be utilized for database mining against the molecular targets and basal gene expression data amassed regarding the tumor cell lines of the NCI60 to identify genes/pathways associated with invasion and possibly to identify compounds in the drug screening database that might inhibit invasion.

---

## 2 Materials

Table 1 lists materials required for the invitro migration or invasion assays. Footnotes to this table provide details and rationale.

---

## 3 Methods

### **3.1 Standardized Conditions for Real-Time Assessment of Migration and Invasion Phenotypes**

Given the large number of variables known to affect in vitro studies of invasion, such as the nature of the chemo-attractant, number of cells loaded, nature of the artificial basement membrane, we established a standardized protocol for use in characterizing the NCI60 phenotypes. Cells were plated at 100,000 cells/well in multi-well plates (CIM-Plate 16, ACEA Biosciences, Inc., San Diego, CA) 1% BSA medium over preformed Matrigel layers (0.3 mg/ml) for invasion assays, or no coating for migration assays, on a membrane containing eight micron pores. Complete growth medium

**Table 1**

**Standardization of the In Vitro Invasion Assay. Components of the assay, their purpose, and the standardized parameters are listed. The footnotes provide details of the rationale for these selections**

Components of the in vitro invasion assay	Purpose	Standardized parameter
Tumor cells	Targets for study	NCI60 tumor cell lines in exponential growth <sup>a</sup>
Complete growth medium	Support viability and growth, Provide chemoattractant	RPMI-1640, 2 mM glutamine, 10% FBS <sup>b</sup>
1% BSA medium	Support viability	RPMI-1640, 1% BSA
Serum-free growth medium	Support viability, vehicle for growth factor supplements	RPMI-1640, 2 mM glutamine
Purified growth factors	Chemoattractants, Support studies of signaling pathways	EGF, bFGF, Gas-6 <sup>c</sup>
Matrigel	Artificial Basement Membrane Matrigel Basement Barrier for invasion studies	0.3 mg/ml BD Membrane Matrix Cat. # 356234 in PBS <sup>d</sup>
Invasion chamber	Culture vessel with 8 micron pore size membrane and detection electrodes	xCELLigence® CIM-16 Plate
Real-time detection instrument	Interfaces with invasion chamber to detect cells that traverse the Matrigel and membrane and impinge on detection electrodes	xCELLigence® RTCA DP <sup>e</sup>

<sup>a</sup>Cells of the NCI60 panel can be obtained from the NCI DCTD Tumor Repository: <https://dtp.cancer.gov/organization/btb/docs/DCTDTumorRepositoryCatalog.pdf>. We recommend establishing a local cryopreserved tumor cell line bank and working within a limited number of serial passages (<20). Harvesting cells in exponential growth phase provides an approach to standardizing the condition of cells when loaded onto the invasion chamber. Several cell lines were initially titered to arrive at 100,000 per well as a standardized input. Varying the input will affect the measured phenotypes

<sup>b</sup>This is the medium routinely used for propagation of NCI60 tumor cell lines. Some of the constituent cell lines were originally cultured in different media and adapted to RPMI-1640 to standardize conditions for use in drug screening. Fetal bovine serum (FBS) lots should be tested for supporting growth and invasion using an indicator cell line such as MDA-MB-231. Growth factor content can be expected to vary by FBS lot.

<sup>c</sup>Informatic analysis of the invasive phenotypes suggested these growth factors as likely determinants of the mesenchymal invasion phenotype. Testing each recombinant human growth factor as chemoattractant confirmed this result

<sup>d</sup>Titration of Matrigel concentrations indicated that 3% provided a barrier of intermediate stringency suitable for use in characterizing the diverse cell lines of the NCI60. Different concentrations may be appropriate for specific cell lines and experimental purposes. Matrigel and dilutions in complete medium must be kept at 0–4 °C until added to the upper surface of the invasion chamber. Chambers are then placed in a 37 °C, humidified incubator, with 5% CO<sub>2</sub> overnight to allow the Matrigel to solidify and equilibrate pH

<sup>e</sup>In order to generate kinetic data, detection grids were queried at 10-min intervals for 48 h

containing 10% fetal bovine serum (FBS) in the bottom chamber was used as a broad-spectrum chemoattractant. Six replicate wells were used for migration and invasion assays to characterize each of the NCI60 tumor lines. Tumor cells were all derived from the NCI Tumor Repository (<https://dtp.cancer.gov/organization/btb/docs/DCTDTumorRepositoryCatalog.pdf>). All cell lines were

assayed on at least two separate occasions. Each CIM-Plate 16 also contained, as a standard, MDA-MB-231 breast cancer cells, plated in duplicate for migration and invasion. The time-course for invasion and migration was monitored every 10 min for 48 h by interrogation of electrical impedance of interdigitated gold microelectrodes on the underside of the membrane using an xCELL<sup>®</sup> RTCA DP instrument (ACEA Biosciences, Inc., San Diego, CA developed by ACEA Biosciences, San Diego, CA). The electrical impedance was converted to a “Cell Index” by the instrument [6, 7]. This Cell Index value is proportional to the number of cells in the vicinity of the gold microelectrodes and the nature of their interaction with the microelectrodes.

A flowchart for the assay is detailed in Table 2.

### **3.2 Visualization of Invading Cells**

While the construction of the CIM-Plate 16 is not amenable to conventional optical microscopy, it is possible to visualize invading cells on the sensor electrode array using scanning electron microscopy (Fig. 1). In this low-magnification illustration, UACC-62 melanoma cells can be observed on the under surface of the membrane and microelectrode array 24 h after addition to the top of the invasion chamber. At higher magnification (Fig. 2a), they can be observed to extend filopodia and lamellipodia as they emerge from pores in and around the detector and move across the surface demonstrating a mesenchymal mode of motility [11]. Several other melanoma cell lines examined, as well as the MDA-MB-232 breast cancer cell line, showed a similar ultrastructural appearance. The HCT-116 colon carcinoma cell line showed a contrasting appearance, with epithelioid groups of cells (Fig. 2b) and scattered cells showing a more mesenchymal appearance. CEM leukemia cells were observed to invade as individual cells and appeared to pass through the pores on the detectors without making close contact or spreading across the detector surface (Fig. 2c). HL-60 leukemia cells showed a similar invasive phenotype, albeit with smoother membrane profiles. KM12 colon carcinoma cells invaded as individuals or groups of cells which also made minimal contact with the detector electrodes (Fig. 2d).

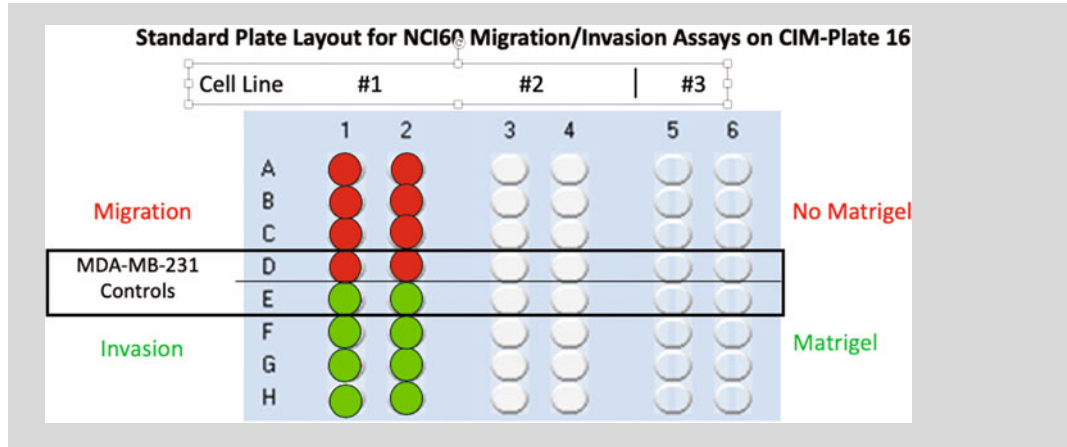
### **3.3 Real-Time Migration and Invasion Phenotypes**

A diverse range of phenotypes was observed across the NCI60 tumor cell line panel. Consistent with the amoeboid mode of invasion observed above, none of the leukemia cell lines produced a signal for migration or invasion on the xCELLigence instrument. Among the solid tumor panels a variety of patterns were observed. Most of the cell lines demonstrated relatively rapid migration followed by invasion. This is illustrated in Fig. 3a for the MDA-MB-231 triple-negative mesenchymal-type breast cancer cell line. Estrogen receptor-positive breast cancer cell lines such as T47-D (Fig. 3b) showed reduced evidence for migration or invasion. The rates and maximum extent for each phenomenon were sufficiently

**Table 2**

**Flowchart for Conduct of In Vitro Migration/Invasion Assays. The sequential process is described in detail. A standardized plate design is illustrated**

Flowchart for real-time in vitro migration/invasion assays								
1. Prepare Matrigel (BD Matrigel basement membrane matrix catalog # 356234) on ice to 0.3 mg/ml in PBS. Pre-chill pipette tips, tubes, all reagents, and CIM plates to avoid premature gelling of the Matrigel								
2. Slowly and gently layer 50µl Matrigel to cover the upper surface of membranes of the CIM plate wells. Remove and discard 30µl Matrigel without disturbing the membrane. Incubate for 4 h at 37 °C in an atmosphere of 5% CO <sub>2</sub> and saturated humidity to allow the Matrigel to solidify								
3. Add 165µl of complete growth medium into lower wells of the CIM plates								
4. Add 25µl 1% BSA medium to the upper chamber for rehydration of membranes								
5. Snap together the top and bottom chambers and incubate for 1 h in instrument in 37 °C, humidified incubator with 5% CO <sub>2</sub> to establish background readings								
6. Prepare tumor cell suspension at 1E06 cells/ml in 1% BSA medium								
7. Add 75µl of cell suspensions at 100,000 c/w and any investigational compounds at appropriate concentrations into upper wells of CIM plate								
8. Mount CIM plates back into instrument and incubate								
9. Monitor detectors at 10 min intervals for 48 h								



diverse to justify detailed treatment of the curves using parameters modeled after those used in analyzing pharmacokinetic data. Thus, a family of parameters was extracted from each curve as illustrated in Fig. 3a. Contrasting phenotypes are illustrated for a renal tumor cell line showing aggressive migration but no invasion (Fig. 3c) and a melanoma (Fig. 3d). In the latter instance (LOX melanoma), the extent of invasion surpassed migration. Reproducibility of the curves for individual cell lines was generally very good, and therefore duplicate experiments were sufficient to establish phenotypes

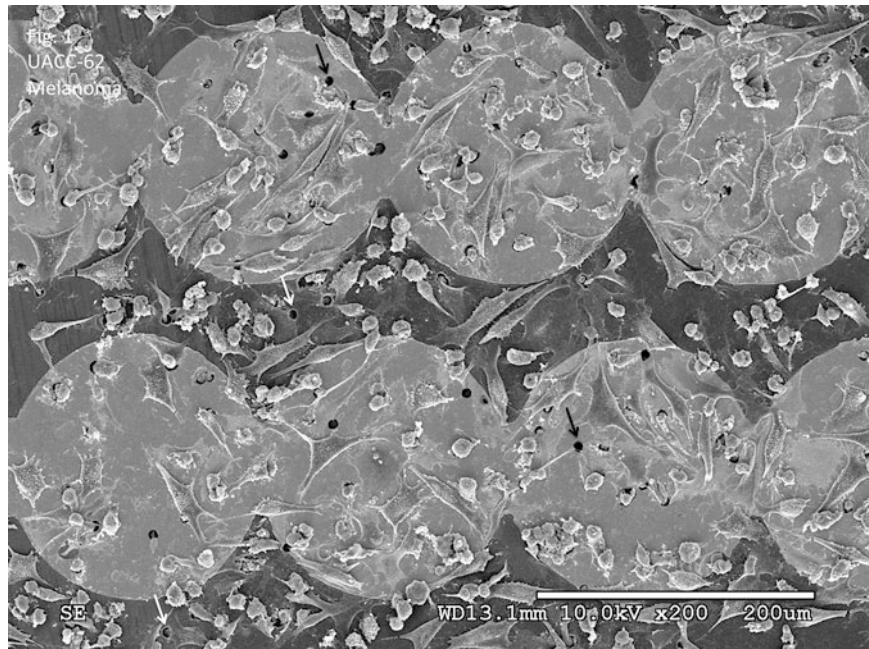


**Fig. 1** Low magnification scanning electron micrograph illustrating UACC-62 melanoma cells invading through pores in and around the microelectrode array on the CIM-Plate 16 invasion chamber. The microelectrode is visible as arrays of connected disks on the under surface of the invasion membrane. Pores not obscured by cells are indicated by black arrows (on the detectors) and white arrows (on the membrane). Imaging conditions, magnification, and scale bar are shown

for the majority of cell lines. Individual data for replicate assays of all of the NCI60 tumor cell lines is provided as an interactive graphic viewer in Supplementary Fig. 1.

### 3.4 Informatic Analysis: Connecting the Invasion Phenotypes with Genes and Pathways

The measured phenotypes reflect the characteristic response of individual cell lines to the array of ligands (growth factors, chemokines, and hormones) present in fetal bovine serum and the interaction of the tumor cells with the sensor electrode array. Informatic analysis of the NCI60 in vitro invasion phenotypes using the area under the curve (AUC) parameter (detailed in Supplementary Table 1) in relation to more than 11,000 previously measured molecular target characteristics (publicly available at <http://dtp.nci.nih.gov>) reveals correlations with many genes/pathways known to be associated with invasion and metastasis. A rank-ordered list of the top 200 positive and negative correlates generated by COMPARE analysis is given in Supplementary Table 2. Among the top ten correlates are expression (assessed by RT-PCR or RNase protection) of AXL, EGF, and FGF receptors. Indeed, some of the most aggressively invading tumor cell lines express all three of these receptors as illustrated in Fig. 4a. Inspection of this figure reveals that all of the cell lines with a more aggressive than

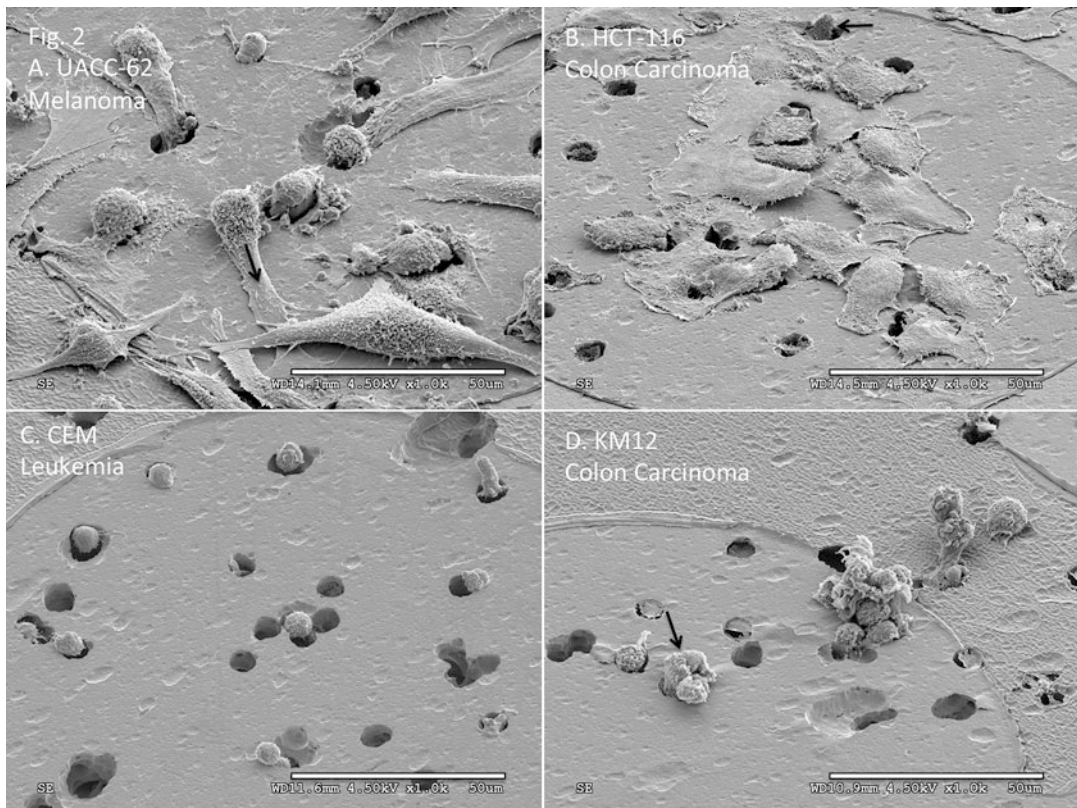


**Fig. 2** Scanning electron micrographs of representative tumor cell lines. **(a)** UACC-62 melanoma cells demonstrating mesenchymal invasion. Cells can be seen to extend lamellipodia (arrow) and filopodia and spread over the surface of the membrane and detector microelectrode, approaching confluence. **(b)** HCT-116 colon carcinoma cells forming an epithelioid cluster on the under surface of the microelectrode. An individual showing a more amoeboid mode cell can be seen emerging from a pore in the electrode (arrow at top of figure). **(c)** CEM leukemia cells invading as individual amoeboid cells. Cells show minimal interaction with the microelectrode and appear to be poised to drift away into liquid medium. **(d)** KM12 colon carcinoma cells demonstrating an amoeboid mode of invasion. Individual cells and groups of cells (arrow) can be seen to emerge from pores in the membrane and detector without making close contact or spreading on the surface. Imaging conditions, magnification, and scale bar are shown

average phenotype express mRNA for at least one of these receptors, except for the melanoma line SK-MEL-28. Since the concentrations of the corresponding bovine growth factors in the FBS used for our studies are not defined, and to establish that human growth factors would exert a similar effect, we evaluated purified recombinant human growth factors as chemoattractants. Results obtained with DU-145 indicated a clear activating effect for each of the three growth factors (Fig. 4b). While all three of these receptors have been previously shown to play a role in invasion [12–14], their functional significance for the measured in vitro phenotype was probed using RNA interference technology. Fig. 4c illustrates the

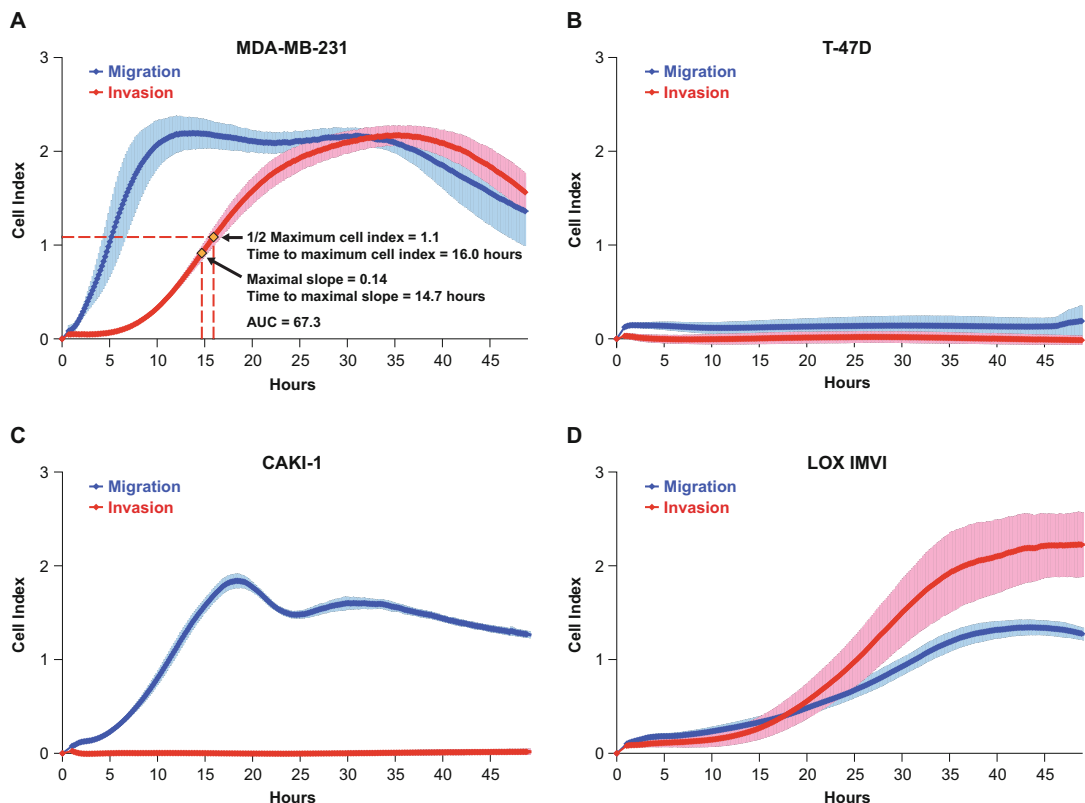
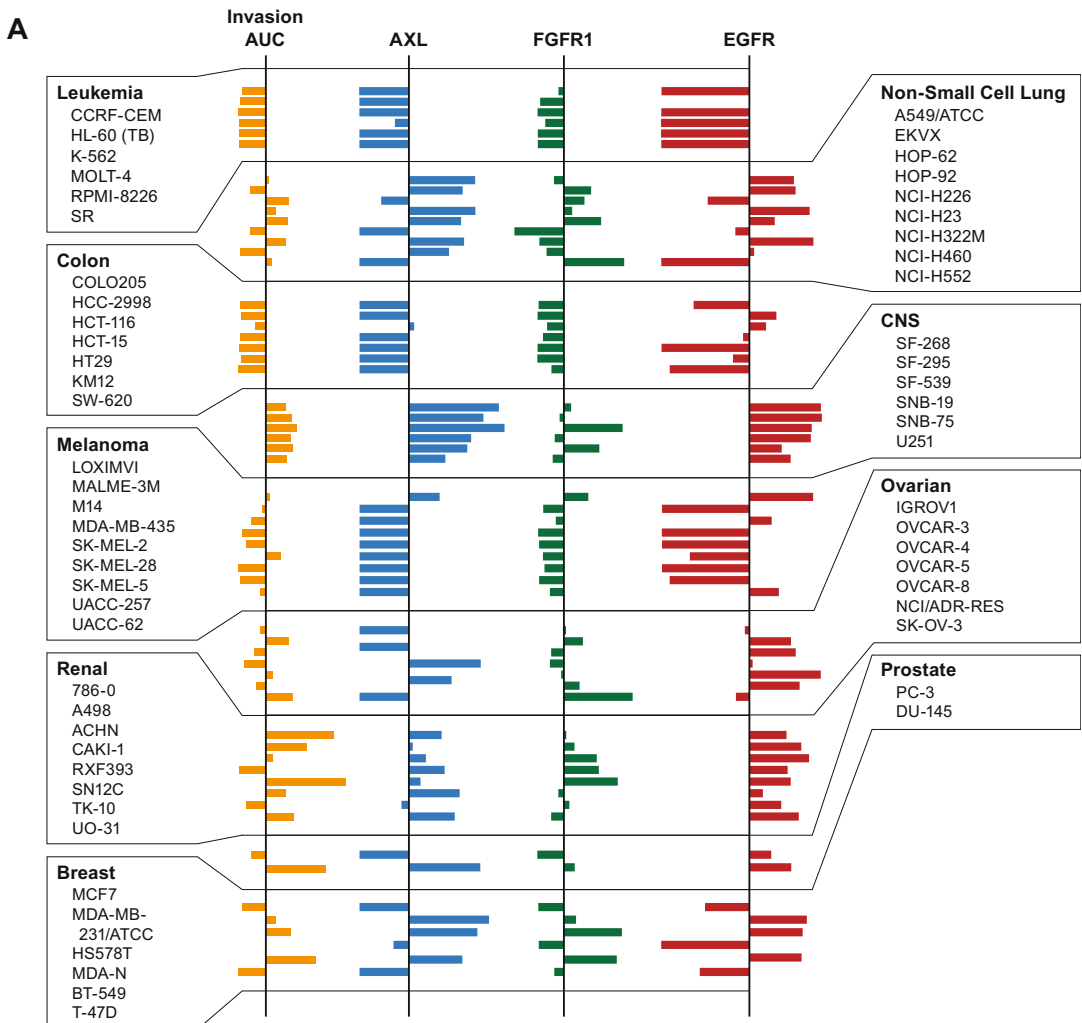


**Fig. 3** Examples of real-time kinetic in vitro migration and invasion phenotypes. (a) Phenotypes of the MDA-MB-231 triple-negative mesenchymal-type breast cancer cell line showing rapid migration (blue line) followed by invasion (red line). Parameters extracted from the migration and invasion curves include maximal slope (relating to rates of migration and invasion), half-maximal cell index (reflecting the mass of cells detected) and the times required to reach these levels, and the area under the curve (AUC) which integrates these phenomena. (b) Phenotypes of the T-47D ER+ luminal-type breast cancer cell line. This and the other ER+ luminal-type breast cancer cell line, MCF-7 showed very weak evidence for in vitro invasion. The triple-negative mesenchymal-type breast cancer cell lines BT-549, HS578T, and MDA-MB-231 all showed aggressive phenotypes for migration and invasion. (c) CAKI-1 renal tumor cell line showing a strong migratory phenotype and no invasion. (d) Phenotypes of the LOX melanoma cell line. This cell line was unique among the NCI60 in that the invasion signal substantially exceeded the migration signal. See Supplementary Fig. 1 for individual experiments with all of the NCI60 tumor cell lines

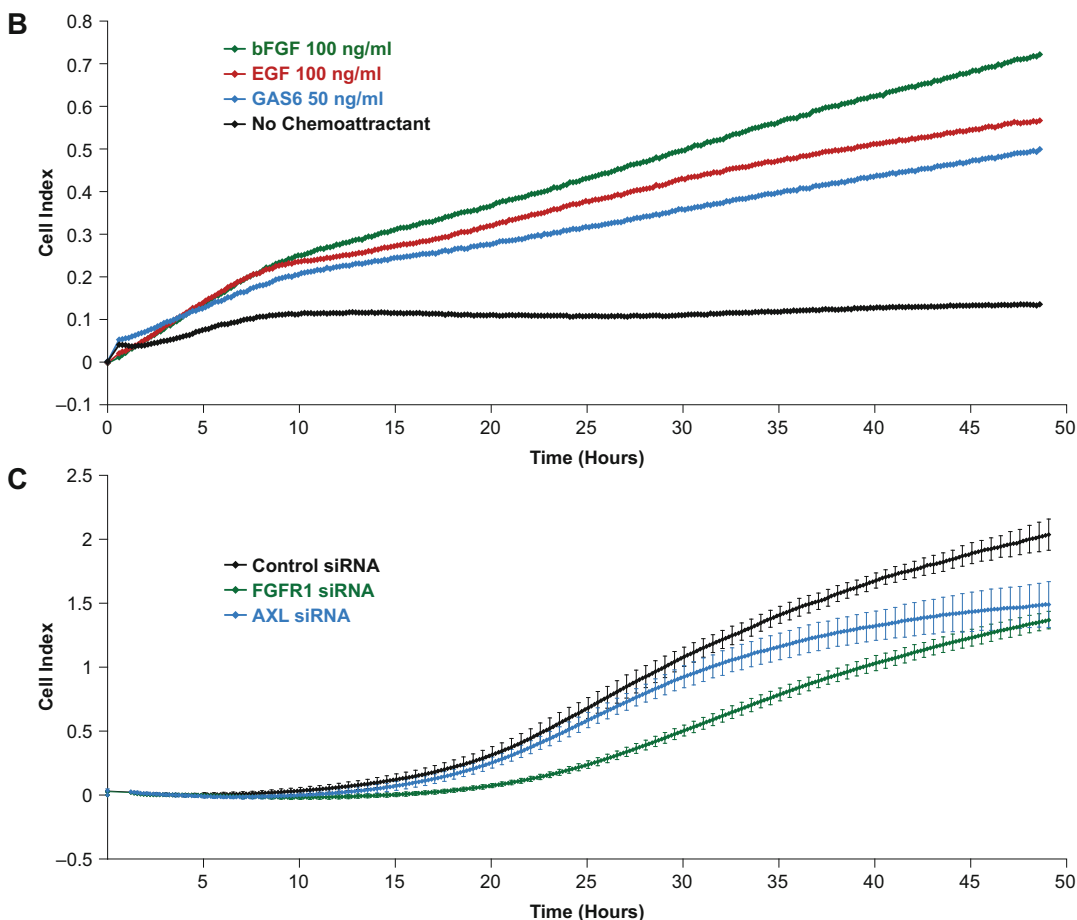
effects of AXL and FGFR1 siRNAs on in vitro invasion of NCI-H226 cells. Both siRNAs produced substantial, but less than complete, knockdown of invasion.

### 3.5 Informatic Analysis: Connecting the Invasive Phenotypes with the NCI Drug Screening Database

Extension of the analysis to the NCI60 drug screening database was addressed, again using the invasion AUC profile as seed in the COMPARE program. Table 3 illustrates some of the top correlates from the synthetic compound database of more than 187,000 compounds. Four of the top ten correlates are in the publicly available database and were screened for activity as inhibitors of



**Fig. 4 (a)** Mean graph representation [5] of the patterns of expression of AXL, FGFR1, and EGFR in comparison to the invasion AUC profile of the NCI60. The overall average of each parameter serves as the vertical line in the center of each profile. For the invasion AUC, gold bars projecting to the right of the line represent cell lines with a more aggressive than average phenotype. Bars projecting to the left represent cell lines with a less aggressive than average phenotype. Gene expression patterns are represented in analogous fashion with blue, green, and red bars representing AXL, FGFR1, and EGFR, respectively. **(b)** Effects of purified human recombinant GAS6 (blue line), bFGF (green line), and EGF (red line) on in vitro migration of DU-145 prostate cancer cells. No migration was observed in the absence of chemoattractant (black line). **(c)** Effects of AXL and FGFR1 siRNAs on in vitro invasion of NCI-H226 lung cancer cells. Control siRNA (black line) had no apparent effect on in vitro invasion, producing a profile similar that observed in untreated cell populations. Transfection with AXL (blue line) or FGFR1 (green line) siRNA produced substantial inhibition of invasion

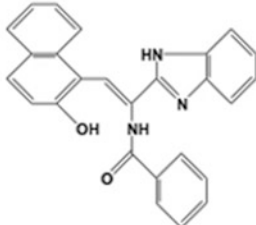
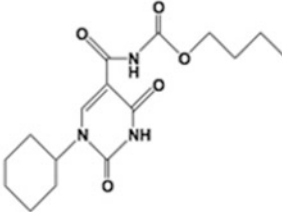
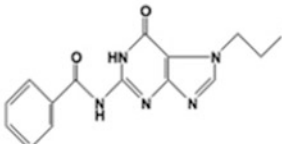
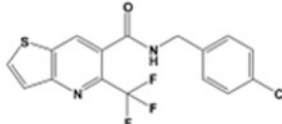
**Fig. 4** (continued)

in vitro invasion on the xCELLigence instrument using concentrations ranging from  $10\mu\text{M}$  to  $100\text{ nM}$ . All four of these compounds showed evidence for inhibition of invasion at one or more concentration in DU-145 and NCI-H226. Results for the top correlate, NSC 624445, are shown in Fig. 5 for the DU-145 prostate cancer cell line. No evidence of growth inhibition was observed in a concurrent growth inhibition assay.

### 3.6 Discussion

The real-time kinetic phenotypes for in vitro migration and invasion were remarkably reproducible and characteristic for each of the NCI60 tumor cell lines. Inspection of the invasion AUC profile, as illustrated in Fig. 4a, indicates relatively aggressive invasive phenotypes for many cell lines in the solid tumor panels and a lack of invasion signal for the leukemia panel, most of the colon cancer cell lines, and the majority of breast cancer cell lines. Visualization by scanning electron microscopy revealed that these latter cell lines

**Table 3**  
**Top Compounds Correlated with Invasion AUC**

Rank	Correlation Coefficient	NSC Number	Structure
1	0.75	624445	
2	0.74	631572	
9	0.70	637529	
10	0.69	680625	

actually do invade, but do so using an amoeboid mode which does not provide for close contact of the invading cells with the micro-detector array. In contrast, the close interaction with the detector associated with mesenchymal motility generates a substantial change in electrical impedance, contributing to efficient detection of migration and invasion of cells which use this mode. Scanning electron microscopy also provided evidence for spreading and interaction of cells as well as replication of cells on the surface of the detectors in the form of apparent postmitotic pairs of cells and morphologic heterogeneity that suggested the existence of subpopulations of cells. Occasionally, individual cells appearing to use amoeboid motility could be observed among cells with a classic mesenchymal appearance. This may reflect an ability of some tumor cells to switch between modes of motility as previously described.

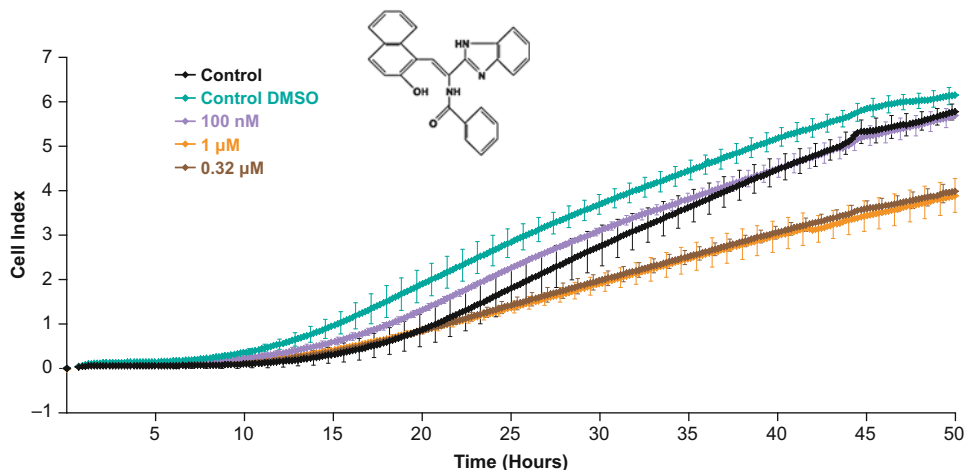


**Fig. 5** Effect of NSC 624445 on in vitro invasion of DU-145 prostate cancer cells. The chemical structure is shown in the inset. Compound was dissolved in DMSO, diluted with RPMI-1640, and added to the upper well of the invasion chamber at the indicated concentrations. 10% FBS was used as chemoattractant in the lower chamber. The DMSO control contained 0.1% final DMSO concentration, as did all test compound dilutions. No evidence for growth inhibition was observed in a concurrent Alamar blue growth inhibition assay

[11]. Nonetheless, it is clear that the kinetic invasion fingerprints generated on the xCELLigence instrument relate primarily to mesenchymal migration and invasion. This is reflected in the nature of the genes and pathways linked to the invasion AUC phenotypes by informatic analysis. Expressions of growth factor receptors, integrins, ILK, FAK, and cytoskeletal elements are classically associated with mesenchymal invasion. It is noteworthy that the kinetics of invasion in response to the purified growth factors are distinctly different from that observed when FBS is used as chemoattractant. This may reflect the combinatorial effect of multiple growth factors in the latter case. It is also possible that, in the absence of FBS, the cells rely more on an amoeboid mode of invasion which has a reduced impact on the detection electrode. The siRNA experiments provide further validation for the importance of growth factors to the in vitro invasion phenotypes. While the knockdown effects were striking in tumor cell lines with aggressive invasive phenotypes and high levels of growth factor receptor expression, such as DU-145, and NCI-H226, other factors are clearly important in these and other cellular contexts. Indeed, the importance of multiple factors for cancer cell invasion is well recognized [16].

Database mining using the invasion AUC phenotypes was effective in identifying compounds capable of inhibiting in vitro invasion at nontoxic concentrations. Notably, NSC 624445 produced an amount of inhibition comparable to that observed for specific growth factor siRNAs. At this point, it is not apparent what receptor or receptors the compound may act on. Further, the

interpretation of these results is complicated by the fact that DMSO (0.1% final concentration), used as vehicle to dissolve the test compound, had an inducing effect on the invasive phenotype as illustrated in Fig. 5. We have also observed this phenomenon in several other tumor cell lines. DMSO, as vehicle, antagonizes the effects of the putative invasion inhibitors. As indicated above, FBS appears to have the potential for inducing the mesenchymal invasion phenotype. Thus, multiple confounding variables are operative in this in vitro model of invasion. Among the other three top correlates from the synthetic drug screening database that also showed inhibition of in vitro invasion, NSC 680625 is of particular interest. This compound was previously identified as an EGFR inhibitor using the COMPARE algorithm [17]. While additional testing will be required to fully characterize the mechanism of action of these compounds, our results provide proof of principle that small molecule leads for inhibition of invasion can be identified using the kinetic invasion phenotypes.

Targeting multiple critical growth factor pathways may represent a useful strategy for treatment or prevention of metastasis. The exact nature of the growth factors may vary substantially with tumor type and pattern of metastasis. Nonetheless, the growing availability of targeted biological agents affecting the bioavailability of growth factors or their receptors and small molecules affecting the functioning of those receptors suggests that such an approach may be feasible. Indeed, the concept of combining kinase inhibitors or exploiting multi-targeting of individual inhibitors is not new. For example, use of a dual kinase inhibitor affecting EGFR and VEGFR has been reported previously [18]. Our results support this approach in that VEGF expression was a prominent feature correlated to the in vitro invasion phenotype. Indeed, it is interesting that this feature, clearly important for successful in vivo metastasis, is retained in the in vitro phenotype. Targeting additional factors such as AXL and FGFR may be necessary to have an optimal therapeutic effect. The prominence of integrin and ILK signaling in relation to in vitro invasion suggests that targeting of this pathway may also have value. Small molecule inhibitors of ILK for cancer treatment have been reported [19]. Whether such molecules could be incorporated into a combination regimen for inhibition of metastasis without engendering toxic effects on normal cells whose function requires motility remains to be established. There may be some basis for a “therapeutic index” in the distinction between mesenchymal and amoeboid phenotypes. As mentioned above, the latter mechanism is associated with motility of blood elements such as neutrophils. Targeting genes and pathways associated with mesenchymal invasion may avoid adverse effects on these normal cells. On the other hand, tumor cells capable of utilizing amoeboid motility or switching from mesenchymal to amoeboid motility may escape such targeted therapy.

In vitro results with bovine growth factors and murine ECM may have limited relevance to clinical metastasis. Use of human growth factors or extracts of human tissues such as lymph node, lung, liver, and brain which are frequent sites of metastasis and human ECM could provide a means of confirming the significance of the present data and extending it to address specific hypotheses regarding therapeutic strategies addressing “soil” factors to inhibit tissue-specific metastasis. Our results provide a starting point for such studies and add a new dimension to the public NCI60 database which can be mined by investigators worldwide to generate hypotheses regarding migration and invasion. Likewise, further database mining may identify additional compounds that may serve as leads for development of a new generation of antimetastatic compounds.

---

#### 4 Notes

To assess the effects of siRNA treatment, transfected cells were plated as described above and monitored for migration and invasion. Evaluation of the effects of recombinant human growth factors as chemoattractants was performed by addition of these materials to the lower chamber in serum-free medium. Small molecules were tested for inhibition of migration and invasion by incorporation into the upper chamber immediately following cell addition. Concurrent cytotoxicity assays were conducted by plating ~1000 cells/well in RPMI-1640 medium supplemented with 10% FBS and 2 mM L-glutamine in 384-well plates, adding dilutions of test compound, and using an Alamar blue assay end point, evaluated at the end of the 48 h incubation period by quantitation of fluorescence using an excitation wavelength of 530 nm and an emission wavelength of 590 nm on a Tecan Spectrafluor Plus Microplate Reader.

For scanning electron microscopy, cells were fixed *in situ* with a solution of 2% glutaraldehyde/4% formaldehyde in PBS, dehydrated through a graded series of alcohols, air-dried from tetramethylsilane, coated with a thin layer of gold/palladium and imaged in a Hitachi S-3000N scanning electron microscope.

---

#### Acknowledgments

The authors thank Adam S. Harned, Kunio Nagashima and Ulrich Baxa for expert assistance with scanning electron microscopy and John Connelly for help with siRNA experiments. Dr. Dominic Scudiero, Anne Monks, Eric Harris and Thomas E. Silvers provided technical and data processing support. This project has been funded in whole or in part with federal funds from the National Cancer

Institute, National Institutes of Health, under Contract HHSN261200800001E. The content of this publication does not necessarily reflect the views or policies of the Department of Health and Human Services, nor does mention of trade names, commercial products, or organizations imply endorsement by the U.S. government. This work was supported in part by Roche Applied Science.

## References

- Talmadge JE, Fidler IJ (2010) AACR centennial series: the biology of cancer metastasis: historical perspective. *Cancer Res* 70(14):5649–5669
- Boyden S (1962) The chemotactic effect of mixtures of antibody and antigen on polymorphonuclear leucocytes. *J Exp Med* 115:453–466
- Albini A, Iwamoto Y, Kleinman HK, Martin GR, Aaronson SA, Kozlowski JM (1987) McEwan RN. A rapid in vitro assay for quantitating the invasive potential of tumor cells. *Cancer Res* 47(12):3239–3245
- Imamura H, Takao S (1994) Aikou T. A modified invasion-3-(4,5-dimethylthiazole-2-yl)-2,5-diphenyltetrazolium bromide assay for quantitating tumor cell invasion. *Cancer Res* 54(13):3620–3624
- Sieuwerts AM, Klijn JG, Foekens JA (1997) Assessment of the invasive potential of human gynecological tumor cell lines with the in vitro Boyden chamber assay: influences of the ability of cells to migrate through the filter membrane. *Clin Exp Metastasis* 15(1):53–62
- Solly K, Wang X, Xu X, Strulovici B, Zheng W (2004) Application of real-time cell electronic sensing (RT-CES) technology to cell-based assays. *Assay Drug Dev Technol* 2(4):363–372
- Xing JZ, Zhu L, Jackson JA, Gabos S, Sun XJ, Wang XB, Xu X (2005) Dynamic monitoring of cytotoxicity on microelectronic sensors. *Chem Res Toxicol* 18(2):154–161
- Monks A, Scudiero D, Skehan P, Shoemaker R, Paull K, Vistica D, Hose C, Langley J, Cronise P, Vaigro-Wolff A, Gray-Goodrich M, Campbell H, Mayo J, Boyd M (1991) Feasibility of a high-flux anticancer drug screen utilizing a diverse panel of cultured human tumor cell lines. *J Natl Cancer Inst* 83:757–766
- Paull KD, Shoemaker RH, Hodes L, Monks A, Scudiero DA, Rubinstein L, Plowman J, Boyd MR (1989) Display and analysis of patterns of differential activity of drugs against human tumor cell lines: development of mean graph and COMPARE algorithm. *J Natl Cancer Inst* 81:1088–1092
- Shoemaker RH (2006) The NCI60 human tumour cell line anticancer drug screen. *Nat Rev Cancer* 6:813–823
- Friedl P, Wolf K (2010) Plasticity of cell migration: a multiscale tuning model. *J Cell Biol* 188(1):11–19
- Vajkoczy P, Knyazev P, Kunkel A, Capelle HH, Behrndt S, von Tengg-Kobligk H, Kiessling F, Eichelsbacher U, Essig M, Read TA, Erber R, Ullrich A (2006) Dominant-negative inhibition of the Axl receptor tyrosine kinase suppresses brain tumor cell growth and invasion and prolongs survival. *Proc Natl Acad Sci U S A* 103(15):5799–5804
- Suyama K, Shapiro I, Guttmann M, Hazan RB (2002) A signalling pathway leading to metastasis is controlled by N-cadherin and the FGF receptor. *Cancer Cell* 2(4):301–314. *Mol Cancer Ther* 2008 Oct;7(10):3408–19
- Fischer H, Taylor N, Allerstorfer S, Grusch M, Sonvilla G, Holzmann K, Setinek U, Elbling L, Cantonati H, Grasl-Kraupp B, Gauglhofer C, Marian B, Micksche M, Berger W (2008) Fibroblast growth factor receptor-mediated signals contribute to the malignant phenotype of non-small cell lung cancer cells: therapeutic implications and synergism with epidermal growth factor receptor inhibition. *Mol Cancer Ther* 7:3408–3419
- Reinhold WC, Sunshine M, Liu H, Varma S, Kohn KW, Morris J, Doroshow J, Pommier Y (2012) CellMiner: a web-based suite of genomic and pharmacologic tools to explore transcript and drug patterns in the NCI-60 cell line set. *Cancer Res* 72(14):3499–3511
- Sahai E (2005) Mechanisms of cancer cell invasion. *Curr Opin Genet Dev* 15:87–96
- Wosikowski K, Schuurhuis D, Johnson K, Paull KD, Myers TG, Weinstein JN, Bates SE (1997) Identification of epidermal growth factor

- receptor and c-erbB2 pathway inhibitors by correlation with gene expression patterns. *J Natl Cancer Inst* 89:1505–1515
18. Yigitbasi OG, Younes MN, Doan D, Jasser SA, Schiff BA, Bucana CD, Bekele BN, Fidler IJ, Myers JN (2004) Tumor cell and endothelial cell therapy of oral cancer by dual tyrosine kinase receptor blockade. *Cancer Res* 64 (21):7977–7984
19. Hannigan G, Troussard AA, Dedhar S (2005) Integrin-linked kinase: a cancer therapeutic target unique among its ilk. *Nat Rev Cancer* 5:51–63



# Chapter 13

## Detection of Tumor Cell-Induced Platelet Aggregation and Granule Secretion

Svenja Schwarz, Martin Schlesinger, and Gerd Bendas

### Abstract

Hematogenous metastatic spread of cancer is strongly dependent on and triggered by an intensive interplay of tumor cells with platelets. Immediately after entering the blood vascular system, tumor cells are surrounded by a platelet cloak, which protects them physically from shear stress and from attacks by the immune surveillance. Furthermore, tumor cell binding activates platelets, which in turn release growth factors and chemokines to recruit myeloid cells into the platelet/tumor cell microemboli, eventually create a permissive microenvironment in the early metastatic niche. Although the molecular mechanisms of tumor cells to activate platelets appear versatile being a matter of further research, interference with platelet activation turns out to be an attractive target to efficiently inhibit tumor metastasis. Some experimental assays are generally recognized to follow tumor cell-induced platelet activation (TCIPA), which provide an insight into the molecular mechanisms of TCIPA and allow searching for potential inhibitors. In this chapter, we describe the two most prominent experimental assays to follow TCIPA, namely platelet aggregation and platelet granule secretion, experimentally realized by dense granules' ATP quantification. Although light transmission aggregometry and ATP detection from dense granule secretion are two age-old techniques, they are still highly relevant to provide reliable information concerning platelet activation status since all tumor cell-derived molecular triggers are covered and monitored in the experimental outcome.

**Key words** Aggregation, ATP release, Cancer metastasis, Platelets, Tumor cell-induced platelet activation (TCIPA)

---

### 1 Introduction

Platelets represent the second most numerous cellular fraction in human blood and possess a pivotal role in physiology and pathology of thrombosis and hemostasis. Platelets are anuclear cells with a discoid shape, which express numerous surface receptors and also contain a multitude of bioactive factors in their intracellular granules. Activation of platelets is crucial for platelet function that subsequently includes a complex interplay of adhesion events, which finally gives rise to platelet aggregation and release of bioactive components triggering procoagulant activity, spreading, and

microparticle release. Platelets have also a strong functional impact on other physiological regulations, such as inflammation, or pathologies like atherosclerosis. Moreover, it is becoming apparent that they have multiple functions in regulation of the innate and adaptive immunity [1, 2].

Remarkably, platelets form a bad alliance with a multitude of malignancy and are especially involved in progression of cancer. There is a body of experimental evidence that platelets strongly support the metastatic spread of tumor cells. Several excellent reviews in that field provide an insight into the different functionalities of platelets to protect circulating tumor cells in their blood passage of hematogenous dissemination [3–6].

Briefly, immediately after entering the blood system, tumor cells were enclosed by platelets, which provide them a physical shield against shear stress and immunological elimination attacks [7–9]. The binding of platelets to tumor cells, leading to platelet activation, has been suggested to be mediated by, e.g., P-selectin and C-type lectin receptor 2 (CLEC-2) expressed on platelets interacting with certain P-selectin ligands or podoplanin, respectively, at the tumor cell surface [10–13]. Direct binding of tumor cells is one option of platelet activation, functionally associated with two other pathways: (1) Many tumor cells express tissue factor which activates the plasmatic coagulation cascade providing a local thrombin formation. Thrombin, in turn, is a highly potent mediator when activating its protease-activated receptor (PARs) pathways in platelets, tumor cells, or endothelium [14]. (2) Different tumor cells are capable of releasing mediators, such as ADP, ATP, thromboxane A<sub>2</sub>, which induce, following their specific receptor pathways, a strong acceleration and increase of the platelet/tumor cell microemboli formation [15–17].

Although the different mechanisms contributing to TCIPA, namely adhesion, thrombin formation, and soluble factor release, strongly depend on tumor entities and several other factors, all TCIPA-inducing pathways can be reflected experimentally by functional assays as a whole process. For this, isolated human platelets can be incubated with tumor cells following the state of platelet activation. However, using those *in vitro* approaches, the impact of platelets on tumor cells can also be detected, e.g., following migratory and invasive properties or the induction of an epithelial to mesenchymal transition program (EMT) in tumor cells [18].

Experimental assays reflecting TCIPA mainly focus on platelet aggregation, which can be detected by light transmission measurements. Furthermore, for quantification of platelet  $\alpha$ -granule releasates, ELISA techniques can be adapted to the indicated type of analyte, e.g., VEGF, EGF, chemokines, respectively [3]. The release of ATP as an indicator for platelet dense granule release can excellently be quantified by luminescence measurements, as indicated below. The secretion of platelets granules often precedes

platelet aggregation but is not necessarily associated with aggregation [19]. Thus, surveillance of platelet granule release besides aggregation is an important and sensitive marker for platelet activation in addition to light transmission measurements.

The application of the indicated approaches to follow TCIPA, ELISAs, ATP quantification, or even aggregometry represents the functional readout of the whole process of platelet tumor cell interaction in a physiologically adapted medium, such as adding platelet-rich or platelet-poor plasma (PRP or PPP, respectively) to the analyte solution. Interference with dominant, tumor cell-derived activation triggers, by, e.g., application of anticoagulants or other receptor pathway inhibitors may provide an insight into the relevance of the different pathways contributing to TCIPA, thus offering novel targets for interference with metastasis.

Here we describe a standard protocol for investigating platelet aggregation by light transmission measurement, which is routinely used in clinics for platelet characterization and is easily adaptable to the aspects of TCIPA. In agreement to many studies in this field, we have good experience in using aggregometry in analyzing TCIPA by numerous tumor cell lines of different entities and origin, indicating this technique as reliable, sensitive, and easy to perform. Furthermore, we also describe a luminescence measurement for quantifying ATP release from platelets, which turns out to be a highly sensitive and cheap detection method using a luminescence plate reader format and which offers additional information concerning tumor cell-induced platelet secretion.

---

## 2 Materials

### 2.1 Platelet Isolation

1. Citrate tubes: e.g., S-Monovette® 8.2 mL 9NC. Final citrate concentration 10.5 mM (*see Note 1*).
2. Appropriate blood collection equipment [20].
3. Apyrase stock solution: Weight 1000 units apyrase and add sterile-filtered ultrapure water to a final volume of 1 mL. Store at –20 °C.
4. Apyrase wash buffer: 5 mM HEPES, 137 mM NaCl, 2.7 mM KCl, 1 mM MgCl<sub>2</sub>, 0.54 mM NaH<sub>2</sub>PO<sub>4</sub>, 2.8 mM D-glucose.

To prepare a 10× stock solution, dissolve 1.192 g HEPES, 7.989 g NaCl, 0.194 g KCl, 0.095 g MgCl<sub>2</sub>, 0.075 g NaH<sub>2</sub>PO<sub>4</sub> × H<sub>2</sub>O, and 0.500 g D-glucose in 100.0 mL ultrapure water in a graduated flask. Filter the solution sterile and store at 4 °C. Before use, dilute the buffer 1:10 with sterile, ultrapure water and adjust pH to 6.5 (by adding HCl or NaOH) (*see Note 2*). Afterwards, add 2 µL apyrase stock solution per mL buffer.

5. Platelet buffer: 10 mM HEPES, 137 mM NaCl, 2.7 mM KCl, 1 mM MgCl<sub>2</sub>, 13.8 mM NaHCO<sub>3</sub>, 0.36 mM NaH<sub>2</sub>PO<sub>4</sub>, 5.5 mM D-glucose.

To prepare a 10× stock solution, dissolve 2.383 g HEPES, 7.989 g NaCl, 0.194 g KCl, 0.095 g MgCl<sub>2</sub>, 1.159 NaHCO<sub>3</sub>, 0.050 g NaH<sub>2</sub>PO<sub>4</sub> × H<sub>2</sub>O, 0.991 g D-glucose in 100.0 mL ultrapure water in a graduated flask. Filter the solution sterile and store at 4 °C. Before use dilute the buffer 1:10 with sterile-filtered, ultrapure water and adjust pH to 7.4 (by adding HCl or NaOH) (*see Note 2*).

6. CaCl<sub>2</sub> solution: 500 mM CaCl<sub>2</sub>.

Dissolve 0.735 g CaCl<sub>2</sub> × 2H<sub>2</sub>O in 10 mL sterile-filtered ultrapure water.

7. Pipettes (tips with large opening to avoid shear stress).

8. Cell counting device (e.g., Neubauer improved counting chamber) (*see Note 3*).

9. Centrifuge (swing bucket rotor, programmable temperature setting, set at 22 °C, compatible with 15 mL tubes).

10. Centrifugation tubes (polypropylene for processing and storage of platelets).

## **2.2 Investigation of a TCIPA Using Light Transmission Aggregometry**

1. Equipment of tumor cell cultivation (e.g., cell culture flasks, media, pipettes).

2. Phosphate-buffered saline (PBS): 140 mM NaCl, 3 mM KCl, 1.5 mM KH<sub>2</sub>PO<sub>4</sub>, 8 mM Na<sub>2</sub>HPO<sub>4</sub>. Dissolve 8.0 g NaCl, 0.2 g KCl, 0.2 g KH<sub>2</sub>PO<sub>4</sub>, 1.14 g Na<sub>2</sub>HPO<sub>4</sub> in 1000.0 mL ultrapure water in a graduated flask and adjust pH to 7.2–7.4 (by adding NaOH or HCl). Filter the solution sterile and store at 4 °C until use.

3. PBS/EDTA solution: 5 mM Na<sub>2</sub>HPO<sub>4</sub>, 1.7 mM KH<sub>2</sub>PO<sub>4</sub>, 150 mM NaCl, 3.76 mM KCl, 0.878 mM EDTA-Na<sub>2</sub>, 10.1 mM LiCl.

To prepare a 10× stock solution, dissolve 0.713 g Na<sub>2</sub>HPO<sub>4</sub>, 0.232 g KH<sub>2</sub>PO<sub>4</sub>, 8.766 g NaCl, 0.280 g KCl, 0.46 g EDTA-Na<sub>2</sub> × 2H<sub>2</sub>O, 0.427 g LiCl in 100.0 mL ultrapure water in a graduated flask. Filter the solution sterile and store at 4 °C. Before use dilute the buffer 1:10 with sterile filtered, ultrapure water and adjust pH to 7.2–7.4 (by adding HCl or NaOH).

4. Centrifugation tubes (polypropylene for processing and storage of platelets).

5. Light transmission aggregometer (e.g., APACT 4004 (LABiTech, Ahrensburg, Germany)) with appropriate cuvettes.

6. Platelet-poor plasma (PPP): Centrifuge the platelet-rich plasma (PRP) (660 × *g*, 10 min, 22 °C), centrifuge the supernatant again (1600 × *g*, 15 min, 22 °C) (*see Note 4*).

### 2.3 Quantification of a Tumor Cell-Induced Platelet Dense Granule Release

1. 1.6 mL polypropylene reaction tubes.
2. Nontreated white 96-well microtiter plate.
3. Reaction buffer ( $20\times$ ): 500 mM tricine buffer (pH 7.8), 100 mM MgSO<sub>4</sub>, 2 mM EDTA, 2 mM sodium azide.  
To prepare a  $20\times$  stock solution, dissolve 8.958 g *N*-(Tri(hydroxymethyl)methyl)glycine (tricine), 1.204 g MgSO<sub>4</sub>, 0.0745 g EDTA-Na<sub>2</sub>  $\times$  2H<sub>2</sub>O, 0.0130 g NaN<sub>3</sub> in 100.0 mL ultrapure water in a graduated flask. Filter the solution sterile and store at -20 °C.
4. D-Luciferin solution: 10 mM d-luciferin.  
Dissolve 30.0 mg (*S*)-2-(6-Hydroxy-2-benzothiazolyl)-2-thiazoline-4-carboxylic acid, 4,5-Dihydro-2-(6-hydroxy-2-benzothiazolyl)-4-thiazolecarboxylic acid (d-luciferin) in 10.0 mL 1× reaction buffer (make 10.0 mL of 1× reaction buffer by adding 500 µL 20× reaction buffer to 9500 µL ultrapure water). Aliquot into ten reaction tubes and store them at -20 °C. The stock solution is reasonably stable for several weeks. Protect from light and avoid freezing and thawing cycles.
5. Firefly luciferase solution: 5 mg/mL recombinant firefly luciferase in 25 mM Tris-acetate (pH 7.8), 200 mM ammonium sulfate, 15% (v/v) glycerol, and 30% (v/v) ethylene glycol.
6. Dithiothreitol (DTT) solution: 100 mM DTT. Dissolve 25 mg DTT in 1.62 mL deionized water. Divide into ten aliquots of 160 µL and store at -20 °C until use. Stock solutions of DTT are stable for 6 months.
7. Luminescence reagent: Prepare the solution shortly prior use. Storage is recommended at 4 °C and protected from light. Prepare 5 mL luminescence reagent for one 96-well plate: 4.45 mL deionized water, 250 µL reaction buffer (20×), 50 µL DTT solution, 250 µL D-luciferin solution, 1.25 µL firefly luciferase solution.
8. Adenosine 5'-triphosphate (ATP) standard: 5 mM in TRIS/EDTA buffer.

---

## 3 Methods

Carry out all procedures at room temperatures unless otherwise indicated.

### 3.1 Platelet Isolation

*See Fig. 1* for an overview of how to isolate platelets and prepare platelet-rich buffer.

1. Collect blood from healthy volunteers (who did not receive any medication 14 days before donation) in citrate tubes [20] (see

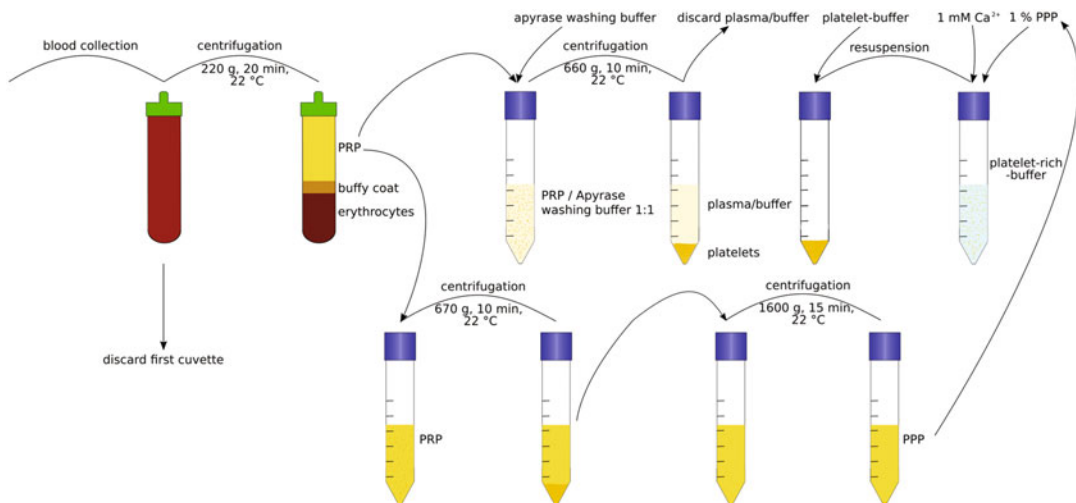


**Fig. 1** Overview of how to isolate platelets and prepare platelet-rich buffer from freshly isolated blood

**Note 5).** The first tube is discarded (*see Note 6*). After blood collection, gently turn over the tubes 3–4 times to ensure mixing of blood and anticoagulant (citrate solution).

2. Centrifuge the tubes as soon as possible after blood collection ( $220 \times g$ , 20 min,  $22^\circ C$ ) (*see Notes 7 and 8*).
3. Leave the tubes upright for 10 min after centrifugation. Transfer platelet-rich plasma (PRP) into centrifugation tubes (*see Notes 9 and 10*).
4. Mix PRP and apyrase washing buffer in a ratio of 1:1 (*see Note 11*).
5. Centrifuge the PRP-buffer mixture ( $660 \times g$ , 10 min,  $22^\circ C$ ).
6. Discard the supernatant. Resuspend platelets in washing buffer (add apyrase if necessary (*see Note 12*)). Use the same volume of buffer as in **step 4**.
7. Centrifugation of platelets in washing buffer ( $660 \times g$ , 10 min,  $22^\circ C$ ).
8. Discard the supernatant. Resuspend platelets in platelet buffer (use half the total volume of **step 4**).
9. Quantify the platelet concentration using a Neubauer improved counting chamber or another counting method (*see Note 3*).
10. Adjust the concentration of platelets to  $300 \times 10^6/\text{mL}$  by adding platelet buffer (*see Note 13*).
11. Add 2  $\mu\text{L}$   $\text{CaCl}_2$  solution per mL platelet-rich buffer (final concentration  $1 \text{ mM Ca}^{2+}$ ) (*see Notes 14 and 15*).

### 3.2 Investigation of a TCIPA Using Light

#### Transmission Aggregometry

##### 3.2.1 Preparation of Platelets and Tumor Cells

1. Cultivate adherent tumor cells until a 90% confluence growth in cell culture flasks (*see Note 16*).
2. Aspirate the cell culture medium and wash the tumor cells three times with warm (37 °C) PBS, to remove remaining media and apoptotic tumor cells.
3. Detach the tumor cells with PBS–EDTA solution at 37 °C and 5% CO<sub>2</sub> for 5–15 min depending on tumor cell line (*see Note 17*).
4. Rinse the tumor cells with PBS and transfer them to a centrifugation tube.
5. Determine the number of tumor cells (*see Note 18*).
6. Centrifuge the tumor cell suspension (450 × *g*, 4 min, 4 °C).
7. Remove the supernatant. Resuspend tumor cell pellet in PBS and adjust desired cell concentration (*see Note 19*).
8. Prepare platelets as described in Subheading 3.1. Add 1% PPP (V/V) to the prepared platelet-rich buffer (10 µL/mL) (*see Note 20*).
9. If necessary, platelets or tumor cells can be incubated with various inhibitors before the subsequent measurement (*see Note 21*).

##### 3.2.2 Induction of a TCIPA and Detection in an LTA Approach

1. TCIPA is determined by a light transmission aggregometer (*see Note 22*). Heat up the device to 37 °C.
2. For a first calibration, a cuvette filled with 200 µL platelet buffer is applied and indicates a transmission corresponding to 100% aggregation (Fig. 2).
3. Prepare a new cuvette for each measurement and fill it with 200 µL platelet-rich buffer. Discard the cuvettes after the measurement (*see Note 23*).
4. Put the cuvette into the aggregometer. Use the aggregometer to determine the zero value of the transmission before induction of platelet activation. This corresponds to the transmission of non-aggregated platelets (0% aggregation) (Fig. 2).
5. Test whether platelets can be activated with an agonist (e.g., TRAP-6, U46619, collagen type I, ADP) to exclude any damage to the platelets during the preparation process (*see Note 24*). Pipette the agonist into the cuvettes. Make sure that the tip of the pipette touches the platelet-rich buffer to ensure the whole volume of agonist is added. Start the measurement immediately after addition of the agonist.
6. Add 20 µL of the prepared tumor cell suspension to another cuvette to induce the TCIPA (*see Note 25*).
7. After adding the tumor cells, start the measurement immediately. The measurement can be followed directly on the device

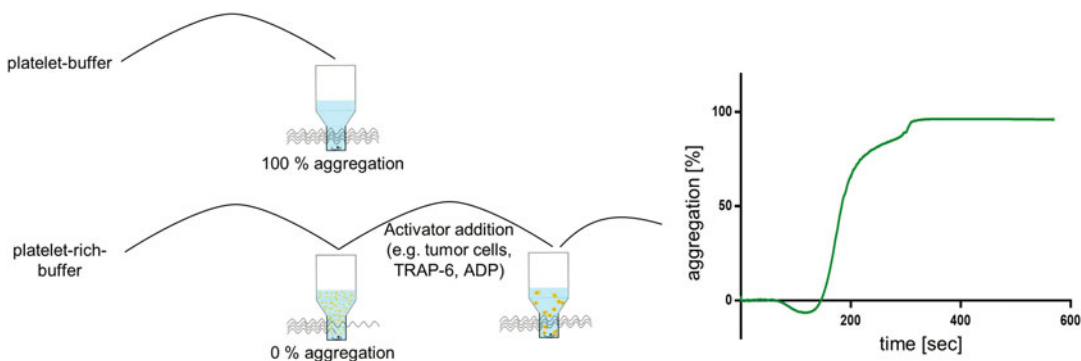


**Fig. 2** Schematic overview of the implementation of a measurement on the light transmissions aggregometer

or using the appropriate software. The measurement should be continued at least until a stable plateau has occurred after the aggregation (*see Note 26*) (Fig. 2).

8. After the measurement, the resulting aggregogram can be evaluated with regard to various parameters (*see Note 27*).

### 3.3 Quantification of a Tumor Cell-Induced Platelet Dense Granule Release

*See Fig. 3 for an overview of performing the quantification of a tumor-cell induced platelet dense granule release.*

1. Prepare tumor cells and platelet-rich buffer according to Subheading 3.2.1.
2. If inhibitors are tested, preincubate tumor cells or platelets with inhibitors (*see Note 21*) in polypropylene reaction tubes. Ensure that appropriate controls were incubated with indicated (organic) solvents, when used. It is advisable to leave platelets or tumor cells for the same period as the other samples without the addition of solvents or inhibitors. Incubation, especially of platelets, should take place at 20–22 °C.
3. Prepare one reaction tube for each desired sample, in which the subsequent activation experiments are performed (*see Note 28*).
4. Place 200 µL platelet-rich buffer, which was previously incubated with or without inhibitor, per reaction tube (*see Note 29*).
5. For the activation experiments, add the corresponding activators (e.g., agonists or tumor cells) to the corresponding reaction tubes. For tumor cells, it is recommended to add 20 µL tumor cell suspension (prepared according to Subheading 3.2.1) per 200 µL platelet-rich buffer (*see Note 25*). Concentrations corresponding to those of the light transmission aggregometry can normally be used for the agonists (*see Note 30*).
6. After adding the activators, close the reaction tubes and mix thoroughly (*see Note 31*).

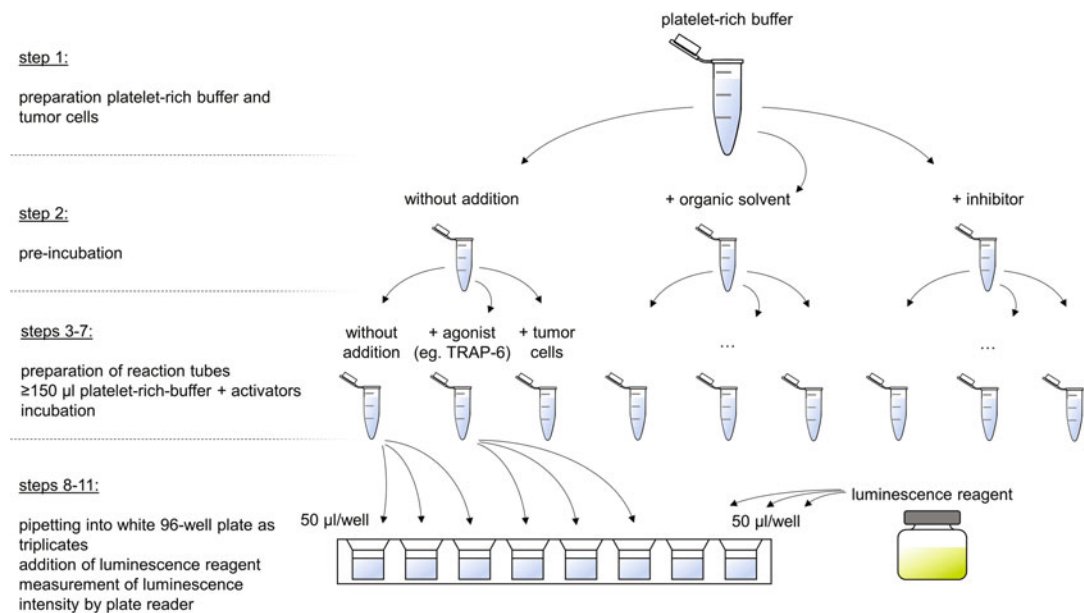


**Fig. 3** Step-by-step process of test execution of the dense granule release assay, starting with the tumor cell suspension and the platelet-rich buffer prepared (Subheading 3.2.1)

7. The incubation times depend on the particular issue and the activators or tumor cell line used (*see Note 32*).
8. The samples can be pipetted into **white** 96-well plate during the previously defined incubation period. Each sample is applied as a triplicate from one reaction tube into three wells containing 50 µL each.
9. In order to evaluate the absolute ATP concentration of the samples, a dilution series of an ATP standard can be measured. Dilute the ATP standard solution in deionized water. The concentrations depend on the design of your assay and the sensitivity of the luminescence measurement device used. Typically, appropriate ATP concentrations range from 1 nM to 1 µM.
10. At the end of the incubation period, 50 µL freshly prepared luminescence reagent is added to each well.
11. The measurement of the luminescence (according to a luciferin–luciferase reaction (Fig. 4)) should be examined immediately in order to avoid a decrease in the luminescence signal. The measurement should be performed at room temperature with the exclusion of light in an appropriate plate reader.

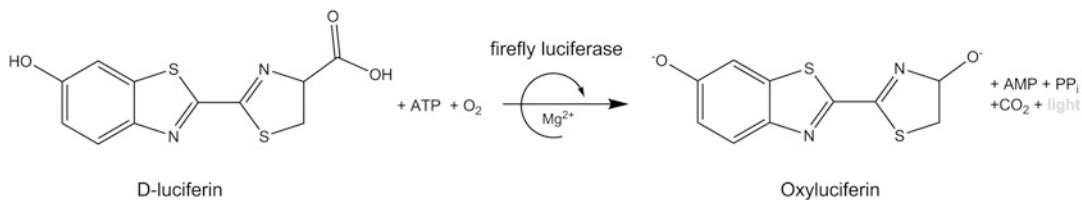


**Fig. 4** Luciferin–luciferase reaction. In the course of bioluminescence, D-luciferin is oxidatively decarboxylated to oxyluciferin by the enzyme luciferase. The quantitative course of the reaction depends on the amount of ATP. The ATP concentration of the sample is proportional to the luminescence detected

#### 4 Notes

1. EDTA tubes (e.g., S-Monovette® 7.5 mL K3E (1.6 mg EDTA/mL)) can also be used instead of citrate tubes.
2. Exact pH of both buffers is highly important. A pH value of 6.5 keeps platelets inactive, pH 7.4 of the platelet buffer is essential for platelet activation.
3. The use of the Neubauer improved counting chamber is the simplest and inexpensive method of quantifying platelets. A variety of other methods are applicable to quantify platelet concentration [21].
4. Initial centrifugation at  $660 \times g$  avoids activation of the platelets and the associated release of mediator substances into the plasma. A second centrifugation at  $1600 \times g$  is used to completely remove remaining platelets from the PPP.
5. Calcium may activate the coagulation system and causes coagulation of the blood. Therefore, calcium has to be complexed by the use of citrate.
6. The first Monovette may contain platelets that have been pre-activated by tissue injury and should therefore not be used.
7. Blood samples must be maintained at temperate conditions (20–24 °C), and platelet preparation should be completed within 2 h after blood collection.
8. Always store, process, and centrifuge platelets at 22 ± 2 °C to avoid activation.
9. Approximately 1.5–2.0 mL PRP can be obtained from 8 mL blood. PRP is the upper phase in the tube after centrifugation (Fig. 1). During careful extraction, do not touch the buffy coat. To enhance the PRP yield, allow the tube to stand vertically for 10 min after centrifugation.
10. Platelets should be handled using pipette tips with an opening as large as practical to avoid activation by shear stress. Use only polypropylene tubes.

11. Apyrase (ATP diphosphohydrolase) is an enzyme that hydrolytically degrades ATP and ADP to AMP. Its activity is dependent on divalent cations. It is used in *in vitro* experiments with platelets to protect the platelets from being activated by ADP (for example, by activation of platelet receptors P2Y<sub>12</sub> and P2Y<sub>1</sub>) [22].
12. It should be evaluated whether activation of the platelets via ADP is desired. If this is the case, platelets should be resuspended in buffer without apyrase after the last washing step.
13. The physiological platelet count is widely quoted as  $150\text{--}400 \times 10^9/\text{L}$  of whole blood.
14. Calcium is essential for both the enzymatic activity of various coagulation factors and the functionality of adhesion receptors that are associated with TCIPA [6, 21]. Normal serum calcium levels are about 2.0–2.5 mmol/L, although the exact range can vary among laboratories. Normal ionized calcium levels are 1–1.4 mmol/L [23].
15. Process platelets in buffer immediately.
16. The protocol can be used with small modifications for suspension cells.
17. Trypsin should not be used because it degrades or modifies the surface of the tumor cells with regard to their ability to activate platelets. In our experience, even strongly adhering tumor cell lines detach after 15 min of EDTA incubation.
18. Use a Neubauer improved counting chamber after trypan blue staining to identify apoptotic cells [24], or a method of your choice (e.g., other hemocytometer devices, or capillary particle counter with pulse area analysis (coulter counter)).
19. When adjusting the cell concentration, note that tumor cells are diluted 1:10 during the assay. We work with a final concentration of  $10^4$  tumor cells/mL and accordingly adjust a stock solution of  $10^5$  tumor cells/mL. The applied cell concentration depends on the tumor cell line. In our experience, it takes approximately  $10^4$  tumor cells/mL to activate platelets in the aggregometer. The maximum concentration of tumor cells used for activation is around  $2.5 \times 10^6$  cells/mL, since light transmission can be severely impaired at higher concentrations.
20. A small amount of plasma in the buffer appears to be essential for TCIPA. The presence of plasma is also necessary when using various direct activators (e.g., collagen type I).

21. In addition to the possibility of testing different tumor cell lines, the method offers the intriguing possibility to evaluate platelet inhibitors. Both, tumor cells and platelets, can be pre-incubated with a wide variety of inhibitors addressing various targets either on the tumor cells or on platelets. In our experience, incubation with inhibitors of extracellular targets for 30 min is recommended. Intracellular targets can also be modulated. The necessary preincubation time depends on the properties of both the target and the inhibitor.

Special care should be taken when using other solvents than water and PBS. A control sample containing the appropriate concentration of solvent should always be examined. In our experience, the concentration of the organic solvent (e.g., DMSO) in platelet suspensions should never exceed 0.5% (V/V).

22. Light transmission (born) aggregometry (LTA). LTA is the gold standard of platelet function assessment. PRP or platelet-rich buffer is stirred in a cuvette that is placed between a light source and a photo cell. The buffer or plasma is cloudy due to suspension of platelets and allows relatively little light to pass through. In response of an activating stimulus, platelets aggregate. By forming the aggregates, the sample becomes clearer, permitting intensified light transmission. Transmission of light is detected by the photo cell and recorded as a function of time (Fig. 2).
23. Insert the plastic cuvettes into the aggregometer so that the flat-ground sides are in the light ray. Before inserting, make sure that there is a stir fish in the bottom of the cuvette. This prevents sinking of the formed aggregates during the measurement. A stir speed of 1000–1200 rpm is recommended.
24. A panel of platelet agonists—ADP, collagen, thrombin receptor-activating peptide (TRAP), the thromboxane A<sub>2</sub> mimetic U46619, and arachidonic acid—is recommended.

We recommend the following concentrations for platelet activation:

TRAP-6 10–45 µM.

Thrombin 0.1–1 NIH/mL.

U46619 2–10 µM.

Arachidonic acid 0.5–5 µM.

ADP 2–20 µM.

Collagen (type I) 2–10 µg/mL.

Required concentrations can vary from measurement to measurement. Among other things, this is due to slightly varying platelet concentrations, individual differences between donors and the type of platelet processing.

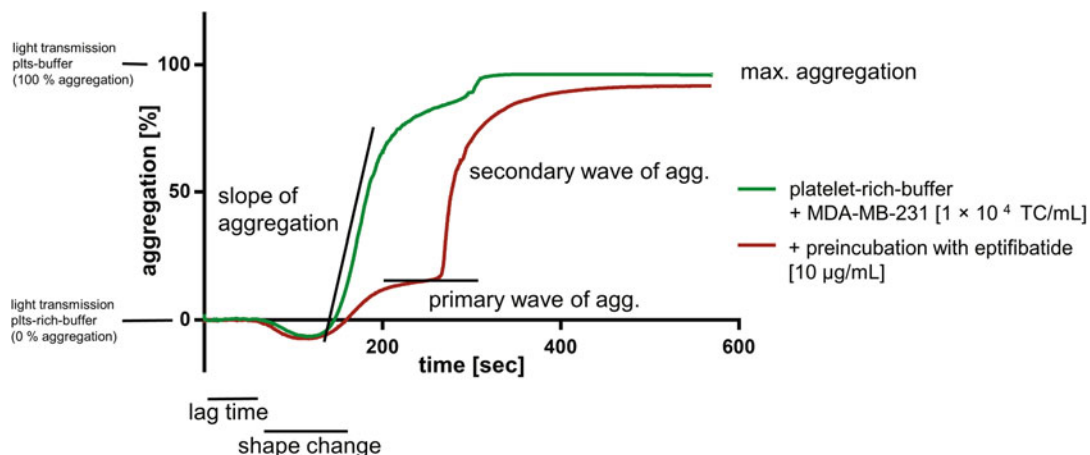


**Fig. 5** Exemplary evaluation of aggregation tracings after addition of MDA-MB-231 breast cancer cells with respect to a number of parameters including shape change, length of lag phase, slope of aggregation, primary aggregation, and presence of a secondary wave of aggregation (after preincubation with eptifibatide), as well as maximal aggregation

25. Note the 1:10 dilution of the tumor cell suspension.
26. A lack of platelet aggregation after tumor cell addition could have different reasons. Check whether calcium and PPP have been added before the measurement. Both are essential for a TCIPA. TCIPA is essentially linked to preactivation of platelets via thrombin. For the initiation of coagulation, coagulation factors and fibrinogen contained in 1% PPP are sufficient. The presence of  $\text{Ca}^{2+}$  as a cofactor is essential for the activity of the coagulation factors. In order to initiate the activation of the extrinsic coagulation cascade, an expression of tissue factor (TF) on the surface of tumor cells is essential. The TF status of the applied tumor cell lines can be checked using flow cytometry or Western blot. In addition, the tumor cell-induced thrombin generation can be quantified in a thrombin generation assay [25].
27. Aggregation tracings (Fig. 5) are evaluated with respect to a number of parameters including shape change; length of lag phase; slope of aggregation; presence of a secondary wave of aggregation produced by weak agonists, such as epinephrine; maximal percent aggregation; and presence of deaggregation.
28. In our experience, samples without inhibitor, with solvent, or with inhibitor, respectively, should be included. It is advisable to perform the following activation experiments with these samples: platelets without activation, to quantify a spontaneous ATP release, especially after incubation with organic solvents and other additives (e.g., inhibitors). In addition, the positive control with defined platelet activators (e.g., thrombin, TRAP-

- 6, collagen type I, U46619 (*see Note 24*) is recommended. These controls can exclude that the functionality of the platelets has been reduced during their preparation. The use of defined agonists in different experiments also offers the possibility of making different experiments comparable among each other. In addition to the two controls, the actual samples can now be prepared by activating them with tumor cells (Fig. 3).
29. 150 µL platelet-rich buffer is sufficient to measure the samples in triplicate. We recommend working with 200 µL in order to avoid possible volume deficits.
  30. In reaction tubes without tumor cells, an appropriate volume compensation with PBS should be ensured. This is necessary to keep a constant concentration of platelets in the buffer.
  31. As always when handling platelets, vigorous shaking or the like should be avoided.
  32. The time point of ATP detection terminates the incubation process and, thus, should be comparable. We mostly examined the maximum ATP release after activation, which may vary depending on the activator. Therefore, it is recommended to determine the release kinetics over different periods. The period of activation is determined based on the release kinetics. If the incubation times vary within an experiment, first add the activator that is to be added longest. In the course of the incubation period, the other activators can then be added at appropriate times.

## References

1. Semple JW, Italiano JE, Freedman J (2011) Platelets and the immune continuum. *Nat Rev Immunol* 11:264–274. <https://doi.org/10.1038/nri2956>
2. Franco AT, Corken A, Ware J (2015) Platelets at the interface of thrombosis, inflammation, and cancer. *Blood* 126:582–588. <https://doi.org/10.1182/blood-2014-08-531582>
3. Gay LJ, Felding-Habermann B (2011) Contribution of platelets to tumour metastasis. *Nat Rev Cancer* 11:123–134. <https://doi.org/10.1038/nrc3004>
4. Labelle M, Hynes RO (2012) The initial hours of metastasis: the importance of cooperative host-tumor cell interactions during hematogenous dissemination. *Cancer Discov* 2:1091–1099. <https://doi.org/10.1158/2159-8290.CD-12-0329>
5. Li N (2016) Platelets in cancer metastasis: to help the “villain” to do evil. *Int J Cancer* 138:2078–2087. <https://doi.org/10.1002/ijc.29847>
6. Schlesinger M (2018) Role of platelets and platelet receptors in cancer metastasis. *J Hematol Oncol* 11:125. <https://doi.org/10.1186/s13045-018-0669-2>
7. Kopp H-G, Placke T, Salih HR (2009) Platelet-derived transforming growth factor-beta down-regulates NKG2D thereby inhibiting natural killer cell antitumor reactivity. *Cancer Res* 69:7775–7783. <https://doi.org/10.1158/0008-5472.CAN-09-2123>
8. Maurer S, Kropp KN, Klein G et al (2018) Platelet-mediated shedding of NKG2D ligands impairs NK cell immune-surveillance of tumor cells. *Oncotargets Ther* 7:e1364827. <https://doi.org/10.1080/2162402X.2017.1364827>
9. Placke T, Kopp H-G, Salih HR (2011) Modulation of natural killer cell anti-tumor reactivity by platelets. *J Innate Immun* 3:374–382. <https://doi.org/10.1159/000323936>
10. Lowe KL, Navarro-Nunez L, Watson SP (2012) Platelet CLEC-2 and podoplanin in cancer metastasis. *Thromb Res* 129(Suppl 1):

- S30–S37. [https://doi.org/10.1016/S0049-3848\(12\)70013-0](https://doi.org/10.1016/S0049-3848(12)70013-0)
11. Stone JP, Wagner DD (1993) P-selectin mediates adhesion of platelets to neuroblastoma and small cell lung cancer. *J Clin Invest* 92:804–813. <https://doi.org/10.1172/JCI116654>
  12. Kim YJ, Borsig L, Varki NM, Varki A (1998) P-selectin deficiency attenuates tumor growth and metastasis. *Proc Natl Acad Sci U S A* 95:9325–9330
  13. Yu Y, Zhou X-D, Liu Y-K et al (2002) Platelets promote the adhesion of human hepatoma cells with a highly metastatic potential to extracellular matrix protein: involvement of platelet P-selectin and GP IIb-IIIa. *J Cancer Res Clin Oncol* 128:283–287. <https://doi.org/10.1007/s00432-002-0325-6>
  14. Rickles FR, Patierno S, Fernandez PM (2003) Tissue factor, thrombin, and cancer. *Chest* 124:58S–68S
  15. Zucchella M, Dezza L, Pacchiarini L et al (1989) Human tumor cells cultured “in vitro” activate platelet function by producing ADP or thrombin. *Haematologica* 74:541–545
  16. Aitokallio-Tallberg A, Kärkkäinen J, Pantzar P et al (1985) Prostacyclin and thromboxane in breast cancer: relationship between steroid receptor status and medroxyprogesterone acetate. *Br J Cancer* 51:671–674
  17. Yu L-X, Yan L, Yang W et al (2014) Platelets promote tumour metastasis via interaction between TLR4 and tumour cell-released high-mobility group box1 protein. *Nat Commun* 5:5256. <https://doi.org/10.1038/ncomms6256>
  18. Labelle M, Begum S, Hynes RO (2011) Direct signaling between platelets and cancer cells induces an epithelial-mesenchymal-like transition and promotes metastasis. *Cancer Cell* 20:576–590. <https://doi.org/10.1016/j.ccr.2011.09.009>
  19. Mitrugno A, Williams D, Kerrigan SW, Moran N (2014) A novel and essential role for Fc $\gamma$ RIIa in cancer cell-induced platelet activation. *Blood* 123:249–260. <https://doi.org/10.1182/blood-2013-03-492447>
  20. Greening DW, Simpson RJ, Sparrow RL (2017) Preparation of platelet concentrates for research and transfusion purposes. *Methods Mol Biol* 1619:31–42. [https://doi.org/10.1007/978-1-4939-7057-5\\_3](https://doi.org/10.1007/978-1-4939-7057-5_3)
  21. Harrison P, Briggs C, Machin SJ (2004) Platelet counting. *Methods Mol Biol* 272:29–46. <https://doi.org/10.1385/1-59259-782-3:029>
  22. Pérez de León AA, Tabachnick WJ (1996) Apyrase activity and adenosine diphosphate induced platelet aggregation inhibition by the salivary gland proteins of Culicoides variipennis, the north American vector of bluetongue viruses. *Vet Parasitol* 61:327–338. [https://doi.org/10.1016/0304-4017\(95\)00828-4](https://doi.org/10.1016/0304-4017(95)00828-4)
  23. Carroll MF, Schade DS (2003) A practical approach to hypercalcemia. *Am Fam Physician* 67:1959–1966
  24. Greenfield EA (2019) Myeloma and Hybridoma cell counts and viability checks. *Cold spring Harb Protoc* 2019:pdb.prot103259. <https://doi.org/10.1101/pdb.prot103259>
  25. Gockel LM, Ponert JM, Schwarz S et al (2018) The low molecular weight heparin Tinzaparin attenuates platelet activation in terms of metastatic niche formation by coagulation-dependent and independent pathways. *Molecules* 23:2753. <https://doi.org/10.3390/molecules23112753>



# Chapter 14

## Fatty Acid–Driven Polarization of Suppressive Bone Marrow–Derived Macrophages Including Metabolic and Functional Analysis

Hao Wu and Rainer Glauben

### Abstract

Macrophages represent not only the first line of defense against pathogens and are the main drivers of inflammation but are also involved in the initiation, immune evasion as well as metastasis of tumors. Therefore, it has been suggested that diminishing the immune regulatory function of macrophages would support the natural immune surveillance or antitumor therapies, respectively. However, the plasticity of macrophages represents an obstacle in understanding and manipulating the role of macrophages in tumor tissue or the tumor microenvironment. Here, we describe a protocol to differentiate macrophages, based on changing their metabolic environment, from bone marrow precursors to tumor-associated macrophage-like cells of an immune suppressive phenotype. Based on these protocols, the inhibitory functional phenotype of macrophages can be manipulated and therefore further analyzed as described, by interrupting metabolic pathways.

**Key words** Tumor-associated macrophages, Lipid droplets, Fatty acid oxidation, T-cell suppression

---

### 1 Introduction

It has been shown that reprogramming of energy metabolism in tumor tissue facilitates tumor development. One of the reasons is that the tumor microenvironment shapes the immune response via production and secretion of metabolites, for instance, lactate and various free fatty acids [1, 2]. Tumor-associated macrophages (TAM) represent a critical cell population among these affected immune cells. They are able to suppress the antitumor response of T cells while in parallel producing growth factors or support angiogenesis. As targets for cancer immunotherapy, their heterogeneity and high plasticity represent major obstacles [3, 4]. Interestingly, several functional subtypes of macrophages demonstrate also distinct metabolic phenotypes. To be noted, both anti-inflammatory macrophages and suppressive myeloid cells show enhanced mitochondrial respiration, suggesting a metabolic-related pathway in

regulating the direction of macrophage polarization [5, 6]. Thus, it is an urgent task to further elucidate how metabolic pathways influence TAM differentiation, polarization, and function in the tumor or the tumor microenvironment. Here we provide a simple protocol to analyze the metabolic pathway and inhibitory function of differentiated macrophages based on a metabolic analyzer (Seahorse XFe96, Agilent, Santa Clara, CA, USA) and the well-known T-cell suppression assay. Sodium oleate will be used here as an example for immune-effective metabolites, as we have proven before that oleate-treated macrophages develop the phenotype of tumor-associated macrophage including their suppressive function [7]. This phenomenon is directly linked to the increased mitochondrial respiration as detected by metabolic analysis. The metabolic environment plays a role not only in tumorigenesis but also in chronic inflammation, where macrophages play a major role in initiation and maintaining inflammation and tissue destruction [8]. Also, in metastasis, regulatory macrophages are critical players and therefore represent interesting targets to be treated on a metabolic level [9–11].

---

## 2 Materials

### 2.1 *Miscellaneous*

1. Mice (here: C57Bl/6J).
2. Cell culture lab (sterile bench, centrifuge, microscope, incubator).

### 2.2 *Buffers*

1. Red cell lysis buffer (155 mM NH<sub>4</sub>Cl, 10 mM KHCO<sub>3</sub>, 0.1 mM EDTA).
2. PBS (phosphate-buffered saline, sterile).
3. Basic bone marrow culture medium: DMEM high glucose medium plus 10% FCS, 1% penicillin/streptomycin, 20 ng/ml GM-CSF (*see Note 1*).
4. Seahorse assay medium: Seahorse XF DMEM medium PH 7.4, 10 mM glucose, 200 mM glutamine, 100 mM sodium pyruvate.
5. MACS buffer: 0.5% BSA, 2 mM EDTA in PBS.
6. T cell culture medium: RPMI (incl. Glutamax) plus 10% FCS, 1% penicillin/streptomycin, 50 µM β-mercaptoethanol.
7. Sodium oleate containing medium: Dissolve sodium oleate in sterile H<sub>2</sub>O to prepare a 100 mM aliquot in 1 ml (*see Note 2*). For the bone marrow treatment, thaw the oleate aliquot at room temperature and add pre-warmed cell culture medium with fatty acid free-BSA at a molar ration of 8:1. For 20 ml medium, dissolve 0.0625 g fatty acid free-BSA in 20 ml basic bone marrow medium and incubate in water bath for 30 min.

Use 0.22 $\mu$ m filter to sterilize the buffer and add sodium oleate from aliquot to prepare the final solution of 20 ml (*see Note 3*). Incubate in 37 °C water bath to stabilize the BSA–Oleate complex in the medium.

8. 10 $\times$  inhibitors for metabolic analysis: Oligomycin (5 mM stock in DMSO), carbonyl cyanide-4-(trifluoromethoxy) phenylhydrazone (FCCP) (7.5 mM stock in DMSO), rotenone (100 mM stock in DMSO) (*see Note 4*), antimycin (1 mM stock in DMSO). All the inhibitors above should be dissolved in 3 ml seahorse assay medium for one assay.

### **2.3 Bone Marrow–Derived Macrophages**

1. 70 $\mu$ m nylon cell strainer.
2. 0.22 $\mu$ m sterile syringe filter.
3. Bone scissor among your dissection tools.
4. 25 G needle.
5. 20 ml syringe.
6. 10 mm petri dish, cell culture treated.
7. Cell culture 6-well plate.

### **2.4 Magnetic Sort**

1. Anti-CD4 antibody (APC-labeled, titrated for magnetic sorting).
2. Anti-Gr1 antibody (APC-labeled, titrated for magnetic sorting).
3. MACS buffer (*see Subheading 2.2*).
4. Anti-APC MicroBeads (Miltenyi Biotec, Bergisch Gladbach, Germany).
5. LS magnets and LS columns (Miltenyi Biotec).

### **2.5 Metabolic Analysis**

1. Seahorse XF DMEM medium pH 7.4 (Agilent).
2. Seahorse mitochondrial stress kit (Agilent, Santa Clara, CA, USA).
3. Seahorse 96-well cell culture plate (Agilent).

### **2.6 Flow Cytometry**

1. Carboxyfluorescein succinimidyl ester (CFSE).
2. BODIPY 493/503.
3. Antibodies for flow cytometry.

### **2.7 Devices**

1. Non-CO<sub>2</sub> incubator.
2. Seahorse XFe96 analyzer (Agilent).
3. Flow cytometer.

---

### 3 Methods

#### 3.1 Bone Marrow Isolation

1. Euthanize one mouse (for  $1-2 \times 10^7$  CD4 $^+$  T cells) via cervical dislocation under CO<sub>2</sub> or isoflurane anesthesia and sterilize the mouse abdomen area and skin of hind limbs with ethanol.
2. Open the skin at the abdomen and hind legs and move the tweezers along the Femur to reach the pelvic-hip joint.
3. Cut off the pelvic-hip joint carefully with a bone scissor.
4. Pull the entire leg bone, including femur, knee, and tibia, up and away from the body, carefully cutting away the connective tissue and muscle connecting the leg to the skin.
5. Grasp the distal end of the tibia and cut it off.
6. Overextend the ankle joint and dislocate the tibia (*see Note 5*).
7. Remove any additional muscle or connective tissue attached to the bone.
8. Cut the ends of tibia and femur.
9. Flush the bone marrow cells by insert 25 gauge needle into marrow cavity and flush with a 20 ml syringe into a petri dish (*see Note 6*).
10. Prepare a single-cell solution by taking up and flushing out the bone marrow clumps using the 20 ml syringe and a 23 G needle. Centrifuge at 4 °C, 400  $\times g$ , 7 min. Cells are ready for differentiation and polarization.

#### 3.2 Macrophage Differentiation and Polarization

1. Seed bone marrow cells from Subheading 3.1 in a cell culture-treated 10 mm petri dish for overnight culture in the presence of 20 ng/ml recombinant murine GM-CSF (*see Note 7*) to get rid of mature adherent macrophages.
2. Next day (day 2), gently flush the dish and harvest nonadherent macrophages with cell culture medium. Centrifuge at 400  $\times g$ , 7 min in 4 °C and discard the medium.
3. Resuspend bone marrow cells in 2 ml red cell lysis buffer for 4 min on ice. Add 10 ml cell culture medium to neutralize the osmotic lysis, centrifuge at 400  $\times g$ , 7 min in 4 °C. Resuspend cell in 10 ml medium.
4. Use 70 $\mu$ m nylon cell strainer to filter the cell suspension.
5. Count the cells, adjust cell density, and seed in 6-well plate at 4 million/well in 3 ml medium per well containing 10 ng/ml recombinant murine GM-CSF plus 0.2 mM sodium oleate (or BSA without oleate as control) as described in Subheading 2.2.
6. Refresh half of the medium every second day, without discarding cells (*see Note 8*).

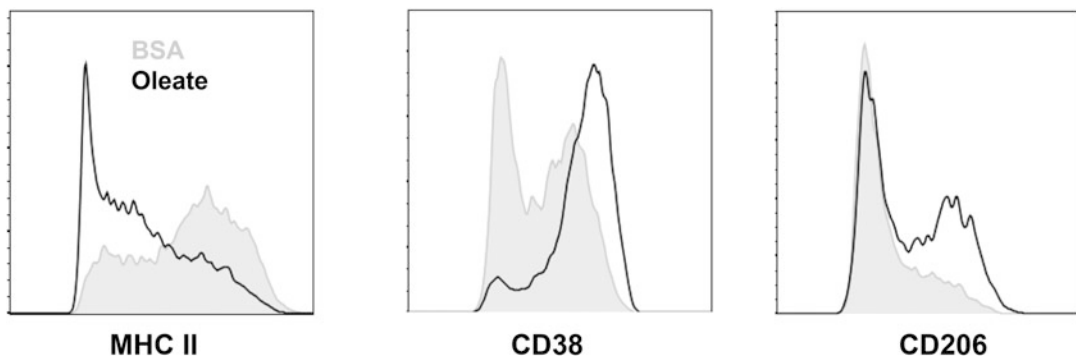


**Fig. 1** Characterization of bone marrow–derived macrophages. Macrophages were differentiated either in the presence of bovine serum albumin (BSA, gray) or sodium oleate (Oleate, black) for 6 days. Cells were stained for indicated markers and analyzed by flow cytometry. Shown are CD11b<sup>+</sup> and Gr1<sup>−</sup> cells, after exclusion of doublets and dead cells

7. On day 6, collect adherent cells (*see Note 9*) and characterize oleate-induced macrophages by determining the expression of CD38, MHCII, and CD206 within the CD11b<sup>−</sup> population via flow cytometry (Fig. 1, *see Note 10*). Additionally, oleate-treated macrophages show increased BODIPY signal due to the formation of lipid droplets (**Step 8**). Metabolic measurement is another method to correlate the metabolic phenotype of macrophages with suppressive function (*see Subheading 3.4*).
8. Alternative step: BODIPY staining for lipid droplets. Collect macrophages from Subheading 3.2 and wash twice with 5 ml PBS in 15 ml tube at  $400 \times g$ , 7 min.
9. Resuspend cells in 5 ml PBS containing 0.2 $\mu$ g/ml BODIPY. Incubate at 37 °C for 30 min.
10. Wash twice with 5 ml PBS and measure the BODIPY signal at flow cytometer (excitation wavelength 480 nm, emission maximum 515 nm, “FITC-channel”).

### 3.3 Gr1<sup>−</sup> Macrophages Purification

1. Collect differentiated macrophages and wash once with MACS buffer (centrifuge at  $400 \times g$ , 7 min in 4 °C).
2. Resuspend macrophages in 1 ml MACS buffer/well in 15 ml tube.
3. Add APC-labeled anti-GR1 antibody in the proper dilution (*see Note 11*). We used 1:1000.
4. Label macrophages for 15 min on ice.
5. Wash once in  $400 \times g$ , 7 min, 4 °C by adding 4 ml sorting buffer.
6. Resuspend cell pellet in MACS buffer and adjust the concentration to  $10^7$ /ml.

7. Label macrophages for 15 min at 4 °C, concentrations according to the anti-APC microbeads kit (Miltenyi).
8. Deplete Gr1<sup>+</sup> cells following the manual (columns, magnets). Collect the negative fraction for metabolic analysis and functional suppressive assay (*see Note 12*).

### **3.4 Metabolic Analysis (Seahorse XFe96 Analyzer, Agilent)**

*Before you start:*

1. Book the machine in your facilities calendar and check the seahorse mitochondrial stress kit (Agilent) for completeness.

*Day 0:*

2. Switch on the instrument 1 day prior to the assay (*see Note 13*).
3. Calibrate the seahorse plate with 200µl/well calibration buffer 1 day prior to the assay according to the manual.

*Day 1:*

4. Seed 1 × 10<sup>5</sup>/well purified Gr1<sup>-</sup> macrophages in seahorse 96-well cell culture plate for 4 h in basal bone marrow medium (*see Note 14*).

5. Prepare seahorse assay medium by adding 0.09 g glucose, 500µl of 200 mM glutamine, and 500µl of 100 mM sodium pyruvate into 49 ml DMEM-based seahorse medium and incubate in 37 °C water bath for 30 min (*see Note 15*).

6. Set up the program of the analyzer.
7. Prepare the 10× inhibitor as the concentration described in Subheading 2.2 in seahorse assay medium.
8. Four hours after incubation, centrifuge and discard the medium in cell culture plate. Add 180µl/well seahorse assay medium. Incubate in non-CO<sub>2</sub> incubator for 1 h.
9. Gently add inhibitors into corresponding ports as described below:

Mitochondrial stress assay:

Port A: Oligomycin 20µl/well.

Port B: FCCP 22µl/well.

Port C: Rotenone + Antimycin 25µl/well.

10. Load inhibitors into correlated port in the sensor cartridge and insert into seahorse instrument for calibration.
11. When the calibration of the instrument is done, insert cell culture plate and start the measurement.
12. Save the plate after measurement for protein or DNA quantification (*see Note 16*).
13. Sodium oleate-treated macrophages show increased basal respiration, maximal respiration as well as spare respiratory capacity (Fig. 2).

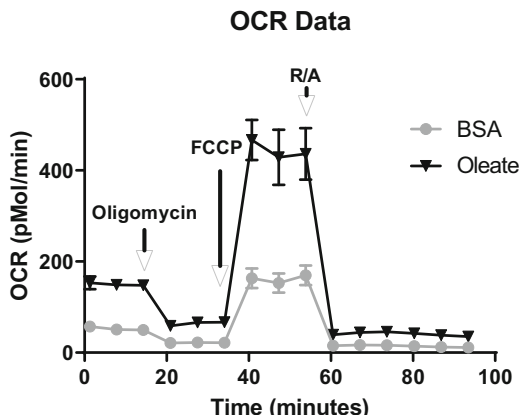


**Fig. 2** Mitochondrial respiration analysis of macrophages. Macrophages were differentiated either in the presence of bovine serum albumin (BSA, gray) or sodium oleate (Oleate, black) for 6 days. CD11b<sup>+</sup>Gr1<sup>-</sup> macrophages were sorted and seeded in seahorse cell culture plates at  $1 \times 10^5$ /well. The mitochondrial respiration was measured in the presence of indicated inhibitors added at indicated time points. FCCP (carbonyl cyanide-4-(trifluoromethoxy) phenylhydrazone), R/A (rotenone + antimycin), OCR (oxygen consumption rate)

### 3.5 T-Cell Suppression Assay

#### 3.5.1 CD4 T Cells Isolation

1. Pre-coat a 96-well plate by using 2 $\mu$ g/ml anti-CD3 antibodies and 5 $\mu$ g/ml anti-CD28 antibodies for 4 h at 37 °C.
2. Euthanize the (wild-type) mouse via cervical dislocation under CO<sub>2</sub> or isoflurane anesthesia and sterilize the mouse abdomen area and skin of limbs with ethanol.
3. Open the skin at the abdomen and isolate spleen and inguinal, axillary lilac, and mesentery lymph nodes.
4. Mash spleen and lymph nodes through a 70 nm nylon filter in a 50 ml tube. Centrifuge 400  $\times$  g, 7 min, 4 °C, resuspend, and transfer in a 15 ml, wash again.
5. Lyse the erythrocytes in 2 ml red cell lysis buffer in a 15 ml tube for 4 min on ice.
6. Stop the osmotic lysis by adding 10 ml PBS on top of the lysis buffer, centrifuge in 400  $\times$  g, 7 min, 4 °C.
7. Resuspend cell pellet in 2 ml MACS buffer (About 5 millions/ml cell density).
8. Add 5 $\mu$ l APC-labeled anti-CD4 antibody to cells (titrated beforehand) and incubate for 15 min at 4 °C.
9. Wash once at 400  $\times$  g, 7 min, 4 °C by adding 4 ml sorting buffer.
10. Resuspend cell pellet in MACS buffer and adjust the concentration to 10<sup>7</sup>/ml.

11. Sort CD4<sup>+</sup> T cells according to the manual of the anti-APC MicroBeads kit (Miltenyi, *see Note 17*).
12. Wash once with PBS in 400 × g, 7 min, 4 °C.
13. Resuspend CD4<sup>+</sup> T cells in 2.5 ml PBS, add 2.5 ml PBS containing 1 mM CFSE, and vortex thoroughly.
14. Incubate in 37 °C for 5 min.
15. Add 10 ml T cell culture medium to stop the reaction.
16. Wash cells twice with T cell culture medium and adjust the concentration to 3 × 10<sup>6</sup>/ml.

### 3.5.2 T-Cell Suppression Assay

1. Discard anti-CD3/CD28 in 96-well plate, wash once with PBS.
2. Seed 3 × 10<sup>5</sup> T cells in 100 µl/well. Set up a negative control without anti-CD3/CD28 pre-coating and a positive control with only CD4<sup>+</sup> T cells seeding.
3. Adjust the concentration of Gr1<sup>-</sup> macrophages accordingly and seed into 96-well plate in 100 µl/well (200 µl in total/well).
4. Culture T cells and macrophages for 72 h and measure the T cell proliferation at the flow cytometer (*see Note 18* and Fig. 3).

## 4 Notes

1. Add GM-CSF freshly when differentiating bone marrow cells.
2. Sodium oleate dissolves in water very well, heating up the temperature will accelerate this procedure.
3. It takes about 30 min to completely thaw a 100 mM sodium oleate aliquot at room temperature. So, it will save some time if one takes the sodium oleate aliquot out from the fridge while the BSA buffer is prepared for incubation.
4. Notice that the solubility of rotenone is lower than other inhibitors, prepare proper aliquots for seahorse assay.
5. After this step, transfer bone in a sterile container (e.g., 50 ml tube) into a clean bench and keep sterile.
6. Hold the bones with stable forceps and try to insert the needle into the smaller opening on the proximal end of the bone. Thus, the bone marrow can be flushed out in one go (and in one piece). Using a 20 ml syringe increases the pressure and you do not have to refill. Smaller syringes are also possible, but 25 G appeared to be the best compromise between high pressure and low thickness.

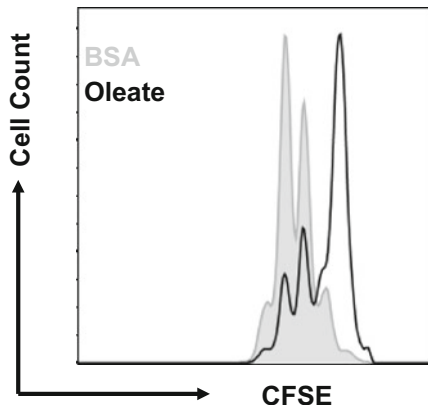


**Fig. 3** T-cell suppression assay. Cells were isolated from spleen, CD4<sup>+</sup> T cells were sorted, labeled with carboxyfluorescein succinimidyl ester (CFSE), and stimulated with anti-CD3/CD28 antibodies. Macrophages were differentiated either in the presence of bovine serum albumin (BSA, gray) or sodium oleate (Oleate, black) for 6 days. CD11b<sup>+</sup>Gr1<sup>-</sup> macrophages were sorted and cocultured with CD4<sup>+</sup> T cells. At day 3, the proliferation of T cells was measured by flow cytometry

7. The adult macrophages adhere stronger to cell culture–treated petri dishes which makes it easier to get rid of adherent cells from bone marrow isolation.
8. Gently suck 1.5 ml medium from each well from the rim to prevent losing cells as differentiating cells are not adherent yet.
9. Differentiated macrophages are adherent cells. Discard the suspension cells here and collect macrophages by flushing cell culture plate with ice-cold PBS. For seahorse analysis in later step, notice to switch on the instrument 1 day before the assay, e.g., day 5 of bone marrow culturing.
10. We do not describe the flow cytometry protocol here as every immunological lab should have this established. The mentioned surface proteins are established markers to determine roughly the regulatory phenotype of macrophages. One can add as many markers as desired and as the respective flow cytometer is able to measure.
11. Antibody concentration should be titrated beforehand. Higher concentration results in better depletion and also in higher cell loss due to false positives. Lower concentration might give you false negatives in the negative population after the sort and therefore bad purity. It is possible here to use differently labeled antibodies than APC, plus the respective sorting beads of course.
12. On day 6, differentiated cells include macrophages (Gr1<sup>-</sup>) and neutrophils (Gr1<sup>+</sup>) in the ratio of 80% to 20%. In oleate-treated

groups, the proportion of Gr1<sup>+</sup> cells could reach 40%. By using magnetic beads, it is possible to negatively sort Gr1<sup>-</sup> population for the suppressive function assay.

13. It takes at least 4 h to stabilize temperature of the seahorse instrument. Switching on overnight will be safe if one wants to start in the morning. Alternatively, it is possible to switch on 4 h prior to the assay. Also, connect the computer to the seahorse instrument and start the software (named “Wave”) to monitor the temperature.
14. For seahorse assay medium, please be aware of the pH, which should be adjusted. Seahorse XF DMEM medium pH 7.4 was ready-made.
15. Cell number for the seahorse test is optimized here based on the confluence under the microscope and basal oxygen consumption rate. Cells should not be plated too dense (~80% confluence) and the basal oxygen consumption rate should be controlled between 100 and 200 pmol/min for a proper assay.
16. All the values in the test are based on exact cell numbers, which are hard to determine, as the cells are adherent and might go into apoptosis or even proliferate further, depending on the assay condition. To get precise results, it is necessary to normalize cell number by quantify protein or DNA after lysis.
17. Usually 10–20 million purified CD4<sup>+</sup> T cells are expected from one mouse in this procedure. It is important to check the purity via flow cytometry before using them. A proper sorting will provide a purity of 90%–99%.
18. T cells show usually 3–4 peaks in the CFSE channel after 72 h when activated with anti-CD/anti-CD28 antibodies and cultured without macrophages. To test the suppressive capacity of macrophages, adjust the macrophage: T cell ratio around 1:10–1:30. This should be sufficient to show suppression. Ideally, depending on the cell number at hand, one uses two or three ratios at once, which gives us the opportunity to plot a curve in the final analysis.

---

## Acknowledgments

This work was supported by the Deutsche Krebshilfe (70112011) as well as the China Scholarship Council and the “Fellowship for Young International Scientists”-program of the Chinese Academy of Science.

## References

1. Bronte V (2014) Tumor cells hijack macrophages via lactic acid. *Immunol Cell Biol* 92:647
2. Wu H, Han Y, Sillke YR, Deng H, Siddiqui S, Treese C, Schmidt F, Friedrich M, Keye J, Wan J (2019) Lipid droplet-dependent fatty acid metabolism controls the immune suppressive phenotype of tumor-associated macrophages. *EMBO Mol Med* 11
3. Mantovani A, Sozzani S, Locati M, Allavena P, Sica A (2002) Macrophage polarization: tumor-associated macrophages as a paradigm for polarized M2 mononuclear phagocytes. *Trends Immunol* 23:549–555
4. Noy R, Pollard JWJ (2014) Tumor-associated macrophages: from mechanisms to therapy. *Immunity* 41:49–61
5. Hossain F, Al-Khami AA, Wyczechowska D, Hernandez C, Zheng L, Reiss K, Del Valle L, Trillo-Tinoco J, Maj T, Zou WJC i r (2015) Inhibition of fatty acid oxidation modulates immunosuppressive functions of myeloid-derived suppressor cells and enhances cancer therapies. *J Immunother Cancer* 3:1236–1247
6. Mills EL, O'Neill LA (2016) Reprogramming mitochondrial metabolism in macrophages as an anti-inflammatory signal. *Eur J Immunol* 46:13–21
7. Wu H, Weidinger C, Schmidt F, Keye J, Friedrich M, Yerinde C, Willimsky G, Qin Z, Siegmund B, Glauben RJS r (2017) Oleate but not stearate induces the regulatory phenotype of myeloid suppressor. *Cell* 7:1–14
8. Medzhitov R (2008) Origin and physiological roles of inflammation. *Nature* 454:428–435
9. Etzerodt A, Moulin M, Doktor TK, Delfini M, Mossadegh-Keller N, Bajenoff M, Sieweke MH, Moestrup SK, Auphan-Anezin N, Lawrence T (2020) Tissue-resident macrophages in omentum promote metastatic spread of ovarian cancer. *J Exp Med* 217
10. Linde N, Casanova-Acebes M, Sosa MS, Mortha A, Rahman A, Farias E, Harper K, Tardio E, Reyes Torres I, Jones J, Condeelis J, Merad M, Aguirre-Ghiso JA (2018) Macrophages orchestrate breast cancer early dissemination and metastasis. *Nat Commun* 9:21
11. Wenes M, Shang M, Di Matteo M, Goveia J, Martin-Perez R, Serneels J, Prenen H, Ghesquiere B, Carmeliet P, Mazzone M (2016) Macrophage metabolism controls tumor blood vessel morphogenesis and metastasis. *Cell Metab* 24:701–715



# Chapter 15

## From Whole Blood to Isolated Pro-Metastasis Immune Cells: An Ex Vivo Approach to Isolate and Manipulate Immune Cells Contributing to Tumor Metastasis

Amany Samir, Aya Aly El Khodiry, and Hend M. ElTayebi

### Abstract

Immune evasion hallmark has grabbed wide attention in cancer progression on the clinical level. Accordingly, innate and adaptive immune cells isolation and manipulation is essential in order to assess their activity and role in the tumor microenvironment (TME). This could open a gate toward a personalized therapy by a simple aspiration of blood sample from patients. Here, we describe the isolation of peripheral blood mononuclear cells (PBMCs) using Ficoll plus media in order to achieve the highest yield of immune cells that can be further processed and used in isolation of specific immune cells such as macrophages and cytotoxic T cells (CD8+ cells). Among the highly metastatic macrophages are the M2. This protocol describes the optimized techniques to isolate monocytes from whole blood, differentiate them into M2. This is followed by genetic and epigenetic (using synthetic nucleotides of noncoding RNAs) manipulation of these isolated immune cells in a tumor culture media, in addition to measurement of released cytokines using specific ELISA kit. In the last decade, new groups of noncoding RNAs have been emerged which are microRNAs and long noncoding RNAs. First, they were known as “junk DNA” with unknown regulatory functions. Despite the limited knowledge of these molecules, basic expression profiling is proving to be clinically relevant to cancer diagnosis, metastasis, and prognosis. Here, we describe methods used in molecular biology to assess the epigenetic expression of ncRNAs and their impact on other messenger RNA transcripts in M2 macrophages that could serve as future biomarkers in the context of tumor biology and metastasis or could open a gate in the treatment of cancer.

**Key words** PBMCs isolation, Macrophages isolation, Cytotoxic T cells, Macrophages differentiation, Transfection, cDNA, qRT-PCR

---

### 1 Introduction

Macrophages and cytotoxic T cells (CD8+) are having powerful cytolytic activity against cancer cells. Thus, restoring cancer recognition by the immune system improves tumor cell killing and elimination as well as avoiding immune escape. This is critical in cancer therapy in order to decrease the side effects of other conventional therapies through boosting the immune response [1]. Isolation of macrophages and T cytotoxic cells is not clearly

optimized. The most common methods of isolation include (1) density gradient separation [2], (2) digestion followed by fluorescence-activated cell sorting (FACS) [3], and (3) magnetic bead-conjugated antibody cell isolation [4]. First, PBMCs are isolated from other components of blood sample according to density gradient with about 75% purity and low concentration of platelets [5]. Here, we demonstrate that PBMCs can be efficiently isolated with highest yield and viability and lowest contamination by platelets using different centrifugation speeds [6]. Furthermore, the isolated PBMCs can be utilized in isolation of specific group of innate or adaptive immune cells. Followed by, culturing of these isolated cells in tumor culture media (TCM) in order to be investigated for genetic manipulation and activity using qRT-PCR and ELISA kits, respectively. Nowadays, there is a growing interest toward understanding tumor pathogenesis and metastasis in order to open a gate for new therapies and counteracting traditional treatment resistance [7]. Noncoding RNAs are newly emerged group, demonstrating a pivotal role in epigenetic regulation at transcriptional and posttranscriptional levels. Mature miRNAs are small single-stranded noncoding RNAs that control cell growth, differentiation, and apoptosis [8]. Another important group is lncRNAs that regulate several processes including cell cycle, gene silencing, transcriptional interference, and disease progression [9]. Some of them serve as oncogenic while others are tumor suppressive. Moreover, numerous interactions between ncRNAs take place such as lncRNA decay by the miRNA, ncRNAs compete for the same mRNA, and lncRNA can act as a precursor for miRNA [10]. Molecular biology techniques enable the detection of such interactions by either mimicking using oligonucleotides or knocking down using short interfering RNAs in M2 macrophages and cytotoxic T cells. Here, we demonstrate simple and efficient molecular biology methods required for gene expression assays starting from cell culture basics until quantification of targeted genes using qRT-PCR.

---

## 2 Materials

Prepare all solutions using ultrapure DPEC-treated water (prepared by incubating with 0.1% diethylpyrocarbonate (DEPC)) (*see Note 1*), shake it vigorously and leave it for 12 h overnight at 37 °C and is then autoclaved (*see Note 2*) for at least 15 min (*see Note 3*). Then, sterile-filter. Additionally, all steps of preparation must be carried out inside the laminar flow unless otherwise stated.

## **2.1 PBMCs Isolation and Counting**

1. Wash mix (full RPMI): In a sterile 50 ml Falcon tube using sterile-filter tips, add 89% RPMI, 10% fetal bovine serum (FBS), and 1% penicillin/streptomycin antibiotics (pen/-strep). Store at 2–8 °C (*see Note 4*).
2. PBMCs isolation media: Ficoll media (Histopaque) (*see Note 5*), density 1.077 g/ml store at 2–8 °C.
3. Freeze mix: In a sterile 15 ml Falcon tube using sterile-filter tips, add 50% RPMI, 40% FBS, and 10% DMSO. Store at –20 °C (*see Note 6*).
4. Autoclaved Eppendorf tubes.
5. Molecular biology degree cryovials.
6. Centrifuge instrument.
7. Hemocytometer chamber for cell counting.
8. Trypan blue dye (*see Note 7*).
9. Freezer –80°C (*see Note 8*).

## **2.2 PBMCs Thawing**

1. Water bath adjusted at 37 °C.
2. Beaker.
3. Centrifuge instrument.

## **2.3 Isolation of Macrophages or Cytotoxic T Cells**

All used solutions and buffers should be stored at 2–8 °C.

1. Polystyrene tube.
2. 15 ml sterile Falcon tubes.
3. MojoSort Buffer 1×: 10 ml buffer in 40 ml ultrapure water.
4. Biotin antibody cocktail.
5. Streptavidin nanobeads.
6. MojoSort Magnet.
7. Fc receptor blocking solution (*see Note 9*).
8. Sterile membrane filter and syringe.

## **2.4 Differentiation of Monocytes into M2 Macrophages**

Store all recombinant proteins at –20 °C.

1. Pyrogen-free tissue culture plate.
2. M-CSF recombinant protein.
3. Interleukin-4 recombinant protein.
4. 10% HAB medium.

## **2.5 Seeding and Transfection of Isolated Cells**

1. 24-well plates.
2. Culture media (full RPMI): 89% RPMI, 10% FBS, 1% pen/strep.
3. Diluted mimics or antagonists: 250 ng/ml.

4. Transfection complex: In a sterile Eppendorf tube, add 1  $\mu$ l miRNA-diluted mimics or antagonists, 1  $\mu$ l HiPerFect, and 30  $\mu$ l free RPMI. Mix well and leave to stand 15 min for complex formation.
5. Incubator 37 °C, 5% CO<sub>2</sub>.

## **2.6 RNA Extraction**

1. BioZol reagent.
2. Chloroform.
3. Isopropanol.
4. Vortexer.
5. Sterile Eppendorf tubes.
6. Centrifuge instrument: Adjusted at 4 °C.
7. 75% ethanol: Add 75 ml of absolute ethanol to 25 ml DEPC water.

## **2.7 RT-PCR for cDNA**

### **Synthesis**

1. Real-time PCR instrument (Thermocycler).
2. Reverse transcription cocktail: RNA solution, DEPC water, RT buffer, RT enzyme, RNase inhibitor, deoxynucleotide triphosphate (dNTPs), and primers. Store at -20 °C.
3. Autoclaved PCR tubes.

## **2.8 qRT-PCR for Quantification of Genes**

1. StepOne Real-time PCR instrument.
2. PCR strips and covers.
3. Amplification cocktail: cDNA sample, TaqMan master mix, DEPC water, and primers of target gene. Store at -20 °C.

## **3 Methods**

Carry out all experiments inside the laminar flow unless otherwise stated.

### **3.1 PBMCs Isolation and Counting**

1. In a 15 ml sterile Falcon tube, transfer 4 ml fresh blood (*see Note 10*) from the EDTA tubes and add 4 ml wash mix (*see Note 11*) then mix well by inversion (*see Note 12*).
2. In another two sterile 15 ml Falcon tubes, using sterile-filter tip, add 3 ml Histopaque in each without touching the walls.
3. Layer carefully 4 ml of diluted blood in each Falcon tube containing Histopaque (*see Note 13*).
4. After layering of diluted blood on Histopaque, the Falcon tube must be immediately placed into the centrifuge (*see Note 14*). Centrifuge at 3315  $\times$  g for 30 min without brakes at 18–20 °C (*see Note 15*).

5. Slowly, aspirate the lymphocyte layer using Pasteur pipette (turbid layer just above the Histopaque layer and under the plasma layer) and transfer it into new sterile Falcon tube (*see Note 16*).
6. Add 3 ml wash mix, then resuspend the cells up and down using pipette. Place the Falcon tube inside the centrifuge at  $466 \times g$  for 10 min. Then, observe the cell pellet.
7. Decant the supernatant, then add 3 ml wash mix, resuspend, and centrifuge at  $298 \times g$  for 5 min then observe the pellet.
8. Decant the supernatant, then add 3 ml wash mix, resuspend.
9. Count the cells using trypan blue dye and hemocytometer chamber. In autoclaved Eppendorf tube, add 90  $\mu l$  trypan blue then 10  $\mu l$  cell suspensions. Mix well and place 10  $\mu l$  in between hemocytometer chamber and the coverslip then count under microscope at  $20\times$  magnification.
10. Centrifuge at 900 rpm for 5 min (*see Note 17*).
11. Discard the supernatant. Add 2 ml freeze mix, mix well using pipette and immediately divide the 2 ml into two cryopreservation vials then store at  $-80^{\circ}\text{C}$ .

### **3.2 PBMCs Thawing**

1. Pre-warm wash mix to  $37^{\circ}\text{C}$  by immersing the Falcon tube in a water bath (*see Note 18*).
2. Thaw the PBMCs cryovial in a beaker containing warm water until small piece of ice is left.
3. Transfer 7 ml of pre-warmed wash mix to 15 ml Falcon tube then transfer the content of cryovial by dropwise addition.
4. Centrifuge at  $829 \times g$  for 10 min.
5. Add 1 ml wash mix then count.

### **3.3 Isolation of Macrophages or Cytotoxic T-Cells**

1. Transfer 1 ml cell suspension to 5 ml polystyrene tube then close the tube firmly.
2. Centrifuge at  $829 \times g$  for 10 min.
3. Discard the supernatant then add 4 ml MojoSort Buffer 5 $\times$ .
4. Centrifuge at  $1865 \times g$  for 5 min.
5. Discard the supernatant and add appropriate amount of buffer suitable for the cell count (*see Note 19*).
6. Only in case of macrophage isolation, Add FcR Blocker (*see Note 20*) then add buffer followed by centrifugation.
7. Discard the supernatant then add 10  $\mu l$  of biotin antibody cocktail, mix well then place the tube in ice for 15 min.
8. Resuspend the nanobeads by using the vortexer and add 10  $\mu l$  of streptavidin nanobeads then mix well and incubate in ice for 15 min.

9. Add 3 ml buffer then centrifuge at  $1865 \times g$  for 3 min then discard the supernatant.
10. Add 3 ml buffer then place the tube in MojoSort Magnet for 5 min.
11. Pour out the liquid in a new polystyrene tube then add 3 ml buffer and place it again in magnet for 5 min.
12. Pour again the liquid in another tube then centrifuge at  $1865 \times g$  for 5 min.
13. Add 1 ml wash mix in one tube and add the content of other tube to it.
14. Count cells and check viability.

### **3.4 Differentiation of Monocytes into M2 Macrophages**

1. Freshly isolated monocytes were cultured in tissue culture plate using 10% HAB medium.
2. For M2-monocyte differentiation, add 1  $\mu\text{g}/\text{ml}$  M-CSF to fresh media every other day.
3. On day 6, refresh media with 1  $\mu\text{g}/\text{ml}$  M-CSF and 1  $\mu\text{g}/\text{ml}$  IL-4 and leave for 24 h.
4. On day 7, use non-cell enzymatic cell dissociation solution for cell harvesting.
5. Flow cytometry should be done to confirm the success of the differentiation before manipulation of genes.

### **3.5 Seeding and Transfection of Isolated Cells**

1. Seed of the cells collected from isolation in a 24-well plate with average 100,000 cells per well (100  $\mu\text{l}$  cell suspension) in full culture media then incubate for 24 h.
2. After 24 h, prepare the transfection complex in an autoclaved Eppendorf tube, vortex for 10 s then leave to stand for 15 min (*see Note 21*).
3. In each well, add 32  $\mu\text{l}$  of transfection complex dropwise on the walls, swirl for proper mixing then place cells in incubator for 6 h.
4. After 6 h, add 400  $\mu\text{l}$  full culture media in each well then incubate for 48 h.

### **3.6 RNA Extraction**

Before starting the experiment, switch on the centrifuge and adjust the temperature at 4 °C (*see Note 22*).

1. 48 h post transfection, using pipette discard media from wells.
2. Add 100  $\mu\text{l}$  Biozol reagent in each well then pipette up and down for 20 s vigorously (*see Note 23*).
3. Transfer the content of each well in an Eppendorf tube, vortex for 15 s then leave to stand 5 min.
4. Add 25  $\mu\text{l}$  chloroform to each Eppendorf tube and invert 10×.

5. Centrifuge at  $29,837 \times g$  for 15 min then observe aqueous and organic layer (*see Note 24*).
6. Transfer the aqueous layer into a new fully labeled autoclaved Eppendorf tube.
7. Add 100  $\mu$ l isopropanol in each Eppendorf tube, invert 10× and incubate in –20 °C for 10 min.
8. Centrifuge at  $29,837 \times g$  for 15 min.
9. Discard the supernatant by decanting (*see Note 25*).
10. Add 200  $\mu$ l 75% ethanol in each Eppendorf tube, invert 5× then centrifuge at  $29,837 \times g$  for 5 min.
11. Remove the supernatant using pipette.
12. Leave RNA Eppendorf tube inside the laminar flow and allow drying for 5 min. Then add 30  $\mu$ l DEPC water in each Eppendorf tube. Store RNA at –80 °C.

### **3.7 RT-PCR for cDNA Synthesis**

1. Thaw each component of reverse transcription kit as well as the RNA sample on ice then mix by vortexing (*see Note 26*).
2. In an Eppendorf tube, prepare the reverse transcription cocktail per sample.  
Add 4.7  $\mu$ l DEPC water, 3  $\mu$ l RT buffer, 1  $\mu$ l random hexamers, 0.8  $\mu$ l dNTPs, and 0.5  $\mu$ l RT enzyme.
3. Transfer 10  $\mu$ l RT cocktail into PCR tubes and add 10  $\mu$ l RNA solution then place the tube in thermocycler adjusted at thermal profile (*see Table 1*).
4. Remove the tubes from the thermocycler and store the cDNA at –20 °C.

### **3.8 qRT-PCR for Quantification of Genes**

1. In autoclaved Eppendorf tube, prepare the amplification cocktail for each sample.  
Add 10  $\mu$ l TaqMan master mix, 7.67  $\mu$ l DEPC water, and 1  $\mu$ l primer (*see Note 27*).
2. In a PCR strip, add in each tube 18.67  $\mu$ l amplification cocktail and 1.33  $\mu$ l cDNA solution then cover the tube directly using the PCR cover (*see Note 28*).
3. Place the PCR strip in StepOne qRT-PCR for quantification of genes using the following parameters for each cycle (*see Table 2*).
4. The StepOne Real-Time PCR yields a value that could be used in mathematical equation to obtain the RQ value.

$$\text{RQ} = 2 - \Delta\Delta \text{CT}$$

**Table 1**

**Reverse transcription of total mRNA into total cDNA program for Thermocycler (RT-PCR).** These conditions are optimized for use with the High Capacity cDNA Reverse Transcription kit. The first 10 min, temperature is set to 25 °C required for reverse transcriptase enzyme activation. Followed by, increasing temperature to 37 °C required for annealing for 120 min. Then, temperature is further increased to 85 °C for enzyme inhibition. Finally, cooling to 4 °C for stopping the reaction

Step	Temperature (°C)	Time (min)
Enzyme activation	25	10
Annealing	37	120
Enzyme inhibition	85	5
Cooling	4	∞

**Table 2**

**qRT-PCR thermal cycling parameters for gene quantification.** The Real-Time PCR run is performed in the standard mode, consisting of two stages: first stage is the activation of Taq-polymerase enzyme by the second stage of 40 amplification cycles (each cycle comprises a denaturation step followed by annealing and extension)

Step	Time	Temperature (°C)
Taq DNA polymerase activation (hold)	10 min	95
Denature Polymerase chain reaction (PCR)–40 cycles	15 s	95
Annealing	60 s	60

#### 4 Notes

1. Diethyl pyrocarbonate or diethyl dicarbonate is essential to inactivate RNase enzymes in water used in molecular biology procedures.
2. Autoclave to decompose the DEPC into ethanol, carbon dioxide, and water, as it is a toxic compound that can interfere with the downstream reactions.
3. Longer duration of autoclaving removes DEPC and inactivates other nucleases.
4. Free RPMI should be stored in refrigerator at 2–8 °C. However, FBS and pen/strep should be kept in freezer –20 °C.
5. Histopaque is more convenient compared to LymphoSep as it allows the usage of 6 ml diluted blood instead of only 4 ml while using the LymphoSep. Thus, achieving high yield of isolated PBMCs in low time and less used consumables.
6. Freeze mix should be stored in freezer due to the presence of DMSO which has cytotoxic effect at room temperature.

7. Trypan blue is an azo compound that should be handled carefully as it has carcinogenic effect, and it is used in counting to differentiate between viable and nonviable cells.
8. It is important to store PBMCs at  $-80^{\circ}\text{C}$  after the addition of freeze mix on the cells, as it contains DMSO which is cytotoxic at room temperature, however inactive at very low temperature degrees.
9. Fc receptor blocking solution is used only in case of macrophages isolation as they express FcR on its surface.
10. Working on fresh withdrawn blood (2–4 h) after surgery ensures higher viability and yield.
11. Wash mix is the cell culture media that is used in dilution instead of balanced salt solution as it increases the cell viability.
12. Wash mix volume should be in ratio 1:1 to blood volume. In other words, the amount of wash mix added should be in equal volume to the required amount of blood that needs to be diluted.
13. While layering the diluted blood on Histopaque, the Falcon tube should be handled at angle that upon the addition of diluted blood it must be sliding on the wall at constant and slow rate to avoid mixing of blood with Histopaque that will result in low yield of isolated cells.
14. By time, the Histopaque layer will be tinged red from the RBCs and this may lower the yield.
15. High centrifugation speed increases the recovery percent of the isolated cells. In addition, Histopaque temperature may cause variation in the yield so in order to avoid low yield of mononuclear cells, Histopaque should be out of refrigerator prior to working in order to maximize the cell recovery.
16. Do not move or shake the Falcon tube after removal from the centrifuge to avoid the disturbance of lymphocyte layer.
17. Centrifugation at low speed (900 rpm) is used for the removal of platelets.
18. Wash mix used in PBMCs thawing is better to be supplemented with 20% FBS that increases the viability.
19. For every 10,000,000 cells, add 100  $\mu\text{l}$  buffer.
20. In order to prevent nonspecific binding of antibodies to the cells.
21. Leave to stand for 15 min to allow complex formation prior to transfection.
22. Low temperature of centrifuge to avoid the degradation of RNA during the extraction procedures.

23. Vigorous up and down pipetting to allow cell lysis and RNA extraction.
24. Aqueous layer is needed as it contains RNA, and organic layer contains other cell components.
25. Sometimes RNA white pellet cannot be visible on the wall of Eppendorf tube so as a precaution while decanting the supernatant, it should be discarded from the opposite side of the pellet to avoid RNA loss.
26. To ensure appropriate resuspension, please vortex each component of the RT kit for 10 s.
27. Master mix and primers are light sensitive, so they should be covered while handling.
28. Avoid the bubbles as it interferes with the results of qRT-PCR.

## References

1. Hsiao CH et al (2020) Isolation and expansion of cytotoxic cytokine-induced killer T cells for cancer treatment. *J Vis Exp* 155
2. Lin EY et al (2007) Vascular endothelial growth factor restores delayed tumor progression in tumors depleted of macrophages. *Mol Oncol* 1(3):288–302
3. Ojalvo LS et al (2009) High-density gene expression analysis of tumor-associated macrophages from mouse mammary tumors. *Am J Pathol* 174(3):1048–1064
4. Kusmartsev S, Gabrilovich DI (2005) STAT1 signaling regulates tumor-associated macrophage-mediated T cell deletion. *J Immunol* 174(8):4880–4891
5. Repnik U, Knezevic M, Jeras M (2003) Simple and cost-effective isolation of monocytes from buffy coats. *J Immunol Methods* 278 (1-2):283–292
6. Salama EA, Adbeltawab RE, El Tayebi HM (2019) XIST and TSIX: novel cancer immune biomarkers in PD-L1-overexpressing breast cancer patients. *Front Oncol* 9:1459
7. Wang P et al (2020) Research progress of epigenetics in pathogenesis and treatment of malignant tumors. *J Lung Cancer* 23 (2):91–100
8. Tufekci KU, Meuwissen RL, Genc S (2014) The role of microRNAs in biological processes. *Methods Mol Biol* 1107:15–31
9. Kopp F (2019) Molecular functions and biological roles of long non-coding RNAs in human physiology and disease. *J Gene Med* 21 (8):e3104
10. Russo F et al (2018) Interplay between long noncoding RNAs and MicroRNAs in cancer. *Methods Mol Biol* 1819:75–92

# **Part III**

## **Prognostication of Metastasis**



# Chapter 16

## A Bioinformatic Pipeline to Identify Biomarkers for Metastasis Formation from RNA Sequencing Data

Mathias Dahlmann and Ulrike S. Stein

### Abstract

Deep molecular characterization of tumors is a prerequisite for precision oncology and personalized anticancer treatment. Analyzing the tumor transcriptome by RNA sequencing (RNAseq) allows the quantification of individual isoforms and also the detection of sequence alteration in the expressed genes. This chapter describes an analysis pipeline that focuses both on accurate quantification of transcripts and on the occurrence of cancer-associated mutations. Another section introduces the analysis of differentially expressed genes for biomarker evaluation on the example of comparing metastasized versus non-metastasized colorectal tumors.

**Key words** RNAseq, Bioinformatics, Expression quantification, Mutation analysis, Differential expression

---

### 1 Introduction

Understanding of aberrant molecular mechanisms in disease, especially in the cancer field, was greatly boosted by the availability of transcriptome-wide gene expression profiling. This methodology can detect individual changes in gene expression activity and regulation of tumors, which determine clinically relevant phenotypes, like growth rate, drug response, and metastatic potential [1], eventually affecting progression and outcome of the disease. In turn, transcriptomic profiling of tumors is used to improve diagnosis or therapy decisions for the individual patient, strongly contributing to the concepts of precision oncology and personalized therapies [2–4].

RNA sequencing (RNAseq) can thereby overcome several limitations of DNA-based assays, like inefficient identification of heterogeneous biomarkers [5], structural variants [6], or prediction of therapy response [7]. In addition, the complexity of genome-wide mutational analysis is reduced to the actively expressed genes, already filtering out genetic alterations of non-transcribed DNA

elements, often representing passenger mutations. Emerging novel RNA-based sequencing technologies, like single-cell sequencing or spatial transcriptomics, will again greatly improve the impact on the understanding of malignant molecular processes for, e.g., development of novel therapeutics, as well as improved prognosis or response prediction in the clinics.

Technically, RNAseq produces millions of short reads from reverse-transcribed (m)RNA fragments, which can be used for transcript quantification, differential expression testing, or to detect novel splicing events which may identify previously unknown isoforms. The individual reads are typically mapped to a reference genome or set of transcripts before expression levels are quantified [8]. The number of sequence aligning tools has grown over time and differ in precision and required technical resources, including run time [9], and this chapter describes the use of Spliced Transcripts Alignment to a Reference (STAR) combining fast alignment with high precision [10]. Similarly, several tools are available to quantify isoform-specific gene expression with or without prior sequence alignment [11], and we describe the use of RNAseq by Expectation Maximization (RSEM) [12] in this chapter. RNAseq is often the only available sequencing dataset for tissue samples and will typically be used for expression quantification. Nevertheless, if the read length and sequencing depth is carefully chosen, genomic variants of the sample can also be identified [13]. Compared to whole-genome or whole-exome sequencing (WGS/WES), only variants of actively transcribed DNA or expressed genes (depending on the library preparation) are detectable, which more closely resembles the altered molecular mechanisms of the tumor. This chapter describes the use of the Genome Analysis Toolkit (GATK) [14] for variant analysis from RNAseq data.

The second part of the chapter describes the use of Differential Expression Analysis for Sequence Count Data (DESeq2) [15] to identify potential biomarkers from expression datasets comparing two or more experimental conditions. This can range from comparing tumors to normal tissues, defining subtypes within a cancer type, evaluating biomarkers for metastasis formation, predicting treatment response to anticancer therapies.

With the data generated above (transcriptomics, variants, differential expression), advanced methods of functional and integrative genomics can be applied to identify underlying molecular mechanisms or pathways associated with the tested hypothesis (subtypes, metastasis, treatment response, etc.), but are beyond the scope of this chapter.

## 2 Materials

Depending on the expected number of samples, the computer hardware can range from a modern Notebook or desktop PCs to workstations. Four CPU cores or more are recommended, as some tools heavily profit from multi-threading. Alternatively, single threads can run in parallel for different samples. The computer should have a minimum of 32 GB RAM and a fast working storage, combined with a larger storage drive. Some tools require a Unix/Linux-based operating system and will be run from a console (*see Note 1*).

The sequencing files of the samples are provided by the sequencing facility mostly in the FASTQ format, consisting of sequence and quality information of each read fragment (*see Note 2*).

The following tools and files should be downloaded and unpacked, decompressed or installed (*see Note 3*).

### 2.1 Tools Required for this Pipeline

FastQC [16]	<a href="https://www.bioinformatics.babraham.ac.uk/projects/fastqc/">https://www.bioinformatics.babraham.ac.uk/projects/fastqc/</a>
fastp [17]	<a href="https://github.com/OpenGene/fastp">https://github.com/OpenGene/fastp</a>
STAR [10]	<a href="https://github.com/alexdobin/STAR">https://github.com/alexdobin/STAR</a>
RSEM [12]	<a href="https://github.com/deweylab/RSEM">https://github.com/deweylab/RSEM</a>
GATK [14]	<a href="https://github.com/broadinstitute/gatk/releases/tag/4.1.0.0">https://github.com/broadinstitute/gatk/releases/tag/4.1.0.0</a>
Samtools [18]	<a href="http://www.htslib.org/">http://www.htslib.org/</a>
R [19]	<a href="https://cran.r-project.org/">https://cran.r-project.org/</a>
Bioconductor	<a href="https://www.bioconductor.org/">https://www.bioconductor.org/</a>
[20]	

### 2.2 Current FASTA and Annotation Files of the Human Genome

<ftp://ftp.ensembl.org/pub/>

- current\_fasta/homo\_sapiens/dna/Homo\_sapiens.GRCh38.dna.toplevel.fa.gz
- current\_fasta/homo\_sapiens/dna/Homo\_sapiens.GRCh38.dna.primary\_assembly.fa.gz
- current\_gtf/homo\_sapiens/Homo\_sapiens.GRCh38.99.gtf.gz
- current\_variation/vcf/homo\_sapiens/homo\_sapiens\_somatic.vcf.gz.

### 3 Methods

To exemplify the processing of sequencing data, all steps have been performed on an exemplary sequenced human CRC tumor tissue (Illumina; 100 bp read length; paired-end; > 60 Mio reads). Differential expression analysis is based on a subset of gene expression data (gene counts) selected from The Cancer Genome Atlas (TCGA) repositories.

#### 3.1 Quality Control and Preprocessing

The first step in the chain of analyses is the quality check and preprocessing of the sequence file. Quality control can be performed with FastQC (graphical interface), and the respective reports can be exported and viewed with any web browser (Fig. 1). Here, the quality of sequences is very high (Fig. 1a), the GC content closely matches the theoretical distribution (Fig. 1b), and the enrichment in duplication indicates variances in gene expression levels (Fig. 1c).

Preprocessing of the paired-end sequencing data is performed by invoking fastp with the command:

```
{PathTo}/fastp --detect_adapter_for_pe --c \
-i SampleName_R1.fastq.gz -I SampleName_R2.fastq.gz \
-o SampleName_R1.fastp.fastq.gz -O SampleName_R2.fastp.
fastq.gz
```

This includes filtering of remaining bad reads, cutting of low-quality bases, end trimming, automatic detection and removal of adapters, and corrects mismatched base pairs in overlapped regions of paired-end reads.

#### 3.2 Quantification of Gene Expression

Quantification of gene expression from preprocessed sequencing files is performed by RSEM.

The following command will prepare a reference index of the human genome, which is used later for mapping the reads to the genome and quantification of the mapped transcripts (*see Note 4*):

```
rsem-prepare-reference --gtf Homo_sapiens.
GRCh38.99.gtf --star --p 4 \
Homo_sapiens.GRCh38.dna.primary_assembly.fa
reference/rsem_GRCh38_ensembl99
```

Gene expression of the sequence file is performed by running (*see Note 5*):

```
rsem-calculate-expression --paired-end --p 4 --
star --star-gzipped-read-file \
--no-bam-output SampleName_R1.fastp.fastq.gz Sample-
Name_R2.fastp.fastq.gz \
reference/rsem_GRCh38_ensembl99 SampleName
```

The resulting files *SampleName.genes.results* and *Sample-
Name.isoforms.results* contain the gene level expression esti-
mates for each gene in total or each transcript isoform, respectively

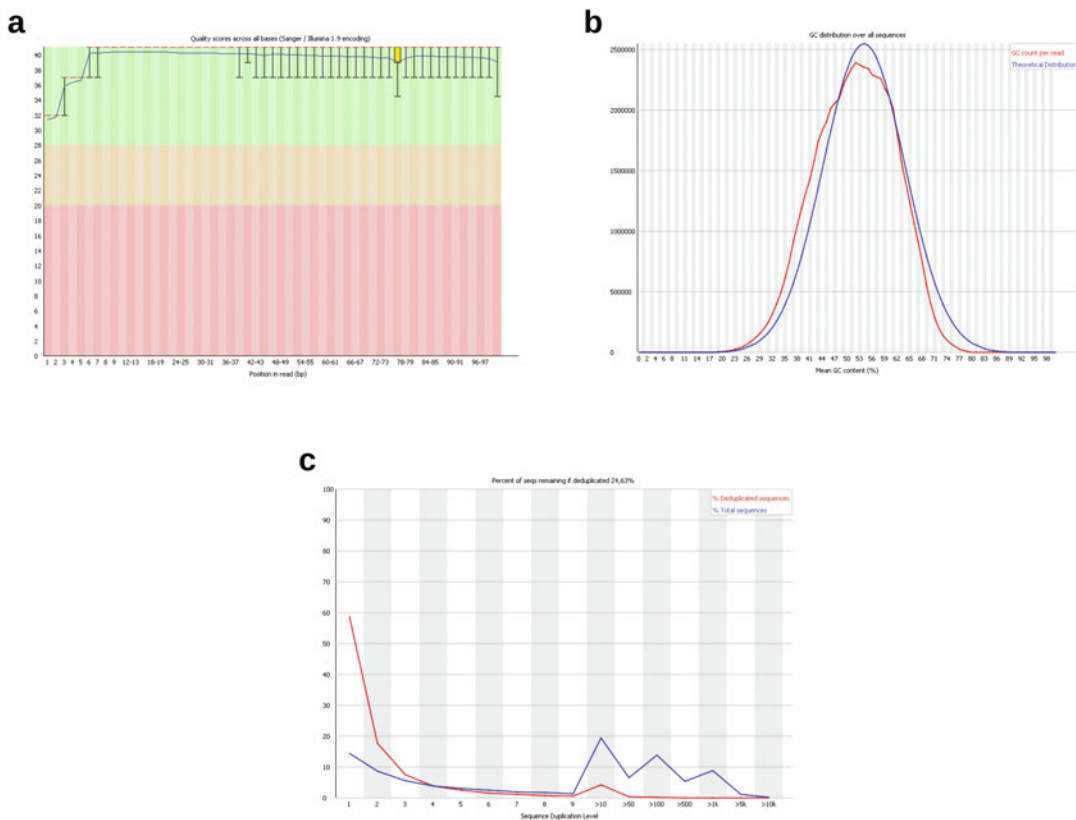


**Fig. 1** Output of FastQC as quality control of sequencing data. **(a)** Per base sequence quality. Quality scores above 30 are preferred for further analysis. **(b)** Per sequence GC content. The GC count of the sequence file should resemble the theoretical GC distribution. Peak shifts or spikes indicate reads of lower quality. **(c)** Sequence duplication levels. In contrast to genomic analyses, transcriptomes will show enrichment in duplicated sequences

(*see Note 6*). Expression data will be provided as estimated counts, transcripts per kilobase million (TPM), and fragments per kilobase million (FPKM). The output files after expression quantification of several samples can now be used to detect transcriptomic similarities of different samples or to identify differentially expressed genes or isoforms (*see Note 7*).

### 3.3 Mutational Analysis of RNAseq Data

Illumina TruSeq RNA libraries consist of nucleotide fragments of approximately 120 – 210 bp without adapters. A paired-end sequencing approach, in combination with a 100 bp read length, results in almost complete fragment sequencing. Taking into account that these fragments largely overlap, an analysis of occurred alterations in expressed genes becomes applicable. For this case, a precise mapping of the read fragments to the standard genome is necessary, before genetic alterations like single nucleotide variations (SNV), genomic insertions/deletions (Indel), novel splice variants, or RNA-editing can be analyzed.

### 3.3.1 Alignment of Fragments to the Reference Genome

The following command generates required index files for the alignment with STAR (*see Note 8*):

```
STAR --runMode genomeGenerate --runThreadN 4 --
genomeDir reference/STAR_ensembl99 \
--genomeFastaFiles Homo_sapiens.GRCh38.dna.primary_assembly.fa \
--sjdbGTFfile Homo_sapiens.GRCh38.99.gtf --sjdbOverhang ReadLength-1
```

The preprocessed FASTQ files will now be mapped to the reference genome in the 2-pass mode by invoking (*see Note 9*):

```
STAR --twopassMode Basic --runThreadN 4 --genome-
Dir STAR_ensembl99 \
--outSAMtype BAM Unsorted --readFilesCommand gun-
zip -c \
--readFilesIn SampleName_R1.fastp.fastq.gz SampleNa-
me_R2.fastp.fastq.gz
```

The aligned, but unsorted reads will be stored in the file `Aligned.out.bam`, which is the basis for the subsequent mutational analysis pipeline by GATK, which includes sorting and deduplication of the reads, base recalibration, and haplotype calling.

### 3.3.2 Addition of Read Groups and Sorting by Coordinates

Sample-specific meta-information provided by the sequencing facility will now be added to the previously generated BAM file, making it unique and traceable when published in appropriate repositories, by the following command (*see Note 10*):

```
{PathTo}/gatk AddOrReplaceReadGroups -I Aligned.
out.bam -O SampleName.RG.sort.bam \
-SO coordinate -PM {platform model} -DT {run date} -ID
{identifier} \
-CN {sequencing center} -LB {library} -PL {platform} -PU
{platform unit} \
-SM {sample name} --CREATE_INDEX true --CREATE_-
MD5_FILE true \
-R Homo_sapiens.GRCh38.dna.toplevel.fa
```

### 3.3.3 Deduplication and Splitting of Reads Containing Undefined Base Calls (N)

Reads are deduplicated and split, if they are containing Ns with the following commands (*see Note 11*):

```
{PathTo}/gatk MarkDuplicates -I SampleName.RG.
sort.bam \
-O SampleName.RG.sort.dedup.bam --CREATE_INDEX
TRUE \
--VALIDATION_STRINGENCY SILENT -M SampleName.dedup.
metrics
samtools faidx Homo_sapiens.GRCh38.dna.tople-
vel.fa
{PathTo}/gatk CreateSequenceDictionary -R Homo_-
sapiens.GRCh38.dna.toplevel.fa \
-O Homo_sapiens.GRCh38.dna.toplevel.dict
```

```
{PathTo}/gatk SplitNCigarReads -R Homo_sapiens.  
GRCh38.dna.toplevel.fa -OBM -OBI \  
-I SampleName.RG.sort.dedup.bam -O SampleName.RG.  
sort.dedup.splitN.bam
```

### 3.3.4 Base Quality Score Recalibration (BQSR) and Haplotype Calling

The following commands create a recalibration table based on several covariates, recalibrate the bases and calls somatic variations via local reassembly of haplotypes (*see Note 12*):

```
{PathTo}/gatk IndexFeatureFile -F homo_sapiens_-  
somatic.vcf  
{PathTo}/gatk BaseRecalibrator -R Homo_sapiens.  
GRCh38.dna.toplevel.fa \  
--known-sites homo_sapiens_somatic.vcf \  
--sequence-dictionary Homo_sapiens.GRCh38.dna.  
toplevel.dict \  
-I SampleName.RG.sort.dedup.splitN.bam -O Sample-  
Name.recal_data.table  
{PathTo}/gatk ApplyBQSR -R Homo_sapiens.GRCh38.  
dna.toplevel.fa -OBI true \  
-OBM true --bqsr-recal-file SampleName.recal_data.  
table \  
--sequence-dictionary Homo_sapiens.GRCh38.dna.  
toplevel.dict \  
-I SampleName.RG.sort.dedup.splitN.bam -O SampleName.  
BQSR.bam  
{PathTo}/gatk HaplotypeCaller -R Homo_sapiens.  
GRCh38.dna.toplevel.fa -OBM true \  
--dont-use-soft-clipped-bases true -OBI true -OVI  
true --OVM true \  
--sequence-dictionary Homo_sapiens.GRCh38.dna.  
toplevel.dict \  
-D homo_sapiens_somatic.vcf -I SampleName.BQSR.bam  
\ \  
-O SampleName.BQSR.vcf
```

The resulting VCF files can then be used for further filtering, indexing, or visualization of called variances with appropriate viewers (*see Note 13*). Optionally, the effect of the identified variances, including gene/transcript names, its relative location, consequence on the expressed proteins, and their function (SIFT, PolyPhen), can be determined by using the Ensembl Variant Effect Predictor (VEP; Fig. 2) [21] (*see Note 14*). The majority of identified somatic variances in the exemplary tumor tissue will not alter the encoded protein sequence (55.1% synonymous variants), followed by missense variants (39.5%) and to lesser extents frameshift variants (4.3%) or Indels (0.9%) (Fig. 2a). The largest category after polymorphism phenotyping (PolyPhen) [22] classifies the identified variants predicts a benign impact on the structure and function

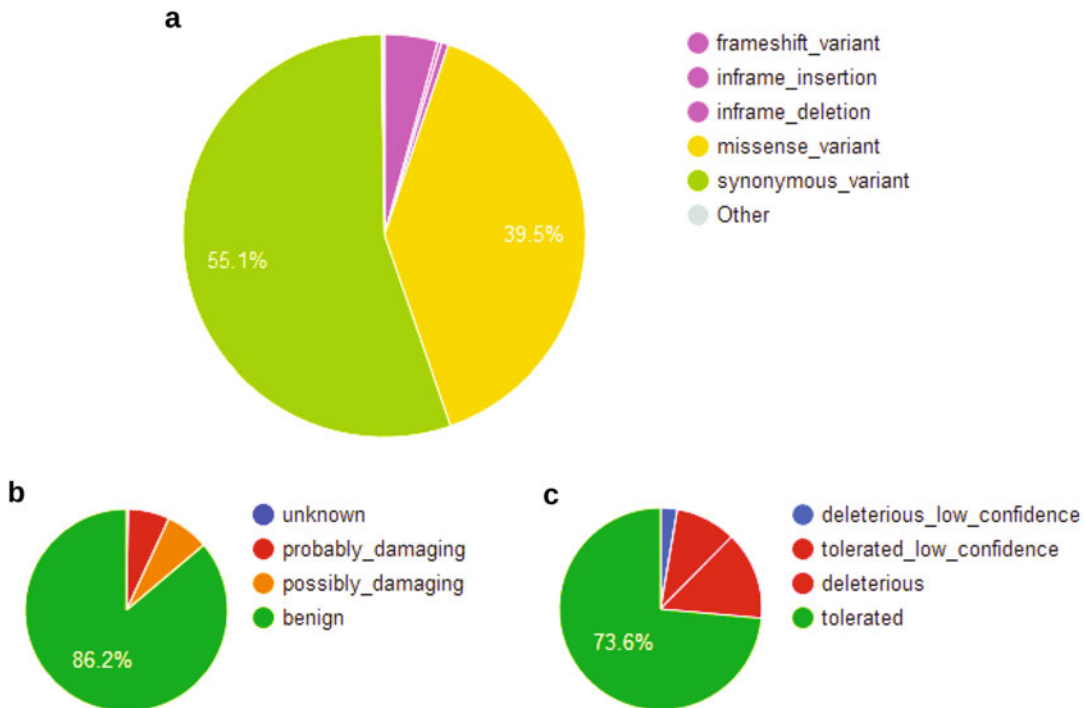


**Fig. 2** Classification of identified somatic variances by VEP. (a) Consequences of variants for protein coding can be classified as synonymous, missense, frameshift alterations of the coding sequence, or the occurrence of insertions/deletions within. (b) Prediction of the impact on protein structure and function by polymorphism phenotyping is classified as benign or damaging. (c) Prediction of altered protein function by the identified variants by SIFT is classified tolerated or deleterious

of the translated protein (86.2%), followed by possibly and probably damaging (6.9% and 6.6%, respectively) (Fig. 2b). The Sorting Intolerant From Tolerant (SIFT) categories [23] are dominated by classification as tolerated for the altered protein sequence (73.6%), followed by deleterious (14.1%) and their low-confidence classifications (9.7% and 2.7%, respectively) (Fig. 2c). Filtering for variants that likely affect the function of the respective protein allows the analysis of potentially affected molecular mechanisms or cellular processes.

### 3.4 Identification of Differentially Expressed Genes with DESeq2

Differentially expressed genes will be calculated from a subset of CRC tumor gene expression, provided by the TCGA Research Network. One sample group consists of 12 non-metastasized (M0) CRC tumors of the UICC stages I (1), II (5), and III (8). Average and median patient age was calculated as 79 years and 78.5 years, respectively. The other sample group consists of 9 metastasized (M1; UICC IV) CRC tumors. Average and median patient age was calculated as 71.4 years and 74 years, respectively. Patients in both groups suffered from adenocarcinoma of the colon, and no

information was found about comorbidities, race, or ethnic groups of the patients.

Quantification of differential expression by DESeq2 [15] requires two datasets: gene counts and the design of the experiment. Examples of the data structure for each dataset are displayed in Table 1 (gene counts) and Table 2 (experimental design) (*see Note 15*).

The DESeq2 packages need to be installed and loaded within an R session (*see Note 16*). The previously prepared table with gene counts will be imported as a matrix, and the samples will be attributed with the previously defined experimental conditions, setting “non-metastasized” as reference condition.

```
#Install and load packages:
BiocManager::install("DESeq2");
library(DESeq2);
#Provide DESeq2 with sample names, gene counts and experiment
conditions
countdata <- as.matrix(read.csv
(file="gene_counts.csv", sep="\t", row.names="ID"));
coldata <- read.csv(file="experimental_design.csv",
row.names=1, sep="\t");
dds <- DESeqDataSetFromMatrix(countData=countdata, colData=coldata,
design=~ condition);
#Set non-metastasized samples as reference condition
dds$condition <- relevel(dds$condition, ref =
"MO");
```

Row sums of gene counts of 10 and below will be removed from the dataset (*see Note 17*), and differentially expressed genes between metastasized and non-metastasized samples will be calculated.

```
#Filter for count sums lower than 10
keep <- rowSums(counts(dds)) >=10;
dds <- dds[keep,];
#Calculate differentially expressed genes and generate
results
dds <- DESeq(dds);
res <- results(dds);
```

The results can be checked for their quality (Fig. 3). The histogram of p-values indicates whether the results allow the analysis of alternative vs. null hypotheses. Here, the p-value distribution is anti-conservative, with a moderate increase of very low p-values (Fig. 3a). Log<sub>2</sub> fold changes (LFC) of genes will be plotted versus the mean of normalized counts to visualize the number of differentially expressed genes, while prior LFC shrinking with the ashR package [24] removes noise from low count genes (Fig. 3b). Principle component analysis (PCA) allows the visualization of overall

**Table 1**  
**“genes\_count.csv”.** This table briefly illustrates the needed data format for DESeq2. Samples are distributed in the columns, estimated gene counts in the rows, identified by ensemble gene IDs and indicator of their version

ID	Tumor. 01	Tumor. 02	Tumor. 03	Tumor. 04	Tumor. 05	Tumor. 06
ENSG00000000003.13	2356	4200	502	3691	4149	6560
ENSG00000000005.5	4	7	1	8	375	103
ENSG00000000419.11	317	852	536	1376	3394	1170
ENSG00000000457.12	301	265	323	391	1077	359
ENSG00000001036.12	3172	2037	1946	1751	3783	2136
ENSG00000001084.9	1139	1369	1116	1549	2532	1169

**Table 2**

“experimental\_design.csv”. This table briefly illustrates the needed data format for DESeq2. Additional information is attributed to each sample. Most importantly the experimental conditions, here M0 (non-metastasized) and M1 (metastasized)

Sample	Condition	Tissue	Donor
Tumor.01	M0	Primary	TCGA-COAD
Tumor.02	M0	Primary	TCGA-COAD
Tumor.12	M0	Primary	TCGA-COAD
Tumor.13	M1	Primary	TCGA-COAD
Tumor.14	M1	Primary	TCGA-COAD
Tumor.21	M1	Primary	TCGA-COAD

effects of experimental covariates or batch effects. The 2D PCA plot of the 21 samples shows generally a high similarity of the analyzed non-metastasized and metastasized tumors (Fig. 3c).

```
#Histogram of p-value
png("Hist-pval.png")
hist(res$pvalue, breaks=20, col="grey")
dev.off();
#LFC shrinking and MA-plot
BiocManager::install("ashr");
resLFC <- lfcShrink(dds,
coef="condition_M1_vs_M0", type="ashr");
png("MA-plot.png")
plotMA(resLFC, ylim=c(-3,3))
abline(h=c(-1,1), lwd=2)
dev.off();
#PCA-plot
vsd <- vst(dds);
png("PCA-plot.png")
plotPCA(vsd, intgroup=c("condition"))
dev.off();
```

In the results table, genes are only labeled with Ensembl gene IDs, including their version number. Adding gene names and descriptions will make it easier to comprehend the results. Additional columns will be created, containing the stripped Ensembl gene ID, the gene name, the biotype, and the description of the respective gene, using stringr and biomaRt [25–27]:

```
#Install and load packages: BiocManager::install
("biomaRt")
library(stringr)
library(biomaRt)
#Strip version numbers of ensemble IDs and add them as column in
results
```

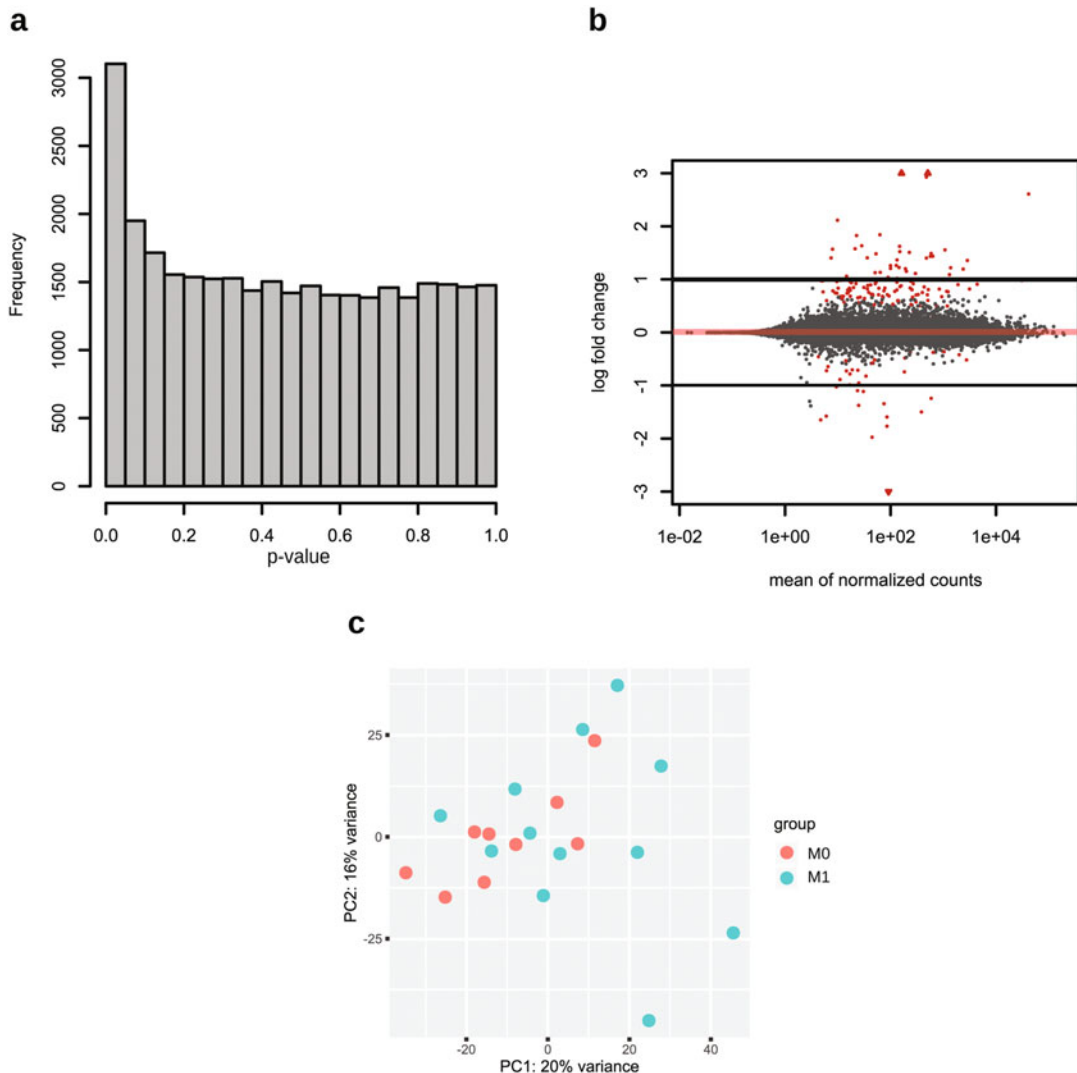


**Fig. 3** Quality control plots after differential expression analysis. (a) Histogram of *p*-values. The distribution of differentially expressed genes over categories of *p*-values gives an indication if subsequent statistical analyses are recommended. (b) The MA-plot of the calculated LFC of differentially expressed genes over the mean of normalized counts helps to estimate the number of genes with a high fold change at a reasonable expression level. (c) The PCA-plot of samples allows the identification of covariates or batch effects by visualizing the general similarity or distance of individual samples

```

res$ensembl <- sapply(strsplit(rownames(res), split="nn+"), "[", 1);
res$ensembl <- str_replace(res$ensembl, pattern=". [0-9]+$", replacement(""));
#Add gene symbols and other information
ensembl = useMart("ensembl",
dataset="hsapiens_gene_ensembl");

```

```

geneinfo <- getBM(attributes=c("ensembl_gene_id",
                               "external_gene_name",
                               "description","gene_biotype"), filters="ensembl_gene_id", values=res$ensembl,
                               mart=ensembl);
index <- match(res$ensembl, geneinfo$ensembl_gene_id);
res$symbol <- geneinfo$external_gene_name[index];
res$biotype <- geneinfo$gene_biotype [index];
res$description <- geneinfo$description [index];
Once the additional gene information is applied, the results can
be filtered according to their levels of significance. One table will
include all differentially expressed genes with a p-value below 0.05,
while the other tables will be filtered with decreasing thresholds of
the adjusted p-value (see Note 18).
#Differentially expressed genes with p-value below 0.05
res.p05 <- results(dds, alpha=0.05);
write.csv(as.data.frame(res.p05), file =
"results_p05.csv");
#Differentially expressed genes with adjusted p-value below
0.1
res.sig <- res[which(res.p05$padj<0.1),];
write.csv(as.data.frame(res.sig), file =
"results_sig.csv");
#Differentially expressed genes with adjusted p-value below
0.05
res.sig05 <- res[which(res.p05$padj<0.05),];
write.csv(as.data.frame(res.sig05), file =
"results_sig05.csv");

```

Plotting the significantly differentially expressed genes in a heatmap allows the clustering of similarly expressed genes (row dendrogram) or samples with similar expression of the gene subset (column dendrogram) (Fig. 4).

```

#Install and load packages:install.packages("pheatmap")
install.packages("reshape2")install.packages("gplots")install.packages("RColorBrewer")
install.packages("ggplot2")library("pheatmap")
#rlog transformation of differential expression
rld <- rlog(dds);
#Select differentially expressed genes with adjusted p-value
below 0.05
DEmatrix = assay(rld)[head(order(res$padj),
sum(res$padj<0.05, na.rm=TRUE)),];
#Subtract the row means from each value
DEmatrix = DEmatrix - rowMeans(DEmatrix);
#Create a dataframe with a column of the conditions
DEframe = as.data.frame(colData(rld)[,c("condition")]);

```

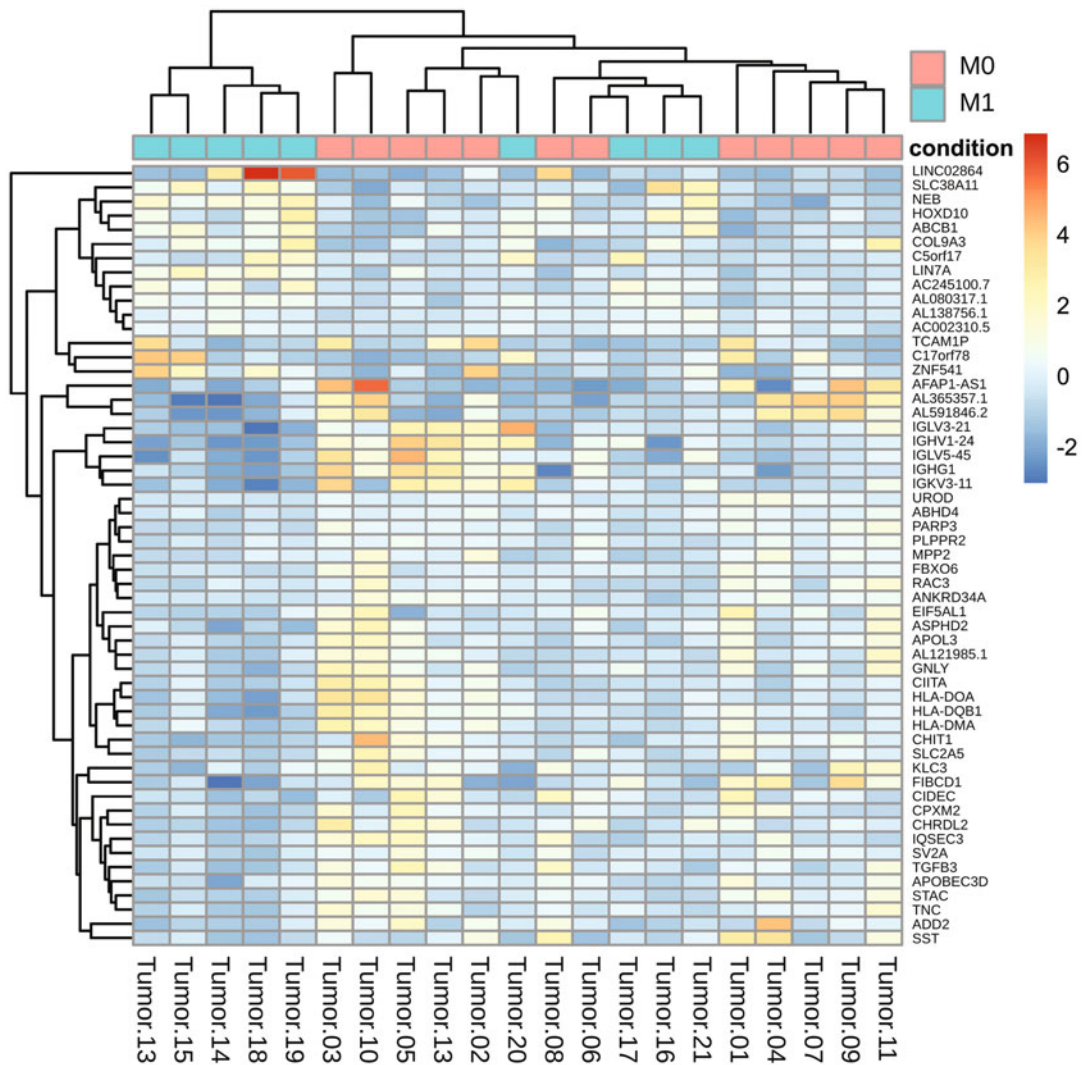


**Fig. 4** Heatmap of significantly differentially expressed transcripts. Color coded fold change of significantly differentially expressed transcripts and clustering of similar transcripts and samples visualize the potential of the gene set to separate the analyzed groups according to their tested condition

```
#Rename the column header, add rownames and plot the heatmap-
colnames(DEframe) = "condition";rownames(DEframe) =
colnames(DEmatrix);png("HeatMap-Sig05.png")pheat-
map(DEmatrix,annotation_col=DEframe);dev.off();
```

#### 4 Notes

1. Running a native Unix/Linux is recommended compared to a virtual system. Scripts of consecutive commands for several samples may need adjustment in conflicting output files.

2. Please mind the specific parameters used for sequencing. Some commands need adjustments when run on either single-end or paired-end sequencing files.
3. Some tools have to be built on the local machine before installation, and detailed instructions can be found in the respective documentation.
4. The process can use more than 4 threads in parallel by increasing the number after option `-p`. The index files are stored under the name `rsem_GRCh38_ensembl99` in the folder `reference`, which needs to exist and to be accessible before running the command.
5. The process can use more than 4 threads in parallel by increasing the number after option `-p`. This process will run very slow on less than 32 GB RAM. To save disk space, the output of a BAM file is suppressed, since this will be later generated with adjusted options by STAR. Additional options for `rsem-calculate-expression` can be found under  
<http://deweylab.biostat.wisc.edu/rsem/rsem-calculate-expression.html>.
6. A detailed description of the results file content can be found under <http://deweylab.biostat.wisc.edu/rsem/rsem-calculate-expression.html#output>.
7. The R package `tximport` allows the easy import of RSEM results into R for DESeq2 analysis. A detailed description can be found under <https://bioconductor.org/packages/release/bioc/html/tximport>.
8. The process can use more than 4 threads in parallel by increasing the number after option `--runThreadN`. The index files are stored under the folder `STAR_ensembl99`, which needs to exist and to be accessible before running the command. The parameter `--sjdbOverhang` should be run with the read length subtracted by 1 (see FastQC output). This process will run very slowly on less than 32 GB RAM.
9. The 2-pass mode allows the detection of novel splice junctions. The process can use more than 4 threads in parallel by increasing the number after option `--runThreadN`. This process will run very slow on less than 32 GB RAM. If run in scripts, please rename `Aligned.out.bam` accordingly or use the `--outFileNamePrefix` parameter to choose the individual output directory.
10. Only some meta-information is required by the tool. The detailed description of individual parameters can be found under  
<https://gatk.broadinstitute.org/hc/en-us/articles/360036360352-AddOrReplaceReadGroups-Picard->.

11. Once the dictionary and index is created for the specific genome FASTA file, these commands can be omitted from the pipeline. Detailed descriptions of the commands are found under.

<https://gatk.broadinstitute.org/hc/en-us/articles/360036359872>CreateSequenceDictionary-Picard->  
<https://gatk.broadinstitute.org/hc/en-us/articles/360036727811>-SplitNCigarReads  
<https://gatk.broadinstitute.org/hc/en-us/articles/360036359852>-MarkDuplicates-Picard- .

12. If needed, the reference list of known variants can also be restricted to either structurally or clinically associated variations, or expanded to all known variants. See [ftp://ftp.ensembl.org/pub/current\\_variation/vcf/homo\\_sapiens/](ftp://ftp.ensembl.org/pub/current_variation/vcf/homo_sapiens/) for additional lists.

Detailed descriptions of the commands are found under.

<https://gatk.broadinstitute.org/hc/en-us/articles/360036726891>-BaseRecalibrator  
<https://gatk.broadinstitute.org/hc/en-us/articles/360036725911>-ApplyBQSR  
<https://gatk.broadinstitute.org/hc/en-us/articles/360036359552>-HaplotypeCaller .

13. A versatile toolbox for working with VCF files is VCFtools, and VCF viewer are available in R (yfcR) or as graphical interface (IGV):

VCFtools	<a href="https://vcftools.github.io/index.html">https://vcftools.github.io/index.html</a>
vcfR:VCF data in R	<a href="https://knausb.github.io/vcfR_documentation/index.html">https://knausb.github.io/vcfR_documentation/index.html</a>
Integrative Genomics Viewer	<a href="https://software.broadinstitute.org/software/igv/VCF">https://software.broadinstitute.org/software/igv/VCF</a>

14. A web-based Variant Effect Predictor is provided under <https://www.ensembl.org/Tools/VEP> but is limited to a VCF file size of 50 MB.

Alternatively, the command line tool can be downloaded under <https://www.ensembl.org/info/docs/tools/vep/index.html> and built, unpacked, or installed as a docker image. Please refer the respective documentation to select the appropriate parameters .

15. Please note that the column names in the gene count table must match with the sample names in the table of the experimental design. The samples can consist of technical replicates, which are later collapsed in the quantification process. Defining more than two experimental conditions is possible, but may

require adjustments in some commands when not all conditions should be compared.

16. Once the packages are installed, the respective commands can be omitted from the pipeline. Nevertheless, loading of the packages with `library()` will be necessary for each new R session.
17. Pre-filtering of low count genes will speed up DESeq2 functions in more complex sample analyses.
18. The filtered results can also be ordered by increasing or decreasing adjusted p-values or LFCs by implementing the `order()` function while filtering or exporting.

## References

1. Ramaswamy S, Ross KN, Lander ES et al (2003) A molecular signature of metastasis in primary solid tumors. *Nat Genet* 33:49–54
2. Byron SA, Van Keuren-Jensen KR, Engelthaler DM et al (2016) Translating RNA sequencing into clinical diagnostics: opportunities and challenges. *Nat Rev Genet* 17:257–271
3. Bild AH, Yao G, Chang JT et al (2006) Oncogenic pathway signatures in human cancers as a guide to targeted therapies. *Nature* 439:353–357
4. Robinson DR, Wu Y-M, Lonigro RJ et al (2017) Integrative clinical genomics of metastatic cancer. *Nature* 548:297–303
5. Choi J, Park S, Yoon Y et al (2017) Improved prediction of breast cancer outcome by identifying heterogeneous biomarkers. *Bioinformatics* 33:3619–3626
6. Yang L, Lee M-S, Lu H et al (2016) Analyzing somatic genome rearrangements in human cancers by using whole-exome sequencing. *Am J Hum Genet* 98:843–856
7. Hutchins G, Southward K, Handley K et al (2011) Value of mismatch repair, KRAS, and BRAF mutations in predicting recurrence and benefits from chemotherapy in colorectal cancer. *J Clin Oncol* 29:1261–1270
8. Conesa A, Madrigal P, Tarazona S et al (2016) A survey of best practices for RNA-seq data analysis. *Genome Biol* 17:13
9. Baruzzo G, Hayer KE, Kim EJ et al (2017) Simulation-based comprehensive benchmarking of RNA-seq aligners. *Nat Methods* 14:135–139
10. Dobin A, Davis CA, Schlesinger F et al (2013) STAR: ultrafast universal RNA-seq aligner. *Bioinformatics* 29:15–21
11. Zhang C, Zhang B, Lin L-L et al (2017) Evaluation and comparison of computational tools for RNA-seq isoform quantification. *BMC Genomics* 18:583
12. Li B, Dewey CN (2011) RSEM: accurate transcript quantification from RNA-Seq data with or without a reference genome. *BMC Bioinformatics* 12:323
13. Piskol R, Ramaswami G, Li JB (2013) Reliable identification of genomic variants from RNA-seq data. *Am J Hum Genet* 93:641–651
14. McKenna N, Hanna M, Banks E et al (2010) The genome analysis toolkit: a MapReduce framework for analyzing next-generation DNA sequencing data. *Genome Res* 20:1297–1303
15. Love MI, Huber W, Anders S (2014) Moderated estimation of fold change and dispersion for RNA-seq data with DESeq2. *Genome Biol* 15:550
16. Trivedi UH, Cézard T, Bridgett S et al (2014) Quality control of next-generation sequencing data without a reference. *Front Genet* 5:111
17. Chen S, Zhou Y, Chen Y et al (2018) Fastp: an ultra-fast all-in-one FASTQ preprocessor. *Bioinformatics* 34:i884–i890
18. Li H, Handsaker B, Wysoker A et al (2009) The sequence alignment/map format and SAMtools. *Bioinformatics* 25:2078–2079
19. R Core Team (2019) R: A Language and Environment for Statistical Computing
20. Morgan M (2019) BiocManager: access the bioconductor project package repository R package version 1.30.10. <https://CRAN.R-project.org/package=BiocManager>
21. McLaren W, Gil L, Hunt SE et al (2016) The Ensembl variant effect predictor. *Genome Biol* 17:122

22. Adzhubei I, Jordan DM, Sunyaev SR (2013) Predicting functional effect of human missense mutations using PolyPhen-2. *Curr Protoc Hum Genet.* Chapter 7:Unit7.20
23. Vaser R, Adusumalli S, Leng SN et al (2016) SIFT missense predictions for genomes. *Nat Protoc* 11:1–9
24. Stephens M, Carbonetto P, Gerard D, et al (2020) ashR: Methods for Adaptive Shrinkage, using Empirical Bayes R package version 2.2-47. <https://CRAN.R-project.org/package=ashr>
25. Durinck S, Moreau Y, Kasprzyk A et al (2005) BioMart and Bioconductor: a powerful link between biological databases and microarray data analysis. *Bioinformatics* 21:3439–3440
26. Durinck S, Spellman PT, Birney E et al (2009) Mapping identifiers for the integration of genomic datasets with the R/Bioconductor package biomaRt. *Nat Protoc* 4:1184–1191
27. Wickham H (2019) stringr: Simple, Consistent Wrappers for Common String Operations R package version 1.4.0. <https://CRAN.R-project.org/package=stringr>



# Chapter 17

## Barcoding Technology for Multiplexed Analysis of Metastatic Ability In Vivo

Philip Dujardin and Barbara M. Grüner

### Abstract

DNA barcoding allows the quantitative, biomarker-free tracking of individual cell populations in mixed/heterogeneous cell pools. Here, we describe a multiplexed *in vivo* screening platform based on DNA barcoding technology to interrogate compound libraries for their effect on metastatic seeding *in vivo*. We apply next-generation sequencing (NGS) technology to quantitatively analyze high-throughput compound screening in mice. Up to 96 compounds and controls can be screened for their effect on metastatic ability in a single mouse.

**Key words** DNA barcoding, Retroviral vector transduction, Next-generation sequencing, Mouse transplantation models, Metastasis, *In vivo* screening, Chemical compound screens

---

### 1 Introduction

High-throughput small molecule screenings are regularly applied to identify novel treatment options or therapeutic targets in disease settings such as cancer. However, most of these *in vitro* screens fail to translate into clinical settings as they are unable to model the complex settings of the *in vivo* situation. On the other hand, conventional *in vivo* experiments are too intricate and expensive for extensive screening. In metastasis research, individual cell culture-based assays like, for example, migration or invasion assays are used to study aspects of this complex, multistage process. Yet, these experiments often do not adequately reflect biological reality. To overcome these limitations, we have developed an *in vivo* multiplexed small molecule screening platform utilizing molecular cell barcoding combined with next-generation sequencing (NGS) to screen for novel modulators or inhibitors of metastatic ability in mice [1]. In molecular barcoding, a random nucleotide barcode sequence (or barcode for short) is used to label individual cells with a unique and inheritable DNA signature. This technology has been successfully established to track individual cells or cell populations

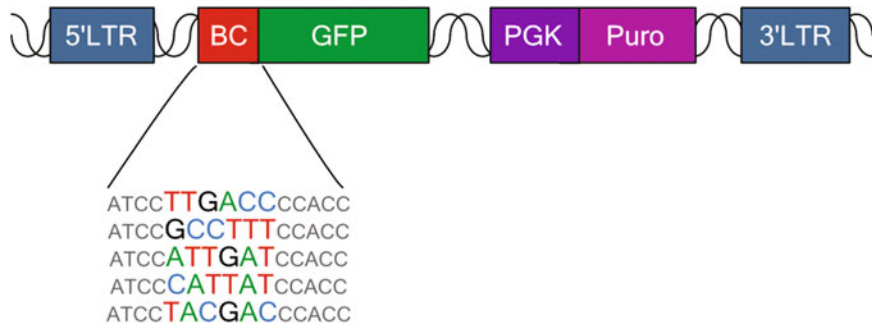


**Fig. 1** Schematic map of the MSCV six-nucleotide barcode-GFP vector. In addition to the barcode and the GFP, a puromycin resistance gene under a PGK promoter is contained in the plasmid. A selection of different barcodes is shown as an example

in heterogeneous cell pools both *in vitro* and *in vivo*. Applications include tracking of hematopoietic or cancer cells and monitoring metastatic ability or therapy response [2–5].

For our barcoding platform, we developed 96 individual plasmids each encoding a random six-nucleotide barcode and a fluorescent marker (green fluorescent protein, GFP) (Fig. 1) and used retroviral transduction to generate 96 uniquely barcoded cell variants of a polyclonal metastatic cancer cell line. These cell line variants can then be frozen and thawed in 96-well format for convenient screening. Each of these variants can be pretreated with a single distinct compound in 96-well format *in vitro*, pooled and injected intravenously into recipient mice to analyze for metastatic seeding to the lungs. After metastatic seeding, the barcoded cells are isolated from the lung as one of the main metastatic sites for many solid cancers. Finally, barcode representation is determined by quantitative sequencing of the DNA barcode in the pre- and postinjection samples, which allows the parallel quantification of the effect of each pretreatment on metastatic seeding ability (Fig. 2). Due to the multiplexed nature of this approach, one is able to analyze hundreds or thousands of molecules rapidly, thereby combining the high throughput of cell-based screening with a sophisticated animal model for metastatic seeding.

## 2 Materials

### 2.1 Barcode Cell Line Generation

1. HEK 293T (CRL-3216) cells cultivated in Gibco™ Dulbecco's Modified Eagle Medium (DMEM) supplemented with 10% fetal bovine serum.
2. PBS: 2.7 mM KCl, 2 mM KH<sub>2</sub>PO<sub>4</sub>, 137 mM NaCl, 10 mM Na<sub>2</sub>HPO<sub>4</sub>, pH 7.4.
3. Trypsin.

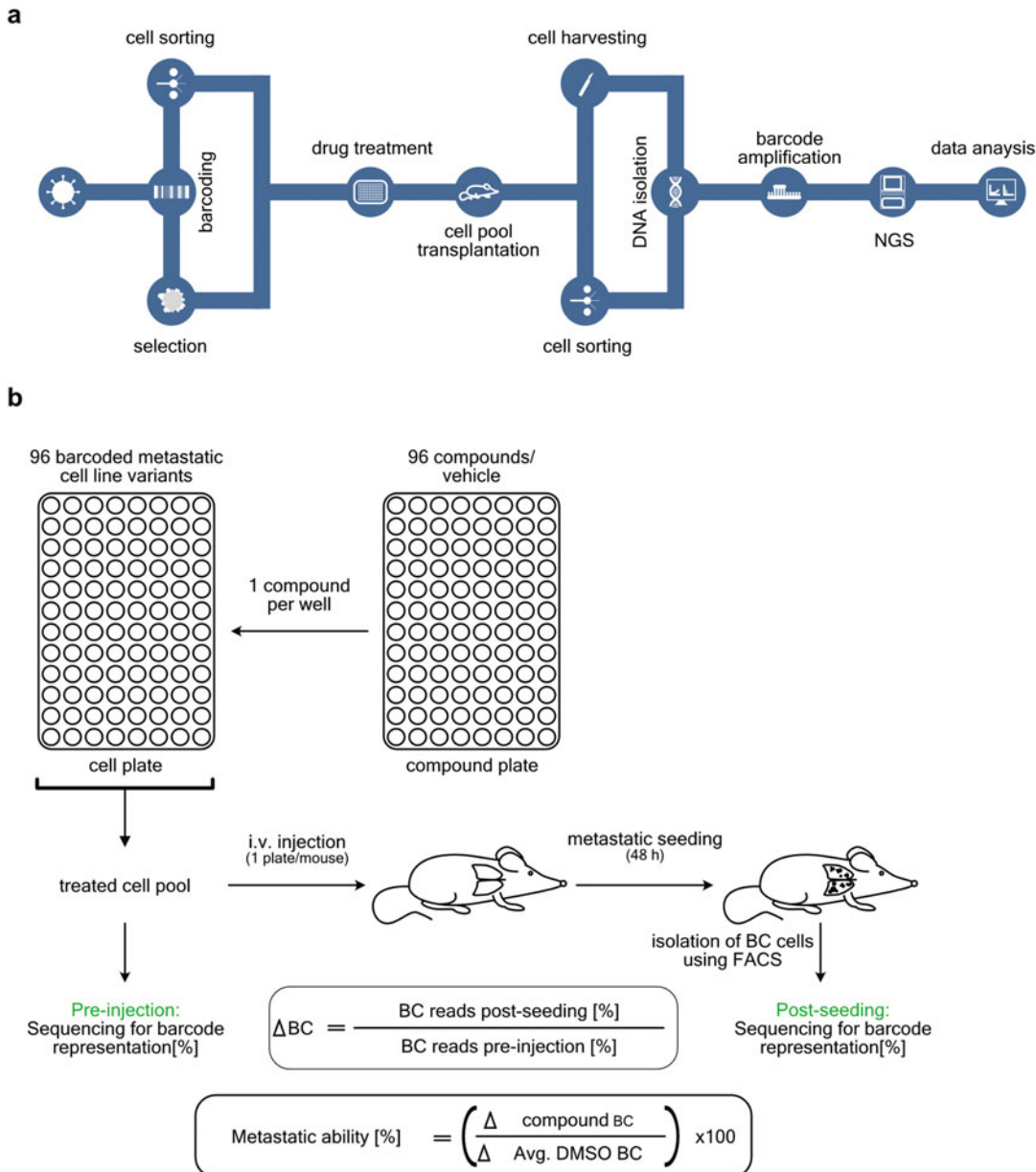


**Fig. 2** Schematic workflow of the multiplexed in vivo small-molecule screen. **(a)** General overview of the individual steps to establish and conduct the screening platform. First, barcoding viruses are produced and used to barcode target cells. Barcoded cells are enriched either by selection or by cell sorting, and each barcoded variant is pretreated in vitro with a distinct compound. Cells of one plate are pooled and intravenously injected into a recipient mouse. After the metastatic seeding, barcoded cells are isolated from the respective organs if necessary by cell sorting. Subsequently, DNA is isolated from both the preinjection and postseeding samples, and the barcode regions are amplified by PCR. NGS libraries are prepared and barcodes are sequenced. **(b)** In-depth schematic overview of the in vitro pretreatment and in vivo drug screening. Compound plates containing the compounds as well as the vehicle controls are prepared and applied on three different layouts of the 96 barcoded cell line variants to exclude specific barcode-compound pairing bias.

4. Cultivation media for the target cells.
5. Packing and envelope plasmids ([www.addgene.org/viral-vectors/retrovirus/](http://www.addgene.org/viral-vectors/retrovirus/)).
6. Barcoding plasmids ([www.addgene.org/browse/article/22414/](http://www.addgene.org/browse/article/22414/)).
7. Opti-MEM™ I Reduced Serum Medium.
8. Transfection reagent (e.g., TransIT-TKO® Transfection Reagent, Mirus).
9. Hexadimethrine bromide (commercial brand name Polybrene).
10. Puromycin.
11. Standard laboratory equipment and consumables for cell culture.

## **2.2 Screening Platform**

1. Drug library.
2. DMSO.
3. Cell viability assay.
4. Pipetting bio-reservoirs.
5. Digestion media (5 mL/sample): 3.5 mL HBSS-free (w/o  $\text{Ca}^{2+}$ , etc.), 500  $\mu\text{L}$  Collagenase IV (Worthington, 10 mg/mL in HBSS with Ca and Mg), 500  $\mu\text{L}$  dispase, 500  $\mu\text{L}$  trypsin 0.25%.
6. Quench solution (10 mL/sample): 9.0 mL L15 media, 1.0 mL FBS, 37.5  $\mu\text{L}$  DNase (5 mg/mL in HBSS-free (- $\text{Mg}^{2+}$ - $\text{Ca}^{2+}$ )).
7. Cell strainers 40  $\mu\text{m}$ .
8. ACK RBC lysis buffer: 0.15 M  $\text{NH}_4\text{Cl}$ , 10.0 mM  $\text{KHCO}_3$ , 0.1 mM  $\text{Na}_2\text{-EDTA}$ .
9. FACS buffer: 1× PBS, 2% FBC, 2 mM EDTA.
10. DNA isolation kit (Gentra Puregene Cell Kit (QIAGEN) or similar).

## **2.3 Barcode Amplification**

1. High-fidelity polymerase.
2. Universal forward primers and reverse primers with different multiplex indices (one individual reverse primer per

**Fig. 2** (continued) Accordingly, each compound is tested in triplicate in three different mice but also with three different barcodes. The average change in barcode representation is calculated between the postseeding and preinjection populations and compared to the average of all vehicle-treated samples to determine the metastatic ability. A compound is considered as a true inhibitor of metastatic ability if the average barcode representation decreases by at least three times the standard deviation of all vehicle controls. In parallel to the drug screening, the effect of each compound on in vitro cell growth is analyzed with a cell viability assay. Cell viability is taken into account to discriminate whether a decrease in barcode representation is caused by cytotoxicity

preinjection or postseeding sample). Primer sequences are listed below, multiplexing indices suitable for Illumina® platforms are highlighted in bold.

3. Gel extraction kit (for instance, QIAquick Gel Extraction Kit, QIAGEN).

Universal FW	AATGATAACGGCGACCACCGAGATCTACACTC TTTCCCTACACGACGCTCTCCGATCTTAGGC GCCGGAATTAGATCC
MP1	CAAGCAGAACAGCGCATACGAGAT <b>C</b> GTGAC TGGAGTT <b>C</b> AGACGTGTGCTCTCCGATCAGCTCG ACCAGGATGGGCAC
MP2	CAAGCAGAACAGCGCATACGAGAT <b>A</b> CGGTGAC TGGAGTT <b>C</b> AGACGTGTGCTCTCCGATCAGCTCG ACCAGGATGGGCAC
MP3	CAAGCAGAACAGCGCATACGAGAT <b>G</b> CCA <b>T</b> GTGAC TGGAGTT <b>C</b> AGACGTGTGCTCTCCGATCAGCTCG ACCAGGATGGGCAC
MP4	CAAGCAGAACAGCGCATACGAGAT <b>T</b> GGTCAGTGAC TGGAGTT <b>C</b> AGACGTGTGCTCTCCGATCAGCTCG ACCAGGATGGGCAC
MP5	CAAGCAGAACAGCGCATACGAGAT <b>C</b> ACTGTGAC TGGAGTT <b>C</b> AGACGTGTGCTCTCCGATCAGCTCG ACCAGGATGGGCAC
MP6	CAAGCAGAACAGCGCATACGAGAT <b>A</b> TTGGCGTGAC TGGAGTT <b>C</b> AGACGTGTGCTCTCCGATCAGCTCG ACCAGGATGGGCAC
MP7	CAAGCAGAACAGCGCATACGAGAT <b>G</b> ATCTGGTGAC TGGAGTT <b>C</b> AGACGTGTGCTCTCCGATCAGCTCG ACCAGGATGGGCAC
MP8	CAAGCAGAACAGCGCATACGAGAT <b>T</b> CAAGTGTGAC TGGAGTT <b>C</b> AGACGTGTGCTCTCCGATCAGCTCG ACCAGGATGGGCAC
MP9	CAAGCAGAACAGCGCATACGAGAT <b>C</b> TGATCGTGAC TGGAGTT <b>C</b> AGACGTGTGCTCTCCGATCAGCTCG ACCAGGATGGGCAC
MP10	CAAGCAGAACAGCGCATACGAGAT <b>A</b> AG <b>C</b> TAGTGAC TGGAGTT <b>C</b> AGACGTGTGCTCTCCGATCAGCTCG ACCAGGATGGGCAC
MP11	CAAGCAGAACAGCGCATACGAGAT <b>G</b> TAGCCGTGAC TGGAGTT <b>C</b> AGACGTGTGCTCTCCGATCAGCTCG ACCAGGATGGGCAC
MP12	CAAGCAGAACAGCGCATACGAGAT <b>T</b> ACAAGGTGAC TGGAGTT <b>C</b> AGACGTGTGCTCTCCGATCAGCTCG ACCAGGATGGGCAC

(continued)

MP13	CAAGCAGAAGACGGCATACGAGATTGACTGTGAC TGGAGTTCAGACGTGTGCTCTCCGATCAGCTCG ACCAGGATGGGCAC
MP14	CAAGCAGAAGACGGCATACGAGAT <b>GGA</b> ACTGTGAC TGGAGTTCAGACGTGTGCTCTCCGATCAGCTCG ACCAGGATGGGCAC
MP15	CAAGCAGAAGACGGCATACGAGATT <b>GAC</b> ATGTGAC TGGAGTTCAGACGTGTGCTCTCCGATCAGCTCG ACCAGGATGGGCAC
MP16	CAAGCAGAAGACGGCATACGAGAT <b>GGAC</b> GGGTGAC TGGAGTTCAGACGTGTGCTCTCCGATCAGCTCG ACCAGGATGGGCAC
MP18	CAAGCAGAAGACGGCATACGAGAT <b>GCGGAC</b> GTGAC TGGAGTTCAGACGTGTGCTCTCCGATCAGCTCG ACCAGGATGGGCAC
MP19	CAAGCAGAAGACGGCATACGAGATTTCACGTGAC TGGAGTTCAGACGTGTGCTCTCCGATCAGCTCG ACCAGGATGGGCAC
MP20	CAAGCAGAAGACGGCATACGAGAT <b>GGCCAC</b> GTGAC TGGAGTTCAGACGTGTGCTCTCCGATCAGCTCG ACCAGGATGGGCAC
MP21	CAAGCAGAAGACGGCATACGAGAT <b>CGAAAC</b> GTGAC TGGAGTTCAGACGTGTGCTCTCCGATCAGCTCG ACCAGGATGGGCAC
MP22	CAAGCAGAAGACGGCATACGAGAT <b>CGTACGG</b> TGAC TGGAGTTCAGACGTGTGCTCTCCGATCAGCTCG ACCAGGATGGGCAC
MP23	CAAGCAGAAGACGGCATACGAGAT <b>CCACTCG</b> TGAC TGGAGTTCAGACGTGTGCTCTCCGATCAGCTCG ACCAGGATGGGCAC
MP25	CAAGCAGAAGACGGCATACGAGAT <b>ATCAG</b> GTGAC TGGAGTTCAGACGTGTGCTCTCCGATCAGCTCG ACCAGGATGGGCAC
MP27	CAAGCAGAAGACGGCATACGAGAT <b>AGGAAT</b> GTGAC TGGAGTTCAGACGTGTGCTCTCCGATCAGCTCG ACCAGGATGGGCAC

## 2.4 Next-Generation Sequencing

1. Sequencing kit (MiniSeq Mid Output Kit (300 cycles) or similar kits for other sequencing platforms with comparable or higher read numbers).
2. PhiX Control v3 (Illumina®).

## 2.5 Laboratory Equipment

1. Standard molecular biology laboratory equipment (centrifuges, PCR cycler, etc.).
2. Cell culture, approved for biosafety level S2 work.

3. Animal facility, approved for biosafety level S1.
4. Cell sorter equipped with laser for GFP.
5. Sequencing platform (Illumina® MiniSeq or higher).

---

### 3 Methods

#### 3.1 Identification of a Suitable Metastatic Cell Line

To screen compound libraries for their effect on metastatic seeding, a suitable cell line must first be selected. If a cell line with a low metastatic potential is chosen, one might primarily identify compounds that increase metastatic potential. Vice versa, a cell line with high metastatic potential is more suited to identify compounds that lower/inhibit the metastatic ability. Among the requirements a cell line must meet are (a) it metastasizes and forms secondary tumors *in vivo* within a reasonable time, (b) at least  $1.0 \times 10^6$  cells can be injected into the lateral tail vein in a maximum volume of 100  $\mu\text{L}$ , and (c) it can be stably transduced with lentiviral vectors.

To test whether a cell line is suitable to use for the multiplexed screening platform, inject each  $1.0 \times 10^6$  cells into the lateral tail vein of four recipient mice (one mouse per time point). Harvest the lungs after 24, 48, 72, and 96 h, respectively, and assess the number of cancer cells that can be found in the lung (for instance, by flow cytometry). It is best to choose a cell line that allows to recover at least  $1 \times 10^5$  cells from the lung by FACS. Furthermore, by combining this preliminary experiment with BrdU labeling *in vivo*, one can choose the most suitable postseeding analysis time point, where cancer cells have actively seeded the lung but have not yet started to proliferate too much to avoid bias (compare to [1]). In addition, the metastatic ability of a cell line can further be analyzed by injecting about tenfold less cells intravenously and observing the formation of macro metastases after several weeks (*see Note 1*).

#### 3.2 Production of Barcode Virus

Each unique barcode containing virus supernatant has to be produced by separate transfection as described below. Virus production (Subheading 3.2) and infection of the target cells (Subheading 3.3) are biosafety level S2 work, as viable infectious virus particles are generated. Once the viral vectors have stably integrated into the target cell genome, the generated barcoded cell lines and all subsequent work are again biosafety level S1, as the barcoded cells cannot produce any more viral particles. Please make sure your laboratory is equipped accordingly and all waste (liquid and solid) is disposed according to S2 regulations (for Subheadings 3.2 and 3.3).

1. One day before transfection, seed  $1.0 \times 10^5$  HEK 293T cells per well of a 12-well plate in 1 mL DMEM. The next day the confluence should be between 50% and 80%.

2. For each well, add 0.4 µg packing plasmid, 0.1 µg envelope plasmid, and 0.5 µg of the respective desired MSCV barcoding plasmid to 50 µL of Opti-MEM I Reduced Serum Medium. Incubate at room temperature for 5 min.
3. For each well, mix 50 µL Opti-MEM I Reduced Serum Medium with 2 µL of transfection reagent.
4. Combine the DNA mix with the transfection reagent mix. Mix gently and incubate for 30 min at room temperature to allow the formation of DNA reagent complexes.
5. After the incubation, add 100 µL of the mixture dropwise to each well containing cells and mix gently by moving the plate back and forth.
6. Incubate the cells for 24 h in a humidified incubator with 5% CO<sub>2</sub> at 37 °C and change media afterwards.
7. Collect the supernatant after 48 h (and again after 72 h [optional] [*see Note 2*]) and centrifuge for at least 10 min at 13,200 rpm to eradicate HEK 293T cells which might be contained in the supernatant (*see Note 3*).

### **3.3 Generation of Barcoded Cell Lines**

Since retroviral integration is random, this protocol aims to generate heterogeneous polyclonal cell populations. Therefore, each individually barcoded cell line variant has to be generated by a separate infection with an individual barcode virus supernatant. Clone picking is expressly not recommended to avoid creating bias.

1. Seed the target cells to the number of wells required for the number of desired individual barcodes (i.e., 96 for screening 96 cell line variants in plate format) in 12-well plates 1 day prior to the infection. Adjust the number of seeded cells so that a confluence of 70% is achieved for transduction.
2. At the next day, aspirate the cultivation media. Prepare fresh cultivation media + 32 µg/mL polybrene (hexadimethrine bromide) (*see Note 4*). Add 250 µL of the polybrene mix to each well and 750 µL virus supernatant (*see Note 2*). Mix by gentle shaking of the plate and incubate overnight.
3. At the next day, wash the cells twice with PBS.
4. Control GFP expression either by microscope or by FACS. Infection rates should at least be 60% for each cell line variant before puromycin selection, to ensure that a heterogeneous population of cells gave rise to each barcoded cell line. At this point, the cells can again be considered as biosafety level S1 (as long as your target cell line also adheres to these regulations, is not otherwise genetically altered, etc.).

### **3.4 Elimination Unbarcoded Cells**

Once the target cells start to express GFP (for most cell lines this takes approximately 2 days), the puromycin selection can be started to eliminate unbarcoded cells. If unknown, the optimal puromycin dose for the target cells should be determined in advance. For this purpose, treat the target cells with a range of different puromycin concentrations and determine the lowest dose that kills all target cells over the course of 2–7 days. The optimal concentration is cell type dependent and can usually range from 0.5 to 10 µg/mL. If the target cells cannot be selected, the GFP-expressing, barcoded cells can alternatively be purified by cell sorting.

### **3.5 Compound Treatment and Cell Pool Injection**

1. Prepare compound plates containing the compound as well as the vehicle controls.
2. Prepare cell plates by seeding  $\sim 2.0 \times 10^3$  cells of one barcoded variant per well in 200 µL cultivation medium and incubate at 37 °C and 5% CO<sub>2</sub> overnight. Use different barcode-arrangement layouts for multiple plates (*see Note 5*).
3. Remove cultivation media and add 100 µL of fresh cultivation media before compound treatment. Add compounds or vehicle controls to well in a 1:100 dilution for the desired final concentration or so that max. 1% vehicle (for example, DMSO) are added per well. Analyze each compound plate in triplicate on three different cell plate layouts to exclude specific barcode-compound pairing biases.
4. Treat cells with compound for a minimum of 6 h at 37 °C when covalent binding molecules are assayed. Expend the treatment period to 48–72 h if non-covalent inhibitors are used instead.
5. In order to discriminate the possibility that a reduced barcode representation in the postseeding samples is due to cytotoxic effects of the tested substances, parallel cell viability assays should be performed. To this end, seed the cells separately in 96-well plates in 200 µL cultivation medium and incubate at 37 °C and 5% CO<sub>2</sub> overnight. Perform the same treatment scheme as described above and use the same treatment time. Then, replace the media after the incubation period with normal cultivation media and wait 48 h (or the same amount of time that is applied to wait between injection and isolation from the lungs in the in vivo experiment) to assess cell viability with a suitable cell viability assay (MTT, PrestoBlue, CellTiter-Glo or similar). Normalize data to the average of the vehicle control wells.
6. After the treatment of the barcoded cell plates, remove the media, wash once with PBS and trypsinize until all cells are detached and in a single-cell suspension.
7. Pool all cells of one plate. For this, it is best to use a multichannel pipette and collect all cells of one plate in a sterile

bio-reservoir before transferring the entire cell solution to a 50 mL Falcon. Rinse the reservoir with PBS and transfer as well. Centrifuge to pellet all cells and resuspend them in ~1 mL PBS.

8. Inject  $1.0 \times 10^6$  of the cell pool into the lateral vein of a recipient mouse.
9. Pellet and isolate the DNA (*see* Subheading 3.7) of the remaining cells to determine the barcode representation in the preinjection pool.
1. Harvest the lungs 48 h (or after the appropriate time point determined by your setup experiment under Subheading 3.1), after the intravenous transplantation of the compound-treated, pooled cancer cells.
2. Transfer each lung to the upper part of an empty 15 mL tube and mince it thoroughly into very small pieces with sterile scissors for several minutes.
3. Once snipping is complete, wash any tissue that sticks to the upper part of the Falcon to the bottom of the tube with 5 mL digestion media (10% trypsin (0.25% in EDTA, Invitrogen), 10% collagenase IV (10 mg/mL in HBSS, Worthington), and 10% dispase (Corning) in HBSS without  $\text{Ca}^{2+}$  and  $\text{Mg}^{2+}$ ), keep on ice until all samples are processed. Digest the samples rotating for 30–60 min at 37 °C in a hybridization oven.
4. Subsequently, cool down the samples on ice for 3 min and quench the digestion with the quenching solution (10% FBS and DNase (5 mg/mL in HBSS) in L15 media).
5. Filter the suspension through a 40 µm mesh, rinse the mesh with 30 mL PBS, and spin down the suspension for 5 min at  $300 \times g$  (*see* Note 6).
6. Discard the supernatant and perform a red blood cell lysis by adding 5 mL of ACK RBC lysis buffer for 10 min. Afterwards, add 30 mL PBS and centrifuge for 5 min at  $300 \times g$ .
7. Discard the supernatant, suspend the cell pellet in 500 µL FACS buffer (1× PBS, 2% FBC, 2 mM EDTA), and transfer the suspension into a FACS tube. Filter again if necessary.
8. Enrich barcoded cells by sorting for GFP. Only sorting for enrichment or yield is required, the barcoded cell solution does not have to be pure, rather try not to lose any potential barcoded cells due to sorting. Pellet the sorted cells and store at –80 °C until DNA isolation.

### 3.7 DNA Isolation

For further analysis, DNA must be isolated from both the preinjection pool and the postinjection samples. A number of kits are commercially available for this purpose. In our experience, good

DNA quantities and qualities are obtained when using the Gentra Puregene Cell Kit (QIAGEN) according to manufacturer's instructions.

### **3.8 Barcode Amplification**

To generate the sequencing libraries from the DNA isolated from the preinjection and postseeding samples, the barcoding region has to be amplified by PCR using primers that add the Illumina sequencing primer-binding sites, the Illumina adapters as well as multiplexing tags in a single PCR (see table above). For the PCR, we recommend using a high-fidelity polymerase. Potential PCR bias can be neglected as the analysis will compare ratios between the pre- and postseeding samples rather than raw read values. Prepare the PCR mixture according to the manufacturer's instructions for the polymerase you are using. Use 1 µg of isolated DNA in a 25 µL PCR mix (*see Note 7*). Use the same universal forward primer for each sample but separate reverse primers containing different indices for each preinjection and postseeding sample. Run the PCR for 30 cycles as depicted below. Make sure to run a negative control for each reverse primer to exclude any potential cross contamination.

Temperature (Time)	Cycle #
95 °C (5 min)	1
95 °C (30 s)	30
58 °C (30 s)	
72 °C (1 min)	
72 °C (7 min)	1
4 °C (continuous)	∞

Separate the amplicons on 2% agarose gels and purify the product (210 bp) using the QIAquick Gel Extraction Kit (QIAGEN). Make sure you have clean, crisp bands. Since the primers are very long (primer dimers will show up at ~150 bp), make sure to run the gel long enough to ensure proper separation. Leave empty wells on the gel between the separate samples to avoid any potential cross contamination. Elute the PCR products twice in 30 µL ddH<sub>2</sub>O and measure the DNA concentration of each sample using a fluorometer (*see Note 8*).

### **3.9 Library Preparation and NGS**

In order to evaluate the effect of the screened compounds on the metastatic ability, changes in the barcode representation under the respective treatments must be determined by next-generation sequencing. Various NGS systems are available on the market and can most likely be adapted for this platform. As the small-molecule screening platform was first established using the MiSeq and the MiSeq Reagent Kit v3 (150 cycle) and later successfully employed

on MiniSeq using the MiniSeq Mid Output Kit (300 cycles), we describe here the primers and setup required for this by Illumina®. Accordingly, the small molecule screening can also be performed with any systems offering a higher read numbers such as the HighSeq platform.

1. Determine the DNA molarity of each sample (*see Note 9*).
2. Pool all samples in equal concentrations, mixed with 50% PhiXv3 control (*see Note 10*).
3. Prepare and dilute the library further according to the instructions of the NGS kit you are using.
4. Load the library according to the manufacturer's instructions.
5. Set read length to a minimum of 50 bp to sequence the barcode and approx. 20 bp up- and downstream of the barcode sequence and choose single read as read type.
6. Set read length of the first index to 6 bp.
7. Generate FASTQ files.

### **3.10 Bioinformatic Analysis/Calculation of Metastatic Ability**

1. Extract the reads per barcode per sample (as identified by the multiplex index) from the FASTQ files.
2. Calculate preinjection to postseeding barcode ratios for each barcode.
3. Normalize each barcode ratio to the average of all vehicle controls included on the analyzed compound plate. The ratios of the vehicle controls should be 1 with a standard deviation of maximum 15%.
4. Calculate the effect on metastatic ability for each compound or control (the average of the corresponding triplicate measurements). The calculation formulas are also depicted in Fig. 2.
5. We recommend to consider a compound as a true inhibitor of metastatic ability if the average barcode representation decreases by at least three times the standard deviation of all vehicle controls.

## **4 Notes**

1. The cell numbers mentioned in this paragraph are only exemplary and should be adjusted accordingly for different cell lines.
2. If the transduction efficiency is insufficient, cells can be transduced for two consecutive days. For this purpose, virus supernatant can be harvested twice after 48 h and 72 h.
3. Either use the supernatant directly or freeze the virus in liquid nitrogen or at –80 °C. Freezing will however decrease virus titer and infection efficiency significantly. Thaw the virus on ice

and use it immediately. Avoid repeated thawing and freezing cycles.

4. Use of polybrene can significantly improve transduction efficiency but it might be cytotoxic. It may therefore be advisable to test different concentrations in advance. The final working concentrations should usually be between 4 and 10 µg/mL.
5. To save work in future screenings, multiple cell plates with different barcode layouts can be produced and can be frozen and stored in 96-well plates containing freezing medium for up to 1 year at -80 °C. When needed, thaw the plates and passage the cells once or twice before using the plates in a screening. This is not possible for all cell lines and has to be tested accordingly.
6. When filtering the digested organ, cell clumps can be forced through the filter with the rubber end of a syringe plunger.
7. We recommend completely amplifying the isolated DNA to not generate a bias in barcode representation.
8. We have good experiences using the Qubit 4 Fluorometer with the Qubit dsDNA HS assay kit (Invitrogen).
9. To calculate the molarity for this purpose, the following formula is an appropriate approximation:  $c[\text{nM}] = \frac{c[\text{ng}]}{136500} \times 10^6$ .
10. Apart from the six-nucleotide barcode, the sequence of all samples is identical. Therefore, the sample sequences are too unbalanced and the PhiX-Library is needed as a control.

## References

1. Gruner BM et al (2016) An in vivo multiplexed small-molecule screening platform. *Nat Methods* 13(10):883–889
2. Wagenblast E et al (2015) A model of breast cancer heterogeneity reveals vascular mimicry as a driver of metastasis. *Nature* 520 (7547):358–362
3. Fan HC, Fu GK, Fodor SP (2015) Expression profiling. Combinatorial labeling of single cells for gene expression cytometry. *Science* 347 (6222):1258367
4. Lu R et al (2011) Tracking single hematopoietic stem cells in vivo using high-throughput sequencing in conjunction with viral genetic barcoding. *Nat Biotechnol* 29(10):928–933
5. Nguyen LV et al (2014) DNA barcoding reveals diverse growth kinetics of human breast tumour subclones in serially passaged xenografts. *Nat Commun* 5:5871



# Chapter 18

## In Vivo Assessment of Metastatic Cell Potential in Prostate Cancer

Marc Nunez-Olle, Marc Guiu, and Roger R. Gomis

### Abstract

Metastasis is the main cause of death for cancer patients, but our ability to improve clinical outcome first requires a better understanding of the dynamics, cellular mechanisms, and kinetics of metastasis. In prostate cancer (PCa), metastatic tumor cells preferentially colonize to bone. However, a lack of applicable mouse models has limited our ability to study this process accurately. Here, we describe a strategy to bypass this limitation: human PCa cells are injected into immunodeficient mice (at tibia, the left ventricle of heart and the iliac artery). Using this novel technique, the metastatic capabilities of these human PCa cells (e.g., colonization and proliferation potential) can be analyzed in bone with an in vivo imaging system.

**Key words** Metastasis, Prostate cancer, Mouse model, In vivo imaging, Bone

---

### 1 Introduction

Prostate cancer (PCa) is the second most prevalent cancer and the second cause of death from cancer, in men worldwide [1]. Although it is a relatively manageable disease, its elevated incidence leads to a high number of patients who have complications due to progression of disease, representing a major medical problem [2, 3]. Progression of disease starts with outgrowth of epithelial cells from the prostate and alterations of the structure of the gland. Progression continues with the formation of invasive PCa lesions, when cancer cells alter the basal lamina structure. These localized invasive lesions can acquire metastatic characteristics, which correlate with the worst prognosis of the disease [4].

Metastasis is a multistep process, consisting of dissemination of cancer cells from the primary tumor and their colonization and growth in other organs. This is a highly inefficient process that requires the cancer cells to survive multiple stresses during dissemination as well as to adapt to the microenvironment conditions of the new niche. Tumor cells adapt to these new conditions by rewiring metabolism, adapting to immune surveillance, exiting

the blood stream, and reinitiating proliferation in the new niche [5, 6]. This process of adaptation also allows tumor cells from patients who have received chemotherapy to adapt to adverse conditions, thereby increasing their resistance to genotoxic drugs. Adaptation of metastatic cells to these situations is promoted by increased mutational rate of cancer cells, providing phenotypic flexibility.

Critically, nearly all patients with metastatic PCa develop resistance to chemotherapy and androgen deprivation therapy (ADT) [7, 8]. Analyses of these lesions show molecular features already identified in the primary tumor and others acquired as a mechanism of resistance to ADT and chemotherapy [9, 10]. Moreover, metastatic cells have tissue-specific tropism and preferentially colonize and grow in certain organs depending on the type of tumor and tissue of origin [11, 12]. In PCa, in particular, metastatic PCa cells tend to colonize the bone in more of the 90% of the cases, followed by the lung and lymph nodes [13, 14]. Altogether suggest that prostate metastatic cells are endowed with particular traits that promote metastatic colonization to particular organs. However, the details of the kinetics and cellular mechanisms driving this specificity are not established.

Currently, a genetically engineered mouse model that faithfully recapitulates metastatic features observed in metastatic PCa patients is not available. There are mouse models that disseminate at the bone and generate micrometastasis or models that generate metastasis in other tissues such as the lung or liver, which are less common in this tumor type [15–19]. Interestingly, immunodeficient mouse models are useful to study metastatic potential of human PCa cells. Different methods of injection have been developed in order to understand and validate the relevance of candidate genes in distinct metastatic prostate cancer-specific processes, including the bone. However, different readouts can be obtained depending on the procedure used leading to conclusions that partially reflect the complexity of the process of metastasis. For example, tail vein injection is useful to understand the capacity of cells to colonize the lungs, but not to understand the proliferation in the bones [20].

In order to study the main features of human PCa metastasis, we have set up in the laboratory several strategies to evaluate the potential of different PCa cells to colonize and growth at the bone. This include: (1) PCa cells injection into the tibia of immunodeficient mice to evaluate the capacity of cancer cells to take and proliferate at the bone, a process that requires the cells to adapt to this specific niche and sustain proliferation; (2) intra-iliac PCa cells injection, it delivers the cells into circulation but lodges them directly at the long bone. This method scores for bone colonization; (3) PCa cells injection via left ventricle, a procedure that allows us to measure the ability of cells to survive in the blood stream and colonize distant organs, including the bone and lungs.

These combined strategies give us a reliable model to evaluate the metastatic potential of PCa cells and also can be used to evaluate the relevance of potential driver genes in the different steps of metastasis.

---

## 2 Material

All solutions and reagents must be prepared under a laminar flow hood in sterile conditions at room temperature and stored at room temperature, unless otherwise indicated.

### 2.1 Cell Culture

1. Cell culture growth medium: DMEM/F-12 supplemented with 10% FBS, 1% L-glutamine (200 mM), and 1% penicillin/streptomycin. Supplements should be stored at -20 °C. After adding supplements to media, store the mix at 4 °C (*see Note 1*).
2. Sterile phosphate saline buffer (PBS).
3. Trypsin-EDTA solution: 0.05% trypsin and EDTA (1:5000) in PBS. Store at -20 °C (*see Note 2*).

### 2.2 Retrovirus Production

1. Sterile NaCl (150 mM).
2. Polyethylenimine (PEI) (1 mg/ml), 2-μm filtered.
3. VSVG-R-expressing vector (purified DNA).
4. GAG-POL-expressing vector (purified DNA).
5. GFP/Firefly luciferase (GFP-LUC)-expressing vector (purified DNA).
6. Polybrene (8 μg/ml).

### 2.3 Fluorescent-Activated Cell Sorting (FACS)

1. 4',6-diamidino-2-phenylindole dihydrochloride (DAPI) (200 mg/ml).
2. BD FACSAria II flow cytometer.

### 2.4 Cell Inoculation In Vivo

Immunodeficient animals (e.g., mice) that require special conditions of maintenance are necessary when using human cancer cells for oncology animal models. An animal house barrier area (SPF) that includes HEP-filtered air is necessary to maintain these animal models.

1. Immunodeficient mice: Balb C/nude mice (*see Note 3*).
2. Anesthesia mix: Mix 1 ml ketamine (100 mg/ml), 0.5 ml xilacine (20 mg/ml), 8.5 ml NaCl (0.009 g/ml solution), pH 6.
3. Buprenorphine: Use 100 μl/mouse (0.01 mg/dl solution) (*see Note 4*).

4. Betadine solution.
5. 70% ethanol.
6. Deionized water ( $H_2O$ d).
7. 10- $\mu$ l Hamilton syringe.
8. 28G/15 mm/pst4 Hamilton needle.
9. 25G syringe needle.
10. 27G syringe needle.
11. 31G syringe needle.
12. Scalpel blades.
13. 5/0 black silk.
14. Sterile cotton swabs.
15. Sterile material for surgery: Surgical scissors, blunt forceps, hemostatic clamps, needle holder.

## **2.5 In Vivo Imaging System**

1. IVIS Spectrum In Vivo Imaging System (PerkinElmer-Caliper).
2. Luciferin solution: Beetle luciferin (15 mg/ml), diluted in PBS (*see Note 5*).
3. Insulin (30G) syringe.

## **3 Methods**

Perform all cell culture steps under a laminar flow hood and at room temperature unless otherwise specified. All cell types are cultured with DMEM/F12 supplemented with 10% FBS, 1% L-glutamine, and 1% penicillin/streptomycin unless otherwise specified.

### **3.1 Transduce Cells with a Luciferase-Expressing Vector**

#### **3.1.1 Produce Retroviral Particles**

1. Seed HEK-293T cells for transfection at 80% confluence in 15 cm Ø culture dish; let cells attach for 8–9 h at 37 °C (*see Note 6*).
2. Prepare transfection solution by mixing the reagents in the following order: 2.32 ml of NaCl (150 mM), 1.2  $\mu$ g of VSVG-R vector, 10.8  $\mu$ g GAG-POL vectors, 12  $\mu$ g of GFP-Luc vector, and 116  $\mu$ l of PEI (for a total volume of 2500  $\mu$ l).
3. Mix well by tapping the tube (do not vortex), and incubate tubes for 15 min.
4. Carefully remove culture media from HEK-293T cells and add 18 ml of fresh complete culture media before adding transfection mix.

5. Add transfection mix dropwise, covering the maximum surface of the culture dish. As viral particles are produced from this step onwards, it is very important to follow appropriate safety guidelines according to your institution instructions (*see Note 7*).
6. Incubate dishes at 37 °C overnight.
7. Carefully remove media and debris, and add 16 ml of fresh complete culture media (*see Note 8*).
8. Incubate 48 h at 37 °C.
9. Harvest media and transfer to a 50 ml Falcon tube (*see Note 9*).
10. Centrifuge at 1200 rpm for 5 min.
11. Collect supernatant containing retroviral particles and pass it through a 0.45 µm filter using a plunger.
12. Aliquot flow-through containing viral particles from previous step and store at –80 °C freezer if not used immediately.

**3.1.2 Transduce PC3, DU145, and 22RV1 Cells with GFP-LUC-Expressing Vector**

1. Collect PC3, DU145, and 22RV1 cells: Wash 1× PBS and incubate with trypsin (prewarmed to room temperature) for 2–5 min.
2. Gently collect the cells from the culture dish and dilute the trypsin-cell mix with at least 5× volumes of fresh complete culture media (*see Note 10*).
3. Seed 500,000 cells/well in a 6-well plate and let them attach overnight (*see Note 11*).
4. Thaw 1 ml of GFP-LUC-encoding retrovirus aliquot for each well.
5. Prepare infection mix by adding 1.6 µl polybrene (8 µg/ml) to 1 ml of GFP-LUC-encoding retrovirus.
6. Remove media from wells with PC3, DU145, or 22RV1 cells and replace with infection mix from previous step.
7. Seal the 6-well plate tightly with parafilm and centrifuge cells at 2250 rpm for 45 min at 33 °C (*see Note 12*).
8. Remove parafilm and place cells in an incubator at 37 °C overnight.
9. Discard the infection cocktail from the 6-well plates and add 2 ml of fresh complete culture media to each well.
10. Incubate the cells for 48 h at 37 °C.
11. Check GFP expression under fluorescence microscope (*see Note 13*).

**3.2 Sort GFP<sup>+</sup> Cells**

1. Before going to the sorter, it is recommended to expand the cells, to obtain at least one 10 cm Ø culture dish for each cell line.

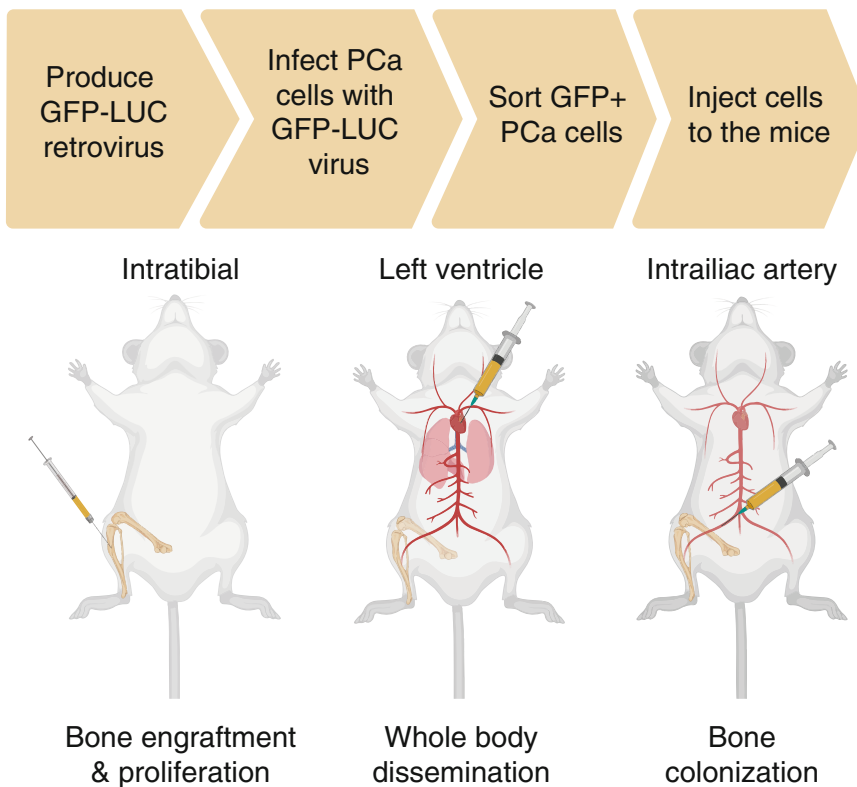


**Fig. 1** Schematic representation of the strategy followed. GFP-Luc retrovirus should be used to infect PCa cells. GFP+ cells are then sorted and expanded before injecting into immunodeficient recipient mice. Depending on the method of injection (intra-tibiae, left ventricle, or intra-iliac artery), different readouts about cell metastatic potential can be obtained

2. Collect PC3, DU145, and 22RV1 cells infected with the GFP-LUC virus and noninfected parental cell lines: Wash cells with 1× PBS and then incubate with trypsin (prewarmed to room temperature) for 2–5 min.
3. Gently collect cells from the dish, and dilute in at least 5× volume of PBS.
4. Spin down cells at 1200 rpm for 5 min.
5. Discard supernatants, and resuspend cell pellets with 1 ml of PBS (depending on the number of cells; *see Note 14*), and transfer to a sorter tube; keep on ice until sorting.
6. Prepare 15 ml conical tubes (Falcon) with 5 ml of fresh culture media to collect cells.
7. Add 3 µl of 200 mg/ml DAPI to cells before sorting.
8. Analyze noninfected parental cell lines by FACS, and set the GFP-negative population for each cell line (Fig. 1a) (*see Note 15*).

9. Sort GFP-positive population from the pool of cells infected with the GFP-LUC virus, and keep cells on ice (Fig. 1b).
10. Centrifuge collection conical tubes with cells at 1200 rpm for 5 min.
11. Resuspend cells with fresh complete fresh media and seed into a 10 cm Ø culture dish (*see Note 16*).
12. Culture cells at 37 °C.
13. Change media the next day and expand.

### **3.3 In Vivo Metastatic Potential**

Before preparing cells for injection, confirm that cells are negative for mycoplasma (*see Note 17*).

#### *3.3.1 Intra-Tibiae Injection*

1. Collect and count cells: Wash cells with 1× PBS and incubate with trypsin (prewarmed to room temperature) for 2–5 min.
2. Gently collect cells from dish, and dilute the trypsin-cell mixture with at least 5× volumes of fresh complete culture media.
3. Count cells and prepare the number of cells needed for each step of administration (as specified in the following).
4. For injecting cells into a live mouse in an animal facility, it is firstly important that the procedure complies with the Institutional Review Board committee approval, following the 3Rs whenever possible (Replacement, Reduction, and Refinement). Further, animals should be procured as needed according to the experimental plan, while ensuring that animal use is minimized. Prepare the mice for injection using the standard approved protocols for anesthesia.
1. Prepare cells at a concentration of 10,000 cells/5 µl (per leg to be injected) in PBS in a 1.5 ml Eppendorf tube; keep on ice until injection (*see Note 18*).
2. Inject 10 µl anesthesia mix/g mouse via intraperitoneal to anesthetize each mouse (*see Note 19*).
3. Wait until the mouse is completely anesthetized before proceeding to the next step (*see Note 20*).
4. Clean thoroughly the leg with betadine solution.
5. Make a 1-cm skin incision on the anteromedial part of the leg.
6. Use blunt forceps to pull the muscles aside during the injection.
7. Drill the bone using a 27G syringe needle.
8. Hydrate the surgical area with NaCl solution.
9. Take out the drilling syringe needle from the bone and immediately inject 5 µl of cell suspension using a Hamilton syringe with a 28G Hamilton needle.
10. Suture back skin using 5/0 black silk.
11. Inject subcutaneously 100 µl of buprenorphine solution.

12. Confirm inoculation by bioluminescent image.
13. Mice will wake up in 20–30 min. Keep mice warm.
14. Wash 5 × 28G needle and Hamilton syringe with 70% ethanol (*see Note 21*).
15. Wash 5 × 28G needle and Hamilton syringe with H<sub>2</sub>Od.

### *3.3.2 Left Ventricle Injection*

1. Prepare cells at a concentration of 200,000 cells/100 µl (per mouse to be injected) in PBS in a 1.5 ml Eppendorf tube, and keep on ice until injection (*see Note 22*).
2. Inject 10 µl anesthesia mix/g mouse via intraperitoneal to anesthetize each mouse (*see Note 19*). Wait until the mouse is completely anesthetized (*see Note 20*).
3. Fix the mouse in X (ventral position) using tape.
4. Clean thoroughly the thoracic area with betadine solution (*see Note 23*).
5. Take 100 µl cell suspension with 1-ml sterile syringe 25G needle (*see Note 24*).
6. Localize fourth left mouse intercostal space.
7. Inject 100 µl of cell suspension into the left ventricle (*see Note 25*).
8. Confirm inoculation by bioluminescent image.
9. Mice will wake up in 20–30 min. Keep mice warm.

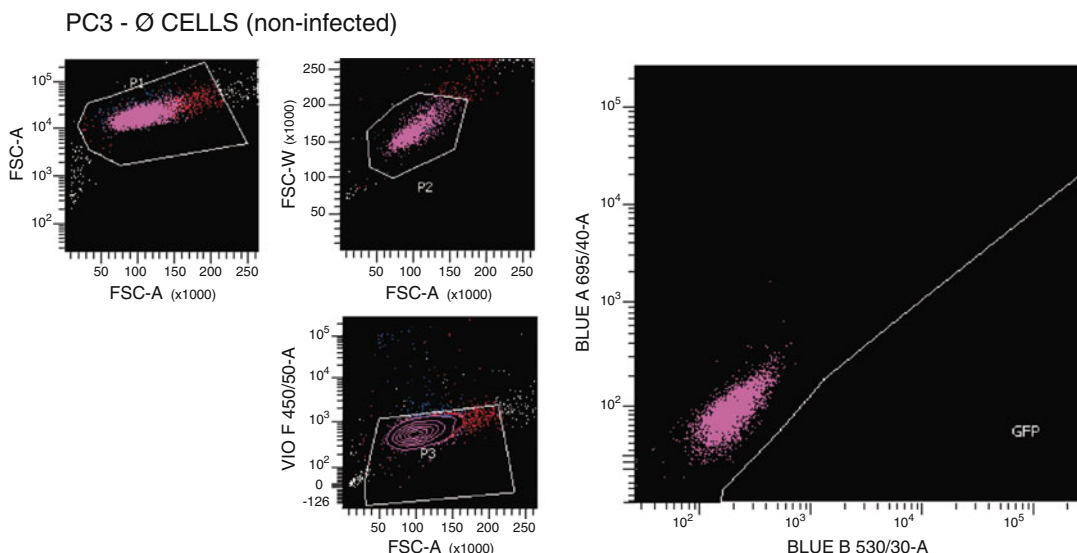
### *3.3.3 Intra-Iliac Injection*

1. Prepare cells at a concentration of 200,000 cells/100 µl (per leg to be injected) in PBS in a 1.5 ml Eppendorf tube, and keep on ice until injection (*see Note 22*).
2. Inject 10 µl anesthesia mix/g mouse via intraperitoneal to anesthetize each mouse (*see Note 19*).
3. Wait until the mouse is completely anesthetized (*see Note 20*).
4. Clean thoroughly the lower abdominal area with betadine solution (*see Note 23*).
5. Fix the mouse in X (ventral position) using tape.
6. Transfer mouse to a binocular magnifying glasses.
7. Make a 1-cm skin incision between fourth and fifth nipple in the lower abdomen.
8. Separate the fat tissue on both sides using blunt forceps, to view iliac vessels and nerves.
9. Use thin forceps to break the connection tissue between vessels and the nerves close to the vessels.
10. Isolate the iliac and vein artery together from the connection tissue and iliac nerve using thin curved forceps (*see Note 26*).
11. Take 100 µl cell suspensions with a 31G insulin syringe.

12. Pass the thin curve forceps back into the iliac vessels and slowly open the forceps tips (*see Note 27*).
13. Push up slowly the thin curve forceps and inject the 100  $\mu$ l cell suspension in the iliac artery between the forceps tips.
14. Remove the needle from artery slowly and quickly apply pressure with a cotton swab.
15. Press the cotton swab for 5–10 min to stop bleeding.
16. Suture back skin using 5/0 black silk.
17. Inject subcutaneously 100  $\mu$ l of buprenorphine solution.
18. Confirm inoculation by bioluminescent image.
19. The mouse will wake up in 20–30 min. Keep the mouse warm.

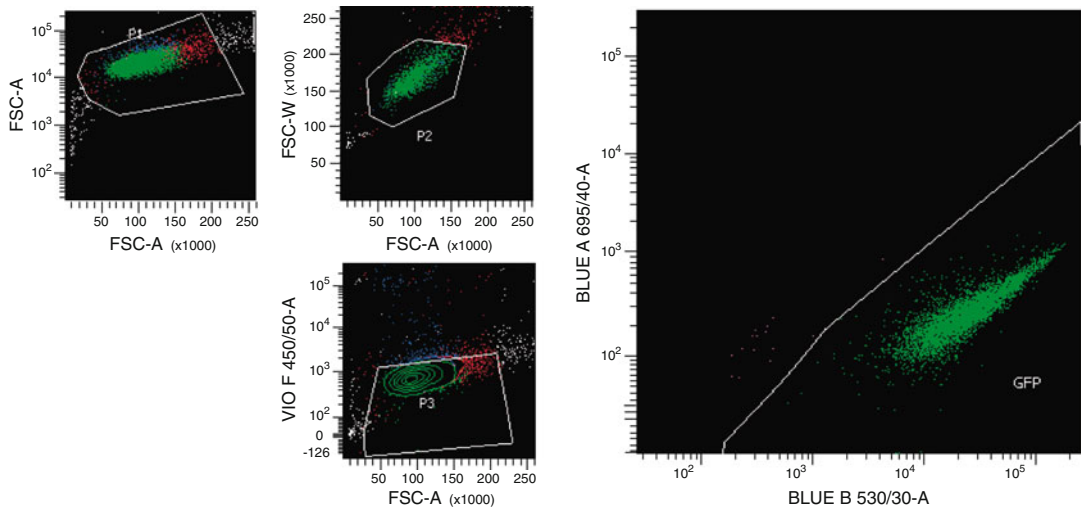
### **3.4 Bioluminescent Imaging and Data Analysis**

1. Anesthetize mice as described above. This step can be done with 5 mice at the same time, which is the IVIS machine system capacity.
2. Place mice in a lateral decubitus position.
3. Inject 50  $\mu$ l of luciferin solution (*see Note 28*).
4. Place mice inside an IVIS machine system in a ventral position if injections were intra-tibiae or intra-iliac (Figs. 2 and 3), or in a dorsal position if injections were in the left ventricle (Figs. 4 and 5).
5. Acquire images. Conditions for acquiring luminescent images:
  - (a) Photographic image time exposure: 0.2 s.
  - (b) Photographic image binning exposure: medium.

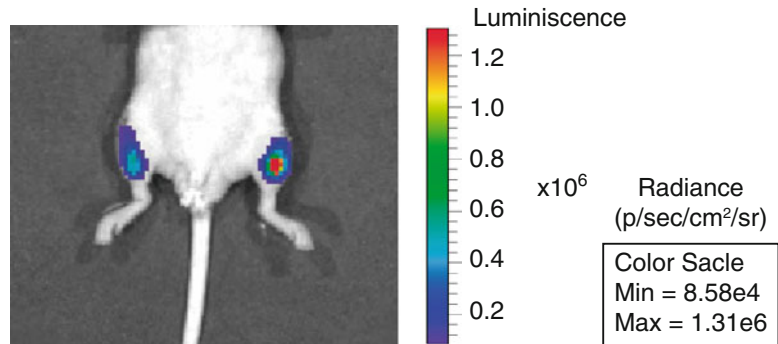


**Fig. 2** GFP+ cell sorting using BD FACSaria II. A parental GFP-cell line (PC3-Ø cells; noninfected) is used to set up sorter conditions to discard doublets, dead cells, and autofluorescence (a). GFP+ positive cells are sorted and collected for subsequent cell culture and expansion (b)

## PC3 - TGL CELLS (infected with TGL)

**Fig. 2** (continued)

## IT INJECTION - VENTRAL VIEW

**Fig. 3** Intra-tibiae injection of PCa GFP-Luc cells. *In vivo* bioluminescent imaging is used to confirm the correct injection of cells into the mouse tibia. Signal must be detected localized at the tibia of the mouse, which is placed in a ventral position

- (c) Photographic image focus: 8.
  - (d) Luminescent image exposure time: 1 min.
  - (e) Luminescent image binning exposure: medium.
  - (f) Field of view: D position (18.5 cm from camera).
6. Repeat acquisition in ventral position for the left ventricle injection with the same IVIS acquiring conditions.

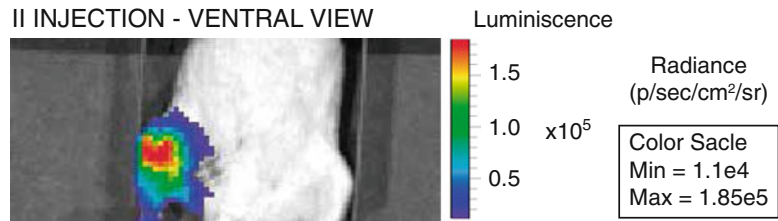


**Fig. 4** Intra-iliac injection of PCa GFP-Luc cells. In vivo bioluminescent imaging is used to confirm the correct injection of cells into the mouse tibia. The signal should be detected as spreading to the leg bones of the mouse, which is placed in ventral position

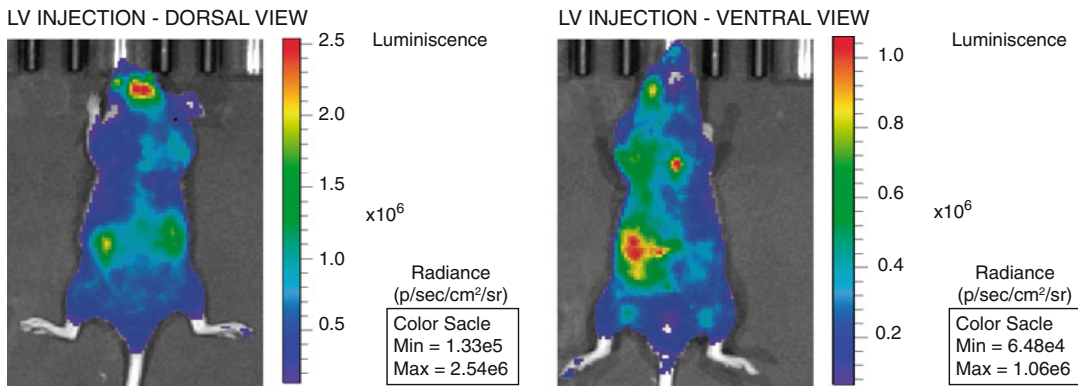


**Fig. 5** Left ventricle injection of PCa GFP-Luc cells. In vivo bioluminescent imaging is used to confirm the correct injection of cells into the mouse tibia. Signal should be detected as spreading to the whole body, with higher intensity at the kidneys when placed in dorsal position (left panel), and spreading to the body with more intensity at liver when analyzed from the ventral position

7. Take pictures every week to score the metastatic capability of different cell lines to whole body dissemination and to form metastasis (left ventricle injection), to proliferate in bone (intra-tibiae injection), or to colonize to bone and form metastasis (intra-iliac injection).
8. Quantify according to the user's manual and plot the luminescent values as a function of time (*see Note 29*).

#### 4 Notes

1. Supplements are required in cell growth media for their survival. Stick to ATCC instructions for each cell population, as requirements might vary.
2. Using a correct time of exposure to trypsin is important for collecting intact cells. Normally, 5–10 min at 37 °C is sufficient;

however, adhesion to the plate will depend on the cell type and confluence. Thus, the incubation time should be prolonged until cells detach, as per visual confirmation under the microscope.

3. Balb C/Nude mice are athymic mice that are deficient for hair, thymus, and T-cells.
4. Buprenorphine is a semisynthetic derivative of thebaine, one of the most chemically reactive opium alkaloids. Buprenorphine is used for pain management in mice and is the favored analgesia if available.
5. Luciferin is the substrate for the luciferase enzymatic reaction expressed in the injected cells. When the reaction occurs, a luminescent light appears that can be captured and measured with an IVIS system.
6. While it is also possible to let HEK-293T cells attach overnight if convenient, this is less preferred as transfection efficiency is more efficient when the cells have been freshly seeded.
7. Although built-in safety measures to prevent retrovirus replication have been taken, it is still a virus able to infect mammalian cells in a single-round. Safety precautions when working with retroviruses, such as using a biosafety cabinet, gloves, lab coats, and decontamination of waste, are strictly necessary.
8. Adding less media volume after transfection results in a higher titer of virus.
9. Media will turn orange or yellow because of acidification. Stressing cells during retroviral production does not significantly affect viral titer.
10. This step can be done the day before harvesting the virus, in order to infect cells with freshly produced viral particles.
11. You can seed several wells to increase the pool of cells, or if you expect the retroviral infection will not very efficient, you can seed with your cell lines.
12. Seal well the plates to avoid any liquid spill into the centrifuge. Alternatively, cells can be infected in 10 cm Ø culture dishes. If this is the case, avoid the centrifugation step.
13. GFP+ expression is sometimes difficult to see under the fluorescent microscope if the expression is low, but detectable when analyzed by flow cytometry. It is recommended to proceed to FACS if possible, even if GFP expression has not been verified under the microscope.
14. Adjust the PBS volume to the cell pellet and number of cells to avoid machine clumping.

15. Each cell line might need different parameters of size, shape, aggregates, and autofluorescence compensations when analyzed in a flow cytometer.
16. Seeding conditions after sorting depend on the yield obtained for each cell line. A minimum concentration of 8000 cells/cm<sup>2</sup> is recommended. A higher density is recommended for 22RV1 cells as well as for cells that do not tolerate strong dilutions when passed. Take into account that sorting considerably impairs cell viability.
17. Testing for mycoplasma is critical before cells are injected into mice, as an infection can alter cell metabolism and change gene expression in our cells, thereby reducing the reliability of our results.
18. Calculate the total number of cells needed, taking into account that two legs per mouse will be injected, and that 2× of this volume is required to avoid running out of cell suspension.
19. You will probably need to repeat the same procedure with several mice (a minimum of 5 mice is recommended to obtain robust results). In this case, inject anesthesia to each mice before to start the procedure.
20. Remember that anesthesia effects in full only lasts 10–15 min when planning the experiment.
21. It is necessary to thoroughly clean the Hamilton syringe and needle to prevent any salt precipitation.
22. Calculate the total number of cells needed, taking into account that 2× of this volume is required to avoid running out of cell suspension, due to the dead volume of the syringe.
23. The surgical or injection area must be cleaned well to prevent any possible infection.
24. It is necessary to have a 100 µl bubble between the syringe mass and the cell suspension, but ensure that no bubbles are inside the needle or in the bottom part of the syringe.
25. During heart injection in left ventricle, the heart will pump blood inside the syringe.
26. The cells will be injected into the artery, but is recommended to isolate both vessels together to save time.
27. Opening the forceps slowly gives you the opportunity to clearly expose the vessels for the injection.
28. Luciferin is the substrate for the luciferase enzymatic reaction expressed in cells injected. When the reaction occurs, luminescent light appears and can be captured and measured with the IVIS system.

29. At 24–48 h postinoculation, there is usually a dramatic reduction in luciferase activity, which eventually will return as different cell lines regrow as a lesion at the distant metastatic niche and/or proliferate to bone.

**Acknowledgments:** We thank V. Raker for manuscript editing. R.R.G. is supported by the Institució Catalana de Recerca i Estudis Avançats. Support and structural funds were provided by the Generalitat de Catalunya (2014 SGR 535) to R.R.G and by the AECC (Asociación Española Contra el Cáncer), BBVA Foundation, the ISCIII/FEDER-CIBERONC, the “la Caixa” Foundation (ID 100010434), under the agreement <HR17-00092>, the Spanish Ministerio de Economía y Competitividad (MINECO), and FEDER funds (CIBEREONC and SAF2016-76008-R) to R.R.G.

## References

1. Bray F, Ferlay J, Soerjomataram I et al (2018) Global cancer statistics 2018: GLOBOCAN estimates of incidence and mortality worldwide for 36 cancers in 185 countries. CA Cancer J Clin 68:394–424. <https://doi.org/10.3322/caac.21492>
2. Morote J, Ropero J, Planas J et al (2012) Metabolic syndrome increases the risk of aggressive prostate cancer detection. BJU Int 111:1031–1036. <https://doi.org/10.1111/j.1464-410X.2012.11406.x>
3. Chang A, Autio K, Roach M, Scher H (2014) High-risk prostate cancer-classification and therapy. Nat Rev Clin Oncol 11:308–323. <https://doi.org/10.1038/nrclinonc.2014.68>
4. Nardella C, Carracedo A, Salmena L, Pandolfi PP (2010) Faithfull modeling of PTEN loss driven diseases in the mouse. Curr Top Microbiol Immunol 347:135–168. [https://doi.org/10.1007/82\\_2010\\_62](https://doi.org/10.1007/82_2010_62)
5. Salvador F, Llorente A, Gomis RR (2019) From latency to overt bone metastasis in breast cancer: potential for treatment and prevention. J Pathol 249:6–18. <https://doi.org/10.1002/path.5292>
6. Massagué J, Obenauf AC (2016) Metastatic colonization by circulating tumour cells. Nature 529:298–306
7. James ND, de Bono JS, Spears MR et al (2017) Abiraterone for prostate cancer not previously treated with hormone therapy. N Engl J Med 377:338–351. <https://doi.org/10.1056/NEJMoa1702900>
8. Sweeney CJ, Chen Y-H, Carducci M et al (2015) Chemohormonal therapy in metastatic hormone-sensitive prostate cancer. N Engl J Med 373:737–746. <https://doi.org/10.1056/NEJMoa1503747>
9. Robinson D, Van Allen EM, Wu YM et al (2015) Integrative clinical genomics of advanced prostate cancer. Cell 161:1215–1228. <https://doi.org/10.1016/j.cell.2015.05.001>
10. Castro E, Romero-Laorden N, Del Pozo A et al (2019) PROREPAIR-B: a prospective cohort study of the impact of germline DNA repair mutations on the outcomes of patients with metastatic castration-resistant prostate cancer. J Clin Oncol 37:490–503. <https://doi.org/10.1200/JCO.18.00358>
11. Obenauf AC, Massagué J (2015) Surviving at a distance: organ-specific metastasis. Trends Cancer 1:76–91
12. Peinado H, Zhang H, Matei IR et al (2017) Pre-metastatic niches: organ-specific homes for metastases. Nat Rev Cancer 17:302–317
13. Bubendorf L, Schöpfer A, Wagner U et al (2000) Metastatic patterns of prostate cancer: an autopsy study of 1,589 patients. Hum Pathol 31:578–583. <https://doi.org/10.1053/hp.2000.6698>
14. Saad F, Olsson C, Schulman CC (2004) Skeletal morbidity in men with prostate cancer: quality-of-life considerations throughout the continuum of care. Eur Urol 46:731–740. <https://doi.org/10.1016/j.eururo.2004.08.016>
15. Hermanova I, Zúñiga-García P, Caro-Maldonado A et al (2020) Genetic manipulation of LKB1 elicits lethal metastatic prostate cancer. J Exp Med 217:e20191787. <https://doi.org/10.1084/jem.20191787>

16. Ku SY, Rosario S, Wang Y et al (2017) Rb1 and Trp53 cooperate to suppress prostate cancer lineage plasticity, metastasis, and antiandrogen resistance. *Science* 355:78–83. <https://doi.org/10.1126/science.aah4199>
17. Hubbard GK, Mutton LN, Khalili M et al (2016) Combined MYC activation and Pten loss are sufficient to create genomic instability and lethal metastatic prostate cancer. *Cancer Res* 76:283–292. <https://doi.org/10.1158/0008-5472.CAN-14-3280>
18. Magnon C, Hall SJ, Lin J et al (2013) Autonomic nerve development contributes to prostate cancer progression. *Science* 12:6142. <https://doi.org/10.1126/science.1236361>
19. Torrano V, Valcarcel-Jimenez L, Cortazar AR et al (2016) The metabolic co-regulator PGC1 $\alpha$  suppresses prostate cancer metastasis. *Nat Cell Biol* 18:645–656. <https://doi.org/10.1038/ncb3357>
20. Gomez-Cuadrado L, Tracey N, Ma R et al (2017) Mouse models of metastasis: Progress and prospects. *Dis Model Mech* 10:1061–1074



# Chapter 19

## Isolation of Nucleoli for Characterization of Nucleolar Contents to Uncover Clues to Metastatic Progression

Shannon E. Weeks and Rajeev S. Samant

### Abstract

Nucleolar isolation is a crucial technique for the study of nucleolar contents and regulation of ribosome biogenesis. Lysed cells are spun through various concentrations of sucrose and magnesium chloride to separate the notoriously dense nucleoli from the rest of the cell. Here we describe isolation of nucleoli from the breast cancer cell line MDA-MB-468. The resulting nucleolar fraction is subjected to immunoblotting to confirm the purity of the nucleolar fraction.

**Key words** Nucleolar isolation, Nucleolus, Metastasis, EMT, Ribosome Biogenesis, Cancer

---

### 1 Introduction

The nucleolus is the largest subnuclear body in the cell and is known primarily for its role in ribosome biogenesis. The nucleolus has been found to play a role in many different human pathologies, including neurological disorders, cardiovascular disease, and cancer [1]. Observations by the Italian pathologist Giuseppe Pianese in the late seventeenth century identified increased number and enlarged nucleoli as one of the first recognized hallmarks of a cancerous lesion [2]. More recent studies have found that patients who have larger and more numerous nucleoli in tumor tissue have a significantly worse prognosis than patients with smaller and less numerous nucleoli [3]. Contemporary research studies continue to support an increasingly important role of the nucleolus in oncogenesis, tumor progression, and EMT [1, 4]. Thus, this reliable nucleolar isolation technique may offer new avenues for the discovery of novel targets and conception of new strategies to treat aggressive, metastatic cancers.

Researchers have been isolating nucleoli from cells since the 1950s when K. J. Monty et al. first published “Isolation and Properties of Liver Cell Nucleoli.” However, their analysis of the

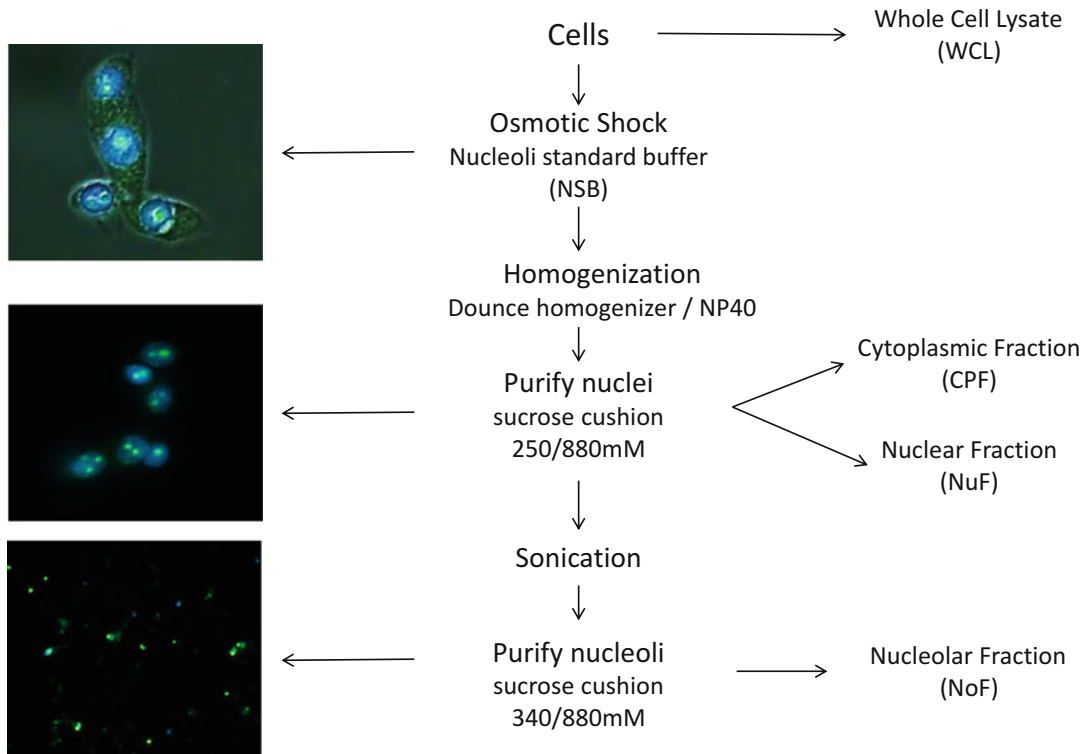


**Fig. 1** Nucleolar isolation. Schematic flowchart of the method for isolation of nucleoli. Nucleolar ID™ (Green) was used to stain nucleoli. NucBlue™ Live ReadyProbes™ reagent was used to stain nuclei

resulting nucleolar fraction was relatively limited compared to today's technical standards. Additional protocols for nucleolar isolation have been published through the years with improvements to the process being made with each adaptation [5, 6]. Nucleolar isolation involves separating lysed cells into cellular fractions by spinning them through various sucrose cushions until the dense nucleolar bodies have been isolated in a nucleolar fraction. Cells are first lysed on ice and undergo dounce homogenization before being spun through the first sucrose cushion to yield cytoplasmic and nuclear fractions. The resulting nuclear fraction is then sonicated several times to sheer the DNA around which the nucleolus forms, before being spun through one final sucrose cushion to separate the nucleolar fractions. Here we demonstrate how clean nucleoli are isolated from tissue-cultured mammalian breast cancer cells and verified for purity and enrichment using immunoblotting. For a graphical representation of this process, see Fig. 1.

---

## 2 Materials

Prepare all solutions in advance unless indicated otherwise and store at  $-20^{\circ}\text{C}$  after use. Unless stated, deionized water ( $18\text{ M}\Omega\text{-cm}$  at  $25^{\circ}\text{C}$ ) and analytical grade reagents are used. We highly recommend following all the institutional biosafety and chemical safety guidelines.

1. Freshly cultured, viable tissue culture cells grown in appropriate media, at approximately 90–95% confluence.
2. Minimum of eight 10 cm plates of cells for each condition.
3. Ice-cold PBS.
4. Three different concentrations of sucrose will be used.
  - (a) 250 mM sucrose in 10 mM MgCl<sub>2</sub>.
  - (b) 880 mM sucrose in 5 mM MgCl<sub>2</sub>.
  - (c) 340 mM sucrose in 5 mM MgCl<sub>2</sub>.
  - (d) 340 mM sucrose (*see Note 1*).

Sucrose can be prepared in advance and stored at  $-20^{\circ}\text{C}$ . Allow sucrose to thaw completely before use.

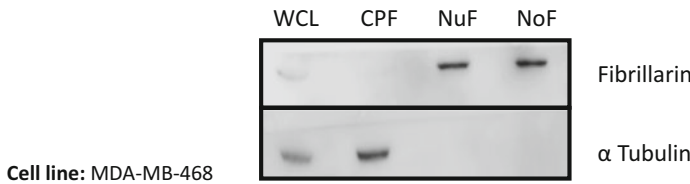
5. Nucleoli standard buffer (NSB):10 mM Tris-Cl, pH 7.4, 10 mM NaCl, 1 mM MgCl<sub>2</sub>, in water, and Halt™ Protease Inhibitor Cocktail (*see Note 2*).
6. Cell scrapers.
7. Halt™ Protease and Phosphatase Inhibitor Cocktail.
8. 15 mL conical tubes.
9. Refrigerated centrifuge.
10. 10% NP-40.
11. 0.4 mm clearance Dounce homogenizer.
12. Miconix sonicator.

---

## 3 Methods

1. Plate cells on 10 cm tissue culture-treated dishes so they will reach approximately 80% confluence within 48 h, at which point nucleoli will be harvested. For this protocol, 8 to 10 tissue culture-treated plates will be needed.
2. Once cells have reached 80% confluence, remove culture media and wash each plate three times with 3 mL of ice-cold PBS to ensure removal of serum and media, leaving a minimum amount of PBS in the dish.

3. Once dishes have been washed, collect cells using a cell scraper and transfer cells in remaining PBS (approximately 1 mL volume is obtained once cells are scraped) from the dish into a 15 mL conical tube on ice.
4. Repeat **steps 2** and **3** until all plates have been washed and pooled in the conical tube. (approximately 10–12 mL will be collected from 10 plates).
5. Pellet cells in centrifuge at 4 °C for 5 min at  $500 \times g$ .
6. Once cells are pelleted, remove supernatant and add 4 mL of NSB (with Halt™: 1× final concentration) for every 10 plates scraped.
7. Incubate cells on ice for 30 min, mixing every 5–10 min.
8. Collect 250 µL sample of cell mixture and store at –80 °C. This is the whole cell fraction (WCF).
9. Lyse remaining cells by adding NP-40 to a final concentration of 0.3%.
10. Invert tube several times to ensure thorough mixing and then decant cell mixture into a Dounce homogenizer with a tight pestle.
11. Homogenize cells with homogenizer for 40–60 strokes or until all cells have been ruptured and separated from the nuclei. Check under inverted microscope. *See Fig. 1* for images of ruptured cells. (Note: fluorescence microscope will be required if the Nucleolar ID™ stain is used as in the Fig. 1).
12. Transfer homogenate into conical tube and spin at 4 °C for 10 min at  $1200 \times g$  to pellet the nuclei.
13. Collect supernatant and store at –80 °C. This is the cytoplasmic fraction (CPF).
14. Resuspend nuclear pellet in 2 mL of 250 mM sucrose in 10 mM MgCl<sub>2</sub> and carefully underlay 2 mL of 880 mM sucrose in 5 mM MgCl<sub>2</sub>.
15. Purify nuclei by centrifuging through the 880 mM sucrose cushion for 10 min at  $1200 \times g$  at 4 °C.
16. Remove supernatant and resuspend purified nuclear fraction in one [1] mL 340 mM sucrose with 5 mM MgCl<sub>2</sub>.
17. Using a light microscope, inspect a drop of the nuclear fraction to ensure that it is devoid of cytoplasmic debris. Please *see Fig. 1* for images of NuF.
18. Keep aside 200 µL sample containing intact nuclei, at –80 °C. This is the nuclear fraction (NuF).
19. Shear remaining NuF using sonication. Sonicate using Misonix, Microson ultrasonic cell disruptor, on setting 5 (5 W) for 10-s bursts with 1 min on ice between bursts (*see Note 3*). The



**WCL:** Whole cell lysate **CPF:** Cytoplasmic Fraction **NuF:** Nuclear Fraction **NoF:** Nucleolar Fraction

**Fig. 2** Western blot analysis for confirmation of nucleolar isolation. Protein samples from whole cell lysate (WCL), cytoplasmic fraction (CPF), nuclear fraction (NuF), and nucleolar fraction (NoF) were resolved using 12% SDS-PAGE. Fibrillarin is an exclusively nucleolar protein. Thus, it is seen in WCL (faint band). NuF and NoF show a noticeable enrichment of fibrillarin whereas it is absent (excluded from) in CPF. Tubulin  $\alpha$  is an exclusively cytoplasmic protein. Thus, it is seen in WCL and CPF but is absent in NuF and NoF

number of bursts will vary depending on cell line. Check a small drop of sonicated lysate under a light microscope to confirm that nuclei are completely lysed. Nucleoli should appear as dark refractile bodies that are devoid of the surrounding nuclei. Fig. 1 shows images of nucleoli separated from nuclei.

20. Add 1 mL of 880 mM sucrose in 5 mM MgCl<sub>2</sub> to a conical tube and gently layer the sonicated NuF on top of the sucrose cushion. Pellet the dense nucleoli through the cushion by centrifuging at 4 °C for 20 min at 2000  $\times \text{g}$ .
21. Remove supernatant and resuspend nucleolar fraction (NoF) in 500  $\mu\text{L}$  of 340 mM sucrose or in PBS depending on intended experiment (*see Note 4*). Verify that the NoF is devoid of any intact nuclei using light microscopy. Halt™ Protease Inhibitor Cocktail (1× final concentration) should be added to the NoF at this time.
22. Store samples at –80 °C until ready for analysis.
23. Validate purity of nucleolar fraction using immunoblotting. The NuF and NoF should be devoid of tubulin which should be easily visualized in the WCL and CPF. Fibrillarin should be easily visualized in the NuF and NoF and to some extent in the WCL but should be absent in the CPF. *See Fig. 2* for an example of Western blot assessment of nucleolar fraction.

#### 4 Notes

1. Sucrose solutions can be stored at –20 °C between experiments.
2. NBS can be prepared in advance without the addition of the protease inhibitor. Halt™ (Protease Inhibitor) should be added fresh at each use.

3. Sonication intensity and number of rounds of sonication will vary depending on machine and cell line.
4. For nucleolar proteomics, it is typically recommended to resuspend NoF in PBS with halt inhibitor.

## References

1. Weeks SE, Metge BJ, Samant RS (2019) The nucleolus: a central response hub for the stressors that drive cancer progression. *Cell Mol Life Sci* 76(22):4511–4524. <https://doi.org/10.1007/s00018-019-03231-0>
2. Ruggero D (2012) Revisiting the nucleolus: from marker to dynamic integrator of cancer signaling. *Sci Signal* 5(241):pe38. <https://doi.org/10.1126/scisignal.2003477>
3. Derenzini M, Montanaro L, Trere D (2009) What the nucleolus says to a tumour pathologist. *Histopathology* 54(6):753–762. <https://doi.org/10.1111/j.1365-2559.2008.03168.x>
4. Prakash V, Carson BB, Feenstra JM, Dass RA, Sekyrova P, Hoshino A, Petersen J, Guo Y, Parks MM, Kurylo CM, Batchelder JE, Haller K, Hashimoto A, Rundqvist H, Condeelis JS, Allis CD, Drygin D, Nieto MA, Andang M, Percipalle P, Bergh J, Adameyko I, Farrants AO, Hartman J, Lyden D, Pietras K, Blanchard SC, Vincent CT (2019) Ribosome biogenesis during cell cycle arrest fuels EMT in development and disease. *Nat Commun* 10(1):2110. <https://doi.org/10.1038/s41467-019-10100-8>
5. Busch H, Muramatsu M, Adams H, Steele WJ, Liau MC, Smetana K (1963) Isolation of nucleoli. *Exp Cell Res* 24(SUPPL9):150–163
6. Hacot S, Coute Y, Belin S, Albaret MA, Mertani HC, Sanchez JC, Rosa-Calatrava M, Diaz JJ (2010) Isolation of nucleoli. *Curr Protoc Cell Biol*. Chapter 3:Unit3 36. <https://doi.org/10.1002/0471143030.cb0336s47>



# Chapter 20

## Analyzing the Role of Proteases in Breast Cancer Progression and Metastasis Using Primary Cells from Transgenic Oncomice

Olga Vasiljeva, Lisa Sevenich, and Thomas Reinheckel

### Abstract

It is becoming increasingly evident that progression and metastasis of solid cancers is driven by the interaction of oncogene-transformed cancer cells and non-malignant host cells in the tumor stroma. In this process, the immune system contributes a complex set of highly important pro- and antitumor effects, which are not readily recapitulated by commonly used xenograft cancer models in immunodeficient mice.

Therefore, we provide protocols for isolation of primary tumor cells from the MMTV-PymT mouse model for metastasizing breast cancer and their resubmission to congenic immunocompetent mice by orthotopic transplantation into the mammary gland or different routes of injection to induce organ-specific experimental metastasis, including intravenous, intracardiac, and caudal artery injection of tumor cells. Moreover, we describe protocols for sensitive detection and quantification of the metastatic burden.

**Key words** Breast cancer, Cathepsin, Experimental metastasis, Lung metastasis, Brain metastasis, Bone metastasis, Mammary adenocarcinoma, Mouse model, Orthotopic transplantation, Polyoma virus middle T antigen, Protease

---

### 1 Introduction

Proteases contribute to invasion and metastasis of solid malignancies by degradation of extracellular matrix proteins and by release of bioactive peptides. Proteases derived from malignant cells have primarily been in the focus of research. More recent results indicate, however, that cells of the tumor stroma produce proteolytic enzymes as well. These activate the tumor microenvironment and propagate invasion and metastasis of cancer cells. In particular, tumor-associated immune cells, i.e., macrophages, promote proliferation and invasion of malignant cells in several mouse models of human cancer.

---

Olga Vasiljeva and Lisa Sevenich contributed equally to this work.

It is remarkable that the human genome encodes for more than 500 proteolytic enzymes [1]. Among them, the protease family C1a comprises 11 cysteine proteases known as cysteine cathepsins, i.e., cathepsins B, C, F, H, K, L, L2/V, O, S, W, and X/Z [2]. In order to elucidate the *in vivo* functions of these enzymes, our lab generated and analyzed multiple mouse lines with deficiencies in cysteine cathepsins as well as cell-type specific transgenic expression of these proteases [3]. These approaches provided evidence for nonredundant, cell-type specific functions for cysteine cathepsins in physiological and pathological processes. Cathepsins have been shown to participate in tumor progression through degradation of extracellular matrix components and modulation of signal transduction pathways that can be also executed through shedding of receptors and adhesion molecules [4]. Numerous clinical data are providing evidence for an association of enhanced cysteine cathepsin expression with poor prognosis of specific malignancies, e.g., mammary cancer. The results of these epidemiological investigations justify detailed analyses of the roles of cathepsins in cancer initiation and progression. Therefore, we crossed several established mouse cancer models with cathepsin-deficient or overexpressing human protease mouse lines and analyzed tumor progression and metastasis in detail [5–14].

For these studies, we often used the transgenic MMTV-PymT model of metastasizing breast cancer. In these mice, the polyoma virus middle T oncogene (PymT) is selectively expressed in mammary epithelial cells under transcriptional control of the mouse mammary tumor virus (MMTV) long terminal repeat (LTR) [15]. Expression of the PymT transgene results in a progression of the neoplasms from benign lesions to invasive carcinomas that can be classified into distinct histopathological stages with similarities to human tumors (Fig. 1). Atypical ductal hyperplasia, which is the first pathological alteration that occurs, is still benign. Ductal carcinoma *in situ* represents a premalignant stage in which the basement membrane is still intact. Breakdown of the basement membrane marks the transition to invasive ductal adenocarcinomas (IDC) (Fig. 1). According to the human histopathology, IDCs can be further categorized as “well differentiated” (G1), “moderately differentiated” (G2), and “poorly differentiated” (G3) with respect to cellular atypia such as tubular formation, nuclear polymorphism, and rate of mitosis [16]. At ~14 weeks of age, all female MMTV-PymT mice exhibit large and mostly poorly differentiated IDCs in each of their ten mammary glands. In contrast to human breast cancer in which metastases are broadly distributed throughout the organism, MMTV-PymT-induced carcinomas almost exclusively metastasize to the lungs. First micro-metastases can be observed microscopically at around 10 weeks of age. With 14 weeks of age, 100% of female mice bear lung metastases. Recent studies also detected metastatic foci in the lymphatic system [17] as well as

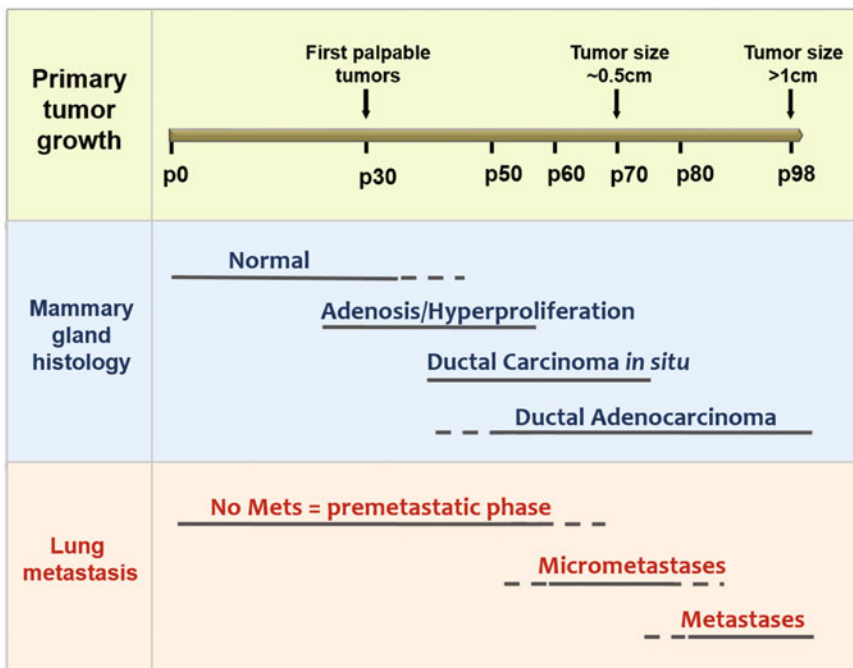


**Fig. 1** Kinetics of tumor growth and lung metastasis in the MMTV-PymT mouse model for breast cancer. Tumor growth data are based on palpation and caliper measurements. Histopathological evaluation was according to Elston and Ellis [16], and assessments of metastasis are based on histology and PymT expression in the lung. p (postpartum) denotes the age in days

disseminated tumor cells in the bone marrow [18]. Experimentally induced organ-specific metastasis models represent valuable tools to expand the scope of metastasis research to organ sites other than the lungs, such as the brain or the bone [12, 19, 20]. Experimentally induced metastasis models are based on different routes of tumor cell inoculation and/or the *in vivo* selection of cell variants with high tissue tropism to specific organs [21–23] (Fig. 2).

Moreover, experimental and clinical studies emphasize the impact of tumor-associated inflammation. Tumor progression of PymT-induced carcinomas is accompanied by sustained infiltration of immune cells such as macrophages, mast cells, and T- and B cells. The role of tumor-associated macrophages (TAMs) is one major focus of current research. It was reported that tumor progression and metastasis of PymT-induced carcinomas is dependent on TAMs [24–26].

In order to study the function of ubiquitously expressed proteins, such as cysteine cathepsins, in the multiple tumor–host interactions during the complex pathogenesis of breast cancer in the MMTV-PymT model, it is often desirable to delete the protein of interest in one cell type, while all other cell types do express it. In principle, this can be achieved by conditional gene targeting or

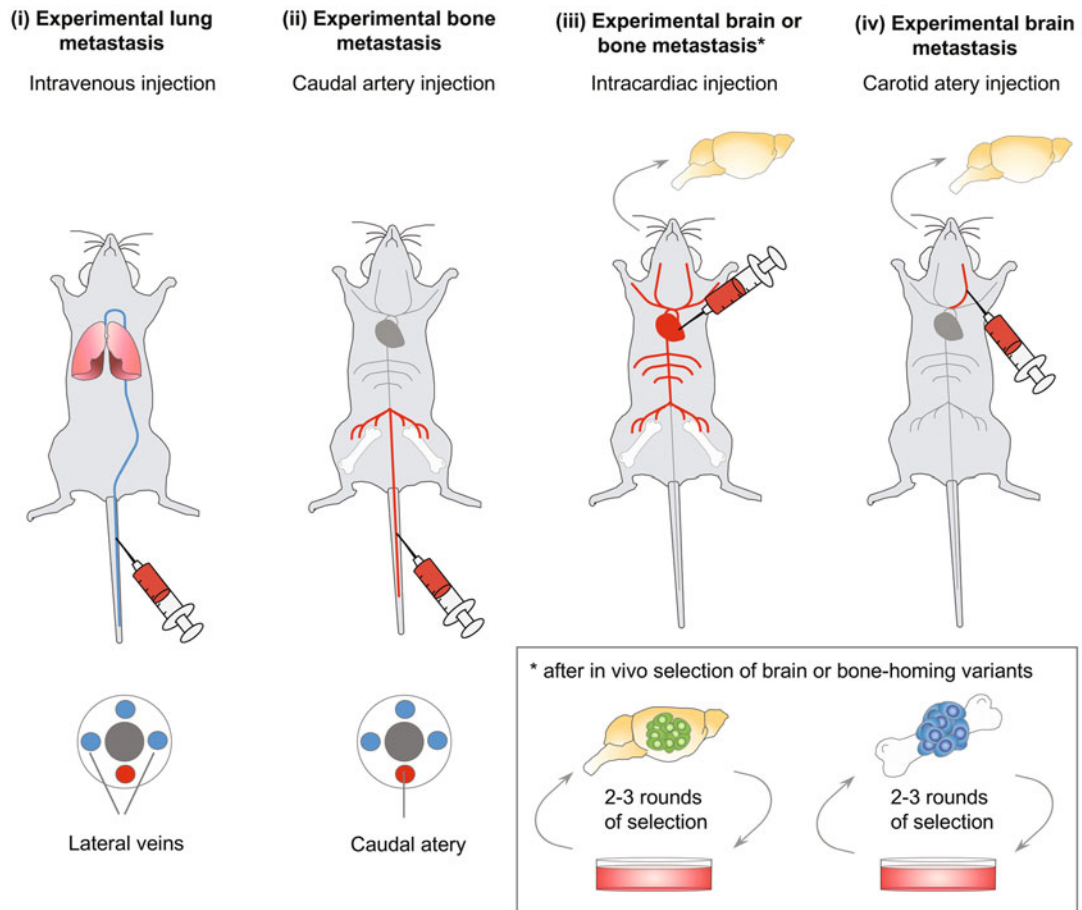


**Fig. 2** Models of experimentally induced metastasis. Schematic of the injections route to induce experimental metastasis to the lungs, the bone, and the brain. Intravenous injection into the lateral tail veins (**i**) results in dissemination of tumor cells predominantly to the lungs, while injection into the caudal artery, (**ii**) delivers tumor cells to the bone marrow of the hind limbs. Intracardiac injection into the left ventricle (**iii**) results in tumor cell dissemination throughout the circulation and gives rise to experimental brain and bone metastasis. Rounds of in vivo selection are needed if cell variants with high tissue tropism to the brain or the bones are desired. Injection into the carotid artery (**iv**) predominantly delivers tumor cells to the brain

transgenesis; however, the appropriately targeted alleles are often not available yet [27]. On the other hand, human cancer cells are often applied to immune-deficient mice (i.e., SCID or *Nude* mice) in a so-called xenograft approach. However, important tumor–host interactions may be impaired in the immunodeficient animals. To address this limitation, a variety of immunologically humanized mouse models have been recently generated and applied in biomedical research [28, 29]. Notably, the injection of mouse cancer cells into recipient to congenic immunocompetent host mice of the same genetic background does not face the challenge of immunological graft rejection. Therefore, these syngeneic allograft models

have been instrumental for the research of host responses to a cancer. In combination with “knockout” or transgenic mice as hosts or source of the cancer cells, these models are powerful tools for functional analysis of proteins involved in tumor–host interactions during cancer development and metastasis.

Here we provide protocols for isolation of primary PymT tumor cells from the MMTV-PymT cancer model, the selection of PymT cell variants with high tropism for specific organ sites, and the resubmission of the PymT cells to congenic immunocompetent mice by intravenous, intracardiac, or caudal artery injection as well as by orthotopic transplantation into the mammary gland fat pad. For more precise tumor cell homing, we describe methods for selection of variants with high tropism for specific organ sites. Moreover, protocols for sensitive detection and quantification of metastatic burden are described.

---

## 2 Materials

### 2.1 Primary PymT Cell Preparation

1. Enzyme cocktail, 5 ml DNase I Type IV (0.25 mg/ml, Sigma, Germany), 5 ml hyaluronidase Type I-S (1 mg/ml, Sigma), 5 ml crude collagenase type IV (6 mg/ml, Sigma), all enzymes diluted in PBS and filter-sterilized (0.22 µm), store 5 ml aliquots at -20 °C.
2. 100 µm and 40 µm [cell strainers](#).
3. Dulbecco’s phosphate-buffered saline (DPBS).
4. Dulbecco’s Modified Eagle Medium (DMEM) supplemented with 10% fetal bovine serum (FBS), 2 mM L-glutamine, 100 units penicillin, 100 µg/ml streptomycin.
5. Freezing medium, complete DMEM with 10% [dimethyl sulfoxide \(DMSO\)](#), keep on ice.
6. Trypsin-EDTA, 0.05% trypsin, 0.01% EDTA.
7. T-175 cm<sup>2</sup> culture flasks.
8. Glass Pasteur pipettes.
9. 50 ml PP-Test Tubes.

### 2.2 Transplantation into Mammary Gland

1. Primary PymT-tumor cells (isolated according to Subheading 3.1).
2. Complete DMEM (*see* Subheading 2.1).
3. Standard Matrigel™ (Corning Life Sciences).
4. Phosphate-buffered saline (PBS), pH 7.2.
5. Trypsin-EDTA, 0.05% trypsin, 0.01% EDTA.
6. Anesthetics: Ketamine (50 mg/ml), xylazine (5 mg/ml) in sterile 0.9% NaCl.

7. T-75 cm<sup>2</sup> cell culture flask.
8. Glass Pasteur pipettes.
9. 15 ml PP-Test Tubes.
10. Syringes 1 ml.
11. Stainless steel wound (7.5 × 1.75 mm; type Michel) clips and remover.
12. Needles, 0.46 × 16 mm.

### **2.3 Experimental Lung Colonization**

1. Complete DMEM (*see* Subheading 2.1).
2. Phosphate-buffered saline (PBS), pH 7.2.
3. Trypsin-EDTA, 0.05% trypsin, 0.01% EDTA.
4. T-75 cm<sup>2</sup> cell culture flask.
5. 15 ml PP-Test Tubes.
6. Syringe, 1 ml.
7. Disposable injection needle (G 26 × 1/2"; ø 0.45–12 mm).

### **2.4 Brain-Homing Variants of PymT Tumor Cells**

1. Complete DMEM (*see* Subheading 2.1).
2. Phosphate-buffered saline (PBS), pH 7.2.
3. Trypsin-EDTA, 0.05% trypsin, 0.01% EDTA.
4. T-75 cm<sup>2</sup> cell culture flask.
5. 15 ml PP-Test Tubes.
6. 1.5 ml reaction tubes.
7. Syringes 1 ml.
8. Disposable injection needle (G 26 × 1/2"; ø 0.45–12 mm).

### **2.5 Experimental Brain Colonization**

1. Complete DMEM (*see* Subheading 2.1).
2. Phosphate-buffered saline (PBS), pH 7.2.
3. Trypsin-EDTA, 0.05% trypsin, 0.01% EDTA.
4. T-75 cm<sup>2</sup> cell culture flask.
5. 15 ml PP-Test Tubes.
6. 1.5 ml reaction tubes.
7. Syringes 1 ml.
8. Disposable injection needle (G 26 × 1/2"; ø 0.45–12 mm).

### **2.6 Experimental Bone Colonization**

1. Complete DMEM (*see* Subheading 2.1).
2. Phosphate-buffered saline (PBS), pH 7.2.
3. Trypsin-EDTA, 0.05% trypsin, 0.01% EDTA.
4. T-75 cm<sup>2</sup> cell culture flask.
5. 15 ml PP-Test Tubes.

6. 1.5 ml reaction tubes.
7. 1 ml insulin syringe (29G) 0.33 mm × 12.7 mm.

### **2.7 Metastatic Burden by Quantitative PCR**

1. MyiQ™ Single-Color Real-Time PCR Detection System (Bio-Rad Laboratories; *see Note 1*).
2. SYBR Green PCR Master Mix (Invitrogen).
3. Primer PymT, 5-CTCCAACAGATACACCCGCACATACT-3 (fw), 5-GCTGGTCTTGGTCGCTTCTGGATAC-3 (rev).
4. Primer GAPDH, 5- TGCACCACCAACTGCTTAG -3 (forward), 5-GATGCAGGGATGATGTTC-3 (reverse).
5. Primer β-actin, 5' ACCCAGGCATTGCTGACAGG 3' (forward), 5'GGACAGTGAGGCCAGGATGG 3' (rev).
6. DNA isolation DNeasy kit (Qiagen, Valencia, CA), alternatively Wizard SV Genomic DNA purification system (Promega).
7. 96-well optical reaction plate.
8. Optical adhesive covers.

### **2.8 Analysis of Metastases by Histology**

1. Phosphate-buffered saline (PBS), pH 7.2.
2. 4% formaldehyde (FA) in PBS.
3. 70% ethanol (EtOH).
4. 10% EDTA pH 7.4.
5. For H&E staining: Xylene, Ethanol: absolute; 96%; 90%; 70%; and 50%, Mayer's Hematoxylin: 1:4 diluted in tap water: nucleus staining: blue, Eosin: 1% in ddH<sub>2</sub>O, 50–100 µl glacial acetic acid: cytoplasm staining: red/pink.
6. Entellan (Merck).
7. Axioskop 2 (Zeiss, Germany).
8. Axiovert LE Rel. 4.4 software (Zeiss, Germany).

## **3 Methods**

### **3.1 Isolation of Primary Tumor Cells from MMTV-PymT-Induced Mammary Carcinomas (See Note 2)**

1. Sacrifice one female MMTV-PymT transgenic mouse with a large tumor burden (i.e., 14 weeks of age).
2. Remove the entire tumor mass from the mammary gland by separating the tumors from the skin and the abdominal wall with tweezers and scalpel (*see Note 3*).
3. Cut the tumor material into small chunks with a sterile disposable scalpel no. 10 and transfer it to a 50 ml Falcon tube.
4. Add 30 ml PBS and gently mix with a pipette.

5. Centrifuge the mixture at  $1200 \times g$  for 5 min at room temperature and discard the supernatant.
6. Repeat steps **4** and **5** twice.
7. Add the enzyme cocktail to the pellet and resuspend it.
8. Transfer the suspension in a sterile glass beaker with glass beads and a magnetic stirring bar and incubate on a magnetic plate stirrer at  $37^\circ\text{C}$  for 1 h.
9. Transfer the suspension with a pipette sequentially through 100- $\mu\text{m}$  and 40- $\mu\text{m}$  cell strainers into a clean 50 ml Falcon tube.
10. Centrifuge at  $290 \times g$  for 5 min at room temperature and discard the supernatant.
11. Add 30 ml PBS and gently mix with a pipette.
12. Centrifuge the mixture at  $290 \times g$  for 5 min at room temperature and discard the supernatant.
13. Repeat steps **11** and **12** once.
14. Resuspend the pellet in 30 ml of cell culture medium.
15. Plate the cells suspension in three T-175  $\text{cm}^2$  culture flasks (each flask 10 ml) with another 30 ml of cell culture medium added in each flask.
16. The three flasks are incubated overnight in a conventional incubator for cell culture with 5%  $\text{CO}_2$  at  $37^\circ\text{C}$  (*see Note 4*).
17. On the next day, remove the medium and wash the cells with PBS twice.
18. Add 3 ml of trypsin-EDTA per culture flask and incubate for 10 min with 5%  $\text{CO}_2$  at  $37^\circ\text{C}$  to detach the cells.
19. Stop the trypsin treatment by adding 10 ml of complete DMEM.
20. Transfer the cell suspension into a clean 50 ml Falcon tube.
21. Count cells using trypan blue staining to exclude dead cells.
22. Centrifuge the cell suspension for 5 min at  $290 \times g$  at room temperature.
23. Discard the supernatant and resuspend cells in freezing medium to a concentration of  $2 \times 10^6$  cells/ml.
24. Aliquot cells suspension into cryogenic storage vials. Use 1 ml per vial.
25. Freeze the cells at  $-70^\circ\text{C}$ , and then transfer to liquid nitrogen storage freezer (*see Note 5*).

**3.2 Orthotopic Transplantation of Primary PymT-Derived Tumor Cells into Mammary Gland of Congenic Mice (See Note 6)**

1. Rapidly thaw  $4 \times 10^6$  primary PymT tumor cells (isolated according to Subheading 3.1). Remove the remaining DMSO from the freezing medium by washing the cells twice with PBS before plating (*see Note 7*).
2. Plate the cells in one T-75 cm<sup>2</sup> culture flask in 12 ml of complete DMEM and culture the cells with 5% CO<sub>2</sub> at 37 °C.
3. When cells are 70–90% confluent (i.e., after 48 h), remove medium and wash cells twice with PBS.
4. Add 1 ml of trypsin–EDTA and incubate for 10 min with 5% CO<sub>2</sub> at 37 °C to detach the cells.
5. Stop the trypsin treatment by adding 6 ml of complete DMEM.
6. Transfer the cell suspension into a clean 15 ml Falcon tube.
7. Count cells using trypan blue staining to exclude dead cells.
8. Centrifuge the cell suspension for 5 min at 290 × g at room temperature.
9. Discard the supernatant and resuspend cells in ice-cold PBS; e.g.,  $2 \times 10^6$  cells/100 µl.
10. Supplement the cell suspension with an equal volume of ice-cold Matrigel™; cell concentration is now  $1 \times 10^6$ /100 µl; store on ice.
11. Induce anesthesia by i.p. injection of 100 µg ketamine + 10 µg xylazine per g animal weight; i.e., inject 40 µl of the premade ketamine/xylazine solution in a 20 g animal.
12. Shave and sterilize the operation area, i.e., left inguinal mammary gland, of the congenic recipient mice (i.e., FVB/N mouse strain) with ethanol.
13. Set a 3–5 mm transversal skin cut and advance the adipose mammary tissue carefully (*see Note 8*).
14. Mix cells and draw about 60 µl cell suspension into a 1 ml syringe without a needle (*see Note 9*).
15. Add a 30-gauge needle to the loaded syringe. Place slowly 50 µl cells (i.e.,  $5 \times 10^5$ ) on the advanced breast tissue of the recipient mouse.
16. Relocate the tissue and close the skin wound by a clip.
17. Remove clip after 7 to 10 days after cell transfer.
18. Tumor diameters are measured with digital calipers, and the tumor volume in mm<sup>3</sup> is calculated by the formula: Volume =  $(a \times b^2)\pi/6$ , where *a* and *b* equal the longer and shorter diameter of the tumor (*see Note 10*).

**3.3 Experimental****Lung Colonization****in Congenic Mice****Using Primary****PymT-Derived Tumor****Cells (See Note 11)**

1. Perform steps 1–8 of Subheading 3.2.
2. Discard the supernatant and resuspend the cells in a volume to give  $2 \times 10^5$  cells in 300  $\mu\text{l}$  PBS per injection (see Note 12).
3. Draw 300  $\mu\text{l}$  of the cell suspension into a 1 ml syringe and attach a 26G needle.
4. Inoculate  $2 \times 10^5$  cells in 300  $\mu\text{l}$  PBS into the tail vein of congenic recipient mice (see Notes 13 and 14).
5. Twenty-one days after tumor cell inoculation sacrifice the mice by PBS perfusion and isolate lungs (see Note 15).
6. Snap-freeze the entire left lobe from each lung in liquid nitrogen for DNA isolation in order to quantify metastatic burden (see Subheading 3.4).
7. To evaluate the volume of lung colonies, the amount of the PymT transgene in genomic DNA from lungs of animals after PymT cell injection can be quantified by quantitative real-time PCR (see Subheading 3.4).
8. The right lung lobes are fixed in 4% FA for 24 h in the dark and subsequently transferred into 70% ethanol prior to paraffin embedding for analyses of lung colonies by histology (see Subheading 3.5).

**3.4 Generation****of Brain-Homing****Variants from****MMTV-PymT Tumor****Cells (See Notes 16–18)**

1. Perform steps 1–5 of Subheading 3.2.
2. Transfer the cells in to 15 ml PP-Tube.
3. Count the cells using trypan blue staining to exclude dead cells.
4. Centrifuge the cell suspension for 5 min at  $290 \times g$  at room temperature.
5. Discard the supernatant and resuspend the cells in a volume to give  $5 \times 10^6$  cells in 1 ml complete DMEM.
6. Transfer 100  $\mu\text{l}$  of the cell suspension into a 1.5 ml reaction tube.
7. Directly before the injection add 900  $\mu\text{l}$  of PBS to the cell suspension and mix thoroughly (see Note 19).
8. Draw 300  $\mu\text{l}$  of the cell suspension into a 1 ml syringe and attach a 26-gauge needle (see Note 20).
9. Clean the chest of the mouse with 70% EtOH (see Note 21).
10. Inoculate 200  $\mu\text{l}$  ( $=1 \times 10^5$  cells) into the left ventricle of an anesthetized mouse (see Notes 22–24).
11. Sacrifice mice 8 weeks after tumor cells inoculation by PBS perfusion and collect the brain (see Note 25).
12. Cut the brain into small pieces using a disposable scalpel (No 10) and transfer the tissue into a 50 ml PP-Tube.

13. Perform **steps 4–14** from Subheading 3.1 to isolate tumor cells from the brain.
14. Plate cells in a T-75 cm<sup>2</sup> flask in 15 ml complete DMEM and let grow to 70–90% confluence.
15. Perform 2–3 rounds of in vivo selection to derive brain-homing variants (*see Note 17*).
16. Cryopreserve the in vivo selected brain-homing variants of the MMTV-PymT tumor cells for further use (*see Note 26*).

### **3.5 Experimental**

#### **Brain Colonization in Congenic Mice by Intracardiac Injection**

1. Perform **steps 1–11** from Subheading 3.4.
2. Snap-freeze one hemisphere of the brain in liquid nitrogen for DNA isolation in order to quantify metastatic burden (*see Subheading 3.6*).
3. Transfer the other brain hemisphere into 4% FA for 24 h in the dark and subsequently transfer the tissue into 70% ethanol before paraffin embedding for analyses of lung colonies by histology (*see Subheading 3.7*).

### **3.6 Experimental**

#### **Bone Colonization in Congenic Mice by Caudal Artery Injection**

1. Perform **steps 1–4** from Subheading 3.4.
2. Discard the supernatant and resuspend the cells in a volume to give  $1 \times 10^5$  cells in 1 ml complete DMEM.
3. Transfer 100  $\mu$ l of the cell suspension into a 1.5 ml reaction tube.
4. Directly before the injection, add 900  $\mu$ l of PBS to the cell suspension and mix thoroughly.
5. Draw 200  $\mu$ l of the cell suspension into an insulin syringe with a 29-gauge needle.
6. Clean the tail of the mouse with 70% ethanol.
7. Inoculate 200  $\mu$ l ( $=2 \times 10^4$  cells) into the caudal artery of a pre-warmed mouse (*see Note 12*).
8. Sacrifice mice 3–4 weeks after tumor cell inoculation by PBS perfusion and collect the bones (*see Note 27*).
9. Snap-freeze one bone in liquid nitrogen and also **one complete** lung in liquid nitrogen for DNA isolation in order to quantify metastatic burden (*see Subheading 3.7*).
10. Transfer the other bone into 4% FA for 24 h in the dark. Subsequently incubate the bone in 10% EDTA pH 7.4 for 1 week for decalcification before transferring it into 70% ethanol prior to paraffin embedding for analyses of lung colonies by histology (*see Subheading 3.8*).

**3.7 Measurement of Lung, Brain, and Bone Metastatic Burden by Quantitative Real-Time PCR (See Note 15)**

1. For quantification of the PymT transgene in experimentally induced metastases or metastases derived from orthotopic transplantation experiments, isolate genomic DNA from lungs, brain, or bones of PymT cell-recipient mice following the kits instructions.
2. Determine the concentration and purity of genomic DNA by the spectrophotometric measurements of the absorbance at 260 nm ( $A_{260}$ ) and ratio between the readings at 260 nm and 280 nm ( $A_{260}/A_{280}$ ), respectively.
3. Setup the experiment, calculate how many reactions you have for each primer set (including the controls) and design a plate template to indicate the reaction that will occur in each well (see Note 1).
 

Each sample is analyzed for (see Note 28):

  - (a) Quantity of the PymT transgene (triplicate; see Note 29).
  - (b) Quantity of the housekeeping gene (triplicate; see Note 30).
  - (c) Include appropriate controls, i.e., a “no template control” (NTC) containing double-distilled sterile water instead of DNA during the amplification step.
4. Prepare a master mix for each primer set; the master mix for one reaction consists of:
  - (a) 12.5  $\mu$ l SYBR green dye.
  - (b) 1.0  $\mu$ l primer pair mix (5 pmol each primer).
  - (c) 1.5  $\mu$ l ddH<sub>2</sub>O.
  - (d) Total volume: 15  $\mu$ l.
5. Add 15  $\mu$ l of the master mix to each well of the 96-well plate.
6. Add 10  $\mu$ l DNA (see Note 29) or ddH<sub>2</sub>O (NTC) per each well, so that the total volume is 25  $\mu$ l. Make sure that you do not cross contaminate your samples.
7. Quickly seal the plate with adhesive cover after pipetting is complete and protect from light.
8. Spin down the reactions in the plate to collect all liquid at the bottom of the plate prior to putting the plate into the qPCR machine. Make sure that the wells are free of bubbles (see Note 30).
9. Create a new template and set up the qPCR program. Default parameters are as follows:
  - (a) 95 °C—15 min.
  - (b) 95 °C—15 s.
  - (c) 60 °C—30 s (modify this if needed for each primer set).
  - (d) 72 °C—30 s.

- (e) Repeat **steps 2** and **4** for 50 cycles.
  - (f) 95 °C—1 min.
  - (g) 55 °C—1 min.
  - (h) Every 10 s increase by 0.5 °C repeated for 80 cycles (to obtain the data for the dissociation curve).
10. Place the plate in the sample block, close lid and run the program.
  11. When the machine has finished cycling, save the data before quitting.
  12. Analyze the real-time PCR data using manufacturer's software (see **Note 1**) and examine the PCR specificity by agarose gel to confirm single correct product.
  13. Normalize the relative amounts of PymT DNA to the levels of housekeeping genes (GAPDH or β-actin; *see Note 28*).

### **3.8 Analysis of Tumor Cell Dissemination to the Lungs, the Brain, and the Bone by Histology**

1. Mice are perfused with PBS via the heart; lung lobes, brain or bone are excised and subsequently fixed in 4% FA for 24 h in the dark and subsequently transferred into 70% EtOH (*see Note 14*). After fixation, the lung lobes or brain hemisphere are dehydrated and paraffin embedded. Bone samples require decalcification via 10% EDTA pH 7.4 treatment for 1 week prior to ethanol fixation and paraffin embedding.
2. For systematic and randomized sampling of lung and brain sections, three sectional planes are chosen as follows. The samples are trimmed by 30 µm sections till the organ is cut. Starting from that sectional plane twelve 5 µm sections are cut from which the first section is taken for H&E staining. Further seven 30 µm sections are cut and discarded followed by twelve 5 µm sections from which the first section is again taken for H&E staining. This procedure is repeated one more time to achieve three independent sectional planes. For bone sections, samples are trimmed by 30 µm sections until the organ is cut. Starting from that sectional plane twelve 5 µm sections are cut from which the first section is taken for H&E staining. Repeat this step two more times without additional trimming. The sections are H&E stained according to the standard protocol.
3. Dewax the sections in 4 changes of xylene for 5 min.
4. Transfer the slides into a descending ethanol series (3 × 1 min absolute ethanol; 1 × 1 min 96% ethanol; 2 × 1 min 70% ethanol; and 2 × 1 min 50% ethanol) and 1 min in deionized water to rehydrate the sections.
5. After the staining of the nucleus in hematoxylin for 5 min, wash the slides under running water for 15 min to blue the tissue sections.

6. Place sections into eosin for 1 min to stain the cytoplasm.
7. Wash slides 2× 1 min in 50% ethanol and transfer sections into an ascending ethanol series (2× 1 min 70% ethanol; 1× 1 min 90% ethanol; 1× 1 min 96%; and 3× 1 min absolute ethanol) to dehydrate the sections.
8. Incubate the sections in xylene 4× 5 min.
9. Cover the slides moistly with 3 drops of Entellan.
10. Let the slides dry at room temperature.
11. Systematic images are taken by Meander sampling using a light microscope with a 2.5× objective. The number of lung metastases is counted on the three non-serial sections and the mean value is taken.
12. Using the tool “contour” of the Axiovert LE Rel. 4.4 software, the area of lung tissue and the area of metastases are estimated.
13. To calculate the average area of lung metastases, the quotient of metastatic area to number of metastases is formed. To estimate the metastatic burden, the ratio of metastatic tissue to lung tissue is calculated.

---

#### 4 Notes

1. We used the Single-Color Real-Time PCR Detection System MyiQ (BioRad). For other equipment, protocols may need adjustment.
2. The primary cell cultures obtained by this protocol represent the cancer stage of the individual mouse. Hence, to generalize findings from this culture, sufficient numbers of independent tumor cell preparations must be performed and compared.
3. For the primary PymT cells preparation at least 4 g of the tumor tissue would be required, whereas with less than 4 g of starting tumor material, we recommend to plate the cell suspension (**step 12**) on two T-175 cm<sup>2</sup> culture flasks and culture them for additional day or two in order to have enough cells for cryopreservation or injections.
4. The primary tumor cells grow in an adherent manner and express epithelial markers such as E-cadherin and keratins. Immunofluorescence detection of these markers is advised for quality control of the cells.
5. As routine we cryopreserve the primary cells only at this stage. Once cells have been thawed, they are immediately used for experiments *in vivo*, i.e., orthotopic transplantation (*see Subheading 3.2*), lung colonization (*see Subheading 3.3*), or *in vitro*, e.g., for invasion assays. We do not recommend prolonged culture or repeated freezing of the cells.

6. By the orthotopic transplantation approach, primary tumor growth, angiogenesis, tumor-associated inflammation, and stromal remodeling can be addressed. Furthermore, a full metastatic process from intravasation of tumor cells to growth at distant sites can be investigated. We observed formation of metastasis in the lungs; however, we did not systematically investigate metastatic dissemination of transplanted PymT tumor cells to other tissues. Since the rapid progression of synchronized tumors and their metastasis can be easily followed, this model is particularly useful for drug efficiency studies in immunocompetent mouse backgrounds. Furthermore, this model enables evaluating the role of different proteins originated either from tumor cells or from tumor microenvironment in tumor progression processes by systematic investigation of genetically modified (e.g., knockout) mice as tumor cell donors or recipient mice.
7. Per mouse  $5 \times 10^5$  PymT cells (orthotopic transplantation; Subheading 3.2) or  $2 \times 10^5$  PymT cells (i.v. injections; Subheading 3.3) are recommended. To achieve an acceptably small variance within an experimental group, minimum of six mice is recommended. When calculating the required cell count for an experiment, we recommend thawing 50% of cells in excess in order to have enough starting material.
8. Alternatively, one can simply inject the cells into the fat pad of the mammary gland. However, in terms of reproducibility of tumor growth and safety of the procedure, we found injections to be inferior to the operative transfer method described here.
9. Using a needle causes a strong, negative pressure potentially causing cell damage and lysis.
10. Therapy trials can start 2–3 weeks after transplantation, when the tumors have reached an average volume of ~60–100 mm<sup>3</sup>. Lung metastases are observed 4–5 weeks after the start of the experiment [30].
11. Complementary to the orthotopic model (Subheading 3.2), this approach allows the study of extravasation of tumor cells and growth of the experimental metastases in the lung independently of cancer growth and invasion in indigenous or transplanted tumors.
12. When calculating the volume for the designated cell count per injection, add at least 4 additional injection volumes.
13. Warm the mice under constant observation 15 min before the i.v. injection under a red light to dilate the tail vein.
14. Cells must be singularized thoroughly to avoid pulmonary embolism after i.v. injection.

15. Anesthesia by i.p. injection of 100 mg/kg body weight Ketavet and 5 mg/kg body weight Rompun in 0.9% NaCl.
16. National law of the animal welfare act might require the use of ultrasound-guided intracardiac injection.
17. Intracardiac injection of tumor cell lines gives rise to brain-homing variants after two to three rounds of in vivo selection. However, certain tumor cell lines do not metastasize to the brain after intracardiac injection. In this case, the alternative route via injection into the carotid artery should be considered.
18. Intracardiac injection can also be used to generate bone-homing variants of the MMTV-PymT cells by isolating cells from the colonized bone and subject those lines for in vivo selection. However, we recommend to use injection into the caudal artery to induce bone colonization.
19. Cells must be carefully singulated in order to avoid cardiac arrest after intracardiac injection.
20. We recommend to prepare the syringe with 100 µl of air between the cell suspension and the plunger to allow sufficient backflow of the arterial blood into the syringe. Avoid bubbles in the syringe.
21. To localize the correct position for injection into the left ventricle, it is helpful to remove the fur on the chest. This step is not necessary for more experienced experimenters.
22. We recommend to fix the mouse on an elastic plastic support on all extremities and under the rip case using adhesive tape. To expose the correct area for injection, it can be useful to place a pencil under the plastic support to carefully bend the mouse.
23. For the injection, slowly insert the syringe at the location of the left ventricle into the heart. The correct positioning of the syringe in the left ventricle is visible through the strong backflow of bright arterial blood. Once the backflow is visible, slowly inject the cell suspension with 25 µl boosts. Do not inject the 200 µl at once.
24. We recommend to use 10–12-week-old mice when injecting Bl6 mice. Younger mice show higher risk of cardiac arrest after the injection into the left ventricle.
25. Depending on the generated cell variant, first tumor lesions can be detected in the brain after 3–5 weeks and tumor progression can be followed for an additional 3–5 weeks before mice develop symptoms. For in vivo monitoring of brain metastasis, cells can be transduced with a luciferase vector and tumor progression can be followed by bioluminescence imaging. We recommend to remove the fur in the head region when using either Bl6 mice or Albino Bl6 mice if bioluminescence imaging is used. Moreover, it has been described that luciferase is immunogenic

and its expression can cause tumor rejection. If available, we recommend to use a Small Animal MRI to monitor tumor progressions to avoid transducing the cells with reporter genes. Details on MRI measurements of brain metastasis can be found in Chae et al. [23] .

26. After the successful establishment of brain- or bone-homing cell variants, cryopreserve the generated lines at low passage number and avoid frequent in vitro passaging.
27. Depending on the generated cell variant, first tumor lesions can be detected in the bone after 2–3 weeks and tumor progression can be followed for an addition 3–5 weeks. For in vivo monitoring of bone metastasis, cells can be transduced with a luciferase vector and tumor progression can be followed by bioluminescence imaging. We recommend to remove the fur in the leg region when using either Bl6 mice or using Albino Bl6 mice if bioluminescence imaging is used. Moreover, it has been described that luciferase is immunogenic and its expression can cause tumor rejection. If available, we recommend to use a PetCT to monitor tumor progressions to avoid transducing the cells with reporter genes.
28. For the evaluation of lung, bone, or brain metastatic burden derived from injection models or orthotopic transplantations of MMT-PymT tumor cells, quantification of the hemizygous PymT transgene by quantitative real-time PCR is used. Since the MMTV-PymT transgenic tumor cells are injected or transplanted into PymT negative (non-transgenic) recipient mice, the presence of PymT transgene unambiguously identifies the tumor cells. The quantity of the PymT transgene is calculated against the quantity of any host gene (we use actin and or GAPDH) in the genomic DNA of the lung. The resulting ratio of PymT/actin is a measure of metastatic burden.
29. In order to enhance the reliability of the analysis, different concentrations of genomic DNA template can be used; i.e., 5 ng, 50 ng, 500 ng. Most real-time PCR systems allow determination of PCR efficiency from the threshold cycle (Ct) values of this dilution series.
30. For optimal results, the reagents (before the preparation of the PCR mix) and the PCR mixture itself (before loading) should be mixed well. Otherwise there may be inefficient amplification during the first PCR cycles.

## Acknowledgment

*Grant Support:* TR is supported by the Deutsche Forschungsgemeinschaft (DFG) SFB 850 subproject B7, GRK 2606 “ProtPath” and the German Cancer Consortium (DKTK) programs Exploitation of Oncogenic Mechanisms project L627 and Radiation Oncology and Imaging project “eRadioImage”. LS is supported by the Deutsche Krebshilfe Max Eder Junior Group Leader Program (70111752) and the Deutsche Forschungsgemeinschaft SPP2084 μbone.

## References

- Puente XS, Sanchez LM, Overall CM, Lopez-Otin C (2003) Human and mouse proteases: a comparative genomic approach. *Nat Rev Genet* 4:544–558
- Turk V, Stoka V, Vasiljeva O et al (2012) Cysteine cathepsins: from structure, function and regulation to new frontiers. *Biochim Biophys Acta* 1824:68–88
- Reinheckel T, Peters C, Krüger A et al (2012) Differential impact of cysteine Cathepsins on genetic mouse models of De novo carcinogenesis: Cathepsin B as emerging therapeutic target. *Front Pharmacol* 3
- Vidak E, Javoršek U, Vizovišek M, Turk B (2019) Cysteine Cathepsins and their extracellular roles: shaping the microenvironment. *Cell* 8:264
- Bengsch F, Buck A, Günther SC et al (2013) Cell type-dependent pathogenic functions of overexpressed human cathepsin B in murine breast cancer progression. *Oncogene* 33:4474–4484. <https://doi.org/10.1038/onc.2013.395>
- Dennemärker J, Lohmüller T, Mayerle J et al (2010) Deficiency for the cysteine protease cathepsin L promotes tumor progression in mouse epidermis. *Oncogene* 29:1611–1621
- Sevenich L, Schurigt U, Sachse K et al (2010) Synergistic antitumor effects of combined cathepsin B and cathepsin Z deficiencies on breast cancer progression and metastasis in mice. *Proc Natl Acad Sci U S A* 107:2497–2502
- Vasiljeva O, Papazoglou A, Krüger A et al (2006) Tumor cell-derived and macrophage-derived cathepsin B promotes progression and lung metastasis of mammary cancer. *Cancer Res* 66:5242–5250
- Gacheva V, Zeng W, Ke D et al (2006) Distinct roles for cysteine cathepsin genes in multistage tumorigenesis. *Genes Dev* 20:543–556
- Vasiljeva O, Korovin M, Gajda M et al (2008) Reduced tumour cell proliferation and delayed development of high-grade mammary carcinomas in cathepsin B-deficient mice. *Oncogene* 27:4191–4199
- Sevenich L, Werner F, Gajda M et al (2011) Transgenic expression of human cathepsin B promotes progression and metastasis of polyomavirus-middle-T-induced breast cancer in mice. *Oncogene* 30:54–64
- Sevenich L, Bowman RL, Mason SD et al (2014) Analysis of tumour- and stroma-supplied proteolytic networks reveals a brain-metastasis-promoting role for cathepsin S. *Nat Cell Biol* 16:876–888
- Tholen M, Wolanski J, Stolze B et al (2015) Stress-resistant translation of Cathepsin L mRNA in breast cancer progression. *J Biol Chem* 290:15758–15769
- Ziegler PK, Bollrath J, Pallangyo CK et al (2018) Mitophagy in intestinal epithelial cells triggers adaptive immunity during tumorigenesis. *Cell* 174:88–101
- Guy CT, Cardiff RD, Muller WJ (1992) Induction of mammary tumors by expression of polyomavirus middle T oncogene: a transgenic mouse model for metastatic disease. *Mol Cell Biol* 12:954–961
- Elston CW, Ellis IO (2002) Pathological prognostic factors in breast cancer. I. the value of histological grade in breast cancer: experience from a large study with long-term follow-up. *Histopathology* 41:154–161
- Almholt K, Lund LR, Rygaard J et al (2005) Reduced metastasis of transgenic mammary cancer in urokinase-deficient mice. *Int J Cancer* 113:525–532
- Hüsemann Y, Geigl JB, Schubert F et al (2008) Systemic spread is an early step in breast cancer. *Cancer Cell* 13:58–68

19. Kang Y, Siegel PM, Shu W et al (2003) A multigenic program mediating breast cancer metastasis to bone. *Cancer Cell* 3:537–549
20. Bos PD, Zhang XH-F, Nadal C et al (2009) Genes that mediate breast cancer metastasis to the brain. *Nature* 459:1005–1009
21. Kuchimaru T, Kataoka N, Nakagawa K et al (2018) A reliable murine model of bone metastasis by injecting cancer cells through caudal arteries. *Nat Commun* 9:2981
22. Bowman RL, Klemm F, Akkari L et al (2016) Macrophage ontogeny underlies differences in tumor-specific education in brain malignancies. *Cell Rep* 17:2445–2459
23. Chae WH, Niesel K, Schulz M et al (2019) Evaluating magnetic resonance spectroscopy as a tool for monitoring therapeutic response of whole brain radiotherapy in a mouse model for breast-to-brain metastasis. *Front Oncol* 9:1324
24. Lin EY, Nguyen V, Russell RG, Pollard JW (2001) Colony-stimulating factor 1 promotes progression of mammary tumors to malignancy. *J Exp Med* 193:727–740
25. Shree T, Olson OC, Elie BT et al (2011) Macrophages and cathepsin proteases blunt chemotherapeutic response in breast cancer. *Genes Dev* 25:2465–2479
26. Qian B-Z, Li J, Zhang H et al (2011) CCL2 recruits inflammatory monocytes to facilitate breast-tumour metastasis. *Nature* 475:222–225
27. Guerin MV, Finisguerra V, Van den Eynde BJ et al (2020) Preclinical murine tumor models: a structural and functional perspective. *elife* 9: e50740
28. Walsh NC, Kenney LL, Jangalwe S et al (2017) Humanized mouse models of clinical disease. *Annu Rev Pathol Mech Dis* 12:187–215
29. Tu W, Zheng J (2016) Application of humanized mice in immunological research. *Methods Mol Biol* 1371:157–176
30. Hillebrand LE, Wickberg SM, Gomez-Auli A et al (2019) MMP14 empowers tumor-initiating breast cancer cells under hypoxic nutrient-depleted conditions. *FASEB J* 33:4124–4140

# **Part IV**

## **Clinical Metastasis**



# Chapter 21

## Nuclear Medicine Imaging Procedures in Oncology

Ajay-Mohan Mohan, Nicola Beindorff, and Winfried Brenner

### Abstract

Nuclear medicine radionuclide imaging is a quantitative imaging modality based on radioisotope-labeled tracers which emit radiation in the form of photons used for image reconstruction. Single photon emission computed tomography (SPECT) and positron emission tomography (PET) are the two noninvasive tomographic three-dimensional radionuclide imaging procedures for both clinical and preclinical settings. In this review on nuclear medicine imaging procedures in oncology, a variety of standard SPECT and PET tracers including radioiodine, <sup>18</sup>Fluorine fluorodeoxyglucose (<sup>18</sup>F-FDG), and <sup>68</sup>Gallium-labeled small proteins like Prostate Specific Membrane Antigen (PSMA) or somatostatin analogues and their application as targeted molecular imaging probes for improved tumor diagnosis and tumor phenotype characterization are described. Absolute and semiquantitative approaches for calculation of tracer uptake in tumors during the course of disease and during treatment allow further insight into tumor biology, and the combination of SPECT and PET with anatomical imaging procedures like computed tomography (CT) or magnetic resonance imaging (MRI) by hybrid SPECT/CT, PET/CT, and PET/MRI scanners provides both anatomical information and tumor functional characterization within one imaging session. With the recent establishment of novel molecular radiolabeled probes for specific tumor diagnosis, prognosis, and treatment monitoring, nuclear medicine has been able to establish itself as a distinct imaging modality with increased sensitivity and specificity.

**Key words** SPECT, PET, <sup>99m</sup>Tc, <sup>123</sup>I, <sup>18</sup>F, <sup>68</sup>Ga, MDP, FDG, PSMA, DOTATOC

---

### 1 Introduction

Nuclear medicine is a field of preclinical and clinical science involving radioisotopes for diagnosis and treatment of cancer as well as many other pathophysiological diseases.

Isotopes in general are elements having the same atomic number ( $Z$  = number of protons) and, thus, the same chemical properties but different mass numbers ( $A$  = total number of protons and neutrons) with different physical characteristics. Radioisotopes are unstable isotopes with excited energy level which emit different types of radiation during the course of transition to a more stable energy state with a specific half-life ( $T_{1/2}$ ).

Radiopharmaceuticals are usually composed of two components namely a radioisotope and a vector for molecular targets [1]. Radioisotopes for diagnostic purposes are usually gamma or positron (“positive” electron) emitters with relatively short half-lives in the range of minutes to hours. The molecular targets can be of various types such as receptors that are expressed in specific tumors, structural analogues of a substance metabolized in the body, or a molecule involved in a pathway pertaining to a pathology. One of the most widely used radiopharmaceuticals for tumor evaluation is  $^{18}\text{F}$ -fluorodeoxyglucose ( $^{18}\text{F}$ -FDG):  $^{18}\text{F}$  is a positron-emitting radioisotope, and fluorodeoxyglucose is an analogue of glucose (molecular target) wherein the second hydroxide ion is replaced by  $^{18}\text{F}$ . It is structurally similar to glucose and follows the first steps of the glycolytic pathway.

Radiolabeling with gamma or positron-emitting radionuclides is used for diagnosis, and beta or alpha emitting radionuclides are used for therapeutic purposes. The radionuclide of choice for SPECT imaging is chosen based on certain necessary characteristics like emitted gamma ray energy (80–300 keV) and physical  $T_{1/2}$  [2]. Based on these characteristics, there are various radionuclides available for SPECT imaging:  $^{99\text{m}}\text{Tc}$ ,  $^{111}\text{In}$ ,  $^{201}\text{Tl}$ , and  $^{123}\text{I}$  (see Table 1). These radionuclides can be produced either in an accelerator like a cyclotron or in a generator system.  $^{99\text{m}}\text{Tc}$  is an almost ideal radionuclide for SPECT imaging and is considered the workhorse of a nuclear medicine facility.

Radiopharmaceuticals are often called tracer, because they are usually applied in trace amounts ranging from micromolar down to picomolar or even less, which do not cause pharmacodynamic or pharmacokinetic effects by themselves. Specific side effects or adverse effects are therefore not observed in tracers, and the tracers do not affect the process to be measured by the tracer. Radiopharmaceuticals are usually specific for the targets or the underlying mechanism but not necessarily for a specific disease.  $^{18}\text{F}$ -FDG, for example, detects elevated glucose metabolism with very high sensitivity and specificity, but cannot differentiate between disease entities with increased glucose metabolisms such as tumor or inflammation.

In nuclear medicine, gamma cameras as well as tomographic Single Photon Emission Computed Tomography (SPECT) and Positron Emission Tomography (PET) scanners are used for non-invasive localization of the radiopharmaceutical within the human body. For imaging in laboratory animals such as mice and rats, dedicated small animal SPECT and PET scanners are available. Both human and small animal scanners nowadays are hybrid scanners such as SPECT/CT, PET/CT, and PET/MRI combining nuclear medicine devices for functional imaging with computed tomography (CT) or magnetic resonance imaging (MRI) for

**Table 1**  
**Physical characteristics of different SPECT radionuclides**

S. No	Radionuclide	Decay mode	Principal photon emissions	Physical half-life	Mode of production
1	$^{99m}\text{Tc}$	Internal conversion	140 keV	6.02 h	Generator
2	$^{111}\text{In}$	Electron capture	173, 247 keV	2.80 days	Cyclotron
3	$^{201}\text{Tl}$	Electron capture	68–80 keV X rays	3.04 days	Cyclotron
4	$^{123}\text{I}$	Electron capture	159 keV	13.2 h	Cyclotron

morphological information. Nuclear medicine imaging procedures are widely performed in a variety of organ disorders pertaining to different organs like the heart, kidney, liver, brain, skeleton, lungs as well as in tumors and inflammatory diseases.

## 2 Gamma Camera

The first radionuclide imaging attempts were performed with a film screen combination as detector in the early 1940s. Gamma cameras are the most widely used nuclear medicine imaging system for clinical applications. The major components of the gamma camera are a collimator, a NaI(Tl) scintillation crystal, photomultiplier tubes (PMT), preamplifier and amplifier, and an analog-to-digital converter (ADC). Collimators made up of lead or tungsten are employed to define the direction of the gamma rays. The gamma rays interact with the scintillation crystal and are converted into light photons and directed toward the PMT wherein they are converted into photoelectrons and then undergo multiplication in the PMT. These electrons cause an electric potential difference which is fed into the preamplifier and the amplifier for signal amplification. This analog signal is finally converted into a digital signal in the ADC which is used for image visualization.

### 2.1 SPECT Systems

SPECT or SPECT/CT is a noninvasive three-dimensional imaging procedure. A gamma camera produces two-dimensional planar images, and nowadays almost all of the commercially available gamma camera systems are able to produce three-dimensional images by rotating around the patient like a CT. A SPECT system is identical to that of a normal gamma camera with either one or two heads equipped with a rotating gantry. In a dualhead SPECT system, the detector heads are placed at  $180^\circ$  apart from each other and the heads follow either a circular or an elliptical orbit around the patient over a region of interest (ROI) acquiring multiple planar images from different angles which are reconstructed into a

tomographic three-dimensional image. SPECT cameras are usually combined with CT for anatomical localization, attenuation correction, and tumor characterization.

### *2.1.1 General SPECT/CT Imaging Protocol*

Tomographic SPECT imaging is performed around an ROI of the target organ or tissue with a 180° or 360° angle of rotation depending upon the type of gamma camera (dual head and single head, respectively). Tomographic image acquisitions can be carried out either in step and shoot or in continuous mode. In continuous mode, the detector heads revolve around the ROI continuously acquiring data in different projection angles; while in step and shoot mode, the gantry stops after each angular increment and data are acquired. Step and shoot method is usually preferred over continuous mode owing to increased resolution which is lost during the continuous rotation of the gantry. SPECT imaging is usually performed with 60–120 stops over the ROI for better image resolution. SPECT studies are usually combined with CT for anatomical information and tissue characterization. Clinical SPECT systems offer a resolution of 8–12 mm while preclinical SPECT systems accomplish a resolution between 0.3 and 0.8 mm based on the use of multi-pinhole collimators. Multi-pinhole collimators with different angles for the different pinholes increase the field of view, acquisition count rates, and sensitivity without degrading spatial resolution compared to standard single pinhole collimators. Another advantage of small animal multi-pinhole SPECT systems is a marked reduction of the number of detector positions needed for quantitative 3D image reconstruction which allows fast dynamic acquisition protocols [3].

## **2.2 Technetium Chemistry and $^{99m}\text{Tc}$ : Compounds for Tumor and Metastasis Diagnosis**

Technetium is a transition metal with the atomic number 43 and has 8 oxidation states namely –1 to +7, of these the +4 and +7 are the most stable states. The coordination number of  $^{99m}\text{Tc}$  complexes can vary between 4 and 9.  $^{99m}\text{Tc}$  decays to  $^{99}\text{Tc}$  with a half-life of 6.02 h, and during this transition it emits a gamma ray photon of 140 keV which is ideally suitable for SPECT imaging. It is readily available at the site of labeling coming from a  $^{99}\text{Mo}/^{99m}\text{Tc}$  generator (Mo: molybdenum).  $^{99m}\text{Tc}$  is eluted with sodium chloride (NaCl) from the generator system in which the parent radionuclide  $^{99}\text{Mo}$  decays with a half-life of 66 hours to  $^{99m}\text{Tc}$  in the form of sodium pertechnetate ( $\text{Na}^{99m}\text{TcO}_4^-$ ) with an oxidation state of +7.

There are different radiopharmaceuticals available labeled with  $^{99m}\text{Tc}$  for the diagnosis of various tumor pathologies owing to the favorable labeling chemistry of technetium.

### *2.2.1 $^{99m}\text{Tc}$ -Phosphonate and Phosphate Compounds*

Carcinomas arising from breast, prostate, lung, kidney, and thyroid gland as well as multiple myeloma usually metastasize to the bones [4, 5] although every malignant tumor—both carcinomas and

sarcomas—can metastasize to the skeleton. It has been reported that around 3.7–11% of colon cancers develop bone metastases [6]. Phosphates and phosphonates are present in the bones naturally and  $^{99m}\text{Tc}$ -labeled phosphonate and phosphate compounds avidly bind to the bones in relation to the local bone metabolism and are thus best suited agents for diagnosis and follow up of bone metastases.

Among the phosphate and phosphonate compounds, the in vivo stability of the phosphonate compounds are higher than the phosphates owing to the P–O–P bond in the latter which is easily cleaved by the phosphatase enzyme but not the P–C–P bond in the phosphonate compounds [1, 7]. Therefore,  $^{99m}\text{Tc}$ -labeled phosphonate compounds are widely used for SPECT imaging of bone metastases such as methylene diphosphonate (MDP), hydroxymethylene diphosphonate (HDP), and diphosphono-1,2-propan-dicarbon acid (DPD). The oxidation state of these bisphosphonate compounds is +3.

### *2.2.2 Mechanism of Localization*

Bone consists of four different types of cells namely osteoblasts, osteoclasts, osteocytes, and osteogenic cells. Osteogenic cells are the primary cells which differentiate and develop into osteoblasts which are involved in the formation of new bones building the organic matrix which undergoes mineralization with primarily calcium and phosphate forming the final hydroxyapatite crystals while the osteoclasts are involved in bone reabsorption [8]. There is usually a highly increased activity of osteoblasts in metastatic sites forming bone matrix which undergoes mineralization to which the phosphonate compounds upon intravenous administration are bound by a process called “chemisorption” on the surface of the newly formed hydroxyapatite crystals.

### *2.2.3 SPECT/CT Protocol*

The administered activity for bone SPECT imaging involving phosphonate compounds in patients is 500–1100 MBq in adults. The activity is administered intravenously, and imaging is performed in supine position after 3–5 h for adequate localization of radiopharmaceuticals in sites of osteoblastic activity and for proper background clearance. Whole-body planar (anterior and posterior view) imaging is performed from head to toe followed by SPECT or SPECT/CT in areas of increased uptake for anatomical definition. The normal biodistribution involves uptake in the appendicular and axial skeleton, and in the kidneys and bladder as the organs of physiological excretion via the urine (Fig. 1).

### *2.2.4 $^{99m}\text{Tc}$ -SESTAMIBI*

$^{99m}\text{Tc}$ -methoxy-isobutyl-isonitrile (SESTAMIBI, often called MIBI) is a lipophilic cationic complex, which contains an isonitrile group that allows the formation of a complex with  $^{99m}\text{Tc}$  after reduction in the presence of stannous ions.  $^{99m}\text{Tc}$ -citrate is formed

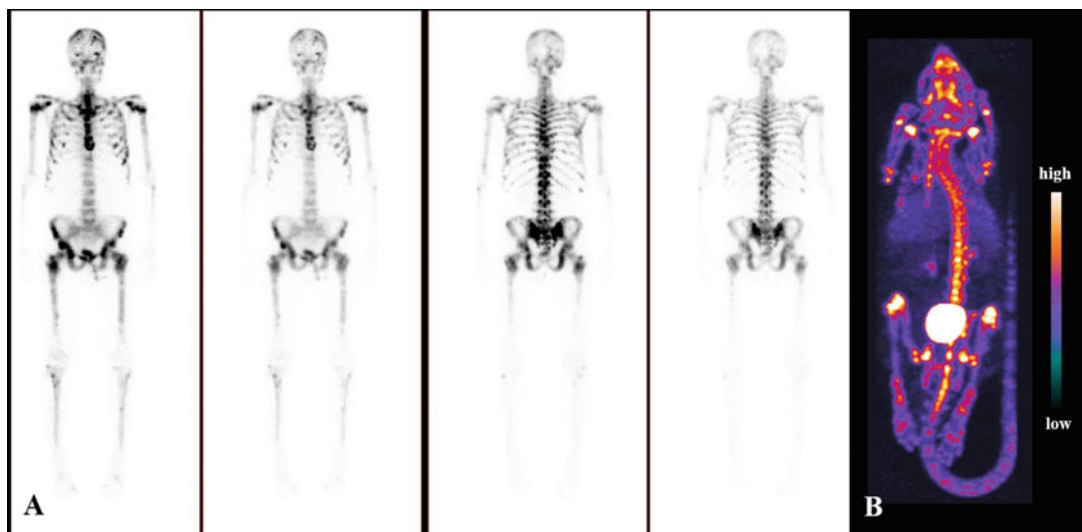


**Fig. 1** Planar whole-body bone scans of a patient (a) from anterior and posterior views displayed in dual intensities each 3 h after intravenous injection of  $^{99m}\text{Tc}$ -DPD depicting multiple skeletal metastases in both the appendicular and axial skeleton. (b) Maximum intensity projection of a healthy mouse after intravenous injection of  $^{99m}\text{Tc}$ -MDP. Normal physiological tracer uptake is visualized in the bones, and tracer excretion via kidneys and the urinary bladder

initially which further undergoes trans-chelation to form  $^{99m}\text{Tc}$ -MIBI. It has a coordination number of 6 containing 6 isonitrile ligands with an oxidation state of +1.

#### 2.2.5 Mechanism of Localization

MIBI is a lipophilic cationic complex which readily localizes in cells by passive diffusion and is bound to the inner membrane of the mitochondria by an active energy-consuming transport driven by a negative membrane potential. Thus, MIBI depicts cells and tissues with high mitochondrial activity [9] such as muscle, heart, and tumor cells. Liver and gut accumulation is also high due to the tracer clearance by the liver and the enterohepatic circulation. Tumor and metastatic cells are in a state of continuous cell division, and therefore there is increased mitochondrial activity in these cells supporting accumulation of MIBI in tumors. MIBI and its analogue tetrofosmin (1,2-bis[di-(2-ethoxyethyl)phosphino]ethane) are unspecific tumor tracers widely employed in breast, brain, lung, and medullary thyroid cancer (MTC) as well as in parathyroid adenomas and also represent the standard tracers for myocardial imaging.

#### 2.2.6 SPECT/CT Protocol

The administered activity for tumor imaging is usually 555–740 MBq in patients. Whole-body planar imaging is performed after 20–60 min post intravenous injection of the tracer. Tumor imaging with MIBI most often involves delayed SPECT or SPECT/CT for exact anatomic information after cellular washout

in non-tumorous cells. MIBI is taken up physiologically in the thyroid and parathyroid glands and the myocardium and is excreted by the liver via gall bladder and the intestines.

### **2.3 Iodine Chemistry and $^{123}\text{I}$ -Labeled Compounds for Diagnosis**

Iodine is a halogen element belonging to the group VIIA of the periodic table with Z number 53. There is only one stable isotope  $^{127}\text{I}$ . Several radioisotopes are available for radioiodination but  $^{123}\text{I}$  is the most convenient radioisotope for diagnosis owing to its half-life of 13.2 h and its photon energy of 159 keV. Since the very beginnings of nuclear medicine, iodine was one of the first radio-nuclides to be exploited for diagnosis ( $^{123}\text{I}$ , and recently  $^{124}\text{I}$  for PET imaging) and therapy ( $^{131}\text{I}$ ) of differentiated thyroid cancer. Labeling of monoclonal antibodies with radioiodine has been carried out successfully for the treatment of lymphoma.

#### **2.3.1 $^{123}\text{I}$ -Sodium Iodide ( $^{123}\text{I}$ -NaI)**

The thyroid gland is an endocrine organ which is primarily involved in the synthesis of the hormones triiodothyronine (T3) and tetra-iodothyronine (T4). The production of these hormones primarily involves three different processes for which iodine is essential, namely trapping, i.e., transmembrane uptake by the sodium-iodide symporter (NIS), organification per thyroid peroxidase, and coupling to the hormones.

##### *Mechanism of Localization:*

Iodine ingested from dietary intake is absorbed from the intestine and transported by NIS into thyroid plasma where it undergoes oxidation and further coupling processes [10]. Based on these physiological processes,  $^{123}\text{I}$ -NaI is either given orally in the form of a capsule or NaI solution or administered intravenously.

##### *SPECT/CT Protocol.*

In oncology,  $^{123}\text{I}$ -NaI is widely used for the diagnosis of well-differentiated thyroid carcinoma. It is also used for the detection of benign thyroid diseases. The administered activity for differentiated thyroid cancer is 185 MBq i.v. [11]. Differentiated thyroid cancer diagnosis involves radioiodine uptake usually performed after 18–24 h. Of importance, intake of iodine-rich drugs, food, and iodinated contrast agents must be strictly avoided at least 8–10 weeks prior to administration of the diagnostic compound because iodine in higher concentration blocks the uptake via NIS. Whole-body planar imaging is usually performed at 6 and 24 (48) h after the administration of  $^{123}\text{I}$ -NaI in anterior and posterior views with additional SPECT or SPECT/CT of the neck and other regions with pathological uptake on the planar images (Fig. 2).

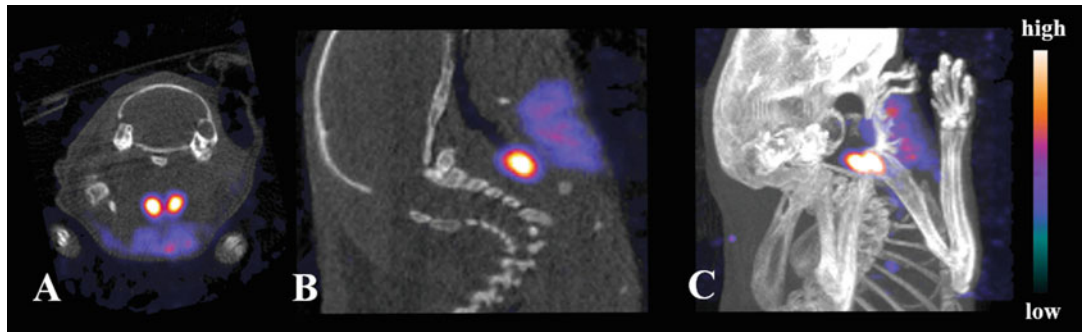


**Fig. 2** Fused SPECT/CT axial (**a**), sagittal (**b**) and maximum intensity projection (**c**) views of a healthy female mouse after intravenous injection of  $^{123}\text{I}$ -NaI. Normal physiological uptake is seen in the thyroid and in the sublingual-submandibular salivary gland complex

### 2.3.2 $^{123}\text{I}$ -Metaiodo-benzyl Guanidine ( $^{123}\text{I}$ -mIBG)

Norepinephrine or noradrenaline, a neurotransmitter, is a hormone synthesized by neuroendocrine cells like adrenergic neurons and adrenal medullary cells. An increased production of this hormone is often observed in tumors originating from these cells.

#### *Mechanism of Localization:*

Metaiodobenzyl guanidine (mIBG) is an analogue of guanidine structurally resembling the hormone norepinephrine. Thus, mIBG is taken up by medullary adrenal gland tumor cells by active transport mechanism allowing to localize the tumor and its metastases.

#### *SPECT/CT Protocol.*

$^{123}\text{I}$ -mIBG is widely used for imaging of pheochromocytoma and medullary thyroid carcinoma in adults and neuroblastoma in children. The administered activity is 150–400 MBq for adults; in case of children, the dosage is adjusted to their body weight [12]. The activity is slowly administered intravenously over 30–120 s in order to avoid “adrenaline crisis.” Thyroid uptake of free  $^{123}\text{I}$  must be prevented by providing thyroid blockade with perchlorate 1 h prior to administration of the tracer and should be continued for at least 48–72 h post administration. Planar imaging is usually performed at 24 and 48 h post administration always complemented by SPECT or SPECT/CT (Fig. 3).

---

## 3 Positron Emission Tomography/Computed Tomography (PET/CT)

Positron emission tomography (PET) is another noninvasive three-dimensional functional tomographic imaging modality in nuclear medicine employing positron-emitting radionuclides. Positrons are positively charged subatomic particles with a mass and a magnitude of charge like negatively charged electrons. A positron interacts with a nearby electron both undergoing mutual annihilation

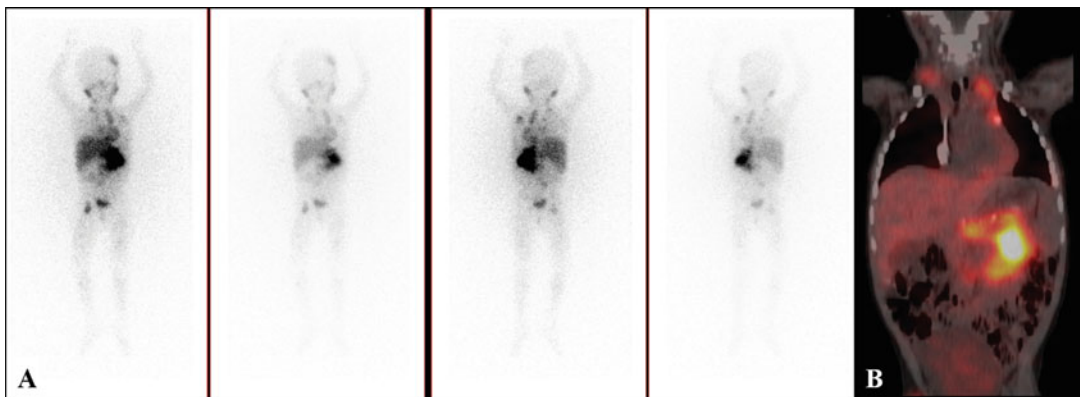


**Fig. 3** Twenty four hour whole-body planar <sup>123</sup>I-MIBG scintigrams (**a**) from anterior and posterior views displayed in dual intensities of a child with metastasized neuroblastoma depicting the primary tumor in the left adrenal gland and metastases in multiple locations including lung and bones. A fused SPECT/CT coronal view (**b**) of the same patient demonstrating a large primary tumor in the left adrenal gland 24 h post administration

where their masses are completely converted into energy, a pair of annihilation photons (511 keV each) which are emitted almost exactly 180° in opposing directions. The range of a positron is usually only a few tenths up to few millimeters to the point of annihilation depending upon the energy of the positron which is nuclide specific.

### 3.1 PET Detectors and Instrumentation

PET systems are equipped with coincidence circuits for detection of these annihilation photons by a ring detector system. The detection mechanism is called annihilation coincidence detection, and the detectors used are called annihilation coincidence detectors (ACD). PET systems thus can trace photons coincidentally detected by two detectors called “line of response.” The scintillation detectors used in PET are block detectors, and the detector crystals are of high Z materials because of the relatively high energy of 511 keV photons. The commonly used scintillator materials for PET imaging are bismuth germanate (BGO) and, nowadays, the faster lutetium oxyorthosilicate (LSO) and lutetium yttrium orthosilicate (LYSO) crystals which enable a higher time resolution, and thus, a more precise measurement of the difference in time between the detection of the two photons. This allows a better definition of the origin point of the annihilation along the line of response which in turn increases the spatial resolution of the scanner. This technology is named time-of-flight (TOF) technique. On the other hand, the range of the positron inevitably decreases the resolution of the PET scanners because only the point of annihilation can be determined by PET but not the point of positron decay. Modern PET scanner systems are always hybrid systems with an additional CT or MRI gantry for fused functional PET and anatomical CT or MR

imaging. Clinical scanners present with a spatial resolution of 3–8 mm; in dedicated small animal PET scanners, the resolution is about 0.8–1.2 mm.

#### *General PET/CT Imaging Protocol.*

PET tomographic imaging is carried out either in 2D (septa between rings) or 3D mode. Modern-day PET systems are 3D systems equipped with time-of-flight technology resulting in high spatial resolution and sensitivity. Whole-body three-dimensional PET tomographic imaging is carried out in multiple bed positions with 2–5 min per bed position each depending upon the count density. PET imaging is always combined with CT or MR imaging to aid in attenuation correction, anatomical information, and for tumor characterization. A normal adult diagnostic CT with intravenous contrast agent (iodinated) and oral contrast agents is performed with 120–180 kVp, 250–400 mA either prior to or after PET imaging, and the reconstructed PET and CT images are fused with specific software tools. Whole-body imaging may be combined with spot imaging in areas of the primary tumor or suspected metastases, e.g., lung or bone optimized CT protocols or contrast-enhanced imaging of the tumor and/or metastases.

### **3.2 PET Radiopharmaceuticals**

A variety of positron emitters are available for radiolabeling of PET tracers. The standard radionuclides involved in PET imaging belong to three major groups of elements namely elements essential for organic substances (carbon  $^{11}\text{C}$ , oxygen  $^{15}\text{O}$ ), halogens (fluor  $^{18}\text{F}$ , iodine  $^{124}\text{I}$ ), and metals (gallium  $^{68}\text{Ga}$ , copper  $^{64}\text{Cu}$ ) (see Table 2).

**Table 2**  
**Physical characteristics of the most widely used PET radionuclides**

S. No	Radionuclide	Decay mode	Principal photon emissions	Physical half-life	Mode of production
1	$^{11}\text{C}$	Positron emission	511 keV annihilation	20 min	Cyclotron
2	$^{15}\text{O}$	Positron emission	511 keV annihilation	2 min	Cyclotron
3	$^{18}\text{F}$	Positron emission	511 keV annihilation	110 min	Cyclotron
4	$^{68}\text{Ga}$	Positron emission	511 keV annihilation	68 min	Generator
5	$^{64}\text{Cu}$	Positron emission	511 keV annihilation	12.7 h	Cyclotron

### 3.2.1 $^{18}\text{F}$ -Labeled PET Radiopharmaceuticals

Fluorine is an element of the halogen group belonging to the group VIIA of the periodic table with atomic number 9. Fluorine is an ideal radionuclide for developing novel PET molecular imaging probes because it is the most electronegative element of all halogens and it can react with both organic and inorganic compounds. And it can act both as an electrophile and a nucleophile partner in a chemical reaction.  $^{18}\text{F}$ luorine ( $^{18}\text{F}$ ) is an ideal radionuclide for PET imaging owing to its low positron energy (0.64 MeV) resulting in a relatively short path length before annihilation which translates into a high spatial resolution. Due to its high chemical reactivity, the labeling yield is usually very high with high specific activity. It has a half-life of 110 min enabling dynamic imaging of up to 3–4 h.

A diverse range of  $^{18}\text{F}$ -labeled imaging probes has been developed for tumor imaging, the clinically most relevant radiopharmaceuticals being  $^{18}\text{F}$ -FDG,  $^{18}\text{F}$ -sodium fluoride ( $^{18}\text{F}$ -NaF),  $^{18}\text{F}$ -fluorothymidine ( $^{18}\text{F}$ -FLT),  $^{18}\text{F}$ -fluoromisonidazole ( $^{18}\text{F}$ -FMISO), and  $^{18}\text{F}$ -fluoroethyl-L-tyrosine ( $^{18}\text{F}$ -FET).

#### $^{18}\text{F}$ -2-Fluoro-2-Deoxyglucose (FDG)

$^{18}\text{F}$ -2-fluoro-2-deoxyglucose is an analogue of glucose, and it is the most widely used PET radiopharmaceutical in oncology for staging, restaging, and treatment monitoring in many different malignant tumors, carcinomas, as well as sarcomas. Structurally it is similar to glucose but the hydroxide ion at position 2 is replaced by a fluorine ion, hence the name 2-fluoro-2-deoxyglucose (2-FDG). Fluorination at several other positions has been tested like 3-FDG and 4-FDG, but 2-FDG is the best suited one with adequate in vivo stability and biokinetics [13].  $^{18}\text{F}$  is usually produced in a cyclotron by irradiation of  $^{18}\text{O}$ -H<sub>2</sub>O with protons, and FDG is then produced on-site by an automated nucleophilic reaction finally resulting in  $^{18}\text{F}$ -FDG.

#### *Mechanism of Localization.*

Glucose is the major source of energy required to maintain the normal metabolism of the body. Glucose is taken up by the cells by specific glucose transporters and converted into glucose-6-phosphate by the hexokinase enzyme, and then undergoes the glycolytic pathway.  $^{18}\text{F}$ -FDG as an analogue of glucose is taken up into the cells by the same glucose transporters, in tumors mostly subtype GLUT-1, and converted into  $^{18}\text{F}$ -FDG-6-phosphate by hexokinase. But due to the absence of the hydroxide ion, it does not undergo further phosphorylation and hence remains trapped in the cells [14–16] (Fig. 4). Glucose metabolism is upregulated in almost all malignant tumors and metastases (Warburg effect).  $^{18}\text{F}$ -FDG therefore is a very sensitive and “universal” tumor marker with however low specificity as it is generally taken up by all glucose-consuming cells and processes such as tumor cells,

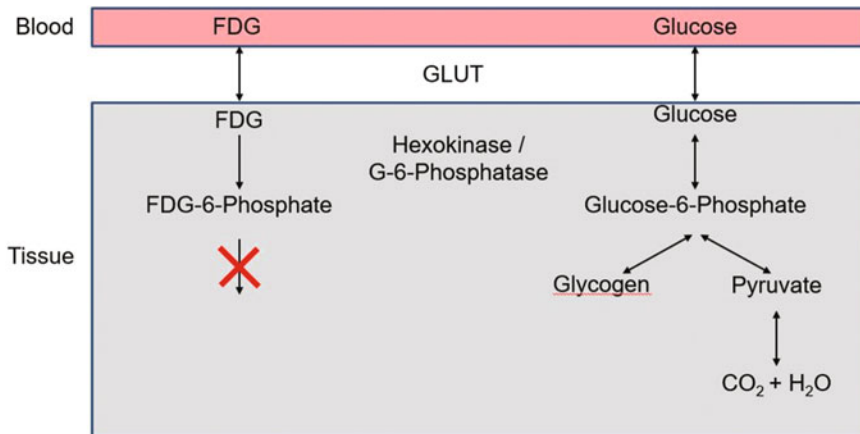


**Fig. 4** Schematic representation of the mechanisms of uptake and metabolism of  $^{18}\text{F}$ -FDG and glucose in the cells. While glucose is fully metabolized,  $^{18}\text{F}$ -FDG-6-phosphate is trapped within the cell. GLUT: glucose transporters

activated immune cells, or activated fibroblasts and macrophages in inflammatory processes and tissue repair. Due to the high glucose metabolism of the brain,  $^{18}\text{F}$ -FDG is also a poor tracer in brain tumors.

#### $^{18}\text{F}$ -FDG PET/CT Protocol.

$^{18}\text{F}$ -FDG has been widely used for the detection of unknown primary tumors with metastasis, differentiating benign from malignant tumors, staging, restaging, and response monitoring in malignant tumors. The administered activity is 250–350 MBq for adults. Intake of external glucose must be avoided because of competitive uptake mechanisms between glucose and  $^{18}\text{F}$ -FDG [17]. Fasting is recommended for 6–8 h prior to  $^{18}\text{F}$ -FDG administration, and the fasting blood glucose level should be less than 160 mg/dL.  $^{18}\text{F}$ -FDG is administered intravenously, and PET imaging is performed after 45–60 min.  $^{18}\text{F}$ -FDG is physiologically taken up in the brain, myocardium, liver, spleen, stomach, and intestines due to their muscular activation as well as activated skeletal muscle, thymus, bone marrow, uterus, and ovaries depending on their hormonal status, and brown adipose tissue (Fig. 5).

$^{18}\text{F}$ -Sodium Fluoride  
( $^{18}\text{F}$ -NaF)

There are two different types of bone metastases namely osteoblastic and osteolytic ones. The osteoblastic metastases arise when there is increased bone formation activity causing sclerotic changes which happens mostly in the case of prostate and breast cancer [18, 19]. Osteolytic lesions arise in case of increased bone resorption which is mostly observed in lung cancer, renal cell carcinoma, and multiple myeloma [18]. Since fluorine is one of the main constituents of the bone matrix,  $^{18}\text{F}$ -NaF is employed for imaging

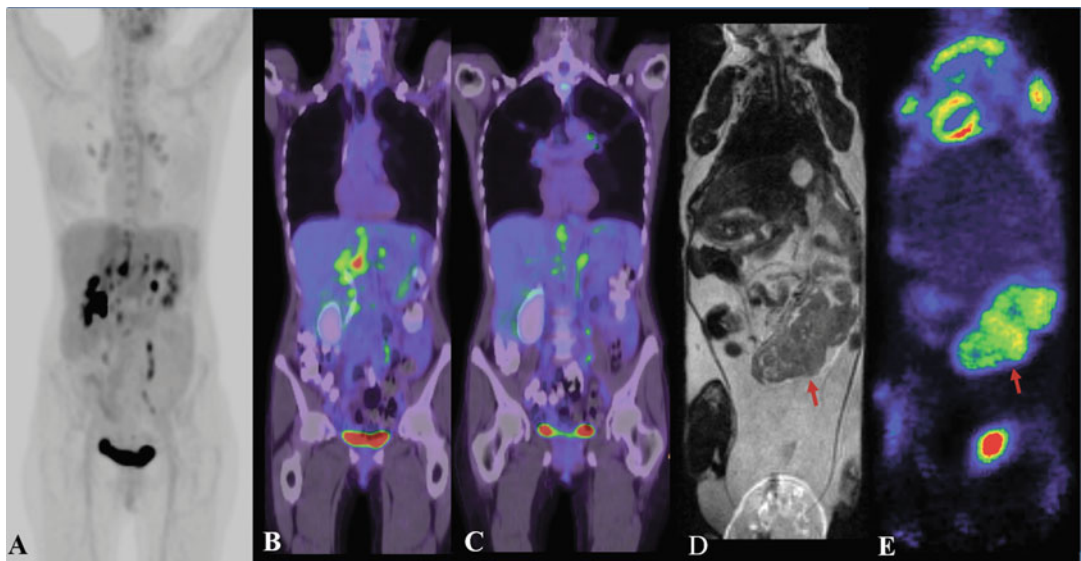


**Fig. 5**  $^{18}\text{F}$ -FDG PET imaging. Maximum intensity projection (**a**) and fused PET/CT coronal views (**b, c**) of a patient with lymphoma after intravenous injection of  $^{18}\text{F}$ -FDG. Pathological uptake is depicted in multiple thoracic, abdominal, and pelvic lymph nodes with physiological uptake in the liver, spleen, kidneys, and urinary bladder. MRI (**d**) and PET (**e**) coronal views of a mouse with an abdominal tumor after intravenous injection of  $^{18}\text{F}$ -FDG. High tracer uptake is seen in the tumor (red arrow) while uptake in the myocardium and bladder is physiological

of bone metabolism in general and for detection of altered bone metabolism in bony metastasis arising from different cancers. Bone scintigraphy with  $^{99\text{m}}\text{Tc}$ -MDP is less sensitive in detecting bone metastases than  $^{18}\text{F}$ -NaF [20].

#### *Mechanism of Localization.*

Bone consists of two components namely the organic matrix and the inorganic hydroxyapatite crystals. The organic matrix is mostly made up of collagens while the inorganic components are mainly composed not only of calcium and phosphate but also of other minerals and elements like bicarbonate, sodium, potassium, citrate, magnesium, carbonate, fluorine, zinc, barium, and strontium [8]. Since the bone matrix contains fluorine,  $^{18}\text{F}$ -NaF is bound to hydroxyapatite in correlation to bone turnover thus indicating bony lesions such as fractures, bone remodeling, and bone metastases.

#### *PET/CT Protocol.*

The administered activity in adults is 185–370 MBq. Since there is rapid accumulation of the tracer in the bones, whole-body PET imaging can be performed after 30–45 min post injection. Uniform physiological uptake is noticed in the skeleton, and uptake is

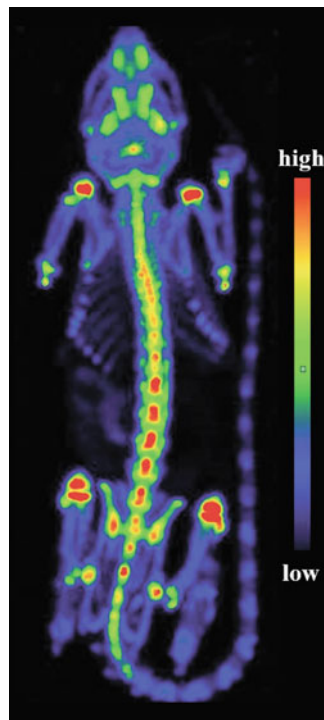


**Fig. 6** Preclinical PET image of a healthy mouse after intravenous injection of  $^{18}\text{F}$ -NaF. Normal physiological uptake is visualized in the bones and joints similar to the uptake of  $^{99\text{m}}\text{Tc}$ -MDP (see Fig. 1b)

increased in areas of new bone formation [21]. Thus,  $^{18}\text{F}$ -NaF PET imaging is very sensitive in detecting alterations in bone metabolism but unspecific for a specific disease (Fig. 6).

#### $^{18}\text{F}$ -Fluorothymidine ( $^{18}\text{F}$ -FLT)

One of the major hallmarks of any cancer is the uncontrolled proliferation of the tumor cells. This requires rapid DNA synthesis coupled with increased glucose metabolism.  $^{18}\text{F}$ -Fluorothymidine is a PET radiopharmaceutical that targets the DNA proliferation.  $^{18}\text{F}$ -FLT is synthesized by a nucleophilic reaction between  $^{18}\text{F}$ -fluoride and a precursor of thymidine.

#### *Mechanism of Localization.*

In malignant tumors, there is uncontrolled division of cells due to the abnormal functioning of genes involved in controlling the cell cycle which is characterized by a mitotic phase and a synthesis phase. The enzyme thymidine kinase 1 (TK1) plays an important role in DNA synthesis, and its activity is significantly increased in malignant cells. Proliferating cells take up FLT in analogy to thymidine which then undergoes phosphorylation to  $^{18}\text{F}$ -FLT monophosphate by TK1. FLT monophosphate is trapped intracellularly [22] although it is not incorporated into the DNA.  $^{18}\text{F}$ -FLT

therefore reflects the activity of the TK1 enzyme which is usually increased in all lesions of malignant tumors and also in proliferating cells, e.g., of the bone marrow.

#### *PET/CT Protocol.*

<sup>18</sup>F-FLT has been successfully used for characterizing a variety of tumors including lung cancer, colorectal cancer, melanoma, lymphoma, breast cancer, laryngeal cancer, and soft-tissue sarcomas [22]. The administered activity is 185–370 MBq, and PET/CT imaging is usually started after an uptake period of 60 min.

#### <sup>18</sup>F-Fluoromisonidazole (<sup>18</sup>F-FMISO)

Cancer cells derive their energy from blood vessels through the tumor-induced process of neoangiogenesis. Cancer progression is greatly affected by oxygenation levels in the cells, and it has been shown that hypoxia (reduced O<sub>2</sub>) is a cofounding factor for tumor progression [23]. Hypoxia is a result of the imbalance between the supply and consumption of oxygen which is primarily caused by aberrant angiogenesis coupled with the high metabolic rate of tumor cells. Hypoxia therefore is a distinctive feature of rapidly progressing, aggressive high-grade solid tumors [23]. Hypoxia also promotes resistance toward chemotherapy and radiotherapy making treatment cumbersome and, thus, is linked to poor prognosis [24–28]. Hence, early identification and the extent of hypoxia are important for effective treatment planning. <sup>18</sup>F-Fluoromisonidazole (<sup>18</sup>F-FMISO) is a PET molecular imaging probe for the detection of hypoxic tissues in different solid carcinomas irrespective of the underlying tumor. It is synthesized by reacting <sup>18</sup>F with the precursor of FMISO, namely 1-(2'-nitro-1'-imidazolyl)-2-O-tetrahydropyranyl-3-O-toluenesulfonylpropanediol (NTTP). The radiochemical yield of this tracer is usually low with only about 34% but a radiochemical purity of more than 97%.

#### *Mechanism of Localization.*

Radiotracers for hypoxia diagnosis most often involve a 2-nitroimidazole structure. The derivatives of 2-nitroimidazole undergo reduction under hypoxic conditions and subsequently accumulate intracellularly because after reduction of the nitro groups, <sup>18</sup>F-FMISO binds covalently to the macromolecules of the hypoxic cell [24].

#### *PET/CT Protocol.*

The mean administered activity of <sup>18</sup>F-FMISO is 370–740 MBq intravenously. PET imaging is usually performed after 60–120 min post administration. The normal biodistribution of the tracer includes uptake in liver, kidney, bladder, blood, spleen, heart, lung, muscle, bone, and brain [29].

*O-(2-[<sup>18</sup>F]-Fluoroethyl)-L-Tyrosine (<sup>18</sup>F-FET)*

Gliomas are a group of cancers arising from the glial cells of the central nervous system. There are different types of gliomas namely astrocytoma, glioblastoma multiforme, oligodendrogiomas, and ependymomas [30]. Gliomas account for 26% of the brain tumors arising from the central nervous system and 81% of gliomas are malignant neoplasms [31, 32]. Glioblastoma multiforme is the most common and most aggressive form comprising 46% of glial tumors [31]. It is always a high-grade tumor in nature with a poor median survival of 15–20 months, despite advanced treatment modalities [31, 33]. MRI is the standard imaging tool in brain tumors [33, 34]. Although the sensitivity of MRI is excellent for primary diagnosis, the efficacy of MRI is limited for treatment monitoring and response evaluation due to post-therapy changes of the blood–brain barrier [31, 33]. Metabolic PET imaging of gliomas usually involves amino acids such as methionine, tyrosine, or phenylalanine radiolabeled with either carbon-11 (<sup>11</sup>C) or <sup>18</sup>F [31]. The reason for this is twofold: First, <sup>18</sup>F-FDG is avidly taken up by normal brain tissue rendering this standard oncologic tracer rather useless in brain tumors. Second, radiolabeled amino acids have a higher specificity than MRI contrast agents owing to their ability to pass the intact blood–brain barrier allowing differentiation of tumor progression from nonspecific, treatment-related changes in the post-therapy setting [35]. O-(2-[<sup>18</sup>F]-fluoroethyl)-L-tyrosine (<sup>18</sup>F-FET) is a fluorinated amino acid, most commonly employed for response evaluation and detection of recurrent disease in gliomas. It is preferred over <sup>11</sup>C-methionine from a practical point of view because of the longer half-life of <sup>18</sup>F compared to <sup>11</sup>C. <sup>18</sup>F-FET PET/MR imaging is the standard imaging method of choice in gliomas providing a higher accuracy in delineation of tumor lesions and recurrences than MRI alone or PET/CT [36, 37].

*Mechanism of Localization.*

The intracellular transport of the amino acid tyrosine occurs largely via the large neutral amino acid transporter (LAT) subtypes LAT1 and LAT2 [35, 37]. These transporters are considerably upregulated in glial tumors compared to a very low expression in normal brain tissue [37]. This upregulation results in an increased uptake of <sup>18</sup>F-FET in gliomas clearly delineating glioblastoma multiforme tumor lesions. <sup>18</sup>F-FET however is not incorporated into proteins making this tracer only a biomarker for amino acid transporter expression and capacity but not for protein synthesis rate [36].

*PET/CT Protocol.*

The mean administered activity of <sup>18</sup>F-FET is 185–200 MBq. A minimum fasting period of 4 h is required before tracer administration. Imaging is performed 20 min post intravenous administration

[31]. The physiological distribution includes vascular structures, basal ganglia, cerebellum, skin, salivary glands, low focal uptake in the pineal body, choroid plexus, and clivus bone marrow [31].

### 3.2.2 $^{68}\text{Ga}$ -Based PET Radiopharmaceuticals

Molecular imaging probes labeled with radiometals are applied in the diagnosis of many different pathologies. Indium (In) and gallium (Ga) are the mostly widely used metals that are involved in tumor imaging. They belong to group IIIB of the periodic table, and gallium has a Z number of 31. There are two different isotopes of gallium used in nuclear medicine,  $^{67}\text{Ga}$ , a gamma emitter, and  $^{68}\text{Ga}$ , a positron emitter with a relatively high positron energy resulting in a much longer pathway than in  $^{18}\text{F}$  ( $^{68}\text{Ga}$ : 1.89 MeV, mean range 1.9 mm;  $^{18}\text{F}$ : 0.64 MeV, mean range 0.2 mm).  $^{68}\text{Ga}$  PET images therefore have systematically a lower resolution than  $^{18}\text{F}$  PET images which is noticeable especially in high-resolution small animal PET scanners. Unlike  $^{18}\text{F}$ ,  $^{68}\text{Ga}$  is readily available from a  $^{68}\text{Ge}/^{68}\text{Ga}$  (Ge: germanium) generator which can be eluted several times per day.  $^{68}\text{Ga}$  has a half-life of 68 min. It is a highly versatile radionuclide for ligand labeling. The commonly used  $^{68}\text{Ga}$ -labeled radiopharmaceuticals are  $^{68}\text{Ga}$ -prostate-specific membrane antigen ( $^{68}\text{Ga}$ -PSMA) for prostate cancer,  $^{68}\text{Ga}$ -DOTATOC for neuroendocrine tumors,  $^{68}\text{Ga}$ -Exendin for imaging insulinomas and congenital hyperinsulinism, and  $^{68}\text{Ga}$ -Pentixafor for chemokine receptor imaging.

#### $^{68}\text{Ga}$ -Prostate-Specific Membrane Antigen ( $^{68}\text{Ga}$ -PSMA)

Prostate-specific membrane antigen (PSMA) is a type II integral membrane glycoprotein which is an analogue to the protein N-acetyl-L-aspartyl-L-glutamate peptidase I (NAALADase I or folate hydrolase I). PSMA protein has a unique structure of three parts, a 19 amino acid internal portion, a 24 amino acid transmembrane portion, and a 707 amino acid external portion. The PSMA gene is located in the short arm of chromosome 11 [38]. It is a reliable tissue marker and an ideal target for diagnostic applications as it exhibits a selective overexpression in 90–100% of local prostate cancer, and it is highly overexpressed both in the primary tumor and metastases.

#### *Mechanism of Localization.*

PSMA is a transmembrane protein present in almost all prostatic tumor tissues and acts as glutamate transferring carboxypeptidase. PSMA expression is inversely related to androgen hormone levels. There is increased expression of PSMA in 90–100% of all prostate cancerous tumors although studies have documented PSMA expression in various other malignancies in which PSMA is highly expressed in the neovasculature of malignant tumors such as clear cell renal carcinoma, transitional cell bladder cancer, testicular embryonal cancer, neuroendocrine tumors, colon cancer, and breast carcinomas [38].

*PET/CT Protocol.*

Various PSMA ligands linked with different chelators have been developed for PET imaging, of which ligand PSMA-11 linked to the chelator *N,N'*-bis[2-hydroxy-5-(carboxyethyl)-benzyl]ethylene diamine *N,N'*-diacetic acid (HBED-CC) is the most suitable one for diagnosis so far owing to its high tumor uptake, rapid blood clearance, high in vivo stability, and decreased liver uptake. Early imaging is possible due to the rapid blood pool clearance. The activity is usually administered based on the body weight, 1.8–2.2 MBq per kg of body weight, and after an uptake period of 60 min, imaging is performed [39]. Normal PSMA ligand uptake can be found in lacrimal and salivary glands, liver, spleen, small intestine, colon, and kidney [39] (Fig. 7).  $^{18}\text{F}$ -labeled PSMA ligands have been introduced very recently which are easier to handle and distribute due to the longer half-life of  $^{18}\text{F}$ .

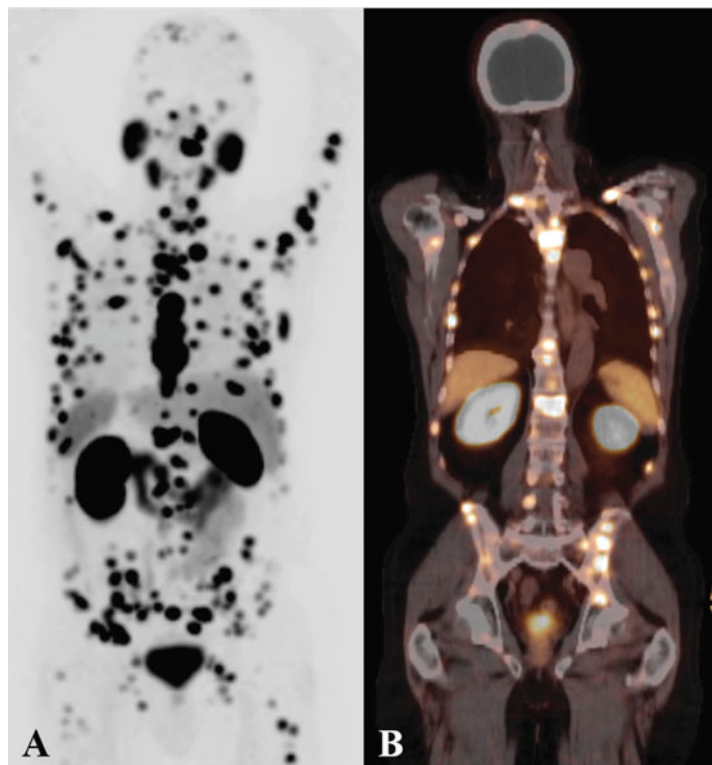


**Fig. 7** PET maximum intensity projection (**a**) and fused PET/CT coronal (**b**) view of a patient with prostate cancer after administration of  $^{68}\text{Ga}$ -PSMA. There are widespread metastases all over the body along with physiological uptake in the salivary glands, liver, spleen, kidneys, and urinary bladder

**<sup>68</sup>Ga-DOTATOC**

Neuroendocrine tumors (NET) originate from both neural and endocrine tissues. NET can be graded as well, moderately and poorly differentiated tumors. The well-differentiated and most of the moderately differentiated tumors express somatostatin receptors, a G-protein-coupled receptor. Basically, five different types of somatostatin receptor subtypes are expressed in these tumors: somatostatin receptor-1 (SSTR)1, SSTR2, SSTR3, SSTR4, and SSTR5. Of these, SSTR2 is the predominant subtype in most NET. There are a variety of somatostatin analogues developed for diagnosis and treatment of NET which target these receptor moieties. The analogues are basically of two types, namely receptor agonists and antagonists. Octreotide was the first somatostatin agonist analogue to be radiolabeled in 1983 with <sup>111</sup>In [40] and had been FDA approved in the early 1990s. Since then, NET diagnosis with SPECT imaging was widely performed with <sup>111</sup>In-Octreotide. The different agonist somatostatin analogues for PET imaging are Phe<sup>1</sup>-Tyr<sup>3</sup>-Octreotide (TOC), NaI<sup>3</sup>-Octreotide (NOC), and Tyr<sup>3</sup>-Octreotate (TATE) which are synthesized by altering the amino acid sequences linked with the chelator 1,4,7,10-tetraazacyclododecane-1,4,7,10-tetraaceticacid (DOTA) for coupling with <sup>68</sup>Ga for PET imaging. These peptides have selective affinity toward the receptors, and it has been shown that DOTATOC exhibits a high affinity for SSTR2 and SSTR5, and DOTANOC for SSTR2, SSTR3, and SSTR5. The analogue DOTATATE has the highest affinity for SSTR2 [41]. For radionuclide treatment however only DOTATOC and DOTATATE can be used while DOTANOC has an unfavorable toxic treatment profile (Table 3).

*Mechanism of localization.*

Somatostatin receptors belong to the family of G-protein-coupled receptors. These receptors are expressed on the cell surface of neuroendocrine cells, and there is a significant overexpression of these receptors in grade I and II NET. Somatostatin is a peptide hormone that binds to these receptors and contributes to signal transmission, cell proliferation, and hormone secretion

**Table 3**  
**Amino acid sequence of the different somatostatin analogues**

Amino acid sequence	Hormone analogue
Ala-Gly-Cys-Lys-Asn-Phe-Phe-try-Lys-Thr-Phe-Thr-Ser-Cys	Somatostatin
DOTA-D-Phe-Cys-Tyr-D-Trp-Lys-Thr-Cys-Thr(ol)	DOTATOC
DOTA-D-Phe-Cys-Tyr-D-Trp-Lys-Thr-Cys-Thr(OH)	DOTATATE
DOTA-D-Phe-Cys-NaI-D-Trp-Lys-Thr-Cys-Thr(ol)	DOTANOC

[40]. Radiolabeled somatostatin analogues also bind to these receptors depending upon their affinity profiles and thus allow SPECT or PET imaging.

*PET/CT Protocol.*

<sup>68</sup>Ga-DOTA-labeled somatostatin agonist analogues are used in gastro–entero–pancreatic tumors, carcinoids, merkel cell carcinoma, medullary thyroid carcinoma, meningioma, and all other NET entities, e.g., NET of the lungs. The administered activity is 100–200 MBq. The activity is administered intravenously, and imaging is performed after an uptake period of 45–60 min. Delayed imaging can be performed for appropriate background clearance. The normal biodistributions of these analogues include liver, spleen, pituitary gland, thyroid, kidneys, adrenal glands, salivary glands, stomach wall, and bowel. The pancreas has a varying uptake for these analogues the highest being in the uncinate process, and there is predominant expression of SSTR2 in the islets of the pancreas [42]

<sup>68</sup>Ga-NODAGA-Exendin

Pancreatic NET (PNET) are a group of endocrine tumors arising in the pancreas and are the most common NET. PNET can be classified as functional and nonfunctional tumors, and functional PNET include gastrinoma, VIPoma, glucagonoma, and insulinoma [43]. Insulinomas arise from the insulin-producing beta cells of the islets of Langerhans. The majority of insulinomas are benign (90%); however, they have a great impact on the quality of life of the patients due to excessive secretion of insulin from the tumor cells resulting in potentially life-threatening hypoglycemia [44]. Benign insulinomas usually demonstrate a decreased receptor density of SSTR2 and SSTR5, thus hampering PET imaging with <sup>68</sup>Ga-somatostatin analogues [45, 46]. In nearly 100% of the cases however there is an increased expression of glucagon-like peptide-1 receptor (GLP-1R) in contrast to the decreased or low SSTR expression, which makes GLP-1R a highly specific target for both diagnosis and treatment. <sup>68</sup>Ga-1,4,7-triazacyclononane,1-gluteric acid-4,7-acetic acid (NODAGA)-Exendin-4 is a high-specific radiotracer developed for imaging of GLP-1R expressed in insulinomas as well as in hyperfunctional islet cells in newborns and children with congenital hyperinsulinism.

*Mechanism of Localization.*

GLP-1R receptor is highly expressed on the surface of almost all benign insulinoma and congenital hyperinsulinism cells. Exendin-4 is a long acting natural ligand of the GLP-1R binding specifically only to this receptor. Since there is a high density and increased expression of this receptor, it is a highly specific molecular target for PET imaging. Radiolabeling has been carried out with various

bifunctional chelators like DOTA and NODAGA, and it has been shown that high-specific activity can be obtained with  $^{68}\text{Ga}$ -labeled exendin-4 analogues using NODAGA as chelator. A high-specific activity reduces the necessary amount of peptide and, thus, minimizes the risk of side effects due to receptor activation such as hypoglycemia [44].

#### *PET/CT Protocol.*

The administered activity is 100–200 MBq for imaging of insulinomas and congenital hyperinsulinism. The activity is administered intravenously, and imaging can be performed after an uptake period of 30 min. For anatomic mapping especially in newborns and children, PET/MR imaging is preferred to PET/CT imaging. The normal biodistribution includes uptake in kidneys, pancreas, and duodenum. Dosimetry studies have confirmed that the radiation exposure from  $^{68}\text{Ga}$ -NODAGA-exendin-4 is several fold lower than from other conventional radiopharmaceuticals [47].

#### $^{68}\text{Ga}$ -Pentixafor

Chemokines are important regulators of tumor environment and play an important role in tumor development. C-X-C motif chemokine receptor 4 (CXCR4), a 40 kDa G-protein-coupled receptor of the chemokine receptor family, is involved in many pathological processes including cancer [48]. CXCR4 overexpression is observed in more than 30 different types of cancer entities such as breast, prostate, lung, ovary, esophagus, renal cell carcinoma, colon cancer, and neuroblastoma [48, 49]. CXCR4 is involved in various pathways which are vital for cell migration, hematopoiesis, angiogenesis, tumor growth, and metastases formation.  $^{68}\text{Ga}$ -Pentixafor is a PET-based radiopharmaceutical that specifically targets the CXCR4 receptor.

#### *Mechanism of Localization.*

CXCR4 belongs to the family of G-protein-coupled receptors. Pathological overexpression has been observed in various solid cancers and also in hematological malignancies such as multiple myeloma and lymphomas [50]. The only natural ligand for the CXCR4 receptor is CXCL12/SDF-1. The binding of SDF-1 to CXCR4 activates many downstream processes involved in cell adhesion and cell migration [50]. In tumor moieties, the adhesion of the ligand CXCL12 and the receptor CXCR4 is a key trigger for tumor growth, invasiveness, and metastasis.

#### *PET/CT Protocol.*

$^{68}\text{Ga}$ -Pentixafor has been shown as a useful tracer for multiple myeloma, gliomas, lung cancer, breast cancer, and also colon cancer. In lymphomas of the central nervous system,  $^{68}\text{Ga}$ -Pentixafor is much more sensitive than  $^{18}\text{F}$ -FDG in tumor detection due to no

uptake of  $^{68}\text{Ga}$ -Pentixafor in normal brain tissue. The activity is administered intravenously, and the activity administered is 100–150 MBq. PET imaging can be started after a minimum uptake period of 30 min. The normal biodistribution includes liver, faint uptake in heart and gall bladder, and high uptake is observed in the kidneys [49].

### **3.3 Positron Emission Tomography/Magnetic Resonance Imaging (PET/MRI)**

PET is a powerful imaging modality that can provide functional information about a specific organ or body at the cellular or molecular level. However, PET imaging does hardly provide any morphological information regarding the anatomical status. This necessitates the need of hybrid imaging systems by combining anatomical imaging like MRI or CT with PET systems. Initially, PET/CT systems were developed which represent nowadays the clinical standard. Technological progress with respect to photomultiplier technology replacing conventional photomultipliers with semiconductor detectors like silicon photomultipliers (SiPM)—conventional photomultipliers are highly susceptible to even small magnetic fields—made PET/MRI systems possible allowing to acquire PET and MR images at the same time in a truly simultaneous modus. The first fully integrated clinical whole-body PET/MR system was commercially available in 2010. This opened up new possibilities for combined morphological and also functional imaging with PET and MR such as diffusion weighted or contrast-enhanced parametric MR imaging in addition to standard morphological T1- and T2-based sequences complementing specific PET tracer information with excellent soft tissue contrast which CT imaging cannot render. These combined PET/MRI systems allow detailed biological characterization of tumors and their phenotypes and, thus, help improving subsequent patient management. Preclinical hybrid systems, on the other hand, foster basic research providing noninvasively longitudinal data of different functional and morphologic aspects of tumors and their development under naive and treatment conditions.

### **3.4 Quantification**

SPECT and especially PET tomographic imaging are quantitative imaging modalities allowing calculation of local tracer accumulation in a region of interest (ROI). Quantification in principle is possible by two different approaches: First, the so-called semiquantitative analysis which includes parameters obtained from single time point images such as the standardized uptake value (SUV) in PET imaging, measures of activity concentrations in kBq per voxel (SPECT, PET), and combined parameters such as metabolic tumor volume. Secondly, absolute quantification methods for PET imaging requiring both dynamic imaging sequences of the region of interest and measurement of an input function driving the tracer uptake within the ROI such as Patlak graphical analysis or nonlinear regression analysis based on compartmental kinetic modelling

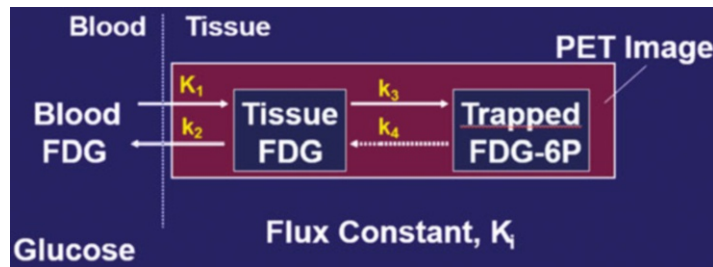


**Fig. 8** Compartment model for calculating  $^{18}\text{F}$ -FDG tumor metabolism

[51, 52]. For  $^{18}\text{F}$ -FDG, the different quantification methods will be briefly explained hereinafter. Although quantification methods are commonly applied in PET imaging, these methods can be used for SPECT as well.

#### 3.4.1 Nonlinear Regression Analysis

The standard compartmental modeling approach for  $^{18}\text{F}$ -FDG is based on a 2 tissue, 4 parameter model (plasma space, unbound, and phosphorylated cell compartments) [53]. The rate constants  $K_1$  and  $k_2$  define the forward and reverse transport of  $^{18}\text{F}$ -FDG between plasma and cell while  $k_3$  represents phosphorylation by hexokinase and  $k_4$ , the rate of dephosphorylation which is often set to zero in tissues other than liver ( $k_4 = 0$ ; prerequisite for Patlak graphical analysis) owing to the very slow dephosphorylation process. Tissue  $^{18}\text{F}$ -FDG net uptake  $K_{\text{NLR}}$  (mmol/min/mL of target tissue) can be calculated by nonlinear regression as well as parameters  $K_1$ ,  $k_2$ ,  $k_3$ , and  $k_4$  with  $K_1$  serving as surrogate parameter for (tracer) blood flow (Fig. 8).

#### 3.4.2 Patlak Analysis

With  $k_4 = 0$ ,  $K_{\text{NLR}}$  can be simply calculated by a graphical approach resulting in the formula:  $K_{\text{NLR}} = K_1 \times k_3 / (k_2 + k_3)$ .

This approach however does not allow calculation of single parameters  $K_1$ ,  $k_2$ , and  $k_3$ .

As both quantitative approaches require a sequence of dynamic PET scans over the tumor of usually 60 min in case of  $^{18}\text{F}$ -labeled tracers for measuring the tumor time-activity curves as well as arterial or venous blood sampling during each time frame of the imaging sequence for tracer concentration determination in the plasma, these time- and labor-consuming approaches are primarily used for research purposes but hardly in the daily clinical routine.

#### 3.4.3 Standardized Uptake Value (SUV)

This semiquantitative measure represents the activity within an ROI corrected for the injected activity and for patient weight or lean body mass as a substitute for the distribution volume of the patient [53]. This parameter is the most widely used quantitative parameter in a routine clinical setting [54]. Tumor SUV calculation requires

both an emission and a transmission scan at one time point only for generating attenuation-corrected images based on the tissue activity:

$$\text{SUV} = A \times m / \text{IA}$$

where “A” is the mean tissue activity (MBq/g) within the ROI, “IA” is the injected activity (MBq), and “m” is the patient body weight (kg). More recently, body weight has been substituted by lean body mass as a more precise substitute for the tracer distribution volume.

## 4 Conclusion

Over the years, nuclear medicine has evolved as a modern imaging methodology with improved diagnostic efficacy in diagnosis and follow-up of malignant tumor entities. There has been a vast technological development in imaging systems and reconstruction algorithms from Anger's first gamma camera to modern-day hybrid PET/CT and PET/MRI systems for both men and mice with increased detection efficiency and decreased imaging time. The field of radiochemistry also witnessed an enormous growth starting from implementation of  $^{131}\text{I}$  for differentiated thyroid cancer diagnosis and therapy to the latest ongoing radiolabeling efforts of novel small-protein-based molecular ligands and probes concerning each specific disease pathology. Thus, radionuclide imaging has established itself as a unique imaging modality providing specific information about a wide variety of molecular pathways and cellular features involved in different cancers which allows improved diagnosis and disease management in tumor patients and fosters basic preclinical research.

## References

1. Saha GB, Saha GB (1992) Fundamentals of nuclear pharmacy, vol 4. Springer, New York
2. Sorenson JA, Phelps ME (1987) Physics in nuclear medicine. Grune & Stratton, New York
3. Lange C, Apostolova I, Lukas M, Huang KP, Hofheinz F, Gregor-Mamoudou B, Brenner W, Buchert R (2014) Performance evaluation of stationary and semi-stationary acquisition with a non-stationary small animal multi-pinhole SPECT system. Mol Imaging Biol 16(3):311–316. <https://doi.org/10.1007/s11307-013-0702-3>
4. Hameed A, Brady JJ, Dowling P, Clynes M, O'Gorman P (2014) Bone disease in multiple myeloma: pathophysiology and management. Cancer Growth Metastasis 7:33–42. <https://doi.org/10.4137/CGM.S16817>
5. Macedo F, Ladeira K, Pinho F, Saraiva N, Bonito N, Pinto L, Goncalves F (2017) Bone metastases: an overview. Oncol Rev 11 (1):43–49. <https://doi.org/10.4081/oncol.2017.321>
6. Babu MCS, Garg S, Lakshmaiah KC, Babu KG, Kumar RV, Loknatha D, Abraham LJ, Rajeev LK, Lokesh KN, Rudresha AH, Rao SA (2017) Colorectal cancer presenting as bone metastasis. J Cancer Res Ther 13(1):80–83. <https://doi.org/10.4103/0973-1482.181177>
7. Khalil M (2010) Basic sciences of nuclear medicine. Springer Science & Business Media, New York
8. Florencio-Silva R, Sasso GRD, Sasso-Cerri E, Simoes MJ, Cerri PS (2015) Biology of bone tissue: structure, function, and factors that

- influence bone cells. *Biomed Res Int.* <https://doi.org/10.1155/2015/421746>
9. Arbab AS, Koizumi K, Toyama K, Arai T, Araki T (1998) Technetium-99m-tetrofosmin, technetium-99m-MIBI and thallium-201 uptake in rat myocardial cells. *J Nucl Med* 39(2):266–271
  10. Rousset B, Dupuy C, Miot F, Dumont J (2000) Chapter 2 Thyroid hormone synthesis and secretion. In: Feingold KR, Anawalt B, Boyce A et al (eds). *Endotext*, South Dartmouth (MA)
  11. Silberstein EB, Alavi A, Balon H, Becker D, Charles N, Clarke S, Divgi C, Donohoe K, Delbeke D, Goldsmith SJSNM (2006) Society of Nuclear Medicine Procedure Guideline for scintigraphy for differentiated papillary and follicular thyroid cancer. 8 [https://s3.amazonaws.com/rdcms-snmri/files/production/public/docs/Scintigraphy%20for%20Differentiated%20Thyroid%20Cancer%20V3%2000%20\(9-25-06\).pdf](https://s3.amazonaws.com/rdcms-snmri/files/production/public/docs/Scintigraphy%20for%20Differentiated%20Thyroid%20Cancer%20V3%2000%20(9-25-06).pdf)
  12. Bombardieri E, Giammarile F, Aktolun C, Baum RP, Bischof Delaloye A, Maffioli L, Moncayo R, Mortelmans L, Pepe G, Reske SN, Castellani MR, Chiti A, European Association for Nuclear Medicine M (2010) 131I/123I-metaiodobenzylguanidine (mIBG) scintigraphy: procedure guidelines for tumour imaging. *Eur J Nucl Med Mol Imaging* 37(12):2436–2446. <https://doi.org/10.1007/s00259-010-1545-7>
  13. Yu S (2006) Review of F-FDG synthesis and quality control. *Biomed Imaging Interv J* 2(4):e57. <https://doi.org/10.2349/bij.2.4.e57>
  14. Buck AK, Reske SN (2004) Cellular origin and molecular mechanisms of 18F-FDG uptake: is there a contribution of the endothelium? *J Nucl Med* 45(3):461–463
  15. Fowler JS, Ido T (2001) DESIGN AND SYNTHESIS OF 2-DEOXY-2 [<sup>18</sup>F] FLUORO-D-GLUCOSE ([<sup>18</sup>F] FDG). Brookhaven National lab., Upton, NY (US)
  16. Kawada K, Iwamoto M, Sakai Y (2016) Mechanisms underlying F-18-fluorodeoxyglucose accumulation in colorectal cancer. *World J Radiol* 8(11):880–886. <https://doi.org/10.4329/wjr.v8.i11.880>
  17. Delbeke D, Coleman RE, Guiberteau MJ, Brown ML, Royal HD, Siegel BA, Townsend DW, Berland LL, Parker JA, Hubner K, Stabin MG, Zubal G, Kachelriess M, Cronin V, Holbrook S (2006) Procedure guideline for tumor imaging with 18F-FDG PET/CT 1.0. *J Nucl Med* 47(5):885–895
  18. Kulshrestha RK, Vinjamuri S, England A, Nightingale J, Hogg P (2016) The role of <sup>18</sup>F-sodium fluoride PET/CT bone scans in the diagnosis of metastatic bone disease from breast and prostate cancer. *J Nucl Med Technol* 44(4):217–222. <https://doi.org/10.2967/jnmt.116.176859>
  19. Roodman GD (2004) Mechanisms of disease: Mechanisms of bone metastasis. *New Engl J Med* 350(16):1655–1664. <https://doi.org/10.1056/NEJMra030831>
  20. Sadeghi MV, Sedaghat S (2018) Is <sup>99m</sup>Tc-methylene diphosphonate bone scintigraphy a sensitive method for detecting bone lesions in multiple myeloma? *Casp J Intern Med* 9(2):140–143. <https://doi.org/10.22088/cjim.9.2.140>
  21. Segall G, Delbeke D, Stabin MG, Even-Sapir E, Fair J, Sajdak R, GTJJoNM S (2010) SNM practice guideline for sodium <sup>18</sup>F-fluoride PET/CT bone scans 1.0. *J Nucl Med* 51(11):1813–1820
  22. Chen W, Cloughesy T, Kamdar N, Satyamurthy N, Bergsneider M, Liau L, Mischel P, Czernin J, Phelps ME, Silverman DH (2005) Imaging proliferation in brain tumors with <sup>18</sup>F-FLT PET: comparison with <sup>18</sup>F-FDG. *J Nucl Med* 46(6):945–952
  23. Campillo N, Falcones B, Otero J, Colina R, Gozal D, Navajas D, Farre R, Almendros I (2019) Differential oxygenation in tumor microenvironment modulates macrophage and cancer cell crosstalk: novel experimental setting and proof of concept. *Front Oncol* 9:43. <https://doi.org/10.3389/fonc.2019.00043>
  24. Masaki Y, Shimizu Y, Yoshioka T, Tanaka Y, Nishijima K, Zhao S, Higashino K, Sakamoto S, Numata Y, Yamaguchi Y, Tamaki N, Kuge Y (2015) The accumulation mechanism of the hypoxia imaging probe "FMISO" by imaging mass spectrometry: possible involvement of low-molecular metabolites. *Sci Rep* 5:16802. <https://doi.org/10.1038/srep16802>
  25. Chanmee T, Ontong P, Konno K, Itano N (2014) Tumor-associated macrophages as major players in the tumor microenvironment. *Cancers (Basel)* 6(3):1670–1690. <https://doi.org/10.3390/cancers6031670>
  26. Gilkes DM, Semenza GL, Wirtz D (2014) Hypoxia and the extracellular matrix: drivers of tumour metastasis. *Nat Rev Cancer* 14(6):430–439. <https://doi.org/10.1038/nrc3726>
  27. Milotti E, Stella S, Chignola R (2017) Pulsation-limited oxygen diffusion in the tumour microenvironment. *Sci Rep* 7:39762. <https://doi.org/10.1038/srep39762>

28. Muz B, de la Puente P, Azab F, Azab AK (2015) The role of hypoxia in cancer progression, angiogenesis, metastasis, and resistance to therapy. *Hypoxia* (Auckl) 3:83–92. <https://doi.org/10.2147/HP.S93413>
29. Xu Z, Li XF, Zou H, Sun X, Shen B (2017) <sup>18</sup>F-Fluoromisonidazole in tumor hypoxia imaging. *Oncotarget* 8(55):94969–94979. <https://doi.org/10.18632/oncotarget.21662>
30. Gladson CL, Prayson RA, Liu WM (2010) The pathobiology of glioma tumors. *Annu Rev Pathol* 5:33–50. <https://doi.org/10.1146/annurev-pathol-121808-102109>
31. Law I, Albert NL, Arbizu J, Boellaard R, Drzezga A, Galldiks N, la Fougère C, Langen K-J, Lopci E, Lowe V (2019) Joint EANM/EANO/RANO practice guidelines/SNMMI procedure standards for imaging of gliomas using PET with radiolabelled amino acids and [18 F] FDG: version 1.0. *Eur J Nucl Med Mol Imaging* 46(3):540–557
32. Maurer GD, Brucker DP, Stoffels G, Filipski K, Filss CP, Mottaghay FM, Galldiks N, Steinbach JP, Hattingen E, Langen KJ (2019) (18)F-FET PET imaging in differentiating glioma progression from treatment-related changes—a single-center experience. *J Nucl Med* 61:505–511. <https://doi.org/10.2967/jnumed.119.234757>
33. Cecon G, Lazaridis L, Stoffels G, Rapp M, Weber M, Blau T, Lohmann P, Kebir S, Herrmann K, Fink GR, Langen KJ, Glas M, Galldiks N (2018) Use of FET PET in glioblastoma patients undergoing neurooncological treatment including tumour-treating fields: initial experience. *Eur J Nucl Med Mol Imaging* 45(9):1626–1635. <https://doi.org/10.1007/s00259-018-3992-5>
34. Pope WB, Brandal G (2018) Conventional and advanced magnetic resonance imaging in patients with high-grade glioma. *Q J Nucl Med Mol Imaging* 62(3):239–253. <https://doi.org/10.23736/S1824-4785.18.03086-8>
35. Langen KJ, Galldiks N (2018) Update on amino acid PET of brain tumours. *Curr Opin Neurol* 31(4):354–361. <https://doi.org/10.1097/WCO.0000000000000574>
36. Koopman T, Verburg N, Schuit RC, Pouwels PJW, Wesseling P, Windhorst AD, Hoekstra OS, de Witt Hamer PC, Lammertsma AA, Boellaard R, Yaquib M (2018) Quantification of O-(2-[(18)F]fluoroethyl)-L-tyrosine kinetics in glioma. *EJNMMI Res* 8(1):72. <https://doi.org/10.1186/s13550-018-0418-0>
37. Stegmayr C, Bandelow U, Oliveira D, Lohmann P, Willuweit A, Filss C, Galldiks N, Lubke JH, Shah NJ, Ermert J, Langen KJ (2017) Influence of blood-brain barrier permeability on O-(2-(18)F-fluoroethyl)-L-tyrosine uptake in rat gliomas. *Eur J Nucl Med Mol Imaging* 44(3):408–416. <https://doi.org/10.1007/s00259-016-3508-0>
38. Chang SS (2004) Overview of prostate-specific membrane antigen. *Rev Urol* 6(Suppl 10): S13–S18
39. Fendler WP, Eiber M, Beheshti M, Bomanji J, Ceci F, Cho S, Giesel F, Haberkorn U, Hope TA, Kopka KJEJonn, imaging M (2017) <sup>68</sup>Ga-PSMA PET/CT: Joint EANM and SNMMI procedure guideline for prostate cancer imaging: version 1.0. *Eur J Nucl Med Mol Imaging* 44(6):1014–1024
40. Hofman MS, Lau WFE, Hicks RJ (2015) Somatostatin receptor imaging with Ga-68 DOTATATE PET/CT: clinical utility, Normal patterns, pearls, and pitfalls in interpretation. *Radiographics* 35(2):500–516. <https://doi.org/10.1148/rug.352140164>
41. Wild D, Bomanji JB, Benkert P, Maecke H, Ell PJ, Reubi JC, Caplin ME (2013) Comparison of Ga-68-DOTANOC and Ga-68-DOTATATE PET/CT within patients with Gastroenteropancreatic neuroendocrine tumors. *J Nucl Med* 54(3):364–372. <https://doi.org/10.2967/jnumed.112.111724>
42. Virgolini I, Ambrosini V, Bomanji JB, Baum RP, Fanti S, Gabriel M, Papathanasiou ND, Pepe G, Oyen W, De Cristoforo CJEJonn, imaging M (2010) Procedure guidelines for pet/ct tumour imaging with 68 Ga-dota-conjugated peptides: 68 Ga-dota-tox, 68 Ga-dota-noc, 68 Ga-dota-tate. *Eur J Nucl Med Mol Imaging* 37(10):2004–2010
43. Ro C, Chai WX, Yu VE, Yu R (2013) Pancreatic neuroendocrine tumors: biology, diagnosis, and treatment. *Chin J Cancer* 32(6):312–324. <https://doi.org/10.5732/cjc.012.10295>
44. Jansen TJP, van Lith SAM, Boss M, Brom M, Joosten L, Behe M, Buitinga M, Gotthardt M (2019) Exendin-4 analogs in insulinoma theranostics. *J Labelled Comp Radiopharm* 62(10):656–672. <https://doi.org/10.1002/jlcr.3750>
45. Reubi JC, Waser B (2003) Concomitant expression of several peptide receptors in neuroendocrine tumours: molecular basis for in vivo multireceptor tumour targeting. *Eur J Nucl Med Mol Imaging* 30(5):781–793. <https://doi.org/10.1007/s00259-003-1184-3>
46. Zimmer T, Stolzel U, Bader M, Koppenhagen K, Hamm B, Buhr H, Riecken EO, Wiedenmann B (1996) Endoscopic

- ultrasonography and somatostatin receptor scintigraphy in the preoperative localisation of insulinomas and gastrinomas. Gut 39 (4):562–568. <https://doi.org/10.1136/gut.39.4.562>
47. Boss M, Buitinga M, Jansen TJP, Brom M, Visser EP, Gothardt M (2020) PET-based human dosimetry of (68)Ga-NODAGA-Exendin-4, a tracer for beta-cell imaging. J Nucl Med 61(1):112–116. <https://doi.org/10.2967/jnumed.119.228627>
48. Breun M, Monoranu CM, Kessler AF, Matthies C, Lohr M, Hagemann C, Schirbel A, Rowe SP, Pomper MG, Buck AK, Wester HJ, Ernestus RI, Lapa C (2019) [(68)Ga]-Pentixafor PET/CT for CXCR4-Mediated Imaging of Vestibular Schwannomas. Front Oncol 9:503. <https://doi.org/10.3389/fonc.2019.00503>
49. Herrmann K, Lapa C, Wester HJ, Schottelius M, Schiepers C, Eberlein U, Bluemel C, Keller U, Knop S, Kropf S, Schirbel A, Buck AK, Lassmann M (2015) Bio-distribution and radiation dosimetry for the chemokine receptor CXCR4-targeting probe 68Ga-pentixafor. J Nucl Med 56(3):410–416. <https://doi.org/10.2967/jnumed.114.151647>
50. Philipp-Abbrederis K, Herrmann K, Knop S, Schottelius M, Eiber M, Lucke K, Pietschmann E, Habringer S, Gerngross C, Franke K, Rudelius M, Schirbel A, Lapa C, Schwamborn K, Steidle S, Hartmann E, Rosenwald A, Kropf S, Beer AJ, Peschel C, Einsele H, Buck AK, Schwaiger M, Gotze K, Wester HJ, Keller U (2015) In vivo molecular imaging of chemokine receptor CXCR4 expression in patients with advanced multiple myeloma. Embo Mol Med 7(4):477–487. <https://doi.org/10.15252/emmm.201404698>
51. Brenner W, Vernon C, Muzi M, Mankoff DA, Link JM, Conrad EU, Eary JF (2004) Comparison of different quantitative approaches to 18F-fluoride PET scans. J Nucl Med 45 (9):1493–1500
52. Weber WA, Schwaiger M, Avril N (2000) Quantitative assessment of tumor metabolism using FDG-PET imaging. Nucl Med Biol 27 (7):683–687. [https://doi.org/10.1016/s0969-8051\(00\)00141-4](https://doi.org/10.1016/s0969-8051(00)00141-4)
53. Graham MM, Peterson LM, Hayward RM (2000) Comparison of simplified quantitative analyses of FDG uptake. Nucl Med Biol 27 (7):647–655. [https://doi.org/10.1016/s0969-8051\(00\)00143-8](https://doi.org/10.1016/s0969-8051(00)00143-8)
54. Lucignani G, Paganelli G, Bombardieri E (2004) The use of standardized uptake values for assessing FDG uptake with PET in oncology: a clinical perspective. Nucl Med Commun 25(7):651–656. <https://doi.org/10.1097/01.mnm.0000134329.30912.49>



# Chapter 22

## From Operating Table to Laboratory Bench: The Path Toward Metastasis Research from the Clinical Setting

Miguel E. Alberto Vilchez and Beate Rau

### Abstract

Presence of metastasis translates unequivocally into worse prognosis for our patients. Translational medicine has been our response to offer patients better therapeutic options. This chapter aims to provide an overview for clinicians to send the necessary metastatic tissue on the right path toward the laboratory bench, overcoming biases and possible data misinterpretations derived from poor sample quality.

**Key words** Biomarker, SOP, Snap-freezing, Biobank, Metastasis

---

### 1 Introduction

“Bench to bedside” is a common term used in translation research to exert the importance of direct collaboration between basic science researchers and clinical researchers. However, with the advance of techniques used on patient-derived tissue, a useful guide to “bedside to bench” may be just as useful. As perhaps already articulately compiled in this book, the presence of metastasis instantly categorizes our patients in the worst disease stadiums and therefore exert reduced overall survival rates.

Metastasectomies are becoming standard of care therapeutic options across various cancer types. Evidence shows that despite metastasectomies being performed in patients presenting with more comorbidities, outcomes are more favorable. These procedures are now safer to carry out than ever before, thus lowering the threshold for other cancer types and resulting in more patients being intervened [1]. Prolonged survival can be seen in patients following resection of metastatic sites in the liver, lung, and brain, among others. Development of more systemic and targeted therapies is prolonging survival rates in patients with various tumor entities, and later resection of residual metastatic disease is being used with increasing frequency [2]. Nevertheless, careful patient

selection and critical decision-making are still necessary to prudently determine patients that will benefit from metastasectomies.

An invaluable resource widely used during this decision-making process are biomarkers, especially those that could predict metachronous metastasis or disease progression after synchronous metastasis. For research in the biomarker field, sample preparation has been pointed out as a major issue during molecular profiling from clinical tissue at any scale. This is due very possibly to a complex workflow from bedside to bench in comparison to the processing endured by cultured cells. For biomarker discovery and/or validation, it is “critical that the protein complement of diseased and healthy tissue is profiled directly *in vivo*, at the site of pathological process.” This makes, for example, the use of frozen tissue samples the gold standard for MS-based proteomic profiling and incredibly valuable for disease-relevant biomarker research [3].

Clinicians are often unaware of optimal or minimal conditions for processing of samples sent by them or their departments. It is essential to provide high-quality samples that are collected and handled under standardized conditions to minimize potential biases or confounding results. This chapter aims to provide a proper start in the path of bedside to bench translational medicine.

---

## 2 Materials

1. Standard operating procedures (SOPs): These are detailed, in written format instructions to achieve uniformity and reproducibility of routine functions. SOPs are to be established conscientiously in a multidisciplinary context. Anesthesiologists, surgeons, OR-nurses, medical technical assistants, and quality control authorities must be engaged in a conjunct and evolving discussion to formulate said “clinical” SOPs. Ideally, these protocols should be revised biannually to improve any and all aspects concerning optimization of routine procedures. In the laboratory context, SOPs should be conjointly developed by researchers, lab technicians, animal caretakers, and quality control authorities.
2. Centralized and/or regional biobank [4].
3. Specialized personnel with experience in sample handling and processing of samples for further laboratory use and long-term storage.

---

## 3 Methods: Processing of Solid Tissue

1. Detailed acquisition of the following information is of paramount importance:

- (a) Tissue of origin.
  - (b) Anatomical situation.
  - (c) Time of anesthesia administration.
  - (d) Time since ligation of vessels.
  - (e) *See Note 1.*
2. All specimens removed during surgery must be submitted to the surgical pathology department for examination. This must be accompanied always with the following information:
    - (a) Patient identification:
      - Name.
      - Medical record number or case number.
      - Age.
      - Sex.
    - (b) Date and time of collection of the specimen.
    - (c) Physicians name, department, and contact number.
    - (d) Medical history:
      - Suspected diagnosis.
      - Clinical history, including previous biopsies, surgeries, chemotherapies, radiotherapies, immunotherapies, etc.
      - Secondary diagnoses the patient might have.
    - (e) Multiple specimens from the same operative procedure must be listed with a precise description of the anatomic site and uniquely labeled.
    - (f) Record of the time of clamping and of excision of the specimen.
    - (g) The surgeon should complete the pathology form, if possible, in advanced.
    - (h) The peri-surgical staff should send the fresh tissue specimen to the pathology department immediately.
    - (i) *See Note 2.*
3. During surgery:
    - (a) The most important aspect to take into consideration when harvesting liver, pancreas, lung, and colorectal metastasis is mainly the amount of tissue that is taken. For example, in lung metastasectomies, “wedge resections” or atypical resections help ensure a good mount of tissue for processing because of the nature of the procedure, using a stapler to excise the tumor leaves you with enough tissue to send for further processing.
    - (b) Peritoneal/pleural metastasis: Make sure to properly record the Peritoneal Carcinomatosis Index (PCI) before

taking any samples. Due to the morphology of the metastasis, procuring a proper sample might prove hard to be. This is especially true for peritoneal or pleural metastasis that are flat, even, and regular rather than voluptuous, classic tumor-like metastases. Such a finding may come up, for example, after receiving intraperitoneal or intrapleural chemotherapy treatment. Attention must be paid to harvest enough material from these lesions to send to the biobank and/or laboratory.

4. With every tissue specimen harvested from a patient, it is our recommendation to collect concomitantly two whole blood samples. These samples can be used for hematology, clinical chemistry, plasma and/or serum preparation, next-generation sequencing (NGS) techniques, among others. Reliability of laboratory values heavily relies on sample integrity, and thus attention must be paid to the following factors:
  - (a) Right choice of container (i.e., EDTA-coated tubes, lithium-heparin-coated tubes). Carefully consider further uses of the sample to choose the correct container.
  - (b) After blood extraction, mix carefully with the coating substance in the tubes.
  - (c) Temperature control between transport and handling steps (2–4 °C) up to long-term storage (−80 °C).
  - (d) *See Note 3.*
5. Pathology department:
  - (a) The pathologist should describe the specimen per custom *see Note 4.*
  - (b) Special care must be taken while dissecting the specimen regarding hygiene and sample integrity. Instruments must be cleaned or changed when changing from normal tissue to tumor tissue and vice versa.
  - (c) Routine diagnostic must be prioritized, hence enough tissue must be taken for fixation and embedding. Afterwards, if there is sufficient material available for the biobank, supply the technicians with representative parts of the tumor (malignant), premalignant conditions (transition zones), and normal tissue.
  - (d) Take representative parts of tissue for routine diagnosis (for fixation and embedding) as a priority and decide whether there is sufficient material available for the tissue bank.
  - (e) Annotation of cryo containers should contain the following information:
    - Patient ID (according to Data Protection Regulations in each country).

- Tissue type.
- Anatomical location.
- Unique cryo container number.

(f) Intraoperative frozen section (FS):

- Intraoperative FS should always be treated as elective procedures. Rarely this procedure will be available in an emergency situation. Therefore, a previous appointment with the pathologist should be arranged:
  - The pathologist must be informed at the beginning of the operation.
  - All samples must be correctly labeled as mentioned previously [5].
  - Information surfaced in the intraoperative FS must be documented and shared with the biobank.
- *See Note 5.*

6. Snap-freezing:

- (a) Prepare the tissue sample for snap-freezing on a clean surface, using clean instruments. Given the case that both normal and tumoral tissue is present in the sample, make sure to use different instruments when preparing each one of them *see Notes 6 and 7*.
- (b) Precool the freezing medium (2-methylbutane) until opaque drops begin to appear and the solution becomes misty; this will bring the medium toward the tissue's optimal freezing point ( $-160^{\circ}\text{C}$ ). The available options are:
  - $\text{LN}_2$ : Suspend a vessel of the freezing medium in  $\text{LN}_2$ .
  - Dry ice: Add dry ice to the freezing medium until a slush is formed.
- (c) Label cryovials, cryomolds, or cryostraws with a barcode and/or sequential code (depending on local laboratory practice). Be sure to use a pen with ink that is able to withstand long-term storage at low temperatures. If a barcode is used, a secondary readable method must be put in place to make the sample identifier readable at institutions where there are no barcode readers.
- (d) Record the following data:
  - Local identifier number.
  - Pathology number.
  - Date.
  - Lag time from arterial clamping and excision to freezing.
  - Type of tissue.

- Site.
  - Characteristics (tumor, normal, and/or premalignant).
  - If a barcode system is in use, the barcode can be scanned, and the abovementioned data recorded.
- (e) Prepare a minimum volume of  $0.5 \text{ cm}^3$  for snap-freezing. This may prove a challenge for specific samples such as peritoneal or pleural metastasis. Therefore, it is of paramount importance that the surgeon be aware of the minimum amount of needed tissue sample. As an example, proteomics facilities may ask for at least  $10 \mu\text{l}$  of a protein at a concentration of  $>1 \text{ mg/ml}$  for adequate sample analysis. It is common that many samples are not processed because the minimal amount is not met *see Note 8*.
- Smaller samples should nevertheless be snap-frozen and stored in the biobank.
  - There should be enough material, freeze duplicate samples.
- (f) Freeze directly in freezing medium. Do not remove the tissue from the medium until freezing is complete (5 s or less, depending on size), but ensure that the sample does not crack. Remove the sample from the medium and enclose it in the labeled cryovial. It is good practice to strive to snap-freeze all tissue within 5 min of excision from the patient. Some protocols are more generous and mention 30 min. Tissue subject to a delay of up to 2 h should still be collected and the delay noted within the inventory database. The available options for freezing are:
- Embed the tissue samples in Optimal Cutting Temperature (O.C.T.) compound and freeze in freezing medium.
  - Freeze directly in the medium. The freezing medium should have been previously cooled either by suspension in  $\text{LN}_2$  or by addition of dry ice.
- (g) Orientate the tissue on a piece of cork and an equally sized piece of Whatman paper soaked in physiological salt solution.
- (h) If the cryostaw system is used to introduce a sample of tissue into the straw, thermally seal each extremity, and place in  $\text{LN}_2$ .

---

## 4 Notes

1. For overall usefulness of the biobank as a continuously and active resource for scientific research, careful and precise documentation for the processing of all tissue specimens is of critical importance. All of the previous data must be recorded in detail, since they are known to have an impact in the quality of posteriorly acquired biomolecules. Of special relevance regarding tissue quality is the warm ischemia time, defined as the period of time between ligation of blood supply and placement in definitive fixative.
2. These protocols for collecting and freezing tissue samples were developed within the European Human Frozen Tumor Tissue Bank (TuBaFrost) project [6] and the Standardization and Improvement of Generic Pre-analytical Tools and Procedures for In Vitro Diagnostics (SPIDIA) project [7]. These recommended protocols contain choices and recommendations for preserving solid tissue and describe the roles of key people involved in the process. Consult the CEN norms for more detailed information on the processing of snap-frozen tissue and FFPE samples for protein DNA and RNA isolation (CEN/TS 16826-1-2 and CEN/TS 16827-1-3).
3. Consult the SOPs for serum and plasma collection [8]
4. According to IARC protocol, the pathologist should be the responsible for assessing quality material to be stored in the biobank and hence used for further research purposes.
5. Intraoperative FS gives out a gross and rapid diagnosis of the pathologic process, giving the surgeon the necessary guidance on intraoperative management and therapeutic decision-making. Clear examples are the need to clarify if the resection margins are free of disease before wound closure and presence or absence of lymph node involvement to determine further resectability or the lack thereof. Known applications are:
  - (a) Establishment of the nature of the tumor, i.e. benign, malign or suspicious.
  - (b) Establishment of the grading of the tumor.
  - (c) Determination of the synchronicity of another tumor in the vicinity.
  - (d) Determination of the organ of origin.
  - (e) Determination of adequate marginal resection.
  - (f) Determination of evidence of invasion into lymph nodes, nerves, vessels, and adjacent or distant organs.
  - (g) Acquiring tissue for special studies [5].

6. The following steps were modified from the IARC Common Minimum Technical Standards and Protocols of Biobanks Dedicated to Cancer Research [4]. It is advisable to consult the published and approved CEN norms for handling of FFPE and Snap-Frozen Tissue for further research.
  - (a) CEN/TS 16826-1:2015: Snap-frozen tissues—RNA isolation.
  - (b) CEN/TS 16826-2:2015: Snap-frozen tissues—Protein isolation.
  - (c) CEN/TS 16827-1:2015: FFPE tissues—RNA isolation.
  - (d) CEN/TS 16827-2:2015: FFPE tissues—Protein isolation.
  - (e) CEN/TS 16827-3:2015: FFPE tissues—DNA isolation.
7. Before tissue stabilization by means of snap-freezing, the protein, RNA, and DNA profiles could change. Mainly dependent on the duration of cold and/or warm ischemia, these changes could significantly alter the scientific outcome. Snap-freezing is the process by which samples are lowered to temperatures below  $-70^{\circ}\text{C}$  very rapidly using dry ice or liquid nitrogen. By doing so, sample integrity can be assured, so that the known wide array of options for tissue analysis, such as extraction of proteins, RNA, and DNA, can be guaranteed. All pre-analytical conditions and time spans should be documented.
8. Fresh frozen tissue is the specimen of choice for mass spectrometry-based proteomics because proteins and other biomolecules are unmodified and preserved in their biological tissue environment. Snap-freezing in liquid nitrogen ( $\text{LN}_2$ ) provides excellent protein integrity and a wide array of options for MS-based proteomic profiling. Fresh frozen specimens are typically processed and analyzed as tissue blocks, thin tissue slices, or laser capture microdissection (LCM) specimens. The availability and storage of FF tissues are issues that should be considered before designing any MS-based biomarker study [3].

---

## Acknowledgments

To the editors of this book: for giving young researchers the opportunity to contribute in every way possible to the well-being of our patients.

## References

1. Bartlett EK et al (2015) The rise in metastasectomy across cancer types over the past decade. *Cancer* 121:747–757
2. Bast RC (2016) Holland-Frei cancer medicine, 9th edn. Wiley-Blackwell, Hoboken, New Jersey
3. Ye X, Prieto DA, Chan KC, Wei B-R, Blonder J (2013) Tissue sample preparation for proteomic analysis. In: Proteomic and Metabolomic approaches to biomarker discovery 39–50. Elsevier, Amsterdam. <https://doi.org/10.1016/B978-0-12-394446-7.00003-0>
4. Mendy M, Caboux E, Lawlor T, Wright R (2017) J. & wild, C. P. common minimum technical standards and protocols for biobanks dedicated to Cancer research, vol 44. IARC technical publications). (International agency for research on cancer, Lyon cedex 5. Jaafar H (2006) Intra-operative frozen section consultation: concepts, applications and limitations. *Malays J Med Sci* 13:4–12
6. Riegman PHJ, Morente MM, Betsou F, de Blasio P, Geary P (2008) Biobanking for better healthcare. *Mol Oncol* 2:213–222
7. Malentacchi F et al (2016) Second SPIDIA-DNA external quality assessment (EQA): influence of pre-analytical phase of blood samples on genomic DNA quality. *Clin Chim Acta* 454:10–14
8. Tuck MK et al (2009) Standard operating procedures for serum and plasma collection: early detection research network consensus statement standard operating procedure integration working group. *J Proteome Res* 8:113–117

# INDEX

## A

- Active invadopodia ..... 161  
Adenosine 5'-triphosphate (ATP) ..... 185  
Adhesion energies ..... 85, 90  
Adhesion molecules ..... 89  
AFM measurements  
    adhesive ..... 82, 85, 87  
    cantilever coating ..... 83  
    cantilever mounting and calibration ..... 83, 84  
    cell seeding ..... 83  
    elastic modulus ..... 82  
    fully adherent cells ..... 85  
    mechanical ..... 82, 85  
    total adhesion energies calculation ..... 89  
    tumor cell biology aspects ..... 82  
        Young's modulus calculation ..... 87, 88  
Agarose blocks ..... 66  
Aggregation tracings ..... 193  
AlamarBlue ..... 38, 39  
Alamar blue assay ..... 175  
Alamar blue growth inhibition assay ..... 176  
Albino Bl6 mice ..... 291  
Alexa Fluor 546 Phalloidin ..... 156, 157  
Alginate hydrogels  
    bioinert polymers ..... 29, 30  
    biological safety cabinet ..... 34  
    divalent cations ..... 29  
    DMEM ..... 36  
    elastic moduli ..... 35  
    frequency-dependent mechanical properties ..... 30  
    luciferase-expressing cell ..... 39  
    single-step method ..... 29  
    stiffness controlled cell ..... 39  
    tissue property ..... 30  
    two-stage preparation method ..... 31  
    workflow ..... 32  
Alginate–bioactive polymer composite systems ..... 30  
*ALU* elements ..... 18  
Amaxa Nucleofector II device ..... 98  
Analog-to-digital converter (ADC) ..... 299  
Analytical grade reagents ..... 271  
Analyze particles ..... 158  
Anatomical CT/MR imaging ..... 305  
Anchorage-independent agar gels ..... 37  
Anchorage-independent assay ..... 37

- Androgen deprivation therapy (ADT) ..... 254  
Anesthesia ..... 265  
Annexin V ..... 141  
Annihilation coincidence detectors (ACD) ..... 305  
Anti-APC MicroBeads kit ..... 204  
Antibody concentration ..... 205  
Antibody incubation ..... 130  
Anti-CD/anti-CD28 antibodies ..... 206  
Anti-inflammatory macrophages ..... 197  
Antimetastatic compounds ..... 178  
Anti-migratory efficacy ..... 140  
Approach curve ..... 85, 86  
Apyrase ..... 191  
Aqueous layer ..... 218  
Area under the curve (AUC) ..... 169, 172  
Arrow TL-2 cantilevers ..... 83, 90  
Aspiration-based medium perfusion ..... 124, 130  
Aspiration perfusion ..... 123  
Atomic force microscope (AFM)  
    adhesions ..... 81  
    cantilever ..... 81  
    measurements (*see* AFM measurements)  
    solid materials ..... 81  
Atomic force microscopy ..... 37  
ATP detection ..... 194  
ATP indicator ..... 182  
ATP quantification ..... 183  
ATP release ..... 193, 194  
AUC phenotypes ..... 176  
Autofluorescence compensations ..... 265  
Axiovert LE Rel. 4.4 software ..... 288

## B

- Balb C/Nude mice ..... 264  
BAM file ..... 226, 235  
Base Quality Score Recalibration (BQSR) ..... 227, 228  
“Bench to bedside” ..... 325  
Bench translational medicine ..... 326  
Bicinchoninic acid assay ..... 145  
Biochemical composition ..... 27  
Bioinert matrices ..... 28  
Bioinert model systems ..... 29  
Bioinert polymers ..... 29  
Bioluminescence imaging ..... 38, 39  
Biomarker discovery ..... 326

Biomarkers	326
Biomechanical stiffness	27
Bioscope Catalyst AFM	82, 83
Bismuth germanate (BGO)	305
Bl6 mice	290, 291
Block detectors	305
BODIPY staining	201
Bone colonization	254
Bone marrow cells differentiation	204
Bone marrow-derived macrophages	199, 201
Bone marrow isolation	205
Bovine serum albumin (BSA)	201
Boyden chamber	165
Brain-homing variants	280, 285
Brain metastases (BM)	
cancer progression	59
cascade	60
intracranial neoplasms	59
metastatic cancer types	60
OHSCs ( <i>see</i> Organotypic hippocampal brain slice cultures (OHSCs))	
paucity	60
<i>vs.</i> primary brain tumors	59
2D and 3D cell culture model	60
Brain metastasis	290
BrdU labeling <i>in vivo</i>	245
Breast cancer cells	6
Breast cancer MDA-MB-231 SRC Y527F cells	160
Buprenorphine	264
<b>C</b>	
CAKI-1 renal tumor cell line	172
Calcium chloride	29
Cancer cell fluorescent labeling	95
Cancer cell metastasis	4
Cancer cell migration	165
Cancer cells	3–6
The Cancer Genome Atlas (TCGA)	224
Cancerous lesion hallmarks	269
Cantilever geometry	89
Carboxyfluorescein diacetate (CFDA)	63, 66, 73
Carboxyfluorescein succinimidyl ester (CFSE)	199, 205
Coverslips acid washing	157
CD4 <sup>+</sup> T cells	203, 204, 206
Cell-cell collision probability	118
Cell-cell contacts	134
Cell culture-based assays	239
Cell Index	168
Cell-line dependence	149
Cell line-derived models	43
Cell-matrix	134
Cell monolayer	143
Cell morphology	162
Cell suspension	288
Cell viability	242
Cell viability assay	247
Cellular adhesion sites	28
CEM leukemia cells	167
Central nervous system (CNS)	60
Centrifugation tubes	184
CFDA fluorescence intensity	73
CFDA-labeled tumor cells	69
Chalice/Genedata Screener	135
Chemisorption	301
Chemoattractants	171, 173, 175, 176
Chemokines	317
Chicken chorioallantoic membrane (CAM)	
advantage	18
chicken eggs	17
chicken embryos	18
consumables	20
eggs	
incubation	21
preparation	21
embryos	18
equipment	19
fertilized eggs	18
genomic DNA	19
grafted tissues	18
<i>in vivo</i> model	17
isolation	
genomic DNA	22, 23, 25
sample	21, 22
metastasis	17
plastic consumables	19
primer/probes	18
reagents	20
real-time PCR	19
SINES	18
TaqMan®-based absolute quantification, invasive cells	24
TaqMan®-based quantitative PCR	
samples	23–25
standard curve	23–25
tumor cells	18
tumor growth	17
Chicken embryo metastasis model	18
5-Chloromethylfluorescein diacetate (CMFDA)	95
Chromosomal centromere region	57
CIM-Plate 16 invasion chamber	170
Circulating tumor cells (CTCs)	
adhesion receptors	112
biomechanical cues	113
capillary beds	112
endothelial cells	113
microfluidic tools	113
selectins	112

Clinical metastasis .....	178
CMFDA-labeled PC3 cells .....	104
Coagulation .....	190, 193
Collimator .....	299
Colony formation.....	31
Combbenefit.....	140, 142
COMPARE analysis .....	169
COMPARE program .....	171
Compartment model .....	319
CompuSyn .....	135
Computed tomography (CT) .....	298
Confocal laser scanning microscope (CLSM).....	65, 69, 73
Confocal microscopy .....	6
Contemporary research studies .....	269
CP-CONT-BSG-A/B/C cantilever.....	83
CRISPR/Cas9.....	113
Crosslink Matrigel.....	28
Cryosection .....	69
Cryostraw system .....	330
C-type lectin receptor 2 (CLEC-2) .....	182
C-X-C motif chemokine receptor 4 (CXCR4).....	317
Cysteine cathepsins .....	276
Cytoplasmic fraction (CPF).....	272, 273
Cytoskeleton.....	90
Cytotoxicity assays .....	175
Cytotoxic T cells (CD8+) .....	209
<b>D</b>	
Database mining .....	176
Decision-making process .....	326
Default thresholding method.....	158
Defense against pathogens .....	93
Density gradient separation .....	210
Deoxynucleotide triphosphate (dNTPs) .....	212
Deproteinization kit.....	144
DESeq2 functions .....	237
D-glucono-delta-lactone (GDL).....	30
4',6-Diamidino-2-phenylindole dihydrochloride (DAPI) .....	161, 255
Diapedesis-extravasation .....	126
Diethylpyrocarbonate (DEPC) .....	210, 212, 215, 216
Differential Expression Analysis for Sequence Count Data (DESeq2)	
biomarkers identification .....	222
data formats .....	230
differentially expressed genes identification .....	228, 229, 231, 233
experimental conditions.....	231
functional and integrative genomics .....	222
gene expression quantification .....	224, 225
mutational analysis ( <i>see</i> RNAseq data mutational analysis)	
quality control and preprocessing .....	224, 232
system/tools requirements .....	223
Differentiated cells .....	205
Differentiated macrophages .....	198, 201, 205
DiI/DiO/MemBright .....	130
Dimethyl sulfoxide (DMSO).....	64, 176
Diphosphono-1,2-propan-dicarbon acid (DPD) .....	301
Dithiothreitol (DTT).....	185
DNA barcoding, <i>see</i> Multiplexed in vivo screening platform	
DNA isolation .....	56, 281
DNeasy Mini spin column .....	54
Dose-response curves.....	137, 140, 141
Dounce homogenizer .....	271, 272
DPEC-treated water .....	210
Drug synergies .....	137
cell cultivation .....	135
cell cultures preparation.....	136–138
cell preparation materials .....	135, 136
data analysis .....	137, 140
outcomes .....	140, 141
qualitative/quantitative migration analysis software.....	136
standard cell culture .....	135
DU-145 prostate cancer cells .....	176
Ductal carcinoma .....	276
Ductal hyperplasia .....	276
Dulbecco's Modified Eagle Medium (DMEM).....	72, 240
Dulbecco's phosphate-buffered saline (DPBS).....	153, 279
<b>E</b>	
ECGM-containing fluorescent beads .....	117
ECM adhesion receptors .....	112
ECM biochemistry .....	28
ECM degradation assay	
acid wash coverslips cleaning .....	153
cell culture .....	153
fluorescence/immunocytochemistry assay .....	153, 154
fluorescent gelatin coating .....	154, 155
fluorescent gelatin degradation .....	155, 156
gelatin coating .....	153
glass coverslips cleaning .....	154
invadopodia formation and function .....	156–158
EDTA incubation .....	191
EDTA tubes .....	190
EGFR inhibitor .....	177
Elastic modulus calculation .....	90
Elbow Luer .....	130
Electric cell-substrate impedance sensing (ECIS) .....	4

# 338 | METASTASIS: METHODS AND PROTOCOLS

## Index

- Electrical impedance ..... 166  
Electroendosmosis (EEO) ..... 63  
Electronic and multichannel pipettes ..... 141  
ELISA techniques ..... 183, 210  
Embryos ..... 11, 14  
Endothelial barrier ..... 112  
Endothelial cell-coated Transwells ..... 94  
Endothelial cells  
  cancer progression ..... 93  
  cell adhesion ..... 93, 94  
  fluorescence and phase contrast  
    detection ..... 100  
  HUVECs ..... 106, 107  
  live cell imaging ..... 96  
  metastasis formation ..... 94  
  monolayer ..... 104  
  preparation assay ..... 103, 104  
  quantification ..... 105  
Energy metabolism reprogramming ..... 197  
Ensembl gene IDs ..... 231  
Ensembl Variant Effect Predictor (VEP) ..... 227  
Enzymatic crosslinking ..... 28  
Epithelial to mesenchymal transition (EMT)  
  program ..... 182, 269  
Eppendorf tube ..... 214  
Estrogen receptor-positive breast cancer  
  cell lines ..... 167  
Ethanol-sterilized needle-nose pliers ..... 127  
European Human Frozen Tumor Tissue Bank  
  (TuBaFrost) project ..... 331  
Exclude edge ..... 158  
Experimental bone colonization ..... 280, 285  
Experimental brain colonization ..... 280, 285  
Experimental lung colonization ..... 280  
Experimentally induced metastasis  
  models ..... 277, 278, 286  
Extracellular matrix (ECM) ..... 28, 111  
  cell matrix contacts ..... 151  
  degradation ..... 151  
  invadopodia ..... 152  
Extravasation ..... 3, 4, 6, 7, 12  
  adhesion steps ..... 112  
  assay ..... 124  
  cancer cell ..... 121  
  CTC arrest ..... 113  
  endothelial layer ..... 112
- F**
- F-actin depolymerization ..... 161  
Falcon tube ..... 217  
FastQC output ..... 223–225  
Fatty acid free-BSA ..... 198  
Fetal bovine serum (FBS) ..... 167  
Fetal calf serum (FCS) ..... 72, 94  
  
<sup>18</sup>F-FDG PET imaging ..... 309  
<sup>18</sup>F-FDG tumor metabolism ..... 319  
<sup>18</sup>F-FET PET/MR imaging ..... 312  
<sup>18</sup>F-Fluorodeoxyglucose (<sup>18</sup>F-FDG) ..... 298, 307  
<sup>18</sup>F-Fluorothymidine (<sup>18</sup>F-FLT) ..... 309  
<sup>18</sup>F-Fluoromisonidazole (<sup>18</sup>F-FMISO) ..... 311  
Fibrillarin ..... 273  
Fibronectin ..... 81  
Field of view (FOV) ..... 127  
Fine-tuned hydrogel stiffening ..... 30  
Firefly luciferase solution ..... 185  
<sup>18</sup>F-labeled PET radiopharmaceuticals  
  <sup>18</sup>F-FET  
    gliomas ..... 312  
    localization mechanism ..... 312  
    MRI ..... 312  
    PET/CT protocol ..... 312  
  <sup>18</sup>F-FLT  
    DNA synthesis ..... 309  
    localization mechanism ..... 309, 311  
    PET/CT protocol ..... 311  
  <sup>18</sup>F-FMISO  
    hypoxia ..... 311  
    localization mechanism ..... 311  
    neoangiogenesis ..... 311  
    PET/CT protocol ..... 311  
    PET molecular imaging probe ..... 311  
  <sup>18</sup>F-NaF  
    bone metabolism ..... 309  
    bone metastases ..... 308  
    localization mechanism ..... 309  
    PET/CT protocol ..... 309  
FDG  
  <sup>18</sup>F-FDG PET/CT protocol ..... 308  
  fluorine ion ..... 307  
  glucose ..... 307  
  irradiation ..... 307  
  localization mechanism ..... 307, 308  
Flow adhesion assay ..... 95, 97  
Flow-based adhesion assay ..... 96, 99, 104, 105, 107  
Flow conditions ..... 124  
Flow system ..... 96, 100, 102  
Fluorescence-activated cell sorting (FACS) ..... 210  
Fluorescence/immunocytochemistry assay ..... 153, 154  
Fluorescent gelatin coating ..... 154, 155  
Fluorescent gelatin degradation assay ..... 155, 156  
Fluorescent microscope ..... 5  
Fluorescent secondary ..... 130  
Fluorine ..... 307  
<sup>18</sup>Fluorine (<sup>18</sup>F) ..... 307  
Fluorodeoxyglucose ..... 298  
Fluorophore-conjugated secondary antibody ..... 161  
FluoSpheres™ Carboxylate-Modified  
  Microspheres ..... 116

- Force-distance curve ..... 85–87, 89  
 Force volume scan ..... 87  
 Fragments per kilobase million (FPKM) ..... 225  
 Frozen section (FS) ..... 329  
<sup>18</sup>F-Sodium Fluoride (<sup>18</sup>F-NaF) ..... 308–310  
 Fully adherent cells ..... 85, 87  
 Functional PNET ..... 316  
 Fused SPECT/CT axial ..... 304
- G**
- <sup>68</sup>Ga-based PET radiopharmaceuticals  
   <sup>68</sup>Ga-DOTATOC ..... 313  
     localization mechanism ..... 315  
     NET ..... 315  
     PET/CT protocol ..... 316  
   <sup>68</sup>Ga-NODAGA-Exendin  
     GLP-1R ..... 316  
     insulinomas ..... 316  
     localization mechanism ..... 316  
     PET/CT protocol ..... 317  
     PNET ..... 316  
   <sup>68</sup>Ga-Pentixafor  
     chemokines ..... 317  
     localization mechanism ..... 317  
     PET/CT protocol ..... 317, 318  
   <sup>68</sup>Ga-PSMA  
     glycoprotein ..... 313  
     localization mechanism ..... 313  
     PET/CT protocol ..... 314  
   group IIIB ..... 313  
   resolution ..... 313
- <sup>68</sup>Ga-DOTA-labeled somatostatin agonist  
   analogues ..... 316
- Gamma camera  
   components ..... 299  
   <sup>123</sup>I ..... 303–304  
   nuclear medicine imaging system ..... 299  
   radionuclide imaging ..... 299  
   SPECT/CT ..... 299–300  
   <sup>99m</sup>Tc (*see* Technetium (<sup>99m</sup>Tc))
- G-block polymers ..... 29  
 Gel extraction kit ..... 243  
 Gelatin-coated coverslips ..... 160  
 Gelatin degradation ..... 159, 162  
 Gelatin degradation assay ..... 153, 154  
 Gene expression patterns ..... 173  
 Genetically engineered mouse model ..... 254  
 Genome Analysis Toolkit (GATK) ..... 222  
 Genome FASTA file ..... 236  
 Genomic DNA ..... 19, 22, 23, 25  
 Genomic insertions/deletions (Indel) ..... 225  
 GentleMACS Dissociator ..... 52  
 GentleMACS Program ..... 52  
 Gentra Puregene Cell Kit (QIAGEN) ..... 249
- GFP<sup>+</sup> expression ..... 264  
 GFP-LUC-encoding retrovirus ..... 257  
 GFP-LUC-expressing vector ..... 257  
 Glass coverslips cleaning ..... 154  
 Glioblastoma (GBM) ..... 59, 71  
 Glioblastoma multiforme ..... 312  
 Gliomas ..... 312  
 Glo assays ..... 147  
 Glucagon-like peptide-1 receptor (GLP-1R) ..... 316  
 Glucose consumption ..... 147, 148  
 Glycoproteins ..... 112  
 Gr1<sup>−</sup> macrophages ..... 204  
 Grafted tissues ..... 18  
 Green fluorescent protein (GFP) ..... 6, 240
- H**
- H&E staining ..... 287  
 Halt™ Protease Inhibitor Cocktail ..... 271, 273  
 Hamilton syringe ..... 265  
 HCT-116 colon carcinoma cells ..... 135, 167, 171  
 Heatmap ..... 233, 234  
 HEK-293T cells ..... 264  
 Hemizygous PymT transgene ..... 291  
 Hepes ..... 129  
 HEP-filtered air ..... 255  
 Hertz model ..... 87, 90  
 High Capacity cDNA Reverse Transcription kit ..... 216  
 HighSeq platform ..... 250  
 High-throughput small molecule screenings ..... 239  
 Histopaque ..... 216, 217  
 HL-60 leukemia cells ..... 167  
 Homogenization ..... 270  
 Human colorectal cancer cell line HCT116 ..... 136, 139  
 Human histopathology ..... 276  
 Human LU9313 PDX-derived tumor cells ..... 51  
 Human pathologies ..... 269  
 Human PCa metastasis ..... 254  
 Human satellite DNA PCR ..... 53  
 Human umbilical vein endothelial cells (HUVECs) ..... 95, 114  
 HUVEC cell culture ..... 98, 99  
 HUVEC complete medium ..... 103  
 HUVEC growth ..... 127  
 HUVEC seeding ..... 99  
 HUVEC shear stress ..... 127  
 Hydrogel softening ..... 30, 37  
 Hydrogel stiffness ..... 38  
 Hydroxymethylene diphosphonate (HDP) ..... 301  
 4-(2-Hydroxyethyl)piperazine-1-ethanesulfonic acid (HEPES) ..... 63  
 Hyperstack display ..... 118  
 Hypoxia ..... 311

## I

- IARC protocol ..... 331  
 ibidi® connectors ..... 96  
 ibidi® flow chamber ..... 94  
 ibidi® μ-Slide channel ..... 100  
 Illumina sequencing primer-binding sites ..... 249  
 Illumina TruSeq RNA libraries ..... 225  
 Image J plugin Ovuscule ..... 73  
 Image J software ..... 144, 162  
<sup>123</sup>I-MIBG scintigrams ..... 305  
 Immune-deficient NOG mice ..... 52  
 Immune-effective metabolites ..... 198  
 Immunoblotting ..... 270, 273  
 Immunodeficient mouse models ..... 254, 255  
 Immunofluorescence staining ..... 65, 70, 71  
 Immunological lab ..... 205  
 Immunostaining ..... 124, 126  
 Immunosurveillance ..... 93  
<sup>111</sup>Indium (<sup>111</sup>In) ..... 298  
 In situ tumor ..... 111  
 In vitro 3D models, tuneable stiffness  
     alginate hydrogel preparation ..... 34, 35  
     alginates ..... 29  
     anionic carboxylic acid groups ..... 29  
     biologically active materials ..... 28  
     calcium carbonate ..... 29  
     calcium chloride ..... 29  
     cation-based gelation procedures ..... 30  
     cationic crosslinking approaches ..... 30  
     collagen/NaOH ratio ..... 36  
     DMEM ..... 37  
     elastic stiffness ..... 30  
     equipments ..... 33  
     fine-tuned biomechanical ..... 30  
     G-block content ..... 36  
     GDL solution ..... 30, 37  
     matrix stiffness ..... 28  
     monitoring spheroid formation ..... 35  
     reagent preparation ..... 33, 34  
     reagents ..... 31, 33  
     RGD sequences ..... 31  
 In vitro migration/invasion phenotypes ..... 166  
 In vivo drug screening ..... 241  
 In vivo metastatic potential  
     intra-iliac injection ..... 260, 261  
     intra-tibiae injection ..... 258, 260  
     left-ventricle injection ..... 260  
 In vivo-like mechanical forces ..... 94  
 In vivo propagation ..... 49  
 IncuCyte® ImageLock Plates ..... 134, 136, 138  
 IncuCyte® WoundMaker tool ..... 134, 136, 138, 141, 142  
 IncuCyte scratch ..... 139

- Incucyte system ..... 134, 141  
 Informatic analysis ..... 169, 176  
 Integrin and ILK signaling ..... 177  
 Intracardiac injection ..... 290  
 Intra-iliac PCa cells injection ..... 254  
 Intravenous injection ..... 302  
 Invadopodia  
     actin-rich membrane protrusions ..... 151  
     cell confluence ..... 160  
     coverslips ..... 156  
     degradation area ..... 156  
     degradation foci ..... 152  
     F-actin ..... 156  
     formation/function ..... 160  
     marker proteins ..... 161  
     rosettes ..... 160  
 Invasion-metastasis cascade ..... 3, 4, 151  
 Invasive ductal adenocarcinomas (IDC) ..... 276  
<sup>123</sup>Iodine (<sup>123</sup>I) ..... 298  
<sup>123</sup>I-mIBG  
     localization mechanism ..... 304  
     SPECT/CT protocol ..... 304  
<sup>123</sup>I-NaI  
     localization mechanism ..... 303  
     SPECT/CT protocol ..... 303  
     diagnosis ..... 303  
     halogen element ..... 303  
 Ismatec Reglo Digital MS pumps ..... 119, 121  
<sup>123</sup>I-Sodium Iodide (<sup>123</sup>I-NaI) ..... 303  
 Isotopes ..... 297  
 IVIS Spectrum In Vivo Imaging System ..... 256
- K**
- Kinase inhibitor ..... 177  
 Kinetic phenotypes ..... 166  
 KM12 colon carcinoma cells ..... 167, 171
- L**
- Lactate production ..... 144, 147  
 Lamellipodia ..... 85, 151, 171  
 Large neutral amino acid transporter (LAT) ..... 312  
 Laser capture microdissection (LCM) ..... 332  
 Life-dead staining ..... 62, 64, 68, 73  
 Light transmission aggregometry (LTA) ..... 184, 187  
     measurement ..... 183  
 PBS/EDTA ..... 184  
 platelets tumor cells preparation ..... 187  
 PPP ..... 184  
 PRP ..... 192  
 TCIPA and detection induction ..... 187  
     tumor cell cultivation ..... 184  
 Lipid droplets ..... 201

Live cell adhesion assay	
adhesion cell	122
CTC perfusion	120
monolayer	120
μSlide VI	120
PBS-EDTA	121
peristaltic pump	115
pushing perfusion	121
transient siRNA	122
tubing	122
Live cell imaging	94, 96, 104, 105
lncRNAs	210
LoG detector	118
Log <sub>2</sub> fold changes (LFC)	229
Long-term cell culture	129
Long terminal repeat (LTR)	276
Luciferase-expressing A549 cells	38
Luciferase-expressing vector	256, 257
Luciferin	264, 265
Luciferin-luciferase reaction	189, 190
Luer connector	107
Luminescence reagent	185, 189
Luminometer	147
Lung carcinoma PDX LU9313	51
Lung colonization	288
Lung metastases	289
Lutetium oxyorthosilicate (LSO)	305
Lutetium yttrium orthosilicate (LYSO) c	305
<b>M</b>	
M2-monocyte differentiation	214
Macrophages/cytotoxic T cells isolation	209, 211, 213, 214
Macroscopic metastasis	54
Magnetic resonance imaging (MRI)	298
Malignancies	276
Malignant cell lines	39
Malignant GBM cells	60
Malignant invasiveness	28
MatLab	87
Matrigel	30, 39, 165
Matrix stiffness	28
Mature miRNAs	210
MDA-MD-232 breast cancer cell line	5, 167, 168
MDA-MB-231 triple-negative mesenchymal-type breast cancer cell line	167, 172
Mean graph representation	173
Mesenchymal invasion	176, 177
Metabolic analyzer	198
Metabolic assays	
deproteinize	147
dilute media	147
equipment	144, 145
interpretation	149
intracellular concentration analysis	147
specific instructions	147
standard lysis buffer	146
substrate consumption	147
Metabolic environment	198
Metabolic-related pathway	197
Metabolic substrates	147
Metabolites	149
Metaiodobenzyl guanidine (mIBG)	304
Metastasectomies	325
Metastases types	44
Metastasis	
microfluidic devices	4
models	44
TME	4
zebrafish (see Zebrafish)	
Metastasis-related immune cells isolation/manipulation	
cDNA synthesis, RT-PCR	212, 215
isolated cells seeding and transfection	211, 212, 214
macrophages/cytotoxic T cells	211, 213, 214
monocytes differentiation, M2	
macrophages	211, 214
PBMCs isolation	211–213
PBMCs thawing	211, 213
qRT-PCR	212, 215
RNA extraction	212, 214, 215
Metastasis research, clinical setting	
bench translational medicine	326
solid tissue processing	326–330
SOPs	326
Metastatic cascade	3, 112, 118
Metastatic mouse mammary carcinoma cell line D2A1	113
Metastatic PCa in vivo imaging	
bioluminescent imaging/data analysis	261–263
cell culture	255
cell inoculation in vivo	255, 256
cells transduction	256–257
FACS	255
GFP <sup>+</sup> cells sort	257, 259
potentials	258–261
retrovirus production	255
systems	256
Metastatic progression	3, 111
Metastatic tumor cells	56
Methylene diphosphonate (MDP)	301
Microchannels	114
Microdetector array	175
Microenvironmental interactions	143
Microfluidic extravasation assay	121, 123
Microfluidics shear stress resistance assay	118, 120
Microfluidics tubing	129
Micrometastasis	254

Micro-milieu.....	82
Migration assays	
cell ability.....	146
cell suspension.....	145
equipment.....	144
medium.....	147
migration chamber.....	145
phase contrast and 4X magnification .....	145
standard culture conditions.....	145
sterile PBS.....	145
timepoints.....	146, 149
4T1 mammary cancer cells.....	146
trypsinizing.....	145
Migration/invasion assays .....	166
Milli-Q grade Ultrapure water .....	122, 128
Minimal Essential Medium (MEM).....	63
MiniSeq using the MiniSeq Mid Output Kit .....	250
miRNA-diluted mimics/antagomirs.....	212
MiSeq and the MiSeq Reagent Kit v3 .....	249
Mitochondrial respiration .....	197, 198, 203
MMTV-PymT-induced carcinomas.....	276
Modern-day hybrid PET/CT .....	320
Modern PET scanner systems .....	305
MojoSort Buffer.....	213
MojoSort Magnet .....	214
Molecular biology techniques .....	210
Molecular characterization .....	166
Molecule inhibitors .....	177
Monovette .....	190
Mosaic plugin in ImageJ.....	129
Mouse mammary tumor virus (MMTV).....	276
Mouse models .....	254
Mouse transplantation models .....	248
MS-based proteomic profiling.....	326
MSCV six-nucleotide barcode-GFP vector .....	240
Multi-pinhole collimators .....	300
Multiple critical growth factor pathways .....	177
Multiple freeze-thaw cycles .....	89
Multiplexed <i>in vivo</i> screening platform	
barcode amplification .....	242, 249
barcode cell line generation.....	240, 242, 246
barcoded cells isolation .....	248
barcode representation .....	240
barcode virus production.....	245, 246
bioinformatic analysis.....	250
cell-based .....	240
cell line variants .....	240
cell pool injection .....	247, 248
compound treatment .....	247, 248
DNA isolation .....	248
elimination unbarcoded cells.....	247
intricate and expensive .....	239
laboratory equipment .....	244
library preparation.....	249, 250
molecular cell barcoding.....	239
next-generation sequencing .....	244
requirements.....	242
schematic workflow .....	241
suitable metastatic cell line identification .....	245
Mycoplasma.....	258, 265
MyiQ™ Single-Color Real-Time PCR Detection System.....	281
<b>N</b>	
N-acetyl-L-aspartyl-L-glutamate peptidase I (NAALADase I).....	313
NaI(Tl) scintillation crystal .....	299
NanoScope .....	87, 89
Natural killer (NK)-cells .....	55
NCI DCTD Tumor Repository .....	167
NCI60 drug screening database .....	171, 174
NCI60 tumor cell lines.....	166, 167, 170, 174, 176
NCI-H226 lung cancer cells .....	173
NCI Tumor Repository .....	167
Neoangiogenesis .....	311
Neubauer chamber.....	103
Neurodegenerative diseases .....	61
Neuroendocrine tumors (NET).....	315
Neuroscience research .....	60
Next-generation sequencing (NGS) .....	239, 244, 249, 328
NMRI nu/nu mice .....	56
1-(2'-Nitro-1'-imidazolyl)-2-O-tetrahydropyranyl-3-O-toluenesulfonylpropanediol (NTTP) .....	311
No AmpErase® UNG for Real-Time PCR	
amplification .....	55
NODAGA .....	317
NOG-F .....	46
Noncoding RNAs .....	210
Nonlinear regression analysis .....	319
Normalization .....	145
No template control (NTC) .....	286
Novel splice junctions .....	235
Novel splice variants .....	225
NSC 624445 .....	176
NucBlue™ Live ReadyProbes™ reagent .....	270
Nuclear fraction (NuF).....	272, 273
Nuclear medicine radionuclide imaging	
CT/MRI .....	298
gamma cameras .....	298
iodine .....	303
isotopes .....	313
modern imaging methodology .....	320
PET .....	304
preclinical and clinical science .....	297
<sup>99m</sup> Tc .....	298

Nucleofector .....	106
Nucleolar fraction (NuF) .....	273
Nucleolar ID™ (Green) .....	270
Nucleolar isolation	
analysis .....	269
lysed cells separation .....	270
novel targets .....	269
procedure/methods .....	271–273
requirements .....	271
schematic flowchart .....	270
tissue-cultured mammalian breast	
cancer cells .....	270
western blot analysis .....	273
Nucleoli standard buffer (NSB) .....	271
Nucleolus .....	269, 270

**O**

O-(2-[ <sup>18</sup> F]-fluoroethyl)-L-tyrosine ( <sup>18</sup> F-FET) .....	312
Offset correction process .....	88
OG 488-conjugated gelatin matrix coating .....	152, 160
Oleate-treated macrophages .....	198
Oligofectamine .....	106
Oligonucleotides .....	47
Operative transfer method .....	289
Optimal cell concentration .....	147
Opti-MEM™ I Reduced Serum Medium .....	242, 246
Oregon green (OG) .....	152, 153
Organ colonization .....	4
Organic solvent .....	192
Organotypic hippocampal brain slice cultures (OHSCs)	
cell seeding .....	63, 66, 68
cornu ammonis .....	61
cryosection .....	65, 69, 70
fixing and staining .....	64, 68, 69
immunofluorescence staining .....	65, 70, 71
immunohistochemical staining .....	62
innovative experimental setup .....	61
life-dead staining .....	64, 68
microenvironment .....	61
neurodegenerative diseases .....	61
preparation .....	62, 63, 65–67
semipermeable membranes .....	61
single brain slice generation .....	61
slicing procedure .....	62
Organ removal .....	71
Orthotopic model .....	289
Orthotopic transplantation .....	279, 288, 289
Osmotic lysis .....	203
Osteogenic cells .....	301
Osteolytic lesions .....	308
Oxidative phosphorylation .....	147

**P**

Pancreatic NET (PNET) .....	316
Parallel cell viability assays .....	247
Pasteur pipettes .....	63, 64, 67, 71
Patient-derived xenograft (PDX) models	
chemosensitivity .....	44
clinically relevant approach .....	43, 44
cytotoxic agents .....	44
development .....	44
DNA methylation pattern .....	43
guide therapy .....	44
hematogenous metastasis ( <i>see</i> PDX-derived metastasis models) .....	
primary tumor cell architecture .....	43
spontaneous metastasis .....	44
subcutaneous tumors .....	44
Patlak analysis .....	319
PBMCs isolation .....	210–213
PBMCs thawing .....	211, 213
PBS–EDTA solution .....	187
PBST blocking solution .....	161
PC3 cell culture .....	96
PC3 prostate cancer cells (ATCC) .....	94, 106
PCa cells injection .....	254
PDX-derived metastasis models	
cells and sample collection .....	46
cryoconservation .....	49, 51
cryoconservation materials .....	45, 46
DNA isolation .....	54
human primary tissue samples .....	45
human satellite DNA .....	55
inoculation .....	52, 53
liver and lung samples collection .....	53
macroscopic metastasis .....	54
media and supplements .....	46
model establishment .....	48
molecular analyses .....	47
mouse strains .....	46
single-cell suspensions .....	51, 52
termination criteria .....	56
tumor tissue harvesting .....	49
xenotransplantation .....	45, 48, 49
PDX subclone LU9313M .....	51
Perchloric acid precipitation .....	149
Peripheral blood mononuclear cells (PBMCs) .....	210, 213, 217
Peritoneal Carcinomatosis Index (PCI) .....	327
Peritoneal/pleural metastasis .....	327
PET radiopharmaceuticals	
Fluorine ( <i>see</i> <sup>18</sup> F-labeled PET radiopharmaceuticals) .....	
<sup>68</sup> Ga-based .....	313–318
organic substances .....	306

# 344 | METASTASIS: METHODS AND PROTOCOLS

## Index

- PET radiopharmaceuticals (*cont.*)  
    PET/MRI systems ..... 318  
    quantification ..... 318–320  
    standard radionuclides ..... 306
- PhiX-Library ..... 251
- Phosphate-buffered saline (PBS) ..... 63, 64
- Photobleaching ..... 152, 160
- Photodetector ..... 83, 89
- Photomultiplier tubes (PMT) ..... 299
- Physiologic processes ..... 134
- Physiological platelet count ..... 191
- Pixel binning ..... 108
- Planar imaging ..... 304
- Plasma membrane permeability ..... 73
- Platelet-poor plasma (PPP) ..... 183, 184
- Platelet-rich buffer ..... 186, 192, 194
- Platelet-rich plasma (PRP) ..... 186
- Platelets  
    activation ..... 181, 192  
    anuclear cells ..... 181  
    cellular fraction ..... 181  
    functional impact ..... 182  
    hematogenous dissemination ..... 182  
    inhibitors ..... 192  
    malignancy ..... 182  
    PARs ..... 182  
    processing ..... 192
- TCIPA (*see* Tumor cell-induced platelet activation (TCIPA))  
    tumor cells ..... 182
- Poiseuille effects ..... 129
- Poiseuille flow ..... 117
- Poiseuilles' equation ..... 129
- Poisson's ratio ..... 88
- Polyamino acids coating ..... 157
- Polydimethylsiloxane (PDMS) ..... 113
- Poly-L-lysine ..... 89, 157, 160
- Polymorphism phenotyping (PolyPhen) ..... 227
- Polyoma virus middle T oncogene (PymT) ..... 276
- Porcine skin gelatin ..... 153
- Positron emission tomography (PET) ..... 298  
    annihilation photons ..... 305  
    detectors and instrumentation ..... 305, 306  
    imaging protocol ..... 306  
    radiopharmaceuticals (*see* PET radiopharmaceuticals)  
        3D functional tomographic imaging ..... 304
- Positron emission tomography/magnetic resonance imaging (PET/MRI) ..... 318
- Positron-emitting radioisotope ..... 298
- Positron-emitting radionuclides ..... 298
- Postinoculation ..... 266
- Postmitotic pairs ..... 175
- Practical Advice on the Determination of  
    Cantilever Spring Constants ..... 90
- Preclinical PET image ..... 310
- Preclinical SPECT systems ..... 300
- Pre-culture ..... 141
- Preheat ECGM medium ..... 123
- Primary antibody anti-invadopodia  
    marker protein ..... 154
- Primary PymT cell preparation ..... 279, 288
- Principle component analysis (PCA) ..... 229
- Probing metastasis using microfluidics  
    cell culture medium ..... 114  
    classical cancer cell lines ..... 113, 114  
    confocal microscopy ..... 116  
    endothelial cell seeding ..... 116, 117  
    equipment ..... 114  
    fluorescent beads ..... 116  
    live cell adhesion assay ..... 120–122  
    live imaging ..... 123, 125  
    live microscopy ..... 114, 116  
    microchannels ..... 114  
    microfluidic extravasation assay ..... 121, 123  
    perfusion and flow profiles ..... 117–119  
    SEM ..... 126, 128  
    SEM reagents ..... 116  
    shear stress resistance assay ..... 118, 120  
    3D confocal imaging ..... 124, 126  
    tubing setup ..... 117
- Promega-Glo assay kits ..... 144
- Prostate cancer (PCa)  
    ADT ..... 254  
    bone ..... 254  
    in vivo imaging (*see* Metastatic PCa in vivo imaging)  
    localized invasive lesions ..... 253  
    lung and lymph nodes ..... 254  
    manageable disease ..... 253  
    metastasis ..... 253  
    metastatic patients ..... 254  
    tumor cell adaptation ..... 254
- Prostate-specific membrane antigen (PSMA) ..... 313
- Protease-activated receptor (PARs) ..... 182
- Proteases  
    11 cysteine ..... 276  
    invasion and metastasis ..... 275  
    malignant cells ..... 275  
    mouse lines ..... 276
- Protocol covering measurements ..... 82
- P-selectin ..... 182
- Public NCI60 database ..... 178
- Pulsatile flows ..... 127
- Pushing perfusion ..... 123, 124
- Putative invasion inhibitors ..... 177
- PymT/actin ..... 291

PymT cell injection .....	284
PymT-induced carcinomas .....	277
<b>Q</b>	
Qiagen DNeasy Blood & Tissue Kit .....	54
Qiagen DNeasy kit .....	56
QIAquick Gel Extraction Kit (QIAGEN) .....	249
qRT-PCR thermal cycling parameters .....	210, 216
Qualitative/quantitative migration analysis software .....	136
Quantification	
activity concentrations .....	318
nonlinear regression analysis .....	318, 319
patlak analysis .....	319
semiquantitative analysis .....	318
SUV .....	319
Quantification cycle (CQ) .....	24
Quantitative cell biology analyses .....	134
Quantitative real-time PCR (qrtPCR) .....	284
Qubit 4 Fluorometer .....	251
Qubit dsDNA HS assay kit .....	251
<b>R</b>	
Radioimmunoprecipitation assay (RIPA) .....	145
Radioisotopes .....	297, 298, 303
Radiolabeled somatostatin analogues .....	316
Radiolabeling .....	298, 316
Radionuclides	
DOTATOC and DOTATATE .....	315
fluorine .....	307
imaging .....	299
imaging modality .....	320
NaCl .....	300
PET imaging .....	306
positron-emitting .....	298
SPECT imaging .....	298, 299
Radiopharmaceuticals .....	298
Real-time in vitro invasive phenotypes	
aggressive migration .....	169
components .....	167
flowchart .....	168, 169
genes and pathways .....	169, 171, 172
growth factor receptor expression .....	176
invading cells visualization .....	167
materials .....	166
migration and invasion .....	166, 168
NCI60 drug screening database .....	171, 174
NCI60 phenotypes .....	166
Real-time PCR .....	19, 20, 216, 291
Recombinant basement membrane .....	28
Region of interest (ROI) .....	299, 318
Resonance peak .....	84
Retract curve .....	85, 86
Retroviral infection .....	264
Retroviral vector transduction .....	240, 250, 251
Reverse transcription cocktail .....	212
Reverse-transcribed (m)RNA fragments .....	222
Rho GTPases	
cancer cell adhesion .....	94
cancer cell fluorescent labeling .....	95
cancer cell preparation .....	102, 103
cancer progression .....	93
cell adhesion molecules .....	93
cell culture .....	94, 95
cycle .....	93
depleted human cancer cells .....	94
endothelial cell preparation .....	103, 104
expression .....	93
flow adhesion assay .....	95, 97
flow-based adhesion assay .....	104, 105
flow system .....	100, 102
HUVEC cell culture .....	98, 99
HUVEC seeding .....	99
microscope setup, live imaging .....	100
PC3 cell culture .....	96
quantification .....	96, 105, 106
shear-stress .....	94
siRNA nucleofection .....	95
siRNA transfection .....	98
Ribosome biogenesis .....	269
RIPA buffer .....	146
RNA extraction .....	212
RNA interference technology .....	171
RNA sequencing (RNAseq)	
DESeq2 ( <i>see</i> Differential Expression Analysis for Sequence Count Data (DESeq2)) .....	221
DNA-based assays .....	221
expression quantification .....	222
GATK .....	222
reference genome .....	222
RSEM .....	222
short reads .....	222
STAR .....	222
technologies .....	222
RNAse enzymes .....	216
RNAseq by Expectation Maximization (RSEM) .....	222
RNAseq data mutational analysis	
BQSR .....	227, 228
fragment alignments .....	226
genetic alterations .....	225
Illumina TruSeq RNA libraries .....	225
read deduplication and splitting .....	226
read groups and sorting .....	226
Rosettes .....	156, 157, 160
R package tximport .....	235

# 346 | METASTASIS: METHODS AND PROTOCOLS

## Index

### S

- Scanning electron microscopy (SEM) ..... 174  
analysis ..... 126–128  
reagents ..... 116
- Scoring system ..... 56
- Scratch assay  
cell's behavior ..... 133  
cellular movement study ..... 133  
format ..... 144  
medium ..... 202, 204  
microscopic techniques ..... 134  
migration ..... 134  
screening tool ..... 134  
traditional ..... 143
- Seahorse XF DMEM medium ..... 206
- Seeding and scratch application ..... 142
- SEM desktop microscope ..... 128
- Semiquantification ..... 51
- Shear rheology ..... 37
- Shear-resistant ..... 101
- Shear stress ..... 93, 94, 102
- Shear stress-resistant firm adhesion ..... 94
- Short interspersed repeated DNA elements  
(SINES) ..... 18
- Silicon nitride ..... 81
- Silicon photomultipliers (SiPMT) ..... 318
- Single-cell solution ..... 200
- Single-Color Real-Time PCR Detection System  
MyIQ (BioRad) ..... 288
- Single nucleotide variations (SNV) ..... 225
- Single photon emission computed tomography  
(SPECT) ..... 298  
CT ..... 300  
dual-headed ..... 299  
image resolution ..... 300  
3D imaging procedure ..... 299
- siRNA nucleofection ..... 95, 98
- siRNA-transfected PC3 cells ..... 102
- siRNA transfection ..... 98
- siRNA treatment ..... 175
- Small Animal MRI ..... 291
- Small animal multi-pinhole SPECT systems ..... 300
- Small-cell lung carcinoma ..... 50, 53
- Small-molecule screening platform ..... 249
- Snap-freezing ..... 329, 330, 332
- Snap-frozen tissue ..... 332
- Sodium borohydride (NaBH<sub>4</sub>) ..... 153, 155, 160
- Sodium-iodide symporter (NIS) ..... 303
- Sodium oleate-treated macrophages ..... 202
- Solid tissue processing  
FS ..... 329  
paramount ..... 326  
pathology department ..... 328, 329

- snap-freezing ..... 329, 330
- surgery ..... 327
- surgical pathology ..... 327
- tissue specimen ..... 328
- Somatic variances ..... 227, 228
- Somatostatin ..... 315
- Sonication ..... 272, 274
- Sorting Intolerant From Tolerant (SIFT) ..... 228
- Specific adhesion events ..... 81
- SPECT imaging ..... 298
- Spectrophotometric analysis ..... 23
- Spheroid characterizations ..... 39
- Spheroid formation  
alginate composite network ..... 31  
cell proliferation ..... 37  
centrifugation ..... 34  
hydrogels ..... 39, 40  
malignant cell lines ..... 39  
mechanical stiffness ..... 31  
microscopy ..... 36  
monitoring ..... 35  
replace media ..... 35  
2D model ..... 28
- Spliced Transcripts Alignment to a Reference  
(STAR) ..... 222, 226, 235
- Stable isotope <sup>127</sup>I ..... 303
- Staining cancer cells ..... 8
- Standard deproteination protocol ..... 147
- Standard operating procedures (SOPs) ..... 326
- Standardization and Improvement of Generic  
Pre-analytical Tools and Procedures for  
In Vitro Diagnostics (SPIDIA) ..... 331
- Standardized uptake value (SUV) ..... 318–320
- Statistical testing ..... 147
- StepOne Real-Time PCR ..... 215
- StepOnePlus™ Real-Time PCR system ..... 55
- Subsequent mutational analysis pipeline ..... 226
- SuperFrost slide ..... 69, 74
- Surrogate models ..... 44
- Synergism ..... 141
- Synergy matrices ..... 140, 141
- SynergyFinder ..... 135
- Syngeneic allograft models ..... 278
- Synthetic drug screening database ..... 177
- T**
- T cell ratio ..... 206
- T175 flasks ..... 136
- Tail vein injection ..... 254
- TaqMan real-time PCR ..... 20, 23, 24
- TaqMan master mix ..... 215
- TaqMan® Universal PCR Master Mix ..... 55
- T-cell suppression assay ..... 204, 205

- TCIPA-inducing pathways ..... 182  
 $^{99m}$ Tc-labeled phosphonate compounds ..... 301  
 $^{99m}$ Tc-SESTAMIBI (MIBI) ..... 301–303  
 Tecan Spectrafluor Plus Microplate Reader ..... 175  
 Technetium ( $^{99m}$ Tc)  
   localization mechanism ..... 301  
   MIBI ..... 301–303  
   NaCl ..... 300  
   phosphonate and phosphate  
    compounds ..... 300, 301  
   radiopharmaceuticals ..... 300  
   SPECT/CT protocol ..... 301  
   SPECT imaging ..... 300  
   transition metal ..... 300  
 Tetraiodothyronine (T4) ..... 303  
 Tetramethylsilane ..... 175  
 $^{201}$ Thallium ( $^{201}$ Tl) ..... 298  
 Thaw frozen genomic DNA ..... 55  
 Therapeutic index ..... 177  
 Thermal tune calibration ..... 84  
 3D cell culture models ..... 60  
 3D confocal imaging ..... 124, 126  
 Three-dimensional extracellular matrix ..... 27  
 Thresholded gelatin image ..... 159  
 Thrombin receptor-activating peptide  
   (TRAP) ..... 192  
 Thymidine kinase 1 (TK1) ..... 309  
 Time-lapse microscope ..... 103, 107  
 Time-lapse movie acquisition ..... 100  
 Time-of-flight (TOF) ..... 305  
 Timepoints ..... 144  
 Tissue culture media ..... 153  
 Tissue factor (TF) ..... 193  
 Tissue stabilization ..... 332  
 Tissue stiffness ..... 28  
 Tissue-Tek ..... 74  
 Tomographic SPECT imaging ..... 300  
 TrackMate plugin ..... 118  
 TrackScheme ..... 118  
 Transcriptome-wide gene expression profiling ..... 221  
 Transcripts per kilobase million (TPM) ..... 225  
 Transfection ..... 214, 217  
 Transgenic MMTV-PymT model  
   brain-homing variants ..... 280, 284, 285  
   breast cancer ..... 277  
   differentiated IDCs ..... 276  
   experimental bone colonization ..... 280  
   experimental brain colonization ..... 280, 285  
   experimental lung colonization ..... 280, 284  
   metastases analysis histology ..... 281  
   orthotopic transplants ..... 283, 291  
   primary PymT cell preparation ..... 279  
   primary tumor cells isolation ..... 281, 282  
   PymT cell variants ..... 279  
   quantitative PC ..... 281  
 quantitative real-time PCR ..... 286, 287  
 transplantation into mammary gland ..... 279, 280  
   tumor cell dissemination analysis ..... 287, 288  
 Transplantation ..... 56  
 Trichloroacetic acid protocols ..... 149  
 Triiodothyronine (T3) ..... 303  
 Triple-negative mesenchymal-type breast  
   cancer cell lines ..... 172  
 Trouble-free representation ..... 134  
 Trypan blue ..... 217  
 Trypsin ..... 191, 262  
 Trypsin-EDTA ..... 136  
 Trypsinize cells ..... 117  
 Tumor-associated immune cells ..... 275  
 Tumor-associated macrophages (TAMs) ..... 277  
   bone marrow-derived macrophages ..... 199  
   bone marrow isolation ..... 200  
   buffers ..... 198, 199  
   CD4 T cells isolation ..... 203, 204  
   cell population ..... 197  
   devices ..... 199  
   flow cytometry ..... 199  
   macrophage differentiation and  
    polarization ..... 200, 201  
   magnetic sort ..... 199  
   metabolic analysis ..... 199  
   metabolic pathways ..... 198  
   oleate-treated macrophages ..... 198  
   purification ..... 201, 202  
   T-cell suppression assay ..... 204  
 Tumor cell-induced platelet activation (TCIPA)  
   ATP release ..... 183  
   granule release ..... 185, 188, 189  
   LTA ..... 184, 187–188  
   pathways ..... 183  
   platelet aggregation ..... 182  
   platelet characterization ..... 183  
   platelet dense granule release ..... 185, 188, 189  
   platelet isolation ..... 183–186  
 Tumor cells ..... 18  
   autonomous ..... 143  
   biology ..... 82  
   invasion ..... 62  
 Tumor culture media (TCM) ..... 210  
 Tumor microenvironment (TME) ..... 4, 197, 289  
 2D cell migration assay ..... 143  
 2D-fluorescent matrix degradation assay ..... 151, 152  
 Two-step cation-based gelation procedures ..... 30  
 Tyr<sup>3</sup>-Octreotide (TATE) ..... 315  
**U**  
 U138-MG glioblastoma cell line ..... 83  
 UACC-62 melanoma cells ..... 170, 171  
 Ultrasound-guided intracardiac injection ..... 290  
 Unix/Linux ..... 229

**V**

- Vascular invasion ..... 4, 5, 8, 13  
VCFtools ..... 236  
VE-cadherin ..... 126  
VEGF expression ..... 177  
Vibratome ..... 71, 72  
Virus production ..... 245  
Vortexing ..... 34  
Vybrant® CFDA SE Cell Tracer Kit ..... 72

**W**

- Weakly adherent cells ..... 85  
Web-based Variant Effect Predictor ..... 236  
Wedge resections ..... 327  
96-Well format ..... 30  
Western blot analysis ..... 273  
Western blot assessment ..... 273  
Whole cell fraction (WCF) ..... 272  
Whole cell lysate (WCL) ..... 273  
Whole-genome or whole-exome sequencing  
(WGS/WES) ..... 222

**X**

- xCELLigence® RTCA DP instrument ..... 168,  
174, 176  
Xenograft approach ..... 278  
Xenograft tumors ..... 56  
Xenotransplantation ..... 48

**Y**

- Young's modulus ..... 82, 87, 90, 91

**Z**

- Zebrafish  
biomedical research ..... 5  
cancer cell invasion ..... 4, 5  
cancer cell metastasis ..... 4  
cost efficient ..... 5  
embryo microinjection ..... 8, 9  
embryos cells ..... 5  
extravasation ..... 4, 6, 7, 12  
fluorescence ..... 12  
fluorescent vasculature ..... 14  
injecting cancer cells, yolk sac ..... 12, 13  
injection station ..... 8  
labeling cells, red lipophilic fluorescent  
dye ..... 9  
manipulating fish ..... 8  
metastasis ..... 5  
microinjection dispense system ..... 10, 11  
single-cell behaviors ..... 5  
temperature ..... 13  
transparent zebrafish strain ..... 5  
tumor cell populations ..... 5, 7  
vascular invasion ..... 5  
visualization ..... 8  
wild-type zebrafish embryos ..... 5